The contribution of immune regulatory microRNAs in endometriosis

Kavita Panir

Robinson Research Institute

Discipline of Obstetrics and Gynaecology

Faculty of Health Science, School of Medicine

The University of Adelaide, South Australia, Australia

A thesis submitted to the University of Adelaide for admission to the degree of Doctor of Philosophy

OCTOBER 2019

Table of contents

List of Figures

List of Tables

Abstract

Endometriosis, the growth of ectopic endometrial tissue, affects 10% of reproductive-aged women. Although disease aetiology is enigmatic, aberrant immune responses within the peritoneal cavity have been implicated. Endometriotic lesion development is broadly classified into two phases; one mediated by a M1-like pro-inflammatory (tissue clearance; which inhibits disease) response and the other a M2-like anti-inflammatory (tissue remodelling; which promotes disease) response. Dysregulated expression of microRNA-155 (*miR-155*) in plasma samples from women with endometriosis is proposed to promote M1-like macrophage activity. Conversely, elevated *miR-223* activity in endometriotic lesions is thought to promote M2-like macrophage activity. Hence, the aims of this doctoral thesis are to initially characterise endometriotic lesion development in an induced 'menstrual' mouse model of endometriosis, and to subsequently evaluate the impact of depleting either *miR-155* or *miR-223* on endometriotic-like lesion development and macrophage activity.

Using the 'menstrual' mouse model of endometriosis, 40mg of decidualised donor endometrium was injected subcutaneously into recipient mice. Lesions that developed from syngeneic transfers (donor and recipient mice of the same genotype) and reciprocal transfers (between wildtype C57 mice and either *miR-155*$^{-/-}$ or *miR-223*$^{-/-}$ mice) were assessed by histochemical and immunohistochemical analysis for macrophage activity, angiogenesis and the extent of fibrosis at day (D)7, D14 and D21 after tissue transfer. To investigate effects on donor tissue gene expression, the differentially expressed genes (DEGs) and molecular pathways associated with the pathogenesis of endometriosis were defined by RNA-Sequencing of donor endometrium, as well as D7 and D14 lesions from syngeneic transfers using the Illumina Next-Seq500 platform at a depth of 50 million reads per samples. Differentially regulated genes were defined as those with a log fold change (log_2FC) of $1 < log_2FC < -1$, and a false discovery rate (FDR) of 0.05.

A reduction in lesion weight and size was seen over time in all groups. Effects of microRNA deficiency were seen on lesion tissue architecture, with an increase in glandular formation only evident in C57 to C57 and C57 to *miR-155*$^{-/-}$ transfers. Systemic deficiency of *miR-155* acted to restrict M1-like macrophage activity and promoted the expression of M2-like macrophage markers. Importantly, blood vessel density increased in *miR-155*$^{-/-}$ to *miR-155*$^{-/-}$ lesions over time, supporting lesion establishment. In contrast, early influx of F4/80^{+} macrophages with increased MHC II and iNOS expression was seen in *miR-223*$^{-/-}$ to *miR-223*$^{-/-}$ lesions, associated with the development of cystic-like lesions devoid of glands. Similarly, by D14, glands were absent in lesions from C57 to *miR-223*$^{-/-}$ transfers. RNA-Seq analysis identified DEGs in

several pathways associated with endometriosis, notably immune regulatory pathways, tissue remodelling, cellular differentiation and proliferation, and angiogenesis.

In summary, this study has shown that microRNA modulation of macrophage polarisation impacts the development of endometriosis-like lesions in a mouse model, with deficiency in *miR-155* increasing M2-like macrophage activity, while deficiency in *miR-223* promotes M1-like macrophage activity. Reciprocal transfer data suggest that microRNA-dependent signalling factors from both the donor tissue and recipient environment influence macrophage activity, and have effects on endometriotic lesion growth. Our findings add to emerging evidence that macrophage phenotype and function are important determinants of endometriosis, and identify *miR-155* and *miR-223* as key microRNAs that regulate macrophage capacity to impact disease establishment and progression. Further studies are now required to determine whether similar microRNA-mediated modulation of macrophages contributes to human disease. In a clinical setting, the targeting of these macrophage-regulating microRNAs may have therapeutic potential, and should be investigated further.

Declaration

I certify that this work contains no material which has been accepted for the award of any other degree or diploma in my name, in any university or other tertiary institution and, to the best of my knowledge and belief, contains no material previously published or written by another person, except where due reference has been made in the text. In addition, I certify that no part of this work will, in the future, be used in a submission in my name, for any other degree or diploma in any university or other tertiary institution without the prior approval of the University of Adelaide and where applicable, any partner institution responsible for the joint-award of this degree.

I acknowledge that copyright of published works contained within this thesis resides with the copyright holder(s) of those works.

I also give permission for the digital version of my thesis to be made available on the web, via the University's digital research repository, the Library Search and also through web search engines, unless permission has been granted by the University to restrict access for a period of time.

I acknowledge the support I have received for my research through the provision of an Australian Government Research Training Program Scholarship.

KAVITA PANIR

OCTOBER 2019

Acknowledgements

Throughout my PhD, so many people have assisted and encouraged me, and they all deserve my sincere gratitude. Most importantly, I'm indebted to A/Prof Louise Hull for her supervision, constant motivation and enthusiasm in my research over the past few years. Thank you for nurturing my independence, allowing me to benefit from your expertise and for the numerous opportunities you continue to provide for me in my research career. Likewise, I am deeply grateful for the guidance and advice received from Prof Sarah Robertson. Thank you for taking the time to provide constructive feedback throughout my PhD and for inspiring me to appreciate the minutia of research while mentoring me to critically analyse and appreciate the impact of my data on a larger scale. I would also like to acknowledge Dr John Schjenken for his glorious supervision and overall awesomeness. Thank you so much for your research wizardry, constant support, patience and tolerance of my terrible jokes, and for being a perpetual source of encouragement and amusement.

I would like to thank Dr Erin Greaves and Dr Jimmy Breen for their major contributions towards this project. Erin's knowledge on the mouse model of endometriosis and Jimmy's bioinformatics skills provided me with a great foundation from which to learn. To the lab members I've had the privilege of working with; Bridget, Ricky, Ella, Tian Zhi, Hanan, Bihong, Loretta, Lachie, Sharkey, Danielle, Ali and Cam, thank you for the camaraderie, commiserations and celebrations shared. Also a special mention to two wonderful women, Michaela Baker and Marie Ritter, who took the time to respond to my numerous emails and schedule meetings with my supervisors.

Finally, I would like to thank those closest to me. Holly and Dexter, thank you for friendship, support and ability to impart a combination of wisdom, inspiration and laughter over numerous lunches and dinners. You have both kept me relatively sane over the course of this PhD and I'm so lucky to have shared this journey with you. To my four-legged family members Darcy and Shadow, thank you for reminding me that some days it's ok to just eat and play and sleep. Alisha and Mohanen, I'll always be grateful for your help, understanding, and encouragement. Above all, a huge thank you to my mum for always believing in me and providing unconditional support throughout all my years of study.

Publications & abstracts from this thesis

PANIR K, SCHJENKEN, J. E., ROBERTSON, S.A. & HULL, M.L. (2018) Non-coding RNAs in endometriosis: a narrative review, *Human Reproduction Update* 24(4): 497–515.

2019

Lesion development in endometriosis is regulated by *miR-223* mediated macrophage activity.

Panir K, Schjenken JE, Breen J, Greaves E, Robertson SA and Hull ML.

Poster presentation at The Society for Reproductive Investigation, March 12th-16th 2019.

2018

The regulation of macrophages *via microRNA-223* impacts lesion development in a mouse model of endometriosis.

Panir K, Schjenken JE, Breen J, Greaves E, Robertson SA and Hull ML.

Poster presentation at The 12th Florey International Postgraduate Research Conference, September 25th 2018.

MicroRNA-223 mediated regulation of macrophages impacts lesion development in a mouse model of endometriosis.

Panir K, Schjenken JE, Breen J, Greaves E, Robertson SA and Hull ML.

Poster presentation at The Society for Reproductive Biology, August 19th - 22th 2018.

2017

Development of endometriotic lesions is significantly increased in *miR-155* deficient mice.

Panir K, Schjenken JE, Greaves E, Robertson SA and Hull ML.

Poster presentation at The Robinson Research Institute Symposium, November 10th 2017.

MicroRNA-155 deficiency increases lesion development in a mouse model of endometriosis.

Panir K, Schjenken JE, Greaves E, Robertson SA and Hull ML.

Poster presentation at The Society for Reproductive Biology, August 27th - 30th 2017.

An altered immune environment in *microRNA-223* deficient mice may contribute to the development of endometriosis-like lesions.

Panir K, Schjenken JE, Greaves E, Robertson SA and Hull ML.

Oral presentation at the World Congress on Endometriosis, May 17th – 20th 2017.

2016

The absence of *miR-223* contributes to the persistence of endometriosis-like lesions.

Panir K, Schjenken JE, Greaves E, Robertson SA and Hull ML.

Poster presentation at The Robinson Research Institute Symposium, November 3rd 2016.

An altered immune environment in *microRNA-223* deficient mice may contribute to the development of endometriosis-like lesions.

Panir K, Schjenken JE, Greaves E, Robertson SA and Hull ML.

Oral presentation at The Epigenetics Conference of South Australia, October 13th 2016.

An altered immune environment in *microRNA-223* deficient mice may contribute to the development of endometriosis.

Panir K, Schjenken JE, Greaves E, Robertson SA and Hull ML.

Poster presentation at The 10th Florey International Postgraduate Research Conference, September 29th 2016.

An altered immune environment in *microRNA-223* deficient mice contributes to the establishment of endometriosis-like lesions.

Panir K, Schjenken JE, Greaves E, Robertson SA and Hull ML.

Oral presentation at The Society for Reproductive Biology, August 21st – 24th 2016.

Abbreviations

°C	degree Celsius
αSMA	alpha smooth muscle actin
AP-1	activator protein-1
Arg1	arginase -1
ASRM	American Society for Reproductive Medicine
AUF	AU-rich element binding factor
BAX	bcl-2-like protein 4
CAM	chicken chorioallontonic membrane
CCL	chemokines chemokine (C-C motif) ligand
CD	cluster of differentiation
cm	centimetre
COX	cyclooxygenase
CPM	counts per million
CSF	colony-stimulating factor
DAB	3,3'-Diaminobenzidine
DEGs	differentially expressed genes
DIE	deep infiltrating endometriosis
DNA	deoxyribonucleic acid
dNTP	deoxyribonucleotide triphosphate
E2	oestrogen
EAOC	endometriosis-associated ovarian cancer
ECM	extracellular matrix
EDTA	ethylenediaminetetraacetic acid
EndoMT	endothelial to mesenchymal transition
ERK	extracellular-signal-regulated kinase
ESC	endometrial stromal cell
FGF	fibroblast growth factor
FOXP1	forkhead box protein P1
FSH	follicle-stimulating hormone
g	gravitational force per unit mass due to gravity
GFP	green fluorescent protein
GnRH	gonadotropin-releasing hormone
GWAS	genome-wide association study

H&E	haematoxylin and eosin
HDAC3	histone deacetylase 3
HIF	hypoxia induced factor
HRP	horseradish peroxidase
IFN	interferon
IL	interleukin
iNOS	intracellular nitric oxide synthase
KLF	Krüppel-like factor
LH	luteinising hormone
LPS	lipopolysaccharide
M0	undifferentiated macrophages
M1-like	classical activation of macrophages
M2-like	alternate activation of macrophages
MCP	monocyte chemotactic protein
mg	milligram
$MgCl_2$	magnesium chloride
MHC II	class II major histocompatibility complex
MIF	macrophage migration inhibitory factor
MIP	macrophage inflammatory protein
miR/miRNA	microRNA
MMP	matrix metalloproteinase
mRNA	messenger RNA
NaCl	sodium chloride
NFκβ	nuclear factor κβ
ng	nanogram
NK	Natural Killer
NO	nitric oxide
O_2	oxygen
OVX	ovariectomy
p	p-value
P4	progesterone
PBS	phosphate buffered saline
PCR	polymerase chain reaction
PPAR-γ	peroxisome proliferator-activated receptor-γ
RANTES	chemokine (C-C motif) ligand 5 (also CCL5)
RNA	ribonucleic acid

RNA-Seq	RNA sequencing
s.c	subcutaneous
SDS	sodium dodecyl sulphate
sFlt-1	soluble fms-like tyrosine kinase-1
SNP	single nucleotide polymorphism
STAT	signal transducer and activator of transcription
TCDD	2, 3, 7, 8-tetrachlorodibenzo-p-dioxin
TGF	transforming growth factor
T_H	T helper cells
TNF	tumour necrosis factor
Tris	tris(hydroxymethyl)aminomethane
TUNEL	terminal deoxynucleotidyl transferase dUTP nick end labelling
V	volts
VEGF	vascular endothelial growth factor
vWF	von Willebrand factor

D14	14 days post-induction of endometriosis
D21	21 days post-induction of endometriosis
D7	7 days post-induction of endometriosis

C57	C57BL/6JArc
miR-155	*microRNA 155*
miR-155$^{-/-}$	*microRNA 155* deficient
miR-155$^{+/+}$	*microRNA 155* sufficient (replete C57 mice)
miR-223	*microRNA 223*
miR-223$^{-/-}$	*microRNA 223* deficient
miR-223$^{+/+}$	*microRNA 223* sufficient (replete C57 mice)

C57 → C57	C57 donor endometrium transferred into C57 recipient
miR-155$^{-/-}$ → *miR-155*$^{-/-}$	*miR-155*$^{-/-}$ donor endometrium transferred into *miR-155*$^{-/-}$ recipient
C57 → *miR-155*$^{-/-}$	C57 donor endometrium transferred into *miR-155*$^{-/-}$ recipient
miR-155$^{-/-}$ → C57	*miR-155*$^{-/-}$ donor endometrium transferred into C57 recipient
miR-223$^{-/-}$ → *miR-223*$^{-/-}$	*miR-223*$^{-/-}$ donor endometrium transferred into *miR-223*$^{-/-}$ recipient
C57 → *miR-223*$^{-/-}$	C57 donor endometrium transferred into *miR-223*$^{-/-}$ recipient
miR-223$^{-/-}$ → C57	*miR-223*$^{-/-}$ donor endometrium transferred into C57 recipient

Chapter 1

Review of literature

1.1. INTRODUCTION

Endometriosis is characterised as a benign gynaecological condition in which endometrial cells from the lining of the uterus are found outside the uterine cavity, commonly presenting as lesions on the peritoneal wall or surface of the ovary (Giudice and Kao, 2004, Zondervan et al., 2018). Throughout the reproductive lifespan of a fertile woman, endometrial cells within the uterus undergo repeated cycles of hormone-induced decidualisation, proliferation, shedding, and remodelling (Maruyama and Yoshimura, 2008). Ectopic endometrial cells are also influenced by hormonal fluctuations and undergo similar cellular responses, giving rise to the most common symptoms of endometriosis – dysmenorrhea, cyclic and acyclic pelvic pain, and dyspareunia (Vercellini, 1997, Ballweg, 2004, Dunselman et al., 2014, Vercellini et al., 2014, Zondervan et al., 2018). In addition to chronic pain, symptoms of endometriosis may include subfertility and irregular uterine bleeding (Giudice and Kao, 2004, Giudice, 2010, Oertelt-Prigione, 2012, Parazzini et al., 2012).

Although endometriosis affects approximately 1 in 10 women of reproductive age, the varying manifestations and intensity of individual symptoms has not been found to be a successful indicator of disease severity (Giudice, 2010, Parazzini et al., 2012, Dunselman et al., 2014). In fact, it has been reported that on average, there is a delay of approximately 6 to 9 years from the early onset of symptoms to a definitive diagnosis of endometriosis (Giudice, 2010, Simoens et al., 2012, Soliman et al., 2017). From a socioeconomic perspective, endometriosis is estimated to cost the Australian healthcare system approximately $6 billion annually, and significantly affects the quality of life of women with the disorder (Bush et al., 2011, Commonwealth of Australia Department of Health, 2018). Symptomatic endometriosis is associated with productivity loss, reduced social interactions, mood swings, pain, and fatigue which may result in work or school absenteeism (Ballweg, 2004, Adamson, 2012, Simoens et al., 2012, Acien and Velasco, 2013, Mehedintu et al., 2014, Bush et al., 2017). A recent economic analysis performed by the EndoActive Society of Australia and New Zealand reported the total impact of endometriosis on the Australian economy for the 2018 financial year to be $7.4 billion, wherein $2.6 billion is derived from productivity losses and the reduction in the quality of life for women with endometriosis is valued at $4.04 billion (EndoActive and Ernst & Young, 2019).

The substantial physical, psychological, and financial burden of endometriosis on both an individual and the community underscores the importance of elucidating the aetiology of this disease. Further studies delineating the interactions between endometrial lesions and the ectopic implantation environment are essential for understanding the establishment and progression of this debilitating disease, as well as to develop targeted diagnostic and therapeutic interventions.

1.1.1 Clinical manifestation of endometriosis

Surgery is essential to obtain a visual identification and diagnosis of endometriosis, with subsequent histological confirmation of disease (Falcone and Flyckt, 2018). The most widely used classification system to record the pathologic findings in endometriosis is the revised American Society for Reproductive Medicine (r-ASRM) classification (American Society for Reproductive Medicine, 1997). This scoring system characterises the stages of endometriosis (I to IV), and is used to quantify endometriosis manifestation and facilitate uniformity in patient care and treatment options (Figure 1.1). Additional classification systems such as the Endometriosis Fertility Index (surgical findings are used to predict fertility outcomes) and the Enzian classification (evaluates the depth of deep infiltrating endometriosis) may also assist in reporting disease burden to better inform clinical management of endometriosis (Falcone and Flyckt, 2018).

The most common sites for endometriosis are the ovaries, pelvic peritoneum, uterosacral ligaments, and uterus (Audebert et al., 2018). Lesions in the pelvic cavity are categorised as either superficial peritoneal lesions, ovarian lesions (endometrioma), or deeply infiltrating endometriosis (DIE) (Vercellini et al., 2014). Although the gross appearance of endometriotic implants are vastly variable at the time of surgery (Clement, 2007), microscopic evaluation of excised lesions share similarities with eutopic endometrial tissue, including endometrial glands and stroma. However, unlike the eutopic endometrium, ectopic endometrial lesions typically contain fibrous tissue, cysts, blood, pigmented histiocytes and hemosiderin-laden macrophages (Schenken, 2018).

Clinical presentation of endometriosis in women usually occurs during the reproductive years with classical symptoms including abdominopelvic pain, dysmenorrhea (painful menstruation), dyspareunia (painful sexual intercourse), infertility or the presence of an ovarian mass (Giudice and Kao, 2004, Vercellini et al., 2014). Additional symptoms include abnormal uterine bleeding, chronic fatigue, low back pain, and bowel and bladder dysfunction (Schenken, 2018). It is important to note that the observed severity or stage of endometriosis is not an accurate correlation to quality-of-life indicators and severity of symptoms experienced. Women with mild endometriosis may experience pain equal to or greater than women with severe endometriosis and conversely, women with extensive endometriosis may present with little or no pain. Therefore, obtaining an early diagnosis and receiving effective treatment options is critical to limit disease progression.

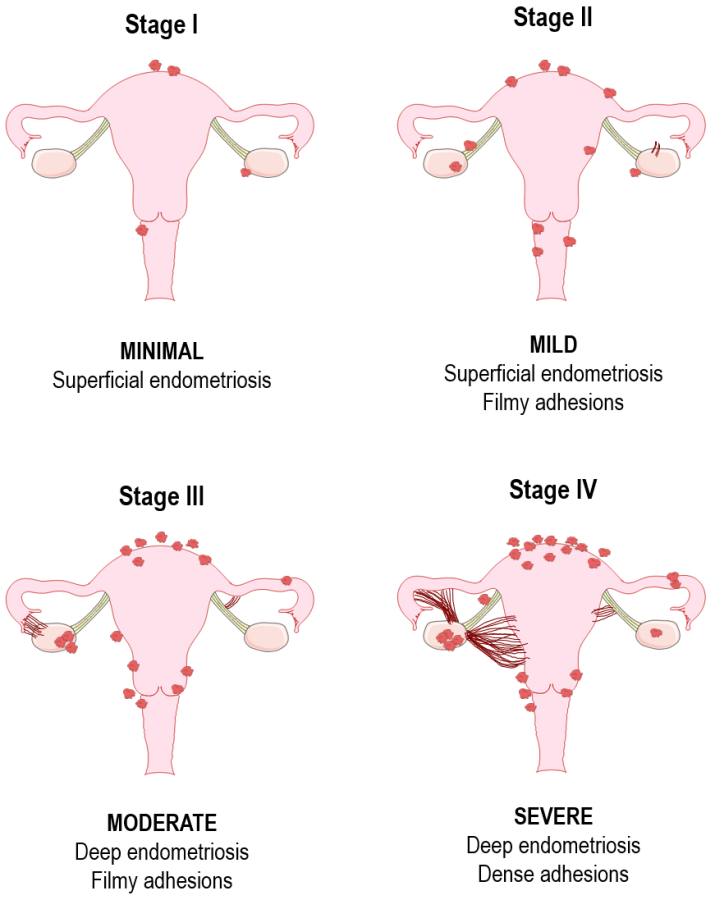

Figure 1.1 ASRM classification of the stages of endometriosis

The revised American Society for Reproductive Medicine classifies endometriosis via a scoring, point based system which takes into account the size, location, severity and depth of the endometriotic growths. The four stages are: Stage I (minimal – isolated implants and no adhesions), Stage II (mild – superficial implants with less than 5cm in aggregate and no significant adhesions), Stage III (moderate – multiple superficial and/or deeply invasive implants with some evidence of adhesions) and Stage IV (severe – multiple superficial and deep implants with large ovarian endometriomas and presence of dense adhesions). Adapted from the American Society for Reproductive Medicine (1997).

1.1.2 Treatment options for endometriosis

As women with endometriosis frequently experience severe pelvic pain and infertility, current treatment options aim to limit disease progression and relieve associated symptoms (Brown and Farquhar, 2015). Surgical intervention is the only option to obtain a definitive diagnosis of endometriosis and remains the 'gold standard' in treatment of this disorder (Giudice, 2010). Laparoscopy is most commonly performed to remove ectopic endometrial lesions and peritoneal tissue from pelvic structures including the bladder, Pouch of Douglas, and pelvic sidewall (Abrão et al., 2012). When compared with open surgery, laparoscopy results in minimal scarring, less discomfort and earlier discharge from hospital. However, laparoscopy is not suitable in all cases, disease recurrence is as high as 18% in women 6 months post-surgery, and up to 75% of women present with endometriomas between 2 to 5 years post-operation (Candiani et al., 1991, Kuohung et al., 2002, Seracchioli et al., 2009, Giudice, 2010, Diamond and Shavell, 2012). To effectively manage pain, non-steroidal anti-inflammatory drugs including aspirin, ibuprofen, diclofenac, and naproxen are commonly prescribed (Seracchioli et al., 2014). Neural-modulating drugs, such as gabapentin and amitriptyline are also used as an analgesic to help manage chronic pain (Evans et al., 2007). Clinical trials utilising Botox injections to reduce associated cramping and assist with pelvic muscle spasms have proved effective in some women (Thomson et al., 2005). Additional therapies, including acupuncture and physiotherapy are also employed in an effort to reduce pain in endometriosis (Seracchioli et al., 2014).

Although the aforementioned therapies help relieve menstrual cramping and pelvic pain, these drugs do not have a direct effect on disease progression, and are commonly used in conjunction with surgical therapy or alternate medical treatments (Johnson and Hummelshoj, 2013). Medical therapy for endometriosis relies on the ability of specific drugs to disrupt the normal cyclic hormone production by ovaries. An example is the mild androgen Danazol, which was the first drug designed specifically for the treatment of endometriosis (Razzi et al., 2007). Following 6-12 months treatment, alleviation of endometriosis-associated pelvic pain is seen in approximately 80% of women (Razzi et al., 2007). However, as its mechanism of action disrupts oestrogen production, side effects including significant bone density loss, oedema, voice deepening, and acne is seen in 75% of women taking this drug (Johnson, 2012). Currently, multiple medications can be prescribed, including Gonadotropin-releasing hormone (GnRH) agonists, oral contraceptives, progesterone-only hormone supplements, and aromatase inhibitors.

GnRH agonists and antagonists suppress oestrogen release by inhibiting release of the menstrual cycle regulatory hormones FSH (Follicle-stimulating hormone) and LH (Luteinising hormone) (Bulun et al., 2012, Platteeuw and D'Hooghe, 2014). *In vitro* studies of eutopic and ectopic endometrial cells treated with GnRH agonists showed a reduced level of proliferation, confirming the efficacy of this treatment (Khan et al., 2010). Similarly, a significant decrease was seen in inflammation and angiogenesis in endometrial tissue of women undergoing this treatment for 3-6 months prior to surgery was seen. GnRH agonist and antagonist treatment effectively mimics a menopausal state, however hypoestrogenic side effects usually limits its use to a six month treatment period (Johnson, 2012). Sustained low oestrogen levels can result in osteoporosis, mood swings, and irregular vaginal bleeding (Makita et al., 2005). 'Add-back' therapy, which involves simultaneous administration of GnRH agonists and low doses of steroid hormones (e.g. oestrogen, progesterone and selective oestrogen receptor modulators), reduces the risk of osteoporosis, as seen in a clinical trial of the oral GnRH antagonist Elagolix (Surrey, 1999, Diamond et al., 2014).

Oral contraceptives, a regulated mixture of oestrogen and progesterone, are often used to limit endometrial tissue growth by disrupting the menstrual cycle and the extent of endometrial tissue remodelling (Platteeuw and D'Hooghe, 2014). The oral contraceptive birth control pill is most commonly used, but in some women, progestins are used as a more potent form to alleviate the symptoms of pelvic pain. Progesterone-only medications (e.g. Dinogest, Norethindrone acetate, and Medroxyprogesterone acetate), can be prescribed to treat endometriosis as they prevent ovulation and subsequent endometrial tissue growth (Horne and Critchley, 2012). In addition, intrauterine devices such as the Mirena coil (levongorgestrel intrauterine system or LNG-IUS) and Implanon are increasingly administered for treatment of endometriosis, as they release low doses of progestogen, a progesterone-like substance, over several years (Ponpuckdee and Taneepanichskul, 2005, Horne and Critchley, 2012, Brown and Farquhar, 2015). However, these treatments do not cure endometriosis, and continuous use may result in weight gain, nausea, acne, and irregular uterine bleeding (Horne and Critchley, 2012).

An alternative treatment option is aromatase inhibitors, which act to disrupt local oestrogen formation within endometriotic lesions (Bulun et al., 2012). The aromatase enzyme catalyses the conversion of adrostenedione to estrone, and testosterone to oestradiol *in situ*, and inhibition of this enzyme results in reduced oestrogen levels (Bulun et al., 2012). For example, the mode of action of the aromatase inhibitor Exemestane involves irreversible binding to aromatase enzymes, rendering them inactive (Mousa et al., 2007). Alternatively, Letrozole and Anastrozole compete with androgens for aromatase binding sites and prevent the production of oestrogen (Mousa et al., 2007). Although this treatment is effective clinically,

the side-effects of aromatase inhibitors include hot flushes, arthralgia, and loss of bone mineral density, which limit their use (Bulun et al., 2012).

In addition to taking prescribed medications, studies have shown that complementary treatments, including alternative medicine (Mira et al., 2018), herbal remedies (Zheng et al., 2018) and changes to diet (Moore et al., 2017), may influence disease progression. To help manage the debilitating chronic pain, mild exercise and/or yoga (Goncalves et al., 2016, Goncalves et al., 2017, Fisher et al., 2018), acupuncture (Wayne et al., 2008, Rubi-Klein et al., 2010), and physiotherapy to manage pelvic pain is beneficial in some patients (Evans et al., 2007, Evans, 2015). Some women with endometriosis also benefit from counselling and support from mental health professionals to alleviate symptoms of depression and low self-esteem associated with this disease (Culley et al., 2013, Facchin et al., 2017).

As the current treatment options for endometriosis may affect individuals in varying ways, most women with endometriosis rely on polytherapy, and use a combination of therapies to manage their disease (Garmendia and De Sanctis, 2012). Furthermore, as the goal of commonly used hormonal therapies is menstrual suppression, with additional medications merely acting to reduce the severity of symptoms associated with endometriosis, the underlying cause of endometriosis is not addressed. Further research into the aetiology of ectopic endometrial tissue implantation is required to provide insights towards the development of a targeted, effective therapeutic intervention.

1.2 THE AETIOLOGY OF ENDOMETRIOTIC LESION DEVELOPMENT

The histological confirmation of endometrial stroma and glands outside the uterine cavity was first described in 1860 (Knapp, 1999). Multiples studies have since evaluated the biological features and molecular characteristics of endometriotic implants in comparison with eutopic endometrial tissue to understand the factors contributing to endometriosis.

1.2.1 Theories of endometriosis establishment

Although the exact mechanisms that give rise to the presence of ectopic endometrial implants remain enigmatic, multiple theories have been proposed to account for the development of endometriosis, including Sampson's theory of retrograde menstruation, the Müllerian remnant theory, the coelomic metaplasia theory, and the theory of induction.

1.2.1.1 Sampson's theory of retrograde menstruation

The most widely accepted theory for the pathogenesis of endometriosis is Sampson's retrograde menstruation theory. Sampson proposed that the reflux of endometrial fragments through the fallopian tubes during menstruation, followed by implantation within the peritoneal cavity, gives rise to ectopic endometriotic lesions (Sampson, 1927). This theory is supported by the fact that approximately 90% of women experience retrograde menstruation, with viable endometrial epithelial cells and glandular structures being found in the menstrual effluent (Halme et al., 1984). In addition, a higher prevalence of basal endometrial fragments have been identified in the menstrual effluent from women with endometriosis compared to women without endometriosis, suggesting that peritoneal endometriosis may result from the trans-tubal dislocation of these fragments (Leyendecker et al., 2002). Furthermore, the site of endometriotic implant adhesion corresponds to the side of tubal reflux; i.e. higher incidence of endometriosis lesions on the left pelvic side in women with an occluded right fallopian tube (Jenkins et al., 1986).

On the other hand, Sampson's theory on its own is an inadequate explanation for the pathogenesis of endometriosis as only 10% of women with retrograde menstruation develop endometriosis and, endometriosis has been known to occur in the absence of menstruation (Schrodt et al., 1980, Halme et al., 1984, Martin and Hauck, 1985). Therefore, several additional theories for the development of endometriosis are based on the assumption that endometriosis develops *in situ* from local tissue in the peritoneal cavity.

1.2.1.2 Müllerian remnant theory

The Müllerian remnant theory postulates that fragments of Müllerian embryonic tissues may undergo metaplastic transformation into endometrial tissues (Ugur et al., 1995). Following clinical examination of the peritoneal cavity in some adolescents and adults, tissue 'pockets' with and without endometriosis have been identified. The manifestation of these tissues were found to be associated with congenital tract malformations (Nap, 2012). This implies a link between endometriosis and embryological abnormalities, and may account for disease sometimes observed in pre-menarche females. However, the presence of this "developmentally misplaced endometrial tissue" defined as Müllerianosis, while histologically similar to endometriotic lesions (containing endometrial stroma and glands), is non-invasive and distinguishable from the classical presentation of endometriosis (Batt et al., 2007).

1.2.1.3 Coelomic metaplasia theory

An alternative theory proposes that the transformation of the ovarian germinal epithelium and/or the serosa of the peritoneum into endometrial cells via metaplasia can give rise to endometriosis (Vinatier et al., 2001, Nap, 2012, Benagiano et al., 2014). This coelomic metaplasia theory provides an explanation for the development of endometriotic lesions outside the pelvic area and, is independent of the process of retrograde menstruation. It also provides an explanation for the presence of endometriotic lesions reported in a small number of males (Schrodt et al., 1980, Martin and Hauck, 1985).

1.2.1.4 Theory of induction

Finally, the theory of induction provides a link between the coelomic metaplasia theory and Sampson's theory of retrograde menstruation. It suggests that one or more endogenous immunological or biochemical factors released from retrograde menstrual fragments may contribute to the induction of endometrial differentiation in the mesothelial layer of the peritoneum (Vinatier et al., 2001, Nap, 2012).

1.2.1.5 Limitations of *in situ* theories

Several criticisms against the *in situ* theories for the pathogenesis of endometriosis exist. The low incidence of endometriosis seen in males does not support the assumption that peritoneal cells can easily undergo transformation into endometrial cells (Martin and Hauck, 1985). Also, as the frequency of metaplastic transformations increases with age (Vinatier et al., 2001), an increase in endometriosis in older women should be observed, but is not. Moreover, the non-uniform distribution of lesions within the

peritoneum, with a higher incidence around the pelvic organs, refutes the concept that the entire coelomic membrane is subject to metaplasia into endometrial tissue (Nap, 2012). In addition, the pathogenesis of endometriosis is postulated to arise from neonatal uterine bleeding. This bleeding represents decidual shedding, and is rich in endometrial stem/progenitor cells, which may implant in the peritoneal cavity, thus giving rise to early-onset (adolescent or premenarcheal) disease development (Gordts et al., 2017). Furthermore, following either caesarean or laparoscopic surgery, the development of subcutaneous endometriosis been observed at the scar site (Denton et al., 1990, Khammash et al., 2003, Hull et al., 2006). The clinical development of subcutaneous endometriosis is believed to be a consequence of exposing endometrial tissue to a surgical site where it establishes ectopically (Liang et al., 1998, Gaunt et al., 2004, Hull et al., 2006). For example, during caesarean section, the transfer of eutopic endometrium to the abdominal wall may occur, giving rise to the development of scar endometriosis in the abdominal wall wound. Therefore, no single theory seems to fully encapsulate the processes leading to endometriosis.

1.2.2 Additional factors contributing to the pathogenesis of endometriosis

While an underlying biological mechanism appears to be the main determinant in developing endometriosis, several additional factors have been linked to disease progression. A growing body of evidence implicates a combination of hormonal (Bulun et al., 2012), genetic (Parazzini et al., 2012), environmental (Rier, 2002), and immunological factors (Klentzeris et al., 1995, Szyllo et al., 2003) in the development of endometriosis.

1.2.2.1 Hormonal influence

Endometriosis is well established as oestrogen-dependent disease, where most ectopic endometrial lesions develop in women of reproductive age and regress after menopause or oophorectomy (Winterhager, 2012). Majority of these lesions contain oestrogen and progesterone receptors as well as aromatase P450, an enzyme that catalyses the conversion of androstenedione and testosterone to oestrogenic compounds. As the expression pattern of these receptors in endometriotic lesions differs from eutopic endometrium, it has been proposed that local oestrogen production may stimulate lesion development. In addition, during endometriosis, activated macrophages in the peritoneal cavity secrete high concentrations of prostaglandins $F_2\alpha$ and E_2 (Ferrero et al., 2014). Prostaglandin E_2 has been found to stimulate aromatase activity and sustain local oestrogen production, thus enhancing the survival of pre-existing lesions or disease recurrence post-treatment (Ferrero et al., 2014).

In addition, a shorter menstrual cycle length (Cramer et al., 1986, Kuohung et al., 2002), earlier age at menarche (Signorello et al., 1997), and delayed childbearing either by choice or infertility (Missmer et al., 2004) may contribute to dysregulated cyclic hormone fluctuations and increased levels of circulating oestradiol and oestrone (Dorgan et al., 1995), and are associated with and increased risk of developing endometriosis (Parasar et al., 2017). On the other hand, current oral contraceptive use (Vercellini et al., 2011), higher body mass index (Ferrero et al., 2005, Shah et al., 2013), and regular exercise (Bonocher et al., 2014) have an inverse association with the development of endometriosis, which may also be linked to hormonal differences and regulation of oestrogen (Parasar et al., 2017).

1.2.2.2 Genetic predisposition

Genetic polymorphisms affecting hormonal and immunological activity may also be risk factors for developing endometriosis (Parazzini et al., 2012). Over the years, large scale studies looking at gene polymorphisms associated with endometriosis have included oestrogen receptor β, vascular endothelial growth factor (VEGF) genes, and cytochrome genes (Montgomery et al., 2008, Zhao et al., 2011, Painter et al., 2014). In particular, cytochrome P450-associated gene, *CYPC2C19* has been linked to an increased prevalence in developing endometriosis (Painter et al., 2014). In 2010, a genome wide association study (GWAS) identified an association between development of endometriosis and genetic variants in the *CDKN2BAS* locus (Uno et al., 2010) and the following year, GWAS conclusively linked a new locus on chromosome 7p15.2 and an increased risk of endometriosis (Painter et al., 2011). To date, while a total of 19 independent genomic regions that display genome-wide significance for endometriosis risk have been identified, with candidate genes associated with hormone regulation (oestrogen receptor 1, follicle stimulating hormone beta subunit, and growth regulating oestrogen receptor binding 1), cell proliferation and migration (cyclin-dependent kinase inhibitor 2B antisense, cell division cycle 42 and kinase insert domain receptor), the majority of these studies have used samples from women with severe endometriosis (Stage III/IV) (Uno et al., 2010, Painter et al., 2011, Nyholt et al., 2012, Rahmioglu et al., 2014, Rahmioglu et al., 2015, Fung et al., 2015, Sapkota et al., 2015a, Sapkota et al., 2015b, Sapkota et al., 2017).

Cancer-associated mutations have been identified in women with endometriosis in the absence of cancer or dysplasia, underscoring the potential for transformation of benign endometriotic lesions into malignant cancers (Anglesio et al., 2017, Suda et al., 2018). Through the use of laser microdissection and sequencing, Anglesio et al. examined samples of deep infiltrating endometriosis, whereas Suda et al. analysed samples of ovarian endometriosis and uterine endometrial epithelium. In these studies, nonsynonymous somatic mutations were identified, including polymorphisms in the cancer-driver genes

ARID1A, *PIK3CA*, *KRAS* and *PPP2R1A* (Anglesio et al., 2017, Suda et al., 2018). Interestingly, clonal expansion of epithelial cells harbouring these cancer-associated mutations was seen (Suda et al., 2018), suggesting that these mutations may confer a survival advantage to refluxed endometrial tissue in the peritoneal cavity.

In addition, the recently proposed genetic/epigenetic theory highlights the importance of both genetic and epigenetic processes in the development of endometriosis (Koninckx et al., 2018). This theory postulates that an induction of genetic or epigenetic changes may potentially be caused by the increased oxidative stress observed in the uterus following menstruation and in the peritoneal cavity following retrograde menstruation (Koninckx et al., 1999, Scutiero et al., 2017, Koninckx et al., 2018). Furthermore, various cellular processes have functional redundancy which effectively masks the phenotypic effect of sequential mutations, and may explain the observation that the cumulative effect of these genetic and epigenetic changes may only become apparent when a 'threshold/tipping-point' is reached (Koninckx et al., 2018). Clinically, the effect of genetic and epigenetic changes result in lesion variations not only between women with endometriosis, but also within the same individual, which could result in variable treatment efficacy over time (Koninckx et al., 2018).

1.2.2.3 Environmental toxin exposure

The increase in global industrialisation and subsequent environmental contamination with man-made chemical compounds has resulted in the exposure and accumulation of these chemicals in both humans and animals. In particular, exposure to organochlorine environmental toxins including polychlorinated biphenyls and dioxins have been widely studied and are found to be associated with endometriosis (Rier et al., 1993, Cummings et al., 1996, Johnson et al., 1997, Cummings et al., 1999, Sofo et al., 2015, Shi et al., 2007).

A study conducted in Rhesus monkeys implicated exposure to the environmental toxin 2, 3, 7, 8-tetrachlorodibenzo-p-dioxin (TCDD or dioxin) with an increased prevalence and severity of endometriosis (Rier et al., 1993, Rier et al., 2001). Exposure to TCDD is also associated with the disruption of cannabinoid signalling pathways, which are utilised for the anti-inflammatory effect of progesterone in inhibiting ectopic endometrial tissue growth (Resuehr et al., 2012). The combination of estrogen and dioxin exposure was found to promote secretion of the chemokines chemokine (C-C motif) ligand 5 (RANTES or CCL5) and macrophage inflammatory protein (MIP)-1α and proteolytic matrix metalloproteinase (MMP)-2 and MMP-9 which promoted the invasion of endometrial stromal cells (Yu et al., 2008).

The mechanism of dioxin action has been linked to disruption of steroid signalling pathways, cell cycle regulation, and immune cell activity (Sofo et al., 2015). Of particular interest is the potential role of dioxin in modulating immune responses via microRNAs, resulting in altered cytokine expression and aberrant mucosal immunity in the reproductive tract (Sofo et al., 2015). In endometriosis, dioxin may disrupt immune cell activity, predominantly by promoting macrophage tolerance towards ectopic endometrial tissue and effectively reducing its clearance from the peritoneal cavity (Rier, 2002).

1.2.2.4 Immunological factors

Endometriosis is classified as an oestrogen-dependent inflammatory disorder, with chronic dysregulation of immune function and vascular signalling (Kralickova et al., 2018, Riccio et al., 2018, Zhang et al., 2018). Research into the role of oestrogen has also shown its marked effect on peritoneal macrophages, whereby the production and secretion of VEGF by macrophages was found to be elevated in the presence of oestrogen (McLaren et al., 1996). In addition, activated macrophages in endometriosis patients were found to secrete Interleukin (IL)-1β (Lebovic et al., 2000) which stimulates endometrial stromal cells to upregulate the expression of the pro-angiogenic cytokine IL-8 (Rossi et al., 2005), which works in tandem with tumour necrosis factor (TNF)-α to promote VEGF-α release from neutrophils (Na et al., 2006). Therefore, the increased levels of VEGF may facilitate the attachment of refluxed endometrial fragments in the peritoneal cavity.

A stage-dependent imbalance in T-helper (T_H)1 and T_H2 ratios has been observed in endometriosis, with a prevalence of T_H1 cytokines present in the peritoneal fluid at Stage I and II, whereas a shift towards increased T_H2 cytokines is noted in Stages III and IV (Andreoli et al., 2011). In endometriotic lesions, the presence of T_H17 cells results in the release of IL-17A, which in turn increases the secretion of CCL20, a T_H17 chemokine, from endometrial cells (Hirata et al., 2008, Hirata et al., 2010). CCL20 feeds-back to induce T_H17 cell migration to endometrial tissue, further enhancing IL-17A activity, which functions synergistically with TNF-α to enhance the secretion of CCL20 and IL-8 (Hirata et al., 2008, Hirata et al., 2010).

Therefore, in endometriosis, significant changes in cellular immunity including elevated numbers and activation status of peritoneal macrophages, decreased natural killer (NK) cell cytotoxicity and dysregulated T cell levels could contribute to disease progression and persistence (Herington et al., 2011, Kralickova et al., 2018). Moreover, epidemiological data links endometriosis with several autoimmune

disorders, including multiple sclerosis, rheumatoid arthritis, and systemic lupus erythematosus (Parazzini et al., 2012), and the increased prevalence of autoantibodies in endometriosis patients (Nothnick, 2001, Matarese et al., 2003, Pathivada and D'Hooghe, 2012) suggests a probable link between autoimmunity and endometriosis. As multiple studies have implicated immune dysfunction as a likely mediator of endometriosis, the following section details the key role facilitated by the immune system during disease pathogenesis and lends support to the premise that an underlying immune aberration contributes to the development of endometriosis.

1.3 ECTOPIC ENDOMETRIAL TISSUE IMPLANTATION IN THE PERITONEAL CAVITY

The peritoneum is the largest serous membrane in the body, comprising the mesothelium, basement membrane, and underlying connective tissue (Kyama et al., 2003, Klemmt and Starzinski-Powitz, 2012, Koninckx et al., 2012, de Arellano ML and Mechsner, 2014). Peritoneal mesothelial cells perform a vital function in maintaining the homeostasis within the peritoneal cavity (de Arellano ML and Mechsner, 2014). This cellular monolayer is joined via tight junctions, a complex association of membrane-bound proteins, and cytoplasmic vesicles which assist in regulating the transport of molecules across the mesothelium (Koninckx et al., 1998). These cells also assist in the peritoneal inflammatory response and attraction of macrophages and neutrophils by secreting multiple cytokines (i.e. granulocyte colony-stimulating factor (CSF), granulocyte-monocyte-CSF, macrophage-CSF, IL-1, and IL-6) (Lanfrancone et al., 1992, de Arellano ML and Mechsner, 2014). The basement membrane plays the dual role of anchoring mesothelial cells to the peritoneal membrane and creates a barrier for diffusion of large molecules through a complex network of connective tissue and aqueous channels (Hull et al., 2008).

The peritoneal fluid, which is rich in immune cells and cytokines, provides a unique environment within the body. Made up of a combination of ovarian exudate, plasma transudate, tubal fluid, retrograde menstruation, and immune cell secretions, the peritoneal fluid from women with endometriosis has been shown to enhance eutopic and ectopic endometrial cell proliferation (Koninckx et al., 1998). Studies have shown that this increased proliferation is influenced by the presence of growth factors such as TNF-α, transforming growth factor (TGF)-β, and steroid hormones which circulate in the peritoneal fluid (Koninckx et al., 2012, Young et al., 2014a, Young et al., 2014b). In addition, the presence of soluble extracellular matrix (ECM) proteins including laminin, hyaluronan, and collagen type IV in the peritoneal fluid has been associated with an increase in the ability of endometrial cells to adhere to surfaces within the peritoneal cavity (e.g. the peritoneum, ovaries, bladder) (Debrock et al., 2002, Kyama et al., 2003, de Arellano ML and Mechsner, 2014).

Research into the role of mesothelial cells during the pathogenesis of endometriosis has provided valuable information regarding the interaction between ectopic endometrial tissue and the site of implantation. From studies using endometrial cells cultured *in vitro*, the mesothelial layer has been implicated as the primary site of adhesion of endometrial fragments, as both endometrial epithelial and stromal cells bind to the mesothelium with high affinity (Dechaud et al., 2001). In 2001, Dunselman *et al.* found that an intact mesothelial layer prevents adhesion of ectopic endometrial tissue and, subsequently concluded that these endometrial fragments establish adhesion sites by exposing the underlying peritoneal ECM by damaging and remodelling the mesothelial layer (Dunselman et al., 2001). In addition,

early analysis of peritoneal fluid from endometriotic women have shown an elevation in several ECM-related proteins including VEGF-A, cysteine-rich angiogenic inducer 61, urokinase plasminogen activator and MMP-3 (Iwabe and Harada, 2014). Although mesothelium reorganisation during attachment of endometrial tissue facilitates disease initiation, the reason behind this attachment and subsequent invasion of endometrial cells in some women and not in others remains unclear.

1.3.1 Aberrant inflammatory response and evasion of immune surveillance

Mounting evidence points towards an underlying immunological aberration that influences endometriotic lesion progression. A combination of factors including aberrant cytokine expression, impaired immune surveillance, and the innate resistance of endometrial tissue against clearance contribute to the pathogenesis of endometriosis (Aznaurova et al., 2014, Benagiano et al., 2014, Bouquet De Jolinière et al., 2014). Multiple studies indicate that the development and maintenance of ectopic endometrial lesions is driven by a mechanism of local peritoneal inflammation, with an altered response or function of immune cells within the peritoneal cavity (Iwabe and Harada, 2014). An *in vitro* culture of primary endometrial cells demonstrated that the cellular component of retrograde menstrual effluent arriving at the peritoneal cavity is prone to necrosis and apoptosis, due to a lack of nutrients and oxygen (Debrock et al., 2002). These cells initiate a cascade of inflammatory responses, with an infiltration of neutrophils and monocytes which subsequently differentiate into macrophages (Janssen and Henson, 2012).

Macrophages have been identified as key players in both the progression and resolution of an inflammatory response (Cao et al., 2004, Jantsch et al., 2014). Macrophages secrete a range of pro-inflammatory cytokines including IL-1, IL-6, IL-12, and TNF which assist in the clearance of damaged tissues (Cao et al., 2004). However, during endometriosis, the phagocytosis of necrotic endometrial cells is associated with a decrease in the pro-inflammatory cytokines IL-1β and TNF-α, suggesting a resolution of inflammation occurs (Capobianco and Rovere-Querini, 2013). The lack of inflammatory chemoattractants may result in impaired immune cell recruitment into the peritoneal cavity, and potentially allow endometrial tissue fragments to attach ectopically (Capobianco and Rovere-Querini, 2013). Furthermore, peritoneal macrophages from women with endometriosis have a reduced ability to phagocytose, clear, and destroy endometriotic cells, thus encouraging ectopic tissue survival and lesion development within the peritoneal cavity (Capobianco and Rovere-Querini, 2013).

Associated with this decrease in pro-inflammatory cytokines, TGF-β, a regulator of cell proliferation and differentiation, was found at elevated levels in peritoneal fluid (Janssen and Henson, 2012). Since TGF-β is a key factor driving the generation of M2-like macrophages, this raises the possibility that during

endometriosis, a shift from pro-inflammatory to anti-inflammatory macrophage activity occurs, supporting disease progression. Further research highlighting the synergistic role of macrophages and TGF-β in endometriotic lesion development was carried out in TGF-β1-null mutant mice on a background of severe combined immunodeficiency (Hull et al., 2012). A reduction in ectopic endometrial lesion size was noted following xenotransplantation of human endometrial cells subcutaneously into these mice, indicating of the likely importance of TGF-β signalling pathways in disease establishment (Hull et al., 2012).

In addition, supporting *in vitro* studies showed CD36-dependent phagocytosis of endometrial cells by peritoneal macrophages is inhibited by the inflammatory mediator prostaglandin E2, which is elevated in the peritoneal fluid of women with endometriosis (Chuang et al., 2010). Similarly, NK cell cytotoxicity towards endometrial tissue is aberrant in women with disease, possibly mediated by the production of intercellular adhesion molecule-1 by endometrial stromal cells (Oosterlynck et al., 1991). NK cell deficiency would reasonably cause a delay in the clearance of endometrial fragments from the peritoneal cavity which may allow ectopic tissue implantation and invasion into the mesothelium.

Although peritoneal macrophages assist in the clearance of endometrial tissue, a vital step towards disease establishment is the innate ability of some of this menstrual effluent to evade immune surveillance and survive in the peritoneal cavity. For example, expression of IL-8 in females with endometriosis was found to enhance endometrial cell proliferation *in vivo* (Arici et al., 1998). Also, endometrial tissue of diseased women was found to have lower TUNEL-positive expression and reduced *BAX* expression, both markers of apoptosis. These innate anti-apoptotic mechanisms in endometrial tissue may increase their ability to evade immune clearance (Johnson et al., 2005). Interestingly, a predisposition towards endometriosis was also found to correlate to other autoimmune disorders (e.g. systemic lupus erythematosus, rheumatoid arthritis) and atopic disease (e.g. asthma, allergies, and eczema), lending support to the concept of a fundamentally altered or dysregulated immune system in women with this disease (Nothnick, 2001, Sundqvist et al., 2011, Pathivada and D'Hooghe, 2012). While targeting these immune mechanisms may ultimately prove to have therapeutic outcomes, significant work still remains to determine the precise underlying mechanisms involved in altered immune response seen in endometriosis. In addition, it remains critical not to discount the possibility that observed changes in immune cell and cytokine abundance in endometriosis could be a consequence of an exacerbated inflammatory response towards the presence of ectopic endometrial tissue, rather than the observed peritoneal inflammation being the cause of disease development.

1.3.2 Lesion maintenance through neurogenesis and angiogenesis

Following the attachment of endometrial fragments to the mesothelium, endometriotic implants manage to thrive in the peritoneal cavity through the development of a vascular supply that provides the lesions with nutrients and oxygen (Giudice and Kao, 2004). Angiogenesis is frequently accompanied by formation of nerve fibres at the site of implantation, possibly contributing to the chronic pain associated with endometriosis (Hey-Cunningham et al., 2013). Importantly, peritoneal fluid from women with endometriosis is found to be more pro-angiogenic than peritoneal fluid from women without endometriosis (Oosterlynck et al., 1993, Groothuis, 2012). A combination of cytokines including VEGF, TNF-α, and IL-8 were found to be elevated in the peritoneal fluid from women with endometriosis compared to those without (McLaren et al., 1996, Maas et al., 2001, Cho et al., 2012). Both TNF-α and IL-8 promote adhesion, proliferation, and angiogenesis of endometrial cells, implying that an overexpression of these cytokines may result in localised vascularisation and remodelling of the mesothelium (Groothuis, 2012). VEGF, an important angiogenic factor, is found to be secreted by activated peritoneal macrophages and is abundantly expressed in the glandular compartment of endometriomas (Groothuis, 2012, Krikun, 2012). The expression of VEGF and its soluble receptor (sFlt-1) was found to be significantly higher in peritoneal endometriotic lesions compared to normal peritoneum biopsies from women without endometriosis (Cho et al., 2012). Interestingly, a comparison of eutopic endometrium from women with and without endometriosis showed a significant reduction in sFlt-1 expression in patients with this disease (Cho et al., 2012). In a nude mouse model of endometriosis, suppression of ectopic endometrial tissue growth via antagonism of VEGF-A (administration of either the truncated sFlt-1 or an anti-VEGF-A antibody) was observed, signifying the crucial role VEGF plays in maintaining ectopic lesion survival (Hull et al., 2003).

Although capillary recruitment to the relatively avascular peritoneal microenvironment initiates remodelling, growth, and survival of invading endometrial tissue, the mechanisms behind this process are poorly understood. A potential theory proposes that endometrial tissues may have progenitor endothelial cells which may form a vascular network in the peritoneal environment (Hull et al., 2003). Alternatively, blood vessels from the mesothelium may infiltrate the attached endometrial tissues, following signals received from the cocktail of cytokines in the peritoneal environment (Braza-Boils et al., 2013). Macrophages have also been implicated as mediators of vascular development, as they are potent sources of VEGF, and can secrete pro-angiogenic, anti-inflammatory factors such as IL-10 and MMP-9 which may assist with vascularisation of the peritoneal surface, making it more prone to endometriotic lesion growth (Lin et al., 2006, Capobianco and Rovere-Querini, 2013, Zajac et al., 2013). Additional work delineating the multifactorial role of macrophages during endometriosis lesion attachment and proliferation is required; especially as targeting this immune cell may be beneficial in improving the understanding of endometriosis establishment, and thus ultimately in treating this disease.

1.4 MACROPHAGE ACTIVITY IN ENDOMETRIOSIS

Macrophages are a heterogeneous population of functionally diverse hematopoietic cells (Gordon and Taylor, 2005). Macrophages differentiate from peripheral monocytes in response to immunological challenges, pathogens, antigenic stimuli, and exposure to cytokines (Gordon and Taylor, 2005). Antigen processing by macrophages and subsequent presentation of these molecules via the Class II Major Histocompatibility Complex (MHC II) to T cells allows for development of a host adaptive immune response (Jantsch et al., 2014). To maintain homeostasis, macrophages perform a vast array of functions including clearance of debris and pathogens, removal of dead cells, and matrix turnover (Wynn et al., 2013). Associated with this functional plasticity is a continuum of macrophage polarisation states, with two extreme activation pathways at either end of this spectrum; classically activated (M1-like) macrophages and the alternatively activated (M2-like) macrophages (Figure 1.2) (Ma et al., 2003, Martinez et al., 2008, Mosser and Edwards, 2008, Italiani and Boraschi, 2014, Jantsch et al., 2014).

Undifferentiated macrophages (M0) derived from bone marrow progenitors can be induced towards the "pro-inflammatory" M1-like macrophage subtype following exposure to IL-1β, TNF-α, Interferon (IFN)-γ or lipopolysaccharide, alone or in combination (Wynn and Barron, 2010, Wynn et al., 2013, Italiani and Boraschi, 2014, Jantsch et al., 2014, Martinez and Gordon, 2014). M1-like macrophages are characterised by their inflammatory cytokine secretion profile (e.g. IL-1β, IL-6, TNF-α and IFN-α) and surface marker expression, including CD40, CD86, and major histocompatibility complex II (MHC II) (Italiani and Boraschi, 2014). These M1-like macrophages are effector cells in the T_H1 cellular immune response and assist in the clearance of pathogens via endocytosis, through the production of inducible nitric oxide synthase (iNOS), which results in oxidative damage (Brune et al., 2013). This helps initiate an antigen-specific T_H1 and T_H17 inflammatory response, and if uncontrolled, can lead to a chronic inflammatory state, which in turn can become pathogenic to the host (Liddiard et al., 2011).

In contrast, M0 macrophages treated *in vitro* with a combination of M-CSF and IL-10 in mice or the T_H2 cytokine IL-4 in humans, produces an "anti-inflammatory" M2-like macrophage subtype (Wynn and Barron, 2010, Wynn et al., 2013, Italiani and Boraschi, 2014, Jantsch et al., 2014, Martinez and Gordon, 2014). Through release of growth factors and cytokines, these macrophages help with pathogen clearance, reduce inflammation, and promote tissue remodelling and regrowth (Italiani and Boraschi, 2014). M2-like macrophages express a range of extracellular markers, including arginase 1 (Arg-1), L-4 receptor, mannose receptor (CD206), resistin-like molecule alpha 1 (Fizz1), and chitinase-like molecule (Ym1/Ym2) (Martinez and Gordon, 2014). Based on gene profiles, inducing agents, and cytokine expression, M2-like macrophages can be further characterised into subsets: M2a, M2b, and M2c.

Exposure to IL-4 or IL-13 elicits an M2a-like response, whereas IL-1R or exposure to LPS elicits an M2b-like response, and M2c-like macrophages form from exposure to IL-10, TGF-β and glucocorticoid hormones (Martinez and Gordon, 2014).

M1-like and M2-like macrophages both play an important role in the initiation and resolution of inflammation. *In vitro* studies have shown that M2-like macrophages are capable of complete repolarisation back to M1-like macrophages, and are able to switch back in response to subtle changes in the cytokine microenvironment (Wang et al., 2014a). The ability of macrophages to express distinct functional phenotypes has been associated with several non-pathogen driven diseases, such as osteoporosis, atherosclerosis, and uncontrolled tissue growth and remodelling, including cancer (Cassetta et al., 2011). During the female reproductive cycle, alterations in macrophage numbers and expression profiles in response to changes in reproductive hormone levels have been observed (Brown et al., 2014).

In endometriosis, the presence of macrophages is a consistent feature of endometriotic lesions and appears to be a significant driving force in the establishment and persistence of disease (Capobianco and Rovere-Querini, 2013). In 1981, Haney *et al.* first described an increase in the number of peritoneal macrophages in women with endometriosis (Haney et al., 1981). Several studies have shown that in women with endometriosis, activated peritoneal macrophages had a reduced capacity to eliminate ectopic endometrial tissue (Kusume et al., 2005, Lee et al., 2005, Yamamoto et al., 2008). These macrophages also appeared to facilitate the survival and proliferation of endometrial cells in the peritoneal cavity, through the release of multiple growth and vascular remodelling factors, thereby contributing to the progression of endometriosis (Ahmad et al., 2014).

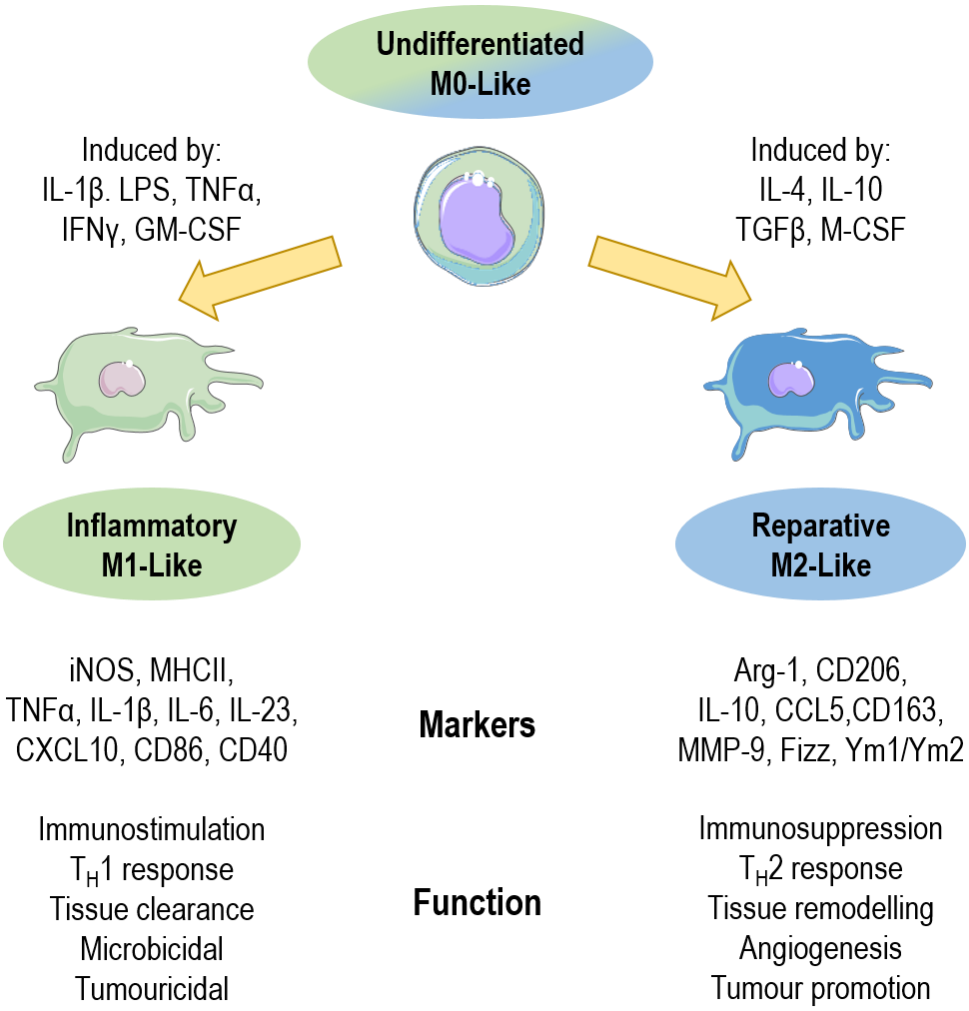

Figure 1.2 Markers of M1-like and M2-like macrophages

The stimulation of undifferentiated M0-like macrophages with M1-like stimuli [Interleukin-1β (IL-1β), lipopolysaccharide (LPS), tumour necrosis factor α (TNFα), interferon γ (IFNγ) and granulocyte-macrophage colony-stimulating factor (GM-CSF)] gives rise to pro-inflammatory M1-like macrophages [characterised by the expression of a range of markers including inducible nitric oxide synthase (iNOS) and major histocompatibility complex class II (MHC II)]. Conversely, the stimulation of M0-like macrophages with M2-like stimuli [IL-4, IL-10, transforming growth factor (TGF-β), and macrophage CSF (M-CSF)] gives rise to tissue healing M2-like macrophages [characterised by the expression of a range of markers including arginase 1 (Arg-1) and CD206.

1.4.1 Endometrial macrophages are elevated during menses

Cyclical changes in hormone levels throughout the menstrual cycle regulate endometrial proliferation, culminating either in successful embryo implantation with associated vascular modifications or in the absence of pregnancy, the withdrawal of progesterone results in myometrial shedding. Multiple studies have demonstrated fluctuating immune cell populations throughout the menstrual cycle (reviewed in Oertelt-Prigione, 2012). Of particular interest is the influx of leukocytes during the secretory and menstrual phases of the cycle (Kamat and Isaacson, 1987, Poropatich et al., 1987), with an elevation in the numbers of tissue-resident endometrial macrophages during the secretory phase (Critchley et al., 2001). This suggests a key role for macrophages in the initiation of menstruation (Critchley et al., 2001) and in the resolution and subsequent repair of the myometrium (Garry et al., 2010, Maybin et al., 2012).

Macrophages have a broad spectrum of activation states, and function as an important source of both pro- and anti-inflammatory mediators in the endometrium (Thiruchelvam et al., 2013). Throughout the menstrual cycle, a steady increase in the proportion of macrophages within the endometrium is observed, with macrophages comprising 6-15% of all endometrial cells following the withdrawal of progesterone (Salamonsen et al., 2002). This increase in macrophage numbers is believed to occur either by in situ proliferation within the endometrium or via chemotaxis of peripheral monocytes into the endometrium (Guo et al., 2011, Jenkins et al., 2011). In the context of endometriosis, it is important to consider the contribution of these immune cells and other cellular components present in the shed menstrual effluent on disease development. A combination of abnormal immune responses, augmented macrophage function, and epigenetic dysregulation throughout the menstrual cycle may facilitate the growth of endometriotic lesions, thus predisposing some women to endometriosis and potentially exacerbating this condition over multiple repeated menstrual cycles.

1.4.2 The inflammatory response and the initiation of endometriosis

Classically activated M1-like macrophages have been implicated in the adherence of endometrial cells in the peritoneal cavity and initial disease establishment (Capobianco and Rovere-Querini, 2013). *In vivo* mouse models of endometriosis have demonstrated that the presence of ectopic endometrial tissue triggers an inflammatory response, characterised by an influx of neutrophils and macrophages into the peritoneal cavity (Bacci et al., 2009). In addition, following intrapelvic injections of endometrial tissue into baboons, a surge in inflammatory mediators is seen, including increased numbers of leucocytes, T-lymphocytes, and TNF-α^{+} cells, with an associated increase in the levels of MIP chemokine (D'Hooghe et

al., 2001). This implies that a large proportion of M1-like macrophages are initially recruited to the localised site of inflammation.

However, as mentioned previously, macrophages from women with endometriosis have a reduced phagocytic ability. Therefore, rather than being efficient effector cells in clearing ectopic endometrial tissue fragments, these macrophages may in fact promote the persistence and survival of displaced endometrial tissue (Capobianco and Rovere-Querini, 2013). Furthermore, studies utilising both human and mouse tissues have shown that the persistence of ectopic endometrial tissue may itself be a driving force for a rapid influx of macrophages (Bacci et al., 2009, Capobianco et al., 2011, Capobianco and Rovere-Querini, 2013, Ahmad et al., 2014). In a mouse model of endometriosis, the monocyte recruitment factor, monocyte chemotactic protein-1 (MCP-1), was significantly higher four hours following intraperitoneal injection of syngeneic endometrial tissue compared to control groups (Cao et al., 2004). The increase of MCP-1 at this time-point is indicative of the role of endometrial tissue exposure in release of this chemokine, and subsequent monocyte recruitment. The chemokine RANTES has also been implicated in the recruitment of M2-like macrophages to the site of lesion development (Hornung et al., 2001). In the peritoneal fluid of women with endometriosis, MCP-1 and RANTES (mediators of acute and chronic inflammation) were found to be present at increased levels, providing insight into the chemokine-driven mechanism behind the macrophage influx during disease initiation (Hornung et al., 2001, Cao et al., 2004, Ahmad et al., 2014).

As extended periods of neutrophil action can result in cellular injury from the presence of reactive oxygen species, anti-inflammatory macrophages are likely to play an important role in limiting neutrophil activity (Hornung and von Wussow, 2012, Brune et al., 2013). In endometriosis, these macrophages assist in the rapid resolution of inflammation, which may contribute to the inefficient clearance of ectopic endometrial tissue (Hornung and von Wussow, 2012, Capobianco and Rovere-Querini, 2013). In a mouse model of tissue repair, it was observed that pro-inflammatory macrophages were present for up to forty eight hours-post injury and were gradually replaced by increasing numbers of anti-inflammatory macrophages (Novak and Koh, 2013). These secondary cells expressed higher levels of TGF-β and IL-10 compared to the initially recruited macrophages, signifying a subtle change from M1-like to M2-like macrophage profile during tissue repair (Sica and Mantovani, 2012, Novak and Koh, 2013).

1.4.3 Resolution of inflammation and tissue remodelling in endometriosis

While M1-like macrophages elevate inflammatory activity in the peritoneal cavity, alternatively activated M2-like macrophages exhibit anti-inflammatory actions and may assist in the resolution of this inflammation, which, paradoxically, may exacerbate the development of endometriosis (Capobianco and

Rovere-Querini, 2013). In 2009, Bacci *et al*. developed a macrophage-depleted endometriosis mouse model to evaluate the contribution of differentially activated macrophages in lesion development (Bacci et al., 2009). In this system, mice were injected with M0, M1-like or M2-like macrophages cultured *in vitro,* and it was shown that M2-like macrophages strongly enhance lesion development. In the absence of M2-like macrophages, ectopic endometrial lesions failed to grow following adherence to the peritoneal membrane. Interestingly, M2-like macrophage depletion resulted in attenuated lesion growth, with fewer blood vessels penetrating the core of the lesion, effectively disrupting its glandular and stromal architecture (Bacci et al., 2009). This indicates a vital role for alternatively activated M2-like macrophages in the neovascularisation and persistence of endometriotic lesions.

M2-like macrophages are found in the peritoneal fluid of humans and experimental animals with endometriosis, indicating a role for these cells in sustaining the growth of ectopic endometrial tissue (Bacci et al., 2009, Capobianco et al., 2011, Capobianco and Rovere-Querini, 2013). Anti-inflammatory macrophages are involved in tissue remodelling and angiogenesis, two essential processes in disease progression (Italiani and Boraschi, 2014). Remodelling of the endometrium occurs naturally during the human menstrual cycle under the control of oestrogen and progesterone, and involves the degradation of the superficial layer of the endometrium and regeneration of a new layer without fibrosis (Oertelt-Prigione, 2012, Hong and Choi, 2018). MMPs are the main tissue-remodelling enzyme family involved in this remodelling process, and in endometriosis, the ectopic endometrium has a higher capacity to produce MMP-2 and MMP-9, compared to eutopic tissues (Halme et al., 1984, Maybin et al., 2011, Guo, 2012, Oertelt-Prigione, 2012). The presence of these enzymes, typically secreted by M2-like macrophages, suggests that the tissue remodelling process may be a precursor which promotes attachment and invasion of ectopic endometrial tissue in the peritoneal cavity (McLaren et al., 1996, Bacci et al., 2009, Capobianco and Rovere-Querini, 2013). Moreover, macrophage infiltration into endometriotic lesions is a key event in disease progression, and M2-like macrophages further promote the vascularisation of these lesions via production of VEGF (McLaren et al., 1996).

1.4.4 Macrophage plasticity in endometriosis

Evidence from *in vivo* mouse and primate studies indicate that M1-like macrophages transform into M2-like macrophages during the progression of endometriosis, but the mechanism behind this phenotype switch remains largely unknown (Figure 1.3) (Capobianco and Rovere-Querini, 2013). In a Rhesus model of endometriosis, macrophages expressing CD163, a M2-like macrophage scavenger receptor, was found to be significantly higher in endometriotic lesions compared to eutopic endometrium (Smith et al., 2012). This data presents the possibility that signalling from the ectopic endometrial tissue or suppression

in the inflammatory cytokine environment may be responsible for macrophage phenotype skewing in endometriosis.

In humans, studying macrophage plasticity during endometriosis is challenging as ectopic lesions are usually surgically removed and evaluated only once the disease is fully established (Bacci et al., 2009). Although Halme *et al.* suggested that recruited macrophages can differentiate into various phenotypes which assist lesion development, samples were analysed from a tissue bank and may not be representative of immunological changes throughout the various stages of disease (Halme et al., 1987). Moreover, macrophage abundance and phenotypes during endometriosis may be altered due to heterogeneity of lesions, disease severity, and hormone cues, which complicates the identification of specific immune cell subsets in these tissues (Capobianco and Rovere-Querini, 2013, Ahmad et al., 2014).

Evaluation of endometrial lesion biopsies has confirmed the presence of HLA-DR, a marker of antigen presenting cell activity (Oosterlynck et al., 1993). Furthermore, expression of M2-like macrophage markers CD206 and CD163 was upregulated in the peritoneum and in lesions during endometriosis compared to in disease-free peritoneum (Bacci et al., 2009). In addition, the M2-like macrophage marker peroxisome proliferator-activated receptor-γ (PPAR-γ) was also found in lesions, glandular epithelial, and stromal cells, implying that this marker is not exclusively expressed by macrophages, but may be indicative of a predominance of 'anti-inflammatory' activity (McKinnon et al., 2010). Collectively, as these studies failed to detect the presence of M1-like macrophage markers within endometriotic tissue samples, this suggests a predominant tissue healing, M2-like immune profile during lesion development.

The evaluation of peritoneal fluid from individuals with endometriosis has helped to determine how the immune microenvironment affects macrophage plasticity. The M1-like macrophage cytokines IL-6 and IL-8 were reported to be higher in women with endometriosis, compared to disease-free counterparts (Harada et al., 2001, Kalu et al., 2007). Expression of MCP-1 by macrophages was also found to be significantly higher in women with severe stage endometriosis, compared to women at a milder stage (Gmyrek et al., 2008). Interestingly, studies have shown that MCP-1 is secreted at a higher level by murine M2-like macrophages compared to M1-like macrophages (Lolmede et al., 2009). These observations are consistent with the proposed theory that M2-like macrophages are important mediators involved with lesion growth and maintenance in endometriosis.

While the classification of M1-like and M2-like subsets simplifies the heterogeneity of macrophages in endometriosis, subtle changes in macrophage phenotype due to tissue signalling, the cytokine microenvironment, or hormone interactions may occur throughout the menstrual cycle (Ahmad et al.,

2014). Macrophage activation is dependent on multiple signals and may dynamically alter throughout disease progression (Cassetta et al., 2011), and although functional testing of the impact of M1-like vs M2-like macrophages in the different stages of endometriosis has been done, activation pathways and markers over time has not been described. Importantly, the sequence of causal pathways linking macrophage phenotype with the development of endometriosis can only be thoroughly defined in animal models, where sequential changes in lesion establishment and immune profiles can be evaluated effectively. In addition, the role of epigenetic regulators, such as microRNAs, in regulating macrophage polarisation during endometriosis has yet to be investigated, and may provide valuable insight into the aetiology of this disease.

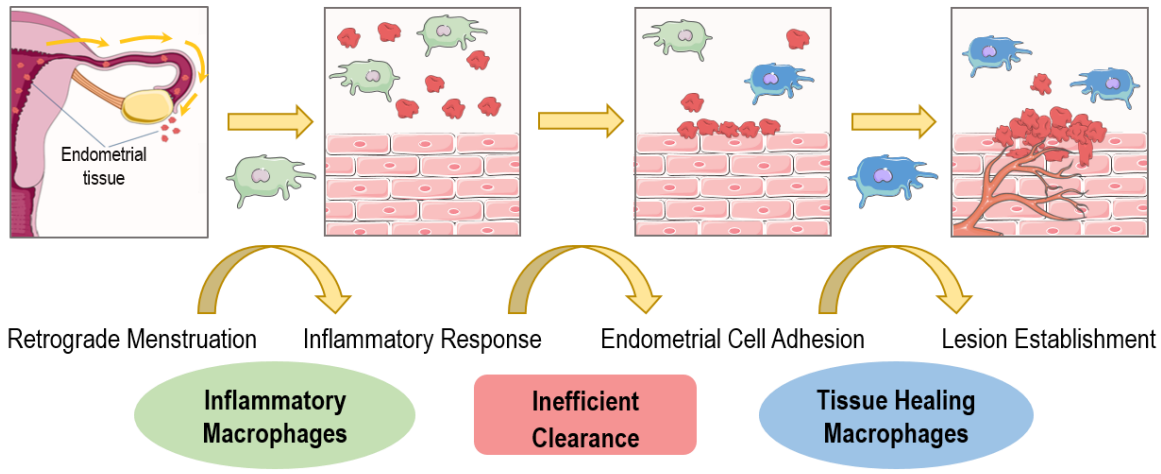

Figure 1.3 View of macrophage plasticity during lesion development in endometriosis

The immune system has a multi-faceted role in the pathogenesis of endometriosis, and macrophages in particular have been shown to be central arbiters of disease progression. Following retrograde menstruation, the presence of ectopic endometrial tissue elicits an influx of inflammatory macrophages in an attempt to clear these fragments. However, in endometriosis, it is believed that inefficient clearance occurs, resulting in endometrial cell survival and adhesion. A second influx of macrophages with anti-inflammatory tissue-healing properties promotes remodelling and lesion establishment.

1.5 ANIMAL MODELS OF ENDOMETRIOSIS

Although peritoneal fluid and endometrial tissue samples are routinely collected from both healthy and affected individuals, this is not sufficient for investigating contributing factors in the establishment and progression of endometriosis. Developing and testing targeted pharmaceutical treatment options remains challenging, as this disease only occurs naturally in humans and some primates (Grümmer, 2006). Human samples can provide descriptive data regarding disease progression but functional studies can only be carried out in manipulable animal models. Using animal models allows for scientific evaluation into the properties of both intrinsic (i.e. genes) and extrinsic (i.e. environment) factors on pathology and progression of diseases. Therefore, over the last few decades, several animal models have been developed to assist in unravelling the enigma of this complex disease, from both pathophysiological and therapeutic aspects (Simitsidellis et al., 2018).

1.5.1 Primate models

The main advantage of studying the pathophysiology of endometriosis in primates is their physical and biological similarity to humans (Fazleabas, 2012). Research on endometriosis has been carried out in female Rhesus monkeys (*Macaca mulatta*), mandrills (*Mandrillus sphinx*), Kenyan baboons (*Papio doguera*), and cynomolgus monkeys (*Macaca fascicularis*). Unlike other animal models used for the study of reproductive disorders, nonhuman primates have endometrial physiology, morphology and undergo menstrual cycles resembling those of humans (Slayden, 2013). Spontaneous development of endometriotic lesions may be observed in animals which have been kept in captivity and are either prevented from mating or undergo controlled/restricted breeding, and similar to endometriosis in humans, nonhuman primates are rarely diagnosed with early-stage disease (Slayden, 2013, D'Hooghe et al., 2009). Endometriosis can also be induced in primates through the intraperitoneal injection of menstrual effluent and endometrial tissue, allowing the progression of endometriosis to be researched for up to 15 months, and examination of lesions *in vivo* to be carried out via laparoscopy (D'Hooghe et al., 2009).

Several studies evaluating the role of the immune system in baboon models of endometriosis have been carried out, with current evidence suggesting that the observed peritoneal inflammation may be a consequence rather than a cause of endometriosis (Kyama et al., 2003). An increase in peritoneal fluid volume, concentration of leukocytes, and inflammatory cytokines was observed following both spontaneous retrograde menstruation (occurs in 83% of baboons (D'Hooghe et al., 1996a)) and induced endometriosis via intraperitoneal injection of donor endometrium (D'Hooghe et al., 1999, D'Hooghe et al., 2001). This elevated inflammatory response appears transient, as it was observed within one month following induced endometriosis (D'Hooghe et al., 2001), however it was absent between 2 to 3 months

following disease establishment (D'Hooghe et al., 1996b). Increased proportions of macrophages and cytotoxic T cells were observed in the peritoneal fluid of baboons with induced endometriosis (D'Hooghe et al., 1996b). Interestingly, low numbers of uterine NK cells were observed in ectopic endometrial lesions from women and baboons, and this was coupled with low expression of NKp30, an activating receptor of uterine NK cells (Drury et al., 2018). If a correlation between low NKp30 expression and reduced uterine NK cell cytotoxicity is proven, this could represent a possible mechanism by which ectopic endometrial cells are able to evade immune clearance and persist in the peritoneal cavity (Drury et al., 2018).

On the other hand, the efficacy of utilising non-human primates as an experimental model of endometriosis has been challenged (Dehoux et al., 2011). The prohibitive financial costs of colony maintenance, ethical considerations regarding primate research, and conservation issues must be taken into account. Furthermore, although spontaneous development of endometriosis does occur, it takes a considerably longer time to establish disease when compared to rodent models. Following induced endometriosis, lesion establishment can take up to 30 days, and has less than a 30% success rate for development of endometriosis in primates (D'Hooghe et al., 2001, Fazleabas, 2012). While slow lesion development implies that progression of endometriosis can be studied at various stages, the cost of housing these animals coupled with the low success rate of disease establishment and the requirement for high technical expertise precludes the use of primate models in most laboratories (Dehoux et al., 2011).

1.5.2 Chicken chorioallantoic membrane

The chicken chorioallantoic membrane (CAM) is the highly vascularised membrane of a fertilised chicken egg that facilitates gas exchange within the developing embryo (Grümmer, 2006). During early development, the embryo does not have a competent immune system, and therefore, xenotransplantation of human tissue is possible. Between 6 to 11 days of incubation, a small portion of a fertilised egg shell is removed and tissue grafts are implanted into the CAM (Borges et al., 2003). In this manner, CAM has been used as an *in vivo* model of endometriosis to study the invasion of implanted endometrial tissue fragments and primary stromal cells (Nap et al., 2003). Utilising CAM as an experimental model is cheaper, and simpler to maintain and manipulate experimentally compared to primate and rodent models (Ribatti et al., 2001).

Although the efficacy of this model in forming lesions from implanted endometrial tissue averages from 68% to 83%, studying lesion growth in CAM is limited to a maximum incubation time of 10 days post-implantation (Borges et al., 2003, Nap et al., 2003, Nap et al., 2005). While CAM has proven to be useful

for elucidating the initial processes involved in endometriosis lesion establishment, it must be noted that implanted tissues are usually placed on an already highly vascularised membrane. Studies in this model have shown that host-derived angiogenesis factors such as VEGF, CD54, and MMP- 1, -2 and -9 regulate the formation of endometriosis-like lesions, but identification of newly formed blood vessels are difficult to distinguish from pre-existing vessels (Borges et al., 2003).

An additional limitation of CAM is its limited ability to support proliferation of endometrial tissue grafts. CAM may lack necessary growth factors to support implanted endometrial tissue growth, as at seventy two hours post-implantation, significantly reduced numbers of proliferative cells are seen (Nap et al., 2003). Moreover, CAM elicits a non-specific inflammatory response following tissue transplantation, which may impede studies on the role of the immune system during endometriosis (Grümmer, 2012). Furthermore, avian immune systems are less widely studied and share less homology with humans compared to primates and rodents. Therefore, although CAM is applicable as a model for early invasion and establishment of endometriosis-like lesions, its ability to represent a complete and accurate model for the progression of endometriosis from an immunological perspective is limited.

1.5.3 Rodent models

Rodents are one of the most abundantly used animals in scientific research. As a disease model, rodents are ideal, in that they are abundant, cost-effective, easy-to-manipulate, and sufficiently mimic human disease (Grümmer, 2012, Bruner-Tran et al., 2018). By using established homologous, xenograft, and/or genetically-modified mouse models of endometriosis, dynamic changes in endometriotic-like lesion development can be evaluated.

1.5.3.1 Homologous rodent models

These models are characterised by tissue transplantation from a donor rodent into a genetically identical or syngeneic immunocompetent recipient animal (Grümmer, 2006). As these mice are immunocompetent, various aspects of the pathogenesis of endometriosis, including angiogenesis, implantation rate, localisation, and any elicited immune response during disease progression has been extensively studied (Bruner-Tran et al., 2012). In addition, the use of homologous rodent models is paving the way to understanding the complexity behind pain and infertility, the most common symptoms of endometriosis (Grümmer, 2012). Using this model, research has shown that reduced fecundity and pain nociception in endometriosis may be attributed to an increased number of luteinised un-ruptured ovarian follicles and/or the feedback effect of gene expression profiles in the eutopic endometrium following endometriotic lesion

formation (Moon et al., 1993). In rats, a subcutaneous model of endometriosis (suturing of 3 x 3 mm autologous uterus fragment to the gastrocnemius muscle), not only identified a strong role for peripheral mechanisms in endometriosis nociception, but also demonstrated the feasibility of using subcutaneous tissue implantation to model disease development in endometriosis (Alvarez et al., 2012).

In addition, the significance of reduced histone deacetylase 3 (HDAC3) protein levels in the eutopic endometrium of infertile women with endometriosis compared to controls was recently evaluated in a mouse with conditional loss of *Hdac3* (Kim et al., 2019). Mice with reduced HDAC3 expression had infertility due to decidualisation defects and implantation failure, suggesting a critical role for HDAC3 in decidualisation and endometrial receptivity (Kim et al., 2019). Furthermore, rodent models have also been widely used to evaluate therapeutic options for the treatment of endometriosis (Bruner-Tran et al., 2012). The effects of steroid hormones, exposure to environmental toxins, immune-modulating drugs, and anti-inflammatory agents on endometriotic lesion establishment have also been investigated (Platteeuw and D'Hooghe, 2014, Seracchioli et al., 2014).

As rodents do not menstruate, with the exception of the Spiny Mouse (Bellofiore et al., 2017), these models are limited in that they do not spontaneously develop endometriosis. The human menstrual cycle (Figure 1.4 A) contrasts significantly from the rodent oestrus cycle (Figure 1.4 B), with the natural decidualisation of stromal cells in murine endometrium transpiring in response to the presence of a blastocyst, whereas in the absence of fertilisation, remodelling of the uterus occurs without shedding of the endometrium (Tranguch et al., 2005). As such, endometrial tissue does not build up in large quantities along the uterus, resulting in a majority of endometriotic-like lesions being established through the transplantation of whole donor uterine fragments, which, unlike human endometriotic lesions, include the myometrium layer (Bruner-Tran et al., 2012, Taniguchi and Harada, 2014). Although this limitation can be overcome through the careful and highly technical procedure of scraping endometrial tissue from the myometrium, this additional step often results in tissue damage and subsequent clearance by phagocytic cells following transplantation (Hirata et al., 2005, Bruner-Tran et al., 2012). Furthermore, to increase the rate of tissue implantation, some studies rely upon suturing tissue fragments (Lin et al., 2006), using fibrin glue (Boztosun et al., 2012), or use media containing extracellular matrix components during transplantation (Cheng et al., 2011). These techniques to induce endometriosis in homologous models differ considerably from the proposed theory of retrograde menstruation, and do not accurately represent the formation of endometriotic lesions.

On the other hand, several steps can be taken to overcome some of these limitations and develop an effective homologous model of endometriosis. Rodents can be ovariectomised to negate the influence of endogenous reproductive hormones and effectively disrupt the oestrus cycle. A protocol outlining the use of scheduled hormone injections and subsequent artificial induction of endometrial stromal cell decidualisation in mice was first described in 1984 (Finn and Pope, 1984). In this model, decidualisation was induced via an injection of oil into the uterus, and following the cessation of a progesterone stimulus, features of the human menstrual cycle were mimicked, including immune cell infiltration and subsequent tissue degeneration (Finn and Pope, 1984). Cousins *et al.* (2014) further refined the timing of hormone delivery in this model (Figure 1.4 C), and at the time of progesterone withdrawal, histological assessment of the uterine lumen was consistent with a robust decidualisation response, as evidenced by the presence of a large decidual cell mass. Moreover, overt vaginal bleeding was observed between four and twenty four hours post-progesterone withdrawal, with portions of uterine stroma being denuded of overlying epithelium due to the shedding of this decidual mass (Cousins et al., 2014, Armstrong et al., 2017).

The aforementioned technique has been used to establish a novel homologous "menstrual" mouse model of endometriosis (Cousins et al., 2014, Greaves et al., 2014). Following induction of "menstruation" in donor mice, the decidualised endometrial tissue was collected, and due to the larger quantity of endometrial tissue available following decidualisation, effective separation of the endometrium from the underlying myometrium was possible. To mimic spontaneous implantation in the peritoneal cavity and to reduce inflammation associated with suturing, an intraperitoneal injection of the donor endometrial tissue into a syngeneic ovariectomised recipient was carried out (Greaves et al., 2014). Three weeks post-transplantation, endometriosis-like lesions were identified on the peritoneal wall covering the uterus, gut and intestines, and on adipose tissues surrounding the bladder and kidney (Greaves et al., 2014). These established lesions exhibited histological similarities with human endometriotic lesions, highlighting the efficacy of this "menstrual" mouse model in studying the development endometriosis (Greaves et al., 2014).

1.5.3.2 Xenograft rodent models

To gain a more comprehensive understanding of the cellular mechanisms involved in in the ectopic implantation and survival of endometriotic lesions, xenograft mouse models have been developed wherein immunocompromised mice are transplanted with human endometrial tissue (Bruner-Tran et al., 2018, Simitsidellis et al., 2018). Strains of immunocompromised mice which have been used as endometriosis models include severe combined immunodeficient (SCID) mice (Hull et al., 2012), athymic/nude mice (Bruner-Tran et al., 2002), and recombinant activating gene 2/common cytokine

receptor γ chain (γc) double null (Rag2 γ(c) mice (Greenberg and Slayden, 2004). As the humoral and cellular immunity is absent, the ability to avoid interspecies graft vs. host disease makes immunocompromised mice useful for examining many aspects of endometriosis.

Both ectopic endometrial lesion tissues as well as eutopic endometrium from women with and without endometriosis have been successfully transplanted into immunocompromised mice (Grümmer, 2012). While the lack of adaptive immunity indicates that the immune response elicited is only an approximation of endometriosis, the lesions that develop in these mice retain characteristic endometrial traits (Zamah et al., 1984, Bruner-Tran et al., 2002, Greenberg and Slayden, 2004). Histological appearance and responsiveness to steroid hormones are maintained following transplantation and, the stage of the menstrual cycle during tissue collection does not appear to impact lesion development (Grümmer, 2006, Laschke and Menger, 2007). In addition, one study using a simultaneous injection of immune cells and transplantation of endometrial tissue from the same human donor showed that the extent of lesion development in this model was limited by the presence of immune cells from disease-free women (Bruner-Tran et al., 2010).

Using this model, it was also noted that vascularisation of the xenografts was due to host vessel invasion, with a corresponding disappearance of native graft vessels (Grümmer et al., 2001, Hull et al., 2003, Eggermont et al., 2005). As angiogenesis is vital for implantation and survival of ectopic endometrial tissue, immunocompromised mouse models have been used extensively to analyse the effects of antiangiogenic compounds (Laschke and Menger, 2007). Moreover, this model has shown that ectopic lesions are inhibited by suppression of MMPs and presents a viable *in vivo* option for analysing biological mechanisms and evaluating the efficacy of therapeutic options on human endometrial tissue (Grümmer, 2012).

1.5.3.3 Genetically-modified rodent models

A major advantage of homologous rodent models is the availability of utilising models with genetic modifications of specific target genes. Genetic manipulation remains the most conclusive method of determining the effect of overexpressed, reduced, or absent gene expression in an animal model (Grümmer, 2006). In endometriosis research, the use of genetically modified mouse models has proven essential in furthering the understanding of disease progression. For example, a 'green-fluorescent protein' (GFP)-expressing transgenic mouse model of endometriosis was developed which emphasised the intricate relationship between the hosts cellular response and lesion development, with particular emphasis on angiogenesis (Wilkosz et al., 2011, Machado et al., 2014). Furthermore, using donor GFP

tissue assists with the identification of induced lesions in non-fluorescent recipient animals. Similarly, a model of endometriosis in mice with green fluorescent-protein labelled macrophages has also been developed (Hull et al., 2012, Greaves et al., 2014). Reciprocal transfers with wildtype mice emphasised the importance of these immune cells in endometriosis, in which both donor and recipient macrophages were positively implicated in the inflammatory microenvironment of endometriotic lesion development (Greaves et al., 2014).

A conditional knockout *Cre/loxP* transgenic mouse model of endometriosis has been used to observe the effect of regulated, cell-specific gene expression during disease establishment (Budiu et al., 2009). Experiments utilising this system have demonstrated the effect of knocking down mouse immune responses, with particular emphasis on reduced macrophage numbers and reduced inflammation outcomes (Budiu et al., 2009, Cheng et al., 2011). Interestingly, the *Cre/loxP* conditional activation of the *K-ras* oncogene in ovarian surface epithelial cells gave rise to the formation of non-cancerous peritoneal and ovarian lesions which shared histological features of human endometriosis, further demonstrating the efficacy of this system as a model for endometriosis (Dinulescu et al., 2005, Cheng et al., 2011, Dinulescu, 2012). Not only can lesion development be analysed alongside changes in immune signalling and inflammatory responses, but further studies exploiting genetic deficiencies can also be easily carried out in rodent models. Using a mouse model with a specific gene mutation can provide substantial insight into disease pathology. For example mice homozygous for CSF1 mutation (*CSF-1*$^{-/-}$) were found to develop significantly fewer endometriotic-like lesions when compared to syngeneic wildtype controls (*CSF-1*$^{+/+}$) (Jensen et al., 2010).

Through cross-transplantation of genetically deficient (gene knockout / null mutant) or wildtype endometrium into homologous mice, the response in the donor endometrium and/or the host can be evaluated (Bruner-Tran et al., 2012). This can give rise to a more replete understanding of the mechanisms involved in the implantation of endometriotic lesions, and their ensuing ability to thrive ectopically. An example of this is the development of a TGFβ1 xenograft mouse model of endometriosis (Hull et al., 2012). A reduction in endometriotic lesion size was noted in a host with a genetic deficiency in TGFβ1, highlighting the importance of TGFβ1 signalling in endometriosis (Hull et al., 2012). In addition, assessment of Krüppel-like factor 9 (KLF9), a progesterone receptor coregulatory in the uterus, was examined through the transplantation of endometrial fragments from wildtype (*Klf9*$^{+/+}$) and *Klf9* null (*Klf9*$^{-/-}$) donor mice into wildtype recipient mice (Heard et al., 2014). In this study, a significant increase in lesion development coupled with a decreased systemic level of TNFα and IL-6 from *Klf9*$^{-/-}$-derived endometrium was observed, suggesting that the absence of *Klf9* reduces the activation of a pro-inflammatory immune response, consistent with the persistence of these lesions (Heard et al., 2014).

Recently, a microRNA null mutant model was used to study the effect of *miR-451* on endometriosis disease progression (Nothnick et al., 2014). In women with endometriosis, *miR-451* was found to be reduced in the eutopic endometrium, and is involved in cell proliferation, differentiation, and invasion (Graham et al., 2015). In this model, uterine fragments from mice deficient in *miR-451* were used to induce endometriosis in genetically replete recipients. Fewer endometriosis-like lesions were observed from microRNA deficient implants compared to wildtype, suggesting a deficiency in *miR-451* expression in endometrial tissue impairs the ability of this tissue to attach ectopically (Nothnick et al., 2014). This finding suggests an important role for microRNAs in the aetiology of endometriosis and, the ability to use microRNA-deficient mice for functional studies of disease progression currently remains unexploited.

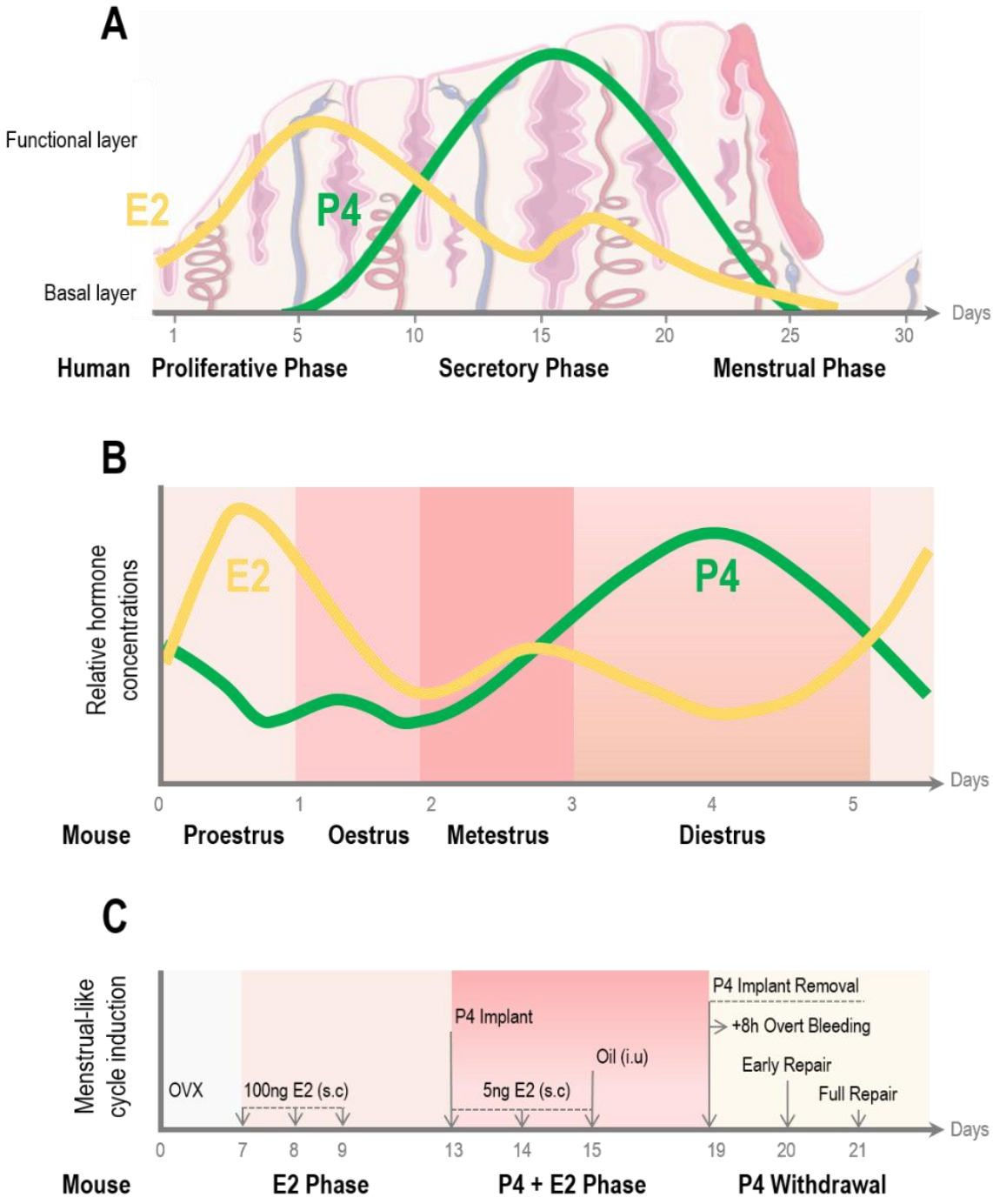

Figure 1.4 **Hormone fluctuations across the human menstrual cycle, mouse oestrus cycle and in the induced 'menstrual' mouse model**

The human menstrual cycle (A) is regulated by oestrogen (E2) and progesterone (P4), which functions in a negative feedback mechanism to regulate the proliferation of the functional layer of the endometrium. The fall in P4 levels results in the breakdown of the functional layer, resulting in menstruation. The oestrus cycle in mice (B) is similarly regulated by E2 and P4, however, unlike menstruation, the endometrial tissue is reabsorbed following the drop in P4. In the induced menstrual mouse model (C), subcutaneous (s.c) injections of E2 and provision of a P4 implant in an ovariectomised (OVX) mouse mimic the hormone changes seen in the human menstrual cycle. The intrauterine (i.u) insertion of oil into the uterus promotes decidualisation of the endometrial stromal cells which subsequently breakdown following the removal of the P4 implant. Within forty eight hours, full repair of the endometrium is observed in this model. Adapted from Armstrong et al. (2017) and Hong and Choi (2018).

1.6 THE ROLE OF MICRORNA IN ENDOMETRIOSIS

MicroRNAs (miRNAs) are a family of highly conserved 19-22 nucleotide sequences that regulate gene expression at the post-transcriptional and translational level (Anglicheau et al., 2010, Bueno and Malumbres, 2011). First identified in *Caenorhabditis elegans* through a genetic screen for developmental transition defects, miRNAs are thought to regulate over 30% of the human genome (Bartel, 2004). In the 21st release of miRBase, 28 645 hairpin miRNA precursors representing 35 853 mature miRNAs have been identified in 223 organism species (Kozomara and Griffiths-Jones, 2014). Functional experiments have shown that the diverse expression patterns exhibited by miRNAs area associated with complex regulatory pathways to control development and maintain homoeostasis (Bartel, 2009).

miRNA genes exist within the genome as either distinct transcriptional units or clusters of polycistronic units containing the information for multiple miRNAs (Bartel, 2004, Fazi and Nervi, 2008). miRNAs are transcribed in the nucleus as primary miRNA, where they undergo maturation steps that utilise the endonucleases, Drosha and Dicer, to attain functional capacity. Briefly, primary miRNA transcripts (pri-miRNA) are transcribed by RNA polymerases II or III and contain a cap structure with polyadenylation. In the nucleus, these pri-miRNA are processed by the Drosha complex to form the characteristic hairpin structured pre-miRNA with a double stranded stem. The Exportin-5/Ran-GTP complex translocates pre-miRNAs to the cytoplasm for Dicer processing in which the pre-miRNA is cleaved near the terminal hairpin loop to from 19-24 nucleotide long miRNA duplexes. A single strand of the duplex is subsequently incorporated into a multiple-protein nuclease complex, the RNA-induced silencing complex, which acts on its target sequence to regulate protein synthesis by either translational repression or messenger RNA (mRNA) degradation (Bartel, 2009, Shukla et al., 2011). However, there have been reports of miRNA acting to enhance target mRNA expression (Bueno and Malumbres, 2011, Green et al., 2016). The precise molecular mechanisms that underpin the ability of miRNAs to modulate post transcriptional repression are still being elucidated, but are thought to be linked to the induction of target mRNA instability (Liu and Abraham, 2013). Importantly, miRNAs are able to simultaneously target several genes within similar or related pathways, where each miRNA may regulate up to 300 different mRNAs (Laffont and Rayner, 2017). Conversely, a single mRNA may contain over 40 binding sites for various miRNAs, which suggests a requirement for functional redundancy amongst miRNAs in maintaining biological homeostasis (Fischer et al., 2015, Laffont and Rayner, 2017).

In addition to their activity within the local cellular environment, miRNAs can be transported across the cell membrane into the systemic blood circulation (Haider et al., 2014), where they can be incorporated into distant cells with functional consequences relevant to disease treatment (Bueno and Malumbres,

2011, Boon and Vickers, 2013). In addition, extracellular miRNAs associated with Argonaute proteins can be shielded from RNAse degradation, and are present at high concentrations in both blood plasma/serum and in tissue culture media (Arroyo et al., 2011, Turchinovich et al., 2011, Meister, 2013). The high stability of miRNAs in circulation and distinctive changes in their plasma profile depending on various disease conditions strongly suggests that they may be ideal biomarkers of disease (Hayes et al., 2014).

Multiple studies have shown that miRNA expression is altered in eutopic endometrium (Toloubeydokhti et al., 2008, Burney et al., 2009, Ramon et al., 2011), in both ectopic and eutopic endometrial tissues (Toloubeydokhti et al., 2008, Ohlsson Teague et al., 2009, Filigheddu et al., 2010) and in circulating miRNAs in women with endometriosis compared to healthy women (Hull and Nisenblat, 2013, Jia et al., 2013a, Wang et al., 2013b, Cho et al., 2015, Rekker et al., 2015). Furthermore, a range of functional studies, including the induction and modulation of miRNA expression levels and the use of luciferase assays *in vitro* (Hawkins et al., 2011, Petracco et al., 2011, Ramon et al., 2011, Lin et al., 2012, Abe et al., 2013), suggest that discrete miRNAs may be able to regulate the dialogue between cellular components within endometriotic lesions, thereby contributing to their persistence. There are several caveats for the design of functional miRNA studies in investigating endometriosis. These include the facts that *in vitro* experiments must be performed in cell lines that express the specified microRNA, that singleplex PCR estimations can be unreliable as they lack a standardised control for miRNA and that single cell cultures do not reflect the complex cellular interplay seen in ectopic tissues. Informative in *vivo* experiments require novel mouse strains or specialised miRNA delivery methodologies that are able to modulate miRNA expression levels, which should be carried out in tandem with *in vitro* functional studies to help comprehend the mechanisms behind the pathogenesis of endometriosis and to exploit the potential of miRNAs as biomarkers of disease progression.

1.6.1 miRNA as biomarkers of endometriosis

A main research priority for endometriosis is to develop a reliable non-invasive diagnostic test, and the concept of using miRNA as biomarkers of this disease is gaining popularity (Hull and Print, 2012, Wang et al., 2013b). Furthermore, the possibility of identifying circulating peripheral miRNA in women with endometriosis that differs significantly from disease-free women could provide valuable insight for both diagnostic and therapeutic options. The use of algorithms to predict target mRNA have uncovered a link between these sequences and a number of cellular events involved in the development of endometriosis, including inflammation, tissue repair and remodelling, hypoxia, DNA methylation, and cell cycle proliferation (Ohlsson Teague et al., 2009, Teague et al., 2010, Hawkins et al., 2011, Gilabert-Estelles et al., 2012, Hull and Nisenblat, 2013).

Although initial studies have identified various miRNAs with potential as circulating biomarkers for endometriosis (Gupta et al., 2016, Nisenblat et al., 2016a), there remains a need for larger transcriptomics studies involving more diverse patient cohorts (Rogers et al., 2016). Efforts have been made to ensure uniformity in specimen collection and processing (Nothnick et al., 2015, Nisenblat et al., 2016b, Gupta et al., 2016, Adamson and Johnson, 2018) and to encourage the deposition of genomic profiling data in repositories (Pereira et al., 2014, van Schaik et al., 2014). Ideally, a collaborative global database of miRNA and long noncoding RNA expression levels in tissues and blood of women with endometriosis and non-diseased controls would inform future biomarker initiatives. A patent was recently filed to utilise leucocyte miRNAs for the diagnosis and treatment of endometriosis (Nagarkatti et al., 2015), demonstrating progress and interest in the commercial development of non-invasive diagnostic tools for endometriosis.

1.6.2 Eutopic endometrial tissue

A number of studies suggest that miRNAs are altered in eutopic endometrial tissue from women with endometriosis (Burney et al., 2009, Aghajanova and Giudice, 2011, Ramon et al., 2011, Ruan et al., 2013, Braza-Boils et al., 2014, Zheng et al., 2014). Initially, six downregulated miRNAs from the *miR-9* and *miR-34* families were identified when eutopic endometrium from women with endometriosis (n = 4) and without endometriosis (n = 3) were compared (Burney et al., 2009). Based on an in silico miRNA target analyses, *miR-34* is thought to potentially regulate progesterone resistance and enhance proliferation and ectopic survival (Burney et al., 2009). Interestingly, *miR-9* overexpression promotes breast cancer development (Gwak et al., 2014), increases cell migration and invasiveness in SW480 human colon adenocarcinoma cells (Park et al., 2016), and works in tandem with *miR-124* to facilitate the conversion of human fibroblasts into neurons (Yoo et al., 2011), suggesting that *miR-9* may have an important role in the persistence of endometriosis lesions and associated nociception.

A larger study, contrasting implantation 'window' eutopic endometrium from women with (n = 36) and without (n = 44) endometriosis, found upregulation of *miR-29c*, *miR-200a* and *miR-145* in endometriosis patients (Ruan et al., 2013). These miRNAs were postulated to contribute to implantation defects and endometriosis-associated subfertility. Additionally, comparison of mRNAs and miRNA profiles in eutopic endometrium from women with mild (n = 19) and severe (n = 44) endometriosis (Aghajanova and Giudice, 2011) has demonstrated upregulation of *miR-21* throughout the menstrual cycle in patients with severe endometriosis, suggesting its use as a potential biomarker for disease progression. There is little overlap in the differentially expressed miRNAs identified by each of these studies, indicating a need for larger

well-powered studies that adequately account for variation in clinical status and tissue biopsy composition to identify the candidate miRNAs that are most relevant for ongoing investigation. Given the lack of consensus amongst these studies, it is possible that further comparisons of eutopic tissue from women with and without endometriosis may demonstrate no substantial difference in miRNA expression patterns attributable to endometriosis. Furthermore, if differential expression of miRNAs in eutopic tissue was to be confirmed, it would be difficult to determine if it was an underlying causal factor driving initiation of disease or a consequence of altered eutopic tissue function that occurs secondary to lesion establishment.

1.6.3 Eutopic vs ectopic microarray analyses

Many research groups have used microarrays or next-generation sequencing techniques to compare miRNA transcripts uniquely expressed within ectopic lesions (ovarian, peritoneal and/or rectovaginal) with paired or unpaired eutopic tissues from women with endometriosis or healthy controls (Ohlsson Teague et al., 2009, Filigheddu et al., 2010, Hawkins et al., 2011, Ramon et al., 2011, Laudanski et al., 2013, Braza-Boils et al., 2014, Zheng et al., 2014). The miRNAs identified again show limited concordance between experiments, which is likely to reflect the considerable heterogeneity in patient selection, experimental design, normalisation methods and bioinformatic assessment of the studies. Additionally there is ongoing debate as to whether lesions at different locations represent different manifestations of the same disease process or distinct disease identities and heterogeneity between lesions from different locations could confound the molecular analyses (Borghese et al., 2017). Across these studies, a total of 132 differentially expressed miRNAs were identified, with 23% of dysregulated miRNAs (31 miRNAs) being present in at least two of the studies (Ohlsson Teague et al., 2009, Filigheddu et al., 2010, Hawkins et al., 2011, Ramon et al., 2011, Laudanski et al., 2013, Braza-Boils et al., 2014, Zheng et al., 2014). Collectively these data suggest that distinct miRNA profiles do indeed exist between ectopic and eutopic tissue, with predicted targets of these miRNA having multi-faceted roles in tissue remodelling, cellular proliferation and angiogenesis (Wei et al., 2015).

Amongst the differentially expressed miRNAs, *miR-29c*, *miR-100* and *miR-143* have emerged as consistently upregulated in ectopic endometrial tissues in four studies (Ohlsson Teague et al., 2009, Filigheddu et al., 2010, Hawkins et al., 2011, Zheng et al., 2014). *miR-29c*, which is known to regulate genes controlling endometrial cell proliferation, apoptosis and invasion (Ohlsson Teague et al., 2009, Filigheddu et al., 2010, Hawkins et al., 2011), targets c-Jun during the late secretory phase (Udou et al., 2004, Long et al., 2015). This is postulated to upregulate anti-apoptotic mechanisms in stromal cells, thereby promoting cellular survival during disease establishment (Long et al., 2015). Upregulation of *miR-*

100 has been found to inhibit cellular proliferation, migration and invasion in a cancer model, whereas downregulation promoted metastasis (Zhou et al., 2014). Similarly, *miR-143* is associated with the development of endometrioid carcinomas (Wang et al., 2014b). The upregulation of *miR-100* and *miR-143* in endometriotic tissues is hypothesised to confer protection from malignant change and promotion of a benign phenotype of endometriosis.

1.6.4 Circulating microRNA in plasma samples

The potential for utilising miRNAs as serum diagnostic markers of disease progression has prompted analysis of dysregulated miRNAs in blood of women with endometriosis. To date, eight studies have examined circulating miRNAs using high throughput assays in either serum (Wang et al., 2013b, Hsu et al., 2014, Cho et al., 2015, Cosar et al., 2016, Wang et al., 2016) or plasma samples (Jia et al., 2013a, Suryawanshi et al., 2013, Nisenblat et al., 2012, Nisenblat et al., 2019) taken from women with and without endometriosis. A further two papers have used singleplex RT-PCR assay methods to demonstrate downregulation of the *miR-200* family in plasma (Rekker et al., 2015) and upregulation of *miR-451a* levels in women with endometriosis (Nothnick, 2017). The results generally show little consistency between these studies. Although several studies identify circulating miRNAs with sensitivities and specificities high enough to suggest utility as a diagnostic tool, the heterogeneity in experimental design, specimen collection, bioinformatic analysis and normalisation methods make the findings difficult to replicate. To date, only one group has evaluated and validated several circulating miRNAs in a large, independent test cohort of women with and without endometriosis (Nisenblat et al., 2019).

Endometriosis has the potential to progress to endometriosis-associated ovarian cancer (EAOC), and plasma miRNAs may prove to be markers for malignant disease progression (Okada et al., 2010, Dinulescu, 2012, Viganò et al., 2012, Suryawanshi et al., 2013, Králíčková and Vetvicka, 2014, Zhao et al., 2014b). Several studies have correlated the progression of EAOC with endometriosis as a precursor stage, and underscores the possibility of using miRNA as a marker for the stage of disease development (Li et al., 2010, Okada et al., 2010, Dinulescu, 2012, Yan et al., 2014). For example, Suryawanshi et al. (2013) compared plasma miRNA levels from women with endometriosis to those with EAOC as well as healthy controls, and found a total of ten miRNAs that were differentially expressed between the three groups, all being higher in patients with endometriosis (Suryawanshi et al., 2013).

Plasma levels of *miR-200a* and *miR-141* were identified as potential biomarkers for endometriosis, but expression levels were found to be altered in response to the time of the day at which blood collection occurred (Rekker et al., 2015). It may be that the impact of circadian rhythms on plasma miRNA levels is

a key factor accounting for inconsistency between studies. Menstrual cycle phase has also been raised as a potential confounding factor, but on investigation, no significant variation in plasma miRNAs across the menstrual cycle was found in one study (Rekker et al., 2013). Notwithstanding, it seems prudent that standardisation of sampling practices and assays for assessment of plasma miRNAs in large cohorts is required to better progress development of informative diagnostic markers.

1.6.5 Pathophysiological processes impacted by differentially expressed miRNAs

The miRNAs identified as dysregulated in endometriosis appear to target mRNAs involved in a range of cellular and biological pathways, several of which are implicated in endometriotic lesion development (Figure 1.5).

1.6.5.1 Hypoxic injury

Hypoxia characterises the early phases of ectopic endometrial tissue survival and hypoxia induced factor (HIF)-1α gene expression is upregulated in endometriotic tissues (Chen et al., 2015c) and in early stage endometriosis-like lesions from mouse models. In endometriotic lesions, high levels of *miR-20a* prolong HIF-1α activation of extracellular-signal-regulated kinase (ERK) (Lin et al., 2012), inducing a signalling cascade which increases fibroblast growth factor (FGF)-9 expression. FGF-9 stimulates endothelial and endometrial stromal cell proliferation and angiogenesis, potentially contributing to ectopic lesion development (Tsai et al., 2002). Elevated *miR-20a* expression suppresses antiangiogenic Netrin-4 gene expression (Zhao et al., 2014a), potentially enhancing angiogenesis in ectopic endometrial lesions. Hypoxic conditions in endometriotic lesions also induce *miR-148a* and AU-rich element binding factor-1 expression *in vitro* (Hsiao et al., 2015), leading to destabilised DNA methyltransferase 1 mRNA expression. This could account for the aberrant epigenetic methylation patterns seen in endometriosis patients.

1.6.5.2 Inflammation

Aberrant immune surveillance is thought to reduce the clearance of endometrial issue within the peritoneal cavity permitting attachment, progression and subsequent disease persistence (Herington et al., 2011, Králíčková and Vetvicka, 2015). The inflammatory mediators IL-1β (Milewski et al., 2008), TNFα (Keenan et al., 1995, Gmyrek et al., 2008) and cyclooxygenase (COX)-2 (Wu et al., 2002) are elevated in peritoneal fluid and ectopic lesions from women with endometriosis, and their inhibition suppresses endometriotic-like lesion development in animal models (Dogan et al., 2004, Kyama et al., 2008). Interestingly, there are studies that suggest that these inflammatory mediators can be targeted by miRNAs in endometrial

tissue, which might then contribute to development of endometriosis. For example, Toloubeydokhti et al. (2008) discovered that *miR-542-3p* interacts with and downregulates COX-2 in ectopic endometrial tissues (Toloubeydokhti et al., 2008). Furthermore, IL-1B, COX-2 and TNF are indirectly targeted by *miR-302a* in endometrial stromal cells (ESCs), where *miR-302a* suppression of chicken ovalbumin upstream promoter-transcription factor II results in induction of these inflammatory mediators (Lin et al., 2014).

1.6.5.3 Steroidogenesis

Aberrant oestrogen and progesterone biosynthesis, metabolism and sensitivity appear to contribute to the development of endometriosis (Bulun et al., 2012). For example, aromatase activity is upregulated in endometriotic lesions as part of a feed forward loop involving COX-2, increasing local oestrogen production and promoting endometriosis development. Increased *miR-142-3p* levels in primary ESCs reduced steroid sulfatase and IL-6 activity, suggesting a dual effect on steroidogenic and inflammatory pathways in endometriosis (Kastingschafer et al., 2015).

Overexpression of *miR-23a* and *miR-23b* which target the NR5A1 gene, leads to the repression of steroidogenic factor-1, resulting in reduced levels of aromatase P450 and steroidogenic acute regulatory protein (Shen et al., 2013). Expression of these miRNAs expression is reduced in eutopic and ectopic endometrium from women with endometriosis (Shen et al., 2013), which is predicted to enhance oestrogen synthesis, promote proliferation in endometriotic tissues and delay endometrial transition from the proliferative to secretory phase, which manifests as progesterone resistance (Gilabert-Estelles et al., 2012, Shen et al., 2013). Progesterone resistance may also be promoted by other miRNA which are increased in eutopic endometrium of endometriosis patients. *miR-135a* and *miR-135b* for example, both target the HOXA10 gene and are involved in uterine stromal cell responsiveness to progesterone (Petracco et al., 2011).

1.6.5.4 Cell proliferation, survival and invasion

Mouse models demonstrate that cellular proliferation is important for the survival and growth of endometrial fragments at ectopic sites (Bruner-Tran et al., 2012, Khanjani et al., 2012, Winterhager, 2012), and miRNA regulation is important to this process. For instance, high expression of *miR-210* in ESCs results in signal transducer and activator of transcription 3 (STAT3) activation and increased proliferation, angiogenesis and resistance to apoptosis (Okamoto et al., 2015), whereas upregulation of *miR-202* modulates sex determining region Y-box 6 expression, increasing the proliferation and invasiveness of ESCs (Zhang et al., 2015). Suppression of *miR-196b* increases the proliferative capacity

and anti-apoptotic mechanisms of endometriotic cells *in vitro* (Abe et al., 2013). Further, the invasive potential of ESCs is enhanced by *miR-183* suppression, which increases integrin β1 expression, a vital component of cell adhesion (Shi et al., 2014, Chen et al., 2015a). Similarly, *miR-10b* and *miR-145* increase ESC proliferation and invasiveness by targeting multiple cytoskeletal elements and metalloproteinases (Adammek et al., 2013, Schneider et al., 2013).

In human endometriotic lesions, *miR-451* expression was inversely correlated with the expression of macrophage migration inhibitory factor (MIF), which contributes to endometrial epithelial cell survival (Graham et al., 2015). Similarly, reduced expression of *miR-451* in lesions from a baboon model of endometriosis (Joshi et al., 2015), corresponds to increases in expression of its predicted targets CDKN2D, GATAD2B and YWHAZ. A recent study also found a significant increase in *miR-451a* levels in serum from women with endometriosis, as well as in baboons with experimentally induced endometriosis (Nothnick et al., 2017). Tumour suppressor activity associated with *miR-451*, including regulation of NOTCH1-induced oncogenesis (Li et al., 2011) and the modulation of IKKβ (Li et al., 2013) and IL6R (Liu et al., 2014) gene expression, also likely contribute to the increased proliferation and anti-apoptotic responses seen in endometriotic lesions. This hypothesis was tested in the only *in vivo* functional miRNA study to date which has utilised a mouse model of endometriosis (Nothnick et al., 2014). Uterine fragments from *miR-451* deficient mice were transplanted to induce endometriosis-like lesions in genetically normal recipients. Ectopic attachment and survival of lesions appeared to be impaired with fewer lesions observed in *miR-451* deficient implants, confirming that *miR-451* confers protection from host clearance mechanisms (Nothnick et al., 2014).

1.6.5.5 Tissue repair, remodelling and angiogenesis

Several factors that promote tissue repair, remodelling and angiogenesis appear to be targeted by miRNAs in endometriosis. VEGF is a critical angiogenic factor expressed in endometriotic tissues and peritoneal macrophages (Laschke and Menger, 2007, Groothuis, 2012, Krikun, 2012) and its inhibition in animal models of endometriosis suppresses lesion development (Hull et al., 2003, Nap et al., 2005). *miR-210* which is induced in ESC cultures, contributes to VEGF regulation as *miR-210* transfection results in induction of VEGF-A and STAT3 (Okamoto et al., 2015), resulting in increased angiogenesis, cell proliferation and reduced apoptosis.

miR-21 and *miR-199a-5p* also appear to contribute to VEGF regulation in endometriosis. *miR-21* is expressed at high levels in exosomes released from primary ESCs, and its overexpression was found to upregulate VEGF leading to enhanced angiogenesis (Harp et al., 2016). Upregulation of *miR-199a-5p*

was shown to repress VEGF-A expression in endometrial mesenchymal stem cells, causing cell proliferation and angiogenesis to be inhibited (Hsu et al., 2014). Functional validation in a mouse model confirmed the pathophysiological relevance of this miRNA, with a reduction in endometriosis-like lesions following repeated delivery of pre-miR-199a (Hsu et al., 2014).

There is evidence that MMPs, which are elevated in endometriosis lesions, are also regulated by miRNAs (Groothuis et al., 2005). These include *miR-93*, the expression of which is suppressed and inversely correlated to MMP-3 and VEGF-A bioactivity in eutopic endometrial cells from women with endometriosis (Lv et al., 2015). Furthermore, systematic evaluation of 17 single nucleotide polymorphisms (SNPs) in the MMP-2 gene identified an aberrant *miR-520g* binding site which is associated with endometriosis susceptibility (Tsai et al., 2013). It was postulated that this SNP predisposes to endometriosis by creating deficiency in the regulatory action of *miR-520g* on MMP-2 synthesis. In this scenario, unregulated levels of MMP-2 could act to enhance degradation of the extracellular matrix and facilitate anchoring of endometrial fragments to ectopic sites and subsequent tissue remodelling (Tsai et al., 2013).

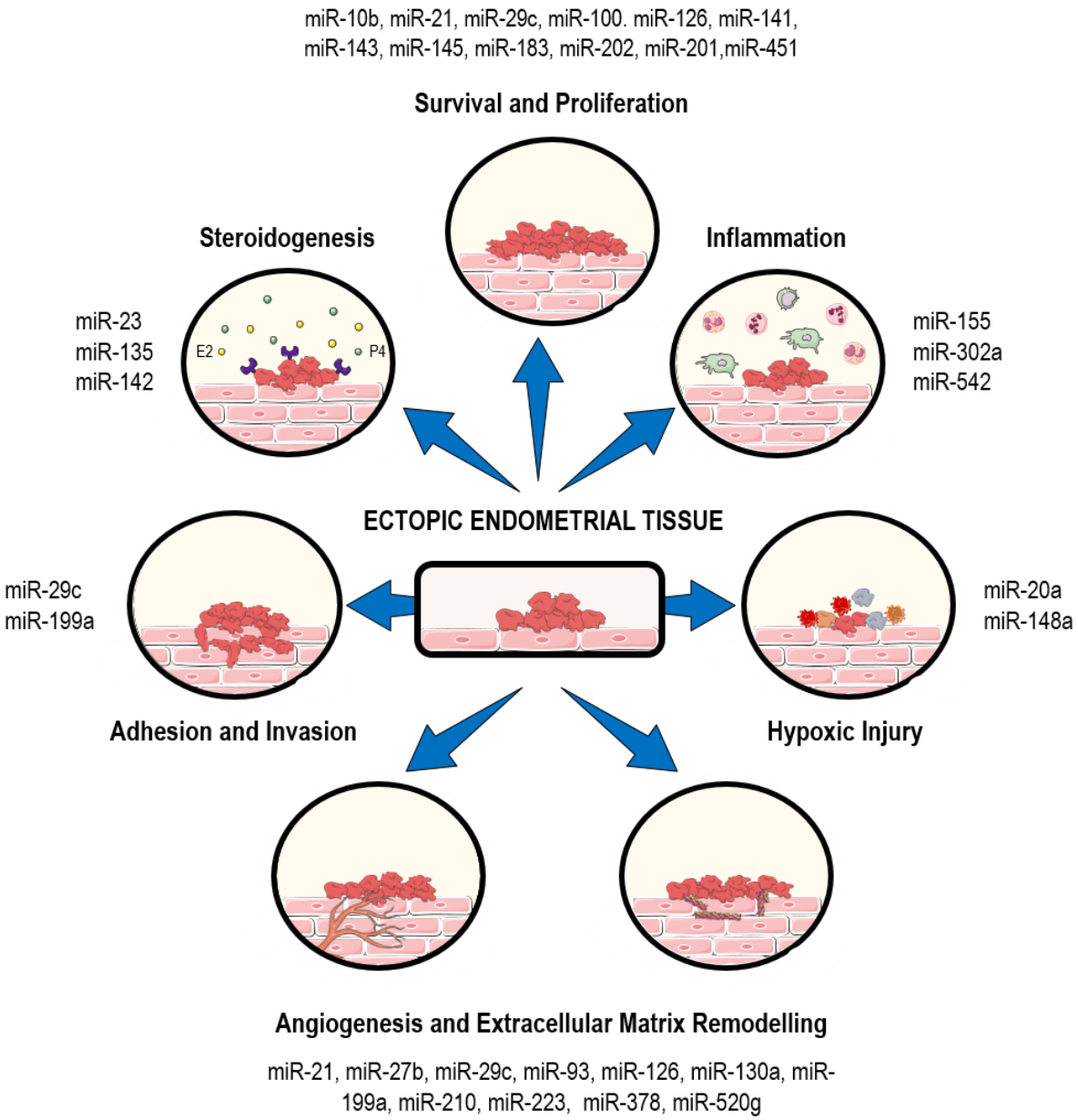

Figure 1.5 A proportion of microRNAs implicated in the development of endometriosis

Experimental validation of microRNAs in endometriosis have shown that multiple biological processes are regulated by miRNAs including survival and proliferation of ectopic endometrial tissue fragments, steroidogenesis, adhesion and invasion, inflammation, hypoxic injury and angiogenesis and extracellular matrix remodelling. Collectively these processes significantly impact lesion development and contribute to the pathophysiology of endometriosis.

1.7 miRNA IN IMMUNE RESPONSE MODULATION AND MACROPHAGE POLARISATION

The transcriptional regulation of macrophage polarisation has been the focus of multiple studies. Among the transcription factors found to promote TLR ligand induced M1-like macrophage activation are nuclear factor κβ (NF-κβ), activator protein-1 (AP-1), and CCAAT/enhancer-binding protein α, while STAT6, PPAR-γ, and KLF4 induce M2-like macrophage polarisation (Brune et al., 2013, Tugal et al., 2013, Jantsch et al., 2014, Wang et al., 2014a). miRNAs are also integral to the regulatory networks of both the innate and adaptive immune systems, and are able to modulate inflammatory responses, shifting between a pro- or anti- inflammatory state (O'Connell et al., 2012, Liu and Abraham, 2013). It has been proposed that specific miRNAs are able to target these important regulators in signalling networks, causing a shift between M1-like and M2-like macrophage phenotypes (Liu and Abraham, 2013). However, to date, only a few miRNAs were found to have a significant differential expression between M1-like and M2-like macrophage subtypes.

1.7.1 Role of *microRNA155* in M1-like macrophage polarisation and endometriosis

The expression of *miR-155* has a pivotal role in Akt kinase-driven polarisation of macrophages (Arranz et al., 2012). Isoforms of Akt kinase have been shown to regulate both pro- and anti-inflammatory immune responses, where an *Akt1*-deficiency resulted in a M1-like macrophage phenotype and conversely, an *Akt2*-deficiency resulted in a M2-like macrophage phenotype (Arranz et al., 2012). In both naïve and LPS-stimulated *Akt2*-deficient macrophages, the expression of *miR-155* is repressed (Arranz et al., 2012). Coinciding with this is the upregulation of C/EBPβ, a hallmark regulator of the M2-like macrophage-associated Arg-1, suggesting a role for *miR-155* in promoting a classical M1-like macrophage phenotype (Arranz et al., 2012).

In vitro studies have also confirmed the ability of *miR-155* to skew macrophages towards the M1-like phenotype (Worm et al., 2009, Martinez-Nunez et al., 2011, Gracias et al., 2013, Wang et al., 2013a). LPS, a classical M1-like inflammatory mediator was shown to upregulate *miR-155* in THP-1 monocyte-derived macrophage cell lines (Das et al., 2013, Gracias et al., 2013). When these cells were transfected with a miR-155 mimic, upregulation of the classical immune pathway transcripts was seen, confirming its role in the M1-like, pro-inflammatory immune response (Das et al., 2013). In addition, *miR-155* is known to regulate macrophage polarisation though translational regulation of IL-13Rα1 gene (Martinez-Nunez et al., 2011). IL-13Rα1 is an important cytokine receptor expressed on monocytes, allowing for M2-like macrophage polarisation following stimulation with IL-13 (Martinez-Nunez et al., 2011). Overexpression of *miR-155* suppresses IL-13Rα1 expression, thus preventing monocyte differentiation into M2-like

macrophages and effectively promoting production of M1-like macrophages. On the other hand, a *miR-155*-deficiency enhances production of IL-13Rα1, thereby promoting M2-like macrophage activation (Martinez-Nunez et al., 2011).

In endometriosis, a miRNA microarray analysis of plasma samples at different phases of the menstrual cycle identified miR-155-5p (miR-155) as being downregulated in women with endometriosis (n = 51) compared to healthy controls (n =27) (Nisenblat et al., 2019). This downregulation of miR-155 expression was further validated in a second cohort of patients, comprising 80 women with endometriosis and 39 women without endometriosis (Nisenblat et al., 2019). Collectively, these findings suggest that downregulation in miR-155 may contribute to the pathogenesis of endometriosis by promoting polarisation of M2-like macrophages, thus inducing a tissue healing and remodelling phenotype eventuating in disease exacerbation, and is discussed further in Chapter 4 of this thesis.

1.7.2 Role of *microRNA-223* in M2-like macrophage polarisation and endometriosis

miR-223 regulates the M1-like vs M2-like immune response through targeting signalling components of the inflammatory pathway (Chen et al., 2012, Zhuang et al., 2012, Ismail et al., 2013). *miR-223* represses the translation of the inhibitory kinase Ikkα; leading to the suppression of downstream signalling nuclear factor κβ (NFκβ) pathways which results in an enhanced alternative immune response (Jia et al., 2011, Haneklaus et al., 2013). On the other hand, in *miR-223* deficient mice, NFκβ pathways are induced, resulting in an enhanced classical, M1-like immune response (Li et al., 2010). These observations were further validated in *miR-233*-deficient macrophages, which were hypersensitive to the classical immune pathway stimulant LPS (Zhuang et al., 2012). In these macrophages, levels of M1-like cytokines IL-1β, IL-6 and TNFα were higher than wildtype controls, indicative of an immune shift towards a pro-inflammatory state. Conversely, *miR-223*-deficient macrophages exhibited delayed responses to the alternative immune pathway stimulant IL-4 compared to controls, and the level of M2-like associated Arg-1 was reduced (Zhuang et al., 2012).

In endometriosis, from a paired eutopic versus ectopic endometrial microarray analysis, miR-223-3p (miR-223), a haematopoietic-specific miRNA, was found to be significantly upregulated by 1.72-fold in endometriotic tissues (n=8) (Ohlsson Teague et al., 2009). Based on predicted mRNA targets (including Nuclear Factor I/A, Myocyte Enhancer Factor 2C, and Leukaemia-Associated Phosphoprotein P18), miR-223 is thought to play a role in cell differentiation, granulopoiesis and myogenesis (Jia et al., 2011, Haneklaus et al., 2013), and is a critical mediator of alternative M2-like macrophage activation (Ying et al., 2015). As miR-223 is upregulated in ectopic endometrial tissue, it is possible that an increased

abundance of M2-like macrophages may be present at the lesion site, and could promote lesion development by shifting the immune response towards a more anti-inflammatory, tissue remodelling state, and is discussed further in Chapter 5 of this thesis.

1.7.3 Regulation of macrophage polarisation by microRNAs as an indicator of ectopic lesion development

The production of new treatment options for endometriosis remains elusive due to the current lack of understanding of the pathophysiology of this disease. While macrophages have been identified as key immune cells influencing the ability of endometrial tissue to attach and thrive ectopically (Bacci et al., 2009, Capobianco and Rovere-Querini, 2013, Ahmad et al., 2014), the underlying mechanisms of macrophage activation during endometriosis have not been thoroughly defined. Although a host of miRNAs have been identified as being dysregulated in endometriosis (Teague et al., 2010, Gilabert-Estelles et al., 2012, Hull and Print, 2012, Hull and Nisenblat, 2013), the current understanding of miRNA pathways in macrophage polarisation combine with miRNA expression profiles obtained from women with endometriosis, leads us to propose that both *miR-223* and *miR-155* are likely to have critical roles in the progression of endometriosis.

Hence, this study aims to evaluate the effect of miRNA-mediated macrophage activation as an indicator of ectopic lesion development in mouse models of endometriosis. Both *miR-223* and *miR-155* deficient mice models are currently used for immunological studies and are well characterised (Faraoni et al., 2009, Haneklaus et al., 2013). We aimed to develop an induced menstrual mouse model of endometriosis in *miR-223* deficient and *miR-155* deficient mice, following techniques descried previously (Greaves et al., 2014). Once this model was established, we determined if a genetic deficiency in *miR-223* or *miR-155* altered macrophage activity and endometriotic lesion development by immunohistochemical evaluation. Subsequently, using RNA-Sequencing, we evaluated the molecular pathways involved in lesion growth and establishment in the absence of either *miR-155* or *miR-223*. Finally, we determined whether a *miR-223* or *miR-155* deficiency only in the donor endometrium or only in the host response altered disease progression via the reciprocal transfer experiments with wildtype C57 mice.

Therefore, by utilising these miRNA deficient mice as models of endometriosis, this project evaluated the hypothesis that a deficiency in *miR-223* will suppress lesion growth via enhancement of pro-inflammatory M1 macrophage activity, and conversely, that a deficiency in *miR-155* will enhance lesion development through upregulation of anti-inflammatory M2 macrophage activity. In turn, the research will inform development of strategies to alter the polarisation status of macrophages in the peritoneal cavity. Novel

therapeutic strategies targeting macrophage polarisation may ultimately improve the lives of women with this debilitating disease.

1.8 HYPOTHESIS

The experiments described in this thesis will address the following hypotheses:

- Lesion development in a subcutaneous menstrual mouse model of endometriosis mimics human disease;
- A *miR-223* deficiency enhances pro-inflammatory M1-like macrophage activity, thereby suppressing endometriotic lesion development via increased ectopic tissue clearance; and conversely,
- A *miR-155* deficiency upregulates anti-inflammatory M2-like macrophage activity, thereby sustaining endometriotic lesion growth through increased remodelling and angiogenesis.

1.9 RESEARCH AIMS

The experiments described in this thesis will address the following experimental aims, in which a menstrual mouse model of endometriosis is used to:

- Characterise the development of endometriotic-like lesions in genetically replete, wildtype mice.
- Determine the effect of a *miR-223* or *miR-155* deficiency on lesion appearance and morphology.
- Assess macrophage localisation and phenotype within lesions, and to evaluate lesion growth and establishment in the absence of either *miR-223* or *miR-155*.
- Investigate the significance of *miR-223* and *miR-155* on molecular signalling pathways contributing to the development of endometriosis.
- Evaluate the contribution of donor endometrial tissue vs recipient environment on the development of endometriotic lesions.

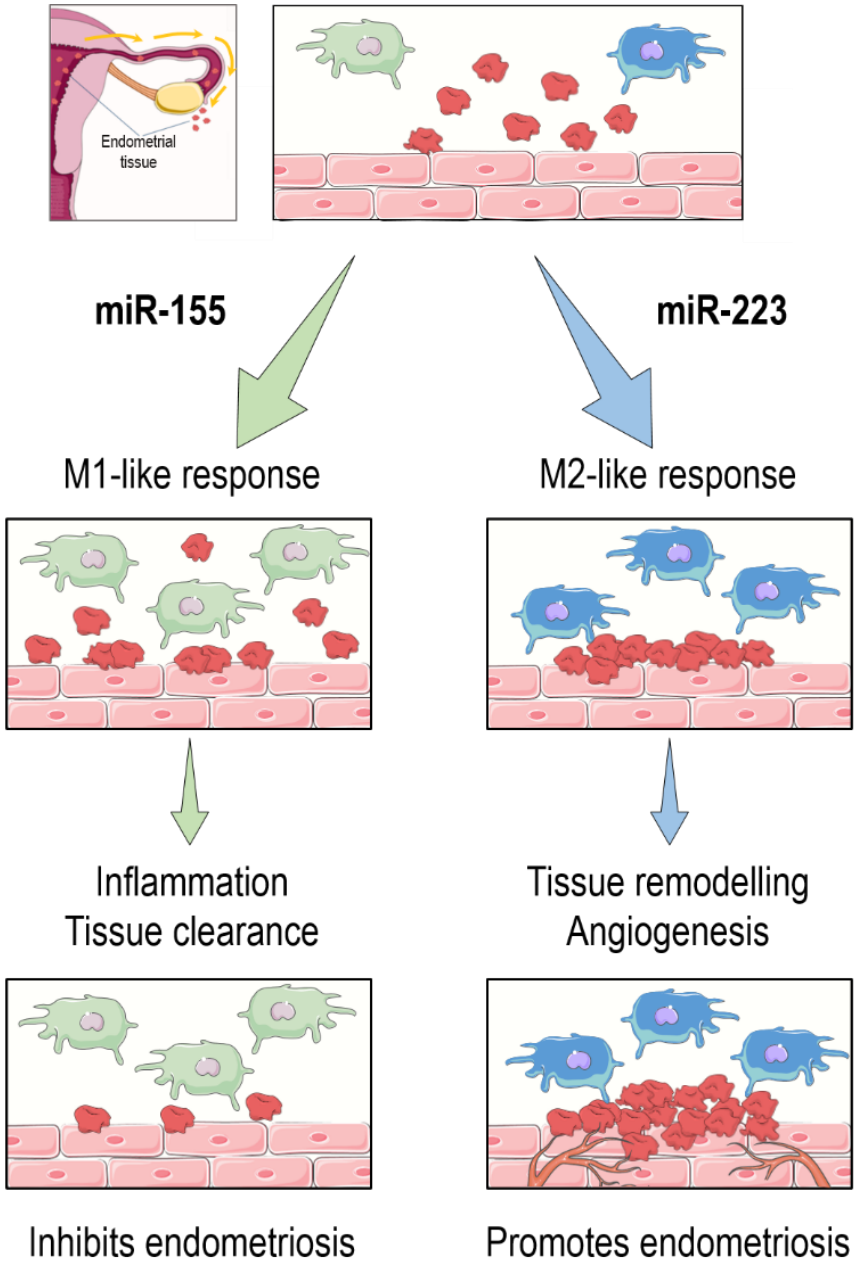

Figure 1.6 **Proposed working model of microRNA regulation of macrophage polarisation in endometriosis**

The presence of ectopic endometrial tissue in the peritoneal cavity results in an influx of immune cells, predominantly, the recruitment of macrophages. In the presence of miR-155, macrophages are preferentially polarised towards an M1-like, pro-inflammatory phenotype, characterised by an increased production of inflammatory mediators such as TNFα, iNOS and IL-1β. This increases inflammation and mediates tissue clearance and destruction, and may result in an inhibition of endometriosis. Conversely, high levels of miR-223 promote an M2-like, anti-inflammatory macrophage phenotype, characterised by elevated levels of TGFβ, Arg-1 and VEGF. This creates a tissue-healing niche and allows for remodelling and angiogenesis to occur, and may result in promoting the development of endometriosis. Adapted from Schjenken et al (2019).

Chapter 2

Materials and methods

2.1. MICE STRAINS

All mice used in this study were kept in same sex group housing and maintained under specific pathogen-free conditions in the Laboratory Animal Services facility at the University of Adelaide, South Australia. Mice were maintained on a twelve hour light / twelve hour dark cycle with sterile breeder chow (10% fat) food (Teklad Diets, Envigo, Madison, WI, USA) and water available *ad libitum*. Sterile filter cages (GM500 Tecniplast IVC Cages, Buguggiate, Italy) were cleaned and changed weekly, or immediately following operative procedures. All experimental mice were weighed and checked daily to monitor condition and healthy appearance. All animals were used according to the Australian Code of Practice for the Care and Use of Animals for Scientific Purposes (8th ed., 2013), with approval from the Animal Ethics Committee, The University of Adelaide (Ethics identifier: m-2015-040). Genetically Modified Organisms Dealing Authorisation was obtained from the Institutional Biosafety Committee, The University of Adelaide (Identifier number: 13354).

2.1.1. C57BL/6JArc mice

C57BL/6JArc (C57) mice were obtained from the Animal Resource Centre (Perth, WA, Australia). Prior to commencing experimental procedures, mice aged between six to eight weeks were given a minimum of one week to recover from transportation and to acclimatise to the facility.

2.1.2. *miR-155* null mutant mice

B6.Cg-*Mirn155*$^{tm1.1Rsky}$/J (*miR-155*$^{-/-}$) mice were bred in-house at the University of Adelaide as homozygous breeding pairs. Founder colony mice were initially obtained from The Jackson Laboratory (Bar Harbor, Maine, USA; Stock Number: 007745 | bic/miR-155). Briefly, using a modified bacterial artificial chromosome (BAC) targeting vector, a 0.97 kb portion of exon 2 of the *bic*/*miR-155* gene on Chromosome 16 was replaced with a β-galactosidase (*lacZ*) reporter gene with polyA sequence followed by a *loxP*-flanked neomycin resistance cassette. To establish mutant mice, this construct was electroporated into embryonic stem cells derived from C57:129 hybrid mice, and chimeras that developed were bred to C57 mice. To remove the *loxP*-flanked neomycin cassette, mice were bred with C57-congenic Cre-deleter strain mice and the resulting *bic/miR-155* mutant mice were subsequently backcrossed for at least five generations to C57 mice (The Jackson Laboratory).

2.1.3. *miR-223* null mutant mice

B6.Cg-*Ptprc*^{a}*Mir223*^{tmFcam}/J (*miR-223*$^{-/-}$) mice were bred in-house at the University of Adelaide as homozygous breeding pairs. Founder colony mice were initially obtained from The Jackson Laboratory (Bar Harbor, Maine, USA; Stock Number: 013198 | miR-223). Briefly, the entire coding region of the *miR-223* gene (110bp locus on Chromosome X) was replaced with a targeting vector containing frt-flanked neomycin resistance cassette. This construct was electroporated into (C57 x 129S4Sv/Jae) F1-derived V6.ES cells. Appropriately targeted ES cells, which resulted in a complete loss of *miR-223* function, were injected into C57 blastocysts. Resulting chimeric male mice were bred to C57 females to generate a colony of *miR-223*$^{-/-}$ mice, which were backcrossed for at least five generations to C57 mice (The Jackson Laboratory).

2.2. GENOTYPING

2.2.1. DNA extraction

Ear notch or tail snip samples were incubated at either 37°C overnight or 55°C for a minimum of four hours in digestion buffer (350µM Proteinase K (Sigma-Aldrich, St. Louis, USA), 20mM EDTA (Sigma-Aldrich), 50mM Tris (Sigma-Aldrich), 120mM NaCl (Chem-Supply, SA, Australia), and 1% [w/v] SDS (Sigma-Aldrich), pH 8.0). To remove undigested material and cellular debris, 250µL of ammonium acetate (4M, pH 7.5; Chem-Supply) was added to the mixture and placed on a shaker for fifteen minutes at room temperature, followed by ten minutes without shaking at room temperature. Samples were centrifuged at 14,000 x g for ten minutes and 400µL of the supernatant was collected. To precipitate the DNA, 800µL of 100% ethanol (Chem-Supply) was added to the supernatant and vortexed briefly. Samples were allowed to sit at room temperature for five minutes, prior to being centrifuged at 14,000 x g for eight minutes. The resulting DNA pellet was washed with 70% ethanol, resuspended in 20-50µL of milliQ water and stored at 4°C for up to two weeks, or at -20°C until required for analysis.

2.2.2. Genotyping PCR

Extracted DNA was amplified using polymerase chain reaction (PCR), following protocols and primers designed by The Jackson Laboratory (Maine, USA) (Table 2.1). All PCRs were run on the GeneAmp PCR System 9700 (Applied Biosystems, subsidiary of Thermo Fisher Scientific, Wilmington, DE, USA) and PCR products were stored at 4°C for up to two weeks prior to being analysed via gel electrophoresis.

Briefly, to detect *miR-155*, 2µl of digested DNA was added to a PCR reaction mixture containing 0.8 X DNA polymerase reaction buffer, 2mM $MgCl_2$, 0.3 U *Taq* polymerase (Thermo Fisher Scientific), 0.2µM dNTPs (Sigma-Aldrich), and 1µM of each primer (forward, reverse and mutant; GeneWorks Pty Ltd, Thebarton, SA, Australia) in a final volume of 12µL. The PCR was carried out with an initial denaturation step at 94°C for five minutes, followed by 35 amplification cycles at 94°C (thirty seconds), 61.8°C (one minute) and 72°C (one minute), and finishing with an elongation step at 72°C for two minutes.

To detect the presence of *miR-223*, 2µl of digested DNA was added to a PCR reaction mixture made out of 1.3 X KAPA 2G HS polymerase reaction buffer, 2.6mM $MgCl_2$, 0.3 U KAPA 2G HS *Taq* polymerase (Kapa Biosystems, subsidiary of Sigma-Aldrich), 0.26µM dNTPs (Sigma-Aldrich), 1µM of each primer (forward, reverse and mutant; GeneWorks Pty Ltd) and 6.5% glycerol (Sigma-Aldrich) in a final volume of 12µL. The PCR was carried out with an initial denaturation step at 94°C for two minutes, 10 amplification

cycles of 94°C (twenty seconds), 65°C (fifteen seconds; with a 1.5°C decrease in temperature per cycle) and 68°C (ten seconds), followed by a further 28 amplification cycles at 94°C (fifteen seconds), 50°C (fifteen seconds) and 72°C (ten seconds), concluding with an elongation step at 72°C for two minutes.

2.2.3. Gel electrophoresis

PCR samples were run on 2% (w/v) agarose gel (Promega, WI, USA) with 1 X GelRed™ nucleic acid gel stain (Biotium, CA, America) in 1 X TBE buffer (45mM Tris base (Sigma-Aldrich), 45mM Boric acid (Chem-Supply), 1mM EDTA (Sigma-Aldrich), pH 8.2) for fifty minutes at 80V alongside pUC19/HpaII molecular weight marker (GeneWorks Pty Ltd). Samples were pre-mixed with 1 X DNA Gel Loading Dye (Sigma-Aldrich) before being loaded onto the gel. After electrophoresis, gels were visualised under UV light using the GelDoc™ EZ Imager (BioRad Laboratories Inc., Hercules, CA, USA) and images were taken for analysis (Figure 2.1 and 2.2).

Table 2.1 PCR primers used to genotype *miR-155*$^{-/-}$ and *miR-223*$^{-/-}$ mice

miRNA	Primer sequence (5' → 3')	Description	Product size (bp)	Genbank number
miR-155	GTG CTG CAA ACC AGG AAG G	Wild type	465	NR_029801.1
	CTG GTT GAA TCA TTG AAG ATG G	Common		
	CGG CAA ACG ACT GTC CTG GCC G	Mutant	600	
miR-223	CAG TGT CAC GCT CCG TGT AT	Wild type	392	NR_029565.1
	TTC TGC TAT TCT GGC TGC AA	Common		
	CTTCCT CGT GCT TTC CGG TAT CG	Mutant	500	

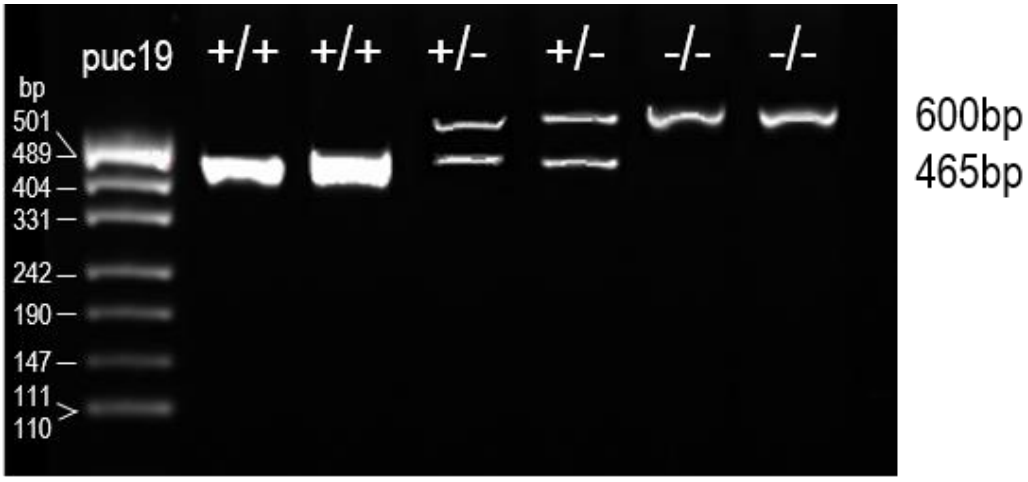

Figure 2.1 Gel electrophoresis image of *miR-155* genotyping

Genotype of *miR-155*$^{-/-}$ mice was confirmed by PCR where a single band at 465bp denoted wild type (*miR-155*$^{+/+}$), double bands at 465bp and 600bp denoted heterozygote mice (*miR-155*$^{+/-}$), and a single band at 600bp denoted null mutants (*miR-155*$^{-/-}$). The DNA ladder pUC19 DNA/Mspl (Hpall) Marker was used to determine band size.

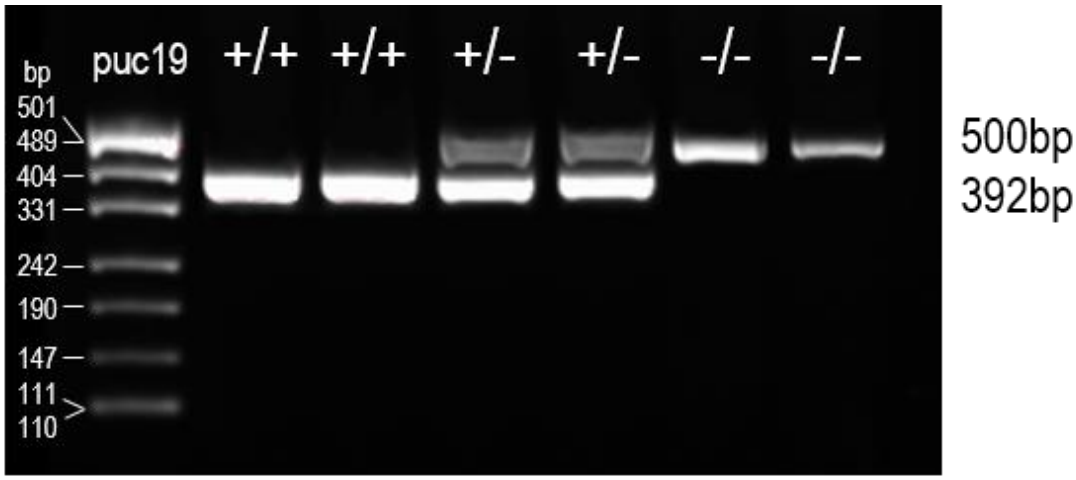

Figure 2.2 Gel electrophoresis image of *miR-223* genotyping

Genotype of *miR-223*$^{-/-}$ mice was confirmed by PCR where a single band at 392bp denoted wild type (*miR-223*$^{+/+}$), double bands at 392bp and 500bp denoted heterozygote mice (*miR-223*$^{+/-}$), and a single band at 500bp denoted null mutants (*miR-223*$^{-/-}$). The DNA ladder pUC19 DNA/Mspl (Hpall) Marker was used to determine band size.

2.3. MENSTRUAL MOUSE MODEL OF ENDOMETRIOSIS

To establish endometriosis in mice, a modified version of The Greaves Saunders Menstrual Mouse Model of Endometriosis (Greaves et al., 2014) was used (Figure 2.3).

2.3.1. Ovariectomy

Female mice aged between eight to ten weeks were ovariectomised under sterile conditions. Mice were anaesthetised under inhalation of 2.5% isoflourane (ISOTHESIA®, Henry Schein®, New York, USA) administered in conjunction with pure oxygen. Anaesthetised mice were placed in a ventral recumbent position and the dorsal mid-lumbar area was swabbed with 70% ethanol. A single surgical incision of 0.5 to 1cm was made on the dorsal midline at the caudal edge of the ribcage, and using blunt forceps, the skin at each end of the cut was separated from the underlying muscle wall. The left ovary, which was embedded in the fat pad, was visible underneath the muscle wall. A retoperitoneal incision of approximately 0.5cm was made on the muscle layer below the last rib, and both the ovary and associated fat pad were gently withdrawn from the peritoneal cavity. Using a surgical cauteriser (Bovie Medical, Clearwater, FL, USA), the entire ovary and oviduct were dissected from the uterine horn. The uterine horn was replaced into the peritoneal cavity, and the muscle wall was brought together. To remove the right ovary, a second incision was made on the opposite side, and the ovary was excised as described above. The skin incision was closed using 9mm stainless steel wound clips (BD Autoclip Wound Closing System, Thermo Fisher Scientific) and mice were injected subcutaneously with carprofen analgesia (Rimadyl; Pfizer, New York, USA) at 0.05mg/10g of body weight. Following anaesthesia, mice were placed into clean cages kept on a 37°C heat pad for a minimum of one hour to recover from surgery. A second dose of carprofen at 0.05mg/10g body weight was administered subcutaneously twenty four hours post-ovariectomy.

2.3.2. Collection of decidualised endometrial tissue from donor mice

Following ovariectomy (day 0), donor mice were given seven days to recover prior to commencing the experimental protocol as illustrated in Figure 2.3A. Briefly, donor mice were injected subcutaneously with 100ng of oestradiol-17β (Sigma-Aldrich) in sesame oil (Sigma-Aldrich) for three consecutive days (days 7 to 9). On day 13, a 140mm SILASTIC pellet (Dow Corning Corp, Midland, MI, USA) containing progesterone (Sigma-Aldrich) was inserted subcutaneously into donor mice (Figure 2.3B). This pellet was made manually in-house, and releases approximately 1mg progesterone per twenty four hours.

Subsequently, mice were injected with 5ng of oestradiol-17β in sesame oil for three consecutive days (days 13 to 15).

Decidualisation of the endometrium in one uterine horn was induced on day 15 using 50μL of sesame oil via the Non-Surgical Embryo Transfer (NSET; ParaTechs, Lexington, KU, USA) device. On day 19, donor mice were euthanised four hours following the withdrawal of progesterone (removal of the pellet). The uterine horns were dissected from the mouse, placed in a petri dish and opened longitudinally (Figure 2.3C). The endometrial tissue from the decidualised uterine horn was scraped away from the myometrial layer using a sterile scalpel and resuspended in sterile Phosphate Buffered Saline (PBS - Calcium and Magnesium Free, Thermo Fisher Scientific), in preparation to be transferred into recipient mice. In addition, approximately 10mg of decidualised tissue was either fixed and processed for histological analysis or snap-frozen in liquid nitrogen for RNA extraction.

2.3.3. Induction of endometriosis in recipient mice

Recipient mice were ovariectomised at the same time as age-matched donor mice. Commencing on day 15, recipient mice received twice weekly subcutaneous injections of 500ng oestradiol valerate (Sigma-Aldrich) in sesame oil for the duration for the experiment (Greaves et al., 2014). On day 19, approximately 40mg (±2mg) of decidualised donor endometrial tissue was finely diced, resuspended in 200μL 1 X PBS (Figure 2.3D) and passed once through a 19-gauge needle (Becton Dickinson, New Jersey, USA) to ensure smooth delivery into recipient mice. Anaesthetised recipient mice received a single subcutaneous injection of donor endometrial tissue on the right flank.

2.3.4. Harvesting lesions from recipient mice

Recipient mice were euthanised at one of three time-points (Figure 2.3E); 7 days (D7), 14 days (D14), or 21 days post-induction of endometriosis (D21). Photographs of the subcutaneous lesions were taken, and the lesion was carefully dissected from the site of attachment, weighed and measured to determine lesion width, length and height (used to calculate lesion volume). Lesions were either fixed and processed for histological analysis or snap-frozen in liquid nitrogen and subsequently stored at -80°C for RNA extraction.

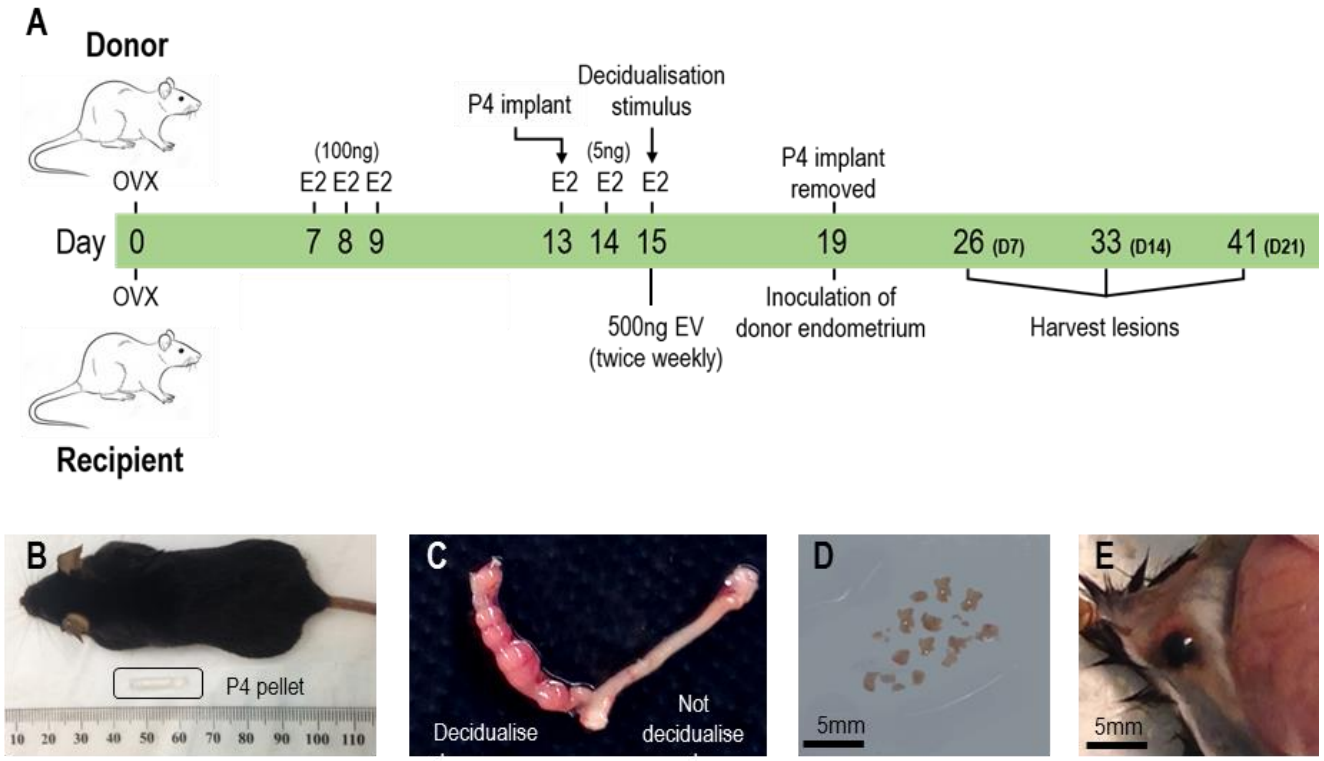

Figure 2.3 The Greaves-Saunders menstrual mouse model of endometriosis

A: Schematic outlining the timeline of procedures performed on donor and recipient mice. **B:** Subcutaneous insertion of a P4 SILASTIC pellet released approximately 1mg of P4 daily for six days. **C:** Four hours following P4 withdrawal, the donor uteri was harvested. The decidualised uterine horn was selected and opened longitudinally. **D:** Decidualised donor endometrial tissue (40mg ± 2mg) was finely diced using a scalpel and resuspended in 200µl PBS, and injected subcutaneously into recipient mice. **E:** Lesions were dissected from recipient mice on either 7, 14 or 21 days–post inoculation of donor endometrium.

2.4. HISTOLOGY

2.4.1. Tissue processing and slide preparation

Decidualised donor endometrial tissue and D7, D14 and D21 lesions were collected and fixed in 4% neutral buffered formalin (Australian Biostain, VIC, Australia) for twenty four hours at 4°C. The tissues were then washed twice in 1 X PBS at 4°C for twenty four hours each, and subsequently transferred into a 70% ethanol solution at 4°C for temporary storage until tissue processing. The Leica TP1020 Tissue Processor (Leica Microsystems, Wetzlar, Germany) was used to process and embed the tissues utilising the following dehydration and embedding protocol: thirty minutes each in 75% ethanol, 80% ethanol, 85% ethanol, 90% ethanol, 95% ethanol and 100% ethanol; 2 x thirty minutes in 100% Xylene (Ajax Finechem, NSW, Australia); 2 x thirty minutes in paraffin wax (Ajax Finechem) under vacuum conditions. The processed tissue was immediately moulded into paraffin blocks and stored at room temperature prior to being sectioned on a Leica Rotary Microtome (Leica Microsystems). Sections were cut at 5µm and transferred onto SuperFrost Plus Advanced Adhesive Microscope Slides (Trajan, VIC, Australia) using a water bath at 45°C. Slides were either dried overnight at 37°C, or allowed to air-dry at room-temperature for a minimum of forty eight hours prior to staining.

2.4.2. Dewaxing and rehydration of slides

Immediately prior to carrying out staining protocols, all slides underwent dewaxing in two washes of Safsolv (Labchem, VIC, Australia) for five minutes each. Slides were then rehydrated in descending concentrations of ethanol, commencing with 2 X 100% ethanol (five minutes each), followed by three minute washes each in 90%, 70% and 50% ethanol. Slides were then placed in milliQ water for a minimum of two minutes to ensure full rehydration of the tissue sections. Staining was then carried out as described in section 2.4.3 to 2.4.5.

2.4.3. Haematoxylin and eosin staining

Haematoxylin and eosin (H&E) staining was carried out as per standard protocols. Briefly, slides were stained in Harris haematoxylin (Sigma-Aldrich) for three minutes, followed by a five minute rinse in tap water. Sections were differentiated in a five second wash of 0.5% ammonia (Sigma-Aldrich) in milliQ water and were rinsed in tap water for two minutes. Sections were placed in 1% hydrochloric acid (Chem-Supply) in milliQ water for five seconds, rinsed in tap water for two minutes, and finally stained in eosin (Sigma-Aldrich) for one minute. Slides were then dehydrated and mounted as described in Section 2.4.6.

2.4.4. Masson's trichrome staining

Masson's trichrome staining was carried out in accordance with standard methodology. Briefly, slides were stained in Weigert's Haematoxylin (Sigma-Aldrich) for fifteen minutes, differentiated in 0.5% hydrochloric acid in 70% ethanol for twenty seconds, and stained in acid ponceau (Sigma-Aldrich) for thirty seconds. Slides were then placed in 1% phosphomolybdic acid aqueous solution (Sigma-Aldrich) for thirty seconds, counterstained in 1% methyl blue (Sigma-Aldrich) in 1% acetic acid (Ajax Finechem) for one minute, and finally washed twice for thirty seconds each in 1% acetic acid. Slides were then dehydrated and mounted as described in Section 2.4.6.

2.4.5. Immunohistochemistry

Immunohistochemistry was performed on dewaxed, rehydrated slides using the following primary antibodies: anti-α-smooth muscle actin (αSMA; Merck Millipore, Darmstadt, Germany), anti-F4/80 (eBioscience, subsidiary of Thermo Fisher Scientific), anti-MHC Class II (MHC II; Abcam, Cambridge, United Kingdom), anti-liver arginase (Arg-1; Abcam), anti-mouse mannose receptor (CD206; R&D Systems, Minneapolis, USA), anti-inducible nitric oxide synthase (iNOS; Merck Millipore), and anti-von Willebrand Factor (vWF; Merck Millipore); with isotype-matched rat, goat or rabbit IgGs used as negative controls. The following biotinylated secondary antibodies were used: rabbit anti-rat IgG (Abcam), goat anti-rabbit IgG (Vector Laboratories, Burlingame, CA, USA), and rabbit anti-goat IgG (Vector Laboratories).

Prior to staining, sections were incubated with 3% hydrogen peroxide (LabServ, Scoresby, VIC, Australia) in 50% methanol (Ajax Finechem) in milliQ water for fifteen minutes to inhibit endogenous peroxidase activity. Utilising serum from the secondary antibody host species (Sigma-Aldrich), sections underwent serum blocking (thirty minutes to an hour at room temperature using 10% host serum in PBS with 1% bovine serum albumin (Sigma-Aldrich)) to limit background and non-specific staining. Following incubation with the primary antibody (concentrations and durations listed in Table 2.2), slides were rinsed three times in PBS for five minutes each. The biotinylated secondary antibody (concentrations and durations listed in Table 2.3) was applied, followed by three PBS washes for five minutes each. Sections were incubated with streptavidin-conjugated horseradish peroxidase (HRP; Vectastain Elite ABC kit, Vector Laboratories) for thirty minutes at room temperature, and were washed three times in PBS for five minutes each. Detection of HRP activity was performed by applying 3,3'-Diaminobenzidine (DAB; Dako North America, Carpinteria, CA, USA) chromogen for five minutes at room temperature, following the

manufacturer's protocol. Finally, sections were counterstained with haematoxylin for a maximum of ten seconds. Slides were then dehydrated and mounted as described in Section 2.4.6.

2.4.6. Dehydration and mounting of slides

Upon completion of staining (section 2.4.3 to 2.4.5), slides were dehydrated for two minutes in 90% ethanol followed by two washes in 100% ethanol for a minute each. Sides were cleared in three washes of Safsolv (Labchem) for five minutes each. Coverslips were mounted onto slides using DPX mounting medium (BDH Industries, Poole, England), and allowed to dry at room temperature for a minimum of twenty four hours prior to image acquisition.

2.4.7. Image acquisition

Slides were imaged using the Nanozoomer-XR Digital slide scanner (Hamamatsu Photonics, Hamamatsu, Japan) at 40 X magnification. Viewing and analysis of captured images was carried out on the NDP.view2 Viewing software (Hamamatsu Photonics), with additional analyses performed using Image J (FIJI software, Wayne Rasband, US National Institutes of Health) as detailed in section 2.4.8 and 2.4.9. Immunohistochemistry staining controls (no primary antibody, no secondary antibody and isotype control) were also imaged (Appendix: Figure 7.1).

2.4.8. Morphometric analyses

A total of six non-serial H&E stained lesion sections per mouse were selected for morphometric analysis. Glandular areas within lesions were identified and measurements of the total area of the glands (encompassing the epithelium and lumen) was obtained (example shown in Figure 2.4). To determine the glandular fraction, the total area of the glands was divided by the total tissue area of the lesion. The average gland size per lesion was determined by dividing the sum total area of all glands with the number of glands present in that lesion. To determine the proportion of glandular epithelial cells within the lesion, the lumen size of individual glands was measured, and subtracted from the total gland area.

2.4.9. Histochemical analysis

To ensure uniformity with analysis, using the NDP.view2 Viewing software (Hamamatsu Photonics), a grid (individual squares measuring 0.25mm^2 (0.5mm x 0.5mm)) was placed over the lesion at a 2.5X

magnification. To analyse the histochemistry of the entire lesion, each square containing a portion of the lesion was the magnified to 20X and an image of the corresponding area was captured and transferred to ImageJ software (FIJI). For each histochemical stain, a minimum of three non-serial lesion sections per mouse were analysed.

To analyse Masson's trichrome staining, the 'Colour Deconvolution' feature set to the vector 'Masson Trichrome' in ImageJ (FIJI) was used. The images of stained lesions were split into two colour streams - blue for collagen fibres and red for cytoplasm (example shown in Figure 2.5). The intensity of each colour stream was adjusted for precision using the threshold option and was measured. To quantify the density of fibrosis, the intensity of blue staining was divided by the intensity of red staining.

To analyse the density of HRP-positive cells, the 'Colour Deconvolution' feature set to the vector 'H DAB' in ImageJ (FIJI) was used. This generated an image with Haematoxylin-only staining and an image with HRP-only staining (example shown in Figure 2.6). The intensity of each colour stream was adjusted for precision using the threshold option and was measured. To quantify the density of HRP-positive cells, the intensity of HRP-only staining was divided by the intensity of Haematoxylin-only staining.

Further quantification of $F4/80^+$ stained cells was carried out to evaluate differences in expression at the lesion periphery (100μM from the edge of the lesion) and at the centre of the lesion (within 500μM from the centre) using ImageJ (FIJI). Additional analysis of vWF staining was carried out, where the total number of vWF^+ blood vessels was counted and the average size of vessels was determined by dividing the total area of vessels per lesion with the number of vessels present. To determine the density of blood vessels, individual blood vessel were traced to obtain the area of vessels per field and this value was divided by the total stromal area in each field.

Table 2.2 List of primary antibodies used for immunohistochemistry

Antigen	Reactivity	Isotype	Concentration	Duration	Manufacturer
αSMA	Mouse / Human	Rabbit IgG	0.5 µg/ml	30 minutes	Merck Millipore
F4/80	Mouse	Rat IgG2a	1 µg/ml	Overnight	eBioscience
MHC II	Mouse	Rabbit IgG	25 µg/ml	30 minutes	Abcam
Arg-1	Mouse	Rabbit IgG	0.8 µg/ml	60 minutes	Abcam
CD206	Mouse	Goat IgG	5 µg/ml	Overnight	R&D Systems
iNOS	Mouse / Human	Rabbit IgG	2 µg/ml	60 minutes	Abcam
vWF	Mouse / Human	Rabbit IgG	1.5 µg/ml	60 minutes	Chemicon

Table 2.3 List of biotinylated secondary antibodies used for immunohistochemistry

Antigen isotype	Reactivity	Concentration	Duration	Manufacturer
Rabbit IgG	Rat IgG	4 µg/ml	40 minutes	Abcam
Goat IgG	Rabbit IgG	3 µg/ml	60 minutes	Vector Labs
Rabbit IgG	Goat IgG	3 µg/ml	60 minutes	Vector Labs

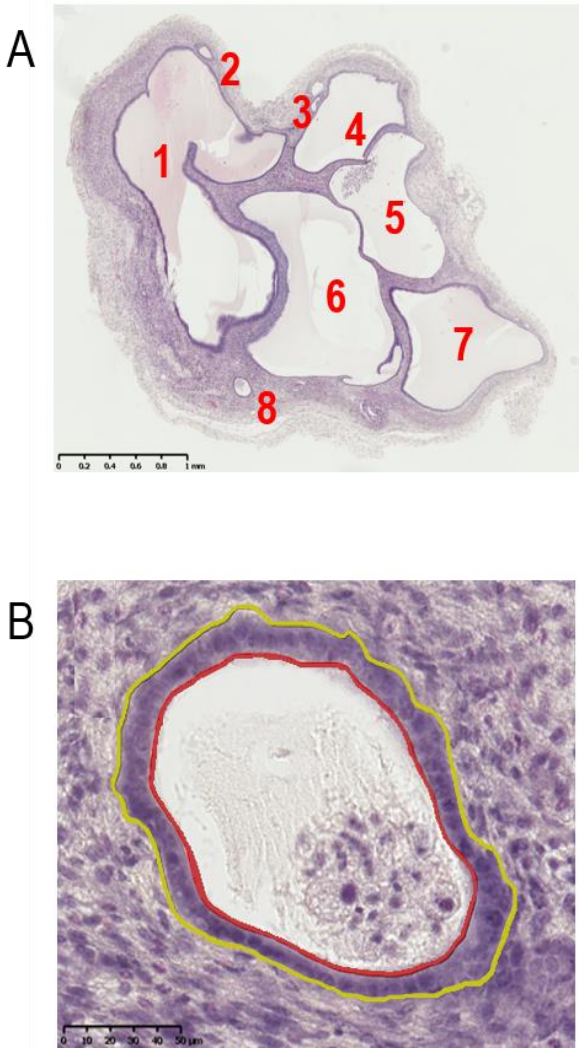

Figure 2.4 Example of morphometric analysis of glandular fractions within lesions

The total number of fully enclosed glands present within each lesion section was counted (**A**). The total area of individual glands (outlined in yellow), as well as the area encompassing the lumen (outlined in red) were measured (**B**). The proportion of epithelial cells within the lesion was determined by subtracting the area of the lumen from the total area of the gland. The average gland size per lesion was determined by dividing the sum total area of the glands with the total number of glands present in that lesion. The glandular fraction was calculated by dividing the total area of the glands with the total lesion area.

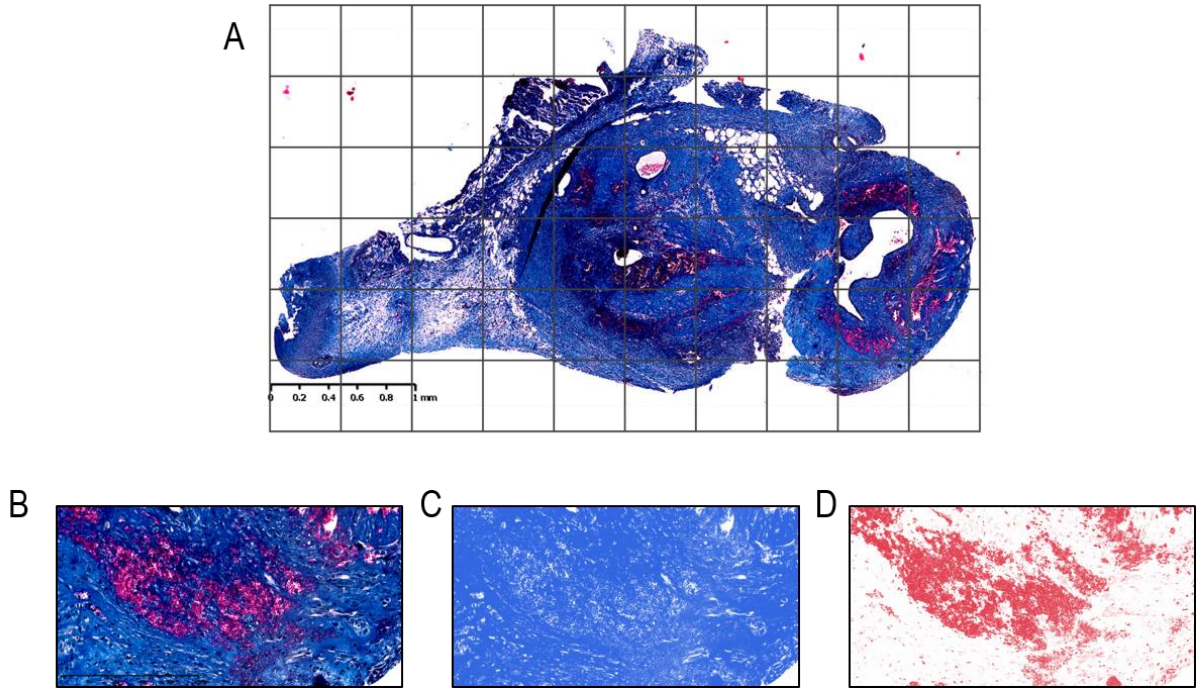

Figure 2.5 Example of Masson's Trichrome quantification

A grid was placed over Masson's Trichrome-stained lesion images (**A**) at 2.5X magnification in NDP.view 2 software (Hamamatsu Photonics). Each square was magnified to 20X (**B**) and images were analysed using ImageJ (FIJI), where images were split into blue for identification of collagen fibres (**C**) or red for identification of cytoplasmic areas (**D**); and the intensity of each component of the individual stains were quantified.

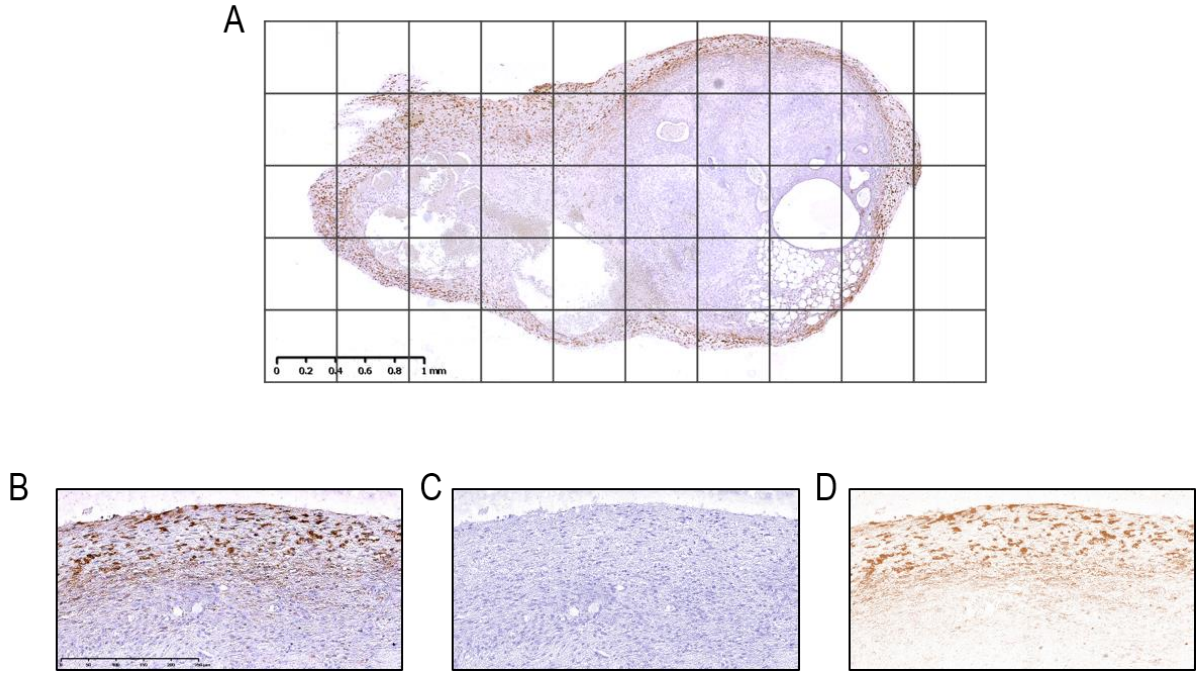

Figure 2.6 Example of quantification of HRP-stained sections

To quantify HRP-stained sections, a grid was placed over lesion images (**A**) at 2.5X magnification in NDP.view 2 software (Hamamatsu Photonics). Each square was magnified to 20X (**B**), and images were analysed using ImageJ (FIJI). Images were split into a haematoxylin-only image (**C**) and a HRP-only image (**D**), which was subsequently analysed to determine the density of HRP-staining.

2.5. RNA EXTRACTION AND PROCESSING

Total RNA from donor decidualised endometrial tissue, D7 and D14 lesions (4 biological replicates each from C57, *miR-155*$^{-/-}$ and *miR-223*$^{-/-}$ mice, totalling 36 samples) was extracted from snap-frozen lesions stored at -80°C. Each sample was homogenised in 700µl of QIAzol Lysis Reagent (Qiagen, Hilden, Germany) using the PowerLyzer 24 Homogenizer (Mo Bio Laboratories, subsidiary of Qiagen) at 3,500 rpm for ten seconds. Following homogenisation, samples were incubated at room temperature for five minutes and total RNA was extracted using the miRNeasy® RNA extraction and purification kit (Qiagen) following the manufacturer's protocol. Briefly, 140µl of chloroform was added to the sample and mixed thoroughly. Samples were incubated at room temperature for three minutes and then centrifuged at 12,000 x g for fifteen minutes at 4°C. The upper aqueous phase was transferred into a fresh Eppendorf tube and 100% ethanol (one and a half times the transferred volume of the aqueous phase) was added and mixed thoroughly. The samples were spun in a miRNeasy® Mini column at 8,000 x g for fifteen seconds at room temperature, with the flow through discarded. The RNA attached to the columns was then washed by centrifugation at 8,000 x g at room temperature with 700µl Buffer RWT for fifteen seconds followed by 500µl Buffer RPE for fifteen seconds and finally with 500µl of Buffer RPE for two minutes, with all flow through discarded. RNA was eluted by adding 50µl RNase-free water into the column and centrifuging at 8,000 x g for one minute at room temperature.

The concentration of extracted RNA was measured using the Nano-drop Spectrophotometer ND-1000 (Thermo Fisher Scientific). Contaminating DNA was removed from the sample using commercially available DNase treatment TURBO DNA-free (Life Technologies, CA, USA) following the manufacturer's instructions. In brief, 5µg of RNA was incubated with 1X TURBO DNase Buffer and 2 units of TURBO DNase, and incubated for thirty minutes at 37°C. DNase activity was stopped by the addition of 0.1 volume of DNase Inactivation Reagent at room temperature for five minutes with regular flicking of the sample. Samples were again centrifuged at 10,000 x g for one and a half minutes, and the DNA-free RNA supernatant was collected.

The final concentration of DNase-treated RNA was determined on the Nano-drop Spectrophotometer and, RNA integrity and purity was assessed on the RNA Agilent Bioanalyser (Agilent Technologies, Santa Clara, CA, USA). All RNA preparations had an RNA integrity number of seven or more, and were stored at -80°C until required.

2.5.1. RNA sequencing

To assess the mRNA profile in donor endometrium and endometriosis-like lesions, 36 DNase-treated RNA samples were subjected to high-throughput RNA Sequencing (RNA-Seq) at the David Gunn Genomics Facility (South Australian Health and Medical Research Institute, SA, Australia).

2.5.1.1. Library preparation

Libraries for a total of 36 samples were made from 1ug total RNA, quantified by Qubit RNA Assay in a Qubit 2.0 Fluorometer (Life Technologies). Following the manufacturer's protocol, the mRNA sequencing library was prepared using Illumina's TruSeq RNA Sample Preparation Kit (Illumina, San Diego, CA, USA). The constructed library was assessed for quality using the Agilent Bioanalyser 2100 (Agilent Technologies). Sequencing of the library preparations was performed on the Illumina Next-Seq 500 platform (Illumina) to obtain 2 x 100 base pair (bp) paired-end reads for mRNA expression at a depth of 50 million reads per sample.

2.5.1.2. *De novo* assembly, alignment and quantification

Initial data analysis was performed by Dr Jimmy Breen from the Bioinformatics Facility at the Robinson Research Institute (Adelaide, SA, Australia). Briefly, the *DESeq2* package in the R Statistical Software Suite (R Foundation for Statistical Computing, Vienna, Austria) was used to estimate sample quality and the expression level of transcripts, and to perform normalisation, variance estimation and differential expression of the raw reads. Briefly, paired-end sequence reads from all 36 libraries were pooled together according to genotype (12 samples each from C57, *miR-155*$^{-/-}$ and *miR-223*$^{-/-}$ mice) to generate a *de novo* transcriptome assembly. The raw FASTQ sequences generated from the Illumina Next-Seq 500 were processed for quality control using *FastQC* and to remove Illumina adapters and primers, redundant reads, poly-N and low quality reads using *AdapterRemoval* Version 2 (Schubert et al., 2016).

Using the RNA mapping program *HISAT2* (Kim et al., 2015), the trimmed RNA-Seq reads were aligned to the mouse reference genome (Genome Reference Consortium GRCm38; Release Name: mm10, The University of California, USA). Genome alignments were processed and sorted to removal optical duplicates using the *sambamba* and *Picard MarkDuplicates* method. To quantify the number of reads that overlap gene regions, *FeatureCounts* function was utilised (Liao et al., 2014), and pseudo-alignment RNA-Seq quantification, where raw data was used to define isoform expression, was performed using *Salmon*.

2.5.2. Differential expression analyses

The R/Bioconductor packages *limma-voom* and *EdgeR* were used to compute counts per million (CPM; defined as "read counts scaled by the number of sequenced fragments times one million" (Sha et al., 2015)), and to carry out analysis of differential expression of genes (Smyth, 2005, Robinson et al., 2010, McCarthy et al., 2012, Ritchie et al., 2015, Law et al., 2016). The deduplicated data was filtered to remove low expressed genes (i.e. only include genes where the CPM was greater than 1 in more than 12 of the 36 samples). Normalisation of the filtered data was carried out using the weighted trimmed mean of M-values to rescale read counts in different samples to comparable levels (Appendix Figure 7.3). The final assembly was used as a reference for the further gene annotation and expression analysis.

Differential isoform expression analyses were carried out using the packages *Sleuth* and *Wasabi*. Raw *p*-values (*p*) were adjusted using the Benjamini-Hochberg false discovery rate method to yield an adjusted *p* (Benjamini and Hochberg, 1995). The criteria for significance of differentially regulated genes was established as having an adjusted *p* value ≤ 0.05 with a ≥ 2-fold change in expression. Differential expression of genes was assessed between the following 15 groups:

1. C57 decidualised endometrium and C57 D7 lesions
2. C57 decidualised endometrium and C57 D14 lesions
3. C57 D7 lesions and C57 D14 lesions
4. *miR-155*$^{-/-}$ decidualised endometrium and *miR-155*$^{-/-}$ D7 lesions
5. *miR-155*$^{-/-}$ decidualised endometrium and *miR-155*$^{-/-}$ D14 lesions
6. *miR-155*$^{-/-}$ D7 lesions and *miR-155*$^{-/-}$ D14 lesions
7. *miR-223*$^{-/-}$ decidualised endometrium and *miR-223*$^{-/-}$ D7 lesions
8. *miR-223*$^{-/-}$ decidualised endometrium and *miR-223*$^{-/-}$ D14 lesions
9. *miR-223*$^{-/-}$ D7 lesions and *miR-223*$^{-/-}$ D14 lesions
10. C57 decidualised endometrium and *miR-155*$^{-/-}$ decidualised endometrium
11. C57 decidualised endometrium and *miR-223*$^{-/-}$ decidualised endometrium
12. C57 D7 lesions and *miR-155*$^{-/-}$ D7 lesions
13. C57 D7 lesions and *miR-223*$^{-/-}$ D7 lesions
14. C57 D14 lesions and *miR-155*$^{-/-}$ D14 lesions

15. C57 D14 lesions and *miR-223*$^{-/-}$ D14 lesions

The Ingenuity Pathway Analysis software (IPA 2018; QIAGEN Inc.) and the Database for Annotation, Visualization and Integrated Discovery (DAVID 6.8; http://david.ncifcrf.gov) were used to identify enriched cellular and molecular functions amongst differentially expressed gene transcripts, and to further classify these genes into functionally related groups.

2.6. STATISTICAL ANALYSIS

All statistical analyses (excluding RNA-Seq - Refer to Section 2.5.2) were conducted using GraphPad Prism version 8 for Windows (GraphPad Software, La Jolla CA, USA). Data obtained from histological analyses were averaged per section analysed, and further averaged to provide a single result for each lesion at each time-point. Following the D'Agostino & Pearson normality test, the distribution of data were found to be non-parametric. To determine statistical significance, data were analysed using either a non-parametric Mann-Whitney U test when comparing between two groups, or a Kruskal-Wallis test followed by Dunn's multiple comparisons test when comparing between three or more groups. To limit bias arising from the development of multiple subcutaneous lesions (≥ 2) in a recipient mouse, only data from mice which had a single endometriotic-like lesion has been included. Data are presented as median (interquartile range). Significance was inferred at $p \leq 0.05$, and is annotated as follows: * (p <0.05), ** (p < 0.01), *** (p < 0.001), and **** (p < 0.0001). Any additional annotations used for specific comparisons are outlined in figure captions.

A summary of the experimental approach taken in this thesis is shown in Figure 2.7.

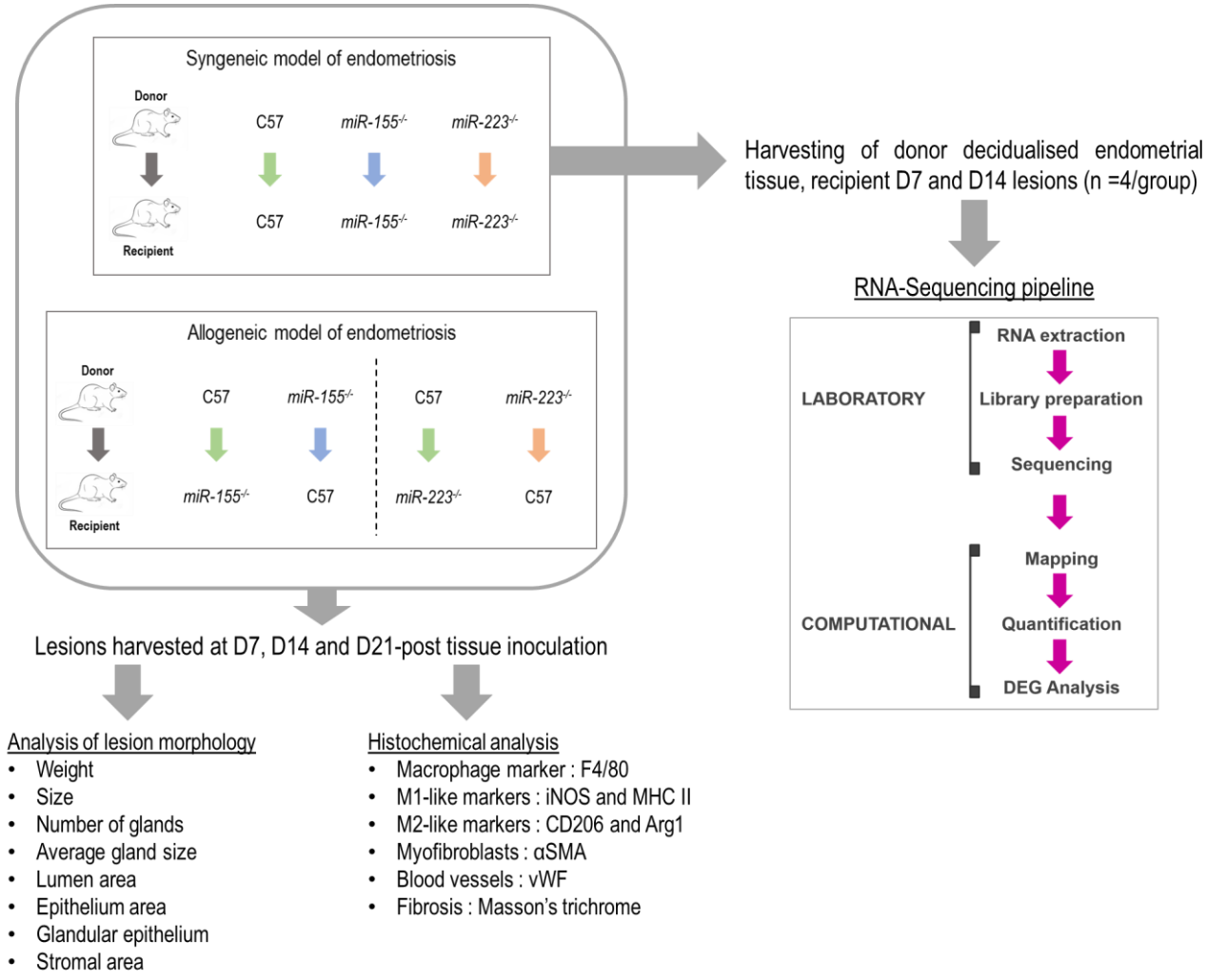

Figure 2.7 Experimental plan schematic

Morphological and histochemical analyses of D7, D14 and D21 subcutaneous lesions harvested from syngeneic and allogeneic mouse model of endometriosis were performed. RNA–Sequencing and analysis of differentially expressed genes (DEGs) was carried out on samples of donor endometrium, D7 and D14 lesions from the syngeneic model of endometriosis.

Chapter 3

Characterisation of endometriotic lesion development in a wildtype menstrual mouse model of endometriosis

3.1. INTRODUCTION

Endometriosis is a complex, multifactorial reproductive disorder specific to humans and some menstruating primates (Giudice and Kao, 2004, Kyama et al., 2007). At the time of visual confirmation for the presence of endometriosis via laparoscopy, evaluation of disease severity is possible and can be classified into several stages (Al-Talib and Tulandi, 2012, Dunselman and Beets-Tan, 2012, Dunselman et al., 2014). Although endometriosis affects approximately 10% of reproductive aged women, the events surrounding disease initiation remains uncertain (Giudice, 2010, Parazzini et al., 2012, Dunselman et al., 2014, Zondervan et al., 2018).

Initial steps in endometriotic lesion development include an ability of ectopic endometrial tissue to evade the immune response, thereby allowing for adherence to surfaces in the peritoneal cavity. Subsequently, invasion of the mesothelial lining allows for further proliferation of ectopic endometrial tissue and this process, coupled with neovascularisation, is essential for endometriotic lesion survival (Hull et al., 2003). Impaired immune surveillance and aberrant cytokine expression contributes to the ability for ectopic endometrial cells to proliferate and thrive (Aznaurova et al., 2014, Benagiano et al., 2014, Bouquet De Jolinière et al., 2014). Higher concentrations of immune cells have been observed in the peritoneal fluid from women with endometriosis compared to women without endometriosis, and as macrophages comprise a majority of peritoneal immune cells, it has been postulated that macrophages are critical players in the pathogenesis of endometriosis (van Furth et al., 1979, Haney et al., 1981, Kyama et al., 2003, Koninckx et al., 2012). Moreover, macrophages secrete high concentrations of prostaglandins F2α and E2 which maintain local oestrogen production and help sustain endometriotic lesion survival (Ferrero et al., 2014).

Macrophages are mononuclear phagocytic cells derived from haematopoietic bone marrow stem cells, and function as immune effector cells (Italiani and Boraschi, 2014, Corliss et al., 2016, Gordon and Plüddemann, 2017). The phenotypic, functional, and metabolic plasticity of macrophages is dictated by their polarisation status (Gordon and Taylor, 2005, Barros et al., 2013, Martinez and Gordon, 2014, dos Anjos Cassado, 2017b). In response to immunological challenges, pathogens, antigenic stimuli, and exposure to cytokines, undifferentiated macrophages can be preferentially activated via distinct polarisation pathways, giving rise to two broad categories; classically activated (M1-like) macrophage phenotype and the alternatively activated (M2-like) macrophage phenotype (Ma et al., 2003, Martinez et al., 2008, Mosser and Edwards, 2008, Italiani and Boraschi, 2014, Jantsch et al., 2014). These two types of macrophages work in a biphasic manner, with the initial arrival of M1-like macrophages mediating a pro-inflammatory response at the site of tissue injury or challenge. The subsequent arrival of M2-like

macrophages elicits an anti-inflammatory response which modulates the extent of inflammation and initiates tissue healing. This critical balance between pro-inflammatory M1-like and anti-inflammatory M2-like macrophage activity appears to be a significant determinant in the establishment and persistence of endometriosis (Bacci et al., 2009, Capobianco and Rovere-Querini, 2013). Therefore, in order to assess mechanisms surrounding the establishment of endometriosis, the use of *in vivo* animal models is essential (Grümmer, 2006, Kyama et al., 2007, D'Hooghe et al., 2009, Greaves et al., 2017).

Rodent models of are excellent candidates for longitudinal studies of disease development including neurodegeneration (Corvino et al., 2011, Harvey et al., 2011), metabolic disorders (Davidson et al., 2014, Derrick-Roberts et al., 2016), orthopaedics (Haffner-Luntzer et al., 2016, Mele et al., 2016), and cancer (Hald et al., 2009, Taylor et al., 2009). However, in the context of endometriosis, few studies have looked at the changes in lesion development over time *in vivo*. Grummer et al. (2001) looked closely at events surrounding initial lesion establishment in a xenograft mouse model of endometriosis. In this model, adhesion of human endometrial fragments and ensuing angiogenesis was observed from 2 days post-inoculation of endometrial tissue (Grümmer et al., 2001). Recently, a study using a homologous mouse model of endometriosis was able to assess the impact of an anti-platelet treatment on the development of lesions at weekly intervals over the course of 6 weeks (Zhang et al., 2017c). This research highlighted the gradual yet progressive development of endometriotic lesions, and suggested that varying the initiation time for a therapeutic intervention may yield entirely different results in resolving the progression of endometriosis (Zhang et al., 2017c). As endometriosis is characterised as an oestrogen-dependent chronic inflammatory disorder, wherein the immune system appears to be a central mediator in disease establishment and progression, studies in homologous mouse models allow for the cascade of inflammatory events associated with endometriosis to be evaluated (Bergqvist et al., 1993, Bacci et al., 2009, Kralickova et al., 2018).

Studies in homologous mouse models of endometriosis have shown a rapid infiltration of macrophages into endometriotic-like lesions within the first few days following disease induction (Lin et al., 2006). A shift in macrophage polarisation status from a predominantly M1-like phenotype to a M2-like phenotype has been shown to occur approximately ten days following disease establishment in mice (Johan et al., 2019). In addition, reciprocal transfers between mice with GFP-labelled macrophages and wildtype mice emphasise the importance of these immune cells in endometriosis, in which both donor and recipient macrophages were positively implicated in the inflammatory microenvironment of endometriotic lesion development (Greaves et al., 2014). Macrophages have also been implicated as mediators of vascular development, as they are potent sources of vascular endothelial growth factor (Capobianco and Rovere-

Querini, 2013). Moreover, neovascularisation is a marker of successful lesion survival, as the development of blood vessels is critical to support lesion growth (Hull et al., 2003). In mice, the depletion of macrophages resulted in disruption of the vascularisation and growth of endometriosis-like lesions over time (Bacci et al., 2009).

In summary, an important factor driving our understanding of endometriotic lesion establishment is the development and characterisation of animal models to mimic disease progression over time. In addition, the series of sequential events surrounding the initiation of endometriosis, beginning with an impaired clearance of ectopic endometrial fragments, followed by the commencement of tissue remodelling, and finally culminating in establishment of a well vascularised lesion, needs to be evaluated at each stage, ideally as a time-course study in an appropriate animal model. Therefore, the experiments in this chapter were devised to characterise the development of subcutaneous endometriotic-like lesions in a syngeneic menstrual mouse model of endometriosis (Refer to Figure 2.3 for protocol; rationale and validation of model discussed in Section 6.2). Donor decidualised endometrial tissue from wildtype C57 mice was injected subcutaneously into syngeneic C57 recipient mice, and resulting endometriosis-like lesions were harvested at either Day 7 (D7), Day 14 (D14) or Day 21 (D21) following disease induction. Lesions were across each of the three time-points for morphometric parameters representative of human endometriosis lesions, including the development of distinctive glandular and stromal areas. In addition, assessment of macrophage localisation via immunohistochemical staining of F4/80 (the F4/80 antibody recognises the EGF-TM7 G protein coupled receptor) was performed, with further identification of M1-like activity (MHC II and iNOS) and M2-like activity (CD206 and Arg-1). Evaluation of additional parameters of lesion establishment (i.e. blood vessel density, myofibroblast abundance and the extent of fibrosis) was performed using vWF and αSMA immunostaining, and Masson's trichrome staining. Finally, RNA-Sequencing (RNA-Seq) was performed on donor decidualised endometrium, D7 and D14 lesions to assess the differential expression of genes between time points, with particular emphasis on macrophage associated and immune related pathways.

3.2. RESULTS

3.2.1. Endometriosis-like lesion development in C57 mice

Previous studies evaluating endometriosis-like lesion development in immunocompetent mice often focus on a single time-point at which to assess disease outcomes. However, lesion development in endometriosis is known to be a dynamic process, characterised by remodelling and gland formation within ectopic endometrial tissue as disease progresses (Hull et al., 2008). Although the 'menstrual' mouse model of endometriosis was first established in 2014 (Greaves et al., 2014), the sequential changes associated with attachment, growth and subsequent maintenance of endometriosis-like lesions have not been described. Therefore, to evaluate the development of endometriosis-like lesions in wildtype, C57 mice, 40mg of decidualised endometrium from ovariectomised C57 donor mice was injected subcutaneously into ovariectomised, oestrogen-supplemented C57 recipient mice. The size and weight of lesions were measured at D7, D14 and D21, and a histological analysis of lesions was carried out at each time-point.

A total of 40 donor mice were required to generate sufficient decidualised endometrial tissue for injection into recipient mice at a ratio of 2 donors to 1.9 recipients (Table 3.1). Overall, 95% of C57 recipient mice had identifiable endometriotic-like lesions over the course of this experiment. At D7 and D14, 100% of recipient mice had lesions. At D21 however, the proportion of recipient mice that had lesions reduced slightly to 82%. A total of 4 mice had more than one lesion and have been excluded from subsequent analyses.

Analysis of the lesions showed differing characteristics across the time course. At D7, lesions were opaque, raised from the skin, and were heme-laden/blood-filled (Figure 3.1 A), whereas by D14, lesions were slightly spread out over the attachment site, and appeared less heme-laden (Figure 3.1 B). By D21, lesions were remained spread out, with the appearance of vascularisation to surrounding areas (Figure 3.1 C). Lesions that developed in C57 mice were 6-fold larger at D7 compared to D14 (15.0 (5.0 – 23.0) mm^3 *versus* 2.5 (2.0 – 4.0) mm^3 respectively, $p = 0.0058$; data presented as median (IQR)). Interestingly, lesion size increased by 2.8-fold from D14 to D21 (7.0 (4.3 – 8.0) mm^3). Overall, lesions were 53% smaller at the end of the time course experiment when compared with D7 values (Figure 3.1 D). Median lesion weight at D7 was reduced by 68% at D14 (15.45 (7.23 – 25.60) mg *versus* 5.00 (3.35 – 12.40) mg respectively). A further reduction in lesion weight was noted at D21 (2.70 (1.55 – 4.08) mg) with lesions being 83% lighter than D7 lesions ($p = 0.0022$) (Figure 3.1 E).

H&E stained lesion sections were analysed for morphological parameters associated with lesion establishment (Figures 3.2 A-C). At D7, lesions were dense (Figure 3.2 A), whereas at both D14 (Figure 3.2 B) and D21 (Figure 3.2 C), lesions appeared less compact, with visible gland formation. The median number of glands per lesion at D7 (0.5 (0 – 1.75) increased significantly at both D14 (5 (2.25 – 11.5), p = 0.0177) and D21 (6.5 (6 – 8.5), p = 0.0006) (Figure 3.2 D). Average gland size, lumen area within glands, and epithelium area of glands was consistent across time points (Figure 3.2 E-G). The median percentage glandular epithelium of lesions increased at D14 (3.87 (0.23 – 23.70) %, p = 0.0315) and D21 (2.93 (1.75 – 5.22) %, p = 0.0358) in comparison to D7 (0.08 (0.00 – 2.05) %) (Figure 3.2 H). However, no change in percentage stromal area was observed over time (Figure 3.2 I). Collectively, this data indicates that the C57 subcutaneous menstrual mouse model of endometriosis is able to mimic disease development, and is an appropriate model to evaluate the progression of lesion establishment over time.

Table 3.1 Endometriosis-like lesion recovery in C57 mice

Lesion collection time point	D7	D14	D21
Total number of donor mice used across all time points: 40			
Number of recipient mice	14	13	11
Number of mice with lesions*	14	13	9
Proportion of mice with lesions (%)	100	100	81.8

* To reduce bias, mice with ≥2 lesions were excluded from subsequent analyses. At D7 - 2 mice excluded; At D14 - 1 mouse excluded; At D21 – 1 mouse excluded.

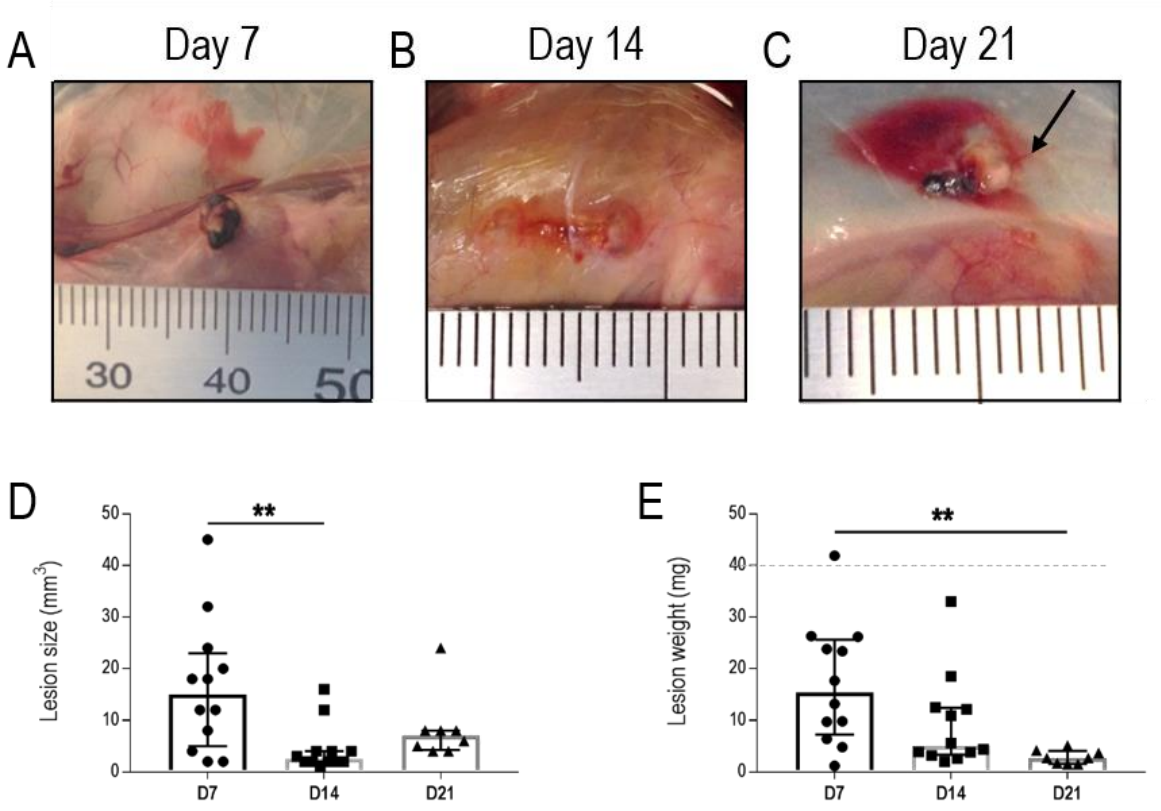

Figure 3.1 Gross morphology of endometriosis-like lesion development in C57 mice

Decidualised C57 donor endometrial tissue was injected subcutaneously into syngeneic recipient mice. Resulting lesions were harvested at either D7 (**A**), D14 (**B**) or D21 (**C**), with representative images shown; arrow indicates evidence of vascularisation. Lesion size was measured (**D**) and lesions were excised and weighed (**E**), with the dotted line indicating the initial weight of donor decidualised endometrial tissue inoculated into recipient mice. Data are presented as median (IQR), with each symbol representative of a single lesion in one mouse (n=12 at D7, n=12 at D14, n=8 at D21). Analysis was done using the Kruskal-Wallis test followed by Dunn's multiple comparison test, with significance denoted as ** ($p < 0.01$).

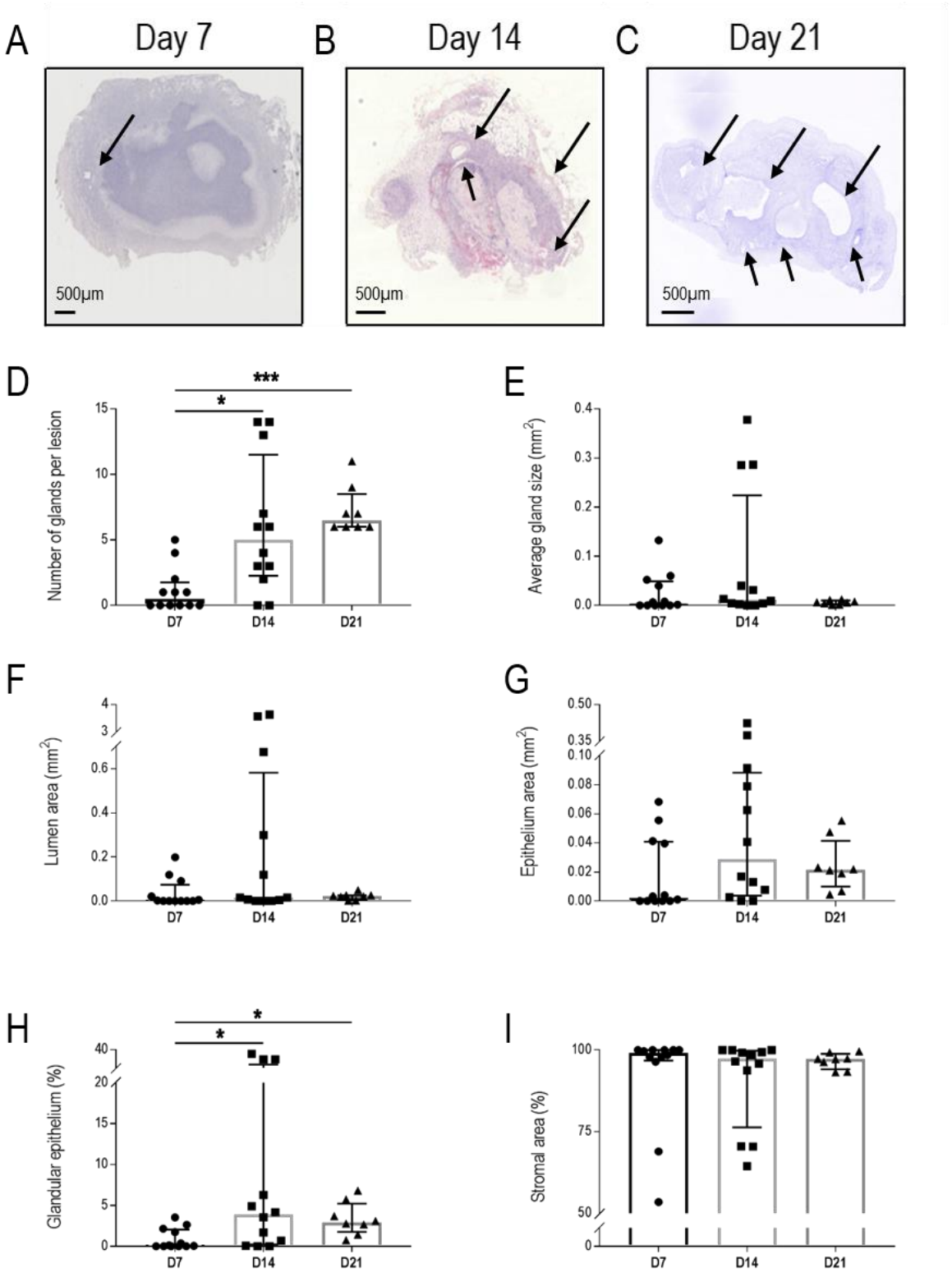

Figure 3.2 **Assessment of morphological parameters in haematoxylin and eosin stained endometriosis-like lesions from C57 mice**

Haematoxylin and eosin stained sections from D7 **(A)**, D14 **(B)**, and D21 **(C)** lesions in C57 mice (representative images shown; arrows indicate glands) were assessed for the following characteristics: number of glands per lesion, **(D)**, average gland size **(E)**, lumen area **(F)**, epithelium area **(G)**, percentage glandular epithelium **(H)** and percentage stromal area **(I)**. Data are presented as median (IQR), with each symbol representative of a single lesion in one mouse (n=12 at D7, n=12 at D14, n=8 at D21). Analysis was done using the Kruskal-Wallis test followed by Dunn's multiple comparison test, with significance denoted as * ($p < 0.05$) and *** ($p < 0.001$).

3.2.2. Macrophage localisation in endometriosis-like lesions from C57 mice

The observed plasticity in macrophage polarisation during the development of endometriosis has been described in mouse models of this disease (Bacci et al., 2009, Johan et al., 2019). A predominant M1-like macrophage phenotype is associated with increased ectopic tissue clearance, and conversely, a predominant M2-like macrophage phenotype is associated with elevated tissue remodelling and lesion persistence (Bacci et al., 2009). To evaluate the contribution of M1-like and M2-like macrophages in lesion development, immunohistochemical analyses were performed. As a previous study noted discrepancies in F4/80$^+$ macrophage distribution throughout lesions at different time points (Johan et al., 2019), quantification of total macrophage density, peripheral density (100µM from the edge of the lesion) and central density (within 500µM from the centre of the lesion) was also performed.

Detection of macrophage phenotype in C57 lesions was performed via quantification of F4/80$^+$ staining (Figure 3.3). Total macrophage density in lesions was unaltered between D7 (11.07 (6.64 – 18.55) %), D14 (17.09 (13.00 – 29.24) %), and D21 (17.84 (15.45 – 22.49) %) (Figure 3.3 G). Evaluation of macrophage density at the lesion periphery (Figure 3.3 A-C) and lesion centre (Figure 3.3 D-F) was also performed. Median peripheral F4/80 density was 39.79 (22.65 – 41.39) % at D7, 40.51 (29.35 – 54.70) % at D14, and decreased to 23.19 (15.29 – 27.76) % at D21 (p = 0.0426 for D14 *vs* D21) (Figure 3.3 H). Interestingly, F4/80 density at the lesion centre significantly increased from D7 (4.01 (2.50 – 6.38) %) to D14 (34.96 (23.72 – 47.83) %, $p < 0.0001$). This increase in central F4/80$^+$ density was sustained at D21 (31.85 (26.47 – 32.48) %, p = 0.0017 for D7 *vs* D21) (Figure 3.3 I).

3.2.2.1. Expression of pro-inflammatory M1-like markers in C57 mice

Quantification of iNOS density in C57 lesions (Figure 3.4 A-C) was unchanged across time points (23.50 (18.96 – 35.99) %, 20.23 (15.31 – 25.27) %, and 16.99 (12.70 – 20.99) % at D7, D14 and D21 respectively) (Figure 3.4 G). Peripheral iNOS density decreased significantly between D7 and D14 (18.83 (17.26 – 22.01) % and 11.10 (6.99 – 15.20) % respectively, $p < 0.0001$), with a subsequent increase at D21 (17.69 (16.44 – 18.21) %, p = 0.0372 for D14 *vs* D21) (Figure 3.4 H). Central iNOS density was consistent at D7 (7.27 (6.30 – 8.74) %) and D14 (6.90 (5.75 – 8.40) %), with a significant increase seen at D21 (10.46 (7.85 – 11.82) %, p = 0.0205 for D7 *vs* D21 and p = 0.0067 for D14 *vs* D21) (Figure 3.4 I).

A trend towards decreased MHC II density was observed between D7 (19.66 (12.49 – 23.27) %) and D14 (12.37 (5.28 – 15.92) %), while a significant increase in MHC II density was seen between D14 and D21

(22.91 (15.94 – 31.90) %, p = 0.0105) (Figure 3.4 D-F, J). Peripheral MHC II density was unchanged at D7 (11.99 (9.55 – 16.37) %) and D14 (10.12 (8.58 – 11.46) %), with a significant increase seen at D21 (21.99 (18.45 – 25.94) %, p = 0.0139 for D7 *vs* D21 and p < 0.0001 for D14 *vs* D21) (Figure 3.4 K). Likewise, central MCH II density was consistent between D7 (8.70 (6.53 – 10.49) %) and D14 (7.36 (6.27 – 8.33) %), with an increase observed at D21 (11.06 (8.62 – 13.35) %, p = 0.0129) (Figure 3.4 L).

3.2.2.2. Expression of alternatively activated M2-like markers in C57 mice

CD206 immunostaining (Figure 3.5 A-C) was quantified across all time points (Figure 3.5 G). Interestingly, a steady increase in the total density of $CD206^+$ cells was noted between D7 (7.43 (6.42 – 11.04) %), D14 (18.75 (11.06 – 33.38) %, p = 0.0531), and was highest at D21 (39.70 (36.21 – 58.72) %, p < 0.0001 for D7 *vs* D14). Peripheral CD206 density increased significantly between D7 (2.54 (1.67 – 3.15) %), D14 (5.99 (4.45 – 6.34) % p = 0.0106 for D7 *vs* D14) and D21 (15.79 (14.24 – 16.52) %, p < 0.0001 for D7 *vs* D21 and p = 0.0449 for D14 *vs* D21) (Figure 3.5 H). Central CD206 density was lowest at D7 (6.68 (4.89 – 8.37) %) and increased significantly at D14 (22.01 (17.35 – 28.32) %, p = 0.0048) and D21 (46.24 (42.24 – 53.20) %, p < 0.0001 for D7 *vs* D21) (Figure 3.5 I).

Detection of total Arg-1 activity in C57 lesions (Figure 3.5 D-F) was not significantly different between D7, D14 or D21 (21.73 (17.17 – 24.62) %, 24.29 (21.08 – 28.34) %, and 24.49 (22.20 – 31.59) % respectively) (Figure 3.5 J). Peripheral Arg-1 density increased significantly between D7 (4.50 (3.89 – 6.35) %), D14 (14.13 (11.46 – 15.69) % p = 0.0005 for D7 *vs* D14) and D21 (15.89 (13.75 – 20.37) %, p < 0.0001 for D7 *vs* D21) (Figure 3.5 K). Central Arg-1 density followed a similar trend, with a significant increase between D7 (11.64 (8.81 – 16.27) %), D14 (19.72 (14.62 – 22.66) %, p = 0.0140 for D7 *vs* D14) and D21 (21.17 (15.10 – 26.11) %, p =0.0040 for D7 *vs* D21) (Figure 3.5 L).

3.2.3. Blood vessel density, myofibroblast abundance and fibrosis in endometriosis-like lesions from C57 mice

Blood vessel density in lesions from C57 mice was assessed using vWF immunostaining (Figure 3.6 A-C). vWF density was consistent between D7 (0.38 (0.00 – 0.50) %) and D14 (0.47 (0.03 – 0.77) %). A significant increase in vWF density was observed at D21 (1.17 (0.87 – 1.47) %, p = 0.0020 for D7 *vs* D21 and p = 0.0208 for D14 *vs* D21) (Figure 3.6 D). The number of vWF^+ blood vessels was lowest at D7 (5 (0 – 11)), increased significantly at D14 (22 (19 – 33), p = 0.0018), and were sustained at D21 (25 (21 – 32), p = 0.0014 for D7 *vs* D21) (Figure 3.6 E). Average vessel size remained consistent between time

points (0.0003 (0.0000 – 0.0005) mm^2 at D7, 0.0004 (0.0003 – 0.0008) mm^2 at D14, and 0.0005 (0.0004 – 0.0009) mm^2 at D21).

The density of myofibroblasts in these lesions was visualised using αSMA immunostaining (Figure 3.7 A-C). Median $αSMA^+$ expression was similar at D7 and D14 (14.93 (11.90 – 21.46) % and 17.76 (11.62 – 22.60) % respectively). Interestingly, by D21, a significant increase in αSMA density was observed (28.20 (24.27 – 33.63) %, $p = 0.0020$ for D7 *vs* D21 and $p = 0.0017$ for D14 *vs* D21) (Figure 3.7 G). Assessment of the extent of fibrosis in C57 lesions was carried out using Masson's trichrome staining (Figure 3.7 D-F). Density of fibrosis was unchanged between D7 (24.25 (17.47 – 30.01) %) and D14 (26.16 (17.61 – 29.84) %). An increase in lesion fibrosis was noted at D21 (30.80 (27.95 – 33.75) %, $p = 0.0324$ for D7 *vs* D21) (Figure 3.7 H).

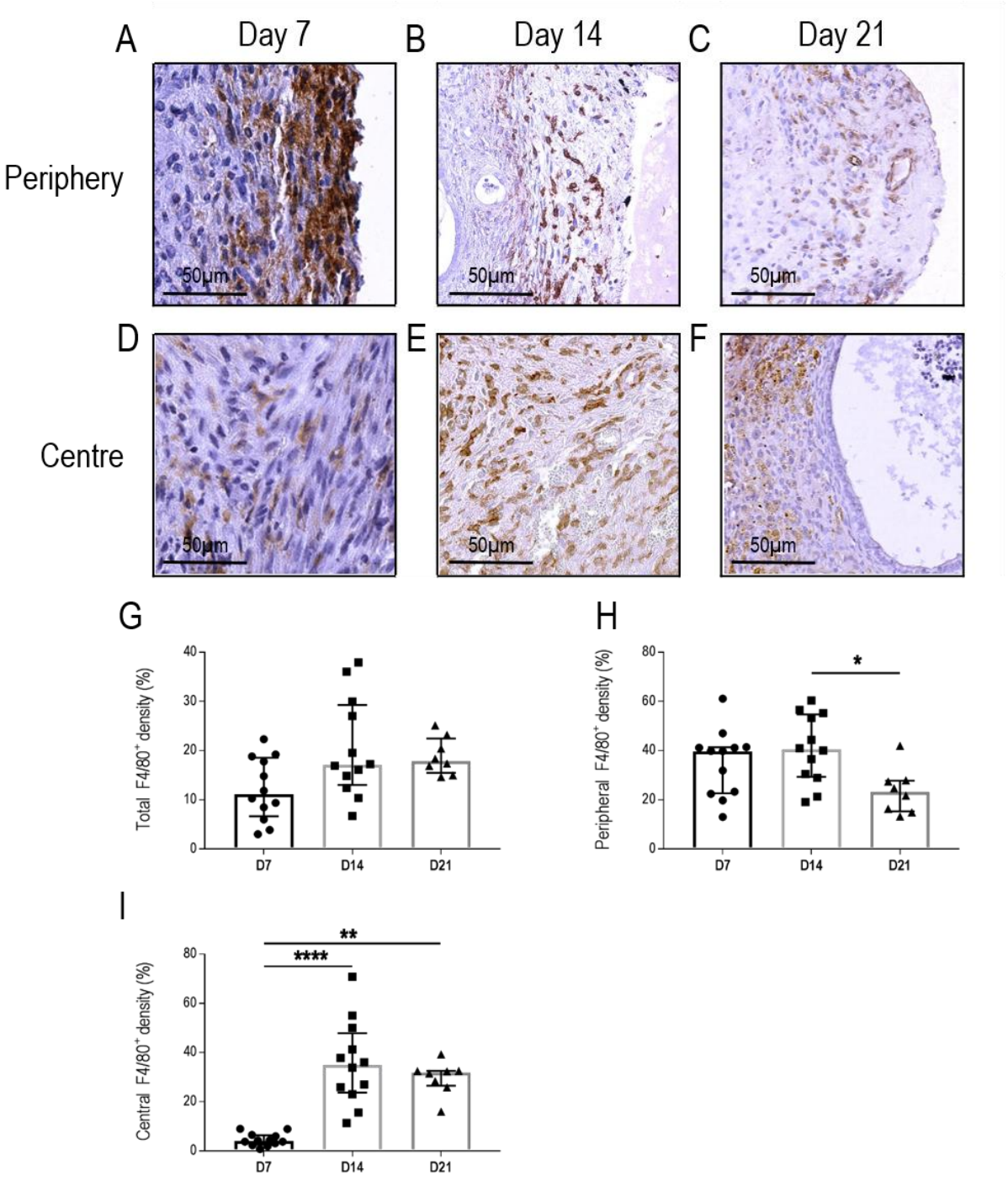

Figure 3.3 F4/80 immunostaining in endometriosis-like lesions from C57 mice

Quantification of total F4/80 density was carried out in lesions from C57 mice (**G**). F4/80 density at the lesion periphery (100µM from the edge of the lesion) at D7 (**A**), D14 (**B**) and D21 (**C**) was evaluated (**H**). F4/80 density at the lesion centre (within 500µM from the centre) at D7 (**D**), D14 (**E**), and D21 (**F**) was also quantified (**I**). Data are presented as median (IQR), with each symbol representative of a single lesion in one mouse (n=12 at D7, n=12 at D14, n=8 at D21). Analysis was done using the Kruskal-Wallis test followed by Dunn's multiple comparison test, with significance denoted as * ($p < 0.05$), ** ($p < 0.001$) and **** ($p < 0.0001$).

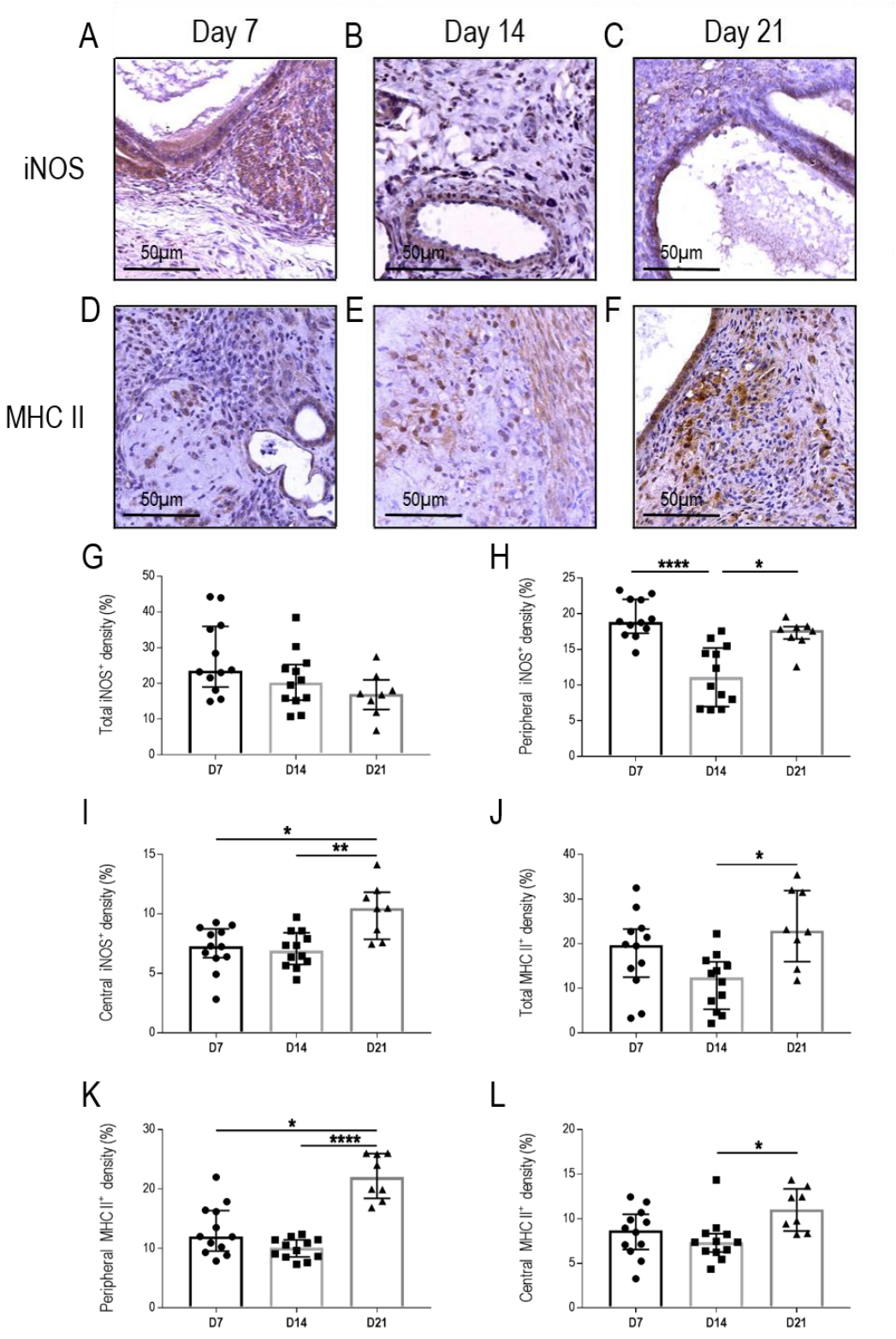

Figure 3.4 M1–like macrophage marker immunostaining in lesions from C57 mice

The expression of inducible nitric oxide synthase (iNOS) at D7 (**A**), D14 (**B**), and D21 (**C**) was quantified in C57 lesions (**G**). Further analysis was performed to determine peripheral (**H**) and central (**I**) iNOS density. Quantification of the Class II Major Histocompatibility Complex (MHC II) was done at D7 (**D**), D14 (**E**) and D21 (**F**) in these lesions (**J**), with peripheral (**K**) and central (**L**) MHC II density determined. Data are presented as median (IQR), with each symbol representative of a single lesion in one mouse (n=12 at D7, n=12 at D14, n=8 at D21). Analysis was done using the Kruskal-Wallis test followed by Dunn's multiple comparison test, with significance denoted as * ($p < 0.05$), ** ($p < 0.001$) and **** ($p < 0.0001$).

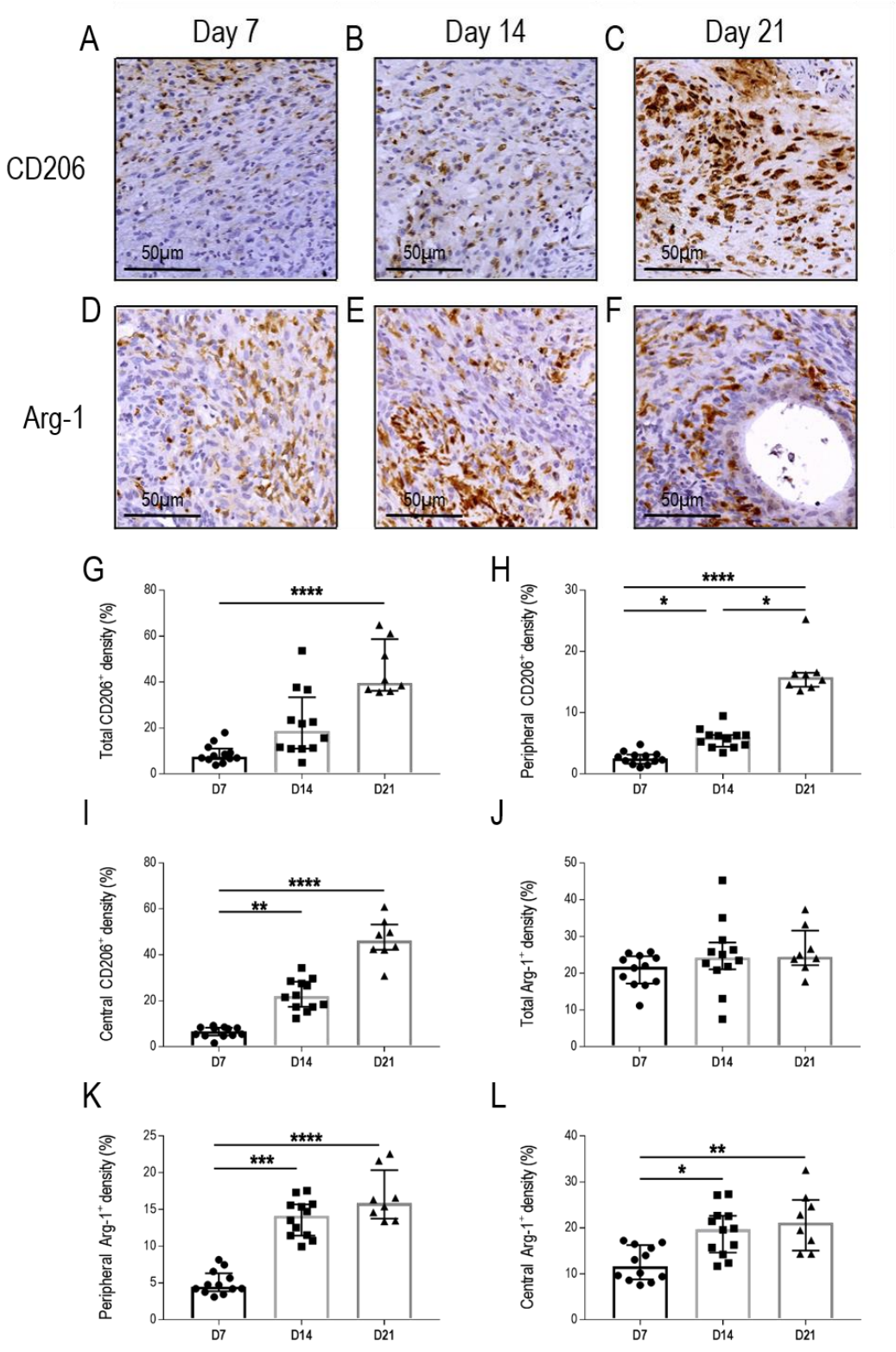

Figure 3.5 M2–like macrophage marker immunostaining in lesions from C57 mice

CD206 density at D7 (**A**), D14 (**B**), and D21 (**C**) was quantified in C57 lesions (**G**), with further analysis of peripheral (**H**) and central (**I**) CD206 density. Expression of Arginase-1 (Arg-1) was evaluated at D7 (**D**), D14 (**E**) and D21 (**F**) in these lesions (**J**), with peripheral (**K**) and central (**L**) Arg-1 density determined. Data are presented as median (IQR), with each symbol representative of a single lesion in one mouse (n=12 at D7, n=12 at D14, n=8 at D21). Analysis was done using the Kruskal-Wallis test followed by Dunn's multiple comparison test, with significance denoted as * ($p < 0.05$), ** ($p < 0.01$), *** ($p < 0.001$) and **** ($p < 0.0001$).

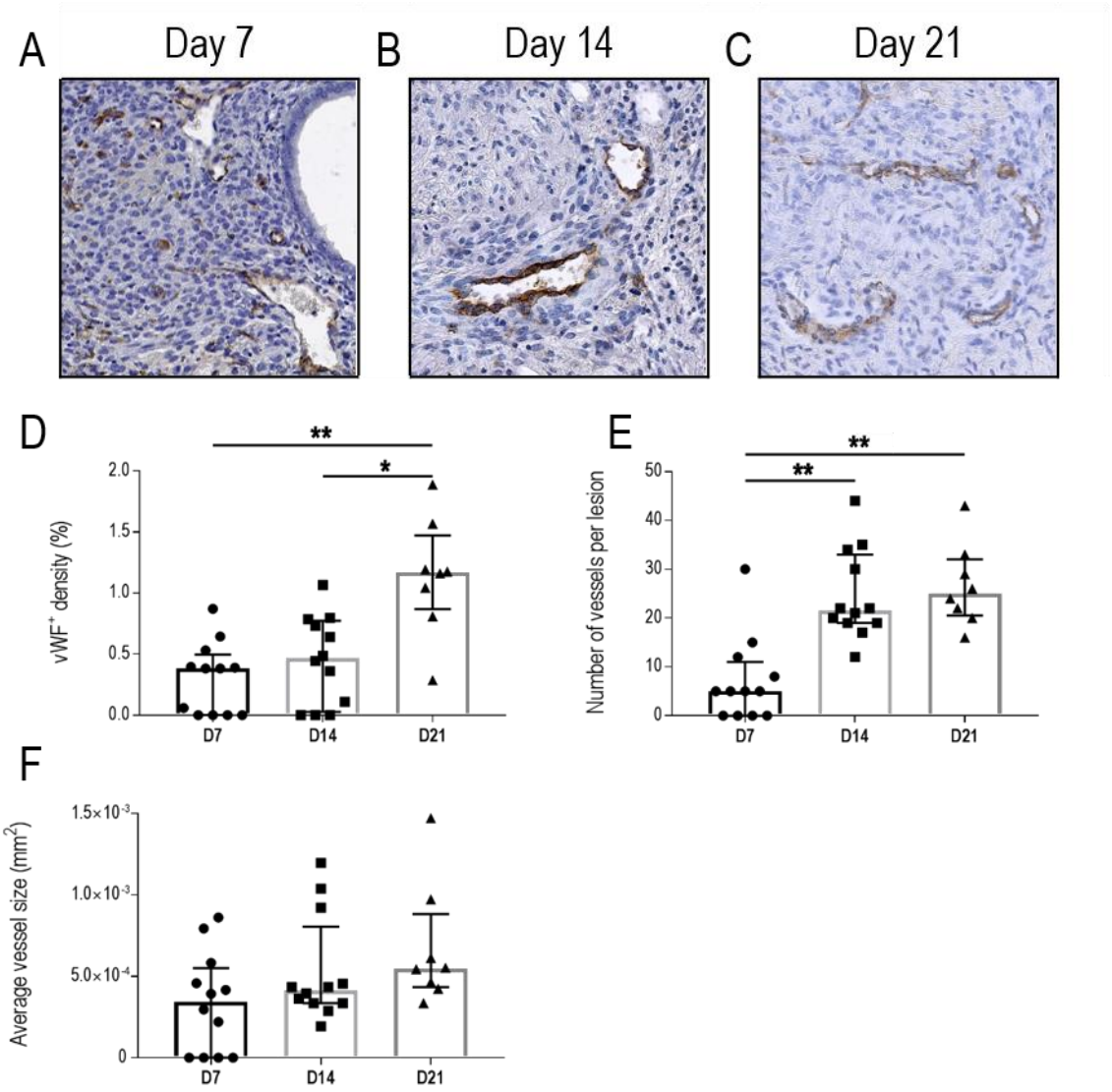

Figure 3.6 Blood vessel localisation in endometriosis-like lesions from C57 mice

Von Willebrand Factor (vWF) staining was used to localise blood vessels in lesions from C57 mice at D7 (**A**), D14 (**B**), and D21 (**C**). The total density of vWF$^+$ vessels was quantified (**D**). The number of vessels per lesion (**E**) and the average vessel size (**F**) was determined. Data are presented as median (IQR), with each symbol representative of a single lesion in one mouse (n=12 at D7, n=12 at D14, n=8 at D21). Analysis was done using the Kruskal-Wallis test followed by Dunn's multiple comparison test, with significance denoted as * ($p < 0.05$) and ** ($p < 0.01$).

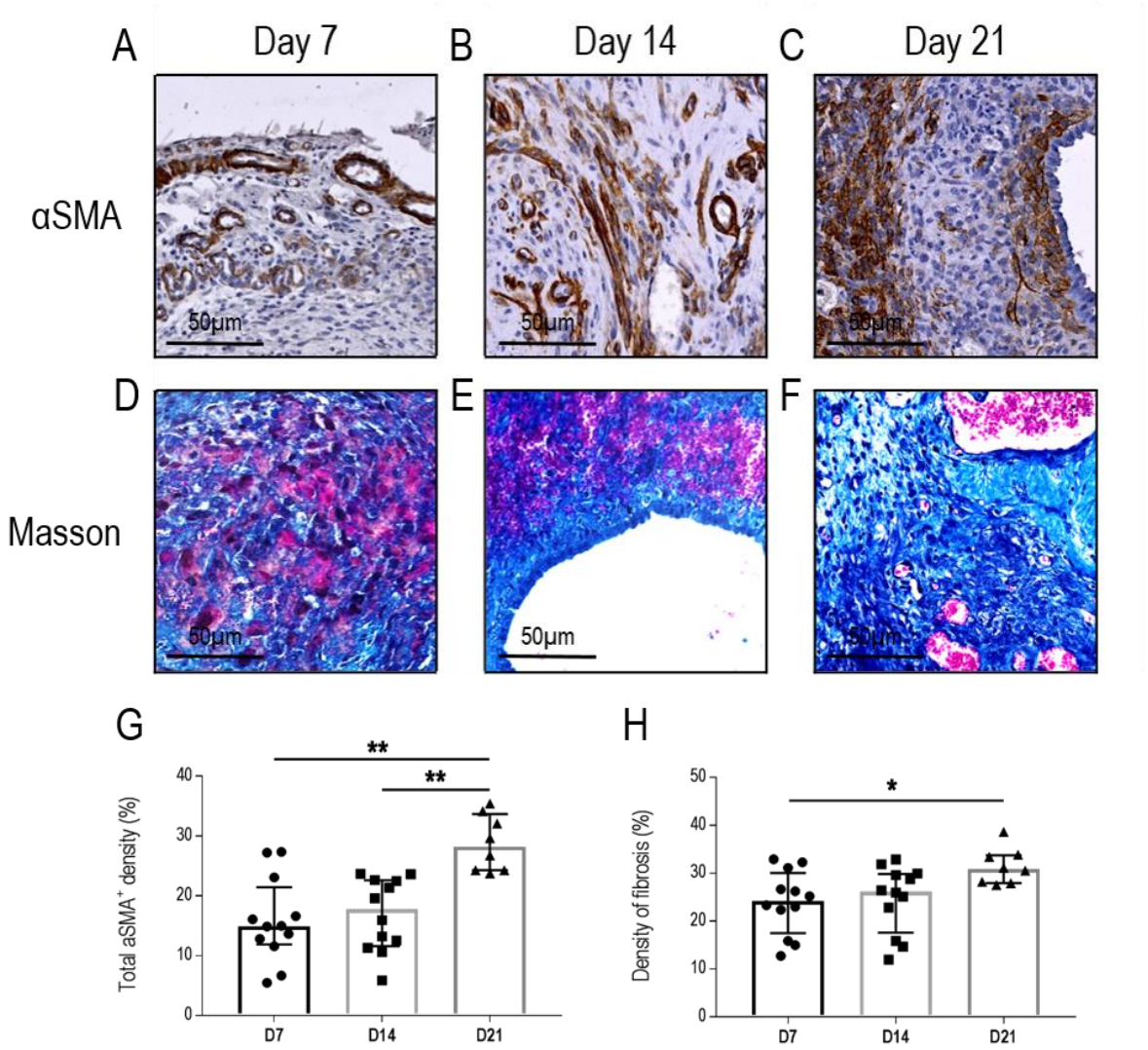

Figure 3.7 Evaluation of fibrosis in endometriosis-like lesions from C57 mice

The density of myofibroblasts in C57 lesions at D7 (**A**), D14 (**B**), and D21 (**C**) was evaluated using alpha smooth muscle actin (αSMA) (**G**). Masson's trichrome staining was used to evaluate the density of fibrosis (**H**) at D7 (**D**), D14 (**E**) and D21 (**F**) in these lesions. Data are presented as median (IQR), with each symbol representative of a single lesion in one mouse (n=12 at D7, n=12 at D14, n=8 at D21). Analysis was done using the Kruskal-Wallis test followed by Dunn's multiple comparison test, with significance denoted as * ($p < 0.05$) and ** ($p < 0.01$).

3.2.4. RNA-Sequencing analysis of lesion progression in C57 mice

To assess the molecular changes associated with lesion development in these mice, RNA-Sequencing (RNA-Seq) was performed on donor decidualised endometrial tissue, D7 and D14 lesions (See Appendix: Figure 7.2 and Figure 7.3 for RNA-Seq metrics). Following alignment to the mouse reference genome and filtering to remove low expressed genes, a total of 16,291 genes were identified from the RNA-Seq. Average gene expression was obtained (n = 4 samples per group of decidualised endometrium, D7 and D14 lesions), and the proportion of differentially expressed genes (DEGs) between groups was determined using a fold change in expression of ≥ 2 with FDR ≤ 0.05 as the cut-off (see attached Supplementary Materials: Table 1 to 3 for complete DEG list). Principal component analysis performed using normalised RNA-Seq data shows a clustering pattern of C57 decidualised endometrial tissue samples on the bottom left, with a distinct separation from both D7 and D14 lesions (Figure 3.8 A). Comparisons between decidualised endometrium and D7 lesions found an upregulation in 12% of detected genes, while 18% of detected genes were downregulated (Figure 3.8 B). Between decidualised endometrium and D14, a total of 14% of detected genes were upregulated while 20% of detected genes were downregulated (Figure 3.8 C). In contrast, between D7 and D14, very few detected genes were differentially expressed (1% upregulated and 1% downregulated) (Figure 3.8 D).

A total of 6,167 genes were differentially expressed between one or more of the three comparisons (Figure 3.8 E). Of this, 2.5% (154 genes) were differentially expressed across all comparisons. The majority of common DEGs were only between the Decidualised *vs* D7 and Decidualised *vs* D14 (4,110 genes) comparisons. A further division of DEGs between Decidualised *vs* D7 and Decidualised *vs* D14 groups into upregulated (2,538 genes) and downregulated (3,625 genes) was performed (Figure 3.8 F and G respectively). A total of 1,739 genes were consistently upregulated, while 2,525 genes were consistently downregulated in lesions at both D7 and D14 when compared to decidualised endometrium.

The genes with the largest fold change in expression between the three samples were identified (Table 3.2). When compared with decidualised endometrium, lesions at both D7 and D14 had an increased expression of prolactin family 3, subfamily c, member 1 (*Prl3c1*; involved in hormone activity, regulation of proliferation and decidual differentiation), tachykinin 2 (*Tac2*; involved in the regulation of blood pressure), prostate stem cell antigen (*Psca*; involved in regulation of neurotransmission), and beta-carotene oxygenase 1 (*Bco1*; involved in beta-carotene metabolic process). Alternatively, the expression of C1q tumour necrosis factor related protein 3 (*C1qtnf3*; involved in gluconeogenesis and cell communication) and superoxide dismutase 3 (*Sod3*; involved in response to hypoxia) was significantly

downregulated at both D7 and D14 compared to decidualised endometrial tissue. Upregulated DEGs between D7 and D14 lesions included genes associated with cellular matrix reorganisation and adhesion (tintin (*Tnn*), serine peptidase inhibitor (*Serpinb2*), integrin binding sialoprotein (*Ibsp*), and mesothelin (*Msln*)), while downregulated genes were involved in immune system regulation (e.g. melan-A (*Mlana*), CD5 antigen-like (*CD5l*), interleukin 31 receptor A (*Il31ra*), and histocompatibility 2, M region locus 2 (*H2-M2*)).

Assessment of canonical pathways in both D7 and D14 lesions compared to decidualised endometrium showed a similar upregulation in multiple cholesterol biosynthesis pathways, antioxidant pathways, and inhibition of matrix metalloproteases (Table 3.3 and Table 3.4). In addition, an upregulation in the Wnt/β-catenin signalling pathway was noted in D7 lesions compared to decidualised endometrium (p = 0.0480, ratio = 8%). A total of 50 similar downregulated canonical pathways were identified in both D7 and D14 lesions compared to decidualised endometrium. The majority of these pathways were associated with immune regulation, including Fcγ receptor-mediated phagocytosis in macrophages and monocytes, NF-κB signalling, and production of nitric oxide and reactive oxygen species in macrophages. Surprisingly, only two canonical pathways were differentially regulated between D7 and D14 lesions, with an upregulation in the inhibition of matrix metalloproteases (p = 0.0014) and a downregulation in G2/M DNA damage checkpoint regulation (p = 0.0040) in D14 lesions (Table 3.5).

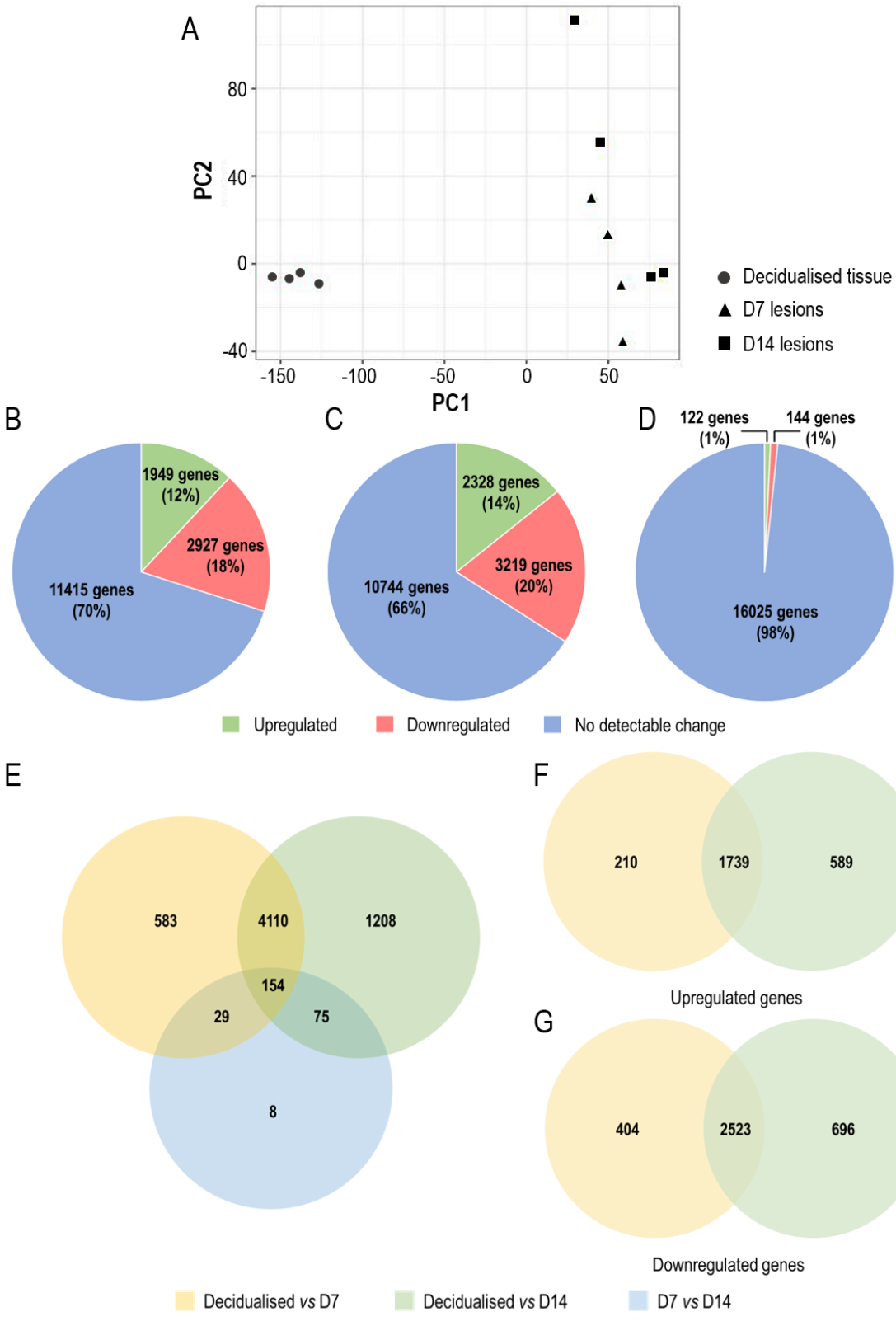

Figure 3.8 Number of differentially expressed genes identified in tissues from C57 mice

Principal component analysis (PCA) was performed using the normalised RNA-Seq data from C57 decidualised endometrium, D7 and D14 lesions (**A**). The proportion of upregulated and downregulated DEGs amongst detected genes between Decidualised *vs* D7 (**B**), Decidualised *vs* D14 (**C**), and D7 *vs* D14 (**D**) was determined. The Venn diagram displays the distribution and overlap of DEGs (both upregulated and downregulated) between each comparison (**E**). Additional Venn diagrams were generated to determine the number of upregulated (**F**) and downregulated (**G**) DEGs during lesion development compared to decidualised endometrial tissue. All genes identified have a ≥ 2-fold change in expression with an adjusted *p* value < 0.05.

Table 3.2 Top ten upregulated and downregulated DEGs in C57 mice during decidualisation and lesion development (FDR <0.05)

Decidualised *vs* D7			Decidualised *vs* D14			D7 *vs* D14		
Gene	**log_2FC**	**FDR**	**Gene**	**log_2FC**	**FDR**	**Gene**	**log_2FC**	**FDR**
Prl3c1	+ 9.58	2.33×10^{-4}	Prl3c1	+ 10.01	1.15×10^{-4}	Nfe2l3	+ 4.04	3.92×10^{-2}
Doxl2	+ 8.87	6.34×10^{-6}	Bco1	+ 9.78	6.97×10^{-10}	Tnn	+ 3.24	5.63×10^{-3}
Cdsn	+ 8.46	2.22×10^{-6}	Psca	+ 9.58	1.08×10^{-8}	Serpinb2	+ 3.11	1.77×10^{-2}
Tac2	+ 8.41	8.78×10^{-10}	Krtdap	+ 9.17	4.31×10^{-5}	Ska3	+ 3.10	3.38×10^{-2}
Psca	+ 8.24	1.89×10^{-8}	Cgn	+ 8.80	4.84×10^{-6}	Exo1	+ 2.75	2.64×10^{-2}
Bco1	+ 8.20	1.97×10^{-10}	Tac2	+ 8.74	6.33×10^{-10}	Ibsp	+ 2.75	4.08×10^{-2}
Dio3	+ 8.12	1.11×10^{-8}	Cdh4	+ 8.54	6.43×10^{-8}	Msln	+ 2.71	2.10×10^{-2}
Krt84	+ 8.00	2.70×10^{-8}	Tacstd2	+ 8.44	4.54×10^{-5}	Sez6l	+ 2.68	6.07×10^{-3}
Spink8	+ 7.96	1.31×10^{-8}	Enpp7	+ 8.43	1.40×10^{-9}	Arg1	+ 2.63	5.40×10^{-3}
Hcn4	+ 7.91	7.54×10^{-9}	Gfy	+ 8.35	1.14×10^{-6}	Erv3	+ 2.58	3.67×10^{-3}
Myh4	- 11.08	3.68×10^{-3}	Clec3b	- 11.08	1.44×10^{-5}	Mlana	- 5.15	1.71×10^{-4}
C1qtnf3	- 11.05	5.57×10^{-5}	Dpt	- 10.78	1.97×10^{-4}	Cd5l	- 4.17	2.14×10^{-4}
Arg1	- 10.83	2.12×10^{-3}	Sod3	- 10.21	3.22×10^{-7}	Il31ra	- 4.16	3.38×10^{-2}
Sod3	- 10.36	3.36×10^{-7}	Mmp3	- 10.06	4.75×10^{-7}	Mcoln3	- 4.01	2.09×10^{-3}
Tbx15	- 10.14	6.43×10^{-5}	C1qtnf3	- 9.96	1.67×10^{-4}	Plppr4	- 3.98	3.36×10^{-2}
Ckm	- 10.11	1.79×10^{-2}	Ptpn5	- 9.92	7.98×10^{-5}	Gm14461	- 3.94	4.18×10^{-3}
Tnni2	- 10.07	3.91×10^{-2}	Tbx15	- 9.87	7.29×10^{-5}	H2-M2	- 3.56	8.59×10^{-3}
Lrrc15	- 10.01	1.06×10^{-5}	Fap	- 9.70	1.92×10^{-11}	Adra1a	- 3.54	3.69×10^{-2}
Tnnt3	- 9.92	1.17×10^{-2}	Mmp12	- 9.58	2.22×10^{-6}	4930512J16Rik	- 3.41	6.80×10^{-3}
Ttn	- 9.90	3.20×10^{-3}	Wisp2	- 9.28	4.87×10^{-6}	Dlgap1	- 3.40	2.54×10^{-2}

Table 3.3 Canonical pathways identified by IPA in D7 lesions compared to decidualised endometrium from C57 mice (*P* < 0.05; -2 > *Z* score > 2)

Canonical Pathway	*Z* score	Ratio	*P* value
Antioxidant Action of Vitamin C	+3.528	33%	5.25×10^{-3}
Superpathway of Cholesterol Biosynthesis	+2.887	44%	6.92×10^{-3}
Cyclins and Cell Cycle Regulation	+2.683	32%	2.24×10^{-2}
Cholesterol Biosynthesis I	+2.121	62%	2.19×10^{-3}
Cholesterol Biosynthesis II (via 24,25-dihydrolanosterol)	+2.121	62%	2.19×10^{-3}
Cholesterol Biosynthesis III (via Desmosterol)	+2.121	62%	2.19×10^{-3}
Wnt/β-catenin Signalling	+2.082	27%	4.79×10^{-2}
Inhibition of Matrix Metalloproteases	+2.065	57%	3.72×10^{-6}
Superpathway of Geranylgeranyldiphosphate Biosynthesis I (via Mevalonate)	+2.000	25%	4.71×10^{-1}
Ceramide Biosynthesis	+2.000	57%	4.47×10^{-2}
Dermatan Sulphate Biosynthesis	-2.000	31%	8.32×10^{-2}
Superoxide Radicals Degradation	-2.000	50%	7.41×10^{-2}
PAK Signalling	-2.030	40%	1.74×10^{-5}
Macropinocytosis Signalling	-2.041	40%	9.55×10^{-5}
GM-CSF Signalling	-2.043	38%	5.25×10^{-4}
fMLP Signalling in Neutrophils	-2.082	37%	1.05×10^{-4}
CREB Signalling in Neurons	-2.101	37%	3.98×10^{-7}
RANK Signalling in Osteoclasts	-2.121	35%	1.15×10^{-3}
Type I Diabetes Mellitus Signalling	-2.132	34%	2.29×10^{-3}
Toll-like Receptor Signalling	-2.132	40%	2.88×10^{-4}
Sperm Motility	-2.197	33%	4.07×10^{-3}
Notch Signalling	-2.236	24%	4.13×10^{-1}
Chondroitin and Dermatan Biosynthesis	-2.236	83%	2.40×10^{-3}
GNRH Signalling	-2.263	39%	3.63×10^{-7}
Eicosanoid Signalling	-2.309	46%	1.02×10^{-5}
P2Y Purigenic Receptor Signalling Pathway	-2.309	39%	2.57×10^{-6}
Synaptic Long Term Depression	-2.324	34%	6.76×10^{-5}
GDNF Family Ligand-Receptor Interactions	-2.353	37%	8.51×10^{-4}
NF-κB Activation by Viruses	-2.401	38%	2.45×10^{-4}
Th2 Pathway	-2.402	40%	8.13×10^{-7}
IL-7 Signalling Pathway	-2.414	34%	5.37×10^{-3}
Calcium-induced T Lymphocyte Apoptosis	-2.449	45%	7.24×10^{-5}
Apelin Cardiomyocyte Signalling Pathway	-2.469	39%	2.45×10^{-5}
Renin-Angiotensin Signalling	-2.469	38%	1.48×10^{-5}
CCR3 Signalling in Eosinophils	-2.475	39%	1.05×10^{-5}
Apelin Liver Signalling Pathway	-2.500	62%	1.32×10^{-5}
Dopamine-DARPP32 Feedback in cAMP Signalling	-2.534	33%	8.71×10^{-4}
NGF Signalling	-2.535	30%	1.86×10^{-2}
Lymphotoxin β Receptor Signalling	-2.558	35%	7.08×10^{-3}
Adrenomedullin signalling pathway	-2.566	36%	4.57×10^{-6}
Gαq Signalling	-2.610	38%	3.02×10^{-6}

Production of Nitric Oxide and Reactive Oxygen Species in Macrophages	-2.626	34%	1.38×10^{-4}
Gluconeogenesis I	-2.646	29%	2.53×10^{-1}
Glycolysis I	-2.646	30%	2.18×10^{-1}
Colorectal Cancer Metastasis Signalling	-2.650	37%	1.91×10^{-8}
Interferon Signalling	-2.673	45%	3.09×10^{-3}
Phospholipase C Signalling	-2.689	35%	3.72×10^{-6}
eNOS Signalling	-2.774	38%	2.19×10^{-6}
Integrin Signalling	-2.782	31%	1.66×10^{-3}
Tec Kinase Signalling	-2.828	39%	1.95×10^{-7}
Fc Epsilon RI Signalling	-2.846	36%	2.45×10^{-4}
B Cell Activating Factor Signalling	-2.887	37%	2.14×10^{-2}
NF-κB Signalling	-2.898	36%	5.37×10^{-6}
Cardiac Hypertrophy Signalling	-2.926	34%	8.51×10^{-6}
p38 MAPK Signalling	-2.959	31%	1.20×10^{-2}
GPCR-Mediated Nutrient Sensing in Enteroendocrine Cells	-3.000	45%	7.41×10^{-8}
PEDF Signalling	-3.024	33%	7.59×10^{-3}
PI3K Signalling in B Lymphocytes	-3.111	41%	2.57×10^{-7}
Glutathione-mediated Detoxification	-3.162	40%	3.02×10^{-2}
Inflammasome pathway	-3.357	79%	1.74×10^{-7}
Th1 Pathway	-3.395	44%	4.27×10^{-8}
CD28 Signalling in T Helper Cells	-3.479	41%	1.51×10^{-6}
B Cell Receptor Signalling	-3.500	38%	3.31×10^{-7}
iCOS-iCOSL Signalling in T Helper Cells	-3.507	47%	1.62×10^{-1}
Leukocyte Extravasation Signalling	-3.623	45%	6.31×10^{-14}
Role of NFAT in Cardiac Hypertrophy	-3.755	41%	5.01×10^{-11}
Role of NFAT in Regulation of the Immune Response	-3.810	40%	7.76×10^{-9}
Role of Pattern Recognition Receptors in Recognition of Bacteria and Viruses	-3.904	45%	4.57×10^{-9}
Fcγ Receptor-mediated Phagocytosis in Macrophages and Monocytes	-4.000	40%	6.76×10^{-5}
GP6 Signalling Pathway	-4.154	55%	3.98×10^{-17}
PKCθ Signalling in T Lymphocytes	-4.160	41%	5.01×10^{-8}
Calcium Signalling	-4.341	36%	1.82×10^{-6}
Neuroinflammation Signalling Pathway	-4.400	38%	1.00×10^{-10}
TREM1 Signalling	-4.964	57%	3.24×10^{-10}
Dendritic Cell Maturation	-5.336	43%	2.82×10^{-10}

Table 3.4 **Canonical pathways identified by IPA in D14 lesions compared to decidualised endometrium from C57 mice (*P* < 0.05; -2 > *Z* score > 2)**

Canonical Pathway	*Z* score	Ratio	*P* value
Superpathway of Cholesterol Biosynthesis	+3.207	52%	2.00×10^{-3}
Antioxidant Action of Vitamin C	+3.024	33%	3.24×10^{-2}
Inhibition of Matrix Metalloproteases	+2.982	57%	2.75×10^{-5}
Mitotic Roles of Polo-Like Kinase	+2.673	39%	6.92×10^{-3}
Cholesterol Biosynthesis I	+2.121	62%	4.90×10^{-3}
Cholesterol Biosynthesis II (via 24,25-dihydrolanosterol)	+2.121	62%	4.90×10^{-3}
Cholesterol Biosynthesis III (via Desmosterol)	+2.121	62%	4.90×10^{-3}
Type II Diabetes Mellitus Signalling	-2.000	42%	1.74×10^{-6}
Heme Degradation	-2.000	100%	3.63×10^{-3}
Chondroitin and Dermatan Biosynthesis	-2.000	67%	3.55×10^{-2}
FGF Signalling	-2.058	38%	2.69×10^{-3}
CREB Signalling in Neurons	-2.066	37%	4.79×10^{-5}
Production of Nitric Oxide and Reactive Oxygen Species in Macrophages	-2.109	37%	6.92×10^{-5}
NF-κB Activation by Viruses	-2.137	41%	2.75×10^{-4}
Apelin Liver Signalling Pathway	-2.138	54%	1.23×10^{-3}
Noradrenaline and Adrenaline Degradation	-2.138	45%	9.55×10^{-3}
Gα12/13 Signalling	-2.188	36%	1.95×10^{-3}
Adrenomedullin signalling pathway	-2.194	39%	1.74×10^{-6}
Superoxide Radicals Degradation	-2.236	63%	2.51×10^{-2}
Colorectal Cancer Metastasis Signalling	-2.251	39%	2.09×10^{-7}
CCR3 Signalling in Eosinophils	-2.263	40%	6.61×10^{-5}
Cardiac Hypertrophy Signalling	-2.278	39%	8.51×10^{-7}
Lymphotoxin β Receptor Signalling	-2.294	37%	1.62×10^{-2}
eNOS Signalling	-2.309	36%	4.07×10^{-4}
Synaptic Long Term Depression	-2.324	35%	1.17×10^{-3}
Eicosanoid Signalling	-2.333	42%	1.86×10^{-3}
Tec Kinase Signalling	-2.335	41%	1.58×10^{-6}
NGF Signalling	-2.343	35%	6.03×10^{-3}
Dopamine-DARPP32 Feedback in cAMP Signalling	-2.359	33%	7.41×10^{-3}
Integrin Signalling	-2.394	33%	3.55×10^{-3}
Sperm Motility	-2.401	34%	1.10×10^{-2}
Fc Epsilon RI Signalling	-2.402	35%	6.03×10^{-3}
GDNF Family Ligand-Receptor Interactions	-2.414	41%	6.92×10^{-4}
Apelin Cardiomyocyte Signalling Pathway	-2.534	42%	4.68×10^{-5}
Renin-Angiotensin Signalling	-2.534	40%	8.71×10^{-5}
Gαq Signalling	-2.540	42%	7.41×10^{-7}
Phospholipase C Signalling	-2.566	37%	3.16×10^{-5}
Th2 Pathway	-2.598	47%	1.23×10^{-8}
IL-7 Signalling Pathway	-2.611	39%	1.32×10^{-3}
PEDF Signalling	-2.694	36%	7.59×10^{-3}
Calcium-induced T Lymphocyte Apoptosis	-2.746	48%	7.24×10^{-5}

GPCR-Mediated Nutrient Sensing in Enteroendocrine Cells	-2.771	43%	2.04×10^{-5}
p38 MAPK Signalling	-2.795	35%	9.12×10^{-3}
Role of NFAT in Cardiac Hypertrophy	-2.929	42%	1.41×10^{-8}
Leukocyte Extravasation Signalling	-3.092	46%	5.01×10^{-12}
PI3K Signalling in B Lymphocytes	-3.159	44%	1.05×10^{-6}
B Cell Receptor Signalling	-3.299	40%	3.63×10^{-6}
NF-κB Signalling	-3.349	37%	7.76×10^{-5}
Role of Pattern Recognition Receptors in Recognition of Bacteria and Viruses	-3.429	49%	8.71×10^{-10}
Glutathione-mediated Detoxification	-3.464	48%	9.12×10^{-3}
Fcγ Receptor-mediated Phagocytosis in Macrophages and Monocytes	-3.550	39%	1.74×10^{-3}
CD28 Signalling in T Helper Cells	-3.592	43%	4.57×10^{-6}
Inflammasome pathway	-3.606	68%	6.61×10^{-5}
iCOS-iCOSL Signalling in T Helper Cells	-3.833	50%	1.86×10^{-9}
Role of NFAT in Regulation of the Immune Response	-4.032	43%	2.19×10^{-8}
Calcium Signalling	-4.082	41%	5.50×10^{-7}
PKCθ Signalling in T Lymphocytes	-4.106	43%	4.17×10^{-7}
Neuroinflammation Signalling Pathway	-4.350	42%	6.31×10^{-11}
Th1 Pathway	-4.429	48%	6.76×10^{-9}
GP6 Signalling Pathway	-4.565	57%	2.00×10^{-15}
TREM1 Signalling	-4.841	59%	6.92×10^{-10}
Dendritic Cell Maturation	-5.498	42%	1.70×10^{-7}

Table 3.5 **Canonical pathways identified by IPA in D14 lesions compared to D7 lesions from C57 mice (*P* < 0.05; -2 > *Z* score > 2)**

Canonical Pathway	*Z* score	Ratio	*P* value
Inhibition of Matrix Metalloproteases	+2.000	11%	1.41×10^{-3}
Cell Cycle: G2/M DNA Damage Checkpoint Regulation	-2.000	8%	3.98×10^{-3}

3.3. DISCUSSION

This is the first study to characterise the development of lesions over time in a subcutaneous menstrual mouse model of endometriosis. The experiments carried out in this chapter demonstrate that successful lesion establishment and morphological changes associated with lesion growth can be effectively characterised across the span of three weeks. The subcutaneous endometriosis-like lesions in C57 mice developed distinctive glandular and stromal areas, and were representative of human endometriosis lesions. Moreover, infiltration of F4/80^{+} macrophages into lesions, with an increase in M2-like macrophage markers was observed over time. Interestingly, from the RNA-Seq data, differential expression of genes was most apparent between the decidualised endometrium and endometriosis-like lesions, while very few DEGs were identified between D7 and D14 lesions, suggesting that the morphological and histological changes observed during lesion development may be predetermined by gene expression in the eutopic endometrium.

3.3.1. Endometriosis-like lesions in C57 mice mimic human disease

In wildtype C57 mice, we observed that lesion recovery rate averaged 95% over the course of three weeks, confirming the efficacy of this model. Distinct changes in the overt appearance of lesions over time highlights the dynamic nature of endometriosis progression. At D7, the observed red, blood-filled opaque lesions are suggestive of the deoxygenation of haemoglobin, which may contribute to the pathogenesis of endometriosis (Van Langendonckt et al., 2002a, Van Langendonckt et al., 2002b). Following the lysis of red blood cells, the presence of haemoglobin is implicated in the activation of cell adhesion molecules, which induce cell proliferation, cytokine production and initiate neovascularisation (Van Langendonckt et al., 2002a, Van Langendonckt et al., 2002b). Indeed, from D14 onwards, we observed colour changes within the lesions, coupled with the appearance of surrounding vasculature. This is indicative of the deoxygenation from haemoglobin to either methaemoglobin or hemosiderin (Khan et al., 2004), and suggests sequential changes from attachment of the ectopic tissue, to heme metabolism and vascularisation which assists in maintaining lesion development (Khan et al., 2014).

Lesion weight and size are important clinical indicators of lesion development. The initial decrease in lesion size between D7 and D14 suggests an attempt to clear the ectopic tissue; however the increase seen in lesion size between D14 and D21 suggests a shift from clearance towards remodelling and establishment which may be driven by immune cell infiltration (Young et al., 2013, Králíčková and Vetvicka, 2015). Endometrial glands are important sources of chemokines, including CCL16 and CCL21 which are secreted by glandular epithelial cells (Chand et al., 2007). These chemokines and additional

associated cytokines, are involved in the regulation and infiltration of immune cells (Chand et al., 2007), and may be vital in supporting the growth of ectopic endometrial tissue. Sustained weight loss over time in C57 lesions was coupled with an inversely proportional increase in the number of glands, luminal and epithelial areas present, suggesting increased lesion remodelling and establishment, potentially mediated by immune cells.

3.3.2. Macrophage activity correlates with lesion development in C57 mice

The multi-faceted role of the immune system mediates the progression of endometriosis. In particular, the presence of macrophages is a consistent feature of endometriotic lesions and appears to be a significant driving force in the establishment and persistence of this disease (Capobianco and Rovere-Querini, 2013). In C57 mice, while total F4/80 macrophage density within lesions was unaltered over the course of the experiment, a significant increase in central F4/80 macrophage density was observed over time, coupled with a reduction in peripheral F4/80 expression. In concordance with previous work, this finding suggests that the presence of ectopic endometrial tissue attracts an influx of macrophages from the surrounding environment (D'Hooghe et al., 2001). Studies have shown that a range of cytokines, including IL-1, Il-17, TNFα, and IL-10–mediated-CCL5 (RANTES), are secreted by infiltrating macrophages, and have roles in both macrophage function as well as further recruitment of macrophages and monocytes (Mori et al., 1992, Khorram et al., 1993, Richter et al., 2005, Barin et al., 2012).

The RNA-Seq data further confirms this observation, with an increase in the IL-17 signalling pathway observed between D7 and D14 (Appendix: Figure 7.4 and Table 7.1 – Cluster 5). Macrophages are associated with IL-17-mediated signalling, wherein IL-17-differentiated macrophages produce inflammatory cytokines in the presence of oxidized low-density lipoprotein (Barin et al., 2012, de la Paz Sánchez-Martínez et al., 2017). During lesion development in this mouse model, the identification of multiple canonical pathways involving cholesterol biosynthesis suggests that the presence of oxidized low-density lipoprotein (or cholesterol) may be driving IL-17-mediated pro-inflammatory macrophage recruitment and activity during endometriosis. In addition, elevated IL-17 signalling is associated with the progression of cancer, autoimmune diseases, and a range of immuno-pathologies, including endometriosis (Ahn et al., 2015, Beringer et al., 2016).

3.3.2.1. Immune activation status remains dynamic throughout lesion development in C57 mice

In endometriosis, macrophages may either promote lesion clearance or regulate endometriotic epithelial remodelling dependent on their activation status (Bacci et al., 2009). Moreover, dynamic changes in macrophage phenotype quantified via immunohistochemical localisation have also been observed in a MacGreen/SCID mouse model of endometriosis (Johan et al., 2019). In this C57 mouse model of endometriosis, the expression levels of the M1-like marker MHC II fluctuated over the three week period. Reduced expression of the MHC II–associated protein HLA-DR was seen in women with endometriosis compared to those without endometriosis (Kusume et al., 2005). In addition, the expression of HLA-DR in the macrophage cell line THP-1, was downregulated following a co-culture with peritoneal fluid from women with endometriosis (Lee et al., 2005). Further investigation has also uncovered roles for IL-10 and RANTES mediated suppression of MHC II expression in macrophages (Lee et al., 2005, Wang et al., 2010). As levels of IL-10 and RANTES are elevated in peritoneal fluid from women with endometriosis (Wang et al., 2010), it is possible that the ectopic implantation environment restricts lesion clearance by reducing M1-like macrophage activity and hence, creates an immune-tolerant milieu that facilitates ectopic tissue survival. Therefore, the expression of MHC II may be an essential step in supporting the clearance of ectopic endometrial tissue and preventing initial disease development. In this study, the observed decline in MHC II expression between D7 and D14 suggests that a resolution of inflammation is occurring, which reduces tissue clearance and supports the survival of ectopic endometrial tissue. Although a subsequent increase in total, central and peripheral MHC II expression is observed between D14 and D21, the respite in immune-mediated clearance at D14 appears to have been sufficient in allowing lesions to become fully established.

Throughout the duration of this study, the total density of the M1-like marker iNOS in lesions remained consistent between D7 and D21. In women, a study evaluating the expression of NO in endometriosis found significantly higher levels in ectopic tissue compared to paired eutopic endometrial samples (Wu et al., 2003). Furthermore, the same study showed elevated expression of NO in endometrial samples from women with endometriosis compared to those without. In addition, higher levels of iNOS were secreted from peritoneal macrophages derived from women with endometriosis compared to women without endometriosis, when stimulated with IFN-α *in vitro* (Osborn et al., 2002). This finding was linked with the observed subfertility seen in women with endometriosis, and is thought to contribute to inflammation and pain in the peritoneal cavity. Thus, macrophage-derived iNOS activity plays a role in the pathogenesis of endometriosis, and regulation of this M1-like immune mediator is critical in managing the symptoms associated with this disorder. Surprisingly, the results from this study contrasts with these findings, wherein a decrease in the canonical pathway 'Production of Nitric Oxide and Reactive Oxygen Species in Macrophages' was seen at both D7 and D14 compared to decidualised endometrium. Similarly,

Immunohistochemical analyses of central iNOS density within lesions was lowest at D7 and D14 and increased significantly at D21. As lesions developed subcutaneously rather than intraperitoneally, it is possible that the availability and/or secretion of iNOS from tissue-resident macrophages may differ from peritoneal macrophages, which may account for fluctuations in the peripheral iNOS density over time. In addition, it is possible that the elevation of NO and iNOS in women with endometriosis may be a consequence of the ectopic endometrial tissue load and chronic inflammation associated with this disease.

A link between endometriosis and Arg-1 expressing M2-like macrophages is yet to be determined. In this study, the expression of total Arg-1 remained comparable at all time points when assessed via immunohistochemistry. In contrast, the RNA-Seq data showed a decrease in *Arg-1* at D7 when compared to decidualised endometrium, while an elevation in *Arg-1* was observed in D14 lesions compared to D7 lesions, which was also observed in analyses of peripheral and central Arg-1 density. During both the proliferative and secretory phases of the human menstrual cycle, detection of *ARG1* mRNA was localised in the epithelial layer of eutopic endometrium (Tajima et al., 2012). In a mouse model of endometriosis, elevated Arg-1 expression was observed in lesions compared to uterine tissue three days following disease initiation, however, Arg-1 levels were unchanged were not significantly different after 29 days (Pelch et al., 2010). In a SCID mouse model of endometriosis, analysis of lesions over four time points (day 4, 7, 10, and 14 – post disease induction) found significantly higher expression of Arg-1$^+$ macrophages at day 7 compared to other time points (Johan et al., 2019). In addition, upregulation of Arg-1 expression was observed in murine peritoneal macrophages exposed to hypoxic conditions (Louis et al., 1998), which is known to occur in endometriosis (Groothuis, 2012). Collectively, these findings suggest that Arg-1 expression may be critical to initiate tissue remodelling during the early stages of endometriotic lesion growth, however more research into the role of Arg-1 is required, particularly at later stages of lesion development.

On the other hand, immunohistochemical quantification showed a significant increase in the expression of the M2-like marker CD206 over time. During disease development, CD206 was expressed at significantly higher levels in peritoneal macrophages from women with endometriosis compared to controls (Bacci et al., 2009). Moreover, immunohistochemical evaluation of endometriotic lesions and peritoneum biopsies from women with endometriosis showed elevated expression of CD206 compared to control peritoneum tissue (Bacci et al., 2009). In addition, the expression and cellular localisation of matrix metalloproteinase (MMP)-27 in ovarian and peritoneal endometriotic lesions was associated with CD206$^+$ macrophages (Cominelli et al., 2014). As MMPs are implicated in tissue remodelling processes associated with invasion and metastasis in endometriosis and cancers (Osteen et al., 2003, Nagase et

al., 2006), elevated expression of M2-like macrophages may contribute significantly in disease pathogenesis and persistence. However, from the RNA-Seq dataset, it is intriguing to note that an elevation in the canonical pathway associated with inhibition of MMPs was observed throughout lesion development, suggesting that MMP-mediated remodelling of endometrial lesions may not be critical during early lesion establishment.

3.3.3. Markers of lesion establishment are observed during disease development in C57 mice

Aside from macrophage infiltration into endometriotic lesions, a study using a nude mouse model of endometriosis identified two additional events which had critical roles in the development of endometriosis (Hull et al., 2008). First, an increase in myofibroblast activity in endometriotic lesions was noted between day 7 and day 14, and second, the formation of blood vessels throughout the ectopic tissue was vital in supporting lesion vascularisation and survival (Hull et al., 2008). In the C57 'menstrual' mouse model of endometriosis, elevation in αSMA as well as an increase in blood vessel formation was observed over time, with a greater extent of fibrosis at D21. In humans, αSMA, the marker used to detect myofibroblast activity, was more abundantly expressed in unaffected peritoneal biopsies from women with endometriosis compared to women without endometriosis (Barcena de Arellano et al., 2011). Furthermore, expression of *ACTA2*, the gene encoding αSMA, was elevated in peritoneal endometriotic lesions compared to paired eutopic endometrium (Sohler et al., 2013), suggesting an important role for myofibroblasts in endometriotic lesion remodelling.

This observation is further supported by the elevation of the tissue remodelling gene *Serpinb2* in lesions at D14 compared to D7. *Serpinb2* has been shown to regulate fibroblast interaction with collagen, thus mediating stromal remodelling and local tissue invasion in a mouse model of pancreatic cancer (Harris et al., 2017). Moreover, following an inflammatory challenge, mice deficient in *Serpinb2* had reduced expression of CCL2 and Arg-1, resulting in impaired macrophage infiltration and reduced M2-like macrophage activation (Zhao et al., 2013). Similarly, several studies have classified *Serpinb2* as an M2-like macrophage associated gene, whereby its expression is important in preventing premature macrophage apoptosis and has a role in inhibiting the early cessation of the innate immune response (Park et al., 2005, de las Casas-Engel et al., 2013, Zhao et al., 2013, Shea-Donohue et al., 2014).

KEGG pathway analysis has shown an upregulation in genes associated with the VEGF signalling pathway at both D7 and D14 (Appendix: Figure 7.4 and Table 7.1 – Cluster 3). Macrophages are a potent source of VEGF, and have roles in vascular development (Capobianco and Rovere-Querini, 2013).

Depletion of macrophages in a mouse model of endometriosis resulted in smaller lesions with reduced vascularisation compared to control mice (Bacci et al., 2009), strongly implicating macrophages in the process of neovascularisation and lesion survival.

Macrophages also contribute to the deposition of collagen and fibrous material. In a mouse wound-healing model, macrophage depletion resulted in reduced collagen intensity as measured by Masson's trichrome staining (Mirza et al., 2009). Interestingly, an association between the time at which macrophages were depleted and their ability to mediate collagen deposition was observed (Mirza et al., 2009, Lucas et al., 2010). In particular, early recruitment of macrophages (within forty eight hours) was essential in collagen synthesis at a later stage, as depletion of macrophages forty eight hours post-injury did not significantly affect tissue healing and remodelling (Lucas et al., 2010). At both D7 and D14, KEGG pathway analysis has shown an upregulation in genes associated with glycosaminoglycan biosynthesis, suggesting that collagen deposition and remodelling may be occurring during lesion development (Appendix: Figure 7.4 and Table 7.1 – Cluster 3 and Cluster 5).

To summarise, the findings from this chapter have shown that the development of glandular fractions occurs gradually in endometriosis-like lesions from C57 mice, corresponding with an increase in vascularisation and myofibroblast activity to support endometriotic lesion growth and survival. These findings have also demonstrated that the gene expression profile between D7 and D14 lesions was comparable, suggesting that subtle shifts in macrophage polarisation status may occur surreptitiously throughout lesion development in endometriosis which may not have been fully captured by the RNA-Seq analysis. Therefore, to better understand the roles of macrophages in endometriosis, it is important that characterisation of lesion progression is undertaken in models in which the impact of sustained expression of either M1-like (pro-inflammatory) or M2-like (anti-inflammatory) immune profiles can be evaluated throughout disease development. Thus, the impact of a systemic *miR-155* or *miR-223* deficiency on endometriotic lesion development in mice is investigated in Chapter 4 and Chapter 5 respectively.

Chapter 4

Evaluating the effect of a *miR-155* deficiency on endometriotic lesion development

4.1. INTRODUCTION

Due to the heterogeneous nature of endometriosis and endometriosis-associated symptoms, achieving an accurate differential diagnosis in the absence of laparoscopic surgery is challenging. The World Endometriosis Research Foundation has highlighted the importance of developing low-invasive tests and biomarkers for endometriosis as a research priority for endometriosis (Adamson and Johnson, 2018). To this extent, multiple studies analysing blood samples from women with and without endometriosis have identified aberrant expression of miRNAs (Suryawanshi et al., 2013, Wang et al., 2013b, Cho et al., 2015, Rekker et al., 2015, Cosar et al., 2016, Nisenblat et al., 2019). Amongst the miRNAs that are dysregulated in plasma from women with endometriosis is miR-155-5p (miR-155) (Nisenblat et al., 2012, Nisenblat et al., 2019).

miR-155 is located within an exon of the B-cell Integration Cluster (BIC) ncRNA, present on chromosome 21 (Lagos-Quintana et al., 2002). BIC is highly expressed in lymphoid organs, with a strong sequence homology among human, chicken, and mouse genomes, indicative of an evolutionary-conserved function (Faraoni et al., 2009). *miR-155* plays important roles in haematopoietic lineage differentiation, vascular remodelling, and response to immunological challenges, and has been implicated in several pathologies including cardiovascular disease, cancer, and chronic autoimmune disorders such as rheumatoid arthritis, multiple sclerosis, and systemic lupus erythematosus (Faraoni et al., 2009, Leng et al., 2011). While *miR-155* is present in endothelial cells and smooth muscle cells (Zhu et al., 2011), the highest expression of this gene is within immune effector cells, including activated B and T cells, monocytes and macrophages (O'Connell et al., 2007, Turner and Vigorito, 2008, Faraoni et al., 2009).

In macrophages, regulation of *miR-155* is initiated via Toll-like receptor (TLR) signalling. TLR activation creates a feed-forward loop, in which the downstream activation of nuclear factor κB (NF-κB) upregulates *miR-155* production, whereas the activation of protein kinase B (AKT1) by TLRs represses *miR-155* expression. In addition, *miR-155* expression inhibits two phosphatases (suppressor of cytokine signalling 1 (SOCS1) and SH2 domain-containing inositol 5'-phosphatase 1 (SHIP1)) which results in a positive feedback loop that increases pro-inflammatory TLR-NF-κB signalling (O'Neill et al., 2011, Mehta and Baltimore, 2016). *miR-155* is upregulated following an inflammatory LPS challenge, and is also a common target of a range of pro-inflammatory mediators, including polyriboinosinic:polyribocytidylic (PI:PC) acid, IFN-β, and TNF-α. (O'Connell et al., 2007, O'Connell et al., 2012).

Within the macrophage lineage, multiple studies have shown that *miR-155* expression preferentially polarises macrophages towards an M1-like phenotype (Worm et al., 2009, Martinez-Nunez et al., 2011,

Arranz et al., 2012, Gracias et al., 2013, Wang et al., 2013a). The silencing of *miR-155* results in increased levels of alternatively-activated M2-like macrophages, with a simultaneous decrease in M1-like macrophage numbers (Zhang et al., 2016c). The expression of *miR-155* has a pivotal role in Akt kinase-driven polarisation of macrophages, wherein an Akt1-deficiency results in a M1-like macrophage phenotype and conversely, an Akt2-deficiency results in a M2-like macrophage phenotype (Arranz et al., 2012). *miR-155* is repressed in Akt-2 deficient macrophages, with the simultaneous upregulation of the transcriptional co-repressor CCAAT/enhancer-binding protein-β (C/EBPβ), an important regulator of the M2-like macrophage-associated *Arg-1*, thus implying a role for *miR-155* in promoting a classical M1-like macrophage phenotype (Arranz et al., 2012). In THP-1 monocyte-derived macrophage cell lines, the transfection of a miR-155 mimic resulted in the upregulation of transcripts associated with the classical M1-like immune response, highlighting the role of *miR-155* in eliciting an M1-like, pro-inflammatory immune response (Das et al., 2013). The overexpression of *miR-155* suppresses IL-13Rα1 (a cytokine receptor expressed on monocytes allowing for M2-like macrophage polarisation), thus inhibiting M2-like macrophage differentiation and effectively promoting M1-like macrophage polarisation. In contrast, a deficiency in *miR-155* enhances the expression of IL-13Rα1, thereby facilitating M2-like macrophage activation (Martinez-Nunez et al., 2011).

In the female reproductive system, the expression of miR-155 in human plasma is comparable across the menstrual cycle (Nisenblat et al., 2019) and miRNA arrays and qRT-PCR validation has demonstrated that oestradiol upregulates *miR-155* in mouse uterine tissues (Nothnick and Healy, 2010). In addition, an upregulation of *miR-155* expression correlates with a poorer prognosis in cervical cancer patients, with an increase in lymph node metastasis and vascular invasion (Fang et al., 2016). Studies have shown that *miR-155* is also upregulated during endothelial to mesenchymal transition (EndoMT), and is further enhanced in hypoxic conditions, such as are present during endometriosis. In addition, *miR-155* is also proposed to be involved in inflammation and fibrosis, and *in vitro* experiments have shown it to be a negative regulator of RhoA signalling in TGFβ-induced EndoMT (O'Connell et al., 2007, Faraoni et al., 2009, Kurowska-Stolarska et al., 2011, Bijkerk et al., 2012, Koch et al., 2012).

In the context of endometriosis, a significant downregulation of miR-155 expression is observed in two separate cohorts of plasma samples from women with (n = 131) and without (n = 66) endometriosis (Nisenblat et al., 2019). Moreover, in a subgroup analysis, expression of miR-155 remained differentially expressed during both mild (Stage I and II) and severe (Stage III and IV) disease (Nisenblat et al., 2019). Collectively, these findings suggest that a downregulation in miR-155 may contribute to the pathogenesis of endometriosis by promoting polarisation of M2-like macrophages, thus inducing a tissue healing and

remodelling phenotype eventuating in disease exacerbation. Therefore, in this chapter, to fully assess the impact of *miR-155* downregulation in endometriosis, a *miR-155*$^{-/-}$ mouse model was utilised.

The physiology of *miR-155*$^{-/-}$ mice has been well characterised, in which a deficiency in *miR-155* does not impact the development and growth of naturally ageing mice (Zhang et al., 2017a). However, the immunological prolife of *miR-155*$^{-/-}$ mice differs from *miR-155* replete mice. *miR-155*$^{-/-}$ mice exhibit reduced eosinophilic inflammation in response to a chronic allergen exposure, with reduced IL-33 signalling (Johansson et al., 2017). A significant reduction in the inflammatory genes *Inos*, *Il-1β*, and *Tnf-α* was observed in M1-like macrophages derived from *miR-155*$^{-/-}$ mice, while the expression of the M2-like macrophage gene *Arg1* was unchanged between *miR-155* deficient and replete mice (Jablonski et al., 2016).

Thus, to evaluate the contribution of *miR-155* on macrophage activity during the development of endometriosis, a *miR-155*$^{-/-}$ menstrual mouse model of endometriosis was developed, in which 40mg of *miR-155*$^{-/-}$ donor decidualised endometrial tissue was injected subcutaneously into syngeneic recipient mice. Characterisation of endometriosis-like lesion size, weight, and glandular fractions was carried out at D7, D14 and D21. Immunohistochemical assessment of macrophage localisation (F4/80 staining), M1-like markers (MHC II and iNOS) and M2-like markers (CD206 and Arg-1), blood vessel density (vWF), and myofibroblast abundance (αSMA) was performed with Masson's trichrome staining to assess the extent of fibrosis. The differential expression of genes between donor decidualised endometrium, D7 and D14 lesions was assessed via RNA-Sequencing (RNA-Seq). Additional comparisons were made between *miR-155*$^{-/-}$ and C57 (wildtype control strain) data at corresponding time points, with the original C57 data presented in Chapter 3 of this thesis. Finally, reciprocal transfers between *miR-155*$^{-/-}$ mice and C57 mice were performed to determine whether a *miR-155* deficiency only in the donor endometrium or only in the host response alters lesion development over the course of three weeks.

4.2. RESULTS

4.2.1. Endometriosis-like lesion development in *miR-155* deficient mice

To assess the contribution of *miR-155* during lesion development in endometriosis, a *miR-155*$^{-/-}$ menstrual mouse model of endometriosis was developed. In this model, 40mg of *miR-155*$^{-/-}$ decidualised donor endometrial tissue was subcutaneously injected into *miR-155*$^{-/-}$ recipient mice. To evaluate the extent of disease establishment, endometriosis-like lesions that developed at D7, D14 and D21 were analysed for size, weight, and glandular fractions.

A total of 53 *miR-155*$^{-/-}$ donor mice were required to generate sufficient decidualised endometrial tissue for transfer into recipient mice at a ratio of 1 donor to 1 recipient. Overall, throughout the duration of this experiment, 91% of *miR-155*$^{-/-}$ recipient mice had identifiable endometriotic-like lesions (Table 4.1). At D7, 90.0% of recipient mice had lesions, at D14, 94.4% of recipient mice had lesions, and at D21, 86.7% of recipient mice had lesions. One mouse had more than one lesion and has been excluded from subsequent analyses.

Lesion morphology was assessed across the time course. At D7, lesions were large, raised from the site of attachment, and appeared white (Figure 4.1 A). At both D14 (Figure 4.1 B) and D21 (Figure 4.1 C), lesions were round, small and opaque, with a black/blood-filled appearance, and showed signs of vascularisation to the surrounding tissue. Lesion size decreased significantly between D7 and D14 (45 (13 – 164) mm^3 *versus* 6 (2.0 – 12.5) mm^3 respectively, $p = 0.0005$), with no differences seen at D21 (12 (8 – 12) mm^3) (Figure 4.1 D). Lesion weight in *miR-155*$^{-/-}$ mice was 37.70 (24.10 – 58.35) mg at D7, and significantly decreased by 82% at D14 (6.90 (4.65 – 12.40) mg, $p = 0.0014$). At D21, lesions weighed 3.90 (3.25 – 4.65) mg, 90% lighter than D7 lesions ($p < 0.0001$) (Figure 4.1 E).

Analysis of morphological parameters from H&E stained lesion sections showed that at D7 (Figure 4.2 A), D14 (Figure 4.2 B), and D21 (Figure 4.2 C), lesions appeared similar, with visible gland formation across all time points (indicated by arrows). No differences were observed in the median number of glands per lesion, gland size, lumen area within glands, epithelium area of glands, percentage glandular epithelium of lesions and the percentage stromal across all time points (Figure 4.2 D-I).

Table 4.1 Endometriosis-like lesion recovery in *miR-155*$^{-/-}$ mice

Lesion collection time point	D7	D14	D21
Total number of donor mice used across all time points: 50			
Number of recipient mice	20	18	15
Number of mice with lesions*	18	17	13
Proportion of mice with lesions (%)	90.0	94.4	86.7

* To reduce bias, mice with ≥2 lesions were excluded from subsequent analyses. At D7 - 1 mouse excluded.

4.2.1.1. Comparison of endometriosis-like lesion progression between C57 mice and *miR-155* deficient mice

Although the systemic depletion of *miR-155* in mice resulted in a significant decrease in both lesion size and weight from D7 to D21, no significant alterations were observed in morphometric parameters within these endometriotic-like lesions. To further evaluate the effect of *miR-155* on the development of endometriosis, a comparative analysis between *miR-155* deficient lesions (*miR-155*$^{-/-}$) and *miR-155* sufficient lesions (C57) was performed.

Lesion size was significantly different between C57 and *miR-155*$^{-/-}$ mice (Figure 4.3 A) on D7, with lesions in *miR-155*$^{-/-}$ mice being 3-fold larger than C57 lesions (p = 0.0165). At D14, lesions reduced in size in both groups, and although *miR-155*$^{-/-}$ lesions were larger than C57 lesions, this was not significantly different. At D21, lesions from *miR-155*$^{-/-}$ mice were 1.7-fold larger than C57 lesions (p = 0.0469). Similarly, lesion weight (Figure 4.3 B) at D7 was significantly heavier in *miR-155*$^{-/-}$ mice compared to C57 mice (increase of 2.4-fold, p = 0.0011). At both D14 and D21, lesions in *miR-155*$^{-/-}$ mice were 1.4-fold heavier than C57 lesions at the same time point, however this did not reach significance (p = 0.5631 and p = 0.0722 respectively).

The median number of glands per lesion (Figure 4.3 C) remained consistent in *miR-155*$^{-/-}$ mice over the all three time points, however in C57 mice, values steadily increased. At D14, *miR-155*$^{-/-}$ lesions had 80% fewer glands than C57 lesions (p = 0.0103), and at D21, *miR-155*$^{-/-}$ lesions had 70% fewer glands than C57 lesions (p < 0.0001). The average gland size (Figure 4.3 D) was comparable between *miR-155*$^{-/-}$ and C57 lesions across all time points. Lumen area (Figure 4.3 E) and epithelium area measurements (Figure 4.3 F) followed a similar trend, wherein at D21, *miR-155*$^{-/-}$ lesions had 90% less lumen area (p = 0.0194) and 87% less epithelial area within glands (p = 0.0009) compared to C57 lesions. The percentage glandular epithelium within lesions (Figure 4.3 G) was not significantly different between *miR-155*$^{-/-}$ and C57 lesions at D7 and D14, however, at D21, *miR-155*$^{-/-}$ lesions had 84% less glandular epithelium than C57 lesions (p = 0.0013). Correspondingly, measurements of percentage stromal area (Figure 4.3 H) was similar between *miR-155*$^{-/-}$ and C57 lesions across D7 and D14, whereas at D21, *miR-155*$^{-/-}$ lesions had 1.02-fold more stromal area (p = 0.0059). These observations suggest that the development of endometriotic-like lesions in C57 and *miR-155*$^{-/-}$ mice may progress in a comparable manner as indicated by comparable morphometric parameters at D14. However, the noticeable difference in size and weight at D7 may be indicative of a delayed immune response which ultimately results in noticeable differences in lesion morphology at D21.

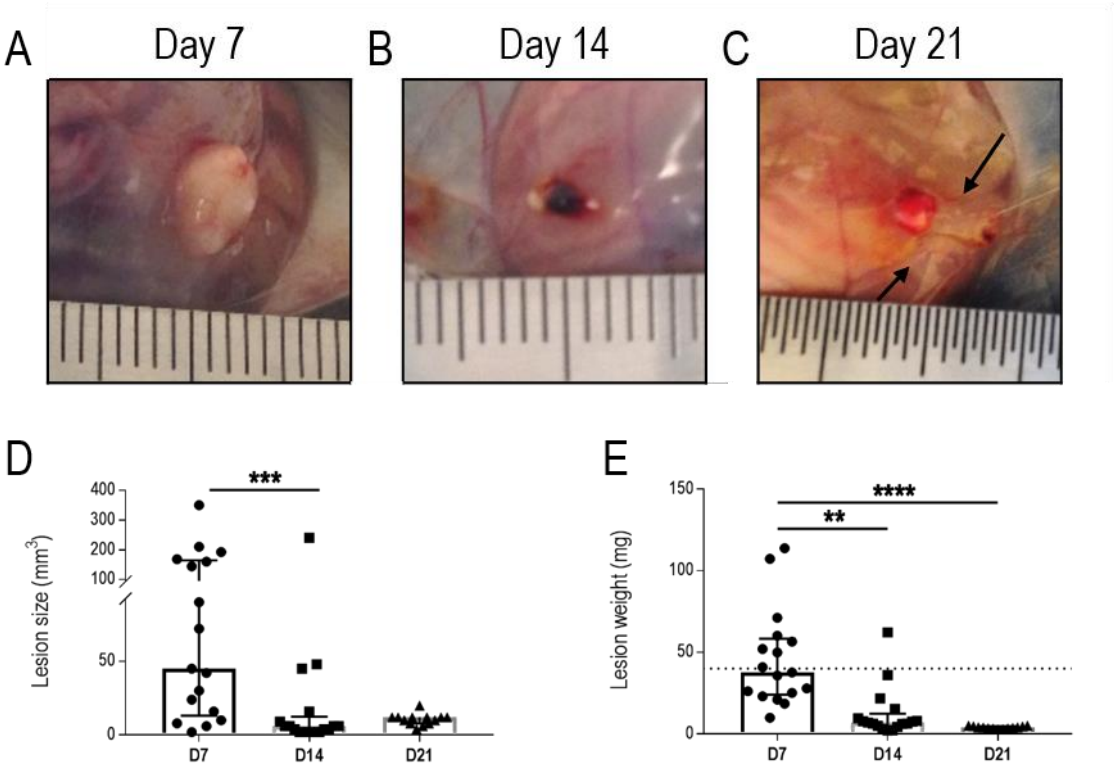

Figure 4.1 Gross morphology of endometriosis-like lesion development in *miR-155*$^{-/-}$ mice

Decidualised *miR-155*$^{-/-}$ donor endometrial tissue was injected subcutaneously into syngeneic recipient mice. Resulting lesions were harvested at either D7 (**A**), D14 (**B**) or D21 (**C**), with representative images shown; arrow indicates evidence of vascularisation. Lesion size was measured (**D**) and lesions were excised and weighed (**E**), with the dotted line indicating the initial weight of donor decidualised endometrial tissue inoculated into recipient mice. Data are presented as median (IQR), with each symbol representative of a single lesion in one mouse (n=17 at D7, n=17 at D14, n=13 at D21). Analysis was done using the Kruskal-Wallis test followed by Dunn's multiple comparison test, with significance denoted as ** ($p < 0.01$), *** ($p < 0.001$), and **** ($p < 0.0001$).

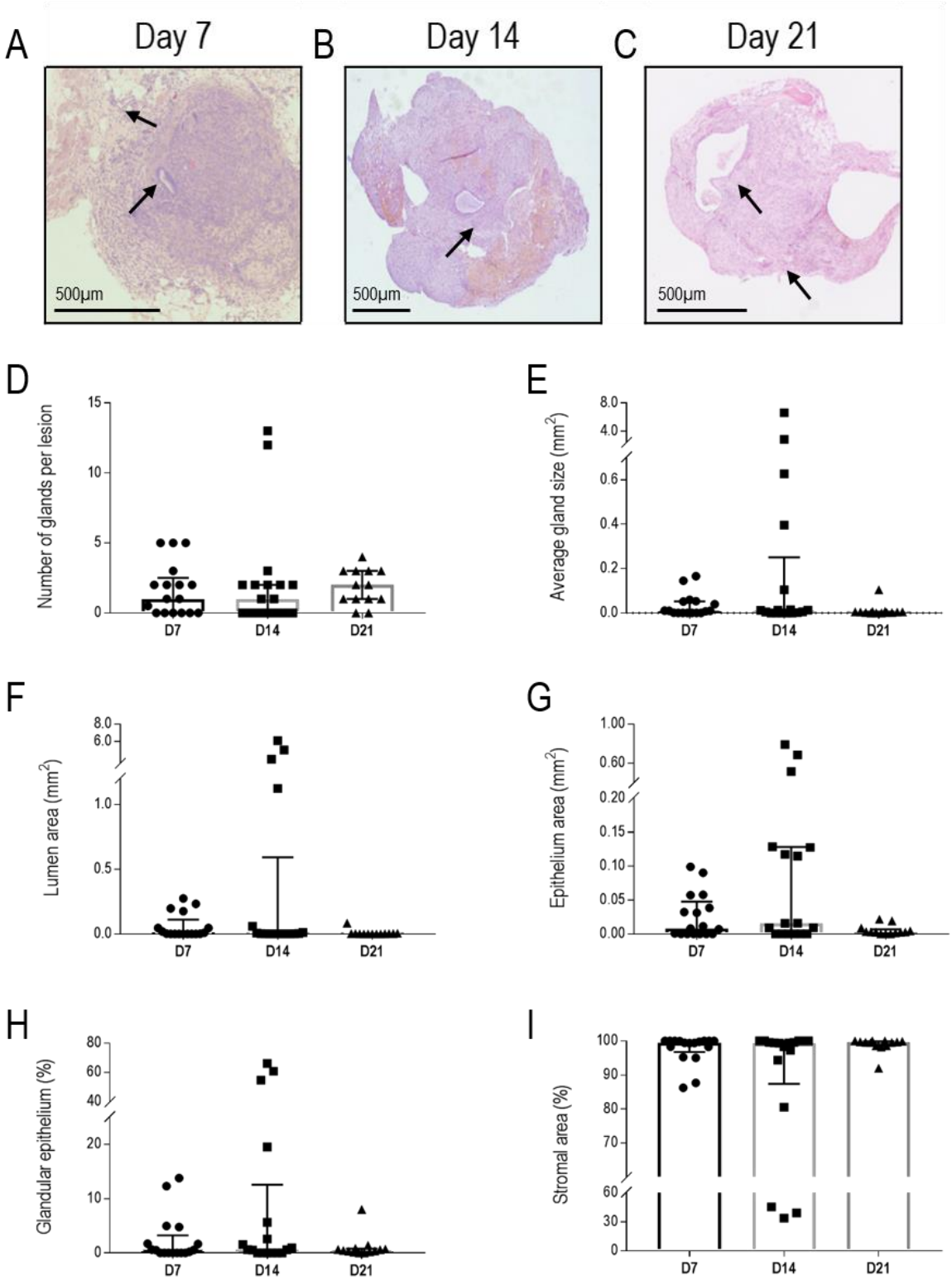

Figure 4.2 **Assessment of morphological parameters in haematoxylin and eosin stained endometriosis-like lesions from *miR-155*$^{-/-}$ mice**

Haematoxylin and eosin stained sections from D7 **(A)**, D14 **(B)**, and D21 **(C)** lesions in *miR-155*$^{-/-}$ mice (representative images shown; arrows indicate glands) were assessed for the following characteristics: number of glands per lesion **(D)**, average gland size **(E)**, lumen area **(F)**, epithelium area **(G)**, percentage glandular epithelium **(H)** and percentage stromal area **(I)**. Data are presented as median (IQR), with each symbol representative of a single lesion in one mouse (n=17 at D7, n=17 at D14, n=13 at D21). Analysis was done using the Kruskal-Wallis test followed by Dunn's multiple comparison test.

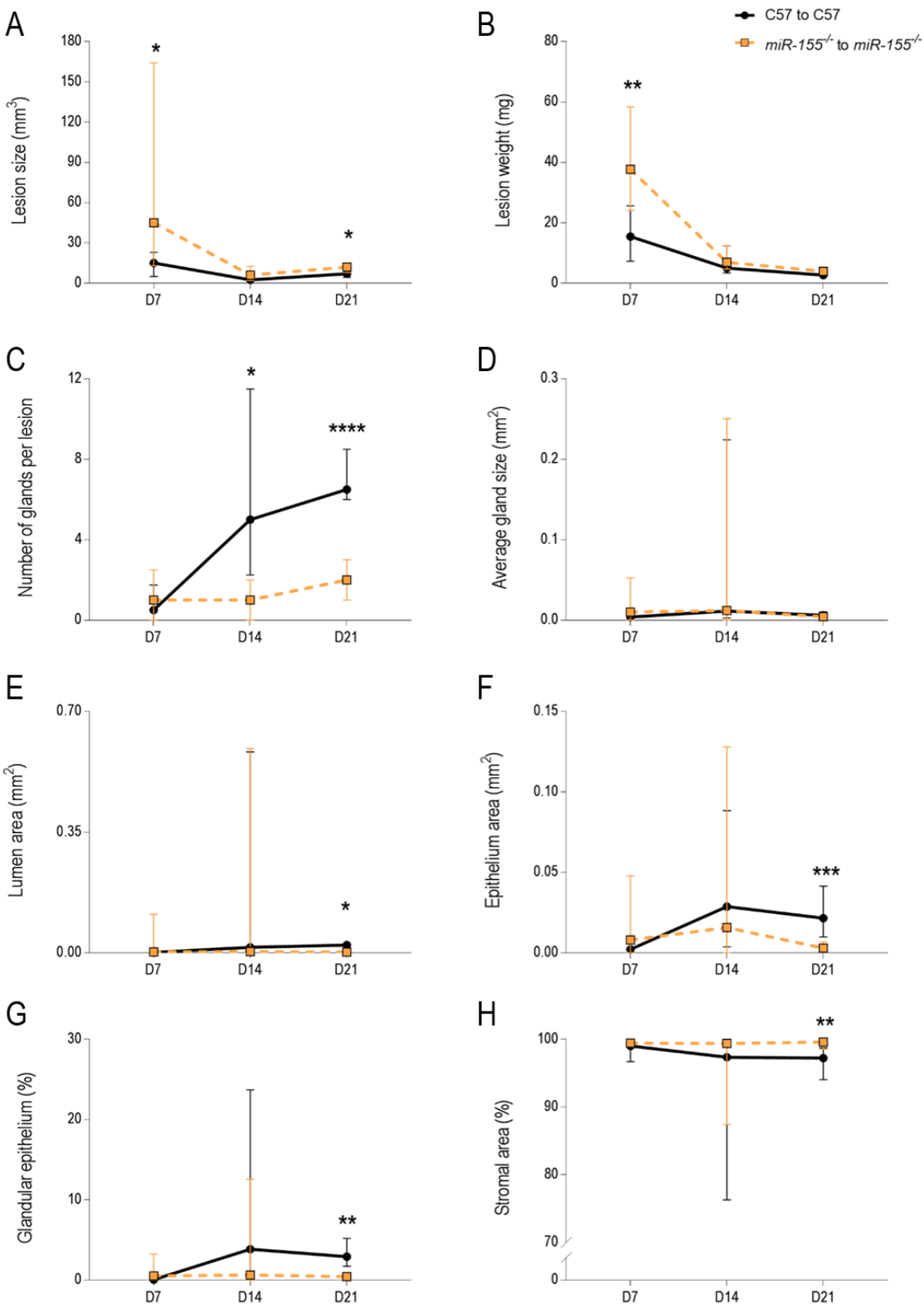

Figure 4.3 **Comparative analysis of morphometric parameters between C57 and *miR-155*$^{-/-}$ endometriosis-like lesions**

Lesion size (**A**), weight (**B**), number of glands per lesion (**C**), average gland size (**D**), lumen area (**E**), epithelium area (**F**), glandular epithelium (**G**), and stromal area (**H**) were compared between C57 mice (; n=12 at D7, n=12 at D14, n=8 at D21) and *miR-155*$^{-/-}$ mice (; n=17 at D7, n=17 at D14, n=13 at D21).Data are presented as median (IQR). Analysis was done using the Mann Whitney U test, with significance denoted as * ($p < 0.05$), ** ($p < 0.01$), *** ($p < 0.001$) and **** ($p < 0.0001$).

4.2.2. Macrophage localisation in endometriosis-like lesions from *miR-155* deficient mice

miR-155 is a crucial regulator of M1-like inflammatory macrophage activity (Faraoni et al., 2009, Kurowska-Stolarska et al., 2011, Tili et al., 2011, Jablonski et al., 2016). Depletion of *miR-155* in macrophages resulted in an increased repolarisation of macrophages from the M1-like phenotype to the M2-like phenotype (Cai et al., 2012). In endometriosis, a predominance of M2-like macrophages supports lesion growth by restricting tissue clearance and increasing tissue healing and remodelling (Bacci et al., 2009). Thus, in this section, macrophage activity and remodelling of endometriosis-like lesions in *miR-155*$^{-/-}$ mice was evaluated.

F4/80 immunostaining was used to detect the presence of macrophages in *miR-155*$^{-/-}$ lesions (Figure 4.4). Density of F4/80^{+} cells across the entire lesion was similar at D7 (8.37 (6.53 – 9.83) %) and D14 (9.51 (6.63 – 14.58) %). A significant increase in F4/80 expression as seen at D21 (16.41 (11.99 – 24.34) %, p = 0.0001 for D7 *vs* D21 and p = 0.0111 for D14 *vs* D21) (Figure 4.4 G). There was a trend towards increased peripheral F4/80 density, with a median of 14.36 (12.46 – 21.97) % at D7, 14.47 (13.06 – 24.78) % at D14 and 20.13 (16.36 – 26.13) % at D21, however this was not significant (Figure 4.4 A-C, H). Central F4/80 density in *miR-155*$^{-/-}$ lesions was lowest at D7 (3.26 (1.75 – 4.35) %), and was similar to D14 values (5.28 (2.61 – 20.53) %). A significant increase in the central distribution of F4/80^{+} cells was seen at D21 (29.67 (22.47 – 41.61) %, p < 0.0001 for D7 *vs* D21 and p = 0.0034 for D14 *vs* D21).

4.2.2.1. Expression of pro-inflammatory M1-like markers in *miR-155* deficient mice

M1-like activity in *miR-155*$^{-/-}$ lesions was evaluated immunohistochemically with antibodies to detect iNOS (Figure 4.5 A-C) and MHC II (Figure 4.5 D-F) expression. The median density of iNOS was similar at D7 and D14 (15.06 (12.46 – 16.87) % and 18.34 (15.03 – 34.34) % respectively), while iNOS density was highest at D21 (27.22 (19.73 – 34.34) %, p = 0.0005 for D7 *vs* D21) (Figure 4.5 G). Peripheral iNOS density followed a similar trend, with similar values at D7 and D14 (14.49 (12.74 – 17.83) % and 17.32 (15.81 – 20.09) % respectively), and a significant increase at D21 (24.26 (18.81 – 25.64) %, p < 0.0001 for D7 *vs* D21) (Figure 4.5 H). Likewise, central iNOS density was consistent at D7 and D14 (9.64 (8.36 – 14.18) % and 11.26 (9.36 – 15.95) % respectively), with a significant increase at D21 (44.00 (39.05 – 50.63) %, p < 0.0001 for D7 *vs* D21 and p < 0.0001 for D14 *vs* D21) (Figure 4.5 I).

Interestingly, in *miR-155*$^{-/-}$ lesions, MHC II density increased significantly between D7 and D14 (1.74 (1.46 – 3.52) % and 5.53 (4.40 – 7.46) %, respectively, p < 0.0001). However, at D21, median MHC II density

reduced to 3.50 (2.58 – 5.84) %, and was not significantly different from either D7 or D14 values (Figure 4.5 J). Peripheral MHC II density was significantly higher at D14 (5.51 (4.29 – 6.23) %) compared to D7 (2.83 (2.19 – 3.53) %, $p < 0.0001$) and D21 (3.73 (3.13 – 4.60) %, $p = 0.0472$) (Figure 4.5 K).Central MHC II density followed a similar trend, with significantly higher D14 values (6.26 (5.35 – 6.83) %) compared to both D7 (4.24 (3.24 – 4.24) %, $p = 0.0111$) and D21 (3.85 (2.99 – 4.49) %, $p = 0.0010$) (Figure 4.5 L).

4.2.2.2. Expression of alternatively activated M2-like markers in *miR-155* deficient mice

Detection of M2-like activity in *miR-155*$^{-/-}$ lesions was performed with antibodies against CD206 (Figure 4.6 A-C) and Arg-1 (Figure 4.6 D-F). CD206 density increased between D7 and D14 (22.14 (17.61 – 27.88) % and 32.48 (20.21 – 42.72) % respectively, $p = 0.0371$). At D21, the density of CD206 was 34.77 (32.51 – 44.50) % which was significantly higher than D7 ($p = 0.0002$), but was similar to D14 (Figure 4.6 G). Peripheral CD206 density was lowest at D7 (9.45 (5.55 – 13.30) %) and significantly increased at D14 (28.90 (26.29 – 33.26) %, $p < 0.0001$) and D21 (28.25 (22.16 – 34.84) %, $p < 0.0001$ for D7 *vs* D21) (Figure 4.6 H). Likewise, central CD206 density was lowest at D7 (9.01 (5.96 – 11.02) %) and significantly increased at D14 (27.26 (22.85 – 31.14) %, $p < 0.0001$) and D21 (32.13 (26.32 – 36.39) %, $p < 0.0001$ for D7 *vs* D21) (Figure 4.6 I).

On the other hand, Arg-1 density was similar at D7 and D14 (37.78 (32.19 – 46.93) % and 44.43 (31.96 – 54.59) % respectively), but increased at D21 (48.77 (40.93 – 62.44) %, $p = 0.0061$ for D7 *vs* D21) (Figure 4.6 J). Peripheral Arg-1 density was consistent at D7 and D14 (39.04 (31.61 – 42.62) % and 38.07 (34.53 – 43.21) % respectively), with a significant increase at D21 (45.26 (38.14 – 48.65) %, $p = 0.0220$ for D7 *vs* D21 and $p = 0.0475$ for D14 *vs* D21) (Figure 4.6 K). Central Arg-1 density increased between D7 (36.23 (33.25 – 46.12) %), D14 (44.89 (40.85 – 51.09) %) and D21 (48.65 (45.19 – 58.10) %, $p = 0.0013$ for D7 *vs* D21) (Figure 4.6 L).

4.2.3. Blood vessel density, myofibroblast abundance and fibrosis in endometriosis-like lesions from *miR-155* deficient mice

Using vWF immunostaining (Figure 4.7 A-C), the total density of blood vessels in *miR-155*$^{-/-}$ lesions was similar across all time points (0.73 (0.53 – 0.90) % at D7, 0.83 (0.59 – 0.91) % at D14, and 0.85 (0.74 – 1.28) % at D21) (Figure 4.7 D). A gradual increase in the number of blood vessels per lesion was observed between D7 (12 (9 – 14)), D14 (15 (12 – 18)), and D21 (21 (15 – 23), $p < 0.0001$ for D7 *vs* D21) (Figure 4.7 E). Surprisingly, an opposite trend was observed in measurements of average vessel size, which

steadily reduced over time (0.0030 (0.0023 – 0.0070) mm^2 at D7, 0.0019 (0.0014 – 0.0024) mm^2 at D14, and 0.0004 (0.0004 – 0.0014) mm^2 at D21; $p < 0.0001$ for D7 *vs* D21 and $p = 0.0101$ for D14 *vs* D21) (Figure 4.7 F).

The expression of αSMA (Figure 4.8 A-C) strongly localised to blood vessels within lesions, and was unchanged across D7 (22.63 (18.34 – 29.45) %), D14 (27.44 (21.55 – 44.27) %) and D21 (30.92 (25.24 – 51.53) %) (Figure 4.8 G). From the Masson's trichrome staining (Figure 4.8 D-F), there was no discernible difference in the density of fibrosis across all time points (17.63 (16.40 – 18.98) % at D7, 15.41 (14.19 – 19.03) % at D14, and 17.65 (15.56 – 19.57) % at D21) (Figure 4.8 H).

4.2.3.1. Comparison of macrophage localisation and cellular parameters between C57 mice and *miR-155* deficient mice

The systemic depletion of *miR-155* resulted in an increase in F4/80 positive cells between D7 and D21, coupled with an increase in M2-like macrophage markers. To further understand the effect of *miR-155* depletion on macrophage phenotype in the development of endometriosis, a comparative analysis between *miR-155* deficient lesions (*miR-155*$^{-/-}$) and *miR-155* sufficient lesions (C57) was performed (Figure 4.9 and 4.10).

At D7 and D21, total F4/80 density in endometriotic-like lesions was similar in both *miR-155*$^{-/-}$ and C57 mice (Figure 4.9 A). Interestingly, at D14, total F4/80 density was 44% lower in *miR-155*$^{-/-}$ lesions compared to C57 lesions ($p = 0.0007$). Peripheral F4/80 density at both D7 and D14 was significantly lower in *miR-155*$^{-/-}$ lesions compared to C57 lesions (64% decrease, $p = 0.0002$ and 64% decrease, $p = 0.0002$ respectively), but no differences were observed at D21 (Figure 4.9 B). Central F4/80 expression was similar between strains at D7 and D21, however *miR-155*$^{-/-}$ lesions had 85% less central F4/80 expression at D21 ($p = 0.0002$) (Figure 4.9 C).

Quantification of M1-like expression showed 36% fewer cells expressing iNOS in *miR-155*$^{-/-}$ lesions compared to C57 lesions at D7 ($p = 0.0009$) (Figure 4.9 D). At D14, iNOS density remained consistent between both groups, whereas, a 1.6-fold increase in iNOS expression was seen in *miR-155*$^{-/-}$ lesions compared to C57 lesions at D21 ($p = 0.0077$). Peripheral iNOS density was 23% lower in *miR-155*$^{-/-}$ lesions compared to C57 lesions at D7 ($p = 0.0037$), however at D14 and D21, *miR-155*$^{-/-}$ lesions had significantly more peripheral iNOS compared to C57 lesions (1.6-fold increase, $p < 0.0001$ and 1.4-fold increase, $p = 0.0126$) (Figure 4.9 E). Central iNOS density remained significantly higher in *miR-155*$^{-/-}$ lesions compared to C57 lesions across all time points (1.3-fold increase, $p = 0.0011$ at D7, 1.6-fold increase, $p < 0.0001$ at D14, and 4.2-fold increase, $p < 0.0001$ at D21) (Figure 4.9 F).

When compared with *miR-155*$^{-/-}$ lesions, MHC II density was significantly lower in *miR-155*$^{-/-}$ lesions compared to C57 lesions at all time points (91% decrease, $p < 0.0001$ at D7, 55% decrease, $p = 0.0208$ at D14, and 85% decrease, $p < 0.0001$ at D21) (Figure 4.9 G). Peripheral MHC II density was significantly lower in *miR-155*$^{-/-}$ lesions compared to C57 lesions at all three time points (76% decrease, $p < 0.0001$ at D7; 46% decrease, $p < 0.0001$ at D14; and 83% decrease, $p < 0.0001$ at D21) (Figure 4.9 H). Similarly, central MHC II density was significantly lower in *miR-155*$^{-/-}$ lesions compared to C57 lesions at all three

time points (51% decrease, $p < 0.0001$ at D7; 15% decrease, $p = 0.0243$ at D14; and 65% decrease, $p < 0.0001$ at D21) (Figure 4.9 I).

Expression of the M2-like marker CD206 was 3-fold higher in *miR-155*$^{-/-}$ lesions compared to C57 lesions at D7 ($p < 0.0001$), and 1.7-fold higher at D14 ($p = 0.0426$), however no differences in CD206 density was observed at D21 (Figure 4.9 J). Peripheral CD206 density was significantly higher in *miR-155*$^{-/-}$ lesions compared to C57 lesions across all time points (3.7-fold increase, $p < 0.0001$ at D7; 4.8-fold increase, $p < 0.0001$ at D14; and, 1.8-fold increase, $p = 0.0003$ at D21) (Figure 4.9 K). Central CD206 density was consistent between strains at D7 and D14, however, a 30% decrease was observed in *miR-155*$^{-/-}$ lesions compared to C57 lesions at D21 ($p = 0.0004$) (Figure 4.9 L).

Arg-1 density was significantly higher in *miR-155*$^{-/-}$ lesions compared to C57 lesions across all time points (1.7-fold increase, $p < 0.0001$ at D7; 2-fold increase, $p < 0.0001$ at D14; and, 2-fold increase, $p < 0.0001$ at D21) (Figure 4.9 M). Similarly, peripheral Arg-1 density was significantly higher in *miR-155*$^{-/-}$ lesions compared to C57 lesions across all time points (8.7-fold increase, $p < 0.0001$ at D7; 2.7-fold increase, $p < 0.0001$ at D14; and, 2.8-fold increase, $p < 0.0001$ at D21) (Figure 4.9 N). Likewise, central Arg-1 density was significantly higher in *miR-155*$^{-/-}$ lesions compared to C57 lesions across all time points (3.1-fold increase, $p < 0.0001$ at D7; 2.3-fold increase, $p < 0.0001$ at D14; and, 2.3-fold increase, $p < 0.0001$ at D21) (Figure 4.9 O).

vWF density was 1.9-fold higher in *miR-155*$^{-/-}$ lesions compared to C57 lesions at D7 ($p = 0.0007$), and 1.8-fold higher at D14 ($p = 0.0106$), whereas similar vWF expression was observed between strains at D21 (Figure 4.10 A). The number of blood vessels per lesion in *miR-155*$^{-/-}$ mice was 2.4-fold higher at D7 ($p = 0104$), 30% lower at D14 ($p = 0.0007$) and unchanged at D21 when compared to lesions from C57 mice (Figure 4.10 B). Average vWF^{+} blood vessel size remained significantly higher in *miR-155*$^{-/-}$ lesions compared to C57 lesions at both D7 and D14 (8.6-fold increase, $p < 0.0001$ and 4.6-fold increase, $p < 0.0001$ respectively), but was similar at D21 (Figure 4.10 C). The density of αSMA was higher in *miR-155*$^{-/-}$ lesions compared to C57 lesions at all time points, however this was only significant at D7 (1.5-fold increase, $p = 0.0380$) and D14 (1.5-fold increase, $p = 0.0002$) (Figure 4.10 D). Interestingly, the extent of fibrosis as quantified using Masson's trichrome staining was significantly lower in *miR-155*$^{-/-}$ lesions compared to C57 lesions at all three time points (27% decrease, $p = 0.0141$ at D7; 41% decrease, $p = 0.0037$ at D14; and 43% decrease, $p < 0.0001$ at D21) (Figure 4.10 E).

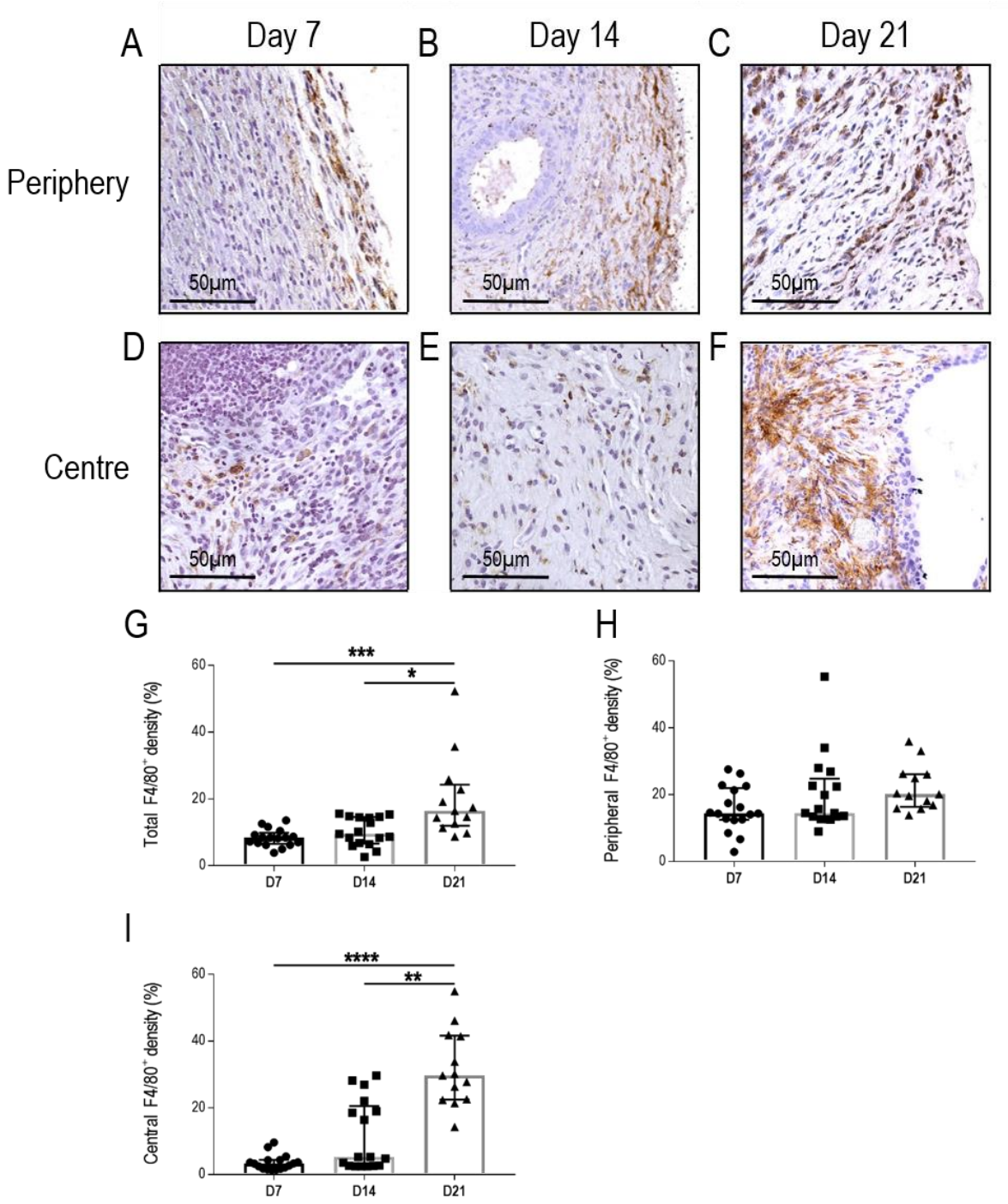

Figure 4.4 F4/80 immunostaining in endometriosis-like lesions from *miR-155*$^{-/-}$ mice

Quantification of total F4/80 density was carried out in lesions from *miR-155*$^{-/-}$ mice (**G**). F4/80 density at the lesion periphery (100µM from the edge of the lesion) at D7 (**A**), D14 (**B**) and D21 (**C**) was evaluated (**H**). F4/80 density at the lesion centre (within 500µM from the centre) at D7 (**D**), D14 (**E**), and D21 (**F**) was also quantified (**I**). Data are presented as median (IQR), with each symbol representative of a single lesion in one mouse (n=17 at D7, n=17 at D14, n=13 at D21). Analysis was done using the Kruskal-Wallis test followed by Dunn's multiple comparison test, with significance denoted as * ($p < 0.05$), *** ($p < 0.001$) and **** ($p < 0.0001$).

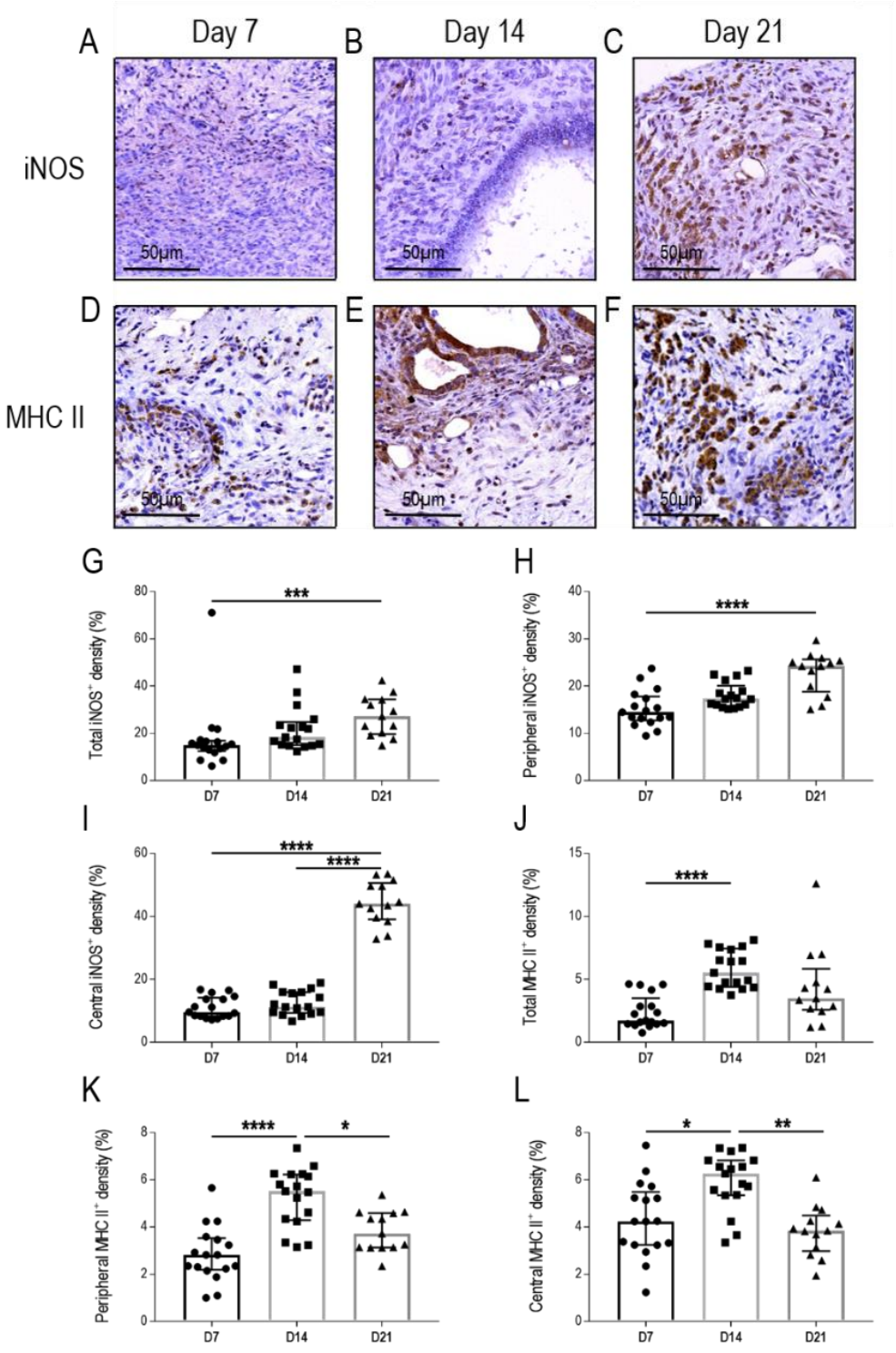

Figure 4.5 M1–like macrophage marker immunostaining in lesions from *miR-155*$^{-/-}$ mice

The expression of inducible nitric oxide synthase (iNOS) at D7 (**A**), D14 (**B**), and D21 (**C**) was quantified in *miR-155*$^{-/-}$ lesions (**G**). Further analysis was performed to determine peripheral (**H**) and central (**I**) iNOS density. Quantification of the Class II Major Histocompatibility Complex (MHC II) was done at D7 (**D**), D14 (**E**) and D21 (**F**) in these lesions (**J**), with peripheral (**K**) and central (**L**) MHC II density determined. Data are presented as median (IQR), with each symbol representative of a single lesion in one mouse (n=17 at D7, n=17 at D14, n=13 at D21). Analysis was done using the Kruskal-Wallis test followed by Dunn's multiple comparison test, with significance denoted as * ($p < 0.05$), ** ($p < 0.001$), *** ($p < 0.001$) and **** ($p < 0.0001$).

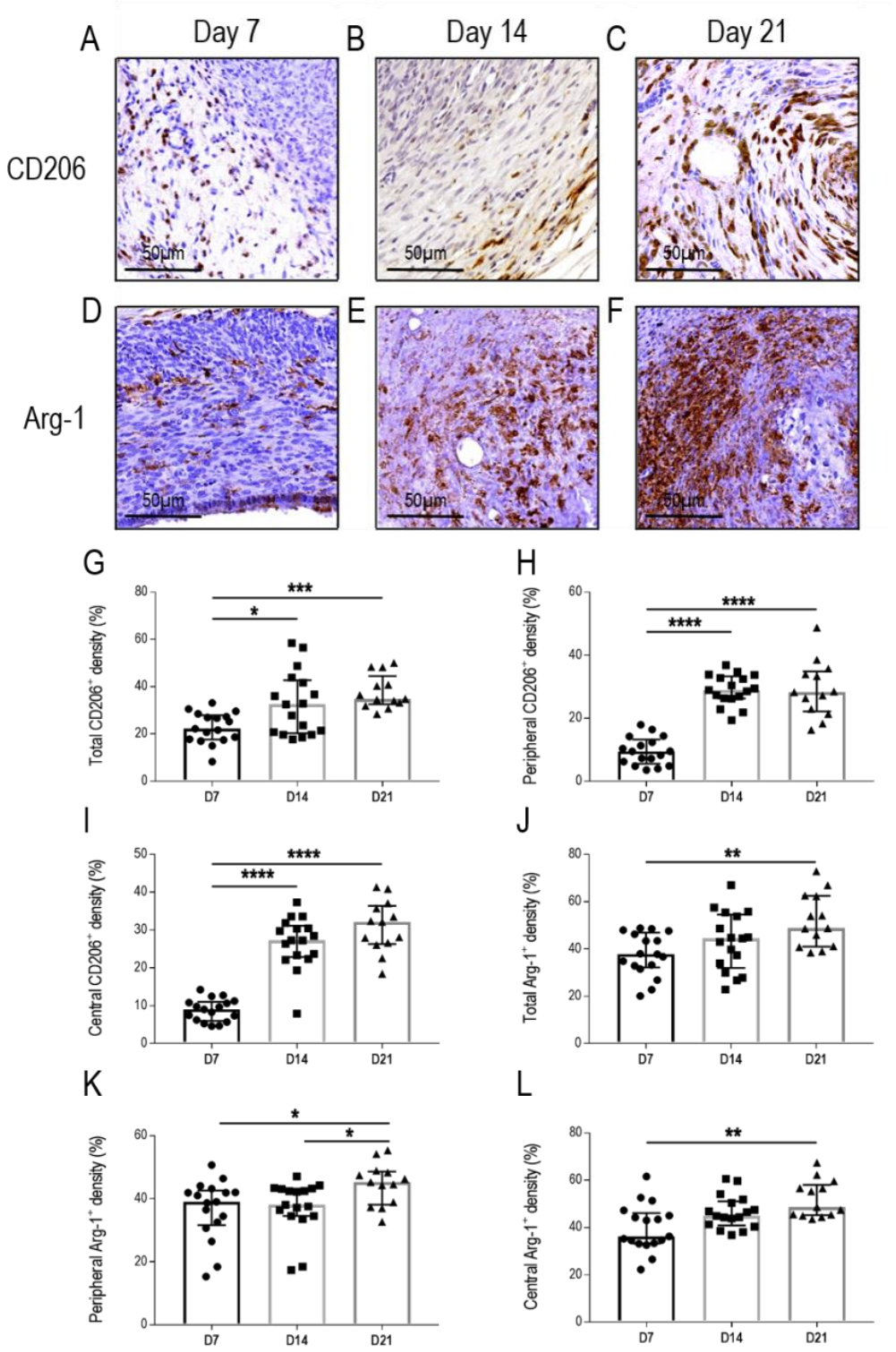

Figure 4.6 M2–like macrophage marker immunostaining in lesions from *miR-155*$^{-/-}$ mice

CD206 density at D7 (**A**), D14 (**B**), and D21 (**C**) was quantified in *miR-155*$^{-/-}$ lesions (**G**), with further analysis of peripheral (**H**) and central (**I**) CD206 density. Expression of Arginase-1 (Arg-1) was evaluated at D7 (**D**), D14 (**E**) and D21 (**F**) in these lesions (**J**), with peripheral (**K**) and central (**L**) Arg-1 density determined. Data are presented as median (IQR), with each symbol representative of a single lesion in one mouse (n=17 at D7, n=17 at D14, n=13 at D21). Analysis was done using the Kruskal-Wallis test followed by Dunn's multiple comparison test, with significance denoted as * ($p < 0.05$), ** ($p < 0.01$), *** ($p < 0.001$) and **** ($p < 0.0001$).

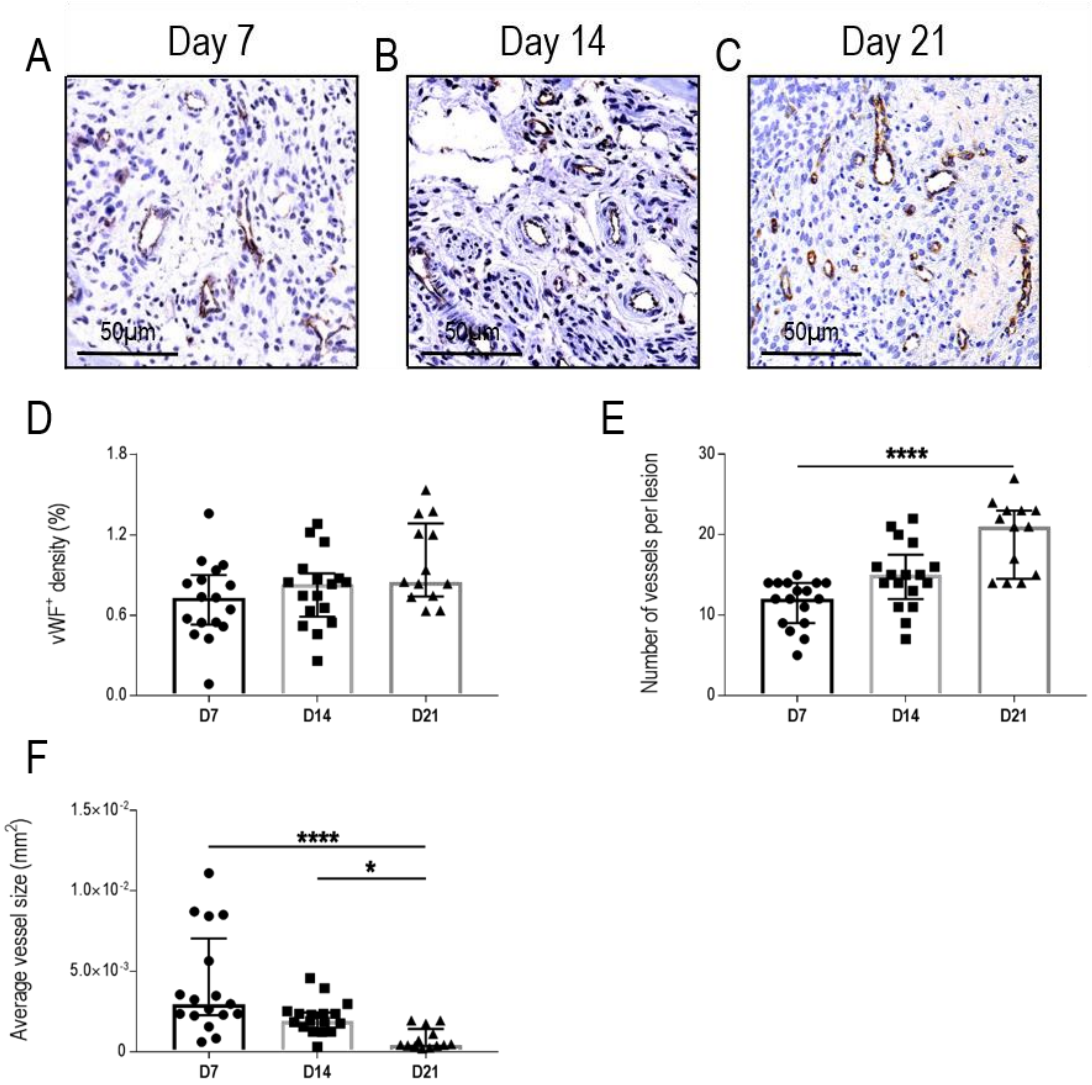

Figure 4.7 Blood vessel localisation in endometriosis-like lesions from *miR-155*$^{-/-}$ mice

Von Willebrand Factor (vWF) staining was used to localise blood vessels in lesions from *miR-155*$^{-/-}$ mice at D7 (**A**), D14 (**B**), and D21 (**C**). The total density of vWF^{+} vessels was quantified (**D**). The number of vessels per lesion (**E**) and the average vessel size (**F**) was determined. Data are presented as median (IQR), with each symbol representative of a single lesion in one mouse (n=17 at D7, n=17 at D14, n=13 at D21). Analysis was done using the Kruskal-Wallis test followed by Dunn's multiple comparison test, with significance denoted as * ($p < 0.05$) and **** ($p < 0.0001$).

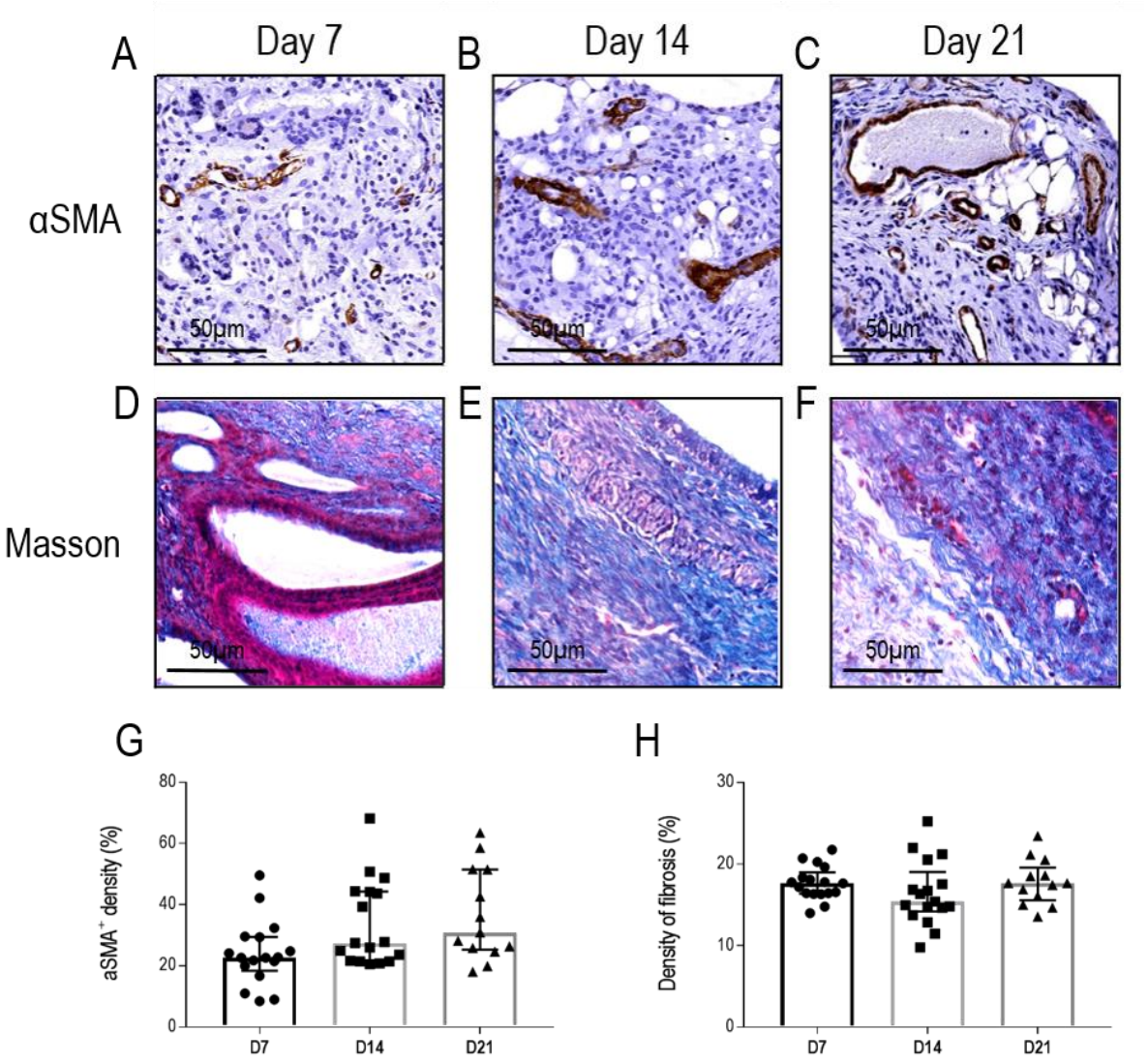

Figure 4.8 Evaluation of fibrosis in endometriosis-like lesions from *miR-155*$^{-/-}$ mice

The density of myofibroblasts in *miR-155*$^{-/-}$ lesions at D7 (**A**), D14 (**B**), and D21 (**C**) was evaluated using alpha smooth muscle actin (αSMA) (**G**). Masson's trichrome staining was used to evaluate the density of fibrosis (**H**) at D7 (**D**), D14 (**E**) and D21 (**F**) in these lesions. Data are presented as median (IQR), with each symbol representative of a single lesion in one mouse (n=17 at D7, n=17 at D14, n=13 at D21). Analysis was done using the Kruskal-Wallis test followed by Dunn's multiple comparison test.

Figure 4.9 Comparative analysis of the expression of macrophage markers between C57 and *miR-155*$^{-/-}$ endometriosis-like lesions

Total (**A**), peripheral (**B**), and central (**C**) F4/80 density were compared between C57 mice (; n=12 at D7, n=12 at D14, n=8 at D21) and *miR-155*$^{-/-}$ mice (; n=17 at D7, n=17 at D14, n=13 at D21). Comparisons between the M1-like macrophage markers inducible nitric oxide synthase (iNOS; total (**D)**, peripheral (**E**), and central (**F**)) and Class II Major Histocompatibility Complex (MHC II; total (**G)**, peripheral (**H**), and central (**I**)) were also performed. The density of the M2-like macrophage markers CD206 (total (**J)**, peripheral (**K**), and central (**L**)) and Arginase-1 (Arg-1; total (**M)**, peripheral (**N**), and central (**O**)) were also compared between strains. Data are presented as median (IQR). Analysis was done using the Mann Whitney U test, with significance denoted as * ($p < 0.05$), ** ($p < 0.01$), *** ($p < 0.001$), and **** ($p < 0.0001$).

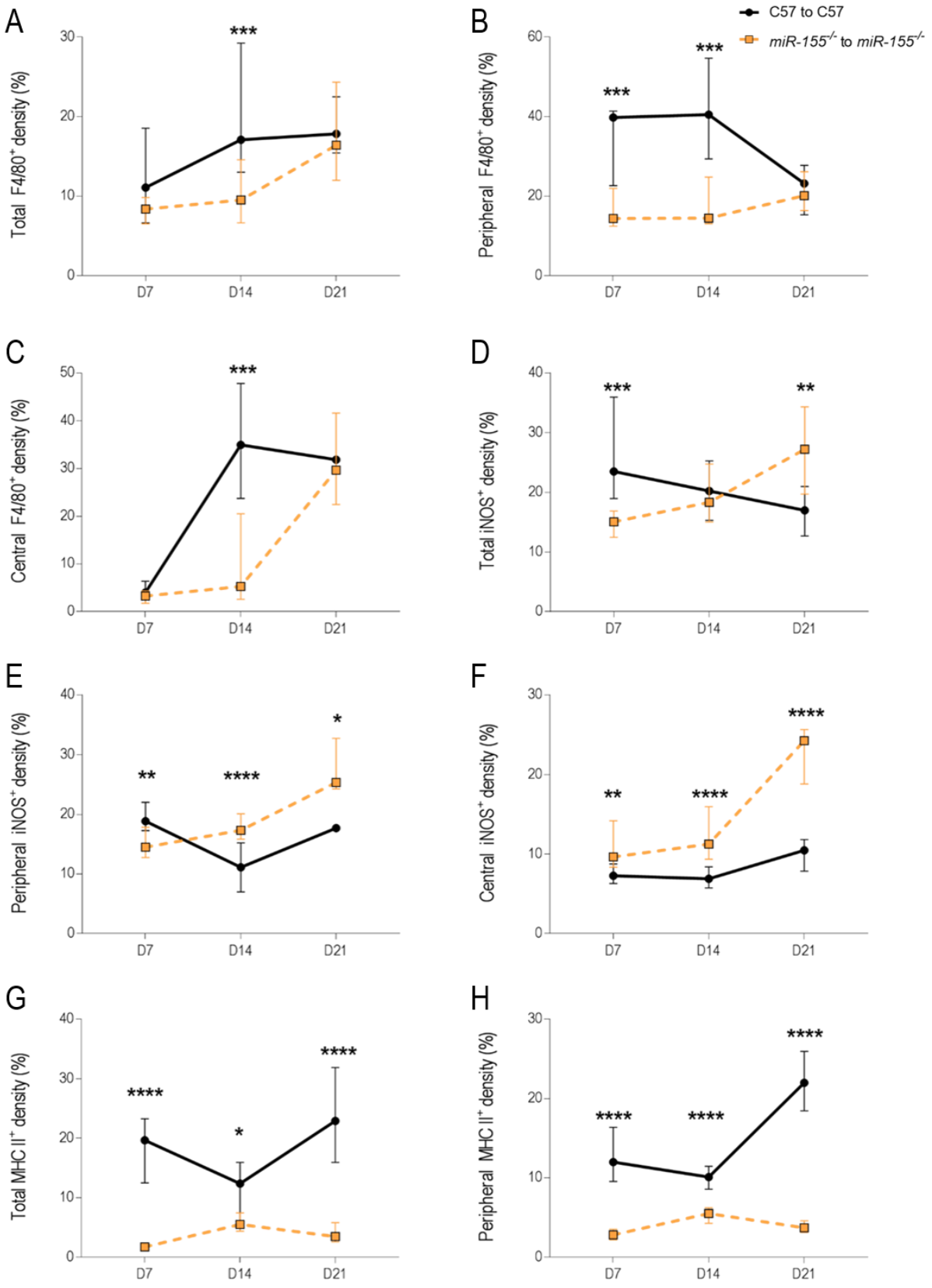

Figure 4.9 (A-H) Comparative analysis of the expression of macrophage markers between C57 and *miR-155*$^{-/-}$ endometriosis-like lesions

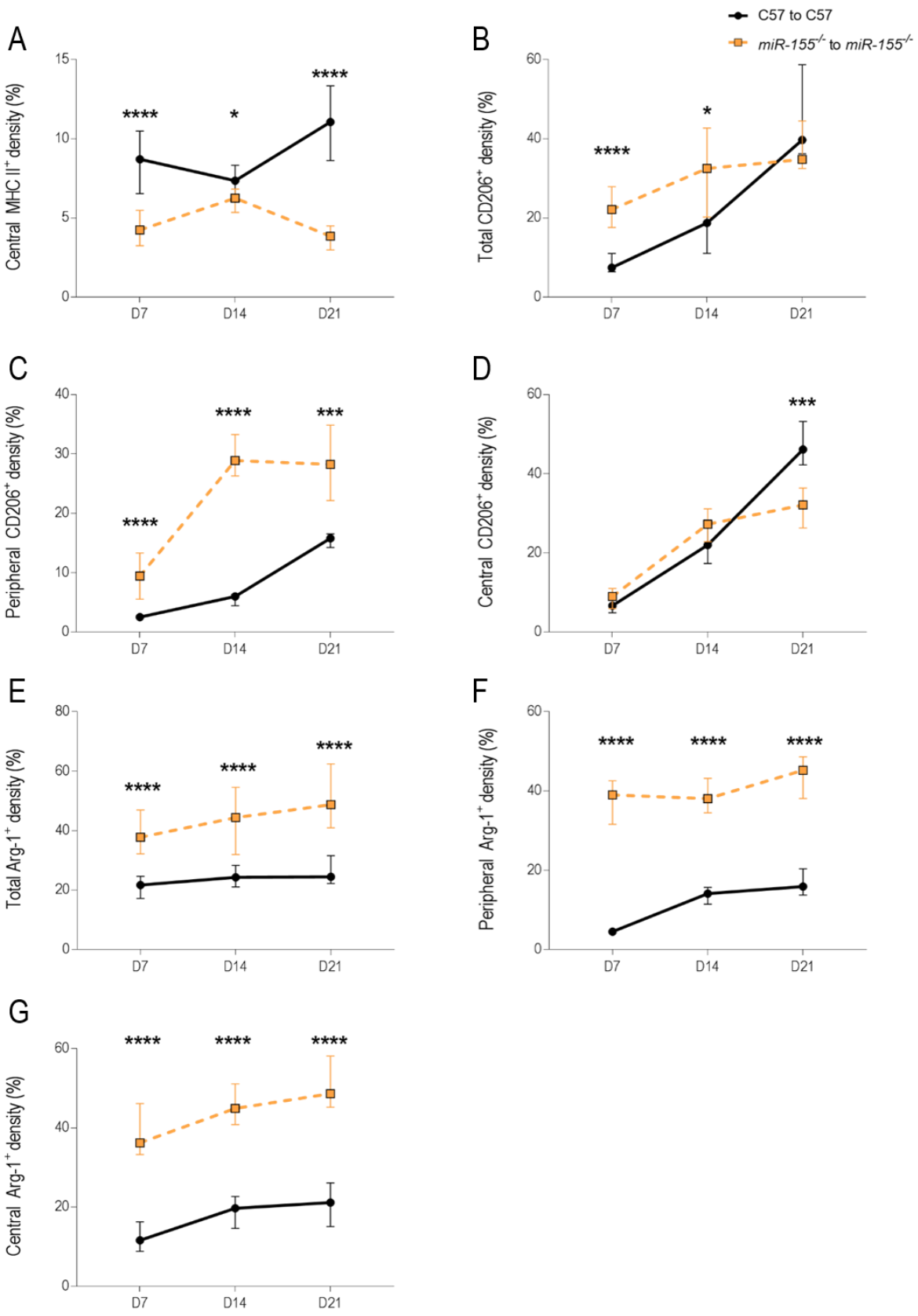

Figure 4.9 (I-O) **Comparative analysis of the expression of macrophage markers between C57 and *miR-155*$^{-/-}$ endometriosis-like lesions**

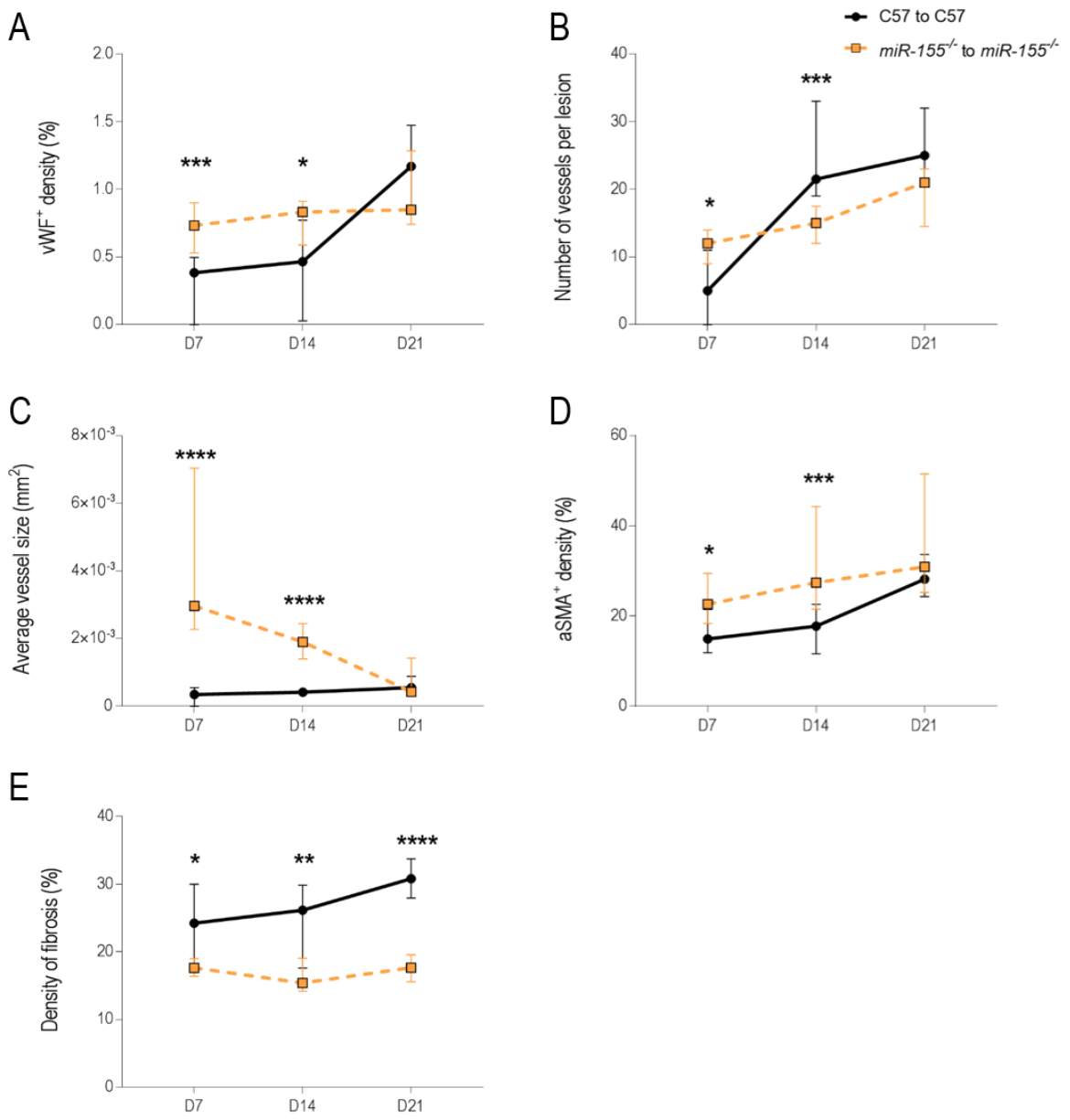

Figure 4.10 **Comparative analysis of blood vessel and fibrosis markers between C57 and *miR-155*$^{-/-}$ endometriosis-like lesions**

Total blood vessel density (**A**), number of vWF^{+} vessels per lesion (**B**), and average vessel size (**C**), density of myofibroblasts (**D**) and extent of fibrosis as measured by Masson's trichrome (**E**) were compared between C57 mice (; n=12 at D7, n=12 at D14, n=8 at D21) and *miR-155*$^{-/-}$ mice (; n=17 at D7, n=17 at D14, n=13 at D21). Data are presented as median (IQR). Analysis was done using the Mann Whitney U test, with significance denoted as * ($p < 0.05$), ** ($p < 0.01$), *** ($p < 0.001$), and **** ($p < 0.0001$).

4.2.4. RNA-Sequencing analysis of lesion progression in *miR-155* deficient mice

To evaluate the molecular changes in lesion development arising from a deficiency in *miR-155*, RNA-Sequencing (RNA-Seq) was performed on donor decidualised endometrial tissue, D7 and D14 lesions (See Appendix: Figure 7.2 and Figure 7.3 for RNA-Seq metrics). The RNA-Seq dataset was filtered to remove genes with a low expression, resulting in 16,291 genes being identified and analysed. The average gene expression of decidualised endometrium, D7 and D14 lesions (n = 4 per group) was obtained, and the proportion of DEGs between groups was determined (fold change in expression of ≥ 2 and FDR ≤ 0.05) (see attached Supplementary Materials: Table 4 to 6 for complete DEG list). Principal component analysis performed using normalised RNA-Seq data shows a clustering pattern of *miR-155*$^{-/-}$ decidualised endometrial tissue samples on the bottom left, with a distinct separation from both D7 and D14 lesions (Figure 4.11 A). Comparisons between decidualised endometrium and D7 lesions found 10% of detected genes upregulated, while 15% of detected genes were downregulated (Figure 4.11 B). Between decidualised endometrium and D14, a total of 13% of detected genes were upregulated whereas 17% of detected genes were downregulated (Figure 4.11 C). In contrast, between D7 and D14, only 2% of detected genes were upregulated, and 2% of detected genes were downregulated (Figure 4.11 D).

A total of 5,608 genes were differentially expressed between one of more of the three comparisons (Figure 4.11 E), with 3.6% (202 genes) differentially expressed in all three groups. The greatest overlap of DEGs (56.2%) was noted between Decidualised *vs* D7 and Decidualised *vs* D14 (3,149 genes). DEGs between Decidualised *vs* D7 and Decidualised *vs* D14 were further categorised into upregulated (2,303 genes) and downregulated (3,271 genes) genes (Figure 4.11 F and G respectively). At both D7 and D14, a consistent upregulation of 1,350 genes and a consistent downregulation of 1,999 genes was observed when compared to decidualised endometrium.

The top genes with the largest fold change in expression between the three samples were identified (Table 4.2). Lesions at D7 and D14 had an increased expression of prolactin family 3, subfamily c, member 1 (*Prl3c1*; involved in hormone activity, regulation of proliferation and decidual differentiation), prostate stem cell antigen (*Psca*; involved in regulation of neurotransmission), wingless-type MMTV integration site family, member 10A (*Wnt10a*; involved in regulation of gene expression during development and implicated in oncogenesis), and keratinocyte differentiation associated protein (*Krtdap*; involved in regulation of keratinocyte differentiation and maintenance of stratified epithelia) when compared to decidualised endometrium. A downregulation of genes involved in the regulation of muscle activity including ATPase, Ca^{2+} transporting, cardiac muscle, fast twitch 1 (*Atp2a1*) and myosin, heavy

polypeptide 4, skeletal muscle (*Myh4*), as well as genes involved in organ development including gremlin 1 DAN family BMP antagonist (*Grem1*) and tintin (*Ttn*), were observed in both D7 and D14 lesions compared to decidualised endometrium.

Comparison of DEGs between D7 and D14 lesions showed an upregulation of small proline-rich protein 2B (*Sprr2b*) and osteoclast stimulatory transmembrane protein (*Ocstamp*) at D14, both of which are associated with the cellular response to oestrogen (Table 4.2). An upregulation of genes involved in cell regulation, organisation, and development such as kinesin family member 14 (*Kif14*), Scl/Tal1 interrupting locus (*Stil*), shugoshin 1 (*Sgo1*), kinetochore scaffold 1 (Knl1), and wingless-type MMTV integration site family, member 2B (*Wnt2b*) was also observed in D14 lesions. In contrast, genes involved in inflammation (melan-A (*Mlana*), histocompatibility 2, M region locus 2 (*H2-M2*), immunoglobulin joining chain (*Jchain*), and CD5 antigen-like (*Cd5l)*) were down regulated in lesions at D14.

Assessment of upregulated canonical pathways during lesion development showed an increase in multiple cholesterol biosynthesis pathways at D7 compared to decidualised endometrium (Table 4.3) At D14, not only was there an increase in a cholesterol biosynthesis super-pathway, but an upregulation in pathways associated with cell cycle regulation and inhibition of matrix metalloproteases was also observed when compared to decidualised endometrium (Table 4.4). Assessment of downregulated canonical pathways identified 37 similar pathways in D7 and D14 lesions compared to decidualised endometrium. These pathways were almost exclusively associated with immune regulation, including B cell signalling, T helper cell signalling, dendritic cell maturation, toll-like receptor signalling, NF-κB signalling, Fcγ receptor-mediated phagocytosis in macrophages and monocytes, and production of nitric oxide and reactive oxygen species in macrophages. Among the five canonical pathways identified in D14 lesions compared to D7 lesions, cyclins and cell cycle regulation pathway was upregulated ($p = 0.0012$), while the G2/M DNA damage checkpoint was downregulated ($p < 0.0001$) at D14 (Table 4.5).

4.2.4.1. Comparison of RNA-Sequencing data between C57 mice and *miR-155* deficient mice

To determine the proportion of DEGs arising from a deficiency in *miR-155*, RNA-Seq data of decidualised endometrium, D7 and D14 lesions in C57 mice and *miR-155*$^{-/-}$ mice were compared, wherein a total of 79 genes were identified (Figure 4.12A). Surprisingly, only four genes (B cell translocation gene 3 (*Btg3*), recombination signal binding protein for immunoglobulin kappa J region (*Rbpj*), recombination signal binding protein for immunoglobulin kappa J region, pseudogene 3 (*Rbpsuh-rs3*), and ATPase, class V, type 10D (*Atp10d*)) were consistently dysregulated between C57 and *miR-155*$^{-/-}$ mice across all samples.

The majority of DEGs were expressed only within the decidualised endometrium, with an upregulation of genes involved in ATP binding activity (heat shock protein 1A and 1B (*Hspa1a* and *Hspa1b*) and tubulin tyrosine ligase-like family, member 11 (*Ttll11*)) (Table 4.6). Interestingly, several of the DEGs identified are classified as either pseudogenes (*Rbpsuh-rs3*), protein-coding genes with an unclassified function (*Gm43039* and *Prr16*), or non-coding RNA genes (*Gm28373*, *0610040F04Rik*, and *2600006K01Rik*) (see attached Supplementary Materials: Table 7 for complete DEG list).

At both D7 and D14, only 8 DEGs were identified between C57 and *miR-155*$^{-/-}$ samples (Figure 4.12). Of these, two genes (*Btg3* and *Rbpj*) were consistently upregulated and two genes (*Rbpsuh-rs3* and *Atp10d*) were consistently downregulated in in *miR-155*$^{-/-}$ lesions (Table 4.6). At D7, an increase in *5830416I19Rik*, a long non-coding RNA was observed, while a downregulation in WD repeat and FYVE domain containing 1 (*Wdfy1*; involved in the positive regulation of toll-like receptor 3 and 4 signalling pathways) was observed in *miR-155*$^{-/-}$ lesions. At D14, an upregulation of leucine rich repeat and fibronectin type III, extracellular 1 (*Elfn1*; protein phosphatase inhibitor activity and involved in synapse organization) and toll-like receptor 1 (*Tlr1*; involved in the regulation of IL-6 biosynthetic process and TNF biosynthetic process) was observed in *miR-155*$^{-/-}$ lesions.

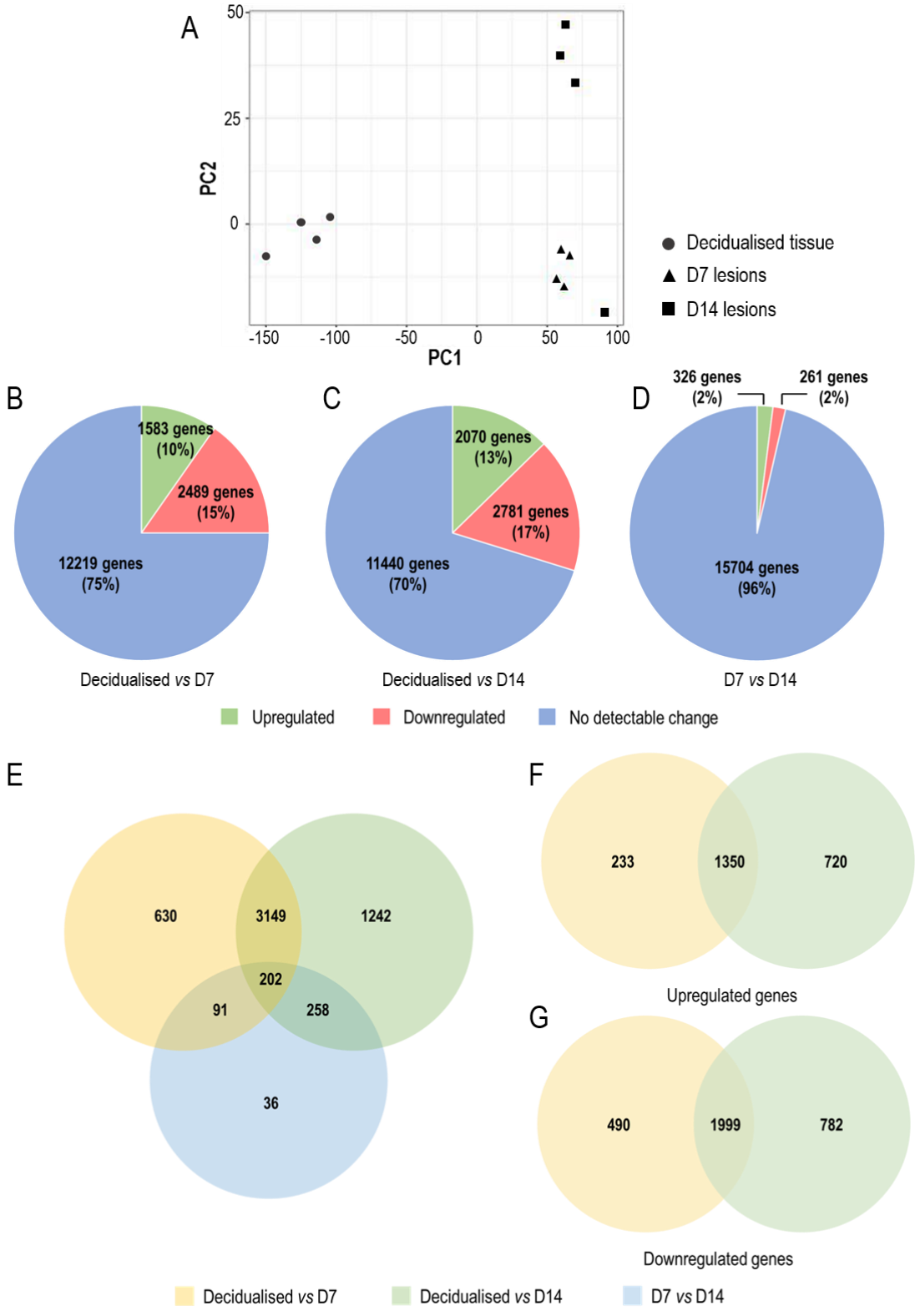

Figure 4.11 Number of differentially expressed genes identified in tissues from *miR-155*$^{-/-}$ mice

Principal component analysis (PCA) was performed using the normalised RNA-Seq data from *miR-155*$^{-/-}$ decidualised endometrium, D7 and D14 lesions (**A**). The proportion of upregulated and downregulated DEGs amongst detected genes between Decidualised *vs* D7 (**B**), Decidualised *vs* D14 (**C**), and D7 *vs* D14 (**D**) was determined. The Venn diagram displays the distribution and overlap of DEGs (both upregulated and downregulated) between each comparison (**E**). Additional Venn diagrams were generated to determine the number of upregulated (**F**) and downregulated (**G**) DEGs during lesion development compared to decidualised endometrial tissue. All genes identified have a ≥ 2-fold change in expression with an adjusted *p* value < 0.05.

Table 4.2 Top ten upregulated and downregulated DEGs in *miR-155*$^{-/-}$ mice during decidualisation and lesion development (FDR <0.05)

Decidualised *vs* D7			Decidualised *vs* D14			D7 *vs* D14		
Gene	**log_2FC**	**FDR**	**Gene**	**log_2FC**	**FDR**	**Gene**	**log_2FC**	**FDR**
Tac2	+ 9.72	6.39×10^{-9}	Psca	+ 10.45	9.00×10^{-9}	Kif14	+ 5.18	2.68×10^{-3}
Doxl2	+ 9.42	4.10×10^{-6}	Bco1	+ 9.74	1.39×10^{-8}	Klra2	+ 4.73	5.82×10^{-3}
Krtdap	+ 9.35	8.23×10^{-5}	Cbln1	+ 9.46	1.13×10^{-7}	Stil	+ 4.46	4.18×10^{-4}
Psca	+ 9.31	9.73×10^{-8}	Wnt10a	+ 9.13	1.08×10^{-10}	Sprr2b	+ 4.24	2.28×10^{-2}
Spink8	+ 9.07	1.94×10^{-9}	Prl3c1	+ 9.04	2.21×10^{-4}	Gm26788	+ 4.06	4.37×10^{-3}
Notum	+ 8.72	1.40×10^{-6}	Cyp11b1	+ 8.80	4.70×10^{-5}	Slc9b2	+ 3.90	2.54×10^{-2}
Prl3c1	+ 8.60	9.90×10^{-5}	Klk7	+ 8.77	5.78×10^{-4}	Sgo1	+ 3.89	6.70×10^{-3}
Cdsn	+ 8.08	1.79×10^{-5}	Krtdap	+ 8.54	1.96×10^{-4}	Knl1	+ 3.89	6.48×10^{-3}
Kcnd3	+ 8.04	1.05×10^{-5}	Cdh4	+ 8.53	5.94×10^{-7}	Ocstamp	+ 3.86	3.50×10^{-2}
Wnt10a	+ 7.97	2.17×10^{-9}	Tac2	+ 8.46	1.62×10^{-9}	Wnt2b	+ 3.86	8.00×10^{-3}
Myh4	- 10.91	1.55×10^{-2}	Mmp12	- 10.72	2.03×10^{-4}	Mlana	- 5.38	1.62×10^{-5}
Atp2a1	- 10.01	6.32×10^{-3}	Myh4	- 9.78	2.55×10^{-2}	Slc18a3	- 5.35	3.38×10^{-2}
Ttn	- 9.88	1.99×10^{-2}	Atp2a1	- 9.52	7.64×10^{-3}	H2-M2	- 5.14	3.15×10^{-5}
Arg1	- 9.42	1.31×10^{-2}	Wisp2	- 8.84	1.71×10^{-4}	Myocos	- 4.76	2.14×10^{-3}
Ano5	- 9.22	2.66×10^{-2}	Mmp13	- 8.69	1.72×10^{-4}	Jchain	- 4.67	2.69×10^{-2}
Grem1	- 8.99	4.86×10^{-6}	Cd5l	- 8.55	1.87×10^{-7}	Gm14461	- 4.44	5.07×10^{-4}
Rbfox1	- 8.88	3.97×10^{-2}	Ttn	- 8.47	3.99×10^{-2}	Gm6939	- 4.22	1.56×10^{-3}
Mybpc2	- 8.83	4.03×10^{-2}	Grem1	- 8.27	1.36×10^{-5}	Cd5l	- 4.04	8.29×10^{-6}
Myl1	- 8.67	4.44×10^{-2}	Gm43909	- 7.84	2.57×10^{-8}	Hc	- 3.68	9.13×10^{-3}
Neb	- 8.65	3.26×10^{-2}	Tnnt3	- 7.60	1.34×10^{-2}	Ptgds	- 3.64	2.19×10^{-3}

Table 4.3 **Canonical pathways identified by IPA in D7 lesions compared to decidualised endometrium from *miR-155*$^{-/-}$ mice (*P* < 0.05; -2 > *Z* score > 2)**

Canonical Pathway	*Z* score	Ratio	*P* value
Antioxidant Action of Vitamin C	+ 2.887	31%	1.12×10^{-3}
Superpathway of Cholesterol Biosynthesis	+ 2.530	37%	1.66×10^{-2}
Wnt/β-catenin Signalling	+ 2.333	25%	1.74×10^{-2}
PPAR Signalling	+ 2.268	28%	9.33×10^{-3}
Cholesterol Biosynthesis I	+ 2.121	62%	6.46×10^{-4}
Cholesterol Biosynthesis II (via 24,25-dihydrolanosterol)	+ 2.121	62%	6.46×10^{-4}
Cholesterol Biosynthesis III (via Desmosterol)	+ 2.121	62%	6.46×10^{-4}
Ceramide Biosynthesis	+ 2.000	57%	2.40×10^{-2}
Dopamine-DARPP32 Feedback in cAMP Signalling	- 2.000	27%	3.80×10^{-3}
Chondroitin and Dermatan Biosynthesis	- 2.000	67%	1.20×10^{-2}
Antiproliferative Role of Somatostatin Receptor 2	- 2.000	28%	2.04×10^{-2}
Superoxide Radicals Degradation	- 2.000	50%	4.17×10^{-2}
Renal Cell Carcinoma Signalling	- 2.065	29%	9.33×10^{-3}
IL-1 Signalling	- 2.111	27%	2.69×10^{-2}
Glioma Invasiveness Signalling	- 2.117	36%	1.26×10^{-4}
PDGF Signalling	- 2.117	29%	7.94×10^{-3}
NRF2-mediated Oxidative Stress Response	- 2.132	23%	4.07×10^{-2}
GPCR-Mediated Nutrient Sensing in Enteroendocrine Cells	- 2.160	38%	6.61×10^{-7}
HGF Signalling	- 2.191	28%	6.03×10^{-3}
FcγRIIB Signalling in B Lymphocytes	- 2.200	40%	1.32×10^{-6}
P2Y Purigenic Receptor Signalling Pathway	- 2.214	32%	7.41×10^{-5}
Oestrogen-Dependent Breast Cancer Signalling	- 2.236	28%	1.78×10^{-2}
Glioma Signalling	- 2.263	34%	2.75×10^{-5}
Type II Diabetes Mellitus Signalling	- 2.268	33%	5.25×10^{-6}
CCR3 Signalling in Eosinophils	- 2.268	32%	1.70×10^{-4}
IL-2 Signalling	- 2.294	33%	1.55×10^{-3}
FGF Signalling	- 2.294	26%	3.89×10^{-2}
IL-9 Signalling	- 2.324	38%	9.77×10^{-4}
Type I Diabetes Mellitus Signalling	- 2.324	30%	1.95×10^{-3}
fMLP Signalling in Neutrophils	- 2.333	33%	3.39×10^{-5}
Eicosanoid Signalling	- 2.333	37%	2.82×10^{-4}
GNRH Signalling	- 2.333	27%	2.29×10^{-3}
Acute Phase Response Signalling	- 2.335	24%	2.88×10^{-2}
SPINK1 General Cancer Pathway	- 2.357	28%	3.72×10^{-2}
GM-CSF Signalling	- 2.449	32%	1.86×10^{-3}
Th2 Pathway	- 2.466	38%	4.07×10^{-8}
CXCR4 Signalling	- 2.469	30%	1.05×10^{-4}
Adrenomedullin Signalling Pathway	- 2.474	31%	6.46×10^{-6}
SAPK/JNK Signalling	- 2.502	26%	2.95×10^{-2}
Toll-like Receptor Signalling	- 2.524	35%	6.31×10^{-4}

Fc Epsilon RI Signalling	- 2.535	32%	2.14×10^{-4}
Chemokine Signalling	- 2.600	35%	6.31×10^{-4}
LPS-stimulated MAPK Signalling	- 2.600	29%	7.24×10^{-3}
IL-8 Signalling	- 2.626	32%	4.68×10^{-6}
Colorectal Cancer Metastasis Signalling	- 2.630	31%	5.13×10^{-7}
April Mediated Signalling	- 2.673	36%	6.76×10^{-3}
Interferon Signalling	- 2.714	36%	1.70×10^{-2}
Renin-Angiotensin Signalling	- 2.722	34%	2.24×10^{-5}
IL-7 Signalling Pathway	- 2.746	32%	1.45×10^{-3}
Cholecystokinin/Gastrin-mediated Signalling	- 2.785	28%	8.71×10^{-3}
NGF Signalling	- 2.828	27%	1.15×10^{-2}
GDNF Family Ligand-Receptor Interactions	- 2.837	31%	2.69×10^{-3}
PEDF Signalling	- 2.858	29%	8.51×10^{-3}
NF-κB Activation by Viruses	- 2.874	39%	1.70×10^{-6}
Integrin Signalling	- 2.887	25%	5.75×10^{-3}
Calcium-induced T Lymphocyte Apoptosis	- 2.982	35%	2.34×10^{-3}
Lymphotoxin β Receptor Signalling	- 2.982	31%	7.94×10^{-3}
Phospholipase C Signalling	- 3.000	28%	1.41×10^{-4}
IL-6 Signalling	- 3.042	32%	1.38×10^{-4}
Gαq Signalling	- 3.130	32%	1.74×10^{-5}
RANK Signalling in Osteoclasts	- 3.138	29%	3.89×10^{-3}
Cardiac Hypertrophy Signalling	- 3.151	28%	2.29×10^{-4}
p38 MAPK Signalling	- 3.157	28%	8.91×10^{-3}
Apelin Liver Signalling Pathway	- 3.207	54%	4.57×10^{-5}
PI3K Signalling in B Lymphocytes	- 3.317	36%	7.59×10^{-7}
Role of NFAT in Cardiac Hypertrophy	- 3.349	33%	1.86×10^{-7}
Tec Kinase Signalling	- 3.395	33%	2.29×10^{-6}
HMGB1 Signalling	- 3.430	26%	1.45×10^{-2}
B Cell Activating Factor Signalling	- 3.464	34%	1.12×10^{-2}
Leukocyte Extravasation Signalling	- 3.491	40%	3.98×10^{-13}
Fcγ Receptor-mediated Phagocytosis in Macrophages and Monocytes	- 3.536	36%	7.08×10^{-5}
Inflammasome pathway	- 3.606	68%	2.19×10^{-6}
Calcium Signalling	- 3.781	27%	1.26×10^{-3}
NF-κB Signalling	- 3.939	34%	6.46×10^{-7}
Role of Pattern Recognition Receptors in Recognition of Bacteria and Viruses	- 4.003	43%	3.98×10^{-11}
GP6 Signalling Pathway	- 4.032	52%	1.00×10^{-18}
iCOS-iCOSL Signalling in T Helper Cells	- 4.110	41%	1.02×10^{-8}
Production of Nitric Oxide and Reactive Oxygen Species in Macrophages	- 4.128	27%	1.95×10^{-3}
CD28 Signalling in T Helper Cells	- 4.333	38%	1.17×10^{-7}
B Cell Receptor Signalling	- 4.533	32%	4.07×10^{-6}
Th1 Pathway	- 4.644	39%	6.61×10^{-8}
Role of NFAT in Regulation of the Immune Response	- 4.901	37%	2.75×10^{-9}
PKCθ Signalling in T Lymphocytes	- 4.919	34%	1.82×10^{-6}
TREM1 Signalling	- 5.096	54%	3.98×10^{-11}

Neuroinflammation Signalling Pathway	- 5.253	33%	3.80×10^{-10}
Dendritic Cell Maturation	- 5.506	38%	1.07×10^{-9}

Table 4.4 **Canonical pathways identified by IPA in D14 lesions compared to decidualised endometrium from *miR-155*$^{-/-}$ mice (*P* < 0.05; -2 > *Z* score > 2)**

Canonical Pathway	*Z* score	Ratio	*P*- value
Superpathway of Cholesterol Biosynthesis	+ 2.887	44%	6.31×10^{-3}
Antioxidant Action of Vitamin C	+ 2.785	35%	1.10×10^{-3}
Mitotic Roles of Polo-Like Kinase	+ 2.668	38%	2.45×10^{-3}
Inhibition of Matrix Metalloproteases	+ 2.183	49%	2.24×10^{-4}
Oestrogen-mediated S-phase Entry	+ 2.111	42%	1.35×10^{-2}
Cyclins and Cell Cycle Regulation	+ 2.065	31%	3.47×10^{-2}
Ceramide Biosynthesis	+ 2.000	57%	4.27×10^{-2}
Heme Degradation	- 2.000	100%	2.14×10^{-3}
Chondroitin and Dermatan Biosynthesis	- 2.000	67%	2.19×10^{-2}
Tec Kinase Signalling	- 2.021	50%	1.58×10^{-6}
RANK Signalling in Osteoclasts	- 2.043	38%	6.92×10^{-3}
Cardiac Hypertrophy Signalling	- 2.109	31%	5.89×10^{-4}
GDNF Family Ligand-Receptor Interactions	- 2.117	39%	2.88×10^{-4}
Type I Diabetes Mellitus Signalling	- 2.132	36%	4.17×10^{-4}
April Mediated Signalling	- 2.138	36%	2.75×10^{-2}
IL-6 Signalling	- 2.188	38%	1.51×10^{-5}
SAPK/JNK Signalling	- 2.191	29%	4.57×10^{-2}
Cholecystokinin/Gastrin-mediated Signalling	- 2.197	34%	2.24×10^{-3}
HMGB1 Signalling	- 2.236	35%	1.91×10^{-4}
PEDF Signalling	- 2.263	38%	1.45×10^{-4}
Leukocyte Extravasation Signalling	- 2.265	43%	2.51×10^{-12}
Phospholipase C Signalling	- 2.324	33%	3.24×10^{-5}
Eicosanoid Signalling	- 2.333	39%	1.32×10^{-3}
Role of Pattern Recognition Receptors in Recognition of Bacteria and Viruses	- 2.412	45%	9.12×10^{-10}
Calcium-induced T Lymphocyte Apoptosis	- 2.449	45%	5.75×10^{-5}
Calcium Signalling	- 2.466	28%	1.51×10^{-2}
Apelin Liver Signalling Pathway	- 2.496	50%	1.20×10^{-3}
Complement System	- 2.530	49%	5.25×10^{-4}
iCOS-iCOSL Signalling in T Helper Cells	- 2.777	27%	1.00×10^{-9}
Toll-like Receptor Signalling	- 2.837	47%	5.75×10^{-4}
Glutathione-mediated Detoxification	- 2.887	39%	2.88×10^{-3}
B Cell Activating Factor Signalling	- 2.887	34%	4.17×10^{-2}
PI3K Signalling in B Lymphocytes	- 2.949	38%	6.61×10^{-6}
GP6 Signalling Pathway	- 2.954	52%	2.51×10^{-14}
FcÎ³ Receptor-mediated Phagocytosis in Macrophages and Monocytes	- 3.000	40%	5.13×10^{-5}
NF-κB Signalling	- 3.048	36%	7.41×10^{-6}
B Cell Receptor Signalling	- 3.098	36%	4.79×10^{-6}
Inflammasome pathway	- 3.464	63%	1.02×10^{-4}
Production of Nitric Oxide and Reactive Oxygen Species in Macrophages	- 3.474	32%	3.31×10^{-4}
CD28 Signalling in T Helper Cells	- 3.479	42%	1.45×10^{-7}

p38 MAPK Signalling	- 3.773	33%	2.95×10^{-3}
Role of NFAT in Regulation of the Immune Response	- 4.000	42%	6.46×10^{-10}
Th1 Pathway	- 4.025	44%	2.69×10^{-8}
Neuroinflammation Signalling Pathway	- 4.243	38%	2.34×10^{-10}
PKCÎ¸ Signalling in T Lymphocytes	- 4.258	37%	5.50×10^{-6}
TREM1 Signalling	- 4.439	54%	4.57×10^{-9}
Dendritic Cell Maturation	- 4.765	42%	1.17×10^{-9}

Table 4.5 **Canonical pathways identified by IPA in D14 lesions compared to D7 lesions from *miR-155*$^{-/-}$ mice (*P* < 0.05; -2 > *Z* score > 2)**

Canonical Pathway	*Z* score	Ratio	*P* value
Cyclins and Cell Cycle Regulation	+ 2.121	10%	1.17×10^{-3}
Mitotic Roles of Polo-Like Kinase	+ 2.111	20%	1.26×10^{-8}
LPS/IL-1 Mediated Inhibition of RXR Function	+ 2.000	5%	4.90×10^{-2}
Glutathione-mediated Detoxification	- 2.000	16%	4.17×10^{-3}
Cell Cycle: G2/M DNA Damage Checkpoint Regulation	- 2.111	22%	5.62×10^{-8}

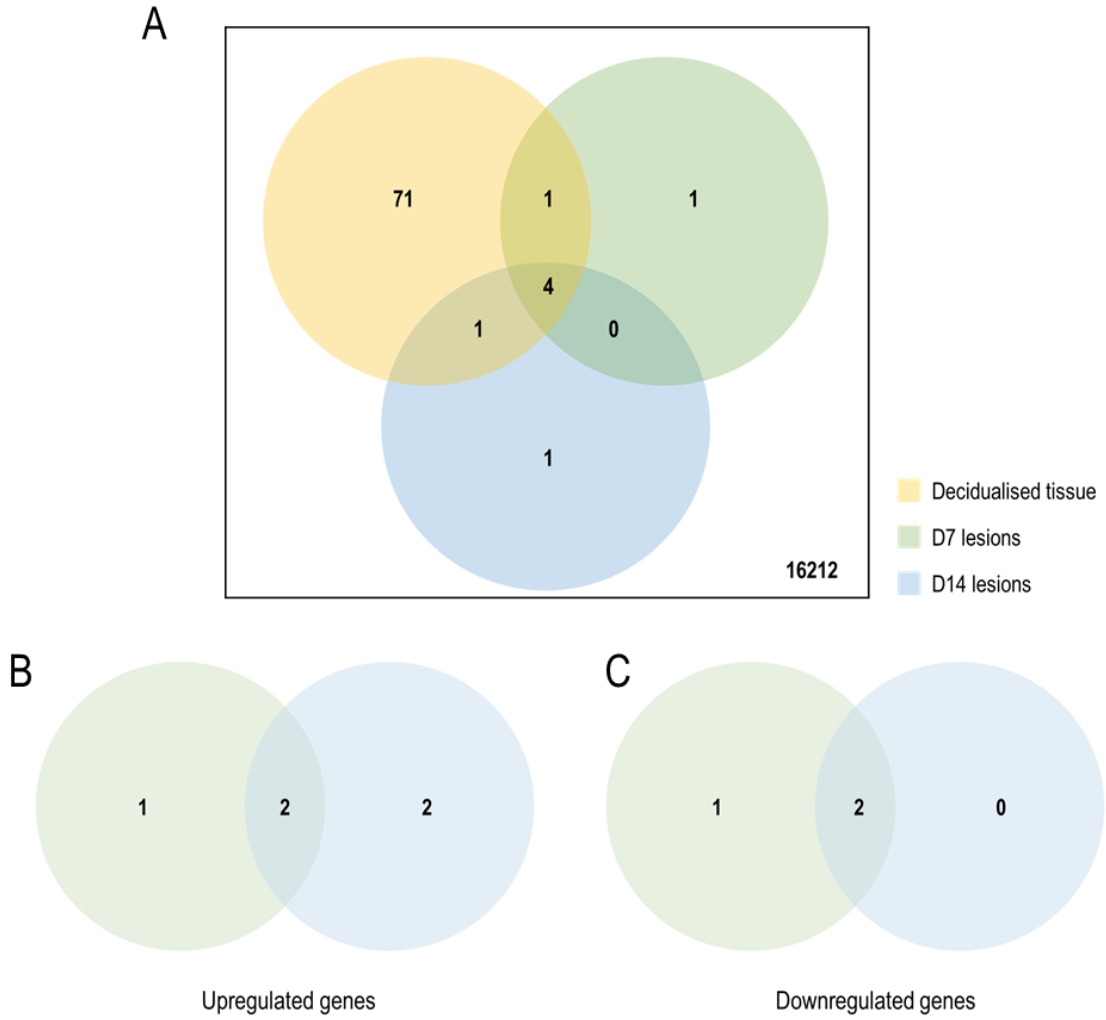

Figure 4.12 Number of differentially expressed genes identified between *miR-155*$^{-/-}$ and C57 mice

RNA-Seq data from decidualised endometrium, D7 and D14 lesions in *miR-155*$^{-/-}$ and C57 mice were compared to determine the proportion of DEGs amongst detected genes. The top Venn diagram displays the distribution and overlap of DEGs (both upregulated and downregulated) between each sample type (A). Additional Venn diagrams were generated to determine the number of upregulated (B) and downregulated (C) DEGs between D7 and D14 lesions. All genes identified have a ≥ 2-fold change in expression with an adjusted *p* value < 0.05.

Table 4.6 Top DEGs genes during decidualisation and lesion development in *miR-155*$^{-/-}$ mice compared to C57 mice (FDR <0.05)

Decidualised endometrium		
Gene	**log_2FC**	**FDR**
Hspa1a	+ 3.63	1.21×10^{-2}
Btg3	+ 3.61	9.52×10^{-3}
Ttll11	+ 3.45	1.01×10^{-2}
Tmem267	+ 2.99	4.44×10^{-2}
Tom1	+ 2.79	1.61×10^{-2}
Hspa1b	+ 2.63	1.91×10^{-2}
Gm43039	+ 2.54	4.46×10^{-2}
Apold1	+ 2.18	2.79×10^{-4}
Gm28373	+ 2.11	4.39×10^{-3}
0610040F04Rik	+ 2.03	1.30×10^{-2}
Optc	- 5.39	4.68×10^{-2}
Rbpsuh-rs3	- 4.67	2.75×10^{-5}
Sgms2	- 3.40	3.59×10^{-2}
2600006K01Rik	- 3.30	2.06×10^{-2}
Sfrp1	- 3.21	2.95×10^{-2}
Prr16	- 2.99	4.23×10^{-2}
Myl9	- 2.80	2.47×10^{-2}
Acta2	- 2.58	3.55×10^{-2}
Lpl	- 2.24	3.41×10^{-2}
Penk	- 2.22	1.12×10^{-2}

D7 lesions		
Gene	**log_2FC**	**FDR**
5830416I19Rik	+ 4.80	2.20×10^{-3}
Btg3	+ 3.77	8.07×10^{-3}
Rbpj	+ 1.28	1.49×10^{-3}
Rbpsuh-rs3	- 3.44	1.49×10^{-3}
Atp10d	- 1.55	8.75×10^{-3}
Wdfy1	- 1.10	3.52×10^{-3}

D14 lesions		
Gene	**log_2FC**	**FDR**
Elfn1	+ 5.00	2.20×10^{-2}
Btg3	+ 4.32	8.09×10^{-3}
Tlr1	+ 2.15	2.19×10^{-2}
Rbpj	+ 1.63	8.54×10^{-5}
Rbpsuh-rs3	- 4.54	1.45×10^{-3}
Atp10d	- 1.31	2.19×10^{-2}

4.2.5. Evaluating the impact of *miR-155* depletion from either the recipient environment or donor endometrium

In a clinical setting, *miR-155* expression is downregulated in plasma from women with endometriosis (Nisenblat et al., 2019). To date, no study has found evidence of dysregulated *miR-155* activity in eutopic *vs* ectopic endometrial tissue. In sections 4.2.1 to 4.2.4 of this thesis, the impact of a systemic depletion of *miR-155 (*i.e. both donor and recipient mice were *miR-155* deficient) on lesion development was evaluated. Thus, to evaluate the contribution of the donor endometrium *vs* recipient environment on the development of endometriosis and expression of M1-like and M2-like markers, this section will evaluate the impact of reciprocal transfers between wildtype mice and mice deficient in *miR-155* (Figure 4.13). To determine the contribution of the recipient environment on the development of endometriosis, *miR-155* sufficient (C57) donor endometrium was transferred into a *miR-155* deficient (*miR-155*$^{-/-}$) recipient (C57 → *miR-155*$^{-/-}$). Conversely, the transfer of *miR-155* deficient (*miR-155*$^{-/-}$) donor endometrium into a replete *miR-155* (C57) recipient (*miR-155*$^{-/-}$ → C57) was performed to determine the contribution of donor endometrial tissue in the pathogenesis of endometriosis.

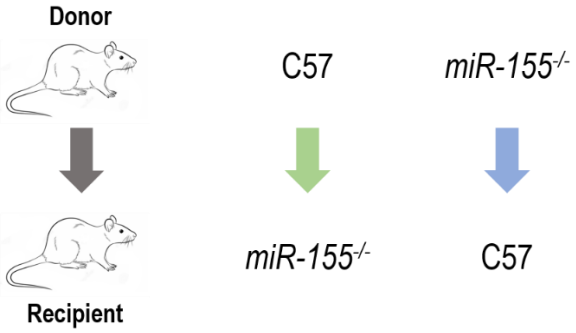

Figure 4.13 Reciprocal transfers between *miR-155*$^{-/-}$ and C57 mice

Utilising the Greaves-Saunders menstrual mouse model of endometriosis (Greaves et al., 2014), 40mg donor decidualised endometrial tissue was injected subcutaneously into an allogeneic recipient. Resulting endometriosis-like lesions from these reciprocal transfers were harvested at either day 7, 14, or 21 post-induction of disease. Refer to Figure 2.3 for the protocol to induce endometriosis in recipient mice.

4.2.5.1. Endometriosis-like lesion development in C57 donor to *miR-155*$^{-/-}$ recipient transfers

A total of 36 C57 donor mice were used to generate sufficient decidualised endometrial tissue for injection into *miR-155*$^{-/-}$ recipient mice (C57 → *miR-155*$^{-/-}$) at a ratio of 2 donors to 1.7 recipients (Table 4.7). Overall, 93% of *miR-155*$^{-/-}$ recipient mice had identifiable lesions over the course of this experiment. At D7, lesions were recovered from 100% of *miR-155*$^{-/-}$ recipient mice. At D14 and D21 however, the proportion of *miR-155*$^{-/-}$ recipient mice that had lesions from C57 donor tissue reduced slightly to 90%.

Endometriosis-like lesions that developed from a C57 → *miR-155*$^{-/-}$ transfer were large, spread out over the attachment site, and blood-filled at D7 (Figure 4.14 A). At D14, lesions remained blood filled, but were small and raised from the attachment site (Figure 4.14 B), while at D21, lesions were small and white (Figure 4.14 C). Lesion size (Figure 4.14 D) was highest at D7 (32 (18 – 36) mm^3), and significantly reduced at D14 (6 (4 – 8) mm^3, $p = 0.0006$), and remained consistent at D21 (4 (4 – 11) mm^3, $p = 0.0008$ for D7 *vs* D21). Lesion weight (Figure 4.14 E) followed a similar trend, with values highest at D7 (26.65 (20.45 – 31.15) mg), and significantly reducing at D14 (9.10 (7.95 – 10.10) mg, $p = 0.0014$) and D21 (7.60 (6.75 – 10.15) mg, $p = 0.003$ for D7 *vs* D21). To assess morphological parameters associated with lesion development in C57 → *miR-155*$^{-/-}$ endometriotic-like lesions, analysis of H&E stained sections was performed (Figure 4.15 A-C). Over the three week time period, no significant differences were observed in the number of glands per lesion (Figure 4.15 D), average gland size (Figure 4.15 E), lumen area (Figure 4.15 F), epithelium area (Figure 4.15 G), percentage glandular epithelium (Figure 4.15 H) or percentage stromal area (Figure 4.15 I).

Quantification of total F4/80 density in lesions steadily increased over time (Figure 4.16 G). At D7, 4.03 (1.04 – 5.48) % of cells were F4/80$^+$, which significantly increased at D14 (12.53 (9.37 – 20.77) %; $p = 0.0189$) and further increased at D21 (24.37 (18.66 – 27.36) %; $p < 0.0001$ for D7 *vs* D21). F4/80 expression at the periphery of C57 → *miR-155*$^{-/-}$ lesions was unchanged over time (Figure 4.16 A-C, H). In contrast, the central F4/80 density in C57 → *miR-155*$^{-/-}$ lesions followed a similar trend to the total expression of F4/80 in these lesions, with a significant increase between D7 and D14 (4.10 (2.26 – 6.44) % and 14.69 (10.03 – 21.23) %; $p = 0.0214$), and a further increase at D21 (38.12 (31.82 – 43.52) %; $p < 0.0001$ for D7 *vs* D21) (Figure 4.16 D-F, I).

A gradual increase in the density of M1-like marker iNOS occurred across the time points (8.55 (6.67 – 13.37) % at D7, 16.67 (12.46 – 23.78) % at D14, and 30.46 (25.88 – 36.74) % at D21; $p < 0.0001$ for D7 *vs* D21) (Figure 4.17 A-C, M). Similarly, expression of the M1-like marker MHC II in C57 → *miR-155*$^{-/-}$

lesions was lowest at D7 (8.89 (6.67 – 10.46) %), increased slightly at D14 (12.65 (9.24 – 15.74) %), and was highest at D21 (15.27 (10.97 – 21.19) %; $p = 0.0033$ for D7 *vs* D21) (Figure 4.17 D-F, N). Over the course of three weeks, the density of the M2-like marker CD206 increased slightly from D7 to D14 (11.90 (10.64 – 12.73) % and 16.91 (14.26 – 24.89) % respectively), and reached maximum expression at D21 (28.96 (25.20 – 31.79) %; $p < 0.0001$ for D7 *vs* D21) (Figure 4.17 G-I, O). In contrast, while the density of the M2-like marker Arg-1 was consistent at D7 and D14 (48.62 (44.58 – 54.35) % and 52.36 (43.94 – 69.17) % respectively), a small but significant decrease in Arg-1 expression was observed between D14 and D21 (39.77 (35.55 – 47.12) %; $p = 0.0274$) (Figure 4.17 J-L, P).

Table 4.7 Endometriosis-like lesion recovery in C57 → *miR-155*$^{-/-}$ mice

Lesion collection time point	D7	D14	D21
Total number of C57 donor mice used across all time points: 36			
Number of *miR-155*$^{-/-}$ recipient mice	10	10	10
Number of mice with lesions	10	9	9
Proportion of mice with lesions (%)	100	90	90

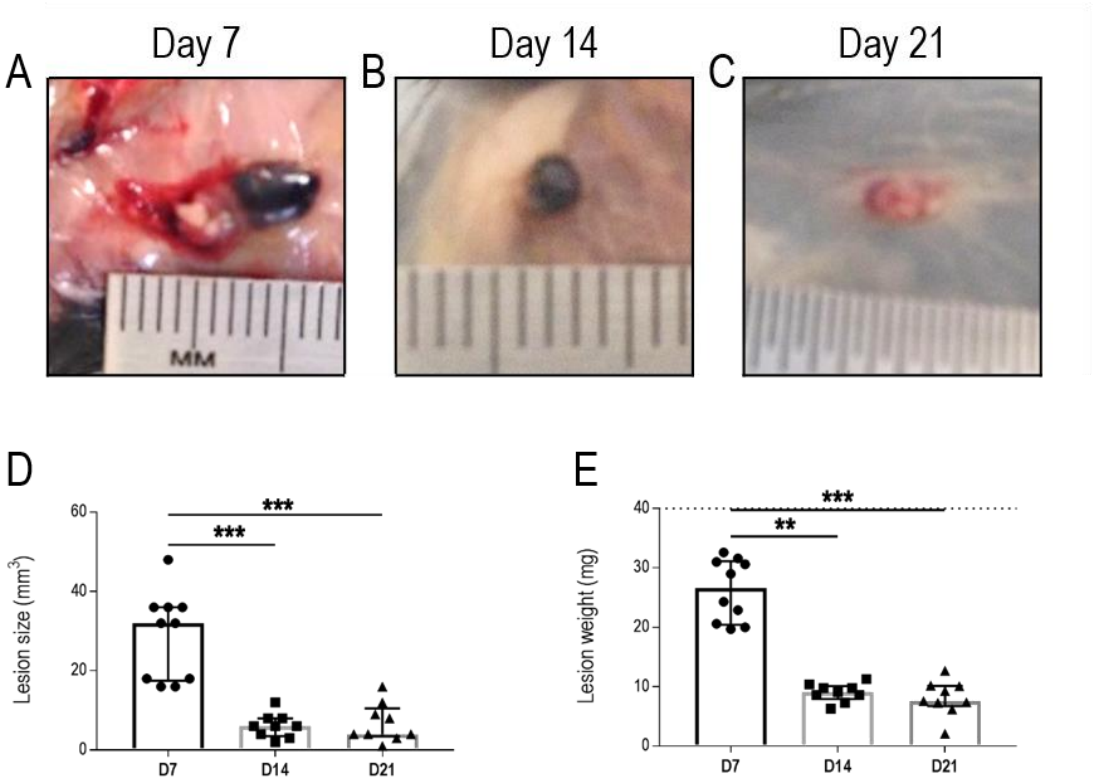

Figure 4.14 **Gross morphology of endometriosis-like lesion development in a transfer from C57 donor to *miR-155*$^{-/-}$ recipient mice**

Decidualised C57 donor endometrial tissue was injected subcutaneously into *miR-155*$^{-/-}$ recipient mice. Resulting lesions were harvested at either D7 (**A**), D14 (**B**) or D21 (**C**), with representative images shown. Lesion size was measured (**D**) and lesions were excised and weighed (**E**), with the dotted line indicating the initial weight of donor decidualised endometrial tissue inoculated into recipient mice. Data are presented as median (IQR), with each symbol representative of a single lesion in one mouse (n=10 at D7, n=9 at D14, n=9 at D21). Analysis was done using the Kruskal-Wallis test followed by Dunn's multiple comparison test, with significance denoted as ** ($p < 0.01$) and *** ($p < 0.001$).

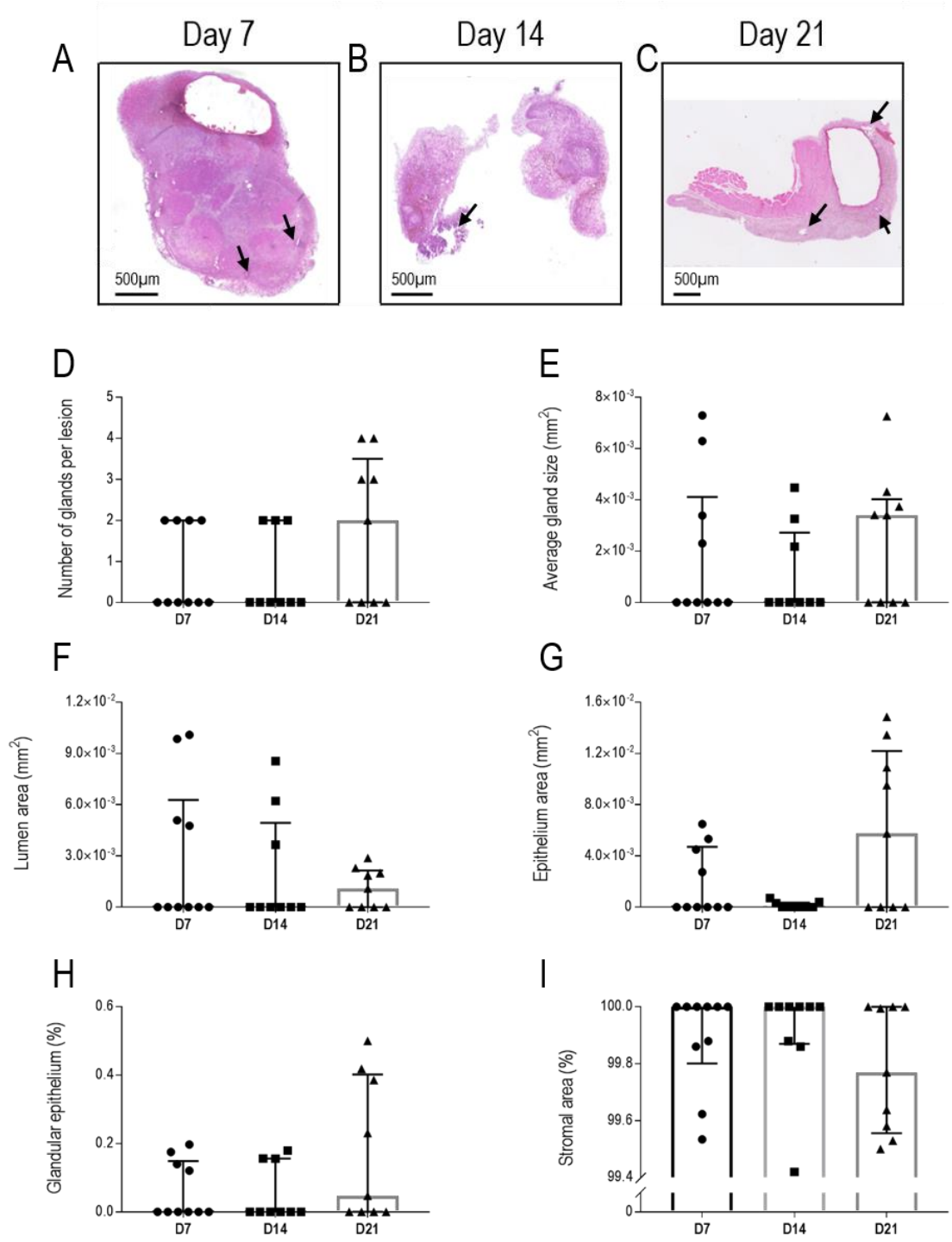

Figure 4.15 Assessment of morphological parameters in haematoxylin and eosin stained endometriosis-like lesions from C57 donor to *miR-155*$^{-/-}$ recipient mice

Haematoxylin and eosin stained sections from D7 **(A)**, D14 **(B)**, and D21 **(C)** lesions (representative images shown; arrows indicate glands) were assessed for the following characteristics: number of glands per lesion **(D)**, average gland size **(E)**, lumen area **(F)**, epithelium area **(G)**, percentage glandular epithelium **(H)** and percentage stromal area **(I)**. Data are presented as media (IQR), with each symbol representative of a single lesion in one mouse (n=10 at D7, n=9 at D14, n=9 at D21). Analysis was done using the Kruskal-Wallis test followed by Dunn's multiple comparison test.

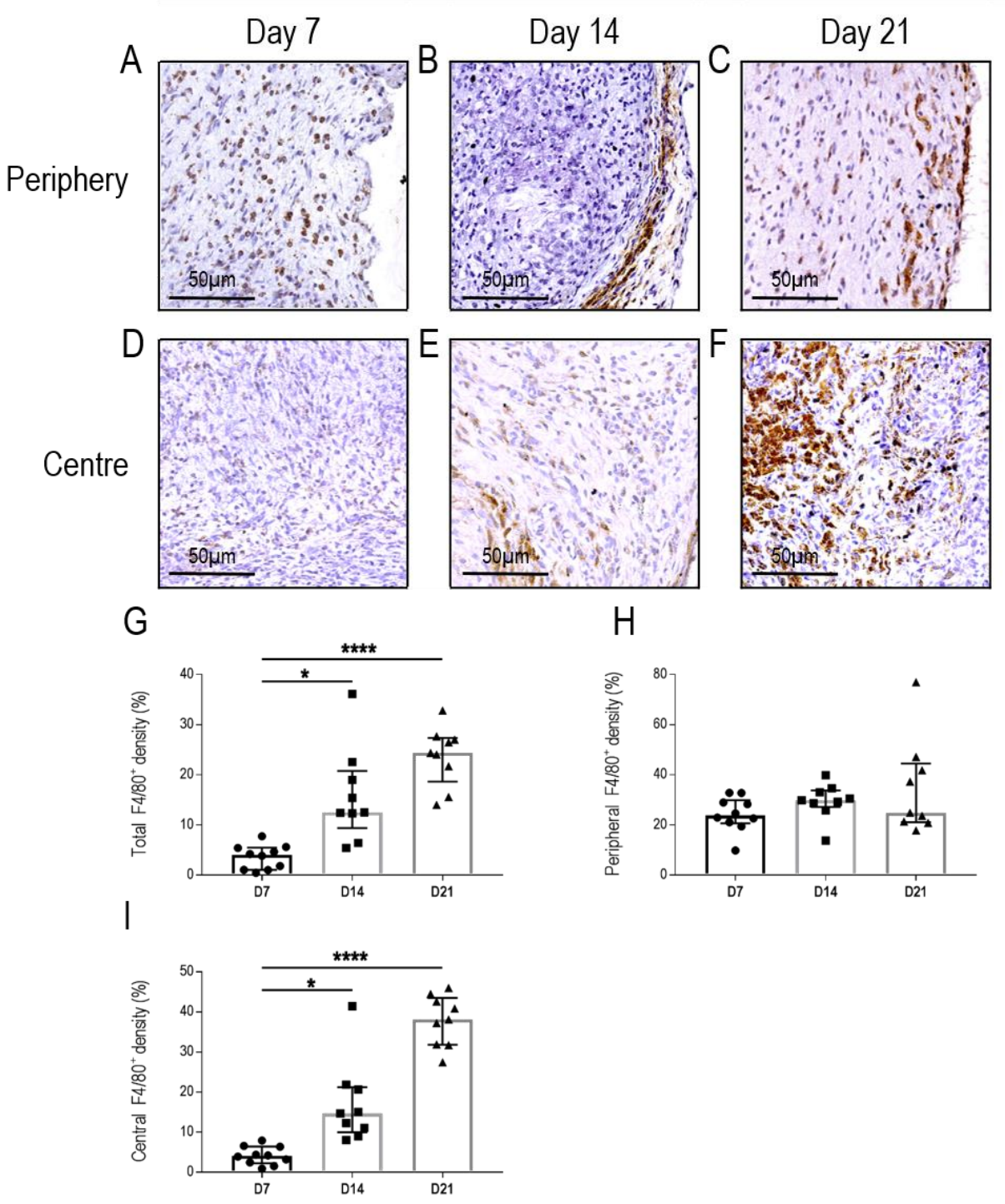

Figure 4.16 **F4/80 immunostaining in endometriosis-like lesions from C57 donor to *miR-155*$^{-/-}$ recipient mice**

Quantification of total F4/80 density was carried out in lesions from C57 donor to *miR-155*$^{-/-}$ recipient mice (**G**). F4/80 density at the lesion periphery (100µM from the edge of the lesion) at D7 (**A**), D14 (**B**) and D21 (**C**) was evaluated (**H**). F4/80 density at the lesion centre (within 500µM from the centre) at D7 (**D**), D14 (**E**), and D21 (**F**) was also quantified (**I**). Data are presented as median (IQR), with each symbol representative of a single lesion in one mouse (n=10 at D7, n=9 at D14, n=9 at D21). Analysis was done using the Kruskal-Wallis test followed by Dunn's multiple comparison test, with significance denoted as * ($p < 0.05$) and **** ($p < 0.0001$).

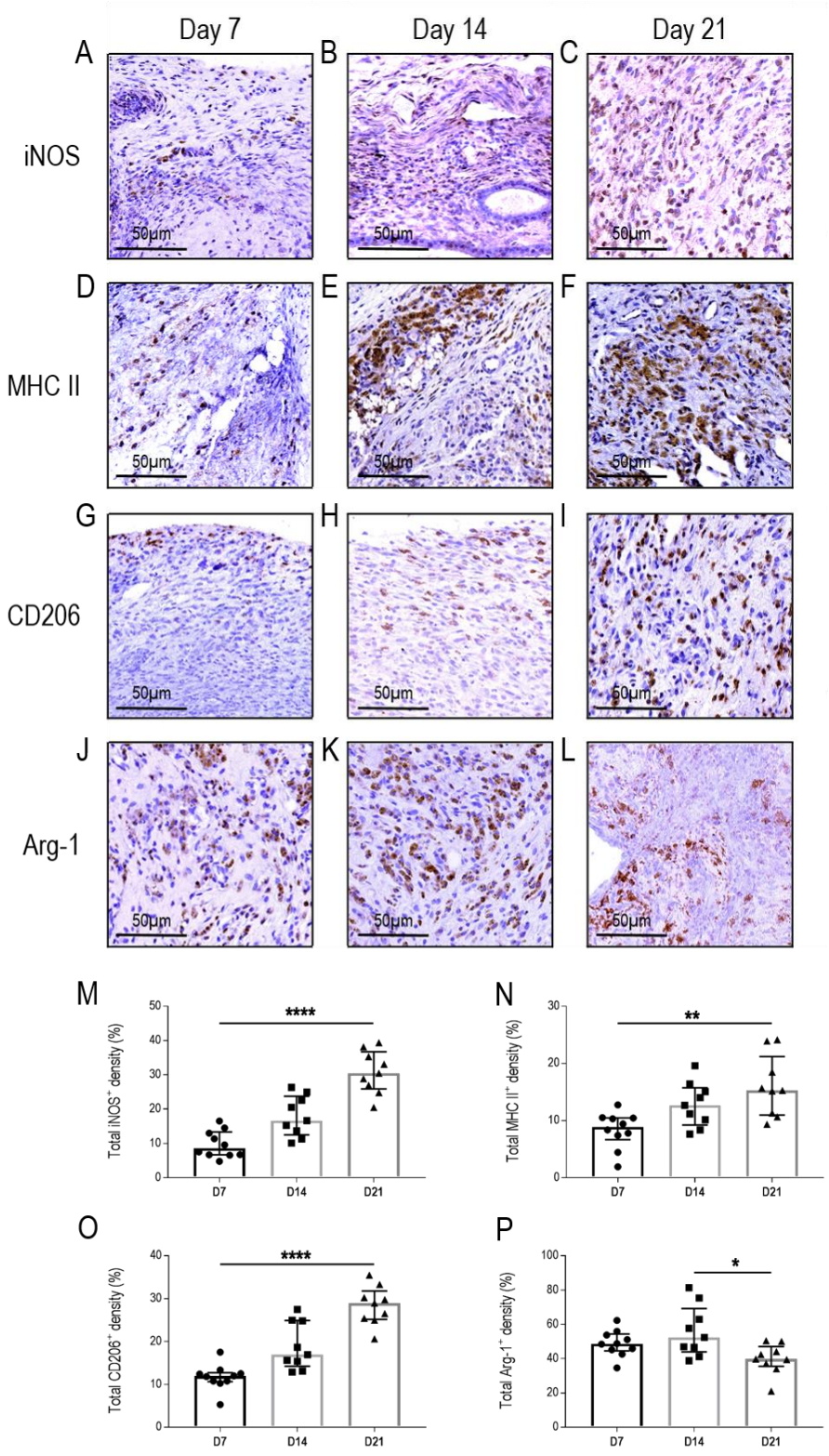

Figure 4.17 **M1-like (iNOS and MHCII) and M2–like (CD206 and Arg-1) immunostaining in endometriosis-like lesions from C57 donor to *miR-155*$^{-/-}$ recipient mice**

The expression of inducible nitric oxide synthase (iNOS) at D7 (**A**), D14 (**B**), and D21 (**C**) was quantified (**M**) in endometriosis-like lesions. Quantification of the Class II Major Histocompatibility Complex (MHC II) (**N**) was done at D7 (**D**), D14 (**E**) and D21 (**F**) in these lesions. CD206 density at D7 (**G**), D14 (**H**), and D21 (**I**) was quantified (**O**) in endometriosis-like lesions. Expression of Arginase-1 (Arg-1) (**P**) was evaluated at D7 (**J**), D14 (**K**) and D21 (**L**) in these lesions. Data are presented as median (IQR), with each symbol representative of a single lesion in one mouse (n=10 at D7, n=9 at D14, n=9 at D21). Analysis was done using the Kruskal-Wallis test followed by Dunn's multiple comparison test, with significance denoted as * ($p < 0.05$), ** ($p < 0.01$) and **** ($p < 0.0001$).

4.2.5.2. Endometriosis-like lesion development in *miR-155*$^{-/-}$ donor to C57 recipient transfers

Thirty two *miR-155*$^{-/-}$ donor mice were required to collect sufficient decidualised endometrial tissue for transfer into C57 recipient mice (*miR-155*$^{-/-}$ → C57) at a ratio of 1 donor to 0.95 recipients (Table 4.8). Overall, 83% of recipient mice developed identifiable lesions. Evaluation of mice at D7, and D14 showed successful lesion recovery in 80% of recipient mice, and at D21, lesions were recovered from 90% of recipient mice. A single mouse had more than one lesion and has been excluded from subsequent analyses.

Lesion appearance from *miR-155*$^{-/-}$ → C57 transfers was similar across all three time points, with a circular blood-filled appearance (Figure 4.18 A-C). Lesions gradually decreased in size over time (D7 (24 (14 – 35) mm^3); D14 (6 (2 – 16) mm^3); D21 (3 (2 – 4) mm^3, p = 0.0145 for D7 *vs* D21)) (Figure 4.18 D). Although a corresponding decrease in lesion weight was observed, this was not significant between time points (Figure 4.18 E).

H&E staining was performed to assess morphological parameters associated with lesion development in *miR-155*$^{-/-}$ → C57 mice (Figure 4.19 A-C). The number of glands per lesion (Figure 4.19 D), lumen area (Figure 4.20 F), epithelium area (Figure 4.19 G), glandular epithelium (Figure 4.19 H) and stromal area (Figure 4.20 I) was similar across all time points. In contrast, the average gland size per lesion reduced slightly between D7 and D14 (0.004 (0.000 – 0.006) mm^2 and 0.001 (0.000 – 0.002) mm^2); however, at D21, average gland size increased significantly to 0.007 (0.001 – 0.012) mm^2 (p = 0.0331 for D14 *vs* D21) (Figure 4.19 E).

F4/80 immunostaining was performed to localise macrophage density in *miR-155*$^{-/-}$→ C57 lesions (Figure 4.20). Total macrophage density gradually increased over the three week time course (3.84 (2.40 – 4.55) % at D7, 12.61 (11.39 – 16.68) % at D14, and 29.51 (21.84 – 41.37) % at D21; p < 0.0001 for D7 *vs* D21) (Figure 4.20 G). Peripheral F4/80 density (Figure 4.20 A-C) followed a similar trend between D7, D14 and D21 (12.21 (8.74 – 13.45) %, 16.35 (7.93 – 23.14) %, and 27.55 (20.72 – 39.12) % respectively; p = 0.0016 for D7 *vs* D21) (Figure 4.20 H). Central F4/80$^+$ density (Figure 4.20 D-F) was lowest at D7 (4.91 (2.91 – 10.84) %) and significantly increased at both D14 and D21 (18.32 (16.38 – 30.72) % and 42.99 (31.81 – 52.41) % respectively; p = 0.0441 for D7 *vs* D41 and p < 0.0001 for D7 *vs* D21) (Figure 4.20 I).

Expression of the M1-like marker iNOS increased significantly over time (4.11 (1.99 – 8.51) % at D7, 16.15 (11.37 – 28.22) % at D14; $p = 0.0486$ for D7 *vs* D14, and 31.45 (28.96 – 35.02) % at D21; $p < 0.0001$ for D7 *vs* D21) (Figure 4.21 A-C, M). Density of the M1-like marker MHC II also gradually increased between D7, D14 and D21 (2.72 (1.13 – 5.69) %, 13.80 (11.47 – 15.02) %, and 21.22 (17.27 – 32.21) % respectively; $p < 0.0001$ for D7 *vs* D21) (Figure 4.21 D-F, N). Expression of the M2-like macrophage marker CD206 gradually increased across the three time points (21.12 (12.45 – 29.02) % at D7, 34.82 (25.97 – 38.43) % at D14, 44.32 (38.46 – 49.80) % at D21; $p = 0.0003$ for D7 *vs* D21) (Figure 4.21 G-I, O). Alternatively the expression of Arg-1 was consistent across all time points (Figure 4.21 J-L, P).

Table 4.8 Endometriosis-like lesion recovery in *miR-155*$^{-/-}$ → C57 mice

Lesion collection time point	D7	D14	D21
Total number of *miR-155*$^{-/-}$ donor mice used across all time points: 32			
Number of C57 recipient mice	10	10	10
Number of mice with lesions*	8	8	9
Proportion of mice with lesions (%)	80	80	90

* To reduce bias, mice with ≥2 lesions were excluded from subsequent analyses. At D21 - 1 mouse excluded.

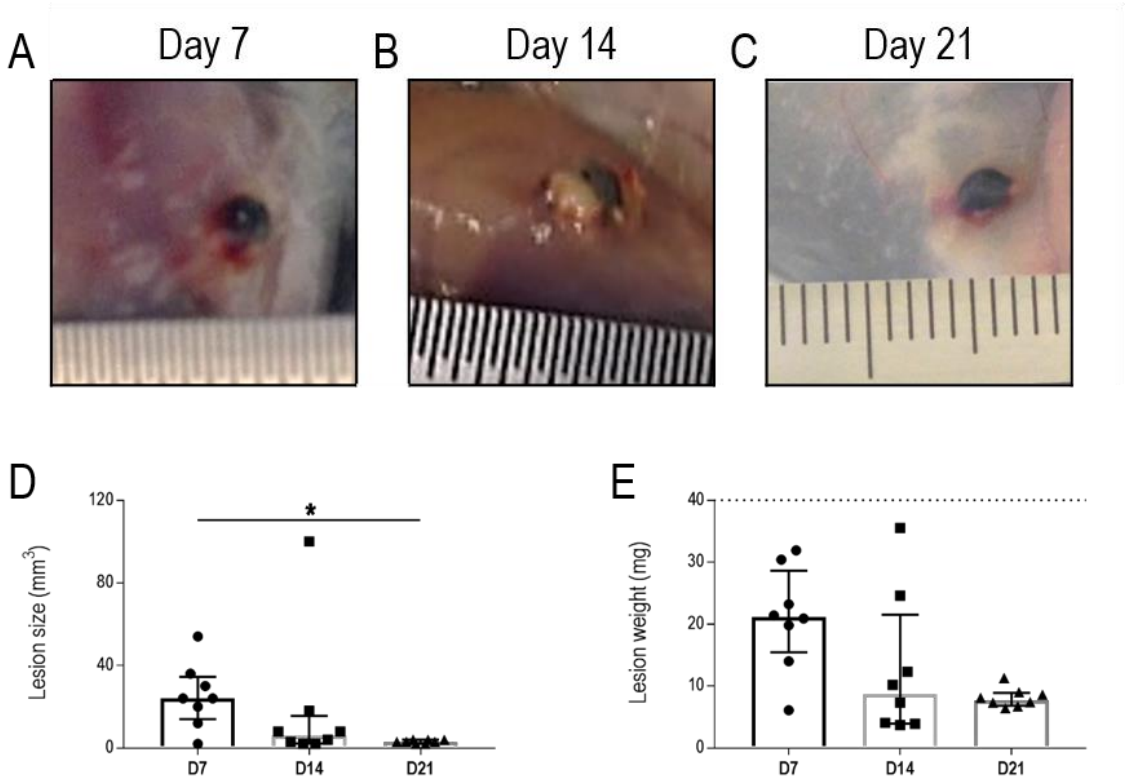

Figure 4.18 Gross morphology of endometriosis-like lesion development in a transfer from *miR-155*$^{-/-}$ donor to C57 recipient mice

Decidualised *miR-155*$^{-/-}$ donor endometrial tissue was injected subcutaneously into C57 recipient mice. Resulting lesions were harvested at either D7 (**A**), D14 (**B**) or D21 (**C**), with representative images shown. Lesion size was measured (**D**) and lesions were excised and weighed (**E**), with the dotted line indicating the initial weight of donor decidualised endometrial tissue inoculated into recipient mice (n=8 at D7, n=8 at D14, n=8 at D21). Data are presented as median (IQR), with each symbol representative of a single lesion in one mouse. Analysis was done using the Kruskal-Wallis test followed by Dunn's multiple comparison test, with significance denoted as * ($p < 0.05$).

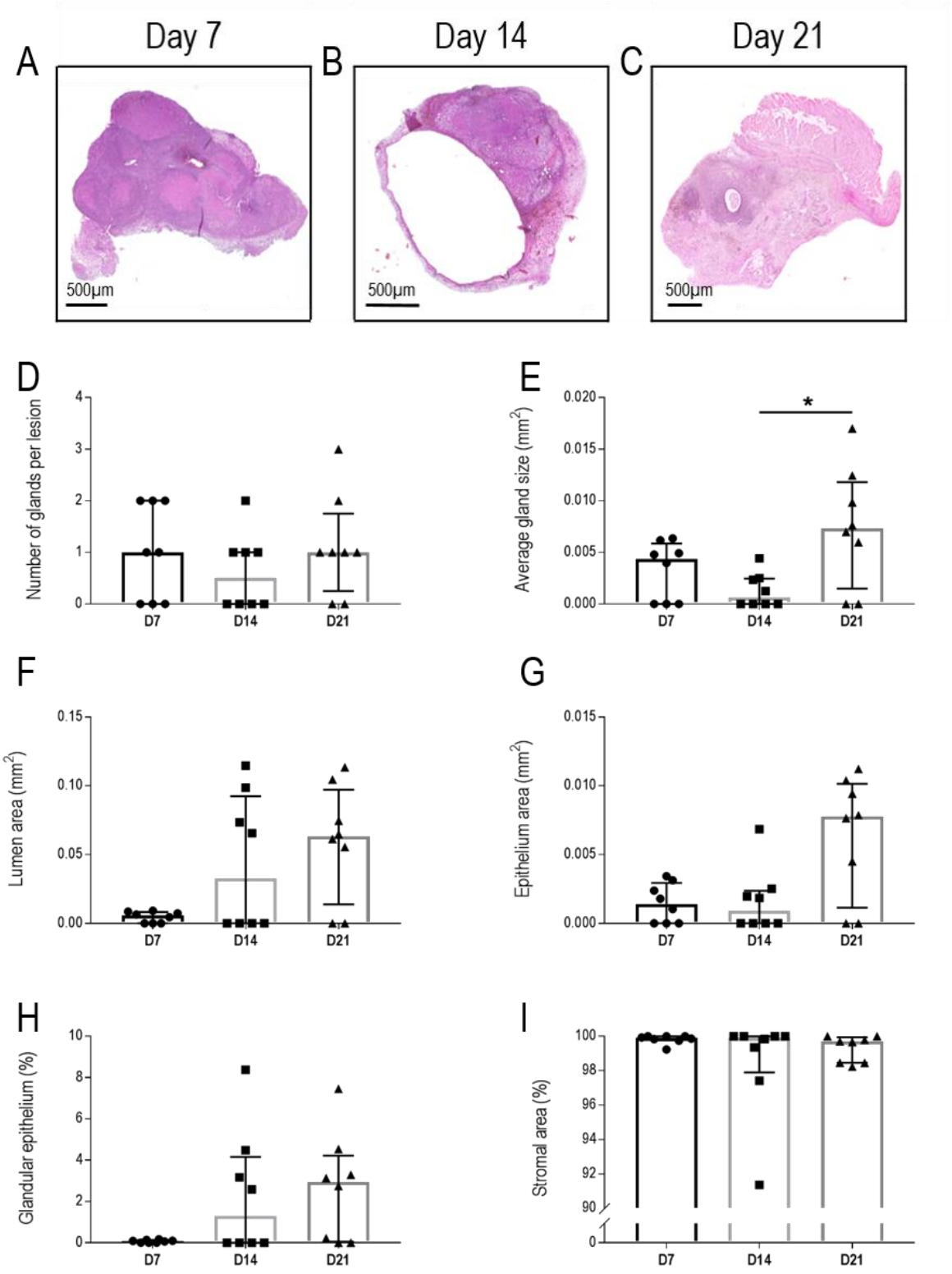

Figure 4.19 **Assessment of morphological parameters in haematoxylin and eosin stained endometriosis-like lesions from *miR-155*$^{-/-}$ donor to C57 recipient mice**

Haematoxylin and eosin stained sections from D7 **(A)**, D14 **(B)**, and D21 **(C)** lesions (representative images shown; arrows indicate glands) were assessed for the following characteristics: number of glands per lesion **(D)**, average gland size **(E)**, lumen area **(F)**, epithelium area **(G)**, percentage glandular epithelium **(H)** and percentage stromal area **(I)**. Data are presented as median (IQR), with each symbol representative of a single lesion in one mouse. Analysis was done using the Kruskal-Wallis test followed by Dunn's multiple comparison test, with significance denoted as * ($p < 0.05$).

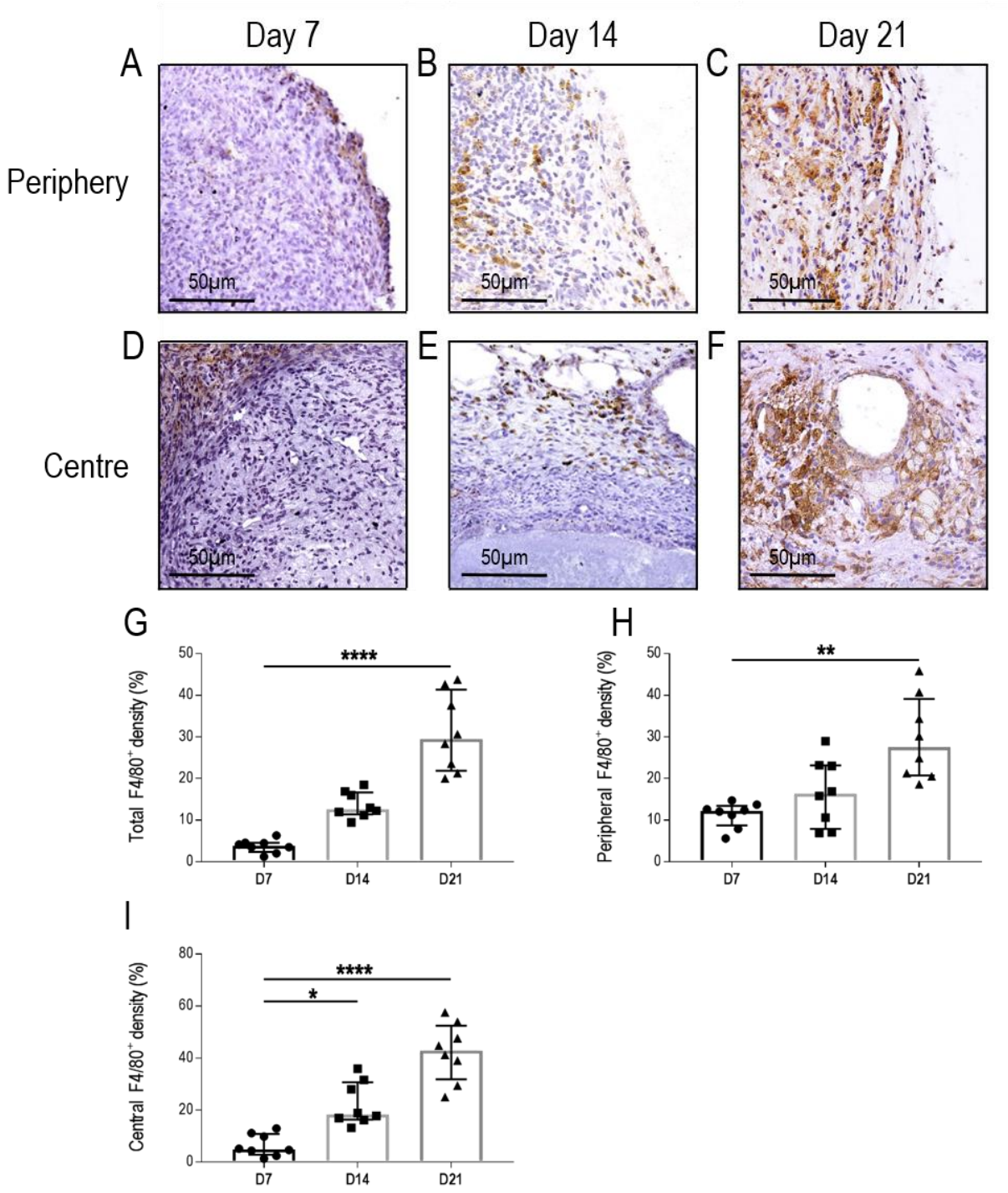

Figure 4.20 **F4/80 immunostaining in endometriosis-like lesions from *miR-155*$^{-/-}$ donor to C57 recipient mice**

Quantification of total F4/80 density was carried out in lesions from *miR-155*$^{-/-}$ donor to C57 recipient mice (**G**). F4/80 density at the lesion periphery (100µM from the edge of the lesion) at D7 (**A**), D14 (**B**) and D21 (**C**) was evaluated (**H**). F4/80 density at the lesion centre (within 500µM from the centre) at D7 (**D**), D14 (**E**), and D21 (**F**) was also quantified (**I**). Data are presented as median (IQR), with each symbol representative of a single lesion in one mouse (n=8 at D7, n=8 at D14, n=8 at D21). Analysis was done using the Kruskal-Wallis test followed by Dunn's multiple comparison test, with significance denoted as * ($p < 0.05$), ** ($p < 0.01$) and **** ($p < 0.0001$).

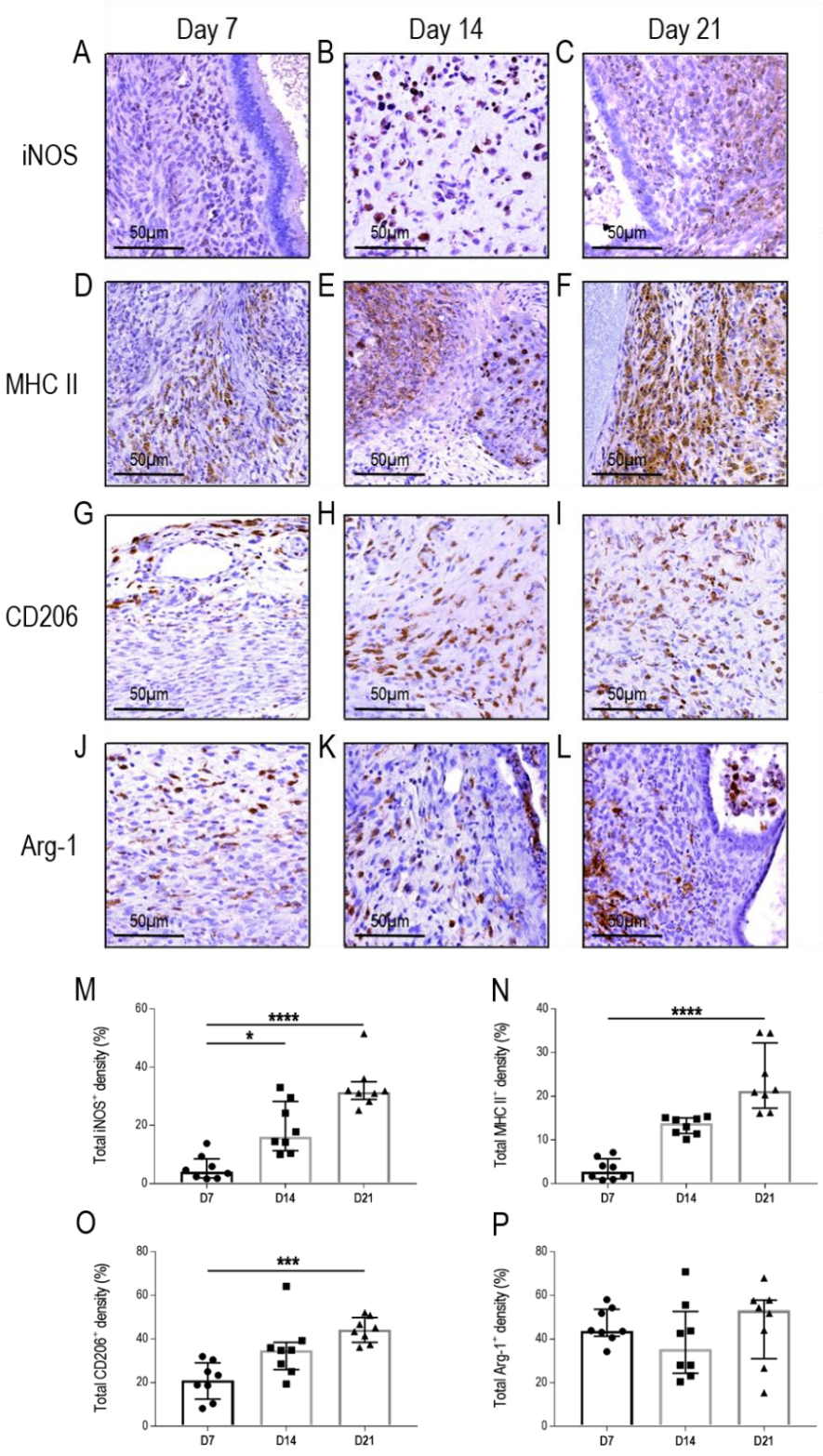

Figure 4.21 **M1-like (iNOS and MHCII) and M2–like (CD206 and Arg-1) immunostaining in endometriosis-like lesions from *miR-155*$^{-/-}$ donor to C57 recipient mice**

The expression of inducible nitric oxide synthase (iNOS) at D7 (**A**), D14 (**B**), and D21 (**C**) was quantified (**M**) in endometriosis-like lesions. Quantification of the Class II Major Histocompatibility Complex (MHC II) (**N**) was done at D7 (**D**), D14 (**E**) and D21 (**F**) in these lesions. CD206 density at D7 (**G**), D14 (**H**), and D21 (**I**) was quantified (**O**) in endometriosis-like lesions. Expression of Arginase-1 (Arg-1) (**P**) was evaluated at D7 (**J**), D14 (**K**) and D21 (**L**) in these lesions. Data are presented as median (IQR), with each symbol representative of a single lesion in one mouse (n=8 at D7, n=8 at D14, n=8 at D21). Analysis was done using the Kruskal-Wallis test followed by Dunn's multiple comparison test, with significance denoted as * ($p < 0.05$), *** ($p < 0.001$) and **** ($p < 0.0001$).

4.2.5.3. Comparison of lesion development in *miR-155*$^{-/-}$ ↔ C57 reciprocal transfer mice with syngeneic C57 and syngeneic *miR-155*$^{-/-}$ mice

To evaluate the effect of a *miR-155* deficiency present either in the recipient environment (C57 → *miR-155*$^{-/-}$ transfer) or in the donor endometrial tissue (*miR-155*$^{-/-}$ → C57 transfer), comparisons of morphometric and immunohistochemical results in these reciprocal transfer models were made against corresponding results from the syngeneic C57 (C57 → C57 transfer) and the syngeneic *miR-155*$^{-/-}$ (*miR-155*$^{-/-}$ → *miR-155*$^{-/-}$ transfer) models.

4.2.5.3.1. C57 → *miR-155*$^{-/-}$ lesion development *vs* C57 → C57 lesion development

While lesion size was similar across time points, C57 → *miR-155*$^{-/-}$ lesions were 2.8-fold larger than C57 → C57 lesions at D21 ($p = 0.0014$) (Figure 4.22 A, B). The number of glands was significantly lower in C57 → *miR-155*$^{-/-}$ lesions compared to C57 → C57 lesions at D14 (100% lower, $p = 0.0023$) and D21 (69% lower, $p < 0.0001$) (Figure 4.22 C). Average gland size was 100% lower in C57 → *miR-155*$^{-/-}$ lesions compared to C57 → C57 lesions at D14 ($p = 0.0032$) but was comparable at other time points (Figure 4.22 D). Lumen area was significantly lower in C57 → *miR-155*$^{-/-}$ lesions compared to C57 → C57 lesions at D14 (100% lower, $p = 0.0072$) and D21 (95% lower, $p = 0.0006$) (Figure 4.22 E). Epithelium area was significantly lower in C57 → *miR-155*$^{-/-}$ lesions compared to C57 → C57 lesions at D14 (100% lower, $p = 0.0013$) and D21 (73% lower, $p = 0.0073$) (Figure 4.22 F). Likewise, glandular epithelium was significantly lower in C57 → *miR-155*$^{-/-}$ lesions compared to C57 → C57 lesions at D14 (100% lower, $p = 0.0032$) and D21 (98% lower, $p = 0.0006$) (Figure 4.22 G). In contrast, stromal area was significantly higher in C57 → *miR-155*$^{-/-}$ lesions compared to C57 → C57 lesions at D14 (1.02-fold higher, $p = 0.0032$) and D21 (1.02-fold higher, $p = 0.0003$) (Figure 4.22 H).

At D7, total F4/80 density was 64% lower in C57 → *miR-155*$^{-/-}$ lesions compared to C57 → C57 lesions ($p = 0.0008$) (Figure 4.23 A). Peripheral F4/80 expression was unchanged between C57 → *miR-155*$^{-/-}$ lesions and C57 → C57 lesions over the three weeks (Figure 4.23 B). Central F4/80 expression was 58% lower in C57 → *miR-155*$^{-/-}$ lesions compared to C57 → C57 lesions at D14 ($p = 0.0056$), but similar at all other time points (Figure 4.23 C). The total density of iNOS was 64% lower in C57 → *miR-155*$^{-/-}$ lesions compared to C57 → C57 lesions at D7 ($p < 0.0001$), whereas by D21, iNOS expression was 1.8-fold higher in C57 → *miR-155*$^{-/-}$ lesions ($p = 0.0010$) (Figure 4.23 D). Total MHC II density was 55% lower in C57 → *miR-155*$^{-/-}$ lesions compared to C57 → C57 lesions at D7 ($p = 0.0056$) (Figure 4.23 E). Total CD206 expression was 27% lower C57 → *miR-155*$^{-/-}$ lesions compared to C57 → C57 lesions at D21 ($p < 0.0001$) (Figure 4.23 F). In contrast, Arg-1 expression was 2.2-fold higher at D7 ($p < 0.0001$) and 2.2-

fold higher at D14 (p < 0.0001) and 1.6-fold higher at D21 (p = 0.0079) in C57 → *miR-155*$^{-/-}$ lesions compared to C57 → C57 lesions (Figure 4.23 G).

4.2.5.3.2. C57 → *miR-155*$^{-/-}$ lesion development *vs miR-155*$^{-/-}$ → *miR-155*$^{-/-}$ lesion development

Lesion development in C57 → *miR-155*$^{-/-}$ and *miR-155*$^{-/-}$ → *miR-155*$^{-/-}$ were comparable across all morphometric parameters, except for lesion weight, wherein lesions were 1.9-fold heavier in C57 → *miR-155*$^{-/-}$ at D21 (p = 0.0014) (Figure 4.22). There was a 52% reduction in total F4/80 density between C57 → *miR-155*$^{-/-}$ lesions and *miR-155*$^{-/-}$ → *miR-155*$^{-/-}$ lesions at D7 (p < 0.0001) (Figure 4.23 A). While peripheral F4/80 density in C57 → *miR-155*$^{-/-}$ lesions was 1.7-fold higher at D7 (p = 0.0056) and 21.-fold higher at D14 (p = 0.0053) compared to *miR-155*$^{-/-}$ → *miR-155*$^{-/-}$ lesions, no differences were observed in central F4/80 density (Figure 4.23 B,C). Total iNOS density was 43% lower in C57 → *miR-155*$^{-/-}$ lesions compared to *miR-155*$^{-/-}$ → *miR-155*$^{-/-}$ lesions at D7 (p = 0.0093) (Figure 4.23 D). MHC II density was significantly elevated in C57 → *miR-155*$^{-/-}$ lesions compared to *miR-155*$^{-/-}$ → *miR-155*$^{-/-}$ lesions at D7, D14 and D21 (5.1-fold higher, p < 0.0001, 2.3-fold higher, p < 0.0001, and 4.4-fold higher, p < 0.0001 respectively) (Figure 4.23 E). In contrast, CD206 density was significantly lower in C57 → *miR-155*$^{-/-}$ lesions compared to *miR-155*$^{-/-}$ → *miR-155*$^{-/-}$ lesions at D7, D14 and D21 (46% lower, p < 0.0001, 48% lower, p = 0.0029, and 17% lower, p = 0.0019 respectively) (Figure 4.23 F). Arg-1 expression 1.3-fold higher in C57 → *miR-155*$^{-/-}$ lesions compared to *miR-155*$^{-/-}$ → *miR-155*$^{-/-}$ lesions at D7 (p = 0.0047) (Figure 4.23 G).

4.2.5.3.3. *miR-155*$^{-/-}$ → C57 lesion development *vs* C57 → C57 lesion development

At D21, although lesions were 57% smaller (p = 0.0016) in *miR-155*$^{-/-}$ → C57 mice, lesions were 2.9-fold heavier (p = 0.0002) compared to C57 → C57 mice (Figure 4.22 A, B). The number of glands per lesion in *miR-155*$^{-/-}$ → C57 mice was 90% lower at D14 (p = 0.0042) and 85% lower at D21 (p = 0.0002) compared to C57 → C57 mice (Figure 4.22 C). Average gland size was 94% smaller in *miR-155*$^{-/-}$ → C57 mice compared to C57 → C57 mice at D14 (p = 0.0107) (Figure 4.22 D). Epithelium area was 97% less at D14 (p = 0.0046) in *miR-155*$^{-/-}$ → C57 mice compared to C57 → C57 mice (Figure 4.22 F). Percentage stromal area was 1.03-fold higher in *miR-155*$^{-/-}$ → C57 mice compared to C57 → C57 mice at D21 (p = 0.0047) (Figure 4.22 H). No differences were observed in lumen area or percentage glandular epithelium between groups (Figure 4.22 E, G).

Total F4/80 density was 65% lower in *miR-155*$^{-/-}$ → C57 lesions compared to C57 → C57 lesions at D7 (p = 0.0030), however, by D21, *miR-155*$^{-/-}$ → C57 lesions hand 1.7-fold more total F4/80 expression (p =

0.0047) (Figure 4.23 A). While peripheral F4/80 density was 69% lower at D7 ($p < 0.0001$) and 60% lower at D14 ($p = 0.0007$) in *miR-155*$^{-/-}$ → C57 lesions, no differences were observed in central F4/80 density (Figure 4.23 B, C). Total iNOS density was 83% lower at D7 ($p < 0.0001$) in *miR-155*$^{-/-}$ → C57 lesions compared to C57 → C57 lesions, whereas by D21, iNOS density was 1.9-fold higher in *miR-155*$^{-/-}$ → C57 lesions ($p = 0.0003$) (Figure 4.23 D). Total MHC II expression was 86% lower in *miR-155*$^{-/-}$ → C57 lesions at D7 ($p = 0.0005$) (Figure 4.23 E). In contrast, total CD206 expression was 2.8-fold higher in *miR-155*$^{-/-}$ → C57 lesions compared to C57 → C57 lesions at D7 ($p = 0.0011$), while Arg-1 density increased 2-fold at D7 ($p < 0.0001$) (Figure 4.23 F,G).

4.2.5.3.4. *miR-155*$^{-/-}$ → C57 lesion development *vs miR-155*$^{-/-}$ → *miR-155*$^{-/-}$ lesion development

Lesions were 75% smaller ($p < 0.0001$) in *miR-155*$^{-/-}$ → C57 mice compared to *miR-155*$^{-/-}$ → *miR-155*$^{-/-}$ mice at D21 (Figure 4.22 A). Although lesion weight in both groups reduced over time, lesions remained 2-fold larger in *miR-155*$^{-/-}$ → C57 mice at D21 ($p < 0.0001$) (Figure 4.22 B). No differences were observed in the number of glands, average gland size, lumen area, epithelium area, percentage glandular epithelium or percentage stromal area between groups (Figure 4.22 C-H).

Total F4/80 density was reduced by 54% in *miR-155*$^{-/-}$ → C57 lesions compared to *miR-155*$^{-/-}$ → *miR-155*$^{-/-}$ lesions at D7 ($p < 0.0001$), however, no differences were observed in either peripheral or central F4/80 density (Figure 4.23 A-C). A 73% reduction in total iNOS expression was noted in *miR-155*$^{-/-}$ → C57 lesions compared to *miR-155*$^{-/-}$ → *miR-155*$^{-/-}$ lesions at D7 ($p = 0.0002$), whereas total MHC II density was 2.5-fold higher at D14 ($p < 0.0001$) and 6.1-fold higher at D21 ($p < 0.0001$) (Figure 4.23 D,E). No differences were observed in either total CD206 or total Arg-1 density (Figure 4.23 F, G).

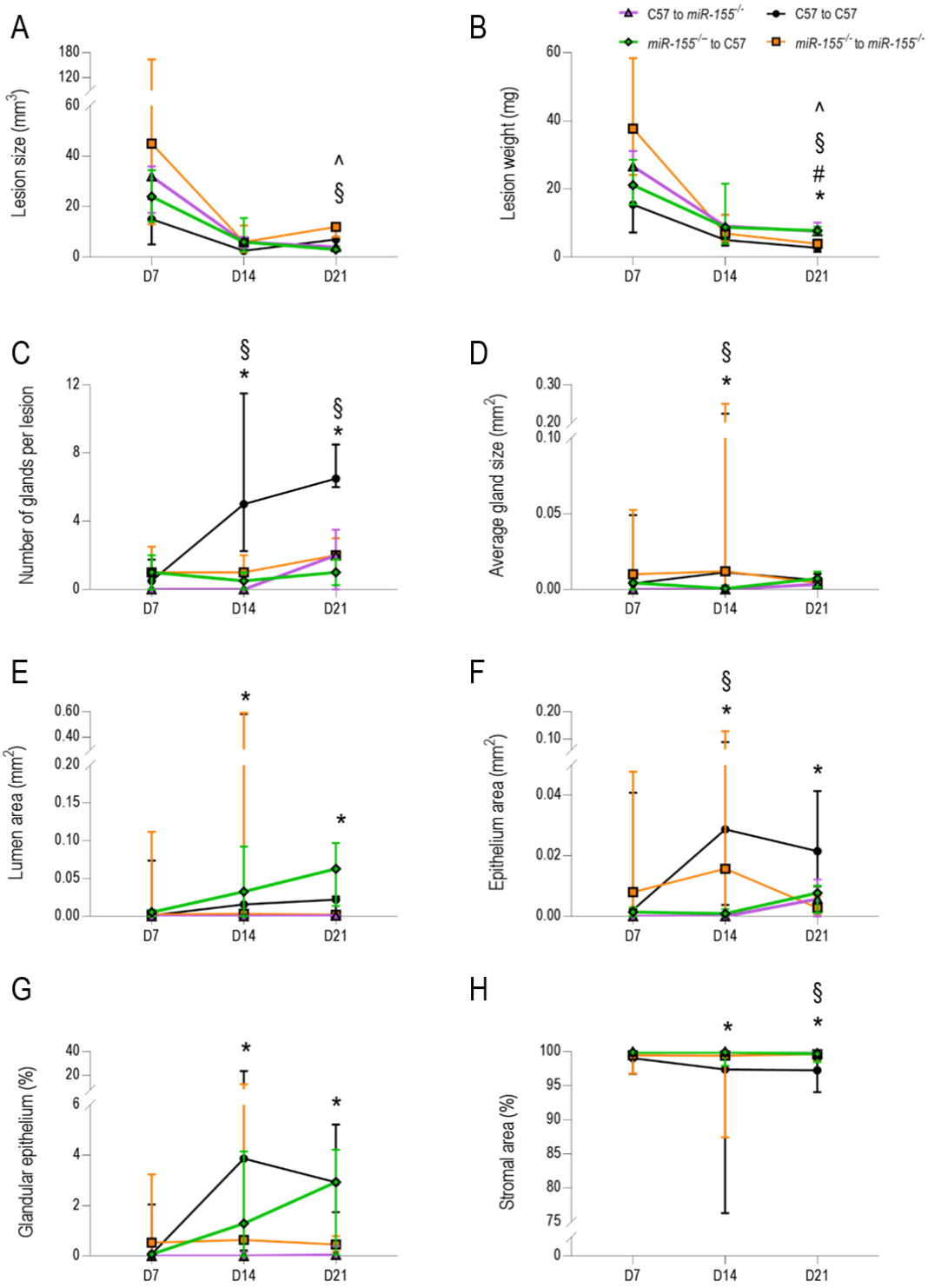

Figure 4.22 **Comparative analysis of morphometric parameters between syngeneic C57 and *miR-155*$^{-/-}$ models with reciprocal *miR-155*$^{-/-}$ cross transfer models**

Comparisons of lesion size (**A**), weight (**B**), number of glands per lesion (**C**), average gland size (**D**), lumen area (**E**), epithelium area (**F**), glandular epithelium (**G**), and stromal area (**H**) between C57 → C57 mice (; n=12 at D7, n=12 at D14, n=8 at D21) and *miR-155*$^{-/-}$ → *miR-155*$^{-/-}$ mice (; n=17 at D7, n=17 at D14, n=13 at D21)) against either C57 → *miR-155*$^{-/-}$ mice (; n=10 at D7, n=9 at D14, n=9 at D21) or *miR-155*$^{-/-}$ → C57 mice (; n=8 at D7, n=8 at D14, n=8 at D21) was performed. Data are presented as median (IQR). Analysis was done using the Kruskal-Wallis test followed by Bonferroni-Dunn's multiple comparison test, with significance inferred at $p < 0.0125$. ***** indicates significance between C57 → C57 and C57 → *miR-155*$^{-/-}$; **#** indicates significance between *miR-155*$^{-/-}$ → *miR-155*$^{-/-}$ and C57 → *miR-155*$^{-/-}$; **§** indicates significance between C57 → C57 and *miR-155*$^{-/-}$ → C57; **^** indicates significance between *miR-155*$^{-/-}$ → *miR-155*$^{-/-}$ and *miR-155*$^{-/-}$ →C57.

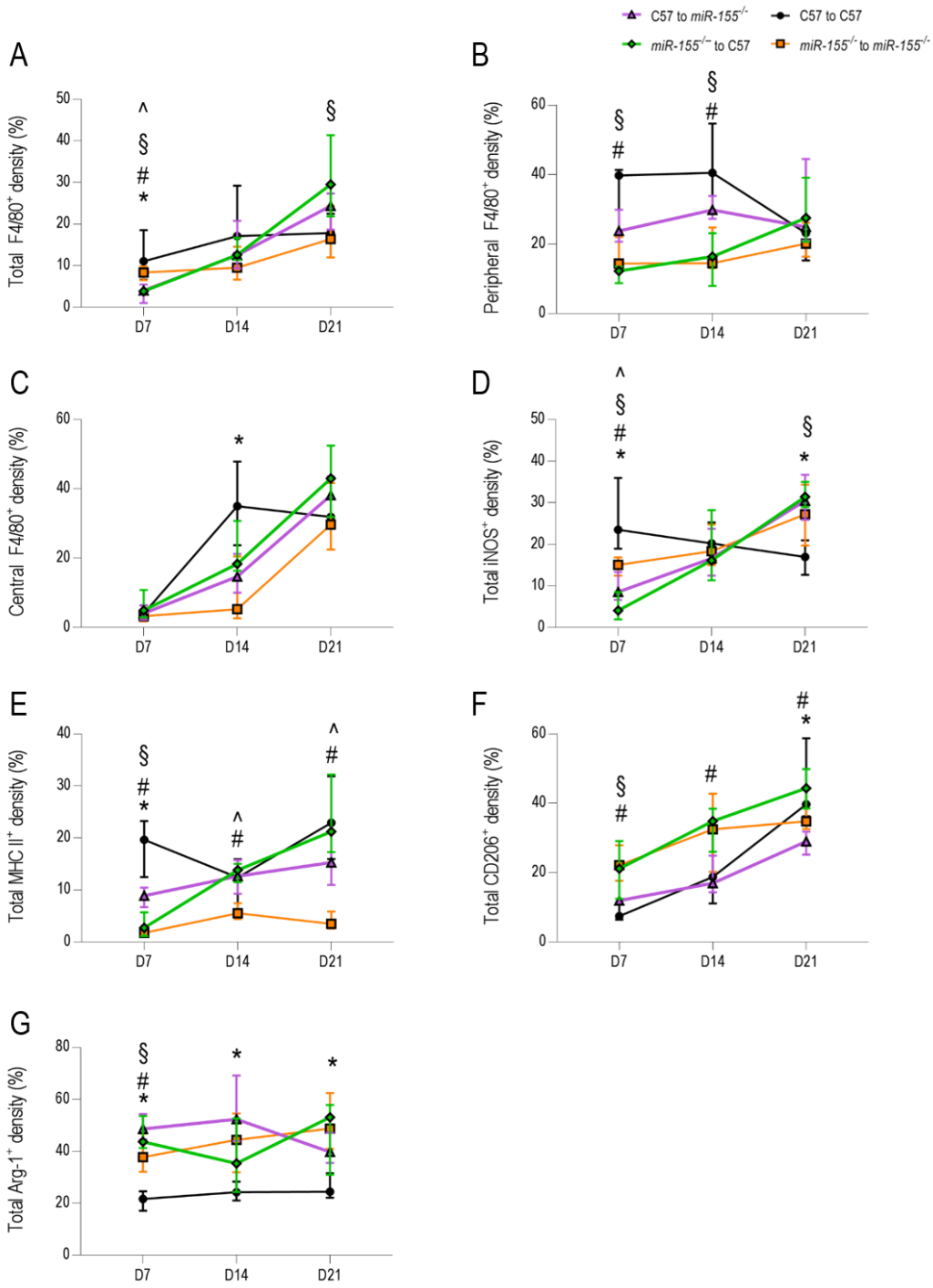

Figure 4.23 **Comparative analysis of macrophage markers between syngeneic C57 and *miR-155*$^{-/-}$ models with reciprocal *miR-155*$^{-/-}$ cross transfer models**

Total (**A**), peripheral (**B**), and central (**C**) F4/80 density were compared between C57 → C57 mice (; n=12 at D7, n=12 at D14, n=8 at D21) and *miR-155*$^{-/-}$ → *miR-155*$^{-/-}$ mice (; n=17 at D7, n=17 at D14, n=13 at D21)) against either C57 → *miR-155*$^{-/-}$ mice (; n=10 at D7, n=9 at D14, n=9 at D21) or *miR-155*$^{-/-}$ → C57 mice (; n=8 at D7, n=8 at D14, n=8 at D21). Comparisons between the M1-like macrophage markers iNOS (**D**) and MHC II (**E**), and the M2-like macrophage markers CD206 (**F**) and Arg-1 (**G**) were also performed. Data are presented as median (IQR). Analysis was done using the Kruskal-Wallis test followed by Bonferroni-Dunn's multiple comparison test, with significance inferred at $p < 0.0125$. ***** indicates significance between C57 → C57 and C57 → *miR-155*$^{-/-}$; **#** indicates significance between *miR-155*$^{-/-}$ → *miR-155*$^{-/-}$ and C57 → *miR-155*$^{-/-}$; **§** indicates significance between C57 → C57 and *miR-155*$^{-/-}$ → C57; **^** indicates significance between *miR-155*$^{-/-}$ → *miR-155*$^{-/-}$ and *miR-155*$^{-/-}$ →C57.

4.3. DISCUSSION

This study was undertaken to investigate the role of *miR-155* in the establishment and progression of endometriotic-like lesions in a subcutaneous menstrual mouse model of endometriosis. *miR-155* is expressed in a range of haematopoietic cells, including stem cells, monocytes, granulocytes, T-cells and B-cells, and has roles in the regulation of myelopoiesis and erythropoiesis (Georgantas et al., 2007, Landgraf et al., 2007, Masaki et al., 2007). The expression of *miR-155* is induced by the presence of inflammatory stimuli, including IL-1α, IL-1β, TNF-α, pathogen-associated molecular patterns and damage-associated molecular patterns (O'Connell et al., 2007, Kurowska-Stolarska et al., 2017), and hypoxic conditions (Bruning et al., 2011). In contrast, the presence of anti-inflammatory cytokines such as TGFβ and IL-10 decrease the expression of *miR-155* (Kong et al., 2008, Quinn et al., 2014).

Following an inflammatory challenge, *miR-155* is induced in monocytes and macrophages, and contributes to the upregulation of an M1-like pro-inflammatory response (Jablonski et al., 2016). Moreover, *miR-155* inhibits the polarisation of M2-like macrophages through the regulation of the TGFβ signalling pathway, in which Smad2 signalling in macrophages is impeded, thereby preventing the expression of IL-4Rα and subsequent development of tissue remodelling macrophages (Louafi et al., 2010). In addition, *miR-155* inhibits the development of STAT6-driven anti-inflammatory macrophages through targeting multiple molecules in the IL-13/IL-4 signalling pathway (He et al., 2009, Martinez-Nunez et al., 2011).

4.3.1. A systemic deficiency of *miR-155* results in endometriosis-like lesions reminiscent of C57 lesions

Approximately 92% of *miR-155*$^{-/-}$ mice had endometriosis-like lesion development, supporting the use of this model to study disease development. In the absence of *miR-155*, developing lesions had characteristic features of endometriosis, however, despite the significant decrease in lesion size and weight between D7 to D21, morphometric analyses did not uncover differences in glandular fractions over time. The overall pattern of lesion development in these mice was consistent with C57 mice at D7 and D14, however differences in gland formation was apparent at D21, with *miR-155*$^{-/-}$ lesions having a lower number of glands present and a lower percentage glandular epithelium. An important observation however, is that the number of glands did not change from D7 to D21 in *miR-155*$^{-/-}$ lesions, and that average gland size remained similar between C57 and *miR-155*$^{-/-}$ lesions over time. In addition, lesions from *miR-155*$^{-/-}$ mice remained dark and opaque throughout this study compared to C57 lesions, which suggests potential differences at a cellular or molecular level.

Clinical evaluation in women with true black opaque endometriotic lesions found reduced concentrations of VEGF, IL-6, MCP-1 and hepatocyte growth factor in the peritoneal fluid, suggesting that these lesions display altered cellular activity and immune activation compared to non-opaque or red lesions (Khan et al., 2004). From the RNA-Seq pathway analysis of *miR-155*$^{-/-}$ lesions, a downregulation of IL-6 signalling was observed at both D7 and D14 compared to the decidualised endometrium. This suggests that the absence of overt changes in gland formation in *miR-155*$^{-/-}$ mice may not be the only indicator of lesion establishment, and could indicate that development of *miR-155*$^{-/-}$ lesions may be progressing at slower rate compared to C57 lesions, as all other parameters were comparable. Therefore, in a clinical setting wherein miR-155 is downregulated in plasma from women with endometriosis (Nisenblat et al., 2019), it is possible that *miR-155* expression may be an indicator of the type of predominant lesion type (e.g. red opaque vs true black) that is present in these women.

In a clinical setting, the Wnt/β-catenin signalling pathway is aberrantly activated in women with endometriosis compared to healthy controls (Pazhohan et al., 2018). Moreover, in mice, endometrial gland formation is linked to the expression of lymphoid enhancing factor 1 (*Lef1*), a known target of the Wnt/β-catenin signalling cascade (Shelton et al., 2012, Zhang et al., 2013). The RNA-Seq data from this study supports this observation, as the canonical Wnt/β-catenin signalling pathway is upregulated in D7 lesions compared to decidualised endometrium, with KEGG pathway analysis showing a consistent increase in the Wnt pathway over time (Appendix: Figure 7.5 and Table 7.2 – Cluster 7). In addition, in the absence of *miR-155*, the expression of *Lef1* is upregulated in D7 lesions ($log_2FC = 3.893$; FDR < 0.0001) and D14 lesions ($log_2FC = 3.617$; FDR < 0.0001) compared to decidualised endometrium (Supplementary material Table 4 and 5). Surprisingly, in contrast with these observations, an *in vitro* study demonstrated that the overexpression of *miR-155* activates the Wnt/β-catenin signalling cascade (Zhang et al., 2013). This discrepancy may be due to miRNA network redundancy (Luck et al., 2015) or a miRNA compensatory mechanism (El-Brolosy et al., 2019), as in addition to *miR-155* regulation of the Wnt/β-catenin signalling pathway, *miR-410* (Zhang et al., 2016b) and *miR-374a* (Cai et al., 2013) positively regulate this pathway, while *miR-200a* (Su et al., 2012) and *miR-34* (Kim et al., 2011) downregulate this pathway. Therefore, while it is possible that endometrial gland development in the absence of *miR-155* may be a consequence of elevated Wnt/ β-catenin signalling, additional epigenetic regulators are likely to be involved in the progression of endometriotic lesions.

4.3.2. The absence of *miR-155* promotes M2-like immune activity in endometriotic lesions

miR-155 is involved in the polarisation of monocytes into M1-like, pro-inflammatory macrophages (Jablonski et al., 2016, O'Connell et al., 2007, Wang et al., 2013a), and in the context of endometriosis, elevated M1-like activity is associated with decreased lesion growth and survival (Bacci et al., 2009). In these mice, systemic depletion of *miR-155* shifts the immune system towards an anti-inflammatory response, with increased levels of M2-like macrophages (He et al., 2015). Previous work has shown that high levels of M2-like macrophages promotes tissue remodelling in endometriosis (Bacci et al., 2009), and thus, could account for the observed survival and growth of endometriosis-like lesions in *miR-155*$^{-/-}$ mice. Therefore, to help understand why gland formation is arrested in *miR-155* lesions, it is important to evaluate the presence and activation status of macrophages in these lesions.

In the *miR-155*$^{-/-}$ mouse model of endometriosis, an increase in total F4/80^{+} macrophages was seen over time, coupled with an influx of macrophages into the centre of the lesion. A study looking at the impact of *miR-155* in monocyte chemokine and chemokine receptor expression found that *miR-155*$^{-/-}$ bone marrow monocytes exhibited downregulated CCR7 and upregulated CCR2 expression (Elmesmari et al., 2016). CCR7 has an important role in lymphocyte recruitment and homing of immune cells, and a CCR7 deficiency has been shown to restrict the migration of dendritic cells (Förster et al., 2008). Similarly, CCR2 harbours a receptor for monocyte chemoattractant protein- 1 (MCP-1), which mediates monocyte chemotaxis and infiltration (Mak and Uetrecht, 2019). Therefore, in this study, the lower macrophage numbers in *miR-155*$^{-/-}$ lesions compared to C57 lesions at D7 may be attributed to a reduced lymphocyte recruitment capacity as a result of downregulated CCR7 (*miR-155*$^{-/-}$ decidualised endometrium *vs* D7 lesions, $\log_2$FC = -2.876; FDR = 0.0167) (Supplementary material Table 4). However, by D21, total macrophage numbers are significantly higher in *miR-155*$^{-/-}$ lesions compared to C57 lesions, suggesting a delayed infiltration of macrophages, which may potentially be mediated by the upregulation of CCR2. This is further supported by the increased expression of CCR2 observed in *miR-155*$^{-/-}$ lesions at D14 compared to D7 ($\log_2$FC = 1.191; FDR = 0.0055) (Supplementary material Table 6).

Following LPS stimulation in mice, *miR-155*$^{-/-}$ bone marrow-derived macrophages exhibited a decrease in the expression of the pro-inflammatory cytokines TNF-α and IL-1β (Kurowska-Stolarska et al., 2011). Moreover, in a *miR-155*$^{-/-}$ model of induced colitis, a decrease in M1-like genes (*IL-1β*, *IL-6*, *IL-12* and *TNF-α*) was observed, while expression of M2-like genes (*Arg-1*, *IL-10*, *Fizz1* and *Mrc1*) were upregulated (Li et al., 2018). As a deficiency in *miR-155* results in the suppression of M1-like macrophage activity, it was unsurprising to note that levels of both M2-like markers, CD206 and Arg-1, increased significantly

over time, with a higher expression of both markers observed in *miR-155*$^{-/-}$ lesions compared to C57 lesions at D7. Data from the *miR-155*$^{-/-}$ RNA-Seq analysis confirms this observation, with a decrease in Arg-1 seen at D7 compared to decidualised endometrium (log_2FC = -9.418; FDR = 0.0131) (Supplementary material Table 4), and an increase of Arg-1 expression observed between D7 and D14 lesions (log_2FC = 2.902; FDR = 0.0040) (Supplementary material Table 6).

While the density of the M1-like macrophage marker MHC II remained significantly lower in *miR-155*$^{-/-}$ lesions compared to C57 lesions, the gradual increase in iNOS expression over the three weeks of lesion development was unexpected, as L-arginine is a common substrate for both arginase and NO synthase (Lee et al., 2017). In contrast to previous work, this study did not observe an inverse relationship between Arg-1 and iNOS expression due to competition for their common substrate L-arginine (McLarren et al., 2011). Nonetheless, information surrounding the role of *miR-155* in regulation of the Arg-1/iNOS balance is conflicting. An upregulation of Arg-1 and Arg-2 in *miR-155* deficient mice has been observed, with a corresponding reduction in iNOS activity (Arranz et al., 2012, Dunand-Sauthier et al., 2014). In contrast, in myeloid-derived suppressor cells, depletion of *miR-155* resulted in the reduction of both Arg-1 and iNOS (Chen et al., 2015b). However, in the context of endometriosis, immunohistochemical analysis of lesions from a mouse model demonstrated an overlap of Arg-1 expression with the inflammatory markers iNOS and MHC II (Johan et al., 2019). This finding suggests a subtle shift between M1-like and M2-like immune activity may occur throughout the development of endometriosis.

At D21, data from this study showed comparable numbers of blood vessels per lesion, average blood vessel size, and αSMA density. Alternatively, the density of fibrosis remained significantly lower in *miR-155*$^{-/-}$ lesions compared to C57 lesions at all time points. This finding is surprising, as a deficiency of *miR-155* has been shown to exacerbate fibrosis, as demonstrated in a pulmonary fibrosis mouse model (Kurowska-Stolarska et al., 2017). Emerging evidence suggests that macrophage-derived exosomes are able to regulate the function of adjacent cells, including fibroblasts (Wang et al., 2017, Alivernini et al., 2017, Sun et al., 2018, Schjenken et al., 2019). In particular, following cardiac injury, cardiac fibroblasts absorb *miR-155*-enriched exosomes secreted by macrophages, resulting in the elevated production of inflammatory mediators with a reduction in SOCS-1 mediated fibroblast proliferation (Wang et al., 2017). Indeed, the results from this chapter show significantly elevated αSMA^{+} myofibroblast activity at D14 in *miR-155*$^{-/-}$ lesions compared to C57 lesions, confirming a role for *miR-155* in the regulation of fibroblast proliferation in the progression of endometriosis. However, the overall lack of fibrosis despite the observed increase in M2-like immune remodelling activity warrants further investigation.

Although chronic pain is a common and debilitating symptom of endometriosis, there remains a poor correlation between symptom severity and lesion load or distribution (Morotti et al., 2017, Coxon et al., 2018). A recent study in a mouse model of endometriosis found that central glial adaptations mediated by changes in microglial CD11b and astrocytic glial fibrillary acidic protein expression occurs in association with endometriosis-like lesions (Dodds et al., 2019). In *miR-155*$^{-/-}$ lesions, a consistent increase in KEGG pathways associated with axon guidance, neuroactive ligand-receptor interaction, and synaptic vesicle cycle was observed over time (Appendix: Figure 7.5 and Table 7.2 – Cluster 7). A study looking at axon regeneration following spinal cord injury in mice demonstrated that a *miR-155* deletion reduced macrophage-mediated inflammation and neuron toxicity, and promoted macrophage-elicited spontaneous axon growth from neurons (Gaudet et al., 2016). Interestingly, studies in rat models of chronic constriction injury have shown that *miR-155* is significantly upregulated in microglia following neuropathic pain (Yin et al., 2017), and the suppression of *miR-155* attenuates this pain (Liu et al., 2015a, Tan et al., 2015). Taken together, this suggests that the decrease in circulating miR-155 seen in women with endometriosis may initially assist in limiting or masking the pain associated with this disease. However, this could eventually be detrimental, as neuron growth appears to be accelerated in the absence of miR-155, and may be a contributing factor to the generation and maintenance of pain in endometriosis.

4.3.3. Depletion of *miR-155* from either donor or recipient environment restricts M1-like immune activity in lesions

Total, peripheral and central F4/80 expression increased in both reciprocal transfer groups over time, following a similar expression pattern to *miR-155*$^{-/-}$ → *miR-155*$^{-/-}$ lesions while contrasting with C57 → C57 lesions. This implies that the absence of *miR-155*, whether in the donor endometrium or in the recipient environment, impacts macrophage recruitment to the lesion site. Indeed, a downregulation of the lymphocyte recruitment chemokine CCR7 was noted in *miR-155*$^{-/-}$ bone marrow monocytes (Elmesmari et al., 2016), supporting this observation. A recent review describing the various processes involved in endometrial cell signalling highlights the importance of the Wnt signalling pathway in the regulation of endometrial cell cycling and communication with adjacent cells (Makieva et al., 2018). As mentioned previously, *miR-155* is implicated in regulation of the Wnt signalling pathway, and as the presence of circulating *miR-155* is not sufficient to restore F4/80^{+} macrophage trafficking in *miR-155*$^{-/-}$ → C57 lesions, this observation strongly suggests that innate signals from the ectopic endometrial tissue itself may regulate macrophage chemotaxis.

The expression of the M1-like markers iNOS and MHC II increased gradually over time in both reciprocal transfer groups. In contrast, MHC II expression in *miR-155*$^{-/-}$ → *miR-155*$^{-/-}$ lesions remained significantly

lower across the duration of the experiment. A series of gain- and loss-of function studies in RAW264.7 cells demonstrated that *miR-155* induced the expression of several surface markers, including MHC II in these cells (Ma et al., 2015). Interestingly, this study also showed that the overexpression of *miR-155* resulted in the morphological and phenotypical transformation of RAW264.7 macrophage-like cells into dendritic-like cells. In women with endometriosis, an increase in dendritic cell numbers has been observed in peritoneal endometriotic lesions compared to paired eutopic endometrium (Schulke et al., 2009). Therefore, the observed increase in MHC II expression in the reciprocal transfer model is likely due to an increase in dendritic cells within these lesions as a consequence of *miR-155* expression, however this remains to be evaluated. This assumption also reconciles the observation of similar levels of F4/80$^+$ macrophages observed in both reciprocal transfer lesions and *miR-155*$^{-/-}$ → *miR-155*$^{-/-}$ lesions.

While the expression of Arg-1 in both reciprocal transfers was similar to *miR-155*$^{-/-}$ → *miR-155*$^{-/-}$ lesions, the expression pattern of CD206 differed between *miR-155*$^{-/-}$ → C57 lesions and C57 → *miR-155*$^{-/-}$ lesions, suggesting that CD206 expression is regulated by signals from the donor endometrial tissue. In the C57 → C57 lesions and C57 → *miR-155*$^{-/-}$ lesions, infiltration of CD206$^+$ cells occurs late in lesion development, suggesting the activation of a phenotypic switch from a M1-like pro-inflammatory immune response to a M2-like anti-inflammatory response. This is further supported by the significant increase in the number of blood vessels per lesion seen between D7 and D21. In a study using a rat model of spinal cord repair, an association between CD206$^+$ macrophages and improved vascularity was observed, with a further correlation to VEGF expression at the site of injury (Bartus et al., 2014). In the context of endometriosis, VEGF-driven neovascularisation promotes the survival and proliferation of endometriotic lesions (Cho et al., 2012). In addition, an upregulation of CD206, M2-like macrophage polarisation, and increased immunoregulatory activity is associated with tissue preservation and neuroprotection (Boven et al., 2006, Bartus et al., 2014). Therefore, it is possible that neurogenesis in endometriosis could be mediated by CD206$^+$ cells, and may contribute to the chronic pelvic pain associated with lesion development in this disease.

In conclusion, the findings from this chapter indicate that the development of glandular fractions occurs progressively in *miR-155*$^{-/-}$ → *miR-155*$^{-/-}$ endometriosis-like lesions, albeit not to the same extent as seen in wildtype mice. Interestingly, the development of glands in C57 → *miR-155*$^{-/-}$ lesions was similar to glandular formation in C57 → C57 lesions, suggesting that the absence of circulating miR-155 observed clinically (Nisenblat et al., 2019) may contribute to increased lesion establishment. High levels of M2-like immune activity was sustained in lesions across D7 to D21, and low expression of the M1-like marker MHC II was observed, confirming that a deficiency in *miR-155* results in the preferential increase in M2-

like immune activity over M1-like immune activity. The RNA-Seq data highlighted the importance of the Wnt/β-catenin signalling pathway in the development of endometriosis, suggesting that the observed systemic downregulation of miR-155 in women with endometriosis may promote glandular development and hence, the survival and proliferation of ectopic endometrial tissue. Having assessed the progression of endometriosis-like lesions in an immune sufficient mouse model (Chapter 3) and in the presence of a sustained M2-like immune environment, the next chapter (Chapter 5) assess the impact of a *miR-223*$^{-/-}$ deficiency (sustained M1-like immune environment) on lesion development.

Chapter 5

Assessing the impact of a *miR-223* deficiency on endometriotic lesion development

5.1. INTRODUCTION

According to Sampson's theory of retrograde menstruation, the reflux of endometrial tissue into the peritoneal cavity gives rise to the formation of endometriotic lesions (Sampson, 1927). As demonstrated in the previous chapters and in multiple independent studies, the infiltration and activation of macrophages are a consistent feature of endometriotic lesions (Lebovic et al., 2001, Zhang et al., 2006, Lawson et al., 2007, Lousse et al., 2008, Capobianco and Rovere-Querini, 2013). In addition, dysfunctional immune responses, including impaired immune surveillance and aberrant cytokine expression contribute to disease pathogenesis (Aznaurova et al., 2014, Benagiano et al., 2014, Bouquet De Jolinière et al., 2014). The contribution of the peritoneal environment in the development of endometriosis has been well studied. The presence of ectopic endometrial tissue in the peritoneal cavity mediates the recruitment of leukocytes, which exhibit a range of functions, broadly characterised as either pro-inflammatory tissue destruction or anti-inflammatory tissue remodelling. A cocktail of cytokines, chemokines and growth factors within the peritoneal cavity facilitates the predominance of either pro-inflammatory or anti-inflammatory immune roles, and is believed to be a determining factor in the clearance or perseverance of ectopic endometrial tissue (Vercellini et al., 1993, Khorram et al., 1993, Koninckx et al., 1998, Kalu et al., 2007, Hull et al., 2008, Riccio et al., 2018).

While the peritoneal environment contributes to the pathogenesis of endometriosis, it is important to consider that changes in immune responses in the peritoneal fluid may be a result of inflammation towards the presence of ectopic endometrial tissue, rather than peritoneal inflammation driving disease establishment. To this extent, it is apparent that eutopic endometrial tissue from women with endometriosis differs from women without endometriosis. Although ectopic endometrial lesions share similar histological features with eutopic endometrium, significant biochemical inconsistencies and differential gene expression profiles between paired eutopic and ectopic samples as well as between eutopic samples from women with and without endometriosis exists (Sha et al., 2007, Filigheddu et al., 2010, Meola et al., 2010, Klemmt and Starzinski-Powitz, 2012, Drury et al., 2018). More recently, several studies have identified nonsynonymous somatic mutations of cancer-driver genes in eutopic endometrial tissue which may provide a survival advantage to refluxed endometrial fragments (Anglesio et al., 2017, Suda et al., 2018). In addition, multiple studies have identified aberrant miRNA profiles between paired eutopic and ectopic endometrial samples from women with endometriosis (reviewed in Panir et al., 2018). Amongst the miRNAs that are dysregulated in endometriotic lesions compared to eutopic endometrium is miR-223-3p (miR-223) (Ohlsson Teague et al., 2009, Nisenblat et al., 2019).

miR-223 is located within the q12 locus of the X chromosome, and is regulated by an independent promoter unrelated to other gene products (Johnnidis et al., 2008, Rodríguez et al., 2012). Both the primary and secondary structure of miR-223 precursors are homologous across 42 vertebrate species, including humans, zebrafish, mice, horses and gorillas, indicative of an evolutionary-conserved function (Roberto et al., 2015). Dysregulated *miR-223* expression is associated with multiple pathologies, including cardiovascular disorders, cancer, type II diabetes, hepatic ischemia, inflammatory bowel disease, and rheumatoid arthritis (Wong et al., 2008, Stamatopoulos et al., 2009, Fulci et al., 2010, Haneklaus et al., 2013, Taibi et al., 2014, Kim et al., 2016, Mangat et al., 2018, Ye et al., 2018). Within the bone marrow, *miR-223* is abundantly expressed in the myeloid compartment, and modulates the differentiation of haematopoietic lineages (Johnnidis et al., 2008, Shi et al., 2015). In particular, *miR-223* is essential for osteoclast and erythrocyte differentiation, and myeloid cell differentiation including granulopoiesis and monocyte/macrophage differentiation and maturation (Johnnidis et al., 2008, Sugatani and Hruska, 2009, Haneklaus et al., 2013, Cantoni et al., 2017).

miR-223 expression is induced by the myeloid transcription factors PU.1 and CAAT/enhancer-binding protein-β (C/EBPβ) (Fazi et al., 2005, Fukao et al., 2007). In contrast, low expression of *miR-223* is maintained by nuclear factor I-A (NFI-A), which is able to stabilise undifferentiated myeloid precursor cells (Fazi et al., 2005). These cells subsequently compete for binding with C/EBPα, an additional inducer of *miR-223* transcription (Eyholzer et al., 2010). Hence, both NFI-A and C/EBPβ are able to regulate *miR-223* expression, forming a negative feedback loop (Haneklaus et al., 2013). *miR-223* is involved in the repression of IκB kinase subunit-α (IKKα), which regulates the differentiation, polarisation, and activation of macrophages. Suppression of *miR-223* induces IKKα, resulting in the repression of nuclear factor κB (NFκB) pathways (Li et al., 2010). *miR-223* mediated regulation of *NFκB* results in the decreased expression of *IL-1β*, *IL-6*, *TNFα*, and *IL-12p40* in U937 macrophage cells (Liu et al., 2015b). Importantly, to attenuate a pro-inflammatory response, miR-223 targets NLR Family Pyrin Domain Containing 3 (NLRP3), an inflammasome sensor, thus repressing inflammation (Bauernfeind et al., 2012, Yang et al., 2015, Neudecker et al., 2017). In addition, miR-223 targets PBX/Knotted 1 Homeobox 1 (Pknox1), promoting the polarisation of macrophages towards an M2-like anti-inflammatory phenotype (Zhuang et al., 2012, Wang et al., 2014a, Yuan et al., 2018).

In tandem with its function in promoting the activation of M2-like macrophages, *miR-223* also reduces macrophage inflammatory responses to Toll-like receptor (TLR) ligand stimulation. Lipopolysaccharide (LPS) and poly (I:C) activation via TLR3 and TLR4 reduced *miR-223* expression in macrophages, accompanied with an increase in signal transducer and activator of transcription 3 (STAT3) (Chen et al., 2012). An increase in STAT3 is accompanied by the production of the pro-inflammatory cytokines IL-1β

and IL-6, with the expression of the IL-6 classical signalling pathway forming a positive feedback loop to simultaneously decrease *miR-223* expression and amplify the pro-inflammatory response (Chen et al., 2012). In addition, upon exposure to LPS, the downregulation of *miR-223* in macrophages leads to an increase in the expression of Ras homolog gene family member B (RhoB), a target of miR-223. This results in the induction of the MAPK and NFκB signalling pathways, promoting the production of IL-1β, IL-6, and TNFα (Zhang et al., 2017b). Collectively, these observations highlight the role *miR-223* plays in regulating the balance between M1-like and M2-like inflammatory responses in macrophages, with elevated expression of *miR-223* promoting M2-like macrophage polarisation, whereas decreased *miR-223* expression promotes M1-like macrophage activity (Sica and Mantovani, 2012, Ying et al., 2015, Zhang et al., 2017b).

In the context of endometriosis, a microarray analysis of paired samples of eutopic and ectopic endometrial tissue identified miR-223 as significantly upregulated by 1.72-fold in endometriotic tissues (n=8) (Ohlsson Teague et al., 2009). From this study, an analysis of predicted mRNA targets (including Nuclear Factor I/A, Myocyte Enhancer Factor 2C, and Leukaemia-Associated Phosphoprotein P18) identified a roles for *miR-223* in cell differentiation, granulopoiesis and myogenesis during lesion development. Additional studies have implicated aberrant *miR-223* expression in as both an indicator and a contributing factor in patients with endometrial cancer (Jia et al., 2013b, Montagnana et al., 2017). Hence, as the expression of *miR-223* is upregulated in ectopic endometrial tissue during endometriosis, this may be linked to the increased abundance of M2-like macrophages observed at the lesion site (Bacci et al., 2009). This could facilitate lesion development by shifting the immune response towards a more anti-inflammatory, tissue remodelling state, and may be indicative of a predisposition towards developing endometrioid endometrial cancer. Therefore in this chapter, to fully evaluate the contribution of miR-223 on lesion development and macrophage recruitment in endometriosis, a *miR-223*$^{-/-}$ mouse model was utilised.

The loss of *miR-223* results in mice with an increased number of granulocyte progenitors, leading to an expanded granulocytic compartment (Johnnidis et al., 2008). In addition, *miR-223*$^{-/-}$ granulocytes are hypersensitive towards activating stimuli and consequently, spontaneously develop inflammatory lung pathology and exhibit exaggerated tissue destruction after an endotoxin challenge (Johnnidis et al., 2008). A knockout of miR-223 further results in an expansion of myeloid progenitors, but had no discernible effects on haematopoietic stem cell quiescence, self-renewal capacity, or long-term repopulating activity (Trissal et al., 2015). *miR-223*$^{-/-}$ mice exhibit significantly enhanced inflammation following high-fat diet feeding, coupled with elevated M1-like macrophage activation and impaired M2-like macrophage function (Zhuang et al., 2012). To assess the development of endometriosis-like lesions in the absence of *miR-*

223, a *miR-223*$^{-/-}$ menstrual mouse model of endometriosis was developed, wherein 40mg of *miR-223*$^{-/-}$ donor decidualised endometrial tissue was subcutaneously injected into syngeneic recipient mice. At D7, D14 and D21- post tissue transfer, characterisation of endometriosis-like lesion size, weight, and glandular fractions was carried out. To assess macrophage localisation and M1-like *vs* M2-like abundance, immunohistochemical assessment of macrophages (F4/80 staining), M1-like markers (MHC II and iNOS) and M2-like markers (CD206 and Arg-1) was performed. Further characterisation of endometriosis-like lesions, including blood vessel density (vWF immunostaining), myofibroblast abundance (αSMA immunostaining) and fibrosis (Masson's trichrome staining) was undertaken. RNA-Sequencing (RNA-Seq) was utilised to determine the differential expression of genes between decidualised donor endometrium, D7 and D14 lesions. Additional comparisons were made between *miR-223*$^{-/-}$ and C57 (wildtype control strain) data at corresponding time points, with the original C57 data presented in Chapter 3 of this thesis. Finally, reciprocal transfers between *miR-223*$^{-/-}$ mice and C57 mice were performed to determine whether a *miR-223* deficiency only in the donor endometrium or only in the host response alters endometriotic-like lesion progression over the course of three weeks.

5.2. RESULTS

5.2.1. Endometriosis-like lesion development in *miR-223* deficient mice

To evaluate the contribution of *miR-223* in the development of endometriosis, a *miR-223*$^{-/-}$ menstrual mouse model of endometriosis was developed. In this model, 40mg of *miR-223*$^{-/-}$ decidualised donor endometrial tissue was subcutaneously injected into *miR-223*$^{-/-}$ recipient mice. To evaluate the extent of disease establishment, endometriosis-like lesions that developed at D7, D14 and D21 were analysed for size, weight, and glandular fractions.

In order to collect sufficient decidualised endometrium in this experiment, a total of 55 *miR-223*$^{-/-}$ donor mice were used, at a ratio of 1 donor to 1 recipient. In total, throughout this study, 78% of *miR-223*$^{-/-}$ recipient mice had lesions (Table 5.1). At D7, 100% of recipient mice had lesions. The proportion of recipient mice that had detectable lesions was reduced to 70% at D14, and further reduced to 60% at D21. A total of 4 mice had more than one lesion and have been excluded from subsequent analyses.

Morphometric analysis of the lesions was performed over the time course. At D7, lesions were large, raised from the skin, and consisted of both blood and pus-filled areas (Figure 5.1 A). At D14, lesions were circular and appeared cystic and fluid-filled (Figure 5.1 B). By D21, lesions were small, opaque and white (Figure 5.1 C). *miR-223*$^{-/-}$ lesions were largest at D7 (45 (19 – 72) mm^3), and underwent a 73% reduction in size by D14 (12 (10 – 21) mm^3, $p = 0.0260$), which further reduced at D21 (9 (6 – 12) mm^3; $p = 0.0009$ for D7 *vs* D21) (Figure 5.1 D). Median lesion weight at D7 was 31.80 (25.40 – 66.85) mg, which reduced by 70% at D14 (9.60 (8.20 – 13.55) mg, $p = 0.0002$). A further 42% reduction in lesion weight was observed between D14 and D21 (5.55 (4.15 – 9.55) mg), with lesions at D21 being 83% lighter than D7 lesions ($p < 0.0001$) (Figure 5.1 E).

H&E stained lesion sections were analysed across the three time points. D7, lesions were large, with the presence of several glands (Figure 5.2 A). However, by D14, large cystic spaces were seen within the lesions (Figure 5.2 B) and by D21, lesions were small and dense, with no visible glands (Figure 5.2 C). The median number of glands per lesion was comparable at D7 (1 (0 – 2)) and D14 (1 (0 – 1)) and was completely absent at D21 (0 (0 – 0), $p = 0.0366$ for D7 *vs* D21) (Figure 5.2 D). Average gland size was not significantly different between D7 (0.003 (0.000 – 0.024) mm^2) and D14 (0.000 (0.000 – 0.003) mm^2) (Figure 5.2 E). At D21, due to an absence of glands, a significant reduction was noted between this time point and D7 values ($p = 0.0164$). Between D7 and D14, no differences in the median measurements of

lumen area within glands was observed (0.0004 (0.0000 – 0.02453) mm^2 and 0.0004 (0.0000 – 0.0005) mm^2 respectively) (Figure 5.2 F). A significant difference in lumen area was noted between D7 and D21 values (p = 0.0132), as no glands were present at D21.

Similarly, the median epithelium area of glands at D7 was 0.0023 (0.0000 – 0.0168) mm^2 which reduced to 0.0001 (0.0000 – 0.0016) mm^2 at D14, and was not present at D21 due to the lack of glands (p = 0.0058 for D7 *vs* D21) (Figure 5.2 G). The percentage glandular epithelium of lesions was highest at D7 (0.04 (0.00 – 1.42) %) when compared to both D14 (0.04 (0.00 – 0.06) %) and D21 (0.00 (0.00 – 0.00) %, p = 0.0168) (Figure 5.2 H). Conversely, the percentage stromal area was highest at D21 (100 (100 – 100) %) compared to D7 (99.95 (99.89 – 100.00) %, p = 0.0071) and D14 (99.95 (99.89 – 100.00) %) (Figure 5.2 I).

Table 5.1 Endometriosis-like lesion recovery in *miR-223*$^{-/-}$ mice

Lesion collection time point	D7	D14	D21
Total number of donor mice used across all time points: 55			
Number of recipient mice	20	20	15
Number of mice with lesions*	20	14	9
Proportion of mice with lesions (%)	100	70	60

* To reduce bias, mice with ≥2 lesions were excluded from subsequent analyses. At D7 – 3 mice excluded; At D14 -1 mouse excluded.

5.2.1.1. Comparison of endometriosis-like lesion progression between C57 mice and *miR-223* deficient mice

Endometriotic-like lesions that developed in mice with a systemic loss of *miR-223* resulted in lesions that had not successfully established, indicated by the reduction in lesion size, coupled with the lack of gland formation at D21. To further delineate the impact of *miR-223* on the progression of endometriosis, a comparative analysis between *miR-223* deficient lesions (*miR-223*$^{-/-}$) and *miR-223* sufficient lesions (C57) was performed.

At D7, lesions in *miR-223*$^{-/-}$ mice were 2.4-fold larger than C57 lesions (p =0.0072) (Figure 5.3 A). At D14, lesions in *miR-223*$^{-/-}$ mice were 4.8-fold larger then C57 lesions (p = 0.0002), however by D21, lesions were similar in size. Lesion weight was 2.1-fold heavier in the *miR-223*$^{-/-}$ mice (p = 0.0003) at D7, but by D14, lesions did not significantly differ in weight between strains (Figure 5.3 B). On D21, lesions were 2.1-fold heavier in *miR-223*$^{-/-}$ mice compared to C57 mice (p= 0.0044).

Interestingly, while the number of glands per lesion steadily increased in C57 mice, an opposite trend was observed in *miR-223*$^{-/-}$ mice (Figure 5.3 C). At D7, the number of glands present in both *miR-223*$^{-/-}$ and C57 lesions were comparable, however, at D14, there were 80% fewer glands in *miR-223*$^{-/-}$ lesions (p = 0.0006). At D21, C57 mice had a median of seven glands per lesion, whereas a significant lack of glands was observed in *miR-223*$^{-/-}$ lesions (p < 0.0001). The average gland size per lesion was similar between *miR-223*$^{-/-}$ and C57 lesions at D7, however gland size was significantly smaller in *miR-223*$^{-/-}$ lesions at D14 (p = 0.00037) (Figure 5.3 D). At D21, although a reduction in gland size was observed in C57 lesions, the total absence of glands in *miR-223*$^{-/-}$ lesions led to a significant difference between the time points (p < 0.0001).

At D7, lumen area (Figure 5.3 E) and epithelium area (Figure 5.3 F) measurements were similar between strains. At D14, lumen area in *miR-223*$^{-/-}$ lesions was 99% smaller than C57 lesions (p = 0.0016), while the epithelium area was 99% smaller in *miR-223*$^{-/-}$ lesions compared to C57 lesions (p = 0.0004). Although both the lumen and epithelium area was reduced at D21 in C57 lesions, measurements remained significantly higher than *miR-223*$^{-/-}$ lesion values (p < 0.0001 for both parameters).

The percentage glandular epithelium was similar at D7, however, at D14, *miR-223*$^{-/-}$ lesions had 99% less glandular epithelium compared to C57 lesions (p = 0.0011), and at D21, the percentage glandular

epithelium in C57 lesions remained significantly higher than *miR-223*$^{-/-}$ lesions ($p < 0.0001$), as no glands were present in *miR-223*$^{-/-}$ lesions (Figure 5.3 G). The percentage stromal area was comparable between strains at D7, whereas by D14, *miR-223*$^{-/-}$ lesions contained 1.01-fold greater stromal area than C57 lesions ($p = 0.0016$) (Figure 5.3 H). *miR-223*$^{-/-}$ lesions comprised entirely of stromal area at D21, which was significantly higher than the proportion of stromal area observed in C57 lesions ($p < 0.0001$). These findings indicate that the development of endometriotic-like lesions in *miR-223*$^{-/-}$ mice does not progress in a similar manner to C57 mice, and suggests that *miR-223* may play an important role in supporting lesion establishment.

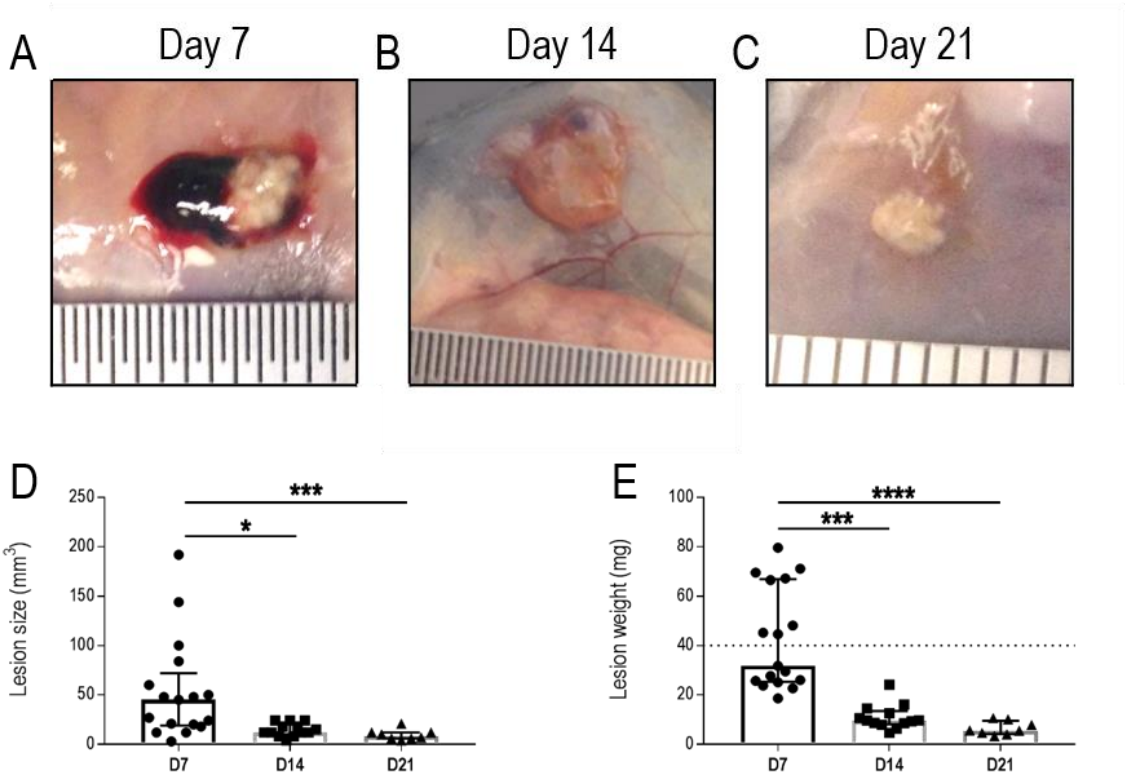

Figure 5.1 Gross morphology of endometriosis-like lesion development in *miR-223*$^{-/-}$ mice

Decidualised *miR-223*$^{-/-}$ donor endometrial tissue was injected subcutaneously into syngeneic recipient mice. Resulting lesions were harvested at either D7 (**A**), D14 (**B**) or D21 (**C**), with representative images shown. Lesion size was measured (**D**) and lesions were excised and weighed (**E**), with the dotted line indicating the initial weight of donor decidualised endometrial tissue inoculated into recipient mice. Data are presented as median (IQR), with each symbol representative of a single lesion in one mouse (n=17 at D7, n=13 at D14, n=9 at D21). Analysis was done using the Kruskal-Wallis test followed by Dunn's multiple comparison test, with significance denoted as * ($p < 0.05$), *** ($p < 0.001$), and **** ($p < 0.0001$).

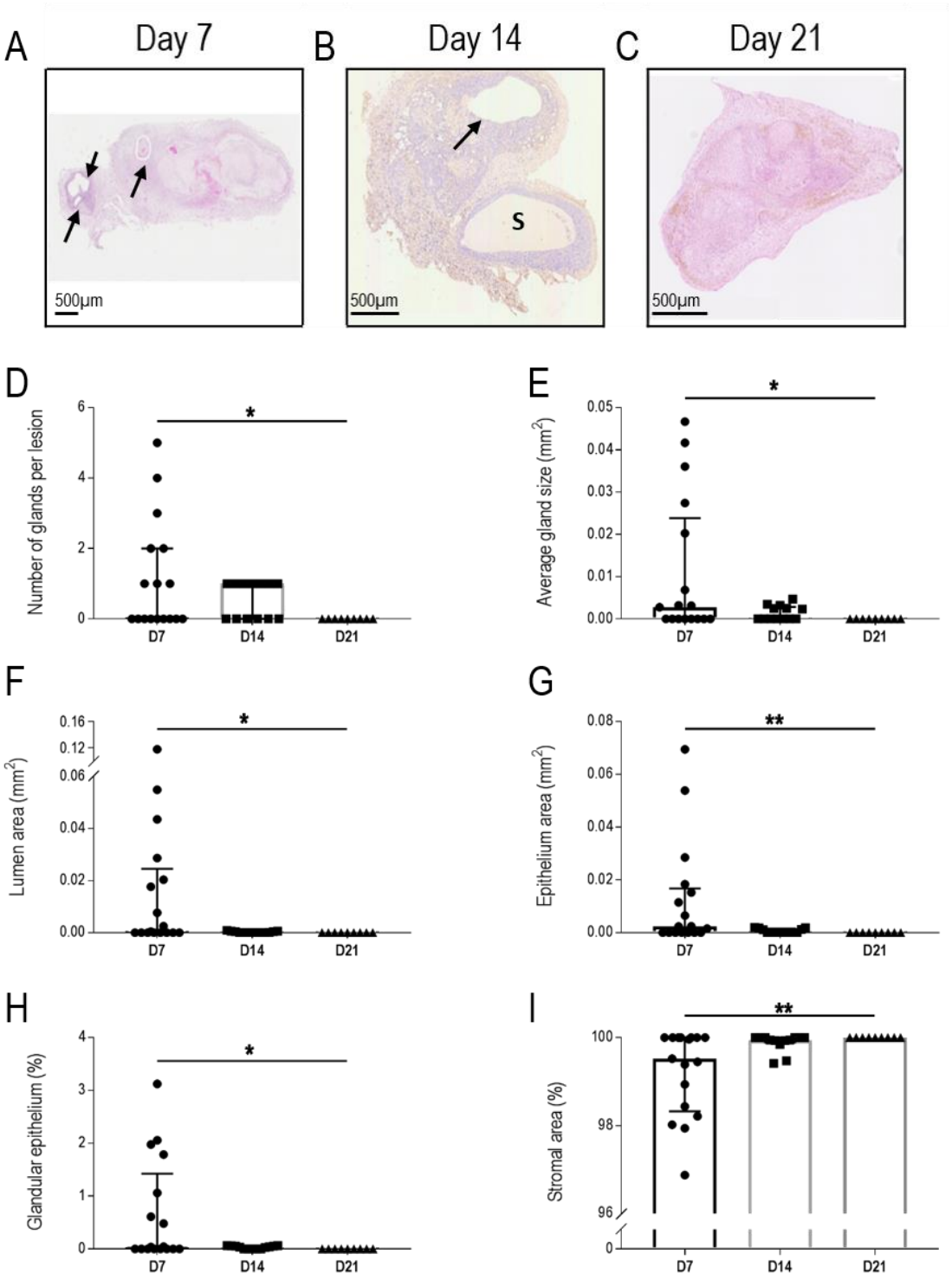

Figure 5.2 Assessment of morphological parameters in haematoxylin and eosin stained endometriosis-like lesions from *miR-223*$^{-/-}$ mice

Haematoxylin and eosin stained sections from D7 **(A)**, D14 **(B)**, and D21 **(C)** lesions in *miR-223*$^{-/-}$ mice (representative images shown; arrows indicate glands; **S** represents cystic space) were assessed for the following characteristics: number of glands per lesion **(D)**, average gland size **(E)**, lumen area **(F)**, epithelium area **(G)**, percentage glandular epithelium **(H)** and percentage stromal area **(I)**. Data are presented as median (IQR), with each symbol representative of a single lesion in one mouse (n=17 at D7, n=13 at D14, n=9 at D21). Analysis was done using the Kruskal-Wallis test followed by Dunn's multiple comparison test, with significance denoted as * ($p < 0.05$).

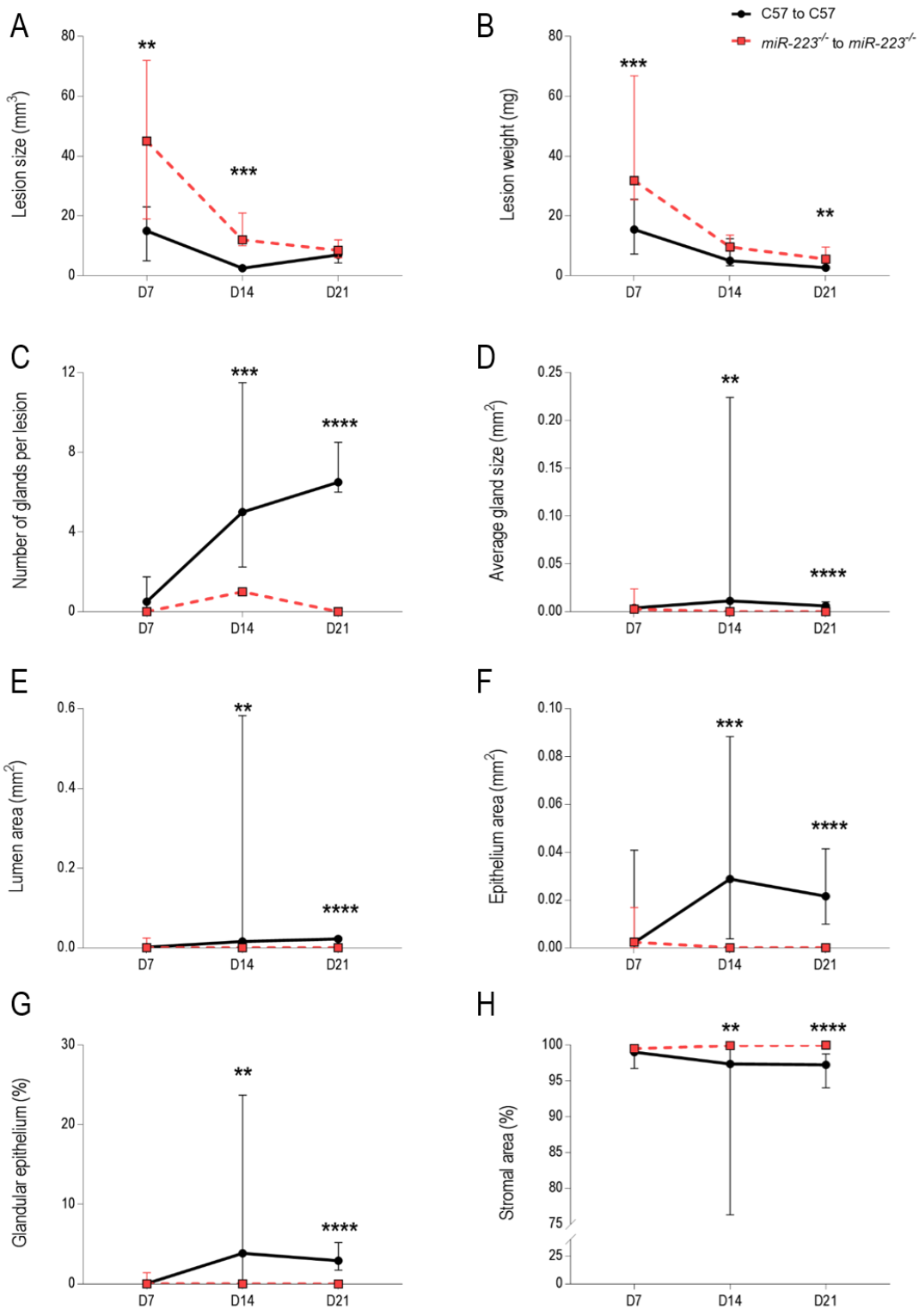

Figure 5.3 **Comparative analysis of morphometric parameters between C57 and *miR-223*$^{-/-}$ endometriosis-like lesions**

Lesion size (**A**), weight (**B**), number of glands per lesion (**C**), average gland size (**D**), lumen area (**E**), epithelium area (**F**), glandular epithelium (**G**), and stromal area (**H**) were compared between C57 mice (; n=12 at D7, n=12 at D14, n=8 at D21) and *miR-223*$^{-/-}$ mice (; n=17 at D7, n=13 at D14, n=9 at D21). Data are presented as median (IQR). Analysis was done using the Mann Whitney U test, with significance denoted as ** ($p < 0.01$), *** ($p < 0.001$) and **** ($p < 0.0001$).

5.2.2. Macrophage localisation in endometriosis-like lesions from *miR-223* deficient mice

miR-223 is involved in the suppression of classic M1-like pro-inflammatory macrophage activation and promotes the polarisation of alternative M2-like anti-inflammatory macrophages (Zhuang et al., 2012, Haneklaus et al., 2013, Ying et al., 2015). In endometriosis, elevation of M1-like macrophage activity inhibits disease development by increasing ectopic tissue clearance (Bacci et al., 2009). Therefore, in this section the impact of a systemic depletion of *miR-223*$^{-/-}$ on macrophage activity and remodelling of endometriosis-like lesions was evaluated.

Quantification of F4/80 immunostaining was used to determine macrophage density in *miR-223*$^{-/-}$ lesions (Figure 5.4). Total F4/80 density in lesions was consistent across all time points (19.73 (16.00 – 24.68) % at D7, 16.15 (7.814 – 24.39) % at D14, and 24.17 (21.30 – 30.40) % at D21) (Figure 5.4G). F4/80 expression at the periphery of *miR-223*$^{-/-}$ lesions (Figure 5.4 A-C) was similar at D7 and D14 (42.00 (37.5 – 47.45) % and 32.76 (20.18 – 43.11) % respectively). However, at D21, peripheral F4/80 expression was 46.5 (44.81 – 60.05) %, 1.4-fold higher than D14 (p = 0.0015) (Figure 5.4 H). The expression of F4/80 at the centre of *miR-223*$^{-/-}$ lesions remained consistent at D7 and D14 (28.76 (22.77 – 33.54) % and 19.05 (6.58 – 26.03) % respectively), and in a similar manner to peripheral F4/80 density, a significant increase in F4/80^{+} cells was observed between D14 and D21 (33.31 (25.64 – 42.91) %, p = 0.0046) (Figure 5.4 I).

5.2.2.1. Expression of pro-inflammatory M1-like markers in *miR-223* deficient mice

Detection of iNOS (Figure 5.5 A-C) and MHC II (Figure 5.5 D-F) expression was used to evaluate the extent of M1-like immune activity in *miR-223*$^{-/-}$ lesions. Total iNOS density was unchanged between D7 and D14 (30.61 (27.42 – 32.36) % and 34.53 (31.05 – 38.04) % respectively). Unexpectedly, a reduction in iNOS expression was seen at D21 (20.56 (15.54 – 25.47) %, p = 0.0002 for D14 *vs* D21) (Figure 5.5 G). Peripheral iNOS density was consistent between D7 (28.54 (24.24 – 31.91) %) and D14 (33.32 (30.02 – 40.69) %), however a significant decrease was seen at D21 (15.43 (12.47 – 16.56) %, p = 0.0018 for D7 *vs* D21 and p < 0.0001 for D14 *vs* D21) (Figure 5.5 H). Similarly, central iNOS density was consistent between D7 (30.84 (24.42 – 33.29) %) and D14 (31.35 (28.34 – 34.00) %), with a significant decrease was seen at D21 (20.62 (16.85 – 22.14) %, p = 0.0013 for D7 *vs* D21 and p = 0.0001 for D14 *vs* D21) (Figure 5.5 I).

On the other hand, expression of MHC II steadily increased between D7 (21.32 (18.89 – 30.85) %), D14 (27.14 (23.02 – 36.71) %) and D21 (35.72 (23.02 – 36.71) %, p = 0.0033 for D7 *vs* D21) (Figure 5.5 J).

Peripheral MHC II density significantly increased between D7 (21.34 (19.41 – 22.71 %) and D14 (32.58 (28.80 – 36.09) %, $p < 0.0001$), however no differences were seen at D21 (25.54 (23.74 – 28.77) %) (Figure 5.5 K). Central MHC II density was significantly lower at D14 (23.23 (20.22 – 26.75) %) when compared to D7 (28.46 (26.69 – 31.44) %, $p = 0.0051$) and D21 (30.87 (28.36 – 33.13) %, $p = 0.0003$) values (Figure 5.5 L).

5.2.2.2. Expression of alternatively activated M2-like markers in *miR-223* deficient mice

Immunostaining for CD206 (Figure 5.6 A-C) and Arg-1 (Figure 5.6 D-F) allowed for quantification of M2-like activity in *miR-223*$^{-/-}$ lesions. Surprisingly, total CD206 density increased significantly between all three time points, with an initial value of 6.66 (4.23 – 8.86) % at D7, rising to 17.11 (12.76 – 21.78) % at D14 ($p = 0.0022$), and finally reaching a peak of 32.44 (24.45 – 35.62) % at D21 ($p < 0.0001$ for D7 *vs* D21 and $p = 0.0396$ for D14 *vs* D21) (Figure 5.6 G). Peripheral CD206 increased significantly between D7 (8.54 (6.90 – 9.52) %) and D14 (15.14 (11.75 – 16.68) %, $p = 0.0007$), reaching a 21.56 (19.49 – 26.54) % at D21 ($p < 0.0001$ for D7 *vs* D21) (Figure 5.6 H). Similarly, central CD206 expression increased significantly between D7 (8.25 (6.47 – 9.76) %), D14 (12.72 (9.46 – 14.38) %, $p = 0.0207$), and D21 (13.69 (10.14 – 16.35) %, $p = 0.0063$ for D7 *vs* D21) (Figure 5.6 I).

The total density of Arg-1 in these lesions increased in a similar pattern (23.38 (18.02 – 26.46) % at D7, 29.39 (26.36 – 31.67) % at D14, and 41.76 (35.95 – 47.02) % at D21), however a significant increase was only seen between D7 and D21 ($p < 0.0001$) (Figure 5.6 J). Peripheral Arg-1 increased significantly between D7 (21.12 (18.66 – 23.98) %) and D14 (29.57 (25.31 – 32.78) %, $p = 0.0014$), reaching a 32.25 (28.56 – 35.64) % at D21 ($p = 0.0001$ for D7 *vs* D21) (Figure 5.6 K). Similarly, central Arg-1 expression increased significantly between D7 (10.35 (7.85 – 13.67) %), D14 (16.24 (14.25 – 19.46) %, $p = 0.0055$), and D21 (22.14 (19.22 – 26.64), $p < 0.0001$ for D7 *vs* D21) (Figure 5.6 L).

5.2.3. Blood vessel density, myofibroblast abundance and fibrosis in endometriosis-like lesions from *miR-223* deficient mice

Immunolocalisation of blood vessels in *miR-223*$^{-/-}$ lesions, performed with an antibody against vWF, (Figure 5.7 A-C) showed significant changes in total blood vessel density (Figure 5.7 D), number of blood vessels per lesion (Figure 5.7 E), and average vessel size (Figure 5.7 F) across time points. Between D7 and D14, vWF density decreased non-significantly from 0.64 (0.46 – 0.97) % to 0.39 (0.28 – 0.85) %, however at D21, a substantial reduction in vWF density was observed (0.00 (0.00 – 0.003) %, $p < 0.0001$ for D7 *vs* D21 and $p = 0.0028$ for D14 *vs* D21). The number of blood vessels per lesion followed a similar

trend, with comparable D7 and D14 values (17 (12 – 33) and 27 (10 – 34) respectively), followed by a significant decrease at D21 (2 (0 – 3), $p = 0.0002$ for D7 *vs* D21 and $p = 0.0002$ for D14 *vs* D21). Average vessel size also decreased over the course of *miR-223*$^{-/-}$ lesion development (0.0013 (0.0008 – 0.0024) % at D7, 0.0006 (0.0004 – 0.0008) % at D14, and 0.0002 (0.0000 – 0.0010) % at D21), however this was only significant between D7 and D21 ($p = 0.0100$).

To evaluate the extent of fibrosis in *miR-223*$^{-/-}$ lesions, αSMA immunostaining (Figure 5.8 A-C) and Masson's trichrome histochemistry (Figure 5.8 D-F) was performed. Expression of αSMA was consistent across D7, D14 and D21 (19.25 (7.11 – 24.56) %, 22.21 (17.87 – 29.49) %, and 22.85 (17.96 – 30.07) % respectively) (Figure 5.8 G). Likewise, the density of fibrosis was unaltered between D7, D14, and D21 (16.8 (12.60 – 19.32) %, 14.46 (12.88 – 23.56) %, and 15.94 (14.32 – 20.75) % respectively) (Figure 5.8 H).

5.2.4. Comparison of macrophage localisation and cellular parameters between C57 mice and *miR-223* deficient mice

Although the systemic depletion of *miR-223* resulted in an unexpected increase in M2-like macrophage markers between D7 and D21, deposition of fibrotic material was not apparent over time. Thus, to better comprehend the impact of *miR-223* depletion on macrophage polarisation in disease pathogenesis, a comparative analysis between *miR-223* deficient lesions (*miR-223*$^{-/-}$) and *miR-223* sufficient lesions (C57) was performed (Figure 5.9 and 5.10).

Total F4/80 density in *miR-223*$^{-/-}$ and C57 lesions was similar at D14, however a 1.8-fold increase was seen at D7 (p = 0.0031) and a 1.4-fold increase at D21 (p = 0.0206) was seen in *miR-223*$^{-/-}$ lesions compared to C57 lesions (Figure 5.9 A). Interestingly, although peripheral F4/80 density in *miR-223*$^{-/-}$ and C57 lesions was comparable at D7 and D14, *miR-223*$^{-/-}$ lesions had 2-fold higher peripheral F4/80 expression (p = 0.0002) (Figure 5.9 B). Conversely, the central expression of F4/80 in *miR-223*$^{-/-}$ lesions was 7.2-fold higher at D7 (p < 0.0001) compared to C57 lesions, whereas at D14, *miR-223*$^{-/-}$ lesions had 46% less central F4/80 expression (p = 0.0055) (Figure 5.9 C). At D21, F4/80 density at the centre of lesions from both strains were similar.

Total expression of the M1-like marker iNOS remained higher in *miR-223*$^{-/-}$ lesions compared to C57 lesions, however this was only significant at D14 (1.7-fold increase in *miR-223*$^{-/-}$, p = 0.0006) (Figure 5.9 D). Peripheral iNOS density in *miR-223*$^{-/-}$ lesions was significantly higher than C57 lesions at D7 (1.5-fold increase, p < 0.0001) and D14 (3-fold increase, p < 0.0001), however a 13% reduction of peripheral iNOS expression was observed in *miR-223*$^{-/-}$ lesions at D21 (p = 0.0464) (Figure 5.9 E). Central iNOS density was consistently higher in *miR-223*$^{-/-}$ lesions than C57 lesions at D7 (4.2-fold increase, p < 0.0001), D14 (4.5-fold increase, p < 0.0001), and D21 (2-fold increase, p = 0.0055) (Figure 5.9 F).

The total density of MHC II, the second M1-like marker used, remained higher in *miR-223*$^{-/-}$ lesions compared to C57 lesions at all time points; in particular, at D14, *miR-223*$^{-/-}$ lesions had 2.2-fold higher expression of MHC II (p < 0.0001), and at D21, *miR-223*$^{-/-}$ lesions had 1.6-fold higher expression of MHC II (p = 0.0111) compared to C57 values (Figure 5.9 G). Peripheral MHC II density in *miR-223*$^{-/-}$ lesions was significantly higher than C57 lesions at D7 (1.8-fold increase, p < 0.0001) and D14 (3.2-fold increase, p < 0.0001) (Figure 5.9 H). Central MHC II density was consistently higher *miR-223*$^{-/-}$ lesions compared to C57 lesions at D7 (3.3-fold increase, p < 0.0001), D14 (3.2-fold increase, p < 0.0001), and D21 (2.8-fold increase, p < 0.0001) (Figure 5.9 I).

On the other hand, the total density of the M2-like macrophage marker CD206, was consistently lower in *miR-223*$^{-/-}$ lesions, with a significant decrease of 41% in expression levels at D21 when compared to C57 lesions (p = 0.0006) (Figure 5.9 J). Interestingly, while peripheral CD206 expression was consistently higher *miR-223*$^{-/-}$ lesions compared to C57 lesions at D7 (3.4-fold increase, p < 0.0001), D14 (2.5-fold increase, p < 0.0001), and D21 (1.4-fold increase, p = 0.0079), central CD206 expression was significantly lower in *miR-223*$^{-/-}$ lesions compared to C57 lesions at D14 (42% lower, p < 0.0001) and D21 (70% lower, p < 0.0001) (Figure 5.9 K,L).

Surprisingly, the depletion of *miR-223* resulted in an increase in total Arg-1 expression in lesions, which was significantly higher than C57 lesions at D14 (1.4-fold increase, p < 0.0001) and D21 (1.7-fold increase, p = 0.0016) (Figure 5.9 G). While peripheral Arg-1 expression was consistently higher *miR-223*$^{-/-}$ lesions compared to C57 lesions at D7 (4.9-fold increase, p < 0.0001), D14 (2.1-fold increase, p < 0.0001), and D21 (2-fold increase, p < 0.0001), central Arg-1 expression was consistent between strains (Figure 5.9 N, O).

While vWF expression in *miR-223*$^{-/-}$ lesions decreased over time, an inverse expression pattern was seen in C57 lesions (Figure 5.10 A). At D7, total vWF density was 1.7-fold higher in *miR-223*$^{-/-}$ lesions compared to C57 lesions (p = 0.0042, however by D21, *miR-223*$^{-/-}$ lesions had 99.9% lower vWF expression compared to C57 lesions (p < 0.0001). A corresponding trend was observed in the number of blood vessels per lesion, with *miR-223*$^{-/-}$ lesions having 3.4-fold more blood vessels at D7 (p = 0.0004) but at D21, *miR-223*$^{-/-}$ lesions had 92% fewer blood vessels (p < 0.0001) when compared to C57 lesions (Figure 5.10 B). The average blood vessel size was 3.8-fold higher in *miR-223*$^{-/-}$ lesions compared to C57 lesions at D7 (p < 0.0001), however no differences were seen between the groups at either D14 or D21 (Figure 5.10 C). αSMA density was comparable between both groups across all time points (Figure 5.10 D). Notably, the density of fibrosis remained significantly lower in *miR-223*$^{-/-}$ lesions compared to C57 lesions across all time points (31% lower at D7, p = 0.0031; 45% lower at D14, p = 0.0188; and 48% lower at D21, p < 0.0001) (Figure 5.10 E).

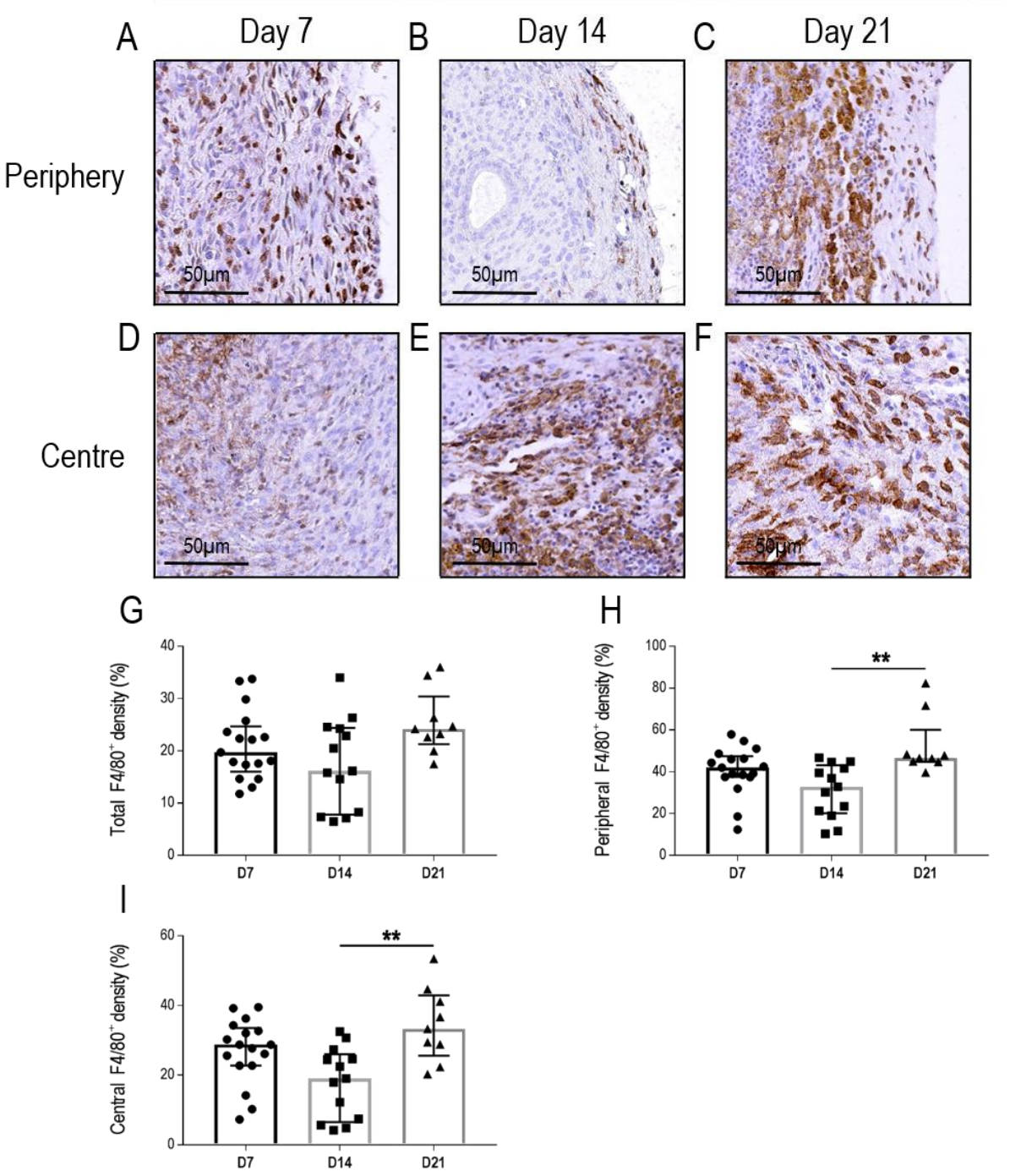

Figure 5.4 F4/80 immunostaining in endometriosis-like lesions from *miR-223*$^{-/-}$ mice

Quantification of total F4/80 density was carried out in lesions from *miR-223*$^{-/-}$ mice (**G**). F4/80 density at the lesion periphery (100µM from the edge of the lesion) at D7 (**A**), D14 (**B**) and D21 (**C**) was evaluated (**H**). F4/80 density at the lesion centre (within 500µM from the centre) at D7 (**D**), D14 (**E**), and D21 (**F**) was also quantified (**I**). Data are presented as median (IQR), with each symbol representative of a single lesion in one mouse (n=17 at D7, n=13 at D14, n=9 at D21). Analysis was done using the Kruskal-Wallis test followed by Dunn's multiple comparison test, with significance denoted as ** ($p < 0.01$).

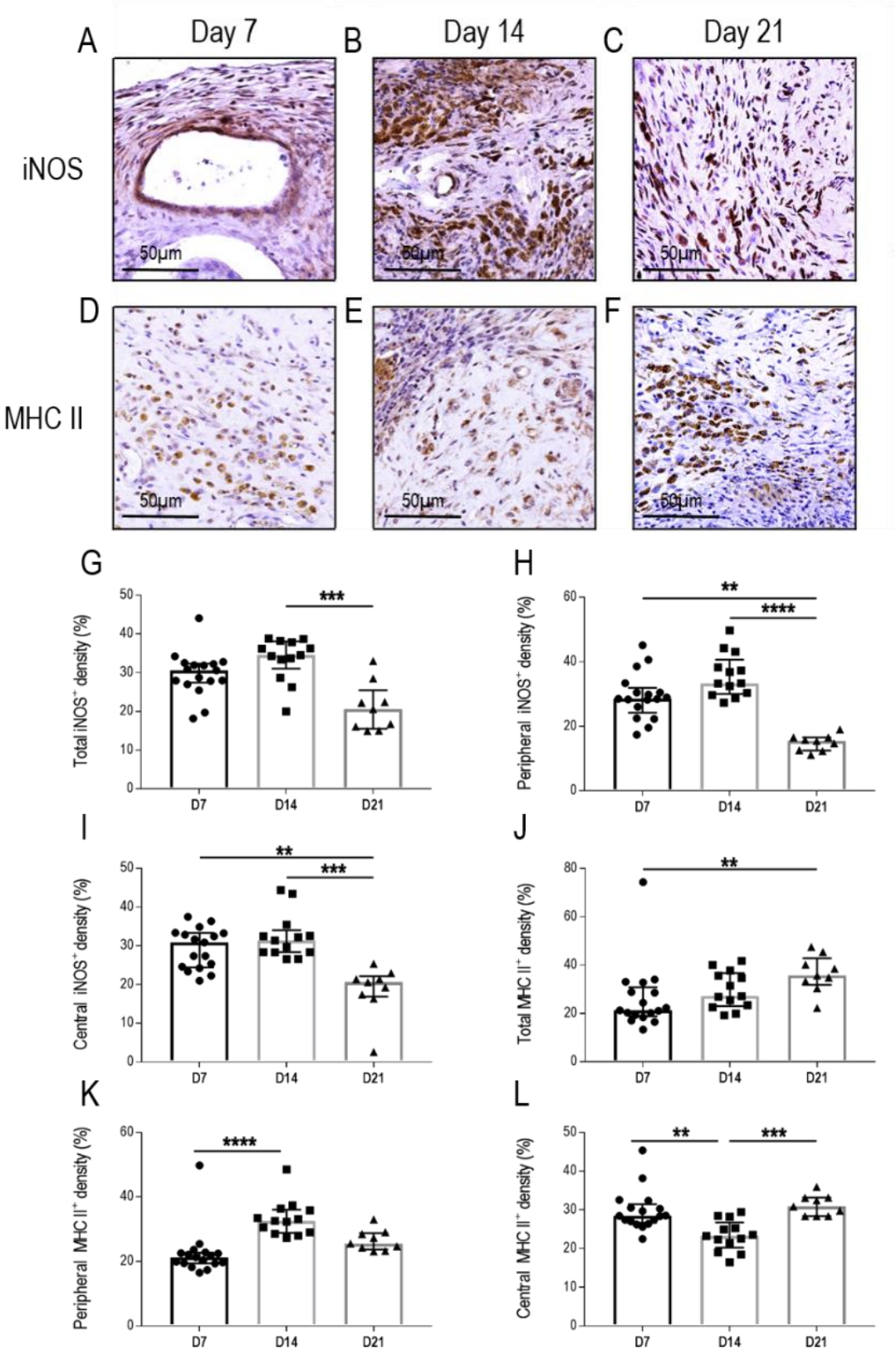

Figure 5.5 M1–like macrophage marker immunostaining in lesions from *miR-223*$^{-/-}$ mice

The expression of inducible nitric oxide synthase (iNOS) at D7 (**A**), D14 (**B**), and D21 (**C**) was quantified in *miR-223*$^{-/-}$ lesions (**G**). Further analysis was performed to determine peripheral (**H**) and central (**I**) iNOS density. Quantification of the Class II Major Histocompatibility Complex (MHC II) was done at D7 (**D**), D14 (**E**) and D21 (**F**) in these lesions (**J**), with peripheral (**K**) and central (**L**) MHC II density determined. Data are presented as median (IQR), with each symbol representative of a single lesion in one mouse (n=17 at D7, n=13 at D14, n=9 at D21). Analysis was done using the Kruskal-Wallis test followed by Dunn's multiple comparison test, with significance denoted as ** ($p < 0.001$), *** ($p < 0.001$) and **** ($p < 0.0001$).

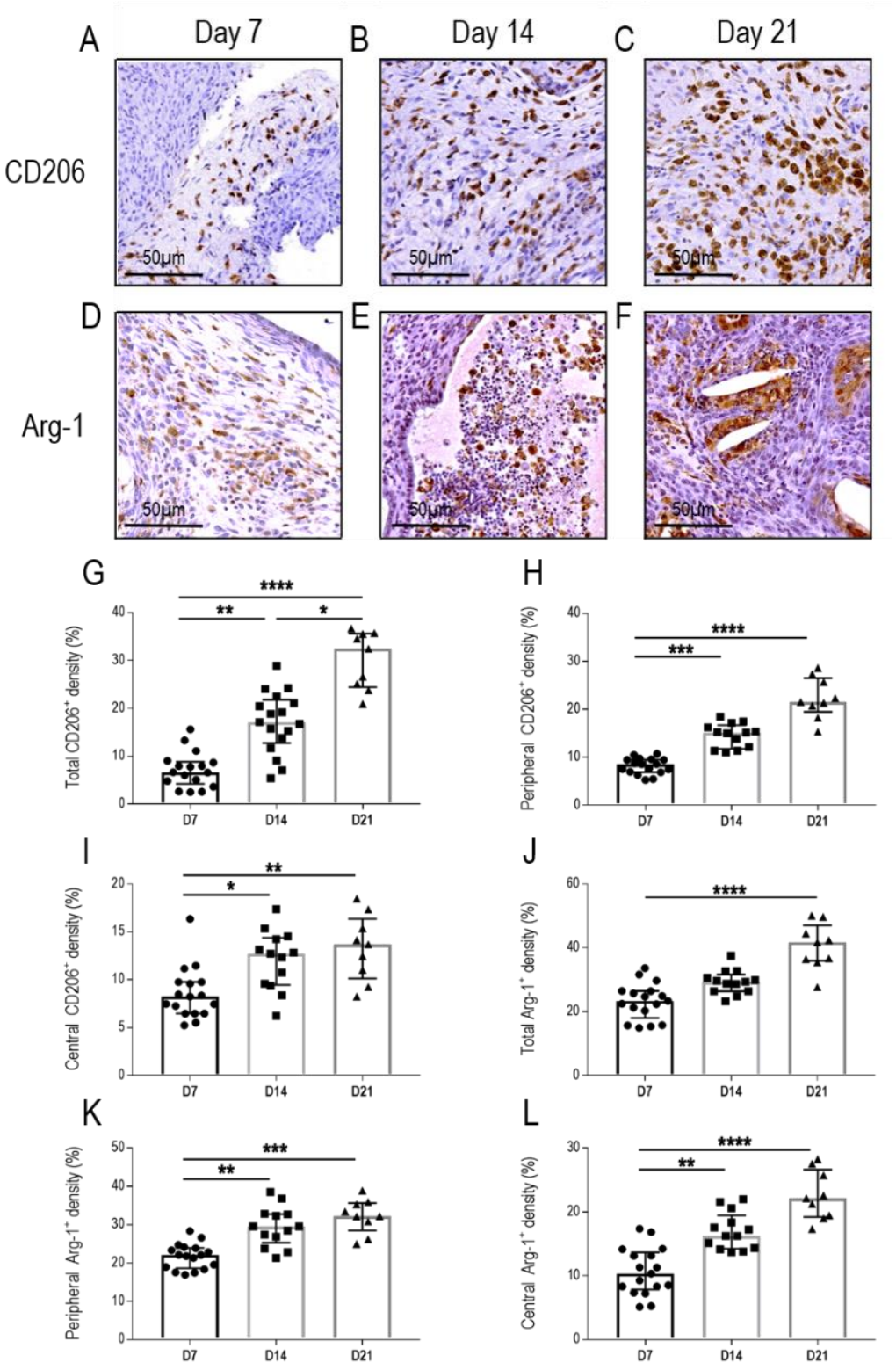

Figure 5.6 M2–like macrophage marker immunostaining in lesions from *miR-223*$^{-/-}$ mice

CD206 density at D7 (**A**), D14 (**B**), and D21 (**C**) was quantified in *miR-223*$^{-/-}$ lesions (**G**), with further analysis of peripheral (**H**) and central (**I**) CD206 density. Expression of Arginase-1 (Arg-1) was evaluated at D7 (**D**), D14 (**E**) and D21 (**F**) in these lesions (**J**), with peripheral (**K**) and central (**L**) Arg-1 density determined. Data are presented as median (IQR), with each symbol representative of a single lesion in one mouse (n=17 at D7, n=13 at D14, n=9 at D21). Analysis was done using the Kruskal-Wallis test followed by Dunn's multiple comparison test, with significance denoted as * ($p < 0.05$), ** ($p < 0.01$), *** ($p < 0.001$) and **** ($p < 0.0001$).

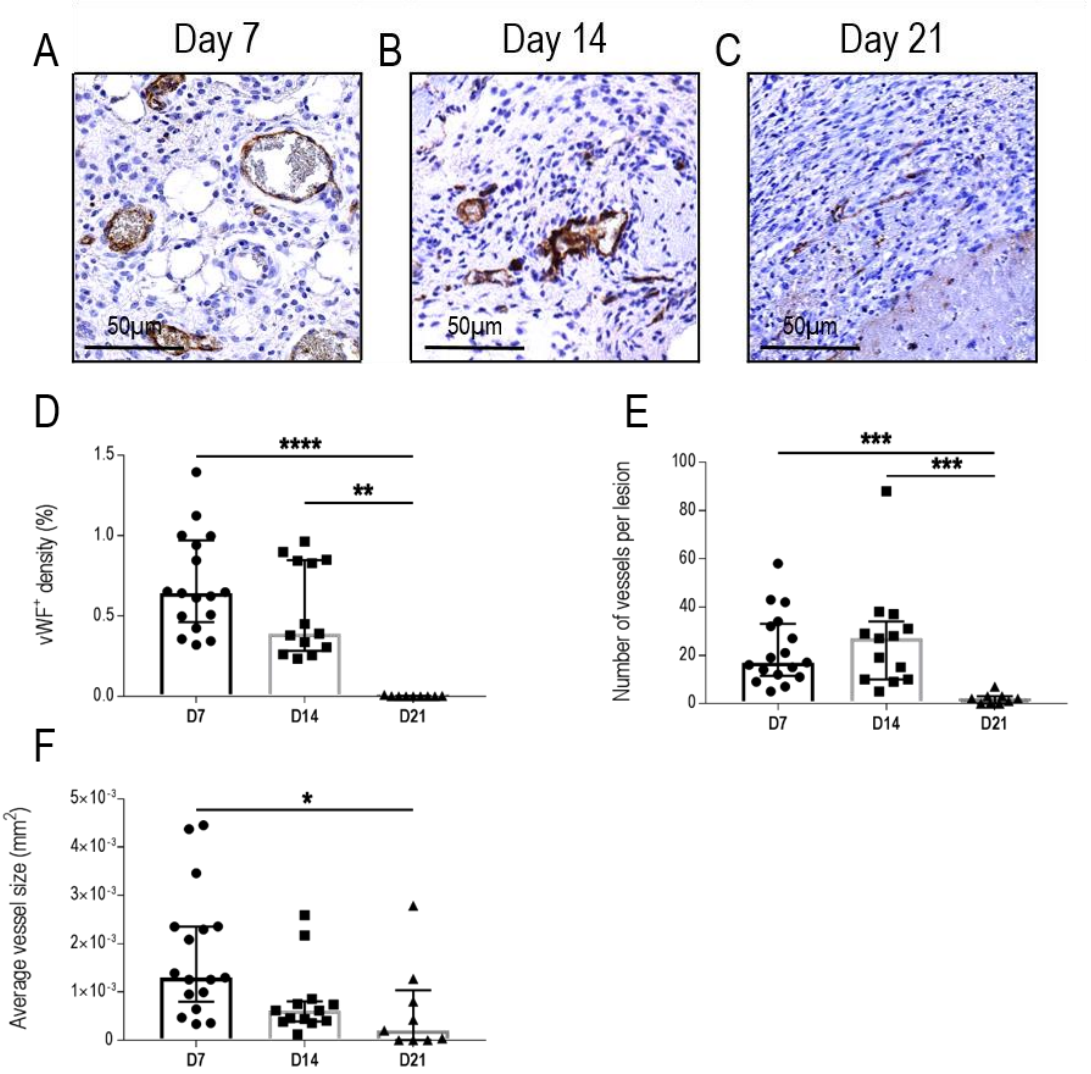

Figure 5.7 Blood vessel localisation in endometriosis-like lesions from *miR-223*$^{-/-}$ mice

Von Willebrand Factor (vWF) staining was used to localise blood vessels in lesions from *miR-223*$^{-/-}$ mice at D7 (**A**), D14 (**B**), and D21 (**C**). The total density of vWF^{+} vessels was quantified (**D**). The number of vessels per lesion (**E**) and the average vessel size (**F**) was determined. Data are presented as median (IQR), with each symbol representative of a single lesion in one mouse (n=17 at D7, n=13 at D14, n=9 at D21). Analysis was done using the Kruskal-Wallis test followed by Dunn's multiple comparison test, with significance denoted as * ($p < 0.05$), ** ($p < 0.01$), *** ($p < 0.001$) and **** ($p < 0.0001$).

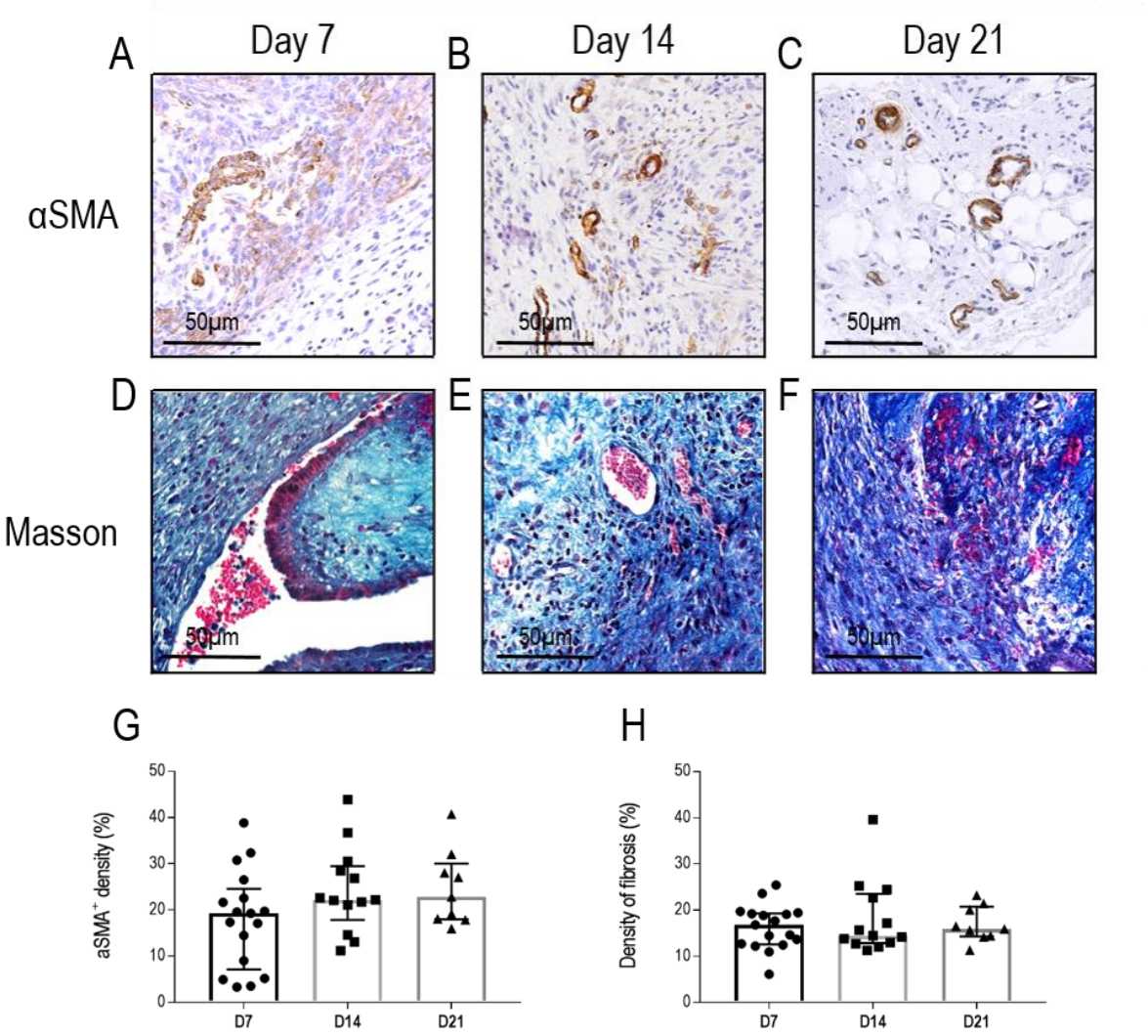

Figure 5.8 Evaluation of fibrosis in endometriosis-like lesions from *miR-223*$^{-/-}$ mice

The density of myofibroblasts in *miR-223*$^{-/-}$ lesions at D7 (**A**), D14 (**B**), and D21 (**C**) was evaluated using alpha smooth muscle actin (αSMA) (**G**). Masson's trichrome staining was used to evaluate the density of fibrosis (**H**) at D7 (**D**), D14 (**E**) and D21 (**F**) in these lesions. Data are presented as median (IQR), with each symbol representative of a single lesion in one mouse (n=17 at D7, n=13 at D14, n=9 at D21). Analysis was done using the Kruskal-Wallis test followed by Dunn's multiple comparison test.

Figure 5.9 Comparative analysis of the expression of macrophage markers between C57 and *miR-223*$^{-/-}$ endometriosis-like lesions

Total (**A**), peripheral (**B**), and central (**C**) F4/80 density were compared between C57 mice (; n=12 at D7, n=12 at D14, n=8 at D21) and *miR-223*$^{-/-}$ mice (; n=17 at D7, n=13 at D14, n=9 at D21). Comparisons between the M1-like macrophage markers inducible nitric oxide synthase (iNOS; total (**D)**, peripheral (**E**), and central (**F**)) and Class II Major Histocompatibility Complex (MHC II; total (**G)**, peripheral (**H**), and central (**I**)) were also performed. The density of the M2-like macrophage markers CD206 (total (**J)**, peripheral (**K**), and central (**L**)) and Arginase-1 (Arg-1; total (**M)**, peripheral (**N**), and central (**O**)) were also compared between strains. Data are presented as median (IQR). Analysis was done using the Mann Whitney U test, with significance denoted as * ($p < 0.05$), ** ($p < 0.01$), *** ($p < 0.001$), and **** ($p < 0.0001$).

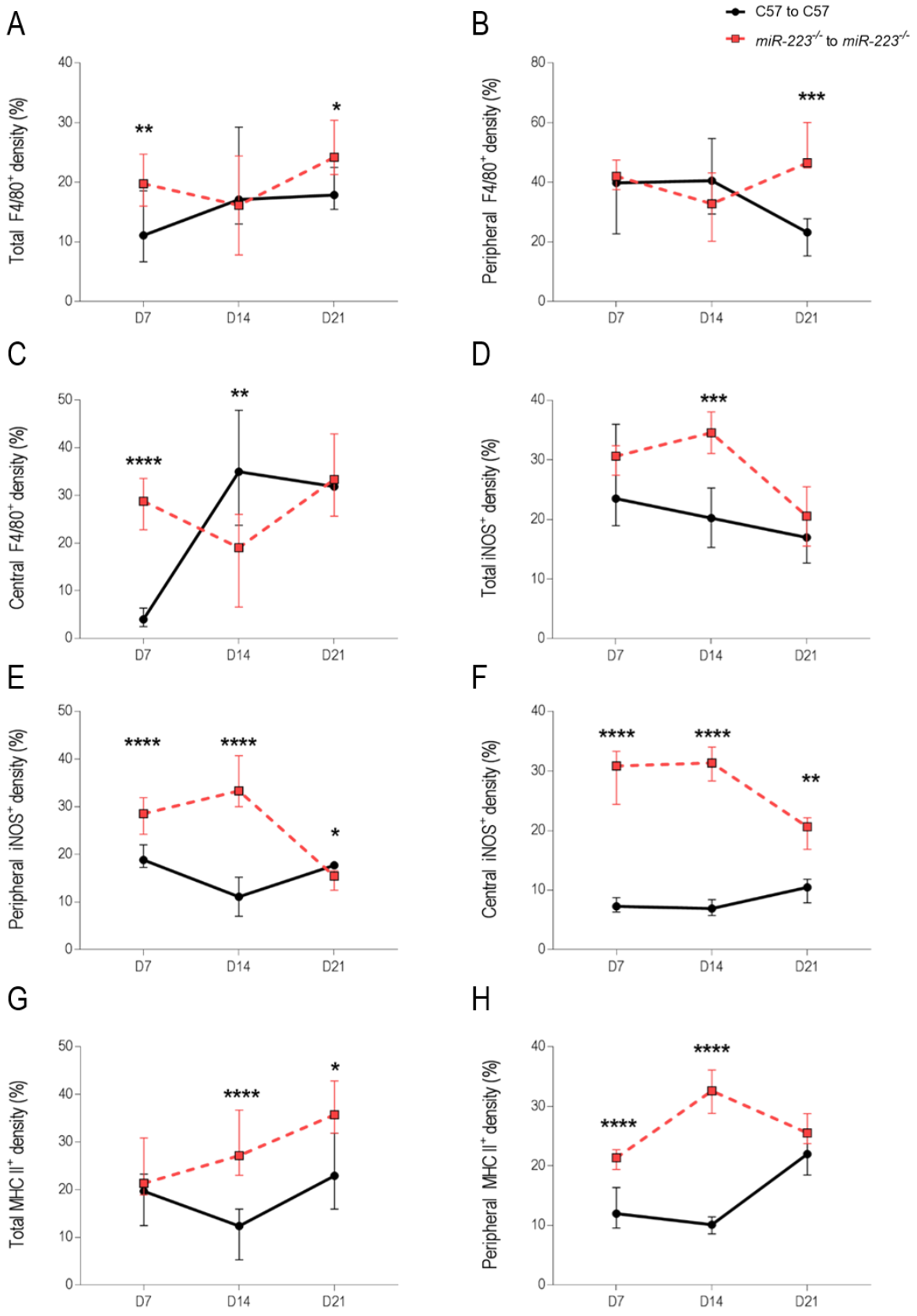

Figure 5.9 (A-H) **Comparative analysis of the expression of macrophage markers between C57 and *miR-223*$^{-/-}$ endometriosis-like lesions**

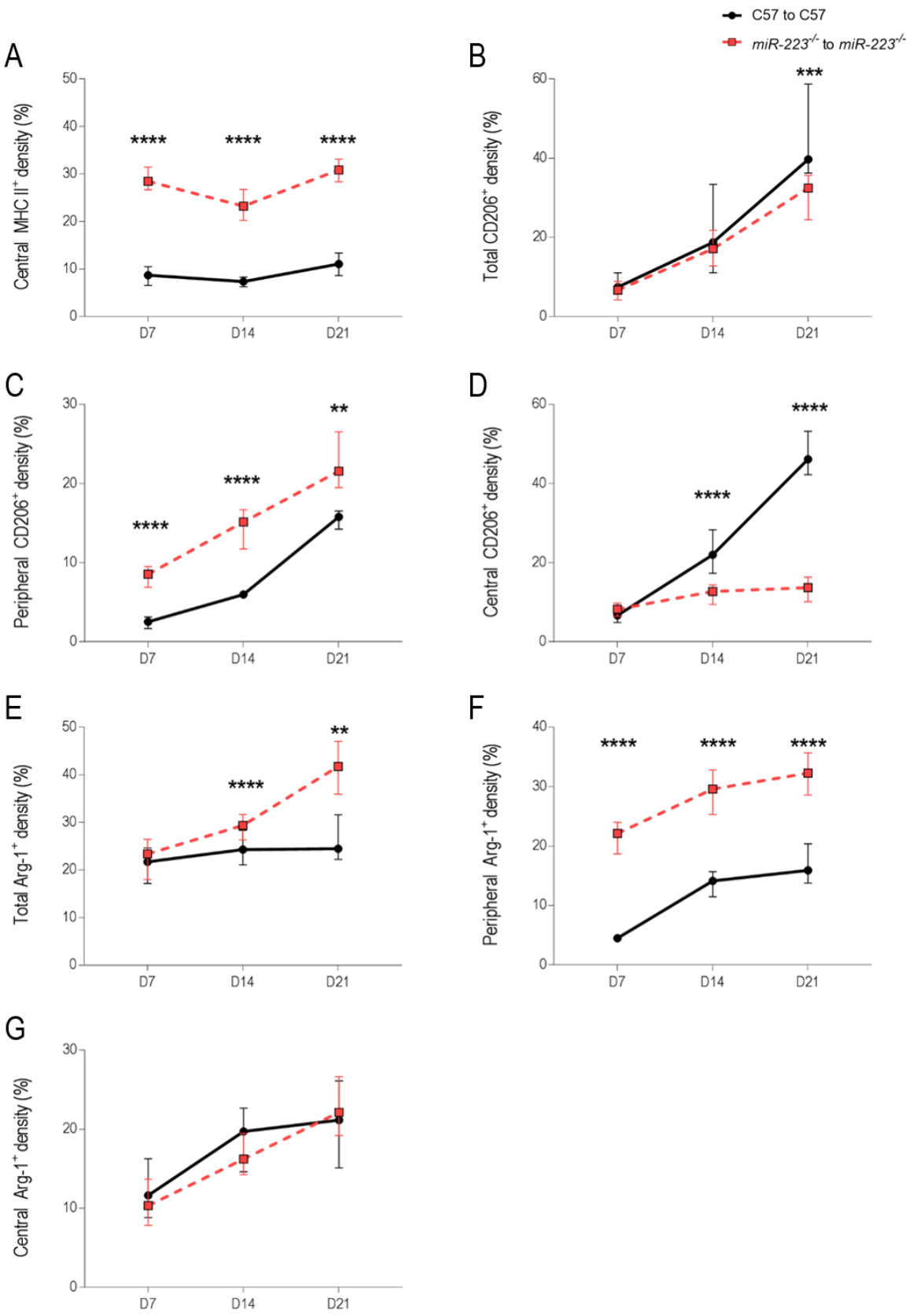

Figure 5.9 (I-O) **Comparative analysis of the expression of macrophage markers between C57 and *miR-223*$^{-/-}$ endometriosis-like lesions**

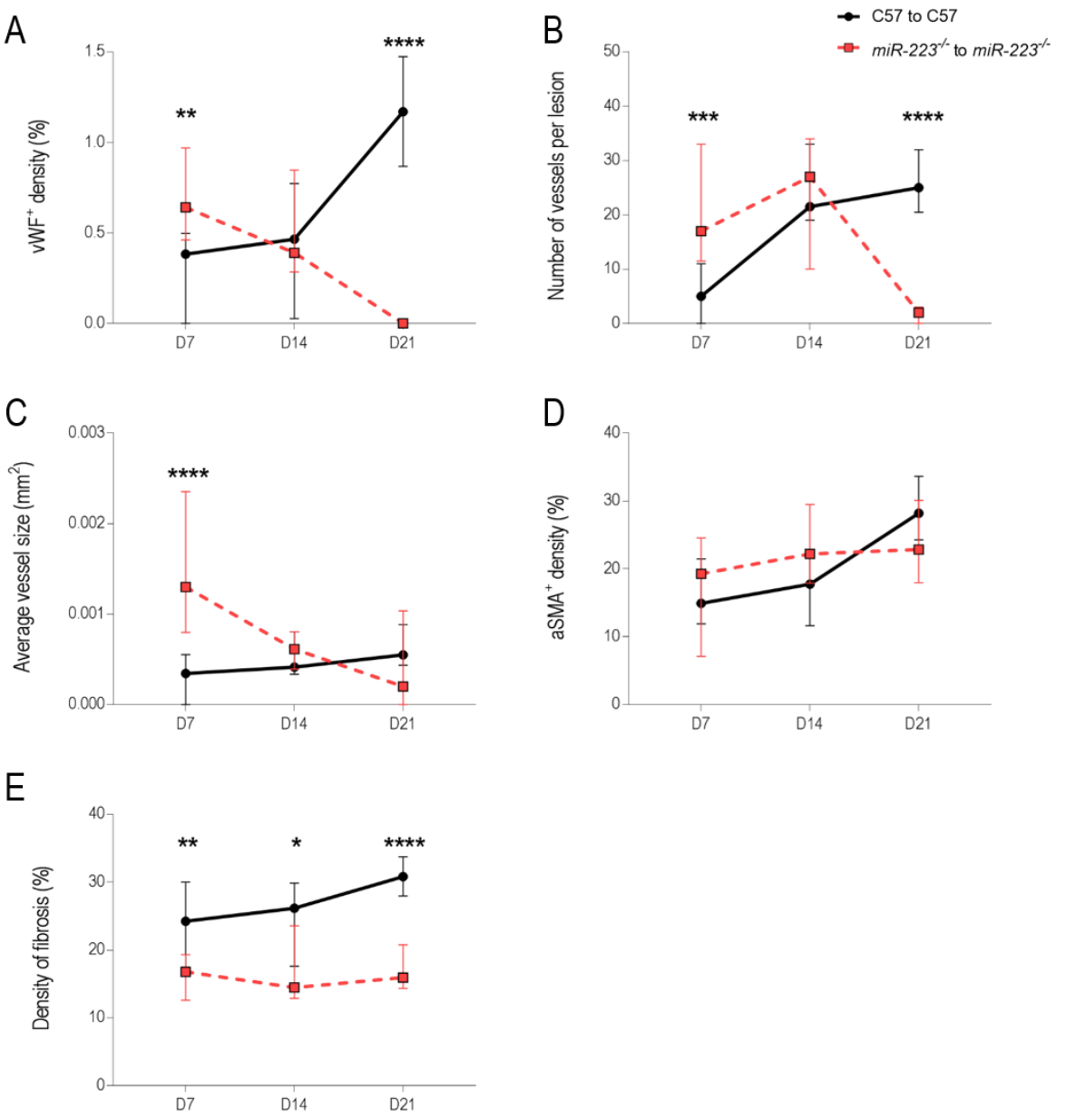

Figure 5.10 **Comparative analysis of blood vessel and fibrosis markers between C57 and *miR-223*$^{-/-}$ endometriosis-like lesions**

Total blood vessel density (**A**), number of vWF^{+} vessels per lesion (**B**), and average vessel size (**C**), density of myofibroblasts (**D**) and extent of fibrosis as measured by Masson's trichrome (**E**) were compared between C57 mice (; n=12 at D7, n=12 at D14, n=8 at D21) and *miR-223*$^{-/-}$ mice (; n=17 at D7, n=13 at D14, n=9 at D21). Data are presented as median (IQR). Analysis was done using the Mann Whitney U test, with significance denoted as * ($p < 0.05$), ** ($p < 0.01$), *** ($p < 0.001$), and **** ($p < 0.0001$).

5.2.5. RNA-Sequencing analysis of lesion progression in *miR-223* deficient mice

To determine the molecular changes associated with lesion development in the absence of *miR-223*, RNA-Sequencing (RNA-Seq) was performed on donor decidualised endometrial tissue, D7 and D14 lesions (See Appendix: Figure 7.2 and Figure 7.3 for RNA-Seq metrics). Post filtering to remove low expressed genes, a total of 16,291 genes were identified and analysed from the RNA-Seq dataset. The average gene expression was obtained from samples of decidualised endometrium, D7 and D14 lesions (n =4 per group), and the number of DEGs amongst detected genes between groups was assessed (FDR ≤ 0.05 and a ≥ 2-fold change in expression) (see attached Supplementary Materials: Table 8 to 10 for complete DEG list). Principal component analysis performed using normalised RNA-Seq data showed a clustering pattern of *miR-223*$^{-/-}$ decidualised endometrial tissue samples on the left, with a distinct separation from both D7 and D14 lesions (Figure 5.11 A). Comparisons between decidualised endometrium and D7 lesions found 10% of detected genes upregulated, whereas 15% of detected genes were downregulated (Figure 5.11 B). Between decidualised endometrium and D14, a total of 12% of detected genes were upregulated while 18% of detected genes were downregulated (Figure 5.11 C). In contrast, between D7 and D14, only 2% of detected genes were upregulated, and 2% of detected genes were downregulated (Figure 5.11 D).

A total of 5,522 genes were differentially expressed between one or more of the three comparisons, wherein 3.4% (190 genes) were differentially expressed in all three groups (Figure 5.11 E). An overlap of 58.4% (3,225 genes) was observed between Decidualised *vs* D7 and Decidualised *vs* D14. These genes were further classified into genes that were upregulated (2,198 genes) and downregulated (3,271 genes) in the dataset (Figure 5.11 F and G respectively). At both D7 and D14, 1330 genes were consistently upregulated while 2083 genes were consistently downregulated when compared to decidualised endometrium.

The genes with the largest fold change in expression between the three samples were identified (Table 5.2). At both D7 and D14, when compared to decidualised endometrium, lesions had an increased expression of prostate stem cell antigen (*Psca*; involved in regulation of neurotransmission), prolactin family 3, subfamily c, member 1 (*Prl3c1*; involved in hormone activity, regulation of proliferation and decidual differentiation), tachykinin 2 (*Tac2*; involved in the regulation of blood pressure), and serine peptidase inhibitor, Kazal type 8 (*Spink8*; involved in the regulation of peptidase activity). Alternatively, a downregulation in the expression of myosin, heavy polypeptide 1 (*Myh1*; involved in actin filament and calmodulin binding), myosin, heavy polypeptide 4 (*Myh4*; involved in response to muscle activity), tintin (*Ttn*; involved in ankyrin binding, actomyosin structure organisation and organ development), creatine

kinase (*Ckm*; involved in phosphocreatine biosynthetic processes), ATPase, Ca^{2+} transporting, cardiac muscle, fast twitch 1 (*Atp2a1*; involved in cellular calcium ion homeostasis and regulation of muscle contraction), and A930016O22Rik (an antisense long noncoding RNA) was observed in lesions at both D7 and D14 compared to decidualised endometrium.

Amongst the DEGs between D7 and D14 lesions, an upregulation in oxidized low density lipoprotein (lectin-like) receptor 1 (*Olr1*; involved in cell death, inflammatory response, and leukocyte cell adhesion), non-specific cytotoxic cell receptor protein 1 homolog (*Nccrp1*; involved in regulation of cell proliferation), and small proline-rich protein 2G (*Sprr2g*; involved in keratinocyte differentiation and peptide cross-linking) was observed as lesions progressed in *miR-223*$^{-/-}$ mice (Table 5.2). In contrast, a downregulation in two antisense long noncoding RNA (*Gm16559* and *Efhd1os*) and genes associated with immune function (histocompatibility 2, M region locus 2 (*H2-M2*), SH3-domain GRB2-like 2 (*Sh3gl2*), and melan-a (*Mlana*)) was observed during lesion progression.

Assessment of canonical pathways in both D7 and D14 lesions compared to decidualised endometrium shared an upregulation in multiple cholesterol biosynthesis pathways, including zymosterol and ceramide, as well as an upregulation in an antioxidant pathway (Table 5.3 and Table 5.4). In addition when compared against decidualised endometrium, an upregulation in Wnt/β-catenin signalling ($p = 0.0120$, ratio = 26%) was observed at D7, whereas an upregulation in pathways associated with cell cycle regulation ($p = 0.0355$, ratio = 31%) and inhibition of matrix metalloproteases ($p < 0.0001$, ratio = 60%) was observed at D14. In contrast, a total of 37 downregulated canonical pathways were similar in D7 and D14 lesions compared to decidualised endometrium (Table 5.3 and Table 5.4). The majority of these pathways were associated with immune regulation, including IL-6 and IL-7 signalling, production of nitric oxide and reactive oxygen species in macrophages, NF-κB signalling, Th1 signalling, dendritic cell maturation, and Fcγ receptor-mediated phagocytosis in macrophages and monocytes. Comparisons between D7 and D14 lesions showed an upregulation in four canonical pathways, including inhibition of matrix metalloproteases ($p < 0.0001$, ratio = 24%), and a downregulation in two canonical pathways, including fibroblast signalling ($p = 0.0032$, ratio = 18%) at D14 (Table 5.5).

5.2.5.1. Comparison of RNA-Sequencing data between C57 mice and *miR-223* deficient mice

To determine the impact of a *miR-223* deficiency on gene expression during the development of endometriosis, RNA-Seq data from decidualised endometrium, D7 and D14 lesions in C57 mice and *miR-223*$^{-/-}$ mice were compared. A total of 240 DEGs were identified (Figure 5.12A), with a consistent dysregulation of ten genes (ATPase, H+ transporting, lysosomal V0 subunit C (*Atp6v0c*), protein tyrosine phosphatase receptor type f polypeptide, interacting protein alpha 4 (*Ppfia4*), cathepsin E (*Ctse*), nicotinamide nucleotide transhydrogenase (*Nnt*), and several pseudogenes (*Tmem181b-ps*, *Gm9825*, *Rps2-ps13*, *Gm13443*, *Gm15487*, and *Gm37333*)) between C57 and *miR-223*$^{-/-}$ mice across all samples

The majority of DEGs were expressed within the decidualised endometrium, with a dysregulation of genes involved in ATP binding activity (heat shock protein 1A and 1B (*Hspa1a* and *Hspa1b*)), immune activity (*Ctse*), signalling pathways (*Tspan11* and *Adgrd1*), non-coding RNA genes (*4931413K12Rik* and *Gm28373*), and genes with unclassified or unknown functions (*Gm20481*, *Tmem26*7, *Fndc9*, and *1810041L15Rik*) (Table 5.6) (see attached Supplementary Materials: Table 11 for complete DEG list).

At D7, 18 genes were differentially expressed between C57 and *miR-223*$^{-/-}$ mice, with five upregulated genes and 13 downregulated genes (Figure 5.12). Alternatively, at D14, 22 DEGs were identified between C57 and *miR-223*$^{-/-}$ mice, with six upregulated genes and 16 downregulated genes (Figure 5.12). An upregulation of three genes (*Ppfia4*, *Atp6v0c*, and ribonuclease T2B (*Rnaset2b*)) and a downregulation of nine genes (*Ctse*, *Nnt*, *Gm9825*, *Gm13443*, *Gm13443*, *Rps2-ps13*, *Gm15487*, *Gm37333*, *Tmem181b-ps*, and *Hmga1-rs1*) was consistent in *miR-223*$^{-/-}$ lesions at both D7 and D14. In addition, at D14, an upregulation in *Mmp11* (involved in collagen fibril organisation) and cytotoxic T lymphocyte-associated protein 2 alpha (*Ctla2a*; involved in regulation of inflammatory response and T cell differentiation) was observed, whereas a downregulation of chitinase-like 1 (*Chil1*; involved in IL-8 secretion) and pleckstrin homology domain containing, family A member 6 (*Plekha6*; interacts with 17β-oestradiol) was observed in *miR-223*$^{-/-}$ lesions (Table 5.6).

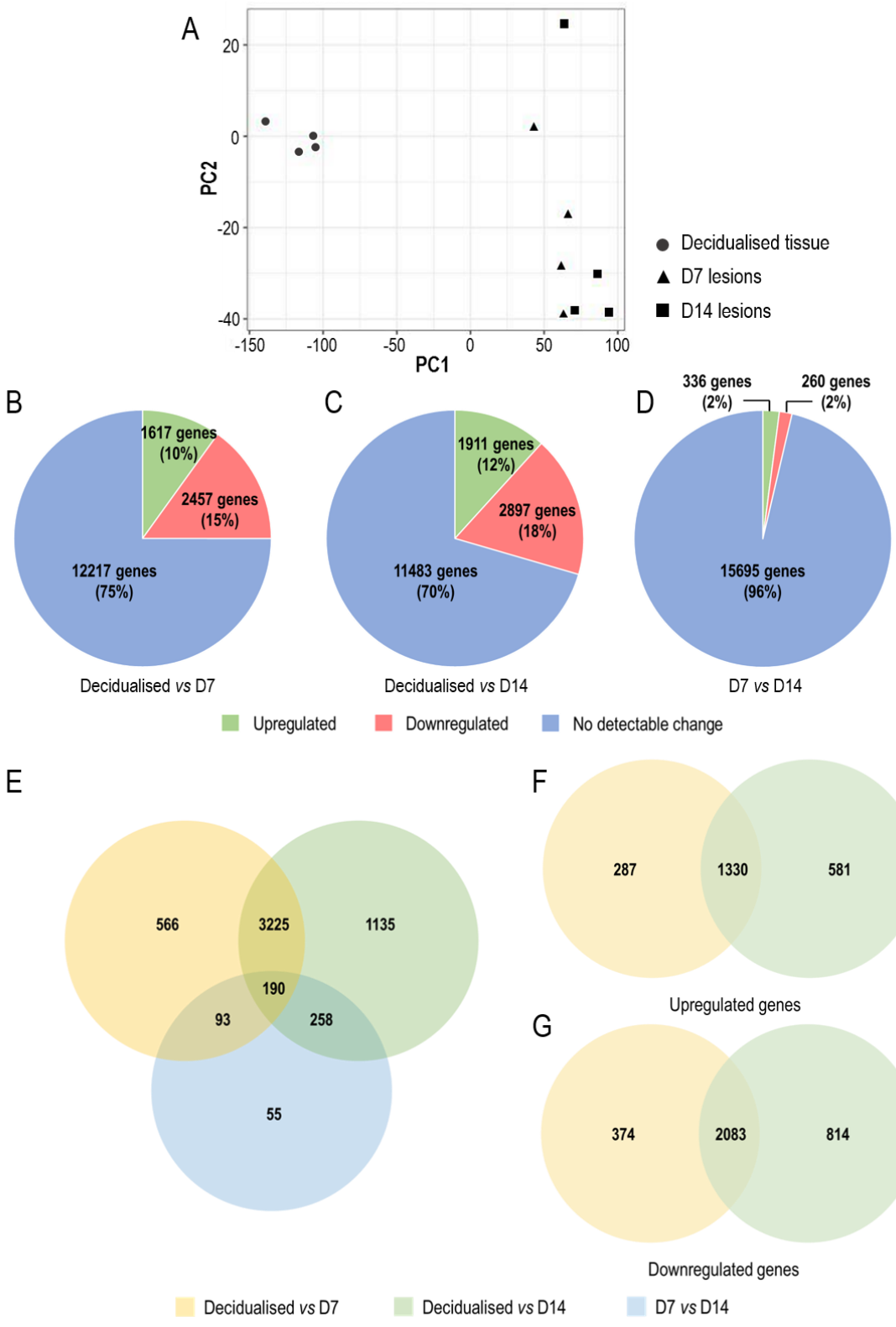

Figure 5.11 Number of differentially expressed genes identified in tissues from *miR-223*$^{-/-}$ mice

Principal component analysis (PCA) was performed using the normalised RNA-Seq data from *miR-223*$^{-/-}$ decidualised endometrium, D7 and D14 lesions (**A**). The proportion of upregulated and downregulated DEGs amongst detected genes between Decidualised *vs* D7 (**B**), Decidualised *vs* D14 (**C**), and D7 *vs* D14 (**D**) was determined. The Venn diagram displays the distribution and overlap of DEGs (both upregulated and downregulated) between each comparison (**E**). Additional Venn diagrams were generated to determine the number of upregulated (**F**) and downregulated (**G**) DEGs during lesion development compared to decidualised endometrial tissue. All genes identified have a ≥ 2-fold change in expression with an adjusted *p* value < 0.05.

Table 5.2 Top ten upregulated and downregulated DEGs in *miR-223*$^{-/-}$ mice during decidualisation and lesion development (FDR <0.05)

Decidualised *vs* D7			Decidualised *vs* D14			D7 *vs* D14		
Gene	**log_2FC**	**FDR**	**Gene**	**log_2FC**	**FDR**	**Gene**	**log_2FC**	**FDR**
Psca	+ 10.31	1.40×10^{-8}	Tac2	+ 10.98	5.90×10^{-9}	Sez6l	+ 4.98	1.07×10^{-3}
Prl3c1	+ 9.67	2.17×10^{-4}	Psca	+ 10.84	4.11×10^{-9}	Klk15	+ 4.97	1.25×10^{-2}
Tac2	+ 9.10	3.92×10^{-9}	Sprr2g	+ 10.32	8.70×10^{-8}	Gm44756	+ 4.79	9.87×10^{-3}
Hsd3b6	+ 8.88	9.72×10^{-6}	Bco1	+ 10.19	2.89×10^{-9}	Nccrp1	+ 4.70	6.89×10^{-4}
Spink8	+ 8.82	2.99×10^{-9}	Prl3c1	+ 10.05	1.88×10^{-4}	Sprr2g	+ 4.52	4.16×10^{-2}
Notum	+ 8.41	9.73×10^{-7}	Nccrp1	+ 9.66	1.51×10^{-11}	Olr1	+ 4.32	3.42×10^{-3}
Wnt10a	+ 8.10	7.91×10^{-10}	Cbln1	+ 9.36	9.17×10^{-8}	Igfn1	+ 4.23	4.15×10^{-2}
Atp7b	+ 8.04	4.04×10^{-8}	Spink8	+ 9.34	7.06×10^{-10}	Otogl	+ 4.08	4.41×10^{-2}
4932415M13Rik	+ 7.84	2.33×10^{-9}	Doxl2	+ 9.30	3.74×10^{-6}	Htr1b	+ 4.02	4.83×10^{-3}
Brinp2	+ 7.65	6.13×10^{-6}	Sprr2h	+ 9.22	3.88×10^{-5}	Ceacam18	+ 3.90	4.90×10^{-2}
Myh4	- 11.01	4.00×10^{-4}	Myh4	- 11.32	2.39×10^{-4}	Asic2	- 6.26	1.71×10^{-3}
Ttn	- 10.95	8.03×10^{-3}	Myh1	- 11.06	2.88×10^{-2}	H2-M2	- 4.08	1.77×10^{-3}
Myh1	- 10.54	4.23×10^{-2}	Ttn	- 10.92	6.94×10^{-3}	Ano4	- 3.94	1.19×10^{-2}
Ryr1	- 10.45	3.70×10^{-2}	A930016O22Rik	- 10.80	3.06×10^{-2}	Mmrn1	- 3.87	1.24×10^{-2}
Ckm	- 10.16	9.65×10^{-3}	Ckm	- 10.80	5.18×10^{-3}	Gm16559	- 3.78	1.28×10^{-2}
A930016O22Rik	- 10.14	4.83×10^{-2}	Tnnc2	- 10.69	3.89×10^{-2}	Adh1	- 3.65	1.01×10^{-2}
Gm44646	- 9.94	4.17×10^{-2}	Ampd1	- 10.53	4.56×10^{-2}	Sh3gl2	- 3.62	1.64×10^{-2}
Atp2a1	- 9.94	9.23×10^{-5}	Atp2a1	- 10.50	3.64×10^{-5}	Efhd1os	- 3.51	1.53×10^{-2}
Ppp1r3a	- 9.84	3.46×10^{-2}	Myhas	- 10.47	4.87×10^{-2}	Myrip	- 3.45	6.79×10^{-3}
Eef1a2	- 9.53	3.79×10^{-2}	Smyd1	- 10.42	4.79×10^{-2}	Mlana	- 3.43	4.81×10^{-3}

Table 5.3 Canonical pathways identified by IPA in D7 lesions compared to decidualised endometrium from *miR-223*$^{-/-}$ mice (*P* < 0.05; -2 > *Z* score > 2)

Canonical Pathway	*Z* score	Ratio	*P* value
Superpathway of Cholesterol Biosynthesis	3.606	48%	3.72×10^{-4}
Antioxidant Action of Vitamin C	3.272	32%	5.01×10^{-4}
Cholesterol Biosynthesis I	2.646	54%	4.07×10^{-3}
Cholesterol Biosynthesis II (via 24,25-dihydrolanosterol)	2.646	54%	4.07×10^{-3}
Cholesterol Biosynthesis III (via Desmosterol)	2.646	54%	4.07×10^{-3}
Wnt/β-catenin Signalling	2.137	26%	1.07×10^{-2}
Zymosterol Biosynthesis	2.000	67%	1.20×10^{-2}
Ceramide Biosynthesis	2.000	57%	2.40×10^{-2}
Chondroitin and Dermatan Biosynthesis	-2.000	67%	1.20×10^{-2}
P2Y Purigenic Receptor Signalling Pathway	-2.030	33%	3.31×10^{-5}
Colorectal Cancer Metastasis Signalling	-2.038	34%	7.76×10^{-10}
GM-CSF Signalling	-2.041	32%	1.82×10^{-3}
LPS-stimulated MAPK Signalling	-2.041	28%	1.35×10^{-2}
Gαq Signalling	-2.064	32%	1.70×10^{-5}
NF-κB Activation by Viruses	-2.117	31%	2.45×10^{-3}
Renin-Angiotensin Signalling	-2.137	34%	9.12×10^{-6}
Apelin Liver Signalling Pathway	-2.138	54%	4.57×10^{-5}
Type I Diabetes Mellitus Signalling	-2.138	28%	7.41×10^{-3}
Toll-like Receptor Signalling	-2.183	32%	3.47×10^{-3}
Integrin Signalling	-2.188	24%	1.38×10^{-2}
IL-7 Signalling Pathway	-2.200	28%	1.17×10^{-2}
HMGB1 Signalling	-2.263	25%	2.40×10^{-2}
CCR3 Signalling in Eosinophils	-2.268	32%	1.66×10^{-4}
GNRH Signalling	-2.271	30%	1.82×10^{-4}
IL-6 Signalling	-2.271	31%	2.82×10^{-4}
Calcium-induced T Lymphocyte Apoptosis	-2.294	41%	3.39×10^{-5}
Phospholipase C Signalling	-2.335	30%	5.25×10^{-6}
GDNF Family Ligand-Receptor Interactions	-2.400	31%	2.69×10^{-3}
Production of Nitric Oxide and Reactive Oxygen Species in Macrophages	-2.429	28%	6.03×10^{-4}
Chemokine Signalling	-2.502	38%	8.91×10^{-5}
Tec Kinase Signalling	-2.530	31%	5.13×10^{-5}
PI3K Signalling in B Lymphocytes	-2.592	35%	4.79×10^{-6}
Role of NFAT in Cardiac Hypertrophy	-2.630	34%	6.17×10^{-9}
Eicosanoid Signalling	-2.714	43%	3.02×10^{-6}
Fc Epsilon RI Signalling	-2.744	30%	9.12×10^{-4}
NF-κB Signalling	-2.832	32%	7.24×10^{-6}
Calcium Signalling	-3.015	31%	6.61×10^{-6}
Role of Pattern Recognition Receptors in Recognition of Bacteria and Viruses	-3.124	41%	1.58×10^{-9}
iCOS-iCOSL Signalling in T Helper Cells	-3.124	41%	1.00×10^{-8}

GP6 Signalling Pathway	-3.250	50%	1.00×10^{-16}
Leukocyte Extravasation Signalling	-3.250	40%	3.98×10^{-13}
p38 MAPK Signalling	-3.272	26%	2.69×10^{-2}
CD28 Signalling in T Helper Cells	-3.307	36%	2.24×10^{-6}
Inflammasome pathway	-3.464	63%	1.82×10^{-5}
B Cell Receptor Signalling	-3.501	31%	1.82×10^{-5}
Th1 Pathway	-3.773	35%	8.91×10^{-6}
Fcγ Receptor-mediated Phagocytosis in Macrophages and Monocytes	-3.773	38%	9.55×10^{-6}
Role of NFAT in Regulation of the Immune Response	-3.810	34%	1.12×10^{-7}
PKCθ Signalling in T Lymphocytes	-4.117	33%	4.17×10^{-6}
Neuroinflammation Signalling Pathway	-4.364	32%	4.17×10^{-9}
Dendritic Cell Maturation	-4.989	36%	5.25×10^{-8}
TREM1 Signalling	-5.000	52%	1.86×10^{-10}

Table 5.4 Canonical pathways identified by IPA in D14 lesions compared to decidualised endometrium from *miR-223*$^{-/-}$ mice (*P* < 0.05; -2 > *Z* score > 2)

Canonical Pathway	*Z* score	Ratio	*P* value
Superpathway of Cholesterol Biosynthesis	3.051	48%	1.91×10^{-3}
Antioxidant Action of Vitamin C	3.024	34%	2.29×10^{-3}
Mitotic Roles of Polo-Like Kinase	2.324	39%	1.05×10^{-3}
Inhibition of Matrix Metalloproteases	2.236	60%	5.89×10^{-7}
Cholesterol Biosynthesis I	2.121	62%	2.04×10^{-3}
Cholesterol Biosynthesis II (via 24,25-dihydrolanosterol)	2.121	62%	2.04×10^{-3}
Cholesterol Biosynthesis III (via Desmosterol)	2.121	62%	2.04×10^{-3}
Cyclins and Cell Cycle Regulation	2.065	31%	3.55×10^{-2}
Zymosterol Biosynthesis	2.000	67%	2.19×10^{-2}
Ceramide Biosynthesis	2.000	57%	4.27×10^{-2}
IL-9 Signalling	-2.000	40%	2.57×10^{-3}
Chondroitin and Dermatan Biosynthesis	-2.000	67%	2.19×10^{-2}
IL-2 Signalling	-2.041	35%	6.61×10^{-3}
NF-κB Activation by Viruses	-2.058	38%	1.91×10^{-4}
Lymphotoxin β Receptor Signalling	-2.065	32%	2.45×10^{-2}
P2Y Purigenic Receptor Signalling Pathway	-2.111	35%	2.14×10^{-4}
Chemokine Signalling	-2.117	38%	1.38×10^{-3}
Gα12/13 Signalling	-2.137	29%	2.88×10^{-2}
Coagulation System	-2.138	40%	1.00×10^{-2}
Gαq Signalling	-2.143	34%	1.82×10^{-4}
Colorectal Cancer Metastasis Signalling	-2.165	35%	4.57×10^{-7}
CCR3 Signalling in Eosinophils	-2.191	34%	7.41×10^{-4}
Toll-like Receptor Signalling	-2.236	36%	3.09×10^{-3}
IL-7 Signalling Pathway	-2.268	34%	4.57×10^{-3}
IL-6 Signalling	-2.287	35%	3.31×10^{-4}
Production of Nitric Oxide and Reactive Oxygen Species in Macrophages	-2.292	32%	6.17×10^{-4}
Cardiac Hypertrophy Signalling	-2.357	30%	1.66×10^{-3}
HMGB1 Signalling	-2.402	31%	8.51×10^{-3}
GPCR-Mediated Nutrient Sensing in Enteroendocrine Cells	-2.469	38%	4.79×10^{-5}
Th2 Pathway	-2.480	45%	4.17×10^{-10}
Eicosanoid Signalling	-2.530	45%	2.51×10^{-5}
Renin-Angiotensin Signalling	-2.530	36%	1.20×10^{-4}
Tec Kinase Signalling	-2.654	35%	3.55×10^{-5}
GDNF Family Ligand-Receptor Interactions	-2.711	34%	6.61×10^{-3}
Calcium-induced T Lymphocyte Apoptosis	-2.858	45%	5.89×10^{-5}
p38 MAPK Signalling	-2.874	33%	3.02×10^{-3}
Fc Epsilon RI Signalling	-2.874	32%	5.25×10^{-3}
Complement System	-2.887	55%	3.24×10^{-5}
Glycolysis I	-3.000	39%	4.17×10^{-2}
Role of NFAT in Cardiac Hypertrophy	-3.064	36%	7.24×10^{-7}

Glutathione-mediated Detoxification	-3.317	44%	9.77×10^{-3}
PI3K Signalling in B Lymphocytes	-3.429	37%	3.55×10^{-5}
Inflammasome pathway	-3.464	63%	1.05×10^{-4}
Leukocyte Extravasation Signalling	-3.487	42%	5.01×10^{-11}
Calcium Signalling	-3.507	34%	4.17×10^{-5}
Role of Pattern Recognition Receptors in Recognition of Bacteria and Viruses	-3.592	45%	9.55×10^{-10}
NF-κB Signalling	-3.615	35%	3.24×10^{-5}
GP6 Signalling Pathway	-3.693	52%	2.51×10^{-14}
CD28 Signalling in T Helper Cells	-3.795	42%	1.51×10^{-7}
B Cell Receptor Signalling	-3.810	33%	2.88×10^{-4}
Fcγ Receptor-mediated Phagocytosis in Macrophages and Monocytes	-3.889	36%	1.51×10^{-3}
iCOS-iCOSL Signalling in T Helper Cells	-3.920	48%	1.00×10^{-10}
Neuroinflammation Signalling Pathway	-4.170	36%	2.63×10^{-8}
Role of NFAT in Regulation of the Immune Response	-4.202	38%	3.80×10^{-7}
Th1 Pathway	-4.808	49%	7.94×10^{-12}
PKCθ Signalling in T Lymphocytes	-4.907	36%	2.69×10^{-5}
TREM1 Signalling	-5.096	54%	4.79×10^{-9}
Dendritic Cell Maturation	-5.333	41%	3.31×10^{-9}

Table 5.5 Canonical pathways identified by IPA in D14 lesions compared to D7 lesions from *miR-223*$^{-/-}$ mice (*P* < 0.05; -2 > *Z* score > 2)

Canonical Pathway	*Z* score	Ratio	*P* value
Inhibition of Matrix Metalloproteases	2.333	24%	7.41×10^{-7}
Mitotic Roles of Polo-Like Kinase	2.121	14%	8.13×10^{-5}
Chondroitin Sulphate Biosynthesis (Late Stages)	2.000	10%	3.16×10^{-2}
Cdc42 Signalling	2.000	6%	4.07×10^{-2}
Apelin Cardiac Fibroblast Signalling Pathway	-2.000	18%	3.24×10^{-3}
Neuregulin Signalling	-2.000	7%	4.90×10^{-2}

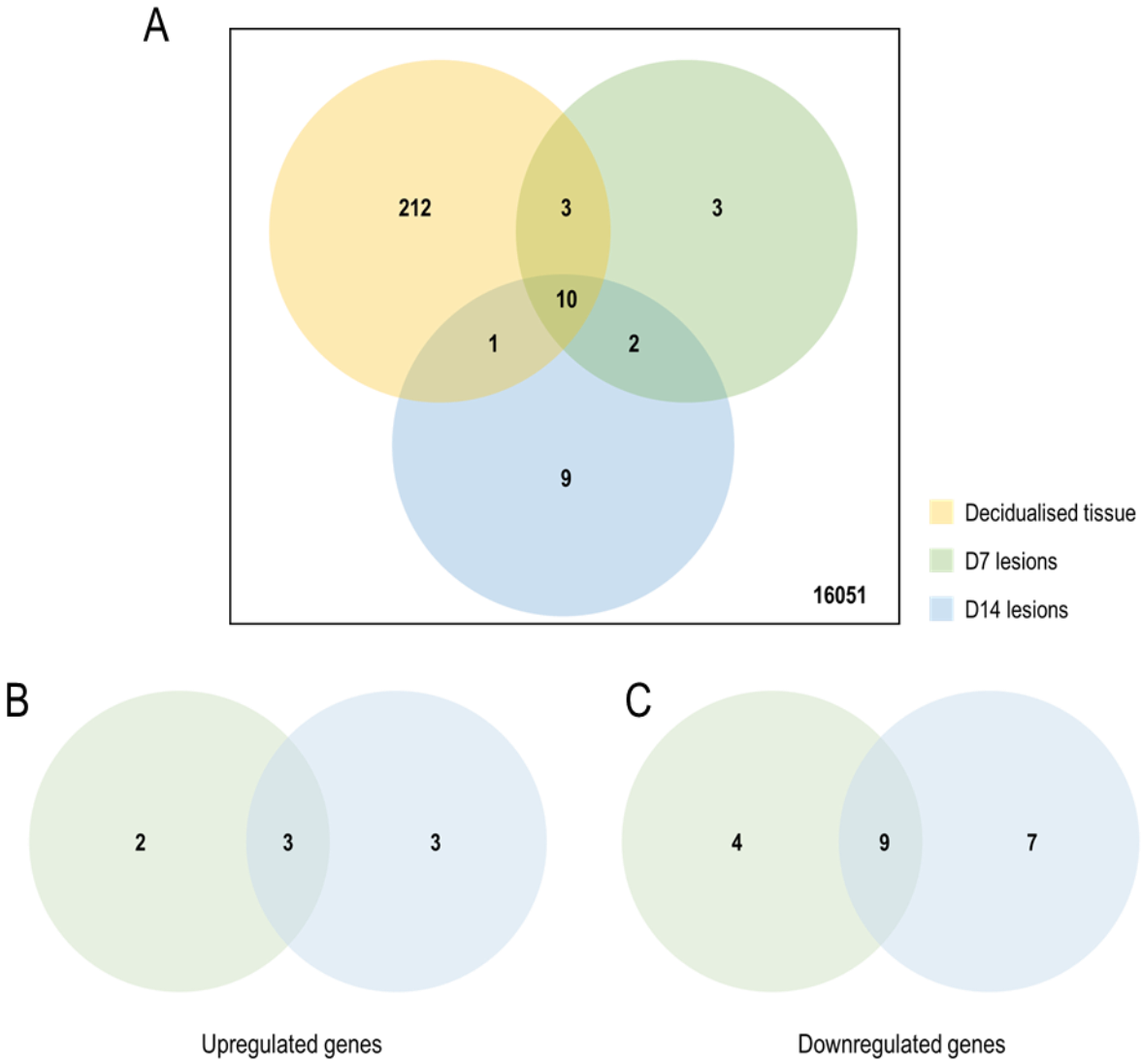

Figure 5.12 Number of differentially expressed genes identified between *miR-223*$^{-/-}$ and C57 mice

RNA-Seq data from decidualised endometrium, D7 and D14 lesions in *miR-223*$^{-/-}$ and C57 mice were compared to determine the proportion of DEGs amongst detected genes. The top Venn diagram displays the distribution and overlap of DEGs (both upregulated and downregulated) between each sample type (A). Additional Venn diagrams were generated to determine the number of upregulated (B) and downregulated (C) DEGs between D7 and D14 lesions. All genes identified have a ≥ 2-fold change in expression with an adjusted *p* value < 0.05.

Table 5.6 Top DEGs genes during decidualisation and lesion development in *miR-223*$^{-/-}$ mice compared to C57 mice (FDR <0.05)

Decidualised endometrium		
Gene	**log_2FC**	**FDR**
4931413K12Rik	+ 3.63	4.84×10^{-2}
Gm20481	+ 3.50	2.46×10^{-2}
Hspa1a	+ 3.03	8.07×10^{-4}
Tmem267	+ 2.87	1.11×10^{-2}
Fndc9	+ 2.63	2.89×10^{-2}
Grm4	+ 2.28	5.84×10^{-3}
Gm28373	+ 2.25	2.17×10^{-4}
Hspa1b	+ 2.15	5.05×10^{-3}
Apold1	+ 1.73	1.02×10^{-4}
Gad1	+ 1.61	2.15×10^{-3}
Syndig1	- 5.95	2.72×10^{-2}
1810041L15Rik	- 5.85	2.03×10^{-2}
Tspan11	- 5.76	1.59×10^{-2}
Ctse	- 5.62	1.46×10^{-3}
Npy	- 5.59	1.56×10^{-2}
Lyz1	- 5.50	7.12×10^{-3}
Myh11	- 5.07	2.09×10^{-2}
Myo5c	- 4.87	4.40×10^{-2}
Nptx2	- 4.84	2.89×10^{-2}
Adgrd1	- 4.47	4.79×10^{-2}

D7 lesions		
Gene	**log_2FC**	**FDR**
Ppfia4	+ 2.17	6.52×10^{-3}
Rnaset2b	+ 2.12	8.66×10^{-3}
Atp6v0c	+ 1.75	9.23×10^{-7}
Rnps1	+ 1.50	5.95×10^{-5}
Rps2	+ 1.41	3.35×10^{-9}
Gm9825	- 5.14	4.91×10^{-4}
Ctse	- 4.91	1.02×10^{-5}
Gm13443	- 4.69	3.37×10^{-3}
Rps2-ps13	- 4.57	5.05×10^{-4}
Tpsab1	- 4.45	3.08×10^{-2}
Hmga1-rs1	- 4.31	2.19×10^{-3}
Gm15487	- 3.22	4.25×10^{-3}
Gm37333	- 3.20	2.71×10^{-2}
Tmem181b-ps	- 2.47	9.23×10^{-7}
Ptprv	- 1.60	2.94×10^{-3}
Nnt	- 1.55	4.93×10^{-5}
Dynlt1-ps1	- 1.46	1.15×10^{-2}
Wdfy1	- 1.42	1.91×10^{-5}

D14 lesions		
Gene	**log_2FC**	**FDR**
Ppfia4	+ 2.01	5.47×10^{-4}
Ctla2a	+ 1.90	1.18×10^{-2}
Rnaset2b	+ 1.71	1.96×10^{-3}
Gdf3	+ 1.65	1.47×10^{-2}
Mmp11	+ 1.28	4.12×10^{-2}
Atp6v0c	+ 1.19	3.02×10^{-4}
Chil1	- 4.84	9.47×10^{-3}
Ctse	- 4.65	7.03×10^{-7}
Hmga1-rs1	- 4.24	3.15×10^{-3}
Asic2	- 3.92	1.69×10^{-2}
Gm13443	- 3.69	2.60×10^{-3}
Gm37333	- 3.67	2.60×10^{-3}
Gm9825	- 3.58	7.12×10^{-3}
Gm15487	- 3.48	1.65×10^{-3}
Gm26892	- 3.33	3.06×10^{-2}
Plekha6	- 3.06	1.46×10^{-2}
Rps2-ps13	- 2.96	9.47×10^{-3}
Tmem181b-ps	- 1.94	8.21×10^{-6}
Nnt	- 1.88	7.03×10^{-7}
Acss2	- 1.42	3.95×10^{-2}
Me1	- 1.39	4.35×10^{-2}
Rab3ip	- 1.25	4.35×10^{-2}

5.2.6. Evaluating the impact of *miR-223* depletion from either the recipient environment or donor endometrium

In a clinical setting, *miR-223* expression is upregulated in ectopic endometrial tissue compared to eutopic endometrial tissue (Ohlsson Teague et al., 2009). To date, correlations between an elevation in serum levels of *miR-223* and endometriosis have been inconclusive. In sections 5.2.1 to 5.2.4 of this thesis, the impact of a systemic depletion of *miR-223* (i.e. deficiency of *miR-223* in both donor and recipient mice) on lesion development was evaluated. Thus, to evaluate the contribution of the donor endometrium *vs* recipient environment on the development of endometriosis and expression of M1-like and M2-like markers, this section will evaluate the impact of reciprocal transfers between wildtype mice and mice deficient in *miR-223* (Figure 5.13). To determine the contribution of the recipient environment on the development of endometriosis, *miR-223* sufficient (C57) donor endometrium was transferred into a *miR-223* deficient (*miR-223*$^{-/-}$) recipient (C57 → *miR-223*$^{-/-}$). Conversely, the transfer of *miR-223* deficient (*miR-223*$^{-/-}$) donor endometrium into a replete *miR-223* (C57) recipient (*miR-223*$^{-/-}$ → C57) was performed to determine the contribution of donor endometrial tissue in the pathogenesis of endometriosis.

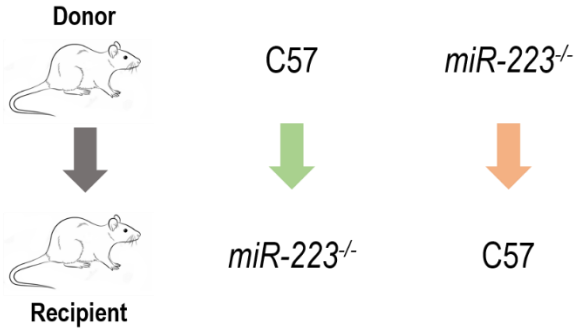

Figure 5.13 Reciprocal transfers between *miR-223*$^{-/-}$ and C57 mice

Utilising the Greaves-Saunders menstrual mouse model of endometriosis (Greaves et al., 2014), 40mg donor decidualised endometrial tissue was injected subcutaneously into an allogeneic recipient. Resulting endometriosis-like lesions from these reciprocal transfers were harvested at either day 7, 14, or 21 post-induction of disease. Refer to Figure 2.3 for the protocol to induce endometriosis in recipient mice.

5.2.6.1. Endometriosis-like lesion development in C57 donor to *miR-223*$^{-/-}$ recipient transfers

A total of 38 C57 donor mice were required to generate enough decidualised endometrial tissue for injection into *miR-223*$^{-/-}$ recipient mice (C57 → *miR-223*$^{-/-}$) at a ratio of 2 donors to 1.8 recipients (Table 5.7). Over the course of the experiment, a total of 97% of *miR-223*$^{-/-}$ recipient mice had identifiable lesions. At both D7 and D14, 100% of *miR-223*$^{-/-}$ recipient mice had lesions, whereas at D21, 83% of *miR-223*$^{-/-}$ recipient mice had lesions. A total of 2 mice had more than one lesion and have been excluded from subsequent analyses.

Endometriosis-like lesions that developed from a C57 → *miR-223*$^{-/-}$ transfer were large, spread out over the attachment site, with a blood and pus-filled appearance at D7 (Figure 5.14 A). At both D14 and D21, lesions appeared small and circular, however still retained a blood and pus-filled appearance (Figure 5.14 B, C). Lesions were significantly larger at D7 (76 (37 – 96) mm^3) compared to both D14 (6 (4 – 8) mm^3, p = 0.0013) and D21 (5 (3 – 7, p = 0.0001 for D7 *vs* D21) (Figure 5.14 D). A similar trend was noted in lesion weight, with heaviest lesions present at D7 (44.65 (36.30 – 48.75) mg), followed by significant reductions in weight at D14 (6.65 (4.75 – 9.43) mg, p = 0.0010) and at D21 (5.40 (4.50 – 7.33) mg, p = 0.0002 for D7 *vs* D21) (Figure 5.14 E).

Assessment of morphological parameters was done in H&E stained lesion sections from C57 → *miR-223*$^{-/-}$ mice (Figure 5.15 A-C). Average gland size per lesion reduced significantly between D7 (0.015 (0.000 – 0.099) mm^2) and D21 (0.000 (0.000 – 0.001) mm^2; p = 0.0443) (Figure 5.15 E). Similarly, lumen area was largest at D7 (0.009 (0.000 – 0.016) mm^2) and reduced significantly at D21 (0.000 (0.000 – 0.000) mm^2, p = 0.0443) (Figure 5.15 F). A corresponding trend was observed in measurements of epithelium area within glands, with a reduction seen between D7 (0.016 (0.000 – 0.037) mm^2) and D21 (0.000 (0.000 – 0.000) mm^2; p = 0.0378) (Figure 5.15 G). Over the three week time period, no significant differences were observed in the number of glands per lesion (Figure 5.15 D), percentage glandular epithelium (Figure 5.15 H) or percentage stromal area (Figure 5.15 I).

Total F4/80$^+$ density was lowest at D7 (16.06 (13.78 – 21.44) %) and significantly increased at both D14 and D21 (25.14 (22.29 – 34.63) % and 33.58 (24.44 – 39.09) % respectively; p = 0.0475 for D7 *vs* D14 and p = 0.0029 for D7 *vs* D21) (Figure 5.16 G). Peripheral F4/80$^+$ density was consistent over all time points (Figure 5.16 A-C, H). Conversely, central expression of F4/80 in these lesions significantly increased between D14 (23.57 (15.69 – 29.98) %) and D21 (47.49 (37.08 – 54.66) %; p = 0.0089) (Figure 5.16 D-F, I).

Expression of the M1-like marker iNOS showed a gradual increase in iNOS$^+$ density was across the time points (18.37 (15.62 – 20.71) % at D7, 24.88 (16.03 – 43.76) % at D14, and 38.17 (34.52 – 43.21) % at D21; p = 0.0006 for D7 *vs* D21) (Figure 5.17 A-C, M). Similarly, expression of the M1-like marker MHC II in C57 → *miR-223*$^{-/-}$ lesions increased significantly over the time course (3.28 (1.83 – 3.99) % at D7, 16.26 (10.79 – 19.63) % at D14, and 23.65 (21.15 – 35.42) % at D21; p = 0.0230 for D7 *vs* D14 and p < 0.0001 for D7 *vs* D21) (Figure 5.17 D-F, N). The density of the M2-like marker CD206 increased over the three weeks (8.10 (5.59 – 8.90) % at D7, 23.33 (16.00 – 34.86) % at D14, and 24.88 (22.48 – 30.67) % at D21; p = 0.0012 for D7 *vs* D14 and p = 0.0002 for D7 *vs* D21). In contrast, the expression of Arg-1 was similar at D7 and D14 (31.66 (26.67 – 40.98) % and 39.58 (33.40 – 43.22) % respectively), with a significant increase observed at D21 (55.82 (49.29 – 66.08) %; p = 0.0003 for D7 *vs* D21 and p = 0.0123 for D14 *vs* D21) (Figure 5.17 J-L, P).

Table 5.7 Endometriosis-like lesion recovery in C57 → *miR-223*$^{-/-}$ mice

Lesion collection time point	D7	D14	D21
Total number of C57 donor mice used across all time points: 38			
Number of *miR-223*$^{-/-}$ recipient mice	11	11	12
Number of mice with lesions*	11	11	10
Proportion of mice with lesions (%)	100	100	83

* To reduce bias, mice with ≥2 lesions were excluded from subsequent analyses. At D7 - 1 mouse excluded; At D14 – 1 mouse excluded.

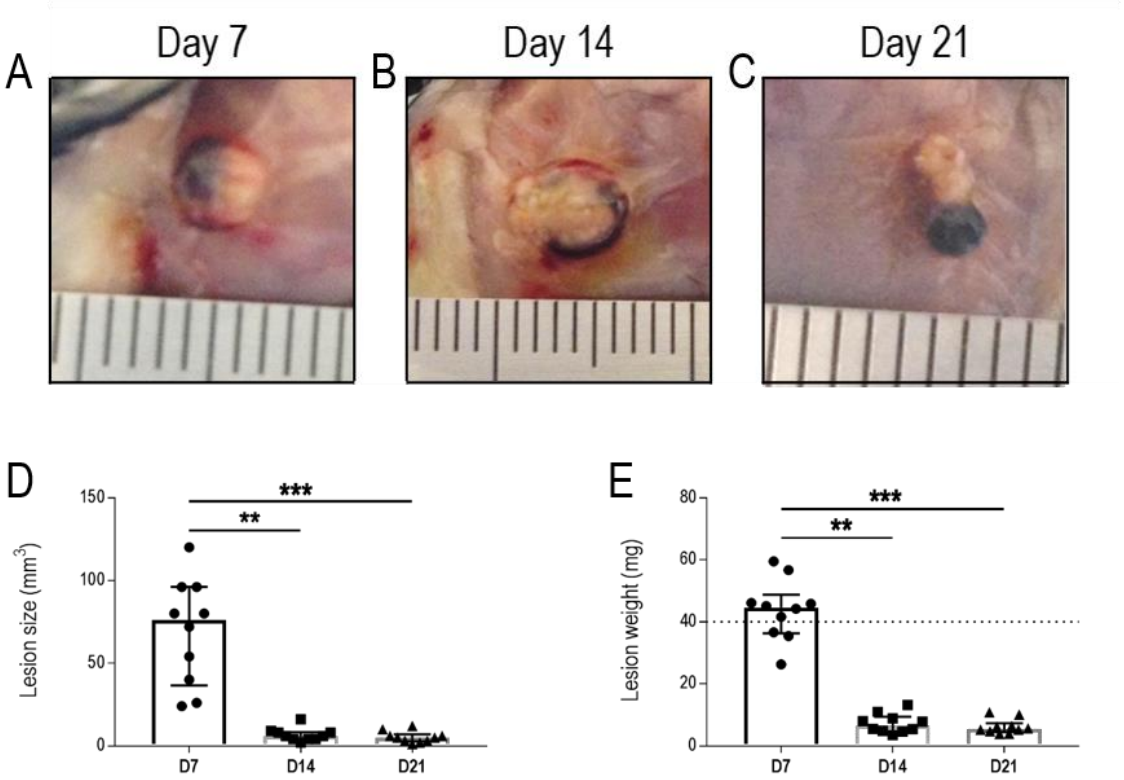

Figure 5.14 **Gross morphology of endometriosis-like lesion development in a transfer from C57 donor to *miR-223*$^{-/-}$ recipient mice**

Decidualised C57 donor endometrial tissue was injected subcutaneously into *miR-223*$^{-/-}$ recipient mice. Resulting lesions were harvested at either D7 (**A**), D14 (**B**) or D21 (**C**), with representative images shown. Lesion size was measured (**D**) and lesions were excised and weighed (**E**), with the dotted line indicating the initial weight of donor decidualised endometrial tissue inoculated into recipient mice. Data are presented as median (IQR), with each symbol representative of a single lesion in one mouse (n=10 at D7, n=10 at D14, n=10 at D21). Analysis was done using the Kruskal-Wallis test followed by Dunn's multiple comparison test, with significance denoted as ** ($p < 0.01$) and *** ($p < 0.001$).

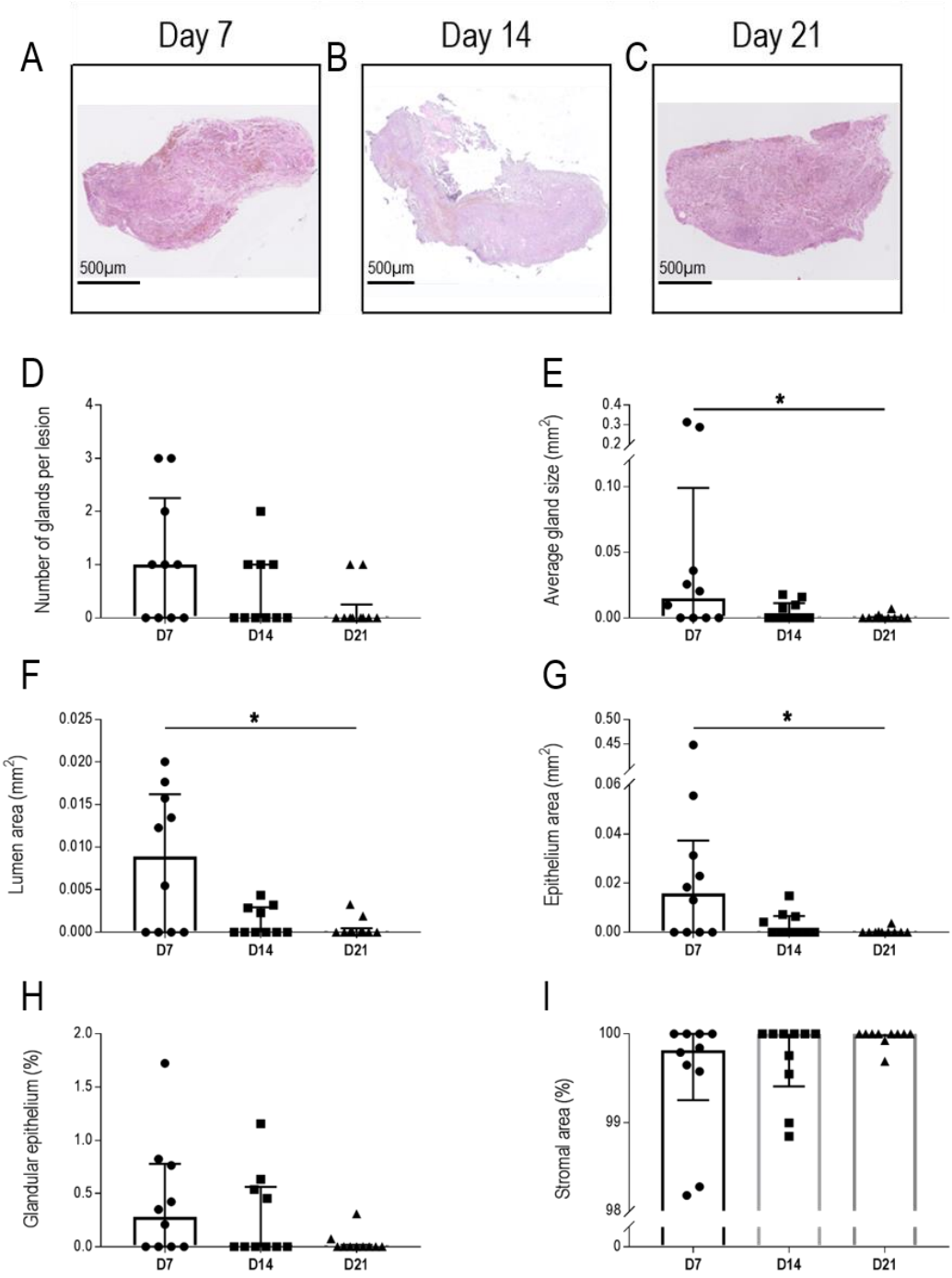

Figure 5.15 Assessment of morphological parameters in haematoxylin and eosin stained endometriosis-like lesions from C57 donor to *miR-223*$^{-/-}$ recipient mice

Haematoxylin and eosin stained sections from D7 **(A)**, D14 **(B)**, and D21 **(C)** lesions (representative images shown; arrows indicate glands) were assessed for the following characteristics: number of glands per lesion **(D)**, average gland size **(E)**, lumen area **(F)**, epithelium area **(G)**, percentage glandular epithelium **(H)** and percentage stromal area **(I)**. Data are presented as median (IQR), with each symbol representative of a single lesion in one mouse (n=10 at D7, n=10 at D14, n=10 at D21). Analysis was done using the Kruskal-Wallis test followed by Dunn's multiple comparison test, with significance denoted as * ($p < 0.05$).

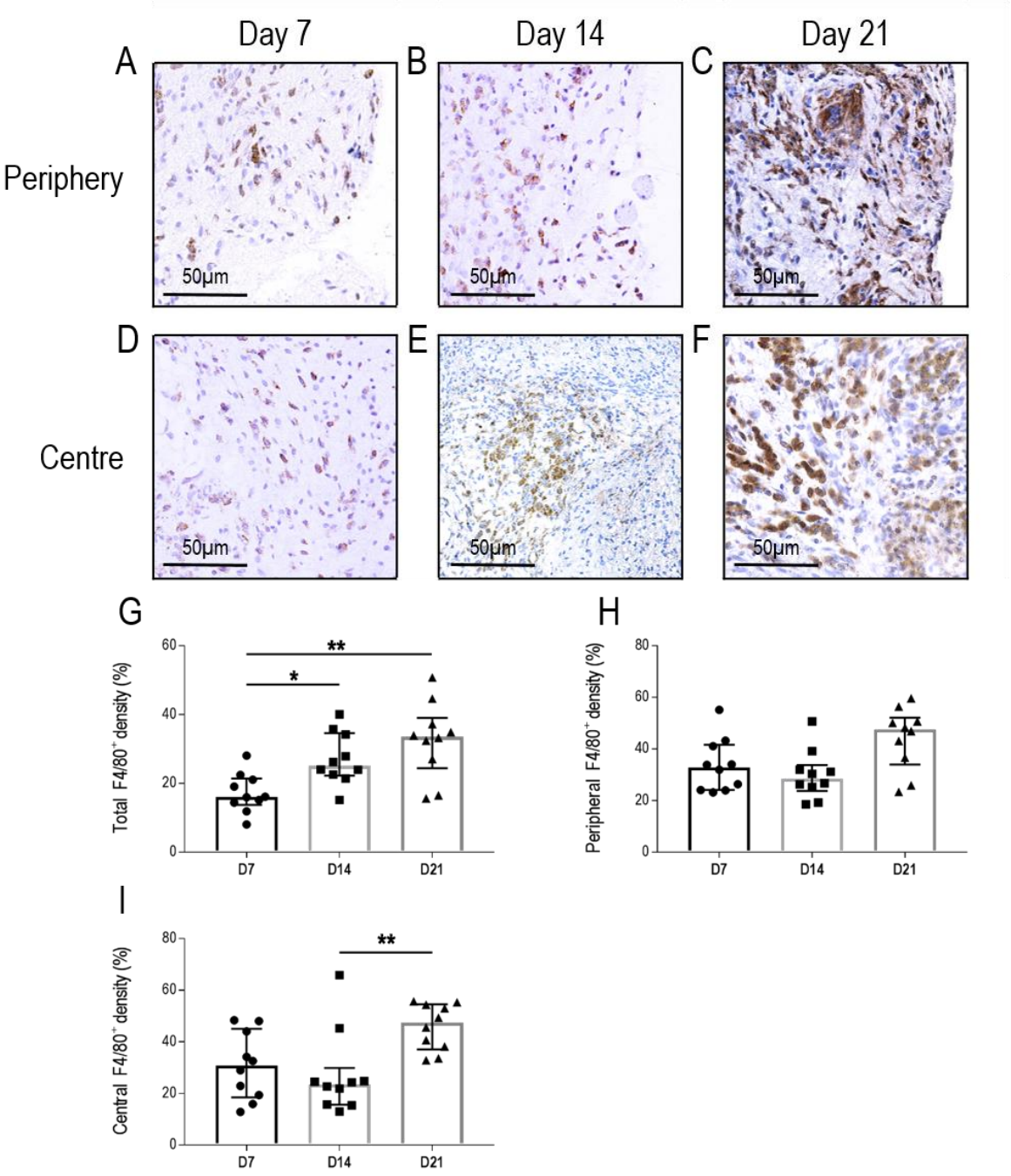

Figure 5.16 **F4/80 immunostaining in endometriosis-like lesions from C57 donor to *miR-223*$^{-/-}$ recipient mice**

Quantification of total F4/80 density was carried out in lesions from C57 donor to *miR-223*$^{-/-}$ recipient mice (**G**). F4/80 density at the lesion periphery (100µM from the edge of the lesion) at D7 (**A**), D14 (**B**) and D21 (**C**) was evaluated (**H**). F4/80 density at the lesion centre (within 500µM from the centre) at D7 (**D**), D14 (**E**), and D21 (**F**) was also quantified (**I**). Data are presented as median (IQR), with each symbol representative of a single lesion in one mouse (n=10 at D7, n=10 at D14, n=10 at D21). Analysis was done using the Kruskal-Wallis test followed by Dunn's multiple comparison test, with significance denoted as * ($p < 0.05$) and ** ($p < 0.01$).

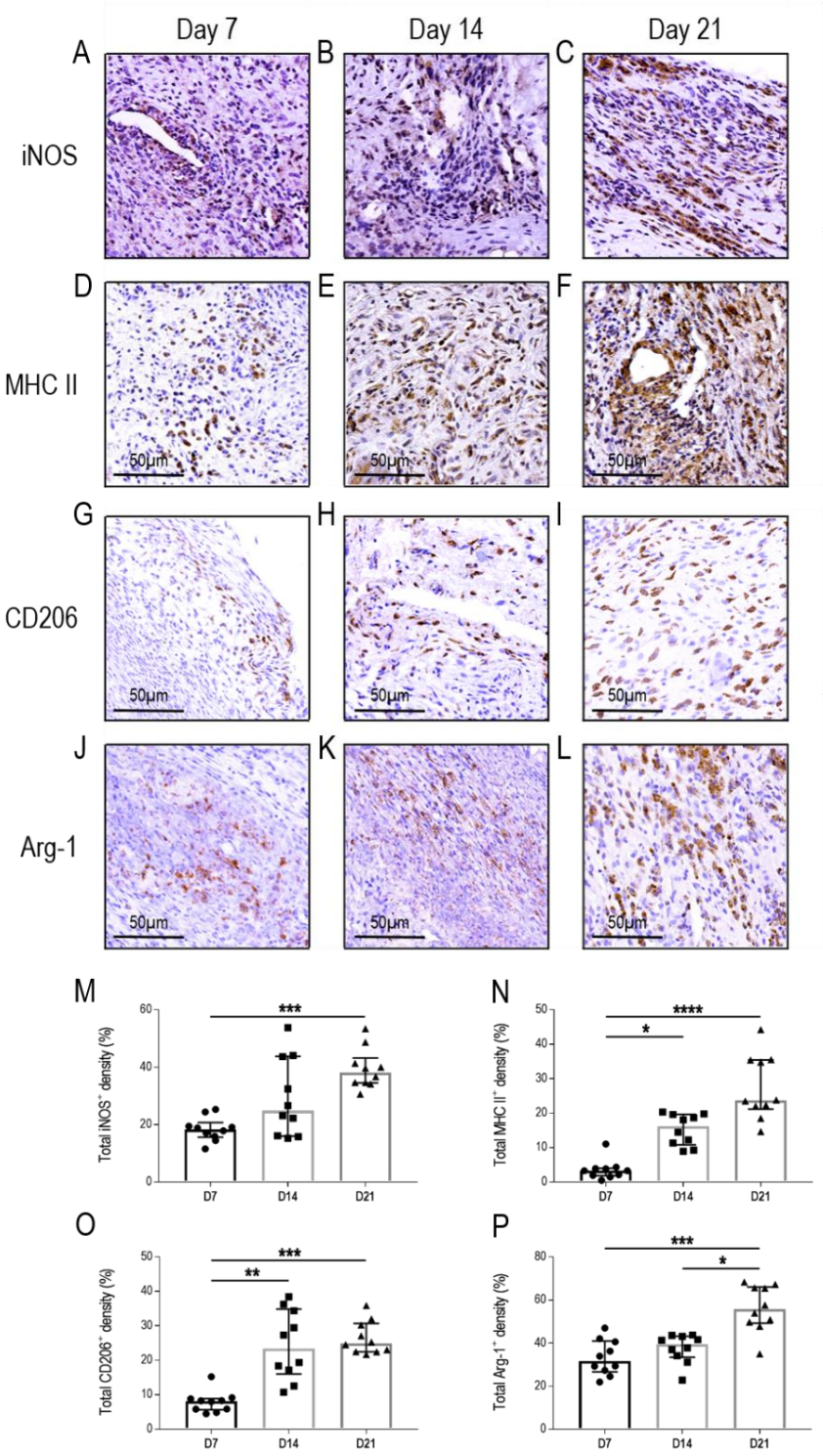

Figure 5.17 **M1-like (iNOS and MHCII) and M2–like (CD206 and Arg-1) immunostaining in endometriosis-like lesions from C57 donor to *miR-223*$^{-/-}$ recipient mice**

The expression of inducible nitric oxide synthase (iNOS) at D7 (**A**), D14 (**B**), and D21 (**C**) was quantified (**M**) in endometriosis-like lesions. Quantification of the Class II Major Histocompatibility Complex (MHC II) (**N**) was done at D7 (**D**), D14 (**E**) and D21 (**F**) in these lesions. CD206 density at D7 (**G**), D14 (**H**), and D21 (**I**) was quantified (**O**) in endometriosis-like lesions. Expression of Arginase-1 (Arg-1) (**P**) was evaluated at D7 (**J**), D14 (**K**) and D21 (**L**) in these lesions. Data are presented as median (IQR), with each symbol representative of a single lesion in one mouse (n=10 at D7, n=10 at D14, n=10 at D21). Analysis was done using the Kruskal-Wallis test followed by Dunn's multiple comparison test, with significance denoted as * ($p < 0.05$), ** ($p < 0.01$), *** ($p < 0.001$), and **** ($p < 0.0001$).

5.2.6.2. Endometriosis-like lesion development in *miR-223*$^{-/-}$ donor to C57 recipient transfers

A total of 35 *miR-223*$^{-/-}$ donor mice were used to generate sufficient decidualised endometrium for transfer into C57 recipient mice (*miR-223*$^{-/-}$ → C57) at a ratio of 2 donors to 1.9 recipients (Table 5.8). Over the course of this experiment, 74% of C57 recipient mice had lesions. At D7, 80% of C57 recipient mice had lesions, which reduced to 73% at D14, and further reduced to 67% by D21. One mouse had more than one lesion and has been excluded from subsequent analyses.

Following the *miR-223*$^{-/-}$ → C57 transfer, endometriosis-like lesions that developed at D7 were large, spread out over the attachment site, and blood-filled (Figure 5.18 A). At D14, lesions remained spread out over the attachment site, and maintained a blood-filled appearance (Figure 5.18 B), while by D21, lesions were small and white (Figure 5.18 C). Lesion size was consistent at D7 and D14 (85 (56 – 115) mm^3 and 48 (36 – 84) mm^3 respectively), however by D21, a significant reduction was noted (4 (2 – 6) mm^3; $p = 0.0002$ for D7 *vs* D21 and $p = 0.0143$ for D14 *vs* D21) (Figure 5.18 D). Correspondingly, lesion weight was similar at D7 and D14 (71.10 (60.53 – 102.70) mg and 59.80 (45.98 – 72.00) mg respectively), while a significant decrease was observed at D21 (6.00 (5.15 – 7.70) mg; $p = 0.0002$ for D7 *vs* D21 and $p = 0.0133$ for D14 *vs* D21) (Figure 5.18 E).

Morphological parameters in endometriosis-like lesions from a *miR-223*$^{-/-}$ → C57 transfer were assessed using H&E staining (Figure 5.19 A-C). The number of glands per lesion was not significantly different between D7, D14 and D21 (1 (0 – 2), 2 (0 – 6), and 2 (1 – 2) respectively) (Figure 5.19 D). Average gland size increased significantly between D7 and D14 (0.002 (0.000 – 0.003) mm^2 and 0.064 (0.006 – 0.274) mm^2 respectively; $p = 0.0063$), however no difference was observed at D21 (0.003 (0.002 – 0.003) mm^2) (Figure 5.19 E). Measurements of lumen area within glands followed a similar trend with a significant increase between D7 and D14 (0.0004 (0.0000 – 0.0007) mm^2 and 0.0064 (0.0033 – 1.1500) mm^2 respectively; $p = 0.0107$) with no differences observed at D21 (0.0006 (0.0003 – 0.0007) mm^2) (Figure 5.19 F). Likewise, the epithelium area within glands increased significantly between D7 and D14 (0.001 (0.000 – 0.004) mm^2 and 0.093 (0.005 – 0.424) mm^2 respectively, $p = 0.0134$), however was unaltered at D21 (0.003 (0.002 – 0.004) mm^2) (Figure 5.19 G). Percentage glandular epithelium also increased significantly between D7 and D14 (0.02 (0.00 – 0.04) % and 0.74 (0.35 – 12.44) % respectively; $p = 0.0010$), whereas values at D21 were not significantly different from either D7 or D14 (0.16 (0.09 – 0.20) %) (Figure 5.19 H). Corresponding measurements of percentage stromal area was highest at D7 (99.97 (99.55 – 100.00) %), and decreased significantly at D14 (98.64 (87.56 – 99.61) %, $p = 0.0188$), but was unaltered at D21 (99.86 (99.81 – 99.94) %) (Figure 5.19 I).

To determine macrophage density in *miR-223*$^{-/-}$ →C57 lesions, quantification of F4/80 immunostaining was performed (Figure 5.20). Total F4/80^{+} density increased significantly from D7 to D14, with sustained expression at D21 (7.61 (5.03 – 8.84) %, 21.17 (12.01 – 29.19) %, and 18.59 (13.22 – 21.94) % respectively; p = 0.0030 for D7 *vs* D14 and p = 0.0089 for D7 *vs* D21) (Figure 5.20 G). Peripheral expression of F4/80 was consistent at all time points (Figure 5.20 A-C, H). In contrast, central F4/80 expression (Figure 5.20 D-F) was lowest at D7 (7.27 (4.06 – 12.40) %) and significantly increased over time (29.70 (20.44 – 41.77) % at D14 and 32.19 (22.66 – 47.56) % at D21; p = 0.0044 for D7 *vs* D14 and p = 0.0009 for D7 *vs* D21) (Figure 5.20 I).

Expression of the M1-like marker iNOS was unchanged across the time course (Figure 5.21 A-C, M). In contrast, density of the M1-like marker MHC II remained low at D7 and D14 (7.79 (5.87 – 10.32) % and 9.45 (6.07 – 12.32) % respectively), a significant increase was observed at D21 (35.84 (27.45 – 39.78) %; p = 0.0008 for D7 *vs* D21 and p = 0.0071 for D14 *vs* D21) (Figure 5.21 D-F, N). A steady increase in the density of the M2-like marker CD206 was observed over the course of the experiment (7.62 (6.10 – 9.30) % at D7, 11.83 (8.70 – 18.10) % at D14, and 21.33 (13.29 – 24.97) % at D21; p = 0.0005 for D7 *vs* D21) (Figure 5.21 D-F, N). Alternatively, the expression of Arg-1 was consistent across all time points (Figure 5.21 J-L, P).

Table 5.8 Endometriosis-like lesion recovery in *miR-223*$^{-/-}$ → C57 mice

Lesion collection time point	D7	D14	D21
Total number of *miR-223*$^{-/-}$ donor mice used across all time points: 32			
Number of C57 recipient mice	10	12	12
Number of mice with lesions*	8	9	8
Proportion of mice with lesions (%)	80	75	67

* To reduce bias, mice with ≥2 lesions were excluded from subsequent analyses. At D14 - 1 mouse excluded.

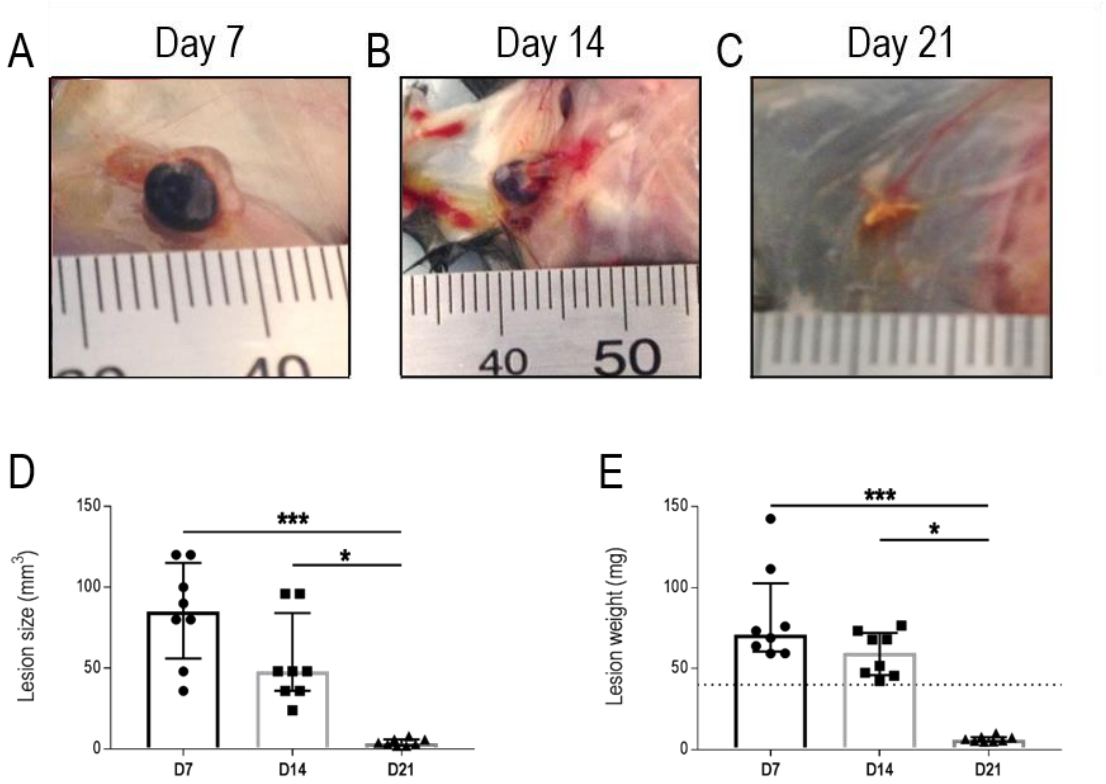

Figure 5.18 Gross morphology of endometriosis-like lesion development in a transfer from *miR-223*$^{-/-}$ donor to C57 recipient mice

Decidualised *miR-223*$^{-/-}$ donor endometrial tissue was injected subcutaneously into C57 recipient mice. Resulting lesions were harvested at either D7 (**A**), D14 (**B**) or D21 (**C**), with representative images shown. Lesion size was measured (**D**) and lesions were excised and weighed (**E**), with the dotted line indicating the initial weight of donor decidualised endometrial tissue inoculated into recipient mice. Data are presented as median (IQR), with each symbol representative of a single lesion in one mouse (n=8 at D7, n=8 at D14, n=8 at D21). Analysis was done using the Kruskal-Wallis test followed by Dunn's multiple comparison test, with significance denoted as * ($p < 0.05$) and *** ($p < 0.001$).

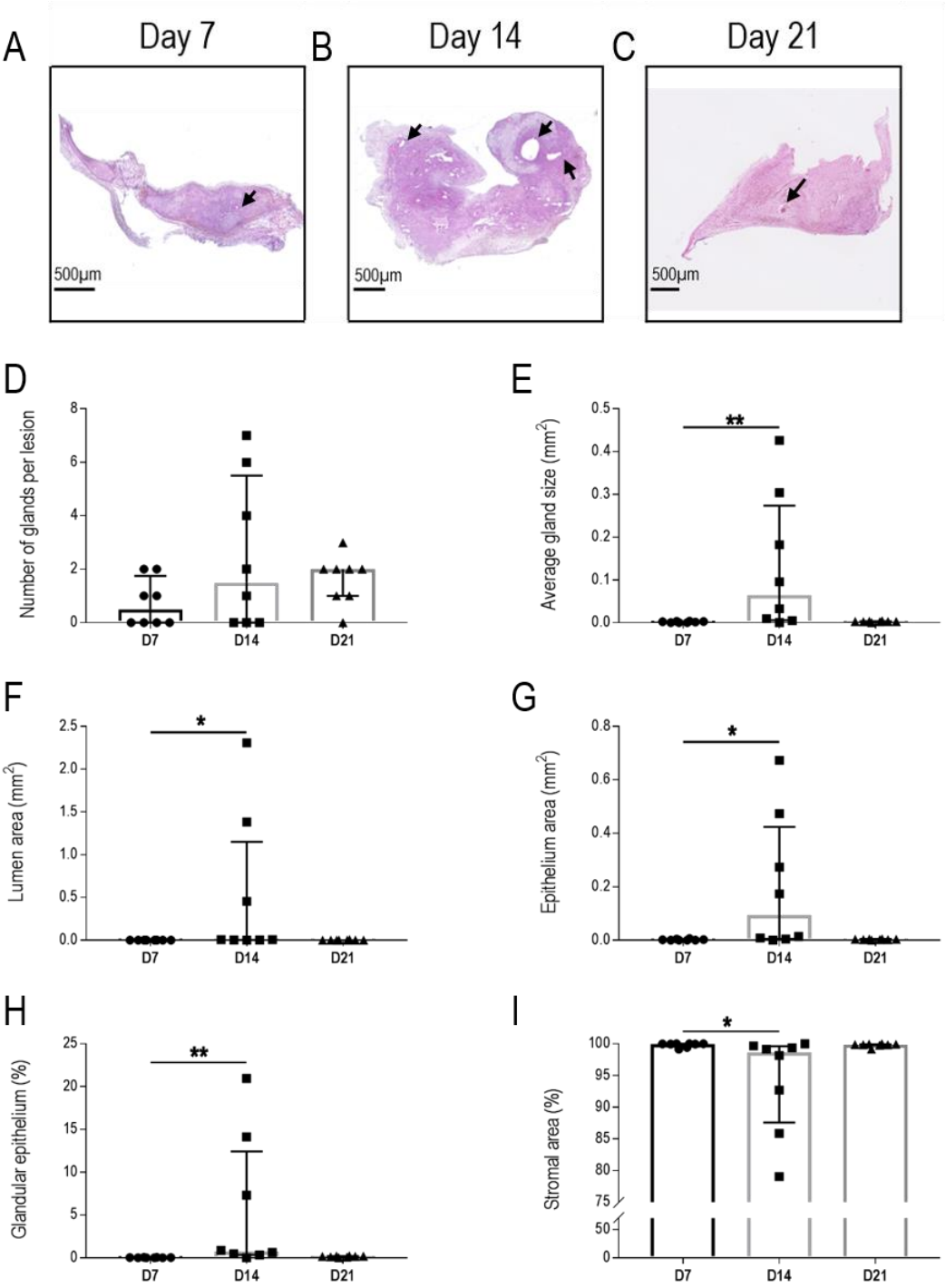

Figure 5.19 Assessment of morphological parameters in haematoxylin and eosin stained endometriosis-like lesions from *miR-223*$^{-/-}$ donor to C57 recipient mice

Haematoxylin and eosin stained sections from D7 **(A)**, D14 **(B)**, and D21 **(C)** lesions (representative images shown; arrows indicate glands) were assessed for the following characteristics: number of glands per lesion **(D)**, average gland size **(E)**, lumen area **(F)**, epithelium area **(G)**, percentage glandular epithelium **(H)** and percentage stromal area **(I)**. Data are presented as median (IQR), with each symbol representative of a single lesion in one mouse (n=8 at D7, n=8 at D14, n=8 at D21). Analysis was done using the Kruskal-Wallis test followed by Dunn's multiple comparison test, with significance denoted as * ($p < 0.05$) and ** ($p < 0.01$).

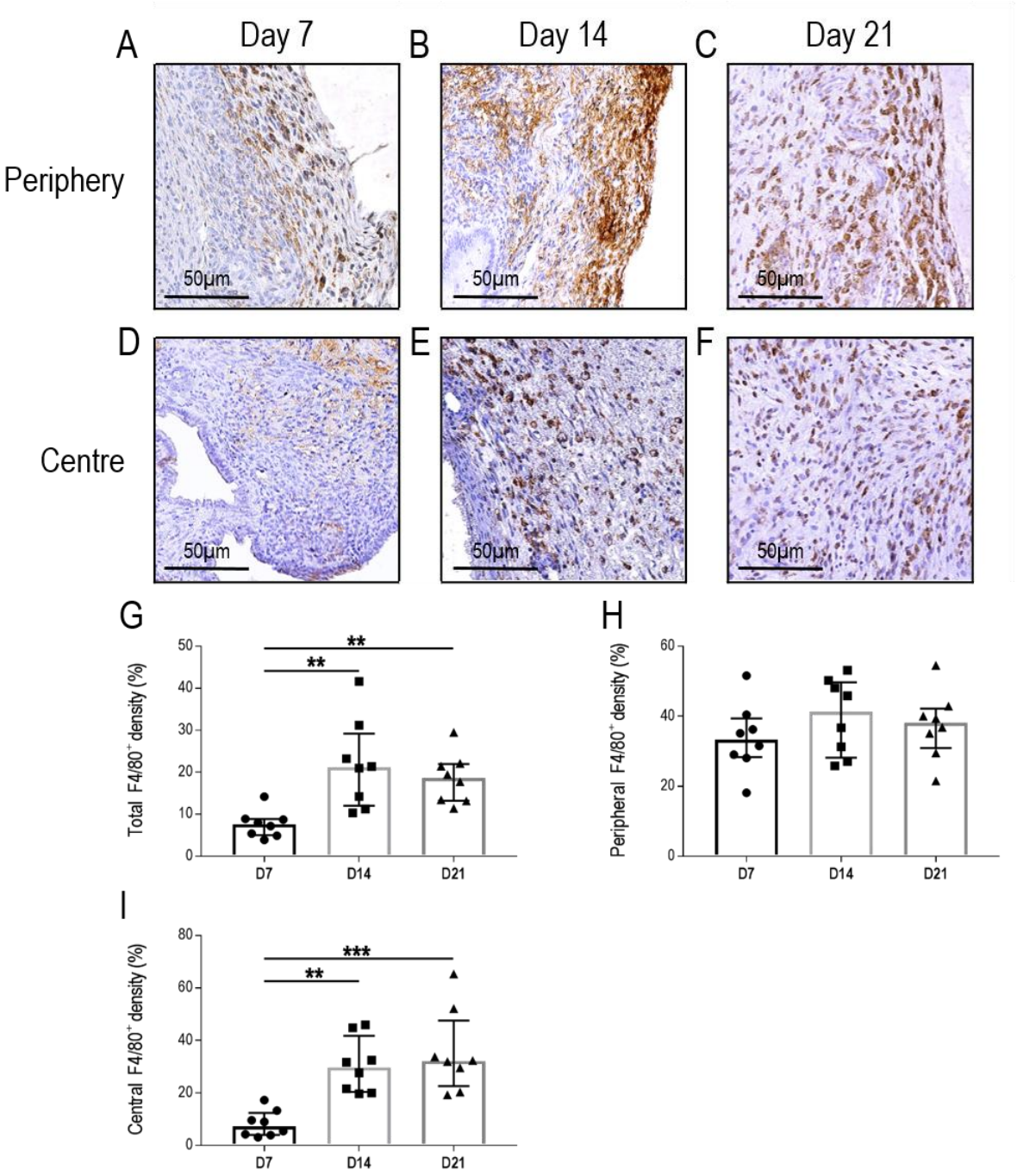

Figure 5.20 **F4/80 immunostaining in endometriosis-like lesions from *miR-223*$^{-/-}$ donor to C57 recipient mice**

Quantification of total F4/80 density was carried out in lesions from *miR-155*$^{-/-}$ donor to C57 recipient mice (**G**). F4/80 density at the lesion periphery (100µM from the edge of the lesion) at D7 (**A**), D14 (**B**) and D21 (**C**) was evaluated (**H**). F4/80 density at the lesion centre (within 500µM from the centre) at D7 (**D**), D14 (**E**), and D21 (**F**) was also quantified (**I**). Data are presented as median (IQR), with each symbol representative of a single lesion in one mouse (n=8 at D7, n=8 at D14, n=8 at D21). Analysis was done using the Kruskal-Wallis test followed by Dunn's multiple comparison test, with significance denoted as ** ($p < 0.01$) and *** ($p < 0.001$).

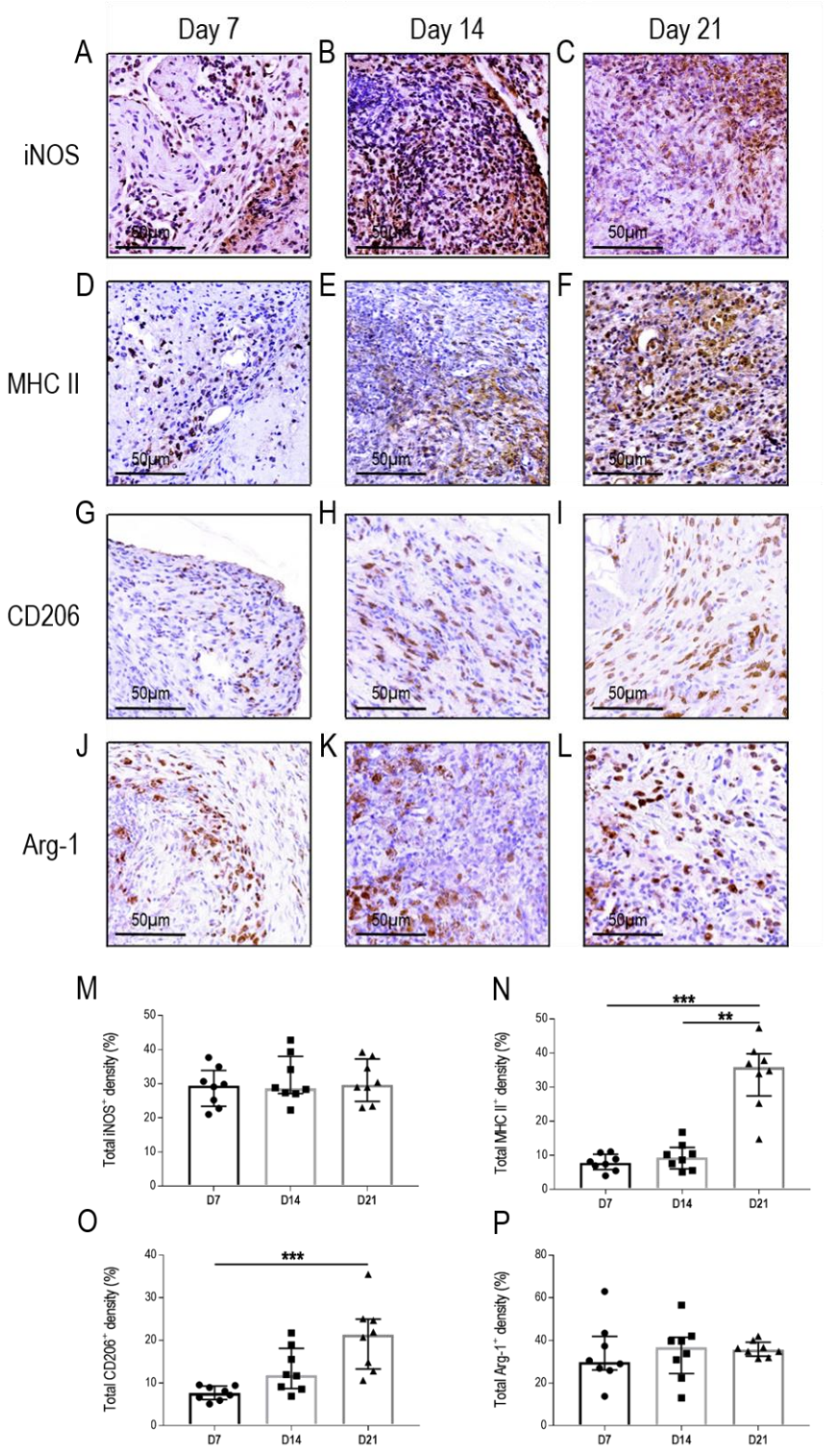

Figure 5.21 **M1-like (iNOS and MHCII) and M2–like (CD206 and Arg-1) immunostaining in endometriosis-like lesions from *miR-223*$^{-/-}$ donor to C57 recipient mice**

The expression of inducible nitric oxide synthase (iNOS) at D7 (**A**), D14 (**B**), and D21 (**C**) was quantified (**M**) in endometriosis-like lesions. Quantification of the Class II Major Histocompatibility Complex (MHC II) (**N**) was done at D7 (**D**), D14 (**E**) and D21 (**F**) in these lesions. CD206 density at D7 (**G**), D14 (**H**), and D21 (**I**) was quantified (**O**) in endometriosis-like lesions. Expression of Arginase-1 (Arg-1) (**P**) was evaluated at D7 (**J**), D14 (**K**) and D21 (**L**) in these lesions. Data are presented as median (IQR), with each symbol representative of a single lesion in one mouse (n=8 at D7, n=8 at D14, n=8 at D21). Analysis was done using the Kruskal-Wallis test followed by Dunn's multiple comparison test, with significance denoted as ** ($p < 0.01$), and *** ($p < 0.001$).

5.2.6.3. Comparison of lesion development in *miR-223*$^{-/-}$ ↔ C57 reciprocal transfer mice with syngeneic C57 and syngeneic *miR-223*$^{-/-}$ mice

To assess the impact of a *miR-223* deficiency present either in the recipient environment (C57 → *miR-223*$^{-/-}$ transfer) or in the donor endometrial tissue (*miR-223*$^{-/-}$ → C57 transfer), comparisons of morphometric and immunohistochemical results in these reciprocal transfer models were made against corresponding results from the syngeneic C57 (C57 → C57 transfer) and the syngeneic *miR-223*$^{-/-}$ (*miR-223*$^{-/-}$ → *miR-223*$^{-/-}$ transfer) models.

5.2.6.3.1. C57 → *miR-223*$^{-/-}$ lesion development *vs* C57 → C57 lesion development

At D7, lesion size in C57 → *miR-223*$^{-/-}$ mice was 5-fold larger at D7 ($p < 0.0001$) compared to lesions from C57 → C57 mice (Figure 5.22 A), with a corresponding 2.9-fold increase in lesion weight ($p < 0.0001$) (Figure 5.22 B). C57 → *miR-223*$^{-/-}$ lesions remained 2-fold heavier at D21 ($p = 0.0008$) compared to C57 → C57 lesions. As no glands were present in C57 → *miR-223*$^{-/-}$ lesions at both D14 and D21, this was significantly lower than values from C57→ C57 lesions ($p = 0.0013$ and $p < 0.0001$ respectively) (Figure 5.22 C). Due to this absence of glands, average gland size was significantly lower in C57 → *miR-223*$^{-/-}$ lesions at D21 ($p = 0.0012$) (Figure 5.22 D). Lumen area was significantly lower at D14 ($p = 0.0034$) and D21 ($p = 0.0001$), as were measurements of epithelium area ($p = 0.0056$ at D14 and $p < 0.0001$ at D21) and percentage glandular epithelium ($p = 0.0044$ at D14 and $p < 0.0001$ at D21) (Figure 5.22 E-G). Corresponding measurements of stromal area showed a 1.02-fold increase at D14 ($p = 0.0089$) and a 1.03-fold increase at D21 ($p < 0.0001$) in C57 → *miR-223*$^{-/-}$ lesions compared to C57 → C57 lesions (Figure 5.22 H).

At D21, C57 → *miR-223*$^{-/-}$ lesions had 1.9-fold more total F4/80 density ($p = 0.0117$), with a 2.1 fold increase in peripheral F4/80 density ($p = 0.0031$) compared to C57 → C57 lesions (Figure 5.23 A, B). Central F4/80 density was 7.7-fold higher in C57 → *miR-223*$^{-/-}$ lesions compared to C57 → C57 lesions at D7 ($p <0.0001$), and 1.5-fold higher at D21 ($p = 0.0003$) (Figure 5.23 C). At D21, iNOS density was 2.2-fold higher in C57 → *miR-223*$^{-/-}$ lesions ($p < 0.0001$) compared to C57 → C57 lesions (Figure 5.23 D). MHC II density was reduced by 83% in C57 → *miR-223*$^{-/-}$ lesions compared to C57 → C57 lesions at D7 ($p < 0.0001$), however expression levels were similar at D14 and D21 (Figure 5.23 E). CD206 expression was 37% lower in C57 → *miR-223*$^{-/-}$ lesions compared to C57 → C57 lesions at D21 ($p < 0.0001$) (Figure 5.23 F). Arg-1 expression was consistently elevated in C57 → *miR-223*$^{-/-}$ lesions compared to C57 → C57 lesions across all time points (1.5-fold increase at D7, $p = 0.0033$; 1.8-fold increase at D14, $p < 0.0001$; 2.3-fold increase at D21, $p < 0.0001$).

5.2.6.3.2. C57 → *miR-223*$^{-/-}$ lesion development *vs* *miR-223*$^{-/-}$ → *miR-223*$^{-/-}$ lesion development

Lesion development in C57 → *miR-223*$^{-/-}$ and *miR-223*$^{-/-}$ → *miR-223*$^{-/-}$ were comparable across all morphometric parameters, except for lesion size, wherein C57 → *miR-223*$^{-/-}$ lesions were 50% smaller at D14 (p = 0.0023) and 41% smaller at D21 (p = 0.0341) compared to *miR-223*$^{-/-}$ → *miR-223*$^{-/-}$ lesions (Figure 5.22). Likewise, total, peripheral and central F4/80 density was consistent at between strains across time points (Figure 5.23 A-C). C57 → *miR-223*$^{-/-}$ lesions had 40% less iNOS expression at D7 (p < 0.0001) however by D21, lesions expressed 1.9-fold more iNOS (p < 0.0001) (Figure 5.23 D). MHC II expression in C57 → *miR-223*$^{-/-}$ lesions was reduced at both D7 and D14 (85% reduction, p < 0.0001; 40% reduction, p < 0.0001 respectively) (Figure 5.23 E). Although expression of CD206 was consistent between groups, Arg-1 expression was consistently elevated in C57 → *miR-223*$^{-/-}$ lesions compared to *miR-223*$^{-/-}$ → *miR-223*$^{-/-}$ lesions at D7 (1.4-fold increase, p = 0.0032), D14 (1.3-fold increase, p = 0.0025) and D21 (1.3-fold increase, p = 0.0041) (Figure 5.23 F,G).

5.2.6.3.3. *miR-223*$^{-/-}$ → C57 lesion development *vs* C57 → C57 lesion development

Lesions in *miR-223*$^{-/-}$ → C57 mice were 5.7 fold larger at D7 (p < 0.0001) and 19.2-fold larger at D14 (p < 0.0001), while lesion weight was significantly heavier across all time points (4.6-fold increase at D7, p < 0.0001; 12-fold increase at D14, p < 0.0001; 2.2-fold increase at D21, p = 0.0005) compared to lesions from C57 → C57 mice (Figure 5.22 A, B). At D21, when compared with C57 → C57 lesions, *miR-223*$^{-/-}$ → C57 lesions had 69% less number of glands (p = 0.0002), 97% less lumen area (p = 0.0006), 86% less epithelium area (p = 0.0003), 95% less glandular epithelium (p = 0.0002) and 1.03-fold more stromal area (p = 0.0006) (Figure 5.22 C, E-H). No differences were observed in average gland size (Figure 5.22 D).

Total, peripheral and central F4/80 density was comparable between groups across all time points (Figure 5.23 A-C). iNOS density was 1.4-fold higher at D14 (p = 0.0073) and 1.7-fold higher at D21 (p = 0.0006) in *miR-223*$^{-/-}$ → C57 lesions compared to C57 → C57 lesions (Figure 5.23 D). At D7, the expression of MHC II in *miR-223*$^{-/-}$ → C57 lesions was reduced by 60% (p = 0.0096) (Figure 5.23 E). CD206 density was 46% lower in *miR-223*$^{-/-}$ → C57 lesions compared to C57 → C57 lesions at D21 (p = 0.0002) (Figure 5.23 F). Arg-1 expression was consistently elevated in *miR-223*$^{-/-}$ → C57 lesions compared to C57 → C57 lesions (1.4-fold increase at D7, p = 0.0030; 1.7-fold increase at D14, p = 0.0124; 1.5-fold increase at D21, p = 0.0104) (Figure 5.23 G).

5.2.6.3.4. *miR-223*$^{-/-}$ → C57 lesion development *vs miR-223*$^{-/-}$ → *miR-223*$^{-/-}$ lesion development

Lesions in *miR-223*$^{-/-}$ → C57 mice were 4-fold larger ($p < 0.0001$) at D14, while at D21, lesions were 59% smaller compared to the syngeneic *miR-223*$^{-/-}$ transfer ($p = 0.0106$) (Figure 5.22 A). Lesions from *miR-223*$^{-/-}$ → C57 mice were 2.2-fold heavier at D7 ($p = 0.0039$) and 6.2-fold heavier at D14 ($p < 0.0001$) (Figure 5.22 B). Due to the lack of glands in *miR-223*$^{-/-}$ → *miR-223*$^{-/-}$ lesions, there were significantly more glands in *miR-223*$^{-/-}$ → C57 lesions at D21 ($p = 0.0004$). Average gland size was significantly higher in *miR-223*$^{-/-}$ → C57 lesions at D14 ($p = 0.0010$) and D21 ($p = 0.0004$) compared to lesions from *miR-223*$^{-/-}$ → *miR-223*$^{-/-}$ mice (Figure 5.22 D). Likewise, lumen area was significantly higher in *miR-223*$^{-/-}$ → C57 lesions at D14 ($p = 0.0011$) and D21 ($p = 0.0004$) compared to *miR-223*$^{-/-}$ → *miR-223*$^{-/-}$ lesions (Figure 5.22 E). Epithelium area followed a similar trend, with significantly higher measurements in *miR-223*$^{-/-}$ → C57 lesions at D14 ($p = 0.0006$) and D21 ($p = 0.0004$) compared to *miR-223*$^{-/-}$ → *miR-223*$^{-/-}$ lesions (Figure 5.22 F). Percentage glandular area was significantly higher in *miR-223*$^{-/-}$ → C57 lesions at D14 ($p = 0.0013$) and D21 ($p = 0.0004$) compared to *miR-223*$^{-/-}$ → *miR-223*$^{-/-}$ lesions (Figure 5.22 G). Percentage stromal area in *miR-223*$^{-/-}$ → C57 lesions was 1.3% lower at D14 ($p = 0.0021$) and 0.15% lower at D21 ($p = 0.0004$) compared to *miR-223*$^{-/-}$ → *miR-223*$^{-/-}$ lesions (Figure 5.22 H).

Total F4/80 density was 61% lower ($p < 0.0001$) in *miR-223*$^{-/-}$ → C57 lesions at D7, with a corresponding 75% decrease in central F4/80 density at D7 ($p < 0.0001$) compared to *miR-223*$^{-/-}$ → *miR-223*$^{-/-}$ lesions (Figure 5.23 A,C). At D21, an 18% decrease of peripheral F4/80 density was observed ($p = 0.0079$) in *miR-223*$^{-/-}$ → C57 lesions compared to *miR-223*$^{-/-}$ → *miR-223*$^{-/-}$ lesions (Figure 5.2B). *miR-223*$^{-/-}$ → C57 lesions had 1.4-fold more iNOS expression at D21 ($p = 0.0037$), while MHC II density was reduced by 63% at D7 ($p < 0.0001$) and 65% at D14 ($p < 0.0001$) compared to *miR-223*$^{-/-}$ → *miR-223*$^{-/-}$ lesions (Figure 5.23 D,E). No differences were observed in CD206 or Arg-1 density between strains across all time points (Figure 5.23 F, G).

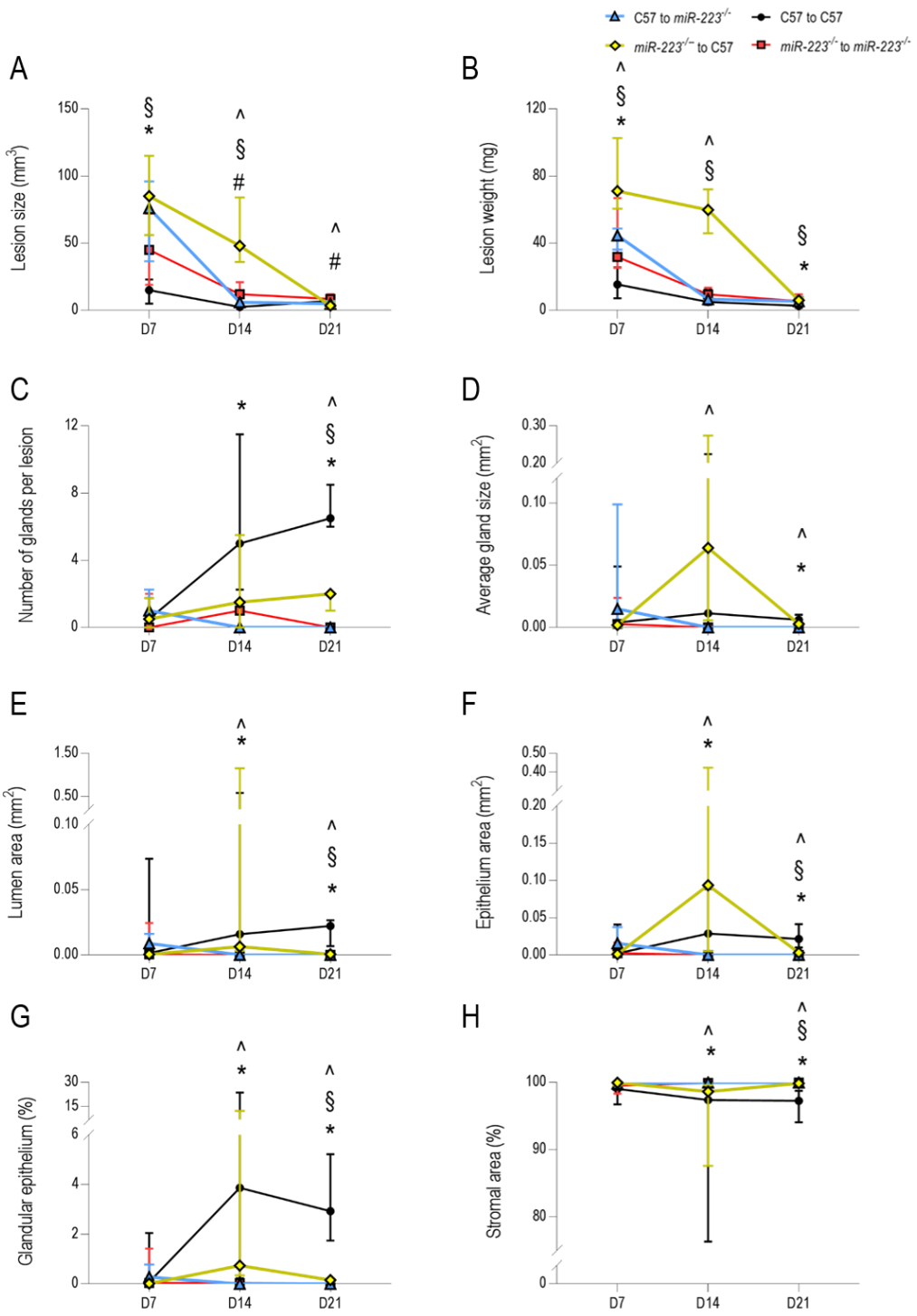

Figure 5.22 **Comparative analysis of morphometric parameters between syngeneic C57 and *miR-223*$^{-/-}$ models with reciprocal *miR-223*$^{-/-}$ cross transfer models**

Comparisons of lesion size (**A**), weight (**B**), number of glands per lesion (**C**), average gland size (**D**), lumen area (**E**), epithelium area (**F**), glandular epithelium (**G**), and stromal area (**H**) between C57 → C57 mice (; n=12 at D7, n=12 at D14, n=8 at D21) and *miR-223*$^{-/-}$ → *miR-223*$^{-/-}$ mice (; n=17 at D7, n=13 at D14, n=9 at D21) against either C57 → *miR-223*$^{-/-}$ mice (; n=10 at D7, n=10 at D14, n=10 at D21) or *miR-223*$^{-/-}$ → C57 mice (; n=8 at D7, n=8 at D14, n=8 at D21) was performed. Data are presented as median (IQR). Analysis was done using the Kruskal-Wallis test followed by Bonferroni-Dunn's multiple comparison test, with significance inferred at $p < 0.0125$. ***** indicates significance between C57 → C57 and C57 → *miR-223*$^{-/-}$; **#** indicates significance between *miR-223*$^{-/-}$ → *miR-223*$^{-/-}$ and C57 → *miR-223*$^{-/-}$; **§** indicates significance between C57 → C57 and *miR-223*$^{-/-}$ → C57; **^** indicates significance between *miR-223*$^{-/-}$ → *miR-223*$^{-/-}$ and *miR-223*$^{-/-}$ →C57.

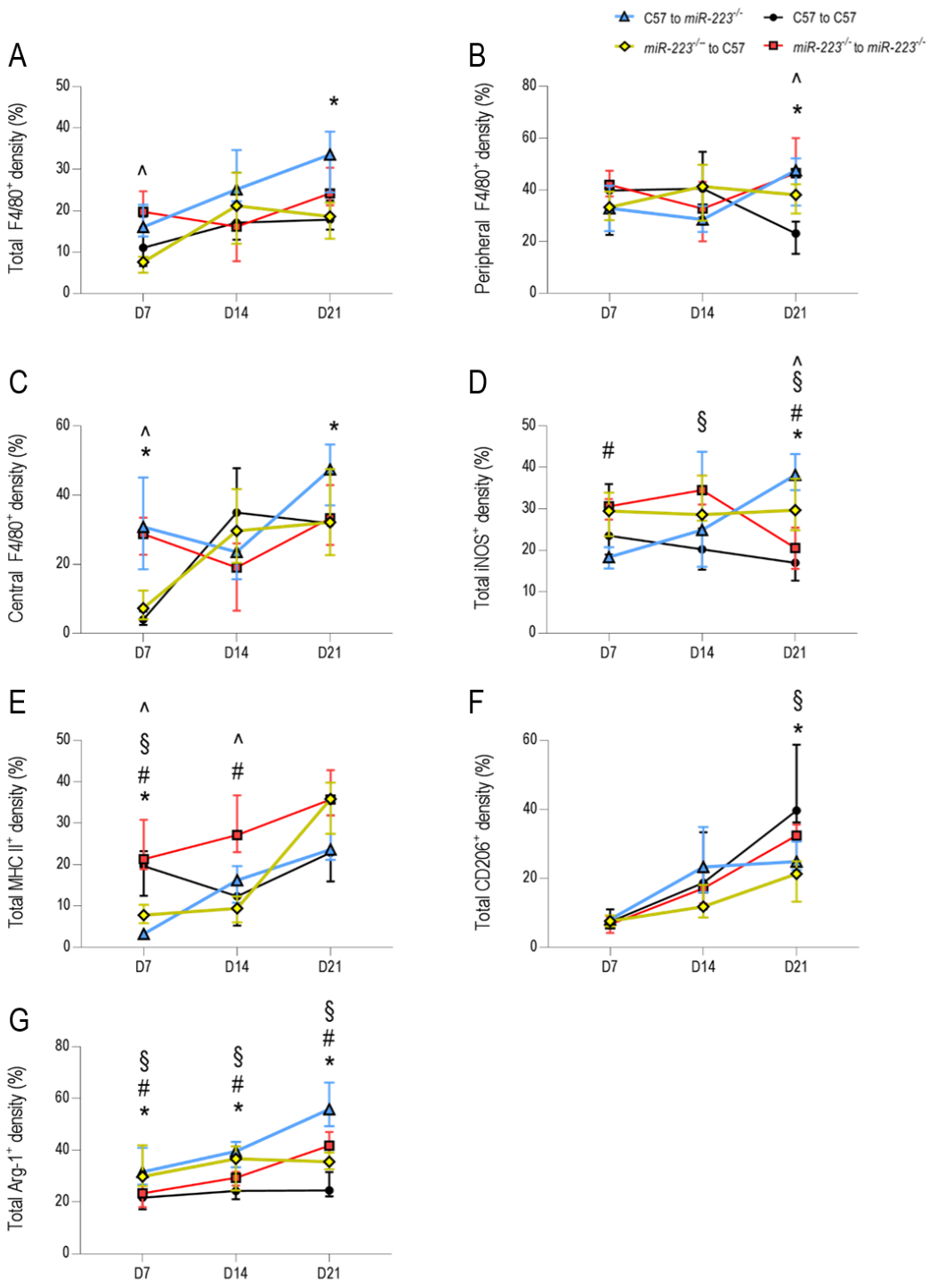

Figure 5.23 **Comparative analysis of macrophage markers between syngeneic C57 and *miR-223*$^{-/-}$ models with reciprocal *miR-223*$^{-/-}$ cross transfer models**

Total (**A**), peripheral (**B**), and central (**C**) F4/80 density were compared between C57 → C57 mice (; n=12 at D7, n=12 at D14, n=8 at D21) and *miR-223*$^{-/-}$ → *miR-223*$^{-/-}$ mice (; n=17 at D7, n=13 at D14, n=9 at D21) against either C57 → *miR-223*$^{-/-}$ mice (; n=10 at D7, n=10 at D14, n=10 at D21) or *miR-223*$^{-/-}$ → C57 mice (; n=8 at D7, n=8 at D14, n=8 at D21). Comparisons between the M1-like macrophage markers iNOS (**D**) and MHC II (**E**), and the M2-like macrophage markers CD206 (**F**) and Arg-1 (**G**) were also performed. Data are presented as median (IQR). Analysis was done using the Kruskal-Wallis test followed by Bonferroni-Dunn's multiple comparison test, with significance inferred at $p < 0.0125$. * indicates significance between C57 → C57 and C57 → *miR-223*$^{-/-}$; # indicates significance between *miR-223*$^{-/-}$ → *miR-223*$^{-/-}$ and C57 → *miR-223*$^{-/-}$; § indicates significance between C57 → C57 and *miR-223*$^{-/-}$ → C57; ^ indicates significance between *miR-223*$^{-/-}$ → *miR-223*$^{-/-}$ and *miR-223*$^{-/-}$ →C57.

5.3. DISCUSSION

This study was performed to evaluate the development of endometriotic-like lesions over time in the absence of *miR-223*. *miR-223* has roles in the regulation of haematopoietic differentiation (Johnnidis et al., 2008), osteoclastogenesis (Chen et al., 2004), human embryonic stem cell differentiation (Yu et al., 2013), and hepatocyte apoptosis and chromosomal stability (Ye et al., 2018). Moreover, the expression of *miR-223* influences immune cell activation and function, especially macrophage polarisation, NF-κB signalling and inflammasome activity (Zhuang et al., 2012, Haneklaus et al., 2013). *miR-223* targets *Pknox1*, an essential regulator of macrophage polarisation, effectively "re-programming" M1-like macrophages towards an M2-like activation profile (Zhuang et al., 2012). In addition, by regulating IKK-α expression, *miR-223* modulates the NF-κB signalling pathway, thus inhibiting macrophage hyperactivation and preventing IL-1β production from the inflammasome (Li et al., 2010). The downregulation of *miR-223* results in the activation of its target, STAT3, thus promoting production of M1-like cytokines IL-6 and IL-1β (Chen et al., 2012). In women with endometriosis, an increase in the expression of *miR-223* was observed in ectopic endometrial tissue when compared against paired samples of eutopic endometrium (Ohlsson Teague et al., 2009), and may contribute towards disease persistence.

5.3.1. A deficiency in *miRNA-223* restricts endometriosis-like lesion development

By depleting *miR-223* systemically, the development of endometriosis-like lesions was impeded in mice, with a significant reduction in lesion size and weight over time. The physical appearance of lesions correlated with H&E morphological observations, in which the large, red lesions at D7 were dense and had glandular areas. At D14, large fluid filled lesions were observed, which could account for the significant loss in lesion weight that was observed, as lesions primarily consisted of large cystic spaces. The small, white opaque lesions seen at D21 were dense with stromal cells and had no visible glands, suggesting the lesions consisted primarily of non-actively proliferating cells or fibrotic tissue. Interestingly, while the subcutaneous lesions in C57 mice appeared to become more established throughout the duration of the experiment, lesions from *miR-223*$^{-/-}$ mice showed signs of regression, evidenced by the gradual loss of glandular areas over time. Collectively, this suggests that inhibition of ectopic endometrial tissue survival occurs within 21 days in the absence of *miR-223*. Furthermore, lesion recovery from *miR-223*$^{-/-}$ mice was progressively worse over time, supporting the hypothesis that a *miR-223* deficiency inhibits the development of endometriosis.

A consistent decrease in the expression of *Nnt* was observed across all samples in *miR-223*$^{-/-}$ mice compared to samples from C57 mice. Nnt is localised to the inner mitochondrial membrane, and functions to maintain mitochondrial membrane potential via proton pumping and as a catalyst to generate nicotinamide adenine dinucleotide (NADH) from nicotinamide adenine dinucleotide phosphate ($NADP^+$) (Hoek and Rydström, 1988, Albracht et al., 2011, Jackson et al., 2015). Cells deficient in *NNT* have a limited capacity to maintain NAD^+ and NADPH levels, resulting in aberrant mitochondrial physiology and increased oxidative phosphorylation (Ho et al., 2017). As a consequence, a decrease in *HIF-1α* and *HDAC1* expression is observed, culminating in a reduction of cellular proliferation and tumourigenicity (Ho et al., 2017). To date, no study has looked at the effect of inhibiting *Nnt* on the development of endometriotic lesions, or the effect of *miR-223* on the expression of *Nnt*. From this chapter, the findings suggest that the absence of *miR-223* results in decreased levels of *Nnt*, which may contribute to the perceived inhibition of endometriotic lesion proliferation, and warrants further investigation.

5.3.2. Elevated M1-like activity in *miR-223*$^{-/-}$ mice may impede endometriotic lesion growth

In this study, lesions deficient in *miR-223* had a significantly higher central density of $F4/80^+$ macrophages compared to C57 lesions at D7. In addition, at D21, total F4/80 density, as well as peripheral F4/80 density, was significantly higher in *miR-223*$^{-/-}$ lesions compared to C57 lesions. Furthermore, as predicted, the expression of the M1-like markers iNOS and MHC II was higher in *miR-223*$^{-/-}$ lesions compared to C57 lesions at all time points. The elevation in pro-inflammatory, M1-like macrophage markers fits well with the current understanding of *miR-223* function. In *miR-223*$^{-/-}$ mice, increased levels of granulocyte progenitors in bone marrow, as well as a hypersensitive and hypermature circulating neutrophil population further contributes to an elevated M1-like immune environment, with enhanced tissue destruction following LPS challenge (Johnnidis et al., 2008). This finding suggests that a predominance of M1-like macrophage infiltration during the initial stages of endometriotic lesion development, coupled with the elevation of additional pro-inflammatory immune cells, could account for the cystic, pus-filled appearance of *miR-223*$^{-/-}$ lesions. Moreover, the overt lack of glandular remodelling observed in *miR-223*$^{-/-}$ lesions supports the observation of sustained ectopic tissue clearance mediated by M1-like immune activity.

While the total and central expression of the M2-like marker CD206 remained significantly lower in *miR-223*$^{-/-}$ lesions compared to C57 lesions at D21, the opposite was seen in Arg-1 expression. From the RNA-Seq data, *Arg-1* decreased in both D7 lesions ($log_2FC = -8.104$; FDR = 0.0005) and D14 lesions ($log_2FC = -5.796$; FDR = 0.0087) compared to decidualised endometrium (Supplementary material Table 8 and 9). However, in concordance with the immunohistochemical staining, there was an increase in *Arg-1* between D7 and D14 ($log_2FC = -8.104$; FDR = 0.0005) (Supplementary material Table 10). As mentioned

previously, Arg-1 and iNOS compete for the same substrate, L-arginine (McLarren et al., 2011), and in these *miR-223*$^{-/-}$ lesions, the observed increase in Arg-1 density was coupled with a significant decrease in iNOS density. Studies have shown that immunosuppression mediated by myeloid-derived suppressor cells require depletion of L-arginine via Arg-1, and the production of NO by iNOS (Peranzoni et al., 2010, Parekh et al., 2013). In addition, the expansion of myeloid-derived suppressor cells in cancer is driven by the expression of STAT3, a known target of *miR-223* which also functions in the regulation of Arg-1 activity (Gabrilovich et al., 2012, Vasquez-Dunddel et al., 2013).

In a *miR-223*$^{-/-}$ mouse model of experimental autoimmune encephalomyelitis, monocytic myeloid-derived suppressor cells demonstrated an increase in the expression of *Arg-1* and *Stat3*, with a simultaneous increase in suppressive function on T-cell proliferation and cytokine production (Cantoni et al., 2017). In this chapter, *miR-223*$^{-/-}$ endometriotic-like lesions exhibited a consistent decrease in KEGG pathways associated with Th1, Th2 and Th17 cell differentiation over time (Appendix: Figure 7.6 and Table 7.3 – Cluster 5). Therefore, the observed increase in Arg-1 density in *miR-223*$^{-/-}$ endometriotic-like lesions over time may be attributed to suppression of T cell mediated immunity. Interestingly, studies have linked elevated regulatory T cell activity with endometriosis (de Barros et al., 2017), and it is possible that suppression of T cell function driven by *miR-223* depletion may contribute to reduced lesion development in this model.

At D7, average vessel size and number of vessels per lesion was significantly higher in *miR-223*$^{-/-}$ lesions compared to C57 lesions, whereas by D21, blood vessel density was significantly higher in C57 lesions. From the RNA-Seq data, an upregulation of *Vegfa* was observed whereas a downregulation of *Vegfb* was noted in both D7 and D14 lesions compared to donor decidualised endometrium (Supplementary material Table 8 and 9). *miR-223* overexpression is known to antagonise angiogenesis via inhibition of VEGF and basic fibroblast growth factor (bFGF) induced phosphorylation of their receptors (VEGFR2 and FRFR1 respectively) (Shi et al., 2013). Therefore, in the absence of *miR-223*, it is possible that an early induction of VEGF and bFGF may occur, accounting for the D7 observations in lesion vasculature. However, as there was a significant increase in M1-like markers over subsequent weeks, it is likely that the expression of pro-angiogenic factors were downregulated, as studies have shown inhibition of VEGF in the presence of pro-inflammatory signals such as TNF-α (Patterson et al., 1996). In addition, a downregulation in the canonical apelin cardiac fibroblast signalling pathway was observed in D14 lesions compared to D7 lesions, which may contribute to the reduced myofibroblast activity and fibrosis seen in *miR-223*$^{-/-}$ lesions compared to C57 lesions.

During lesion development, the remodelling of ectopic endometrial tissue is important for lesion establishment and persistence. The activation of a range of MMPs assist with ectopic tissue invasion and facilitate disease progression (Osteen et al., 2003, Yang et al., 2016). Endometriosis-like lesions which developed in the absence of *miR-223* had a reduced expression of *Mmp3*, *Mmp12*, and *Mmp27* in D14 lesions compared to D7 lesions (Supplementary material Table 10). Elevated MMP3 protein levels have been observed in greater than 50% of ectopic endometrial tissue samples (Lv et al., 2015), and allelic polymorphisms in *MMP3* are associated with the development of genital endometriosis (Yarmolinskaya et al., 2014). Increased expression of *MMP12* is associated with the invasion and differentiation of endometrial adenocarcinoma cells (Yang et al., 2007), with genetic polymorphisms in *MMP12* may have a potential role in the progression of superficial endometriosis (Borghese et al., 2008). Similarly, MMP27 is detected in ovarian an peritoneal endometriotic lesions, and importantly, is expressed in $CD163^{+}/CD206^{+}$ M2-like endometrial macrophages (Cominelli et al., 2014). Collectively, this data suggests that the lack of lesion establishment and fibrosis over time in *miR-223*$^{-/-}$ mice could be a consequence of the reduced expression of MMPs, which may potentially be mediated by the deficiency in M2-like macrophages in this model.

5.3.3. Depletion of *miR-223* from the recipient environment restricts endometriotic lesion growth

miR-223 suppresses the canonical NF-κB pathway to restrict the magnitude of inflammation (Haneklaus et al., 2013). However, in the absence of *miR-223*, an increase in granulopoiesis coupled with an elevation in hyper-mature and hyper-responsive neutrophils was observed in mice (Johnnidis et al., 2008). Women with endometriosis have an increased number of neutrophils in the peritoneal fluid (Tariverdian et al., 2009, Milewski et al., 2011), as well as an increased neutrophil-to-lymphocyte ratio in the blood (Cho et al., 2008). In a mouse model of endometriosis, antibody mediated depletion of neutrophils during early stage disease development resulted in a significant reduction in the weight and total number of lesions formed (Takamura et al., 2016). The findings from our study support this, as *miR-223*$^{-/-}$ → C57 lesions were significantly heavier and larger at D7 and D14, and had increased glandular formation at D14 compared to both C57 and *miR-223*$^{-/-}$ syngeneic lesions. In contrast, although C57 → *miR-223*$^{-/-}$ lesions were large at D7, by D14 lesions had reduced significantly in size, and an absence of glandular formation was noted. Although this study did not assess the presence of neutrophils, our findings suggests that elevated neutrophil activity in itself is insufficient to maintain lesion growth and survival over time.

Lesions from *miR-223*$^{-/-}$ → C57 mice exhibited a gradual increase in total and central F4/80 expression over time, however, it is surprising to note that MHC II expression remained low at D7 and D14. The increase in MHC II expression appears to correlate with a decrease in lesion weight and size at D21,

suggesting that the recruitment of M1-like macrophages in these lesions is delayed, thereby preventing the clearance of ectopic tissue. Importantly, following M1-like macrophage and neutrophil-mediated tissue degradation and clearance, the presence of M2-like macrophages is required to restore homeostasis and initiate tissue regeneration (Prame Kumar et al., 2018). It was interesting that the expression of both M2-like markers remained consistently low in *miR-223*$^{-/-}$ → C57 lesions.

In a mouse model of endometriosis, the infiltration of VEGF-secreting neutrophils and macrophages was observed within 5 days following disease induction, subsequently promoting lesion development, neoangiogenesis and ectopic tissue survival (Lin et al., 2006). During macrophage polarisation, a deficiency of *miR-223* expression induces IKK-α, resulting in the suppression of NF-κB pathways, preventing the induction of an M2-like response (Li et al., 2010). Thus, the inability to recruit M2-like tissue-remodelling macrophages early during *miR-223*$^{-/-}$ → C57 lesion development impacts the ability for sustained lesion growth and survival, despite the possible increase in neutrophil numbers. Our findings imply that signals from the donor endometrium may govern the recruitment and polarisation of macrophages within the lesion. Therefore, regardless of the availability of M2-like macrophages from the recipient environment, a deficiency of *miR-223* results in a lack of M2-like macrophage activity within the lesion. This observation supports clinical findings, as elevated *miR-223* expression is observed in endometriotic lesions, and suggests that repression of *miR-223* within these lesions may hold potential in reducing the extent of tissue remodelling and lesion growth.

Alternatively, in C57 → *miR-223*$^{-/-}$ lesions, similar proportions of F4/80^{+} cells were observed at lesion periphery and centre at D7 and D14, with low expression of both M1-like markers iNOS and Arg-1 at D7. This finding was surprising as it contrasted with observations from both the syngeneic C57 → C57 lesions and *miR-223*$^{-/-}$ → *miR-223*$^{-/-}$ lesions, and similarly, does not conform to the idea that a predominance of M1-like macrophages are present early in lesion growth (Bacci et al., 2009). A possible explanation is that following transfer into a *miR-223*$^{-/-}$ pro-inflammatory recipient environment, signals from the donor replete endometrium attempt to restrict the extent of M1-like activity. This may account for the high lesion weight and size observed at D7, which may be indicative of reduced tissue clearance at this time point, as the replete ectopic tissue is attempting to evade clearance and survive. However, lesions are unable to maintain glandular areas in the sustained M1-like pro-inflammatory environment, and ultimately regress.

In conclusion, the findings from this chapter indicate that a deficiency in *miR-223* significantly attenuates lesion progression in a menstrual mouse model of endometriosis. *miR-223* is involved in promoting an anti-inflammatory, tissue healing immune environment by polarising monocytes into M2-like macrophages (Chen et al., 2012, Ismail et al., 2013, Ying et al., 2015). Bacci *et al.* (2009) showed that increased tissue remodelling mediated by M2-like macrophages promotes the development of endometriosis lesions. In these mice, systemic depletion of *miR-223* results in an elevated pro-inflammatory immune response, with increased levels of M1-like macrophages (Zhuang et al., 2012), which could account for the rapid lesion clearance seen in the menstrual mouse model of endometriosis used in this chapter. In a clinical setting, *miR-223* is upregulated in ectopic endometrial lesions compared to paired eutopic endometrial biopsies, suggesting that elevated levels of this microRNA supports lesion survival (Ohlsson Teague et al., 2009). Furthermore, a sustained elevation in the expression of *miR-223* has harmful physiological effects. In the RL95-2 human endometrial carcinoma cell line, overexpression of *miR-223* was found to significantly inhibit cell proliferation and cell cycle progress via regulation of the insulin-like growth factor 1 receptor (IGF-1R) (Huang et al., 2014). IGF-1R signalling has been implicated in various cancers, and is often associated with an increased resistance to conventional treatments (Jones et al., 2004, Warshamana-Greene et al., 2005, Vella and Malaguarnera, 2018). As cancer-associated mutations have been identified in both eutopic and ectopic endometrium of women with endometriosis in the absence of cancer or dysplasia (Anglesio et al., 2017, Suda et al., 2018), it is possible that *miR-223* expression may have a role in inhibition of the transformation of benign endometriotic lesions into malignant carcinomas. Hence, the apparent paradoxical role of *miR-223* in the progression of endometriosis should be analysed further. It is possible that a therapeutic strategy to inhibit *miR-223* expression could result in a reduction in endometriotic lesion growth as seen in this mouse model, and characterisation of the long term effects of *miR-223* suppression on endometriotic lesion development should be performed.

Chapter 6

General discussion and conclusion

6.1. INTRODUCTION

Endometriosis, the ectopic growth of endometrial tissue outside the uterine cavity, afflicts 10% of reproductive-aged women, and remains a complex, chronic and debilitating disorder (Giudice, 2010, Zondervan et al., 2018). The exact mechanisms governing the development of this disease are still uncertain, but have been linked to dysregulated immune responses within the peritoneal cavity (Capobianco and Rovere-Querini, 2013). From an immunological standpoint, lesion development in endometriosis can be broadly classified into two stages which are governed by either a pro-inflammatory (M1-like) response or a tissue remodelling (M2-like) response. An imbalance in the M1/M2 response may result in the survival, attachment and proliferation of ectopic endometrial tissue in the peritoneal cavity, when normally this tissue would be actively cleared by host immune cells.

Macrophages have been implicated as central arbiters and enablers of disease progression, as an increased number of these immune cells are present within the peritoneal cavity of women with endometriosis compared to healthy controls (Haney et al., 1981, Capobianco and Rovere-Querini, 2013). Macrophages are key players in both the progression and resolution of inflammatory responses (Cao et al., 2004, Jantsch et al., 2014). In endometriotic lesion development, *in vivo* studies have demonstrated that a predominance of M1-like macrophages results in inhibition of lesion growth via increased tissue clearance, while an increase in M2-like macrophages supports lesion survival, remodelling and establishment (Bacci et al., 2009). Thus, the regulatory mechanisms driving macrophage polarisation in endometriosis should be evaluated *in vivo* to better understand the impact of an M1/M2 imbalance during disease development.

MicroRNAs, a subset of epigenetic regulators, play a physiological role in regulating and mediating the polarisation of macrophages (O'Connell et al., 2012, Liu and Abraham, 2013). For example, *miR-155* is important in facilitating pro-inflammatory M1-like macrophage polarisation (Worm et al., 2009, Martinez-Nunez et al., 2011, Arranz et al., 2012, Gracias et al., 2013, Wang et al., 2013a), whereas the haematopoietic-specific microRNA *miR-223* is crucial in the programming of anti-inflammatory, tissue healing M2-like macrophages (Zhuang et al., 2012, Wang et al., 2014a, Yuan et al., 2018). Moreover, multiple studies have demonstrated an aberrant microRNA expression profile in women with endometriosis. The expression of *miR-155* is downregulated in the plasma of women with endometriosis compared to disease-free controls, suggesting disease progression is associated with reduced M1-like immune activity (Nisenblat et al., 2019). Additional studies have demonstrated an upregulation of *miR-223* in ectopic endometrial tissue compared to paired eutopic samples, further implicating an M2-like immune environment in the pathogenesis of endometriosis (Ohlsson Teague et al., 2009).

Therefore, the experiments described in this thesis were undertaken to investigate the establishment and progression of endometriotic-like lesions in a subcutaneous menstrual mouse model of endometriosis in the absence of either *miR-155* or *miR-223*, with the hypotheses that a deficiency in *miR-155* will enhance lesion development through upregulation of anti-inflammatory M2-like immune activity, and conversely, that a deficiency in *miR-223* will suppress lesion growth via enhancement of pro-inflammatory M1-like immune activity. Collectively, this data contributes to the growing evidence implicating a shift in the M1/M2 macrophage phenotype balance as an important determinant of endometriotic lesion establishment and survival (Figure 6.1).

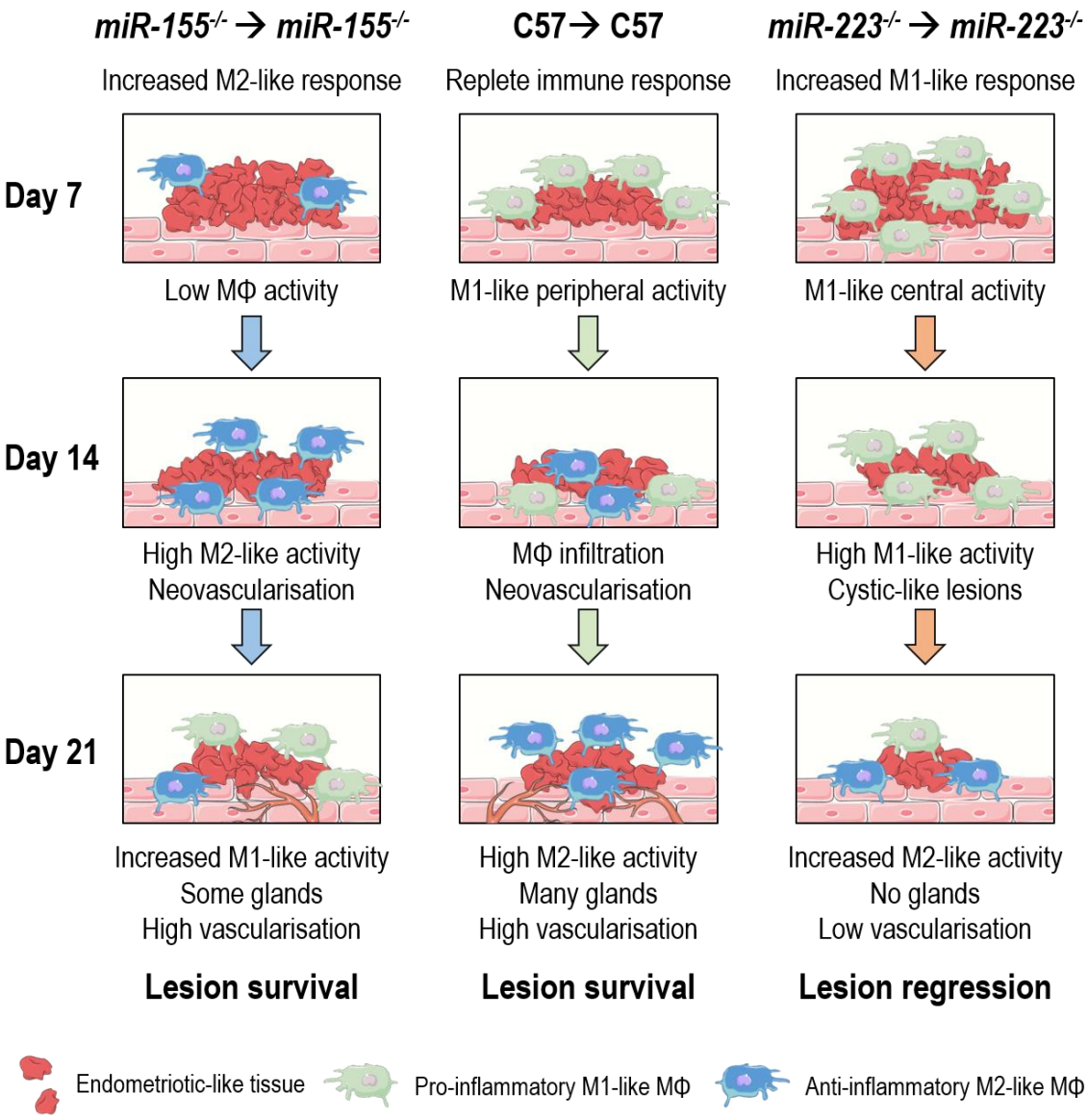

Figure 6.1 **Summary of the impact of a systemic *miR-155* or *miR-223* knockout on macrophage activity in endometriotic-like lesion development**

In wildtype (C57) mice, a replete immune system results in an initial M1-like response at the lesion periphery, followed by macrophage (MΦ) infiltration and neovascularisation at day 14. By day 21, lesions have elevated M2-like MΦ activity, along with the presence of numerous glands and extensive vascularisation, indicative of successful lesion survival and establishment. The systemic absence of *miR-155* promotes an M2-like immune response, characterised by low MΦ activity in lesions at day 7. However, at day 14, high M2-like immune activity is observed with blood vessel development, and although lesions at day 21 have increased M1-like activity, the presence of glands and high levels of vascularisation indicates successful lesion survival. In contrast, in the absence of *miR-223* facilitates an elevated pro-inflammatory immune response, and early MΦ infiltration into endometriotic-like lesions is coupled with high M1-like immune activity. At day 14, lesions appear cystic and high M1-like immune activity is sustained. At day 21, M2-like immune activity is increased, however as low vascularisation and no glandular formation is evident, lesions are unable to establish successfully, suggesting disease regression.

6.2. RATIONALE AND VALIDATION OF MODEL

As it is challenging to understand the significance of M1/M2 macrophage phenotype in the pathogenesis of endometriosis from human clinical studies alone, animal models are useful to demonstrate correlations, causalities, and consequences of skewing immune polarisation on disease development. The main criticism of using rodents to mimic endometriosis is the absence of a menstrual cycle in these animals. Multiple studies in both autologous and homologous mouse models of endometriosis often require uterine fragments to be sutured onto the peritoneal wall or intestinal mesentery, as endometrial scrapings alone rarely formed quantifiable lesions (Grümmer et al., 2001, Lin et al., 2006, Cheng et al., 2011). To overcome this limitation, we used an induced menstrual mouse model of endometriosis, in which decidualised endometrial fragments readily adhere to the peritoneal surface (Greaves et al., 2014). In this model, insertion of oil into the uterine lumen, in conjunction with hormone manipulation to mimic the hormonal environment of early pregnancy in donor mice, allowed induction of an extensive and sustained decidual response. Within four hours of progesterone withdrawal, large numbers of proliferating cells were observed in the basal stroma and luminal epithelium of donor mice, and the expression profile of epithelial and junctional proteins mimicked features of human menstruation (Cousins et al., 2014). Therefore, the transfer of donor decidualised endometrium into a recipient mouse simulates the process of retrograde menstruation which gives rise to the development of endometriosis. In addition, we found that the loss of either *miR-155* or *miR-223* did not impede the induced decidualisation of stromal cells in donor mice, as evidenced by the respective donor:recipient ratios. Moreover, previous studies have shown that a minimum of 40mg of donor endometrial tissue is sufficient for development of endometriotic-like lesions in a homologous mouse model (Greaves et al., 2014, Dodds et al., 2019).

A further challenge faced in modelling endometriosis in rodents is that intraperitoneal inoculation of endometrial tissues may not successfully attach within the peritoneal cavity, resulting in non-vascularised, necrotic fragments devoid of proliferating cells (Burns et al., 2012), coupled with a low lesion recovery rate of approximately 33-66% (Grümmer et al., 2001). In a clinical setting, subcutaneous endometriosis may occur following either caesarean or laparoscopic surgery (Denton et al., 1990, Khammash et al., 2003, Hull et al., 2006). Subcutaneous endometriosis, or scar endometriosis, is believed to arise from the exposure and subsequent transfer of either eutopic endometrium (during caesarean section) or pre-existing ectopic endometrial tissue to the surgical site, where it incorporates into the abdominal wall wound (Liang et al., 1998, Gaunt et al., 2004, Hull et al., 2006). Therefore, when modelling endometriosis in rodents, subcutaneous inoculation of endometrial fragments effectively mimics disease development. Moreover, this approach allows for encapsulation of these fragments between the skin and peritoneal

layer, increasing the lesion recovery rate to 63-100% (Hull et al., 2012) and allowing for a more accurate correlation between the amount of tissue injected and the size of the resulting lesion.

In addition, to increase the rate of tissue implantation, several studies have relied upon suturing endometrial fragments to the peritoneal wall (Lin et al., 2006), using fibrin glue (Boztosun et al., 2012), or injecting tissue in conjunction with extracellular matrix-enriched media such as Matrigel (Cheng et al., 2011). Although these approaches increase ectopic tissue attachment frequencies, the supplementation of enriched media and the artificial adherence of these fragments are likely to confound the evaluation of innate mechanisms upregulated during the establishment of endometriosis (e.g. effectiveness of immune-mediated clearance; MMP expression). Thus, to overcome the influence of growth-stimulating or enhancing factors which may compromise the validity of endometriotic-like lesion development, the use of PBS, saline, or ECM-free media as the injection diluent is critical (Capobianco et al., 2011, Greaves et al., 2014).

Therefore, to ensure adequate lesion recovery in this study, we used a menstrual mouse model of endometriosis in which 40mg of decidualised donor endometrial tissue in PBS was injected subcutaneously into recipient mice. Following this method, we obtained an overall lesion recovery rate of 87% (94% in C57 mice; 92% in *miR-155*$^{-/-}$ mice; 78% in *miR-223*$^{-/-}$ mice), confirming the efficacy of this method in modelling endometriotic disease progression. Furthermore, the endometriotic-like lesions which developed over the course of three weeks post-induction of disease in this model displayed typical endometriotic histomorphology, characterised by the formation of quantifiable glandular and stromal areas.

6.3. KEY FINDINGS AND SIGNIFICANCE OF STUDY

This is the first study to characterise the development of lesions over time in a menstrual mouse model of endometriosis. Collectively, the experiments carried out in this thesis demonstrate that successful lesion establishment, morphological, immunological, and molecular changes associated with endometriotic-like lesion development can be effectively investigated in this model. Importantly, we have shown that miRNA-mediated epigenetic regulation of the immune system impacts the development of endometriosis, highlighting the potential of miRNA-mediated or miRNA-targeting therapeutics in managing this disease.

Endometrial glands are important sources of chemokines and cytokines, which collectively monitor and regulate the infiltration of immune cells into endometrial tissue (Chand et al., 2007). In women with endometriosis, spontaneous apoptosis of endometrial glands was decreased in the late secretory and early proliferative phases of the menstrual cycle compared to disease-free women (Dmowski et al., 2001). The development of glands in ectopic endometrial tissue is a hallmark of successful lesion survival and establishment, and an inverse correlation between endometrial gland apoptosis and severity/stage of endometriosis has been observed (Dmowski et al., 2001). Although the complex physiological events underlying the development of uterine glands are not well delineated, a sustained activation of TGF-β signalling is associated with endometrial dysfunction (Ni et al., 2018). TGF-β, an inducer of M2-like macrophage polarisation (Zhang et al., 2016a), promotes tumour cell invasion and metastasis by inducing epithelial-mesenchymal transition (Johansson et al., 2013), and is associated with the survival and establishment of ectopic endometrial tissue (Hull et al., 2012, Dela Cruz and Reis, 2015, Young et al., 2017). As demonstrated by Bacci et al. (2009), a dysfunction of macrophage activity and an imbalance in macrophage polarisation can result in exacerbation of endometriosis, with M2-like macrophage activity promoting lesion development.

In women with endometriosis, a downregulation of circulating miR-155 levels is observed (Nisenblat et al., 2019). In our mouse model of endometriosis, a systemic deficiency of *miR-155* resulted in a significant increase in the expression of two M2-like immune markers, CD206 and Arg-1, in endometriotic lesions between D7 and D21. miR-155 targets the transcription factor SMAD5, disrupting TGF-β activity via the non-canonical TGF-β1/SMAD5 signalling pathway (Rai et al., 2010). Thus, during the pathogenesis of endometriosis, reduced miR-155 expression may result in elevated TGF-β activity, with a corresponding increase in M2-like immune activity, likely caused by the increase in TGF-β. However, it is important to note that the number of glands per lesion in these mice did not alter across the time course. This may in part be due to a reduced lymphocyte recruitment capacity, as *miR-155*$^{-/-}$ bone marrow monocytes exhibit

downregulated CCR7 expression, which is important in lymphocyte recruitment (Elmesmari et al., 2016). Thus, despite an increase in the levels of M2-like tissue remodelling activity, impaired lymphocyte recruitment may impede the sustained influx M2-like macrophages, suggesting that a *miR-155* deficiency is in itself insufficient to promote the formation of endometrial glands.

From the plethora of circulating lymphocytes, an elevation of M2-like macrophage activity in *miR-155*$^{-/-}$ mice has been noted (He et al., 2015). M2-like macrophages are implicated as mediators of vascular development, as they are potent sources of VEGF (Capobianco and Rovere-Querini, 2013). VEGF, an important angiogenic factor, is found to be secreted by activated peritoneal macrophages and is abundantly expressed in the glandular compartment of endometriomas (Groothuis, 2012, Krikun, 2012). In endometriosis, neovascularisation is an additional marker of successful lesion survival, as the development of blood vessels is critical to support lesion growth (Lebovic et al., 2000, Hull et al., 2003). In the syngeneic *miR-155*$^{-/-}$ mouse model, we observed an increase in blood vessel formation between D7 and D21, suggesting that the observed elevation of M2-like immune markers promotes the vascularisation and survival of endometriotic-like lesions in these mice. However, this finding contrasts with published literature, in which a down-regulation of miR-155 reduced VEGF-induced proliferation, migration and tube formation abilities of human retinal microvascular endothelial cells via the PI3K/Akt pathway (Zhuang et al., 2015). To reconcile this observation, it is important to consider the unique conditions in which endometriotic lesions become established, with particular focus on the hypoxic environment that facilitates the attachment, proliferation and progression of ectopic endometrial tissue.

Under hypoxic conditions, ectopic endometrial cells undergo complex gene regulation and epigenetic modulation, evoking a range of survival mechanisms, including metabolic switching, steroidogenesis, and angiogenesis (Wu et al., 2019). During prolonged hypoxia, miR-155 promotes resolution of HIF-1α activity in an isoform-specific negative feedback loop (Bruning et al., 2011). Thus, in a clinical setting, the downregulation of miR-155 may promote a hypoxic environment in women with endometriosis via HIF-1α activation. In addition, HIF-1α activation of ERK induces a signalling cascade which increased FGF-9 expression (Lin et al., 2012). FGF-9 stimulates endothelial and endometrial stromal cell proliferation and angiogenesis, potentially contributing to ectopic lesion development (Tsai et al., 2002). Indeed, when compared to C57 lesions, the results from this thesis show elevated αSMA^{+} myofibroblast activity in *miR-155*$^{-/-}$ → *miR-155*$^{-/-}$ lesions, as well as in both *miR-155*$^{-/-}$/C57 reciprocal transfer groups, confirming a role for *miR-155* in the regulation of fibroblast proliferation in the progression of endometriosis. Moreover, immunohistochemical analysis these lesions showed a large extent of vasculature present, further supporting the role of neoangiogenesis in lesion establishment and progression. In addition, the existence of functional redundancy amongst miRNAs is essential to maintain biological homeostasis (Fischer et al.,

2015, Laffont and Rayner, 2017). For example, both miR-148a and miR-155 are found to be upregulated in acute viral myocarditis with both miRs directly targeting RelA, a subunit of NF-κB. Hypoxic conditions in endometriotic lesions induce *miR-148a*, leading to destabilised DNA methyltransferase 1 mRNA expression *in vitro* (Hsiao et al., 2015). Therefore, in the absence of miR-155, it possible that miR-148a and/or additional miRNAs may be induced following hypoxia, contributing to increased angiogenesis and survival of endometriotic lesions in hostile ectopic environments. Thus, clinical evaluation of dysregulated epigenetic modulators within endometriotic lesions may provide further insights into mechanisms driving disease establishment. It remains imperative to understand the contribution of these factors which may in turn be harnessed therapeutically to limit disease progression.

To this extent, the expression of the epigenetic regulator miR-223 is upregulated in ectopic endometrial lesions compared to paired eutopic samples (Ohlsson Teague et al., 2009). miR-223 modulates the differentiation of haematopoietic lineages, and attenuates pro-inflammatory immune responses while concurrently promoting the polarisation of M2-like macrophages (Zhuang et al., 2012, Ying et al., 2015, Yuan et al., 2018). Hence, the observed upregulation of miR-223 may result in an increased abundance of M2-like macrophages within endometriotic lesions, thus facilitating lesion development though the release of tissue remodelling and pro-angiogenic factors (Bacci et al., 2009). In mice, the loss of *miR-223* results in an increase of M1-like pro-inflammatory immune activity (Johnnidis et al., 2008, Sica and Mantovani, 2012, Trissal et al., 2015, Ying et al., 2015), and using a *miR-223* deficient mouse model of endometriosis allowed us to assess the effect of a sustained M1-like immune response on lesion development.

Syngeneic lesions from *miR-223*$^{-/-}$ mice showed signs of regression, evidenced by the gradual loss of glandular areas over time. These lesions consisted of large cystic spaces at D14, and by D21, a large proportion these lesions were fibrotic, with a complete absence of glandular formation. Previous work has shown that the presence of ectopic endometrial tissue attracts an influx of macrophages from the surrounding environment (D'Hooghe et al., 2001). In these mice, F4/80^{+} macrophages were dispersed throughout lesions at D7, and both peripheral and central F4/80 density remained significantly higher in D21 lesions from *miR-223*$^{-/-}$ mice compared to C57 mice. The observed infiltration of F4/80^{+} macrophages in *miR-223*$^{-/-}$ endometriotic-like lesions corresponds with an increase in the expression of the M1-like immune markers iNOS and MHC II over time. This observation concurs with previous work showing that *miR-223* deficient mice have an increased M1-like, hypersensitive pro-inflammatory immune response (Johnnidis et al., 2008). This finding further suggests that an early infiltration of macrophages may impact lesion development, particularly when coupled with a sustained M1-like immune environment. This prolonged M1-like status could account for the cystic, pus-filled appearance and the overt lack of glandular

remodelling observed in *miR-223*$^{-/-}$ lesions, strongly suggesting that early macrophage infiltration with an elevation in M1-like immune responses restricts ectopic endometrial tissue growth.

As mentioned previously, hypoxic conditions contributes to the induction of survival-associated gene networks to promote the development of endometriosis (Wu et al., 2019). The overexpression of miR-223 is able to antagonize the hypoxic effects seen in pulmonary arterial smooth muscle cells (Zeng et al., 2016). In addition, the upregulation of miR-223 *in vivo* results in the reversal of pulmonary arterial hypertension, including beneficial effects on vascular remodelling (Meloche et al., 2015). In our mouse model of endometriosis, we observed a regression in the number of blood vessels in *miR-223*$^{-/-}$ lesions, further impeding the survival ability of these lesions. Collectively, this suggests that the observed upregulation of miR-223 clinically may attenuate hypoxia within the endometriotic lesion microenvironment while simultaneously inducing angiogenesis to promote lesion survival.

While analyses from the systemic *miR-223*$^{-/-}$ mouse model highlights the significance of reducing miR-223 expression to limit the development of endometriosis, the most compelling data to support this inference comes from the reciprocal transfer model in which miR-223 sufficient donor endometrium was transferred into a miR-223 deficient recipient (C57 → *miR-223*$^{-/-}$). The absence of glands in C57 → *miR-223*$^{-/-}$ lesions from D14 onwards has significant clinical implications. In women with endometriosis, elevated miR-223 expression is noted in the ectopic endometrial tissue, but not in the eutopic endometrium (Ohlsson Teague et al., 2009). Our study shows that the lack of *miR-223* in the recipient environment following lesion transfer impedes the survival and progression of endometriosis, suggesting that a knockdown of miR-223 activity in the peritoneal cavity of women with endometriosis may assist in lesion clearance. These findings provide credence to an epigenetic-mediated approach in treating endometriosis, with particular emphasis on utilising miRNA-antagonists to manipulate the immune response towards ectopic endometrial tissue.

Multiple research groups are exploring the applicability and clinical translation of RNA-based therapeutics. Technological advances in the development of efficient, targeted drug delivery systems involving liposomes and nanoparticles, have facilitated human clinical trials of antagomirs, miRNA sponges, miRNA masking, and miRNA mimics (Baumann and Winkler, 2014, Christopher et al., 2016, Chakraborty et al., 2018). The first group to demonstrate efficient miRNA-mediated silencing utilised intravenous delivery of a locked nucleic acid modified oligonucleotide (LNA-antimiR) to antagonise hepatic miR-122 activity in non-human primates (Elmen et al., 2008). Not only did this therapeutic approach reversibly decrease

plasma cholesterol levels, but crucially, there were not toxic side effects of histopathological changes observed *in vivo*.

In the context of endometriosis, the inhibition of mature microRNA which promote disease progression may have therapeutic utility. Moreover, the experiments in this thesis identified a role for miR-223 downregulation in limiting endometriotic lesion development via modulation of the immune response. Clinically, the targeted delivery of miR-223 antagomirs to the site of lesion growth may simultaneously decrease M2-like tissue remodelling while increasing the recruitment of M1-like pro-inflammatory mediators to assist with lesion regression and clearance. The recently developed LODER™ (Local Drug EluteR manufactured by Silenseed©) cancer drug delivery platform enables direct insertion of RNA-based therapeutics into tumour cores to ensure therapeutic release over the course of several months (Shemi et al., 2015). A similar approach could be used for delivery of miRNA-based therapeutics in endometriosis, to allow for the sustained treatment of this recurrent, chronic disease. Thus, strategies to modulate the inflammatory response associated with endometriosis should consider targeting epigenetic regulators, and additional studies looking at dysregulations in non-coding RNA pathways which impact activation profiles of macrophages, lymphocytes or related immune cell subsets may be a useful avenue in the treatment of endometriosis.

6.4. IMPLICATIONS AND CLINICAL RELEVANCE

Altered immune parameters observed in women with endometriosis allude to an ineffective immune response as the underlying causal pathway in disease development. Mounting evidence from animal studies implicate infiltrating macrophages in endometriotic lesion establishment and underscores the importance of an appropriate M1/M2 macrophage phenotype response in exacerbating or reducing disease burden (Bacci et al., 2009, Capobianco et al., 2011, Greaves et al., 2014, Johan et al., 2019). In a mouse model of endometriosis, adoptive transfer of pro-inflammatory M1-like macrophages and alternatively activated M2-like macrophages resulted in impaired or enhanced establishment of endometriotic lesions respectively (Bacci et al., 2009). Thus, the manipulation of the M1/M2 macrophage phenotype balance contributes significantly to endometriosis disease outcome, suggesting a correlation between aberrant macrophage polarisation and lesion survival.

These observations are clinically relevant as they suggest that the susceptibility to developing endometriosis as well as the diverse manifestation of endometriotic lesion presentation could be in part attributed to an imbalance in the M1/M2 macrophage phenotype. Our findings support this assumption, and further indicate that the lesion-implantation environment controls macrophage polarisation potential, wherein a predominance of M2-like macrophages enhanced lesion growth and vascularisation while an abundance of M1-like macrophages impaired lesion establishment. However, although animal studies have demonstrated an association between M1/M2 macrophage imbalance and endometriosis, it is important to consider human heterogeneity, specifically with regard to the immune system.

The ontogeny of the immune system is influenced by genetic and epigenetic variations between individuals, with physiological, environmental and lifestyle factors affecting immune response modulation. It is possible that different women are more or less predisposed to endometriosis by genetic and/or environmental factors affecting their M1/M2 balance, but it is also possible that changes in their balance are a consequence, not a cause of disease. That is, the complexity of discrete individual responses towards inflammatory challenge gives rise to the possibility that observed changes in M1/M2 macrophage phenotype abundance in women with endometriosis may arise as a consequence of an exacerbated inflammatory response towards ectopic endometrial tissue, rather than an M1/M2 macrophage imbalance being causal in disease pathogenesis. Similarly, it remains challenging to conclude if differential expression of immune regulatory miRNAs in women with endometriosis is an underlying causal factor driving initiation of disease or a consequence of altered hormonal or immune function that occurs following lesion establishment.

To this extent, while multiple studies have investigated correlations between endometriosis and autoimmune diseases (Shigesi et al., 2019), there is insufficient understanding of the aetiology of endometriosis to account for increased comorbidities associated with endometriosis. It is probable that the convergence of genetic, environmental, physiological, and lifestyle factors influence the propensity to develop endometriosis via the M1/M2 immune response, which may similarly contribute to the development of additional immune-associated diseases. For example, the worldwide increase in the incidence of many chronic inflammatory diseases is postulated to be due, in part, to a significant reduction of bacterial microbiome diversity associated with a metropolitan environment (Blaser and Falkow, 2009, Hand et al., 2016). Likewise, urban lifestyles are linked with reduced exposure to parasites, microbes and other pathogens, and as described elegantly in the 'hygiene hypothesis', early exposure to antigens may be crucial in priming the immune system to respond to inflammatory challenges in later life (Alexandre-Silva et al., 2018, Beenhouwer, 2018). In addition, exposure to endocrine disruptor compounds, commonly found in plastics, solvents and pesticides, affects macrophage phagocytosis via an oestrogen receptor dependent pathway (Couleau et al., 2015), and may contribute to a M1/M2 macrophage phenotype imbalance. Therefore, although aberrant macrophage function is implicated in the pathogenesis of endometriosis, pinpointing the exact mechanisms driving this shift in immune function remains challenging in affected women.

Whilst acknowledging that the presence of a chronic disease like endometriosis necessitates that the immune system remains in a constant state of flux, strategies which shift the M1/M2 balance may prove therapeutic by inhibiting the reparative function of M2-like macrophages which promotes disease progression. As mentioned previously, RNA-based therapeutics have potential in modulating macrophage phenotype balance, and additional macrophage-based clinical interventions for endometriosis should be investigated. Macrophage-associated therapeutic strategies employed in pathologies with characteristic macrophage-driven inflammatory responses, such as type 2 diabetes, atherosclerosis, and cancer (Parisi et al., 2018), should be further researched to determine suitability for clinical translation in endometriosis. For example, parallels between the heterogeneous tumour microenvironment in cancer and endometriotic lesions comprising similarly diverse cell populations suggests that pharmacological approaches targeting macrophages within the tumour microenvironment (i.e. manipulating macrophage recruitment, macrophage depletion, and macrophage reprograming (Poh and Ernst, 2018)) may be beneficial in treating endometriosis.

Despite the significant contribution of macrophages in endometriosis, it is important to consider the multifactorial nature of this disease. Although studies in animal models have demonstrated correlations between macrophage polarisation imbalances and lesion development, it is yet unknown if manipulation

of the M1/M2 macrophage balance would be sufficient to reverse established disease, and should be evaluated. Hence, to achieve the best clinical outcome for women with endometriosis, multi-targeted approaches to regulate macrophage activity should be employed in conjunction with current therapeutic strategies such as excision of pre-existing lesions and hormone manipulation. In addition, considering the multitude of factors regulated by the immune system, studies looking at the long-term impact of macrophage modulation on physiological and neurological outcomes should also be undertaken.

6.5. LIMITATIONS AND FUTURE DIRECTIONS

While the findings from this thesis highlight the important role of specific miRNAs in immune modulation during the progression of endometriosis, several caveats and limitations exist, necessitating further experimentation to validate these observations. Although subcutaneous rodent models are frequently utilised to study the pathogenesis of endometriosis, we do acknowledge that this is not an entirely accurate representation of the disease in humans as it does not encapsulate the peritoneal environment. However, a pilot study using an intraperitoneal menstrual mouse model of endometriosis in *miR-223*$^{-/-}$ mice found that D7 lesions were predominantly cystic, whereas D14 lesions were fibrotic and devoid of both cysts and glands (Unpublished data). These early observations from the intraperitoneal model concur with the findings presented in this thesis, indicating that the data gathered from the subcutaneous model remains valid in modelling early endometriotic-like lesion development. An additional caveat regarding this model is that there was no continuous monitoring of individual lesions over time, as is possible in large primate models. However, the approach undertaken in this thesis allowed for histochemical assessment to be performed at each time point, which has provided valuable information regarding endometriotic lesion development.

In addition to the aforementioned limitation is the methodological approach used to identify macrophages and their M1-like and M2-like immune activation status. In particular, the expression of the M1-like (iNOS and MHC II) and M2-like (CD206 and Arg-1) immune markers investigated are not limited to macrophages. Fluorescent-mediated dual-labelling studies in murine models of endometriosis have demonstrated that in addition to macrophages and immune cells, iNOS is co-expressed by epithelial cells; MHC II is co-expressed by dendritic cells; and Arg-1 is co-expressed by fibroblasts (Johan et al., 2019). In this thesis, endometriotic-like lesions were stored in formalin and processed for paraffin embedding and sectioning. During immunohistochemical optimisation trials, the formalin-paraffin crosslinking imparted a high level of non-specific background staining, thus impacting our ability to perform fluorescent dual-labelling. However, the single labelling approach and quantification of staining performed in this thesis indicated differences in the abundance of cells expressing each marker, suggesting that the expression of these markers may impart a potential functional consequence on the progression of endometriosis.

Similarly, the use of a single marker (F4/80) to identify the entire macrophage population is an additional limitation of this thesis. Although multiple peer-reviewed studies have only utilised F4/80 as a macrophage marker, it is important to note that macrophages express a range of different markers at varying concentrations throughout their development, polarisation, and activation (Hume, 2006). Furthermore,

emerging evidence suggests that F4/80 may not be constitutively expressed by all macrophage populations (Dos Anjos Cassado, 2017a). Hence, the discrepancy between the total density of F4/80 positive cells and cells expressing M1-like and M2-like markers should be recognised, as some macrophages within these endometriotic-like lesions may be positive for the examined markers, but negative for F4/80 expression. An alternative approach to immunohistochemical assessment for macrophages and M1-like vs M2-like immune activity would be to perform fluorescence activated cell sorting (Flow cytometry/FACS). While FACS allows for superior isolation and quantification of cell populations within endometriotic lesions, the critical advantage imparted by immunohistochemistry is that the localisation of cellular subsets and interactions within a tissue sample can be visualised. For example, in this thesis, the influx of macrophages from the periphery into the centre of the lesion would not be detectable via FACS. Thus, future work in this model should utilise FACS as a complementary method to quantify additional immune subsets within these endometriotic-like lesions.

The final limitation of this study centres on the presence of artefacts within the RNA-Seq data, wherein all samples had more than 70% clonal duplication (Appendix Figure 7.2). The read duplication rate is affected by the sequencing depth, read length, transcript abundance, and most commonly by artificial generation as a result of PCR amplification. A consequence of over 50% duplicated sequences suggests a bias in the sequencing library, and may be indicative of a failure to randomly sample the target sequence (Li et al., 2015). To overcome this limitation, we have applied the Picard MarkDuplicates method to remove optical duplicates, and subsequently filtered and normalised the dataset (Appendix Figure 7.3). Importantly, irrespective of mouse genotype, we observed that all samples of decidualised endometrium clustered together while all lesion samples grouped in a similar position in both the multi dimension scaling plot and individual principal component analyses plots. This key observation indicates that ectopic endometrial tissue undergoes significant molecular changes to facilitate its survival outside the uterus, and is confirmed by the large number of DEGs present between decidualised endometrial samples and D7/D14 lesions.

It was surprising to note that the low number of canonical pathways identified between D7 and D14 lesions within each genotype, given the vast differences observed morphometrically and histochemically. Likewise, very few DEGs were identified between C57 mice and miR-deficient mice at either D7 or D14. It is possible that the depletion of these microRNAs may result in subtle changes in the molecular profile of endometriotic-like lesions over time, however genes with a low but potentially significant expression level may have been masked in this dataset. It is also possible that changes occurring at an epigenetic level do not necessarily translate to observable differences at a transcript level. Alternatively, it is possible that changes in gene expression may be fluctuating over the course of lesion development, and might

have been more readily apparent at a different sampling time point (e.g. D5 or D10). Importantly, as we observed the greatest number of DEGs between the donor decidualised endometrial tissue and the resulting lesions at both D7 and D14, the contribution of genes from the donor endometrial tissue may be considered as a major factor in determining the capacity for endometrial tissue to survive ectopically.

The high number of clonal duplications also suggests the possibility that genes with a low but potentially significant expression level may have been masked in the dataset. For example, there are noticeable differences in the histology of lesions between D7 and D14, however the RNA-Seq dataset does not identify many DEGs between these time points. It is further possible that alternate compensatory epigenetic mechanisms may be driving these observed changes in lesion development. Future work should utilise the option of laser microdissection to isolate glandular fractions from stromal fractions prior to sequencing, as both tissue compartments may have a unique expression profile which could be masked during the sequencing of the total endometriotic-like lesion. An alternative approach would be to perform single cell RNA-Seq (scRNA-Seq). Although scRNA-Seq is associated with several duplication issues, this approach is advantageous over conventional RNA-Seq, as it allows for the identification of new, complex or rare cell populations or subsets and allows for regulatory relationships between genes to be discovered (Hwang et al., 2018). Finally, it would be advantageous not only to sequence endometriotic-like lesions at D21, but the gene expression profile in lesions derived from the reciprocal transfers should also be assessed to better understand the relative importance of the donor endometrium *vs* the recipient environment in disease development.

6.6. SUMMARY AND CONCLUSION

The complex, heterogeneous manifestation and symptoms of endometriosis contributes to the challenge of understanding the aetiology of this disease. This thesis has shown that the development of endometriotic-like lesions can be evaluated effectively over three weeks in a subcutaneous 'menstrual' mouse model of endometriosis. RNA-Seq analysis identified DEGs in several pathways associated with endometriosis, notably immune regulatory pathways, tissue remodelling, cellular differentiation and proliferation, and angiogenesis.

In addition, the contribution of the epigenetic regulators *miR-155* and *miR-223* was assessed in knockout mice, indicating the efficacy of rodent models in understanding the significance of microRNA influence on the pathogenesis of endometriosis. A reduction in lesion weight and size was seen over time in all groups, however glandular formation only increased in C57 mice. Systemic depletion of *miR-155*$^{-/-}$ restricted M1-like immune activity and promoted the expression of M2-like immune markers, with an increase in blood vessel density over time, further supporting lesion establishment. In contrast, early influx of F4/80^{+} macrophages with an increase in MHC II and iNOS expression was seen in *miR-223*$^{-/-}$ lesions, resulting in cystic-like lesions devoid of glands.

Significantly, we have demonstrated the critical role of *miR-223* in promoting endometriotic glandular development, suggesting that silencing of *miR-223* is a therapeutic approach that has potential to suppress lesion growth in women with endometriosis. Therefore, future experiments should be tailored to better understand the impact of depleting *miR-223* in human ectopic endometrial tissue, both *in vitro* and *in vivo* via xenograft models. As our comprehension on the role of epigenetic regulators increases, the clinical applicability of utilising these factors in the diagnosis and treatment of endometriosis will ideally become an increasingly appropriate and realistic outcome.

Chapter 7

Appendices

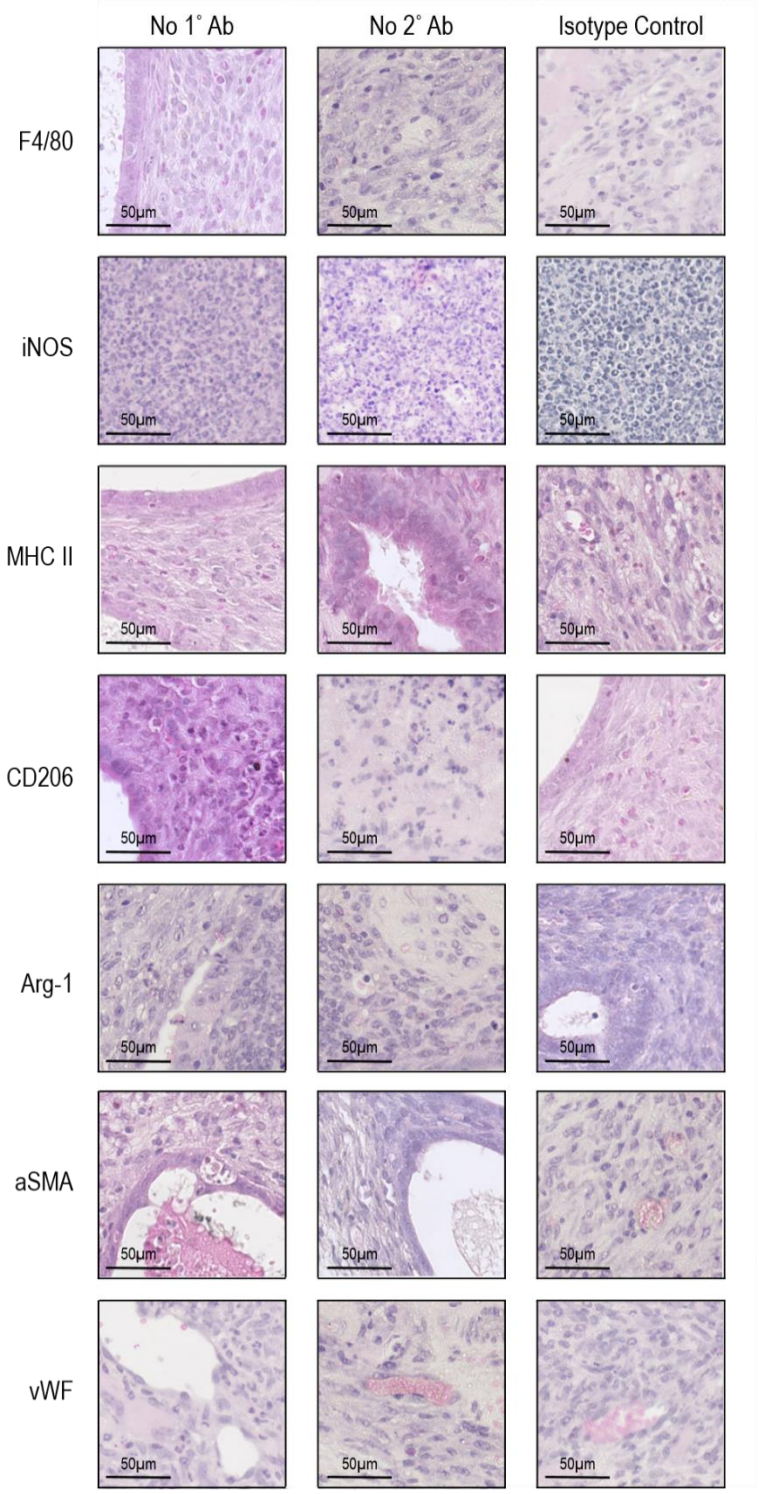

Figure 7.1 Control sections from immunohistochemistry staining

The specificity of each primary antibody (1° Ab) used for immunohistochemical staining was assessed by substituting the primary antibody with a serum-only control (no 1° Ab) or an isotype-matched control (Isotype Control). To assess the specificity of the secondary antibody (2° Ab), the secondary antibody was substituted with a serum-only control (no 2° Ab).

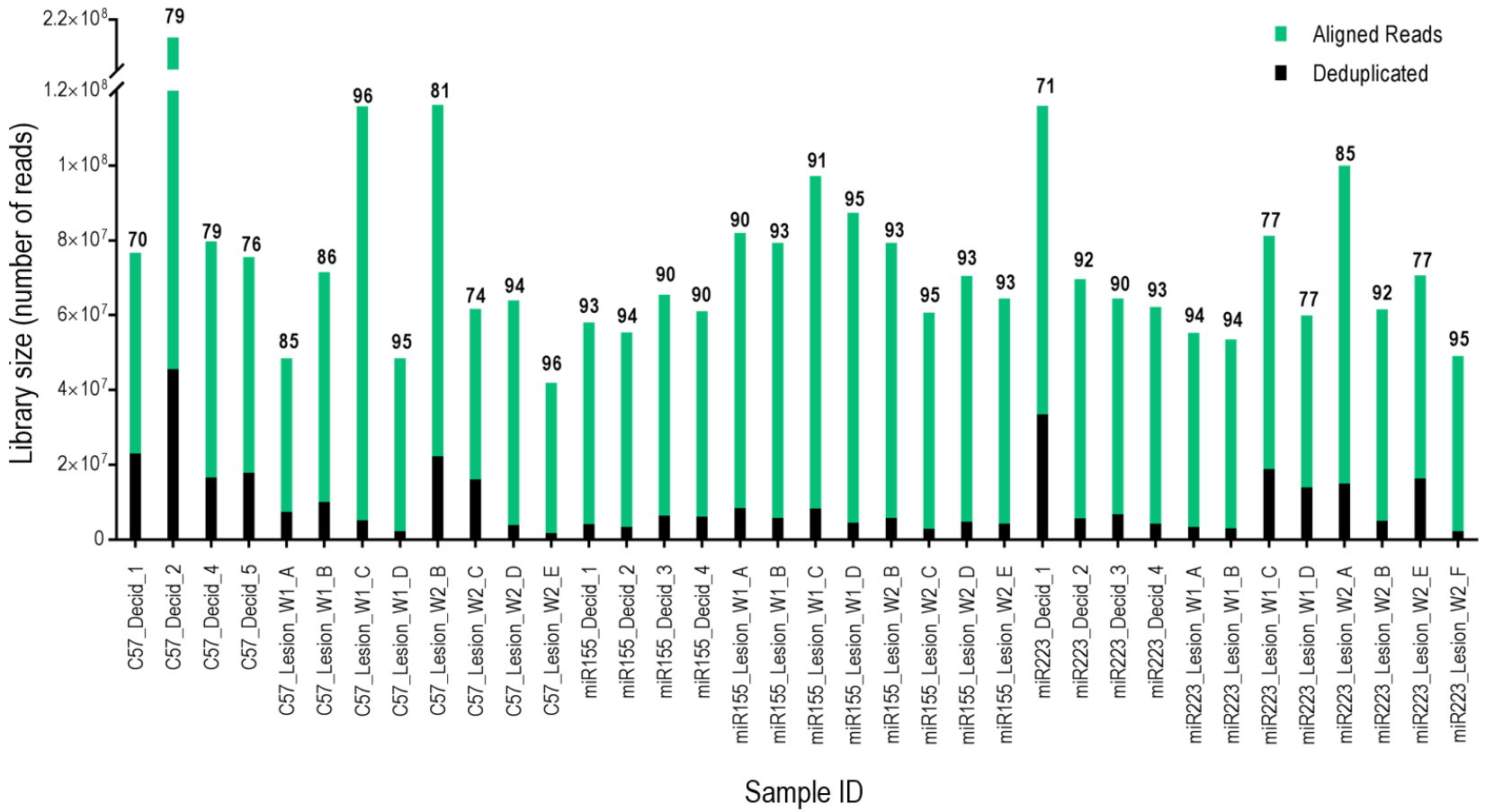

Figure 7.2 RNA-Sequencing library size

Donor decidualised endometrial tissue, D7 and D14 lesions (4 biological replicates each from C57, *miR-155*$^{-/-}$ and *miR-223*$^{-/-}$ mice) were sequenced on the Illumina Next-Seq 500 platform to obtain paired-end reads for mRNA expression. Green bars represent the total library size following alignment to the mouse reference genome. Black bars represent the library size following deduplication (removal of optical duplicates). Numbers above bars represent the percentage of clonal duplication within each sample.

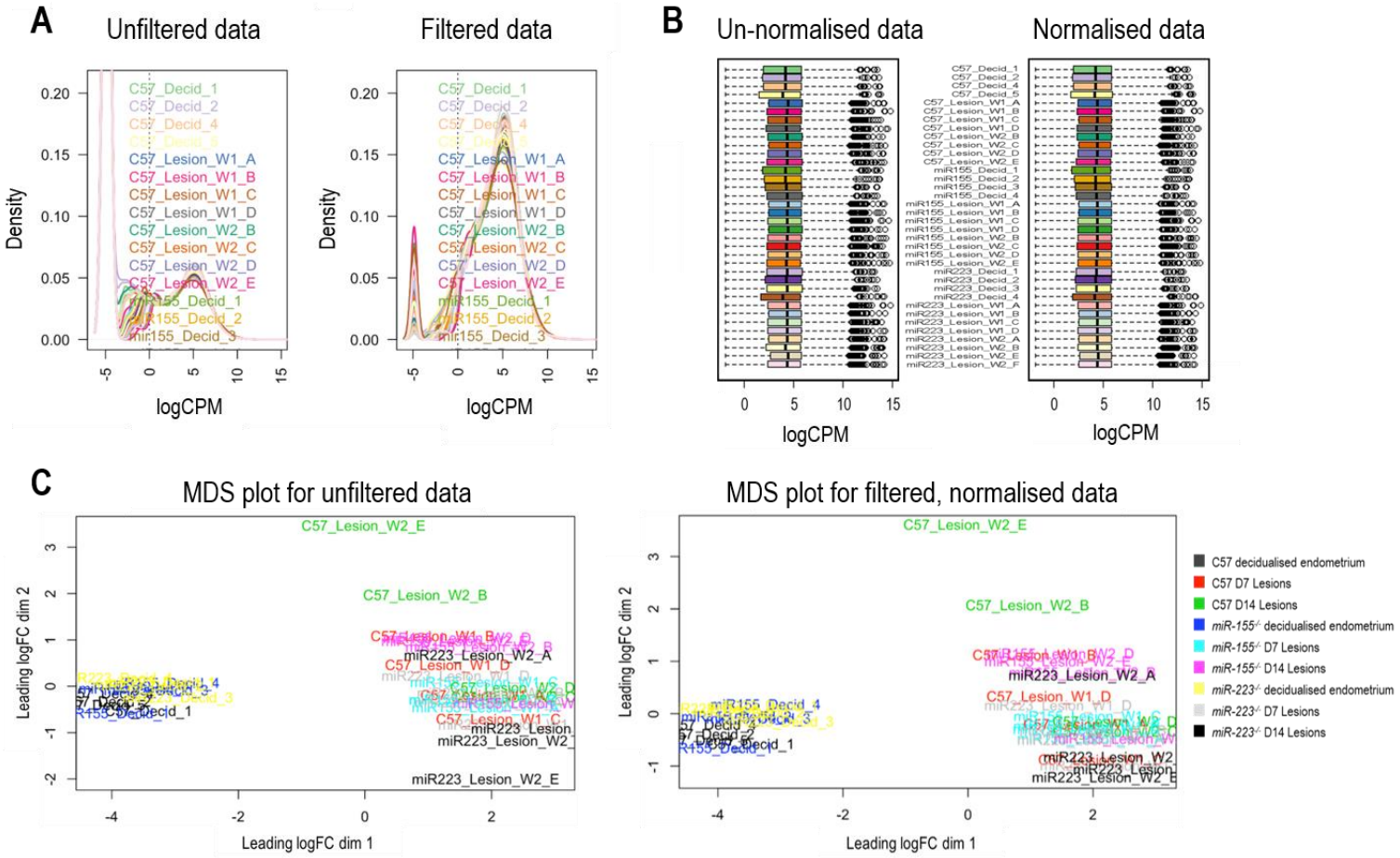

Figure 7.3 **Filtering and normalisation of RNA-Seq data**

The deduplicated RNA-Seq dataset was filtered to remove low expressed genes (CPM >1 in more than 12 samples) (**A**). Box plots show normalisation of the filtered data, which was carried out using the weighted trimmed mean of M-values to rescale read counts in different samples to comparable levels (**B**). A multi dimension scaling plot (MDS) was created to observe data clustering patterns among the different samples, wherein decidualised endometrial tissue samples cluster independently of lesion samples (**C**).

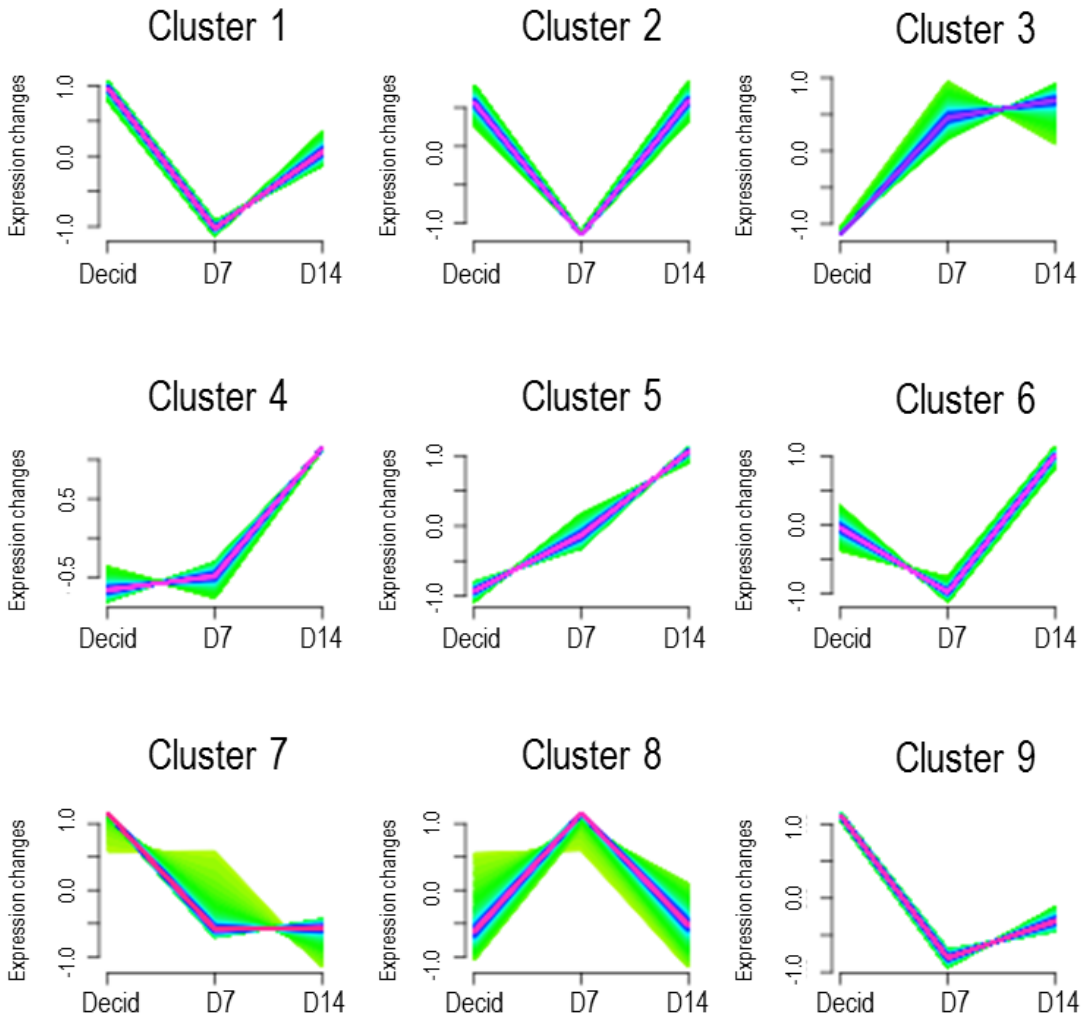

Figure 7.4 Patterns of gene clustering during lesion development in C57 mice

Computational analyses detected nine clusters of gene expression profiles in C57 samples from the RNA-Seq dataset. Further analysis of each gene cluster was performed to identify KEGG pathways associated with each expression pattern (Table 7.1).The total of number of genes assessed was 16, 291 genes.

Table 7.1 Top 25 KEGG Pathways identified from nine gene expression clusters during lesion development in C57 mice

C57 Cluster 1		C57 Cluster 2		C57 Cluster 3	
KEGG Pathway	***P* Value**	**KEGG Pathway**	***P* Value**	**KEGG Pathway**	***P* Value**
Ribosome	5.04×10^{-7}	Osteoclast differentiation	2.02×10^{-9}	Lysosome	3.70×10^{-10}
Nucleotide excision repair	3.02×10^{-6}	Phagosome	1.15×10^{-8}	Metabolic pathways	7.21×10^{-5}
Basal transcription factors	1.69×10^{-5}	Cytokine-cytokine receptor interaction	1.49×10^{-8}	SNARE interactions in vesicular transport	1.05×10^{-4}
Protein processing in endoplasmic reticulum	1.59×10^{-4}	Chemokine signalling pathway	6.60×10^{-8}	Glycosaminoglycan degradation	2.98×10^{-4}
Ubiquitin mediated proteolysis	1.60×10^{-4}	Focal adhesion	1.09×10^{-7}	Notch signalling pathway	1.77×10^{-3}
RNA degradation	1.63×10^{-4}	Malaria	7.65×10^{-7}	Inositol phosphate metabolism	1.77×10^{-3}
Spliceosome	1.91×10^{-4}	HTLV-I infection	1.05×10^{-6}	Endocytosis	1.79×10^{-3}
mRNA surveillance pathway	3.38×10^{-4}	Antigen processing and presentation	1.75×10^{-6}	Phosphatidylinositol signalling system	1.95×10^{-3}
Endocytosis	4.09×10^{-4}	Kaposi's sarcoma-associated herpesvirus infection	2.51×10^{-6}	Synaptic vesicle cycle	2.18×10^{-3}
Autophagy – animal	9.11×10^{-4}	Viral myocarditis	4.47×10^{-6}	Glycosylphosphatidylinositol (GPI)-anchor biosynthesis	5.31×10^{-3}
RNA transport	9.82×10^{-4}	TNF signalling pathway	6.63×10^{-6}	Folate biosynthesis	6.33×10^{-3}
Cell cycle	1.22×10^{-3}	Natural killer cell mediated cytotoxicity	7.50×10^{-6}	Sphingolipid metabolism	6.46×10^{-3}
RNA polymerase	1.54×10^{-3}	ECM-receptor interaction	8.07×10^{-6}	Fatty acid metabolism	1.00×10^{-2}
RIG-I-like receptor signalling pathway	1.83×10^{-3}	Human papillomavirus infection	1.62×10^{-5}	Regulation of actin cytoskeleton	1.12×10^{-2}
Mitophagy – animal	2.80×10^{-3}	PI3K-Akt signalling pathway	2.29×10^{-5}	Ferroptosis	1.12×10^{-2}
SNARE interactions in vesicular transport	2.97×10^{-3}	cGMP-PKG signalling pathway	2.72×10^{-5}	Sphingolipid signalling pathway	1.14×10^{-2}
Adherens junction	3.11×10^{-3}	Graft-versus-host disease	2.80×10^{-5}	mTOR signalling pathway	1.21×10^{-2}
Homologous recombination	3.43×10^{-3}	Rheumatoid arthritis	3.30×10^{-5}	Glycosaminoglycan biosynthesis – chondroitin sulphate / dermatan sulphate	1.25×10^{-2}
Pancreatic cancer	4.48×10^{-3}	Melanoma	4.35×10^{-5}	Valine, leucine and isoleucine degradation	1.48×10^{-2}
NOD-like receptor signalling pathway	4.93×10^{-3}	NF-kappa B signalling pathway	4.93×10^{-5}	VEGF signalling pathway	1.77×10^{-2}
Circadian rhythm	8.11×10^{-3}	Platelet activation	5.44×10^{-5}	Pentose and glucoronate interconversions	1.97×10^{-2}
Ras signalling pathway	8.69×10^{-3}	Cellular senescence	5.68×10^{-5}	Amino sugar and nucleotide sugar metabolism	2.56×10^{-2}
Cytosolic DNA-sensing pathway	9.18×10^{-3}	Type I diabetes mellitus	6.69×10^{-5}	Cholesterol metabolism	2.56×10^{-2}
Autophagy – other	9.71×10^{-3}	NOD-like receptor signalling pathway	7.69×10^{-5}	Fatty acid degradation	2.80×10^{-2}
Apoptosis – multiple species	9.71×10^{-3}	Cell adhesion molecules (CAMs)	8.46×10^{-5}	Biosynthesis of unsaturated fatty acids	3.96×10^{-2}

Table 7.1 continued

C57 Cluster 4

KEGG Pathway	*P* Value
Adrenergic signalling in cardiomyocytes	2.28×10^{-9}
Cardiac muscle contraction	6.03×10^{-9}
Hypertrophic cardiomyopathy (HCM)	1.98×10^{-8}
Calcium signalling pathway	1.81×10^{-7}
Dilated cardiomyopathy (DCM)	2.95×10^{-7}
Tight junction	8.08×10^{-6}
Glucagon signalling pathway	9.45×10^{-6}
Oxytocin signalling pathway	2.94×10^{-5}
Apelin signalling pathway	2.96×10^{-5}
Glycolysis / Gluconeogenesis	5.27×10^{-5}
Malaria	1.03×10^{-4}
Arrhythmogenic right ventricular cardiomyopathy	1.04×10^{-4}
Insulin signalling pathway	1.26×10^{-4}
Proximal tubule bicarbonate reclamation	1.55×10^{-4}
AMPK signalling pathway	4.11×10^{-4}
Adipocytokine signalling pathway	4.22×10^{-4}
African trypanosomiasis	4.26×10^{-4}
PPAR signalling pathway	4.65×10^{-4}
Proteoglycans in cancer	4.67×10^{-4}
Starch and sucrose metabolism	1.60×10^{-3}
Fatty acid biosynthesis	1.72×10^{-3}
Insulin secretion	1.76×10^{-3}
Fructose and mannose metabolism	2.19×10^{-3}
cGMP-PKG signalling pathway	2.50×10^{-3}
IL-17 signalling pathway	2.94×10^{-3}

C57 Cluster 5

KEGG Pathway	*P* Value
Ribosome	2.32×10^{-10}
Vasopressin-regulated water reabsorption	6.84×10^{-6}
Neurotrophin signalling pathway	1.24×10^{-4}
Lysosome	4.08×10^{-3}
Bacterial invasion of epithelial cells	4.92×10^{-3}
Autophagy – other	4.92×10^{-3}
Endocytosis	5.38×10^{-3}
SNARE interactions in vesicular transport	5.76×10^{-3}
Glycosphingolipid biosynthesis – ganglio series	5.77×10^{-3}
Sulphur relay system	6.05×10^{-3}
Autophagy – animal	6.22×10^{-3}
Lipoic acid metabolism	7.50×10^{-3}
Purine metabolism	9.07×10^{-3}
Peroxisome	9.93×10^{-3}
Amino sugar and nucleotide sugar metabolism	1.14×10^{-2}
Other glycan degradation	1.15×10^{-2}
Pancreatic cancer	1.34×10^{-2}
Salmonella infection	1.71×10^{-2}
Chronic myeloid leukaemia	1.71×10^{-2}
Small cell lung cancer	1.81×10^{-2}
RIG-I-like receptor signalling pathway	2.15×10^{-2}
Pathways in cancer	2.26×10^{-2}
mTOR signalling pathway	2.37×10^{-2}
Glycosaminoglycan biosynthesis – heparan sulphate / heparin	3.13×10^{-2}
Pyrimidine metabolism	3.24×10^{-2}

C57 Cluster 6

KEGG Pathway	*P* Value
Protein processing in endoplasmic reticulum	1.35×10^{-19}
RNA transport	4.52×10^{-12}
Spliceosome	4.31×10^{-10}
Proteasome	6.50×10^{-9}
RNA degradation	9.67×10^{-7}
Terpenoid backbone biosynthesis	1.83×10^{-6}
Ribosome biogenesis in eukaryotes	1.44×10^{-5}
Endometrial cancer	4.61×10^{-5}
Breast cancer	2.44×10^{-4}
N-Glycan biosynthesis	3.59×10^{-4}
Hepatocellular carcinoma	8.02×10^{-4}
Cell cycle	8.48×10^{-4}
Protein export	1.11×10^{-3}
Thyroid cancer	1.46×10^{-3}
ErbB signalling pathway	1.68×10^{-3}
Gastric cancer	1.71×10^{-3}
Chronic myeloid leukaemia	1.72×10^{-3}
Ubiquitin mediated proteolysis	2.05×10^{-3}
Homologous recombination	3.34×10^{-3}
Autophagy – animal	3.64×10^{-3}
Amino sugar and nucleotide sugar metabolism	4.26×10^{-3}
Notch signalling pathway	4.26×10^{-3}
Valine, leucine and isoleucine degradation	4.33×10^{-3}
Endocrine resistance	4.51×10^{-3}
Glioma	4.77×10^{-3}

Table 7.1 continued

C57 Cluster 7

C57 Cluster 8

C57 Cluster 9

KEGG Pathway	*P* Value	KEGG Pathway	*P* Value	KEGG Pathway	*P* Value
Lysosome	2.63×10^{-10}	Spliceosome	2.03×10^{-14}	Metabolic pathways	3.15×10^{-21}
Intestinal immune network for IgA production	9.18×10^{-9}	mRNA surveillance pathway	4.49×10^{-8}	Oxidative phosphorylation	1.99×10^{-20}
Pathways in cancer	2.52×10^{-8}	Ubiquitin mediated proteolysis	4.75×10^{-8}	Parkinson's disease	1.89×10^{-19}
Staphylococcus aureus infection	3.91×10^{-8}	AMPK signalling pathway	1.45×10^{-5}	Alzheimer's disease	5.38×10^{-19}
Cytokine-cytokine receptor interaction	7.19×10^{-8}	Protein processing in endoplasmic reticulum	6.07×10^{-5}	Huntington's disease	7.51×10^{-16}
Hematopoietic cell lineage	2.18×10^{-7}	Autophagy – animal	7.24×10^{-5}	Carbon metabolism	3.66×10^{-15}
Pertussis	3.83×10^{-6}	Herpes simplex infection	7.64×10^{-5}	Citrate cycle (TCA cycle)	1.02×10^{-13}
NOD-like receptor signalling pathway	6.56×10^{-6}	Oocyte meiosis	7.77×10^{-5}	Non-alcoholic fatty liver disease (NAFLD)	4.06×10^{-11}
Inflammatory bowel disease (IBD)	8.67×10^{-6}	Cell cycle	8.65×10^{-5}	Pyruvate metabolism	4.86×10^{-7}
Phospholipase D signalling pathway	9.83×10^{-6}	HTLV-I infection	8.85×10^{-5}	Biosynthesis of amino acids	6.07×10^{-7}
Leishmaniosis	1.21×10^{-5}	Ribosome	8.88×10^{-5}	Cell cycle	3.20×10^{-6}
Rheumatoid arthritis	1.87×10^{-5}	Mitophagy – animal	9.88×10^{-5}	DNA replication	5.29×10^{-6}
Tuberculosis	2.19×10^{-5}	Endocytosis	1.33×10^{-4}	2-Oxocarboxylic acid metabolism	6.16×10^{-6}
Chemokine signalling pathway	2.21×10^{-5}	RNA polymerase	1.82×10^{-4}	Retrograde endocannabinoid signalling	7.13×10^{-5}
Th17 cell differentiation	3.82×10^{-5}	Hippo signalling pathway	2.19×10^{-4}	Fanconi anaemia pathway	1.64×10^{-4}
Primary immunodeficiency	6.76×10^{-5}	Basal transcription factors	3.56×10^{-4}	Propanoate metabolism	1.96×10^{-4}
Relaxin signalling pathway	8.07×10^{-5}	Hedgehog signalling pathway	3.56×10^{-4}	Mismatch repair	2.17×10^{-4}
AGE-RAGE signalling pathway in diabetic complications	8.94×10^{-5}	RNA transport	3.82×10^{-4}	Pyrimidine metabolism	2.67×10^{-4}
Chagas disease (American trypanosomiasis)	1.03×10^{-4}	Sphingolipid signalling pathway	1.12×10^{-3}	Glycosylate and dicarboxylate metabolism	4.99×10^{-4}
Osteoclast differentiation	1.53×10^{-4}	Epstein-Barr virus infection	1.13×10^{-3}	Cysteine and methionine metabolism	1.05×10^{-3}
Morphine addiction	2.65×10^{-4}	Nucleotide excision repair	1.37×10^{-3}	HIF-1 signalling pathway	1.36×10^{-3}
Influenza A	2.94×10^{-4}	Autophagy – other	1.52×10^{-3}	Amoebiasis	3.15×10^{-3}
Natural killer cell mediated cytotoxicity	3.36×10^{-4}	Adherens junction	1.54×10^{-3}	MAPK signalling pathway	3.58×10^{-3}
NF-kappa B signalling pathway	4.53×10^{-4}	Lysine degradation	1.83×10^{-3}	Alanine, aspartate and glutamate metabolism	3.97×10^{-3}
Viral myocarditis	4.56×10^{-4}	Longevity regulating pathway	2.39×10^{-3}	Oocyte meiosis	4.44×10^{-3}

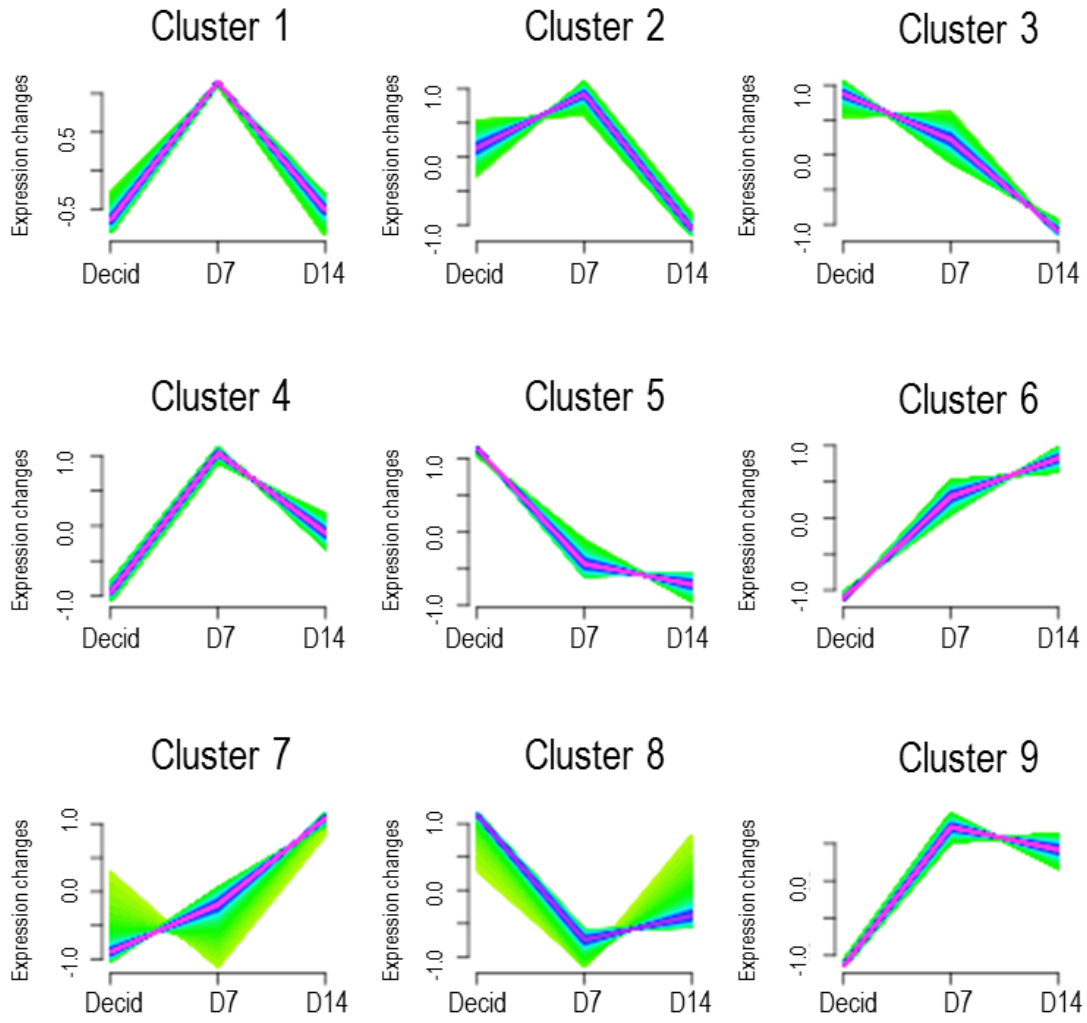

Figure 7.5 Patterns of gene clustering during lesion development in *miR-155*$^{-/-}$ mice

Computational analyses detected nine clusters of gene expression profiles in *miR-155*$^{-/-}$ samples from the RNA-Seq dataset. Further analysis of each gene cluster was performed to identify KEGG pathways associated with each expression pattern (Table 7.2).The total of number of genes assessed was 16, 291 genes.

Table 7.2 Top 25 KEGG Pathways identified from nine gene expression clusters during lesion development in *miR-155*$^{-/-}$ mice

***miR-155*$^{-/-}$ Cluster 1**		***miR-155*$^{-/-}$ Cluster 2**		***miR-155*$^{-/-}$ Cluster 3**	
Pathway	***P* Value**	**Pathway**	***P* Value**	**Pathway**	***P* Value**
Endocytosis	1.14×10^{-8}	Lysosome	6.51×10^{-16}	Spliceosome	8.93×10^{-10}
Lysosome	2.42×10^{-8}	Other glycan degradation	5.11×10^{-5}	Proteasome	3.41×10^{-9}
Fc gamma R-mediated phagocytosis	4.19×10^{-8}	Natural killer cell mediated cytotoxicity	7.85×10^{-5}	Citrate cycle (TCA cycle)	6.58×10^{-8}
Phospholipase D signalling pathway	4.03×10^{-7}	Th17 cell differentiation	1.20×10^{-4}	Cell cycle	7.68×10^{-7}
HTLV-I infection	2.02×10^{-6}	Ferroptosis	1.24×10^{-4}	RNA degradation	2.27×10^{-6}
Longevity regulating pathway	5.73×10^{-6}	Glycosaminoglycan degradation	1.59×10^{-4}	RNA transport	2.62×10^{-6}
B cell receptor signalling pathway	9.56×10^{-6}	Staphylococcus aureus infection	2.27×10^{-4}	Metabolic pathways	1.06×10^{-5}
Chemokine signalling pathway	1.05×10^{-5}	Thyroid cancer	1.39×10^{-3}	Carbon metabolism	1.76×10^{-5}
Antigen processing and presentation	2.46×10^{-5}	Hepatocellular carcinoma	1.40×10^{-3}	Protein processing in endoplasmic reticulum	5.56×10^{-5}
Tuberculosis	2.63×10^{-5}	Transcriptional misregulation in cancer	1.55×10^{-3}	Aminoacyl-tRNA biosynthesis	1.19×10^{-4}
Phagosome	4.11×10^{-5}	Leishmaniosis	2.12×10^{-3}	Protein export	1.21×10^{-4}
Bacterial invasion of epithelial cells	7.83×10^{-5}	Cholesterol metabolism	2.39×10^{-3}	Epstein-Barr virus infection	2.09×10^{-4}
Autophagy - animal	8.23×10^{-5}	Malaria	2.39×10^{-3}	Cellular senescence	3.69×10^{-4}
Viral myocarditis	1.66×10^{-4}	Adherens junction	3.79×10^{-3}	Purine metabolism	4.43×10^{-4}
Herpes simplex infection	1.91×10^{-4}	Rheumatoid arthritis	4.05×10^{-3}	Basal transcription factors	6.21×10^{-4}
Pathways in cancer	2.13×10^{-4}	Mitophagy – animal	4.28×10^{-3}	Huntington's disease	7.11×10^{-4}
Rheumatoid arthritis	2.46×10^{-4}	Focal adhesion	4.43×10^{-3}	Ribosome biogenesis in eukaryotes	8.50×10^{-4}
Choline metabolism in cancer	2.65×10^{-4}	Osteoclast differentiation	4.44×10^{-3}	Fanconi anaemia pathway	2.07×10^{-3}
Intestinal immune network for IgA production	4.20×10^{-4}	Hematopoietic cell lineage	4.60×10^{-3}	mRNA surveillance pathway	2.09×10^{-3}
Allograft rejection	4.22×10^{-4}	Autophagy – animal	5.17×10^{-3}	RNA polymerase	3.47×10^{-3}
Glycosylphosphatidylinositol (GPI)-anchor biosynthesis	5.07×10^{-4}	Pertussis	5.21×10^{-3}	Alzheimer's disease	4.00×10^{-3}
Apelin signalling pathway	6.05×10^{-4}	Gastric cancer	5.42×10^{-3}	Colorectal cancer	4.15×10^{-3}
Colorectal cancer	6.31×10^{-4}	Phosphatidylinositol signalling system	6.00×10^{-3}	Oocyte meiosis	5.44×10^{-3}
Leishmaniosis	6.90×10^{-4}	Pathways in cancer	6.11×10^{-3}	Homologous recombination	5.87×10^{-3}
Platelet activation	7.55×10^{-4}	Chronic myeloid leukaemia	7.03×10^{-3}	Pyrimidine metabolism	8.62×10^{-3}

Table 7.2 continued

***miR-155*$^{-/-}$ Cluster 4**		***miR-155*$^{-/-}$ Cluster 5**		***miR-155*$^{-/-}$ Cluster 6**	
Pathway	***P* Value**	**Pathway**	***P* Value**	**Pathway**	***P* Value**
TNF signalling pathway	5.63×10^{-8}	Oxidative phosphorylation	3.03×10^{-10}	Ribosome	9.93×10^{-8}
Neurotrophin signalling pathway	7.29×10^{-7}	Huntington's disease	5.38×10^{-10}	Insulin signalling pathway	2.28×10^{-5}
Osteoclast differentiation	2.42×10^{-6}	Parkinson's disease	8.36×10^{-9}	Non-alcoholic fatty liver disease (NAFLD)	3.17×10^{-5}
Kaposi's sarcoma-associated herpesvirus infection	5.22×10^{-6}	Alzheimer's disease	2.43×10^{-7}	Alzheimer's disease	3.49×10^{-5}
Rap1 signalling pathway	2.01×10^{-5}	Ribosome	3.16×10^{-7}	Glucagon signalling pathway	4.62×10^{-5}
Other types of O-glycan biosynthesis	4.05×10^{-5}	Ubiquitin mediated proteolysis	3.09×10^{-6}	Measles	8.71×10^{-5}
Ras signalling pathway	4.32×10^{-5}	Non-alcoholic fatty liver disease (NAFLD)	3.97×10^{-6}	Fructose and mannose metabolism	1.14×10^{-4}
NOD-like receptor signalling pathway	7.19×10^{-5}	Protein processing in endoplasmic reticulum	2.30×10^{-5}	NOD-like receptor signalling pathway	2.30×10^{-4}
Salmonella infection	7.25×10^{-5}	RNA transport	7.12×10^{-5}	Parkinson's disease	2.30×10^{-4}
T cell receptor signalling pathway	1.28×10^{-4}	RNA polymerase	8.11×10^{-5}	Hypertrophic cardiomyopathy (HCM)	2.43×10^{-4}
GnRH signalling pathway	1.41×10^{-4}	Metabolic pathways	2.27×10^{-4}	Huntington's disease	2.64×10^{-4}
Toll-like receptor signalling pathway	2.11×10^{-4}	Cell cycle	3.82×10^{-4}	Cardiac muscle contraction	2.90×10^{-4}
Tuberculosis	2.11×10^{-4}	Epstein-Barr virus infection	4.58×10^{-4}	Dilated cardiomyopathy (DCM)	5.13×10^{-4}
Sphingolipid signalling pathway	2.16×10^{-4}	Renal cell carcinoma	1.47×10^{-3}	Influenza A	5.29×10^{-4}
Insulin resistance	2.95×10^{-4}	Spliceosome	2.33×10^{-3}	Ubiquitin mediated proteolysis	8.60×10^{-4}
Fc gamma R-mediated phagocytosis	3.17×10^{-4}	Pyruvate metabolism	2.61×10^{-3}	Hepatitis C	1.07×10^{-3}
Endocytosis	3.57×10^{-4}	Cysteine and methionine metabolism	3.33×10^{-3}	Pentose phosphate pathway	1.18×10^{-3}
Pathways in cancer	4.58×10^{-4}	Pyrimidine metabolism	5.54×10^{-3}	Glycolysis / Gluconeogenesis	1.51×10^{-3}
MAPK signalling pathway	5.19×10^{-4}	Cardiac muscle contraction	1.16×10^{-2}	Herpes simplex infection	1.62×10^{-3}
Autophagy - animal	5.60×10^{-4}	Malaria	1.29×10^{-2}	Apelin signalling pathway	1.78×10^{-3}
Small cell lung cancer	6.45×10^{-4}	Homologous recombination	1.54×10^{-2}	Peroxisome	2.00×10^{-3}
AGE-RAGE signalling pathway in diabetic complications	6.75×10^{-4}	Ribosome biogenesis in eukaryotes	1.80×10^{-2}	Transcriptional misregulation in cancer	2.05×10^{-3}
Phagosome	6.98×10^{-4}	Oocyte meiosis	1.80×10^{-2}	MAPK signalling pathway	2.41×10^{-3}
Dopaminergic synapse	8.67×10^{-4}	Nucleotide excision repair	2.22×10^{-2}	Oxidative phosphorylation	2.46×10^{-3}
Glycosaminoglycan biosynthesis - chondroitin sulphate / dermatan sulphate	9.14×10^{-4}	Biosynthesis of amino acids	2.68×10^{-2}	cGMP-PKG signalling pathway	2.47×10^{-3}

Table 7.2 continued

***miR-155*$^{-/-}$ Cluster 7**		***miR-155*$^{-/-}$ Cluster 8**		***miR-155*$^{-/-}$ Cluster 9**	
Pathway	***P* Value**	**Pathway**	***P* Value**	**Pathway**	***P* Value**
cGMP-PKG signalling pathway	1.59×10^{-4}	RNA transport	2.89×10^{-12}	Tight junction	1.31×10^{-5}
Basal cell carcinoma	4.83×10^{-4}	DNA replication	3.47×10^{-10}	Basal cell carcinoma	1.61×10^{-5}
Rheumatoid arthritis	9.45×10^{-4}	Cell cycle	1.26×10^{-9}	Hippo signalling pathway	4.63×10^{-5}
Vascular smooth muscle contraction	2.97×10^{-3}	Spliceosome	1.15×10^{-7}	Axon guidance	8.61×10^{-5}
cAMP signalling pathway	6.50×10^{-3}	Protein processing in endoplasmic reticulum	1.27×10^{-7}	Rap1 signalling pathway	3.24×10^{-4}
Base excision repair	8.88×10^{-3}	Fanconi anaemia pathway	7.17×10^{-6}	Pathways in cancer	4.29×10^{-4}
Neuroactive ligand-receptor interaction	9.64×10^{-3}	Protein export	2.31×10^{-5}	Signalling pathways regulating pluripotency of stem cells	6.24×10^{-4}
Amphetamine addiction	1.27×10^{-2}	Pyrimidine metabolism	6.64×10^{-5}	Steroid biosynthesis	7.05×10^{-4}
Axon guidance	1.32×10^{-2}	Mismatch repair	7.63×10^{-5}	Proteoglycans in cancer	7.80×10^{-4}
Glycosaminoglycan biosynthesis - keratin sulphate	1.36×10^{-2}	Homologous recombination	8.70×10^{-5}	Melanogenesis	8.18×10^{-4}
Fluid shear stress and atherosclerosis	1.64×10^{-2}	Terpenoid backbone biosynthesis	1.10×10^{-4}	Histidine metabolism	8.65×10^{-4}
TNF signalling pathway	1.87×10^{-2}	Nucleotide excision repair	1.74×10^{-4}	EGFR tyrosine kinase inhibitor resistance	3.21×10^{-3}
IL-17 signalling pathway	1.94×10^{-2}	Ribosome biogenesis in eukaryotes	4.37×10^{-4}	Endocytosis	3.24×10^{-3}
Wnt signalling pathway	1.98×10^{-2}	N-Glycan biosynthesis	4.79×10^{-4}	PI3K-Akt signalling pathway	3.39×10^{-3}
Hepatocellular carcinoma	2.43×10^{-2}	mRNA surveillance pathway	1.00×10^{-3}	Wnt signalling pathway	3.41×10^{-3}
Long-term depression	2.50×10^{-2}	Propanoate metabolism	1.07×10^{-3}	Protein digestion and absorption	4.14×10^{-3}
Synaptic vesicle cycle	2.69×10^{-2}	Oocyte meiosis	1.18×10^{-3}	Human papillomavirus infection	4.33×10^{-3}
Hippo signalling pathway	2.81×10^{-2}	Prostate cancer	3.05×10^{-3}	Regulation of actin cytoskeleton	5.49×10^{-3}
ABC transporters	2.93×10^{-2}	Adherens junction	4.14×10^{-3}	TGF-beta signalling pathway	5.80×10^{-3}
Sphingolipid metabolism	3.18×10^{-2}	Valine, leucine and isoleucine degradation	5.19×10^{-3}	cAMP signalling pathway	1.09×10^{-2}
AGE-RAGE signalling pathway in diabetic complications	3.21×10^{-2}	Carbon metabolism	9.78×10^{-3}	ECM-receptor interaction	1.12×10^{-2}
HTLV-I infection	3.33×10^{-2}	Base excision repair	9.88×10^{-3}	Glycerolipid metabolism	1.45×10^{-2}
Prion diseases	3.60×10^{-2}	Metabolic pathways	1.18×10^{-2}	Complement and coagulation cascades	1.67×10^{-2}
NF-kappa B signalling pathway	3.92×10^{-2}	RNA degradation	1.29×10^{-2}	Glycine, serine and threonine metabolism	1.94×10^{-2}
Platelet activation	4.09×10^{-2}	Glycosylate and dicarboxylate metabolism	1.40×10^{-2}	MAPK signalling pathway	1.96×10^{-2}

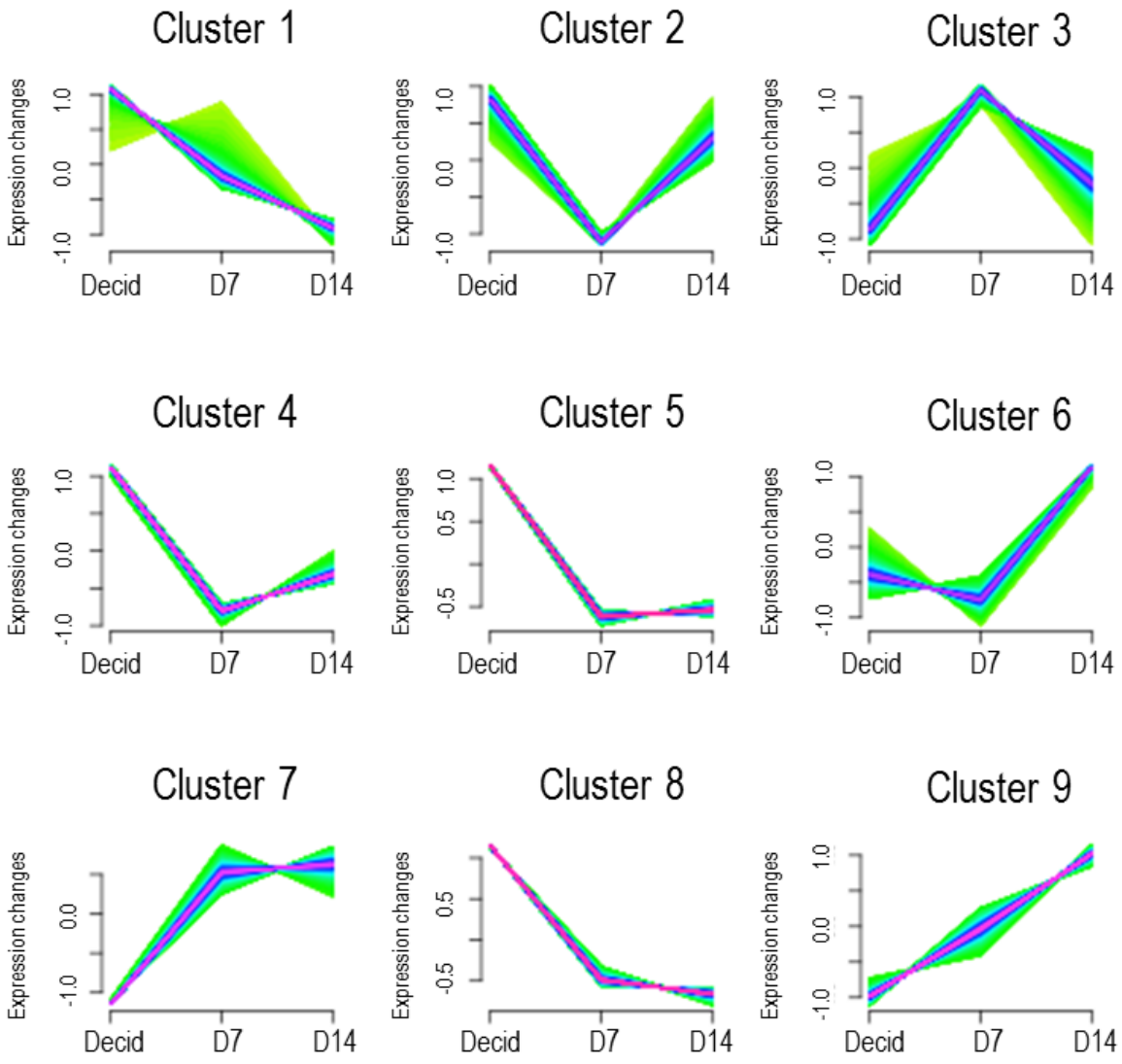

Figure 7.6 Patterns of gene clustering during lesion development in *miR-223*$^{-/-}$ mice

Computational analyses detected nine clusters of gene expression profiles in *miR-223*$^{-/-}$ samples from the RNA-Seq dataset. Further analysis of each gene cluster was performed to identify KEGG pathways associated with each expression pattern (Table 7.3).The total of number of genes assessed was 16, 291 genes.

Table 7.3 Top 25 KEGG Pathways identified from nine gene expression clusters during lesion development in *miR-223*$^{-/-}$ mice

***miR-223*$^{-/-}$ Cluster 1**		***miR-223*$^{-/-}$ Cluster 2**		***miR-223*$^{-/-}$ Cluster 3**	
Pathway	***P* Value**	**Pathway**	***P* Value**	**Pathway**	***P* Value**
Cell cycle	8.53×10^{-16}	Dilated cardiomyopathy (DCM)	6.92×10^{-8}	Lysosome	6.13×10^{-6}
Protein processing in endoplasmic reticulum	7.26×10^{-14}	Chemokine signalling pathway	1.82×10^{-7}	Hepatocellular carcinoma	5.89×10^{-5}
Ubiquitin mediated proteolysis	1.89×10^{-11}	Oxytocin signalling pathway	3.42×10^{-7}	Metabolic pathways	3.13×10^{-4}
Spliceosome	1.25×10^{-10}	Adrenergic signalling in cardiomyocytes	6.69×10^{-7}	Glutathione metabolism	5.76×10^{-4}
RNA transport	3.76×10^{-7}	Cytokine-cytokine receptor interaction	1.66×10^{-6}	Pathways in cancer	1.00×10^{-3}
Ribosome	8.99×10^{-7}	NOD-like receptor signalling pathway	1.85×10^{-6}	mTOR signalling pathway	1.01×10^{-3}
DNA replication	2.28×10^{-6}	Platelet activation	1.09×10^{-5}	Fatty acid elongation	1.47×10^{-3}
Protein export	7.33×10^{-6}	Apelin signalling pathway	1.50×10^{-5}	Basal cell carcinoma	2.90×10^{-3}
Pyrimidine metabolism	2.27×10^{-5}	Hypertrophic cardiomyopathy (HCM)	2.14×10^{-5}	Fatty acid metabolism	3.07×10^{-3}
Nucleotide excision repair	7.40×10^{-5}	Cardiac muscle contraction	4.22×10^{-5}	Sulphur relay system	5.12×10^{-3}
Small cell lung cancer	7.99×10^{-5}	Osteoclast differentiation	6.14×10^{-5}	Biotin metabolism	6.66×10^{-3}
TGF-beta signalling pathway	1.51×10^{-4}	Staphylococcus aureus infection	9.39×10^{-5}	Biosynthesis of unsaturated fatty acids	9.75×10^{-3}
Mismatch repair	2.02×10^{-4}	Fc gamma R-mediated phagocytosis	1.35×10^{-4}	Platinum drug resistance	1.01×10^{-2}
Hippo signalling pathway - multiple species	2.12×10^{-4}	HTLV-I infection	1.83×10^{-4}	Insulin resistance	1.51×10^{-2}
p53 signalling pathway	2.33×10^{-4}	Gastric acid secretion	4.60×10^{-4}	Gastric cancer	1.57×10^{-2}
Base excision repair	2.73×10^{-4}	Phagosome	5.76×10^{-4}	Glycosaminoglycan degradation	1.63×10^{-2}
Huntington's disease	2.76×10^{-4}	cGMP-PKG signalling pathway	5.87×10^{-4}	Valine, leucine and isoleucine degradation	1.69×10^{-2}
Oocyte meiosis	3.37×10^{-4}	Intestinal immune network for IgA production	5.98×10^{-4}	Insulin signalling pathway	1.76×10^{-2}
Homologous recombination	4.41×10^{-4}	Relaxin signalling pathway	8.35×10^{-4}	Peroxisome	1.87×10^{-2}
Adherens junction	6.61×10^{-4}	Legionellosis	1.09×10^{-3}	beta-Alanine metabolism	1.94×10^{-2}
RNA degradation	7.33×10^{-4}	Rheumatoid arthritis	1.23×10^{-3}	Vascular smooth muscle contraction	2.07×10^{-2}
Cellular senescence	8.40×10^{-4}	Malaria	1.47×10^{-3}	B cell receptor signalling pathway	2.13×10^{-2}
Fanconi anaemia pathway	1.62×10^{-3}	Calcium signalling pathway	1.59×10^{-3}	ABC transporters	2.38×10^{-2}
Ribosome biogenesis in eukaryotes	1.70×10^{-3}	Toll-like receptor signalling pathway	1.66×10^{-3}	Cysteine and methionine metabolism	2.62×10^{-2}
Progesterone-mediated oocyte maturation	2.30×10^{-3}	Cell adhesion molecules (CAMs)	1.67×10^{-3}	Carbon metabolism	2.87×10^{-2}

Table 7.3 continued

***miR-223*$^{-/-}$ Cluster 4**		***miR-223*$^{-/-}$ Cluster 5**		***miR-223*$^{-/-}$ Cluster 6**	
Pathway	***P* Value**	**Pathway**	***P* Value**	**Pathway**	***P* Value**
Other glycan degradation	1.58×10^{-5}	Antigen processing and presentation	3.66×10^{-13}	Pathways in cancer	1.41×10^{-5}
Lysosome	2.04×10^{-4}	Viral myocarditis	1.13×10^{-12}	Proteoglycans in cancer	4.34×10^{-4}
Glycosaminoglycan degradation	4.85×10^{-4}	Lysosome	1.82×10^{-10}	Small cell lung cancer	4.65×10^{-4}
Phosphatidylinositol signalling system	1.35×10^{-3}	Graft-versus-host disease	2.13×10^{-10}	Signalling pathways regulating pluripotency of stem cells	6.49×10^{-4}
Fluid shear stress and atherosclerosis	2.40×10^{-3}	Natural killer cell mediated cytotoxicity	2.82×10^{-10}	Hippo signalling pathway	2.15×10^{-3}
Pertussis	3.06×10^{-3}	Cell adhesion molecules (CAMs)	1.11×10^{-9}	Ras signalling pathway	2.46×10^{-3}
Propanoate metabolism	3.10×10^{-3}	Allograft rejection	1.20×10^{-9}	Regulation of actin cytoskeleton	4.12×10^{-3}
Glutathione metabolism	3.64×10^{-3}	Hematopoietic cell lineage	1.87×10^{-9}	PI3K-Akt signalling pathway	4.33×10^{-3}
Inositol phosphate metabolism	9.08×10^{-3}	Cytokine-cytokine receptor interaction	5.83×10^{-9}	Breast cancer	4.66×10^{-3}
Pathways in cancer	9.55×10^{-3}	Type I diabetes mellitus	6.38×10^{-9}	Fanconi anaemia pathway	5.31×10^{-3}
Porphyrin and chlorophyll metabolism	1.05×10^{-2}	Staphylococcus aureus infection	1.41×10^{-8}	Cell cycle	6.09×10^{-3}
Inflammatory bowel disease (IBD)	1.24×10^{-2}	Phagosome	1.02×10^{-7}	Ubiquitin mediated proteolysis	6.22×10^{-3}
Focal adhesion	1.39×10^{-2}	Leishmaniosis	1.20×10^{-7}	MAPK signalling pathway	6.31×10^{-3}
Glycosylate and dicarboxylate metabolism	1.41×10^{-2}	Th1 and Th2 cell differentiation	2.84×10^{-7}	p53 signalling pathway	6.98×10^{-3}
Glycerolipid metabolism	1.45×10^{-2}	Autoimmune thyroid disease	2.98×10^{-7}	Leishmaniosis	6.98×10^{-3}
ECM-receptor interaction	1.89×10^{-2}	Primary immunodeficiency	3.51×10^{-7}	Hypertrophic cardiomyopathy (HCM)	8.78×10^{-3}
Metabolism of xenobiotics by cytochrome P450	1.94×10^{-2}	Intestinal immune network for IgA production	4.13×10^{-7}	Focal adhesion	1.01×10^{-2}
NF-kappa B signalling pathway	2.07×10^{-2}	Rheumatoid arthritis	6.55×10^{-7}	Arrhythmogenic right ventricular cardiomyopathy	1.07×10^{-2}
Metabolic pathways	2.20×10^{-2}	Tuberculosis	7.36×10^{-7}	Mineral absorption	1.11×10^{-2}
Aldosterone synthesis and secretion	2.25×10^{-2}	Th17 cell differentiation	8.75×10^{-7}	Dilated cardiomyopathy (DCM)	1.26×10^{-2}
PI3K-Akt signalling pathway	2.43×10^{-2}	Chemokine signalling pathway	1.53×10^{-6}	Base excision repair	1.50×10^{-2}
Amyotrophic lateral sclerosis (ALS)	2.72×10^{-2}	Toxoplasmosis	2.25×10^{-6}	Endocrine resistance	1.65×10^{-2}
Renin secretion	3.04×10^{-2}	Herpes simplex infection	3.90×10^{-6}	Chronic myeloid leukaemia	1.68×10^{-2}
MAPK signalling pathway	3.16×10^{-2}	Asthma	5.15×10^{-6}	Glycosylphosphatidylinositol (GPI)-anchor biosynthesis	1.97×10^{-2}
Thyroid cancer	3.21×10^{-2}	Osteoclast differentiation	9.32×10^{-6}	Non-small cell lung cancer	2.09×10^{-2}

Table 7.3 continued

***miR-223*$^{-/-}$ Cluster 7**		***miR-223*$^{-/-}$ Cluster 8**		***miR-223*$^{-/-}$ Cluster 9**	
Pathway	***P* Value**	**Pathway**	***P* Value**	**Pathway**	***P* Value**
Autophagy - animal	6.55×10^{-9}	Malaria	4.90×10^{-8}	Spliceosome	1.14×10^{-14}
Metabolic pathways	1.36×10^{-7}	Focal adhesion	7.70×10^{-7}	Protein processing in endoplasmic reticulum	7.87×10^{-11}
Peroxisome	1.87×10^{-7}	Proteoglycans in cancer	1.39×10^{-6}	RNA transport	9.65×10^{-10}
Autophagy - other	1.56×10^{-6}	ECM-receptor interaction	3.34×10^{-6}	mRNA surveillance pathway	3.42×10^{-7}
Non-alcoholic fatty liver disease (NAFLD)	8.88×10^{-6}	Hypertrophic cardiomyopathy (HCM)	2.10×10^{-5}	Endocytosis	3.54×10^{-7}
Parkinson's disease	9.66×10^{-4}	Gap junction	2.68×10^{-5}	Metabolic pathways	4.65×10^{-7}
mTOR signalling pathway	1.07×10^{-3}	Dilated cardiomyopathy (DCM)	3.80×10^{-5}	Oxidative phosphorylation	3.56×10^{-6}
Mitophagy – animal	1.15×10^{-3}	TNF signalling pathway	6.13×10^{-5}	Basal transcription factors	4.75×10^{-6}
Oxidative phosphorylation	1.77×10^{-3}	Human papillomavirus infection	1.12×10^{-4}	Ribosome	1.49×10^{-5}
Alzheimer's disease	1.81×10^{-3}	African trypanosomiasis	1.61×10^{-4}	Nucleotide excision repair	2.04×10^{-5}
SNARE interactions in vesicular transport	1.95×10^{-3}	Protein digestion and absorption	1.97×10^{-4}	Alzheimer's disease	2.32×10^{-5}
RIG-I-like receptor signalling pathway	2.49×10^{-3}	PI3K-Akt signalling pathway	3.48×10^{-4}	Proteasome	4.33×10^{-5}
Toll-like receptor signalling pathway	2.84×10^{-3}	Cholinergic synapse	3.87×10^{-4}	Citrate cycle (TCA cycle)	4.74×10^{-5}
Thyroid hormone signalling pathway	2.94×10^{-3}	Adrenergic signalling in cardiomyocytes	4.03×10^{-4}	Huntington's disease	5.15×10^{-5}
Endocytosis	3.44×10^{-3}	Glycosaminoglycan biosynthesis - chondroitin sulphate / dermatan sulphate	4.21×10^{-4}	Terpenoid backbone biosynthesis	7.40×10^{-5}
Amino sugar and nucleotide sugar metabolism	3.49×10^{-3}	Arrhythmogenic right ventricular cardiomyopathy	6.33×10^{-4}	RNA degradation	1.75×10^{-4}
Adipocytokine signalling pathway	3.78×10^{-3}	cAMP signalling pathway	9.37×10^{-4}	RNA polymerase	4.00×10^{-4}
Vasopressin-regulated water reabsorption	4.02×10^{-3}	Osteoclast differentiation	1.19×10^{-3}	Mitophagy – animal	6.22×10^{-4}
NOD-like receptor signalling pathway	4.13×10^{-3}	Wnt signalling pathway	1.21×10^{-3}	Lysine degradation	6.52×10^{-4}
Glycosylphosphatidylinositol (GPI)-anchor biosynthesis	5.24×10^{-3}	Calcium signalling pathway	1.23×10^{-3}	Pyrimidine metabolism	1.06×10^{-3}
Fatty acid metabolism	5.65×10^{-3}	Amphetamine addiction	1.88×10^{-3}	Parkinson's disease	1.17×10^{-3}
HIF-1 signalling pathway	6.01×10^{-3}	MAPK signalling pathway	1.98×10^{-3}	Neurotrophin signalling pathway	1.32×10^{-3}
Phosphatidylinositol signalling system	6.02×10^{-3}	Mucin type O-glycan biosynthesis	2.14×10^{-3}	Non-alcoholic fatty liver disease (NAFLD)	1.56×10^{-3}
FoxO signalling pathway	6.85×10^{-3}	Glucagon signalling pathway	2.16×10^{-3}	Pyruvate metabolism	1.67×10^{-3}
Insulin signalling pathway	7.22×10^{-3}	Apelin signalling pathway	2.41×10^{-3}	Tight junction	1.84×10^{-3}

The additional supplementary material listed below can be found in the attached Microsoft Excel spreadsheet.

SM Table 1: List of DEGs between decidualised endometrium and D7 lesions in C57 mice

SM Table 2: List of DEGs between decidualised endometrium and D14 lesions in C57 mice

SM Table 3: List of DEGs between D7 and D14 lesions in C57 mice

SM Table 4: List of DEGs between decidualised endometrium and D7 lesions in *miR-155*$^{-/-}$ mice

SM Table 5: List of DEGs between decidualised endometrium and D14 lesions in *miR-155*$^{-/-}$ mice

SM Table 6: List of DEGs between D7 and D14 lesions in *miR-155*$^{-/-}$ mice

SM Table 7: List of DEGs in decidualised endometrium between C57 mice and *miR-155*$^{-/-}$ mice

SM Table 8: List of DEGs between decidualised endometrium and D7 lesions in *miR-223*$^{-/-}$ mice

SM Table 9: List of DEGs between decidualised endometrium and D14 lesions in *miR-223*$^{-/-}$ mice

SM Table 10: List of DEGs between D7 and D14 lesions in *miR-223*$^{-/-}$ mice

SM Table 11: List of DEGs in decidualised endometrium between C57 mice and *miR-223*$^{-/-}$ mice

Chapter 8

Bibliography

ABE, W., NASU, K., NAKADA, C., KAWANO, Y., MORIYAMA, M. & NARAHARA, H. 2013. miR-196b targets c-myc and Bcl-2 expression, inhibits proliferation and induces apoptosis in endometriotic stromal cells. *Hum Reprod,* 28**,** 750-61.

ABRÃO, M. S., PODGAEC, S. & FERNANDES, L. F. C. 2012. Surgical Therapies: Pouch of Douglas and Uterovaginal Pouch Resection for Endometriosis. *Endometriosis.* Wiley-Blackwell.

ACIEN, P. & VELASCO, I. 2013. Endometriosis: a disease that remains enigmatic. *ISRN Obstet Gynecol,* 2013**,** 242149.

ADAMMEK, M., GREVE, B., KASSENS, N., SCHNEIDER, C., BRUGGEMANN, K., SCHURING, A. N., STARZINSKI-POWITZ, A., KIESEL, L. & GOTTE, M. 2013. MicroRNA miR-145 inhibits proliferation, invasiveness, and stem cell phenotype of an in vitro endometriosis model by targeting multiple cytoskeletal elements and pluripotency factors. *Fertil Steril,* 99**,** 1346-1355 e5.

ADAMSON, G. D. 2012. Endometriosis: Disease Classification and Behavior. *Endometriosis.* Wiley-Blackwell.

ADAMSON, G. D. & JOHNSON, N. P. 2018. *Diagnostic biomarkers for endometriosis* [Online]. World Endometriosis Research Foundation. Available: https://endometriosisfoundation.org [Accessed].

AGHAJANOVA, L. & GIUDICE, L. C. 2011. Molecular evidence for differences in endometrium in severe versus mild endometriosis. *Reprod Sci,* 18**,** 229-51.

AHMAD, S. F., MICHAUD, N., RAKHILA, H. & AKOUM, A. 2014. Macrophages in Pathophysiology of Endometriosis. *In:* HARADA, T. (ed.) *Endometriosis: Pathogenesis and Treatment.* Tokyo: Springer Japan.

AHN, S. H., EDWARDS, A. K., SINGH, S. S., YOUNG, S. L., LESSEY, B. A. & TAYADE, C. 2015. IL-17A Contributes to the Pathogenesis of Endometriosis by Triggering Proinflammatory Cytokines and Angiogenic Growth Factors. *J Immunol,* 195**,** 2591-600.

AL-TALIB, A. & TULANDI, T. 2012. Surgical Historical Overview. *Endometriosis.* Wiley-Blackwell.

ALBRACHT, S. P., MEIJER, A. J. & RYDSTROM, J. 2011. Mammalian NADH:ubiquinone oxidoreductase (Complex I) and nicotinamide nucleotide transhydrogenase (Nnt) together regulate the mitochondrial production of H(2)O(2)--implications for their role in disease, especially cancer. *J Bioenerg Biomembr,* 43**,** 541-64.

ALEXANDRE-SILVA, G. M., BRITO-SOUZA, P. A., OLIVEIRA, A. C. S., CERNI, F. A., ZOTTICH, U. & PUCCA, M. B. 2018. The hygiene hypothesis at a glance: Early exposures, immune mechanism and novel therapies. *Acta Trop,* 188**,** 16-26.

ALIVERNINI, S., GREMESE, E., MCSHARRY, C., TOLUSSO, B., FERRACCIOLI, G., MCINNES, I. B. & KUROWSKA-STOLARSKA, M. 2017. MicroRNA-155-at the Critical Interface of Innate and Adaptive Immunity in Arthritis. *Front Immunol,* 8**,** 1932.

ALVAREZ, P., CHEN, X., HENDRICH, J., IRWIN, J. C., GREEN, P. G., GIUDICE, L. C. & LEVINE, J. D. 2012. Ectopic uterine tissue as a chronic pain generator. *Neuroscience,* 225, 269-282.

AMERICAN SOCIETY FOR REPRODUCTIVE MEDICINE 1997. Revised American Society for Reproductive Medicine classification of endometriosis. *Fertil Steril,* 67**,** 817-21.

ANDREOLI, C. G., GENRO, V. K., SOUZA, C. A., MICHELON, T., BILIBIO, J. P., SCHEFFEL, C. & CUNHA-FILHO, J. S. 2011. T helper (Th)1, Th2, and Th17 interleukin pathways in infertile patients with minimal/mild endometriosis. *Fertil Steril,* 95**,** 2477-80.

ANGLESIO, M. S., PAPADOPOULOS, N., AYHAN, A., NAZERAN, T. M., NOE, M., HORLINGS, H. M., LUM, A., JONES, S., SENZ, J., SECKIN, T., HO, J., WU, R. C., LAC, V., OGAWA, H., TESSIER-CLOUTIER, B., ALHASSAN, R., WANG, A., WANG, Y., COHEN, J. D., WONG, F., HASANOVIC, A., ORR, N., ZHANG, M., POPOLI, M., MCMAHON, W., WOOD, L. D., MATTOX, A., ALLAIRE, C.,

SEGARS, J., WILLIAMS, C., TOMASETTI, C., BOYD, N., KINZLER, K. W., GILKS, C. B., DIAZ, L., WANG, T. L., VOGELSTEIN, B., YONG, P. J., HUNTSMAN, D. G. & SHIH, I. M. 2017. Cancer-Associated Mutations in Endometriosis without Cancer. *N Engl J Med,* 376**,** 1835-1848.

ANGLICHEAU, D., MUTHUKUMAR, T. & SUTHANTHIRAN, M. 2010. MicroRNAs: small RNAs with big effects. *Transplantation,* 90**,** 105-12.

ARICI, A., SELI, E., ZEYNELOGLU, H. B., SENTURK, L. M., ORAL, E. & OLIVE, D. L. 1998. Interleukin-8 induces proliferation of endometrial stromal cells: a potential autocrine growth factor. *J Clin Endocrinol Metab,* 83**,** 1201-5.

ARMSTRONG, G. M., MAYBIN, J. A., MURRAY, A. A., NICOL, M., WALKER, C., SAUNDERS, P. T. K., ROSSI, A. G. & CRITCHLEY, H. O. D. 2017. Endometrial apoptosis and neutrophil infiltration during menstruation exhibits spatial and temporal dynamics that are recapitulated in a mouse model. *Scientific reports,* 7**,** 17416-17416.

ARRANZ, A., DOXAKI, C., VERGADI, E., MARTINEZ DE LA TORRE, Y., VAPORIDI, K., LAGOUDAKI, E. D., IERONYMAKI, E., ANDROULIDAKI, A., VENIHAKI, M., MARGIORIS, A. N., STATHOPOULOS, E. N., TSICHLIS, P. N. & TSATSANIS, C. 2012. Akt1 and Akt2 protein kinases differentially contribute to macrophage polarization. *Proc Natl Acad Sci U S A,* 109**,** 9517-22.

ARROYO, J. D., CHEVILLET, J. R., KROH, E. M., RUF, I. K., PRITCHARD, C. C., GIBSON, D. F., MITCHELL, P. S., BENNETT, C. F., POGOSOVA-AGADJANYAN, E. L., STIREWALT, D. L., TAIT, J. F. & TEWARI, M. 2011. Argonaute2 complexes carry a population of circulating microRNAs independent of vesicles in human plasma. *Proc Natl Acad Sci U S A,* 108**,** 5003-8.

AUDEBERT, A., PETOUSIS, S., MARGIOULA-SIARKOU, C., RAVANOS, K., PRAPAS, N. & PRAPAS, Y. 2018. Anatomic distribution of endometriosis: A reappraisal based on series of 1101 patients. *Eur J Obstet Gynecol Reprod Biol,* 230**,** 36-40.

AZNAUROVA, Y. B., ZHUMATAEV, M. B., ROBERTS, T. K., ALIPER, A. M. & ZHAVORONKOV, A. A. 2014. Molecular aspects of development and regulation of endometriosis. *Reproductive Biology and Endocrinology,* 12**,** 1-25.

BACCI, M., CAPOBIANCO, A., MONNO, A., COTTONE, L., DI PUPPO, F., CAMISA, B., MARIANI, M., BRIGNOLE, C., PONZONI, M., FERRARI, S., PANINA-BORDIGNON, P., MANFREDI, A. & ROVERE-QUERINI, P. 2009. Macrophages are alternatively activated in patients with endometriosis and required for growth and vascularization of lesions in a mouse model of disease. *Am J Pathol,* 175.

BALLWEG, M. L. 2004. Impact of endometriosis on women's health: comparative historical data show that the earlier the onset, the more severe the disease. *Best Pract Res Clin Obstet Gynaecol,* 18**,** 201-18.

BARCENA DE ARELLANO, M. L., GERICKE, J., REICHELT, U., OKUDUCU, A. F., EBERT, A. D., CHIANTERA, V., SCHNEIDER, A. & MECHSNER, S. 2011. Immunohistochemical characterization of endometriosis-associated smooth muscle cells in human peritoneal endometriotic lesions. *Hum Reprod,* 26**,** 2721-30.

BARIN, J. G., BALDEVIANO, G. C., TALOR, M. V., WU, L., ONG, S., QUADER, F., CHEN, P., ZHENG, D., CATUREGLI, P., ROSE, N. R. & CIHAKOVA, D. 2012. Macrophages participate in IL-17-mediated inflammation. *Eur J Immunol,* 42**,** 726-36.

BARROS, M. H., HAUCK, F., DREYER, J. H., KEMPKES, B. & NIEDOBITEK, G. 2013. Macrophage polarisation: an immunohistochemical approach for identifying M1 and M2 macrophages. *PLoS One,* 8**,** e80908.

BARTEL, D. P. 2004. MicroRNAs: genomics, biogenesis, mechanism, and function. *Cell,* 116.

BARTEL, D. P. 2009. MicroRNAs: target recognition and regulatory functions. *Cell,* 136**,** 215-33.

BARTUS, K., JAMES, N. D., DIDANGELOS, A., BOSCH, K. D., VERHAAGEN, J., YÁÑEZ-MUÑOZ, R. J., ROGERS, J. H., SCHNEIDER, B. L., MUIR, E. M. & BRADBURY, E. J. 2014. Large-scale chondroitin sulfate proteoglycan digestion with chondroitinase gene therapy leads to reduced pathology and modulates macrophage phenotype following spinal cord contusion injury. *The Journal of neuroscience : the official journal of the Society for Neuroscience,* 34**,** 4822-4836.

BATT, R. E., SMITH, R. A., BUCK LOUIS, G. M., MARTIN, D. C., CHAPRON, C., KONINCKX, P. R. & YEH, J. 2007. Mullerianosis. *Histol Histopathol,* 22**,** 1161-6.

BAUERNFEIND, F., RIEGER, A., SCHILDBERG, F. A., KNOLLE, P. A., SCHMID-BURGK, J. L. & HORNUNG, V. 2012. NLRP3 inflammasome activity is negatively controlled by miR-223. *J Immunol,* 189**,** 4175-81.

BAUMANN, V. & WINKLER, J. 2014. miRNA-based therapies: strategies and delivery platforms for oligonucleotide and non-oligonucleotide agents. *Future medicinal chemistry,* 6**,** 1967-1984.

BEENHOUWER, D. O. 2018. Chapter 17 - Molecular Basis of Diseases of Immunity. *In:* COLEMAN, W. B. & TSONGALIS, G. J. (eds.) *Molecular Pathology (Second Edition).* Academic Press.

BELLOFIORE, N., ELLERY, S. J., MAMROT, J., WALKER, D. W., TEMPLE-SMITH, P. & DICKINSON, H. 2017. First evidence of a menstruating rodent: the spiny mouse (Acomys cahirinus). *Am J Obstet Gynecol,* 216**,** 40.e1-40.e11.

BENAGIANO, G., BROSENS, I. & LIPPI, D. 2014. The history of endometriosis. *Gynecol Obstet Invest,* 78**,** 1-9.

BENJAMINI, Y. & HOCHBERG, Y. 1995. Controlling the False Discovery Rate: A Practical and Powerful Approach to Multiple Testing. *Journal of the Royal Statistical Society. Series B (Methodological),* 57**,** 289-300.

BERGQVIST, A., LJUNGBERG, O. & SKOOG, L. 1993. Immunohistochemical analysis of oestrogen and progesterone receptors in endometriotic tissue and endometrium. *Hum Reprod,* 8**,** 1915-22.

BERINGER, A., NOACK, M. & MIOSSEC, P. 2016. IL-17 in Chronic Inflammation: From Discovery to Targeting. *Trends Mol Med,* 22**,** 230-241.

BLASER, M. J. & FALKOW, S. 2009. What are the consequences of the disappearing human microbiota? *Nat Rev Microbiol,* 7**,** 887-94.

BONOCHER, C. M., MONTENEGRO, M. L., ROSA, E. S. J. C., FERRIANI, R. A. & MEOLA, J. 2014. Endometriosis and physical exercises: a systematic review. *Reprod Biol Endocrinol,* 12**,** 4.

BOON, R. A. & VICKERS, K. C. 2013. Intercellular transport of microRNAs. *Arterioscler Thromb Vasc Biol,* 33**,** 186-92.

BORGES, J., TEGTMEIER, F. T., PADRON, N. T., MUELLER, M. C., LANG, E. M. & STARK, G. B. 2003. Chorioallantoic membrane angiogenesis model for tissue engineering: a new twist on a classic model. *Tissue Eng,* 9**,** 441-50.

BORGHESE, B., CHICHE, J. D., VERNEREY, D., CHENOT, C., MIR, O., BIJAOUI, G., BONAITI-PELLIE, C. & CHAPRON, C. 2008. Genetic polymorphisms of matrix metalloproteinase 12 and 13 genes are implicated in endometriosis progression. *Hum Reprod,* 23**,** 1207-13.

BORGHESE, B., ZONDERVAN, K. T., ABRAO, M. S., CHAPRON, C. & VAIMAN, D. 2017. Recent insights on the genetics and epigenetics of endometriosis. *Clin Genet,* 91**,** 254-264.

BOUQUET DE JOLINIÈRE, J., AYOUBI, J. M. B., GIANAROLI, L., DUBUISSON, J. B., GOGUSEV, J. & FEKI, A. 2014. Endometriosis: A New Cellular and Molecular Genetic Approach for Understanding the Pathogenesis and Evolutivity. *Frontiers in Surgery,* 1**,** 16.

BOVEN, L. A., VAN MEURS, M., VAN ZWAM, M., WIERENGA-WOLF, A., HINTZEN, R. Q., BOOT, R. G., AERTS, J. M., AMOR, S., NIEUWENHUIS, E. E. & LAMAN, J. D. 2006. Myelin-laden macrophages are anti-inflammatory, consistent with foam cells in multiple sclerosis. *Brain,* 129**,** 517-26.

BOZTOSUN, A., OZER, H., ATILGAN, R., ACMAZ, G., YALTA, T., MUDERRIS, II & YANIK, A. 2012. Effect of fibrin glue and comparison with suture on experimental induction of endometriosis in a rat endometrial autograft model. *Clin Exp Obstet Gynecol,* 39**,** 107-11.

BRAZA-BOILS, A., GILABERT-ESTELLES, J., RAMON, L. A., GILABERT, J., MARI-ALEXANDRE, J., CHIRIVELLA, M., ESPANA, F. & ESTELLES, A. 2013. Peritoneal fluid reduces angiogenesis-related microRNA expression in cell cultures of endometrial and endometriotic tissues from women with endometriosis. *PLoS One,* 8**,** e62370.

BRAZA-BOILS, A., MARI-ALEXANDRE, J., GILABERT, J., SANCHEZ-IZQUIERDO, D., ESPANA, F., ESTELLES, A. & GILABERT-ESTELLES, J. 2014. MicroRNA expression profile in endometriosis: its relation to angiogenesis and fibrinolytic factors. *Hum Reprod,* 29**,** 978-88.

BROWN, J. & FARQUHAR, C. 2015. An overview of treatments for endometriosis. *JAMA,* 313**,** 296-7.

BROWN, M. B., VON CHAMIER, M., ALLAM, A. B. & REYES, L. 2014. M1/M2 macrophage polarity in normal and complicated pregnancy. *Front Immunol,* 5**,** 606.

BRUNE, B., DEHNE, N., GROSSMANN, N., JUNG, M., NAMGALADZE, D., SCHMID, T., VON KNETHEN, A. & WEIGERT, A. 2013. Redox control of inflammation in macrophages. *Antioxid Redox Signal,* 19**,** 595-637.

BRUNER-TRAN, K. L., CARVALHO-MACEDO, A. C., DULEBA, A. J., CRISPENS, M. A. & OSTEEN, K. G. 2010. Experimental endometriosis in immunocompromised mice after adoptive transfer of human leukocytes. *Fertil Steril,* 93**,** 2519-24.

BRUNER-TRAN, K. L., MCCONAHA, M. E. & OSTEEN, K. G. 2012. Models of Endometriosis: Animal Models I – Rodent-Based Chimeric Models. *Endometriosis.* Wiley-Blackwell.

BRUNER-TRAN, K. L., MOKSHAGUNDAM, S., HERINGTON, J. L., DING, T. & OSTEEN, K. G. 2018. Rodent Models of Experimental Endometriosis: Identifying Mechanisms of Disease and Therapeutic Targets. *Curr Womens Health Rev,* 14**,** 173-188.

BRUNER-TRAN, K. L., WEBSTER-CLAIR, D. & OSTEEN, K. G. 2002. Experimental endometriosis: the nude mouse as a xenographic host. *Ann N Y Acad Sci,* 955**,** 328-39; discussion 340-2, 396-406.

BRUNING, U., CERONE, L., NEUFELD, Z., FITZPATRICK, S. F., CHEONG, A., SCHOLZ, C. C., SIMPSON, D. A., LEONARD, M. O., TAMBUWALA, M. M., CUMMINS, E. P. & TAYLOR, C. T. 2011. MicroRNA-155 promotes resolution of hypoxia-inducible factor 1alpha activity during prolonged hypoxia. *Mol Cell Biol,* 31**,** 4087-96.

BUDIU, R. A., DIACONU, I., CHRISSLUIS, R., DRICU, A., EDWARDS, R. P. & VLAD, A. M. 2009. A conditional mouse model for human MUC1-positive endometriosis shows the presence of anti-MUC1 antibodies and Foxp3+ regulatory T cells. *Dis Model Mech,* 2**,** 593-603.

BUENO, M. J. & MALUMBRES, M. 2011. MicroRNAs and the cell cycle. *Biochim Biophys Acta,* 1812**,** 592-601.

BULUN, S. E., ATTAR, E., GURATES, B., CHEN, Y.-H., TOKUNAGA, H., MONSIVAIS, D. & PAVONE, M. E. 2012. Medical Therapies: Aromatase Inhibitors. *Endometriosis.* Wiley-Blackwell.

BURNEY, R. O., HAMILTON, A. E., AGHAJANOVA, L., VO, K. C., NEZHAT, C. N., LESSEY, B. A. & GIUDICE, L. C. 2009. MicroRNA expression profiling of eutopic secretory endometrium in women with versus without endometriosis. *Mol Hum Reprod,* 15**,** 625-31.

BURNS, K. A., RODRIGUEZ, K. F., HEWITT, S. C., JANARDHAN, K. S., YOUNG, S. L. & KORACH, K. S. 2012. Role of estrogen receptor signaling required for endometriosis-like lesion establishment in a mouse model. *Endocrinology,* 153**,** 3960-71.

BUSH, D., BRICK, E., EAST, M. C. & JOHNSON, N. 2017. Endometriosis education in schools: A New Zealand model examining the impact of an education program in schools on early recognition of symptoms suggesting endometriosis. *Aust N Z J Obstet Gynaecol,* 57**,** 452-457.

BUSH, D., EVANS, S. & VANCAILLIE, T. G. 2011. The $6 Billion Woman and the $600 Million Girl - the PELVIC PAIN report. *the PELVIC PAIN report.*

CAI, J., GUAN, H., FANG, L., YANG, Y., ZHU, X., YUAN, J., WU, J. & LI, M. 2013. MicroRNA-374a activates Wnt/β-catenin signaling to promote breast cancer metastasis. *The Journal of clinical investigation,* 123**,** 566-579.

CAI, X., YIN, Y., LI, N., ZHU, D., ZHANG, J., ZHANG, C. Y. & ZEN, K. 2012. Re-polarization of tumor-associated macrophages to pro-inflammatory M1 macrophages by microRNA-155. *J Mol Cell Biol,* 4**,** 341-3.

CANDIANI, G. B., FEDELE, L., VERCELLINI, P., BIANCHI, S. & DI NOLA, G. 1991. Repetitive conservative surgery for recurrence of endometriosis. *Obstetrics and Gynecology,* 77**,** 421-424.

CANTONI, C., CIGNARELLA, F., GHEZZI, L., MIKESELL, B., BOLLMAN, B., BERRIEN-ELLIOTT, M. M., IRELAND, A. R., FEHNIGER, T. A., WU, G. F. & PICCIO, L. 2017. Mir-223 regulates the number and function of myeloid-derived suppressor cells in multiple sclerosis and experimental autoimmune encephalomyelitis. *Acta Neuropathol,* 133**,** 61-77.

CAO, X., YANG, D., SONG, M., MURPHY, A. & PARTHASARATHY, S. 2004. The presence of endometrial cells in the peritoneal cavity enhances monocyte recruitment and induces inflammatory cytokines in mice: implications for endometriosis. *Fertil Steril,* 82 Suppl 3**,** 999-1007.

CAPOBIANCO, A., MONNO, A., COTTONE, L., VENNERI, M. A., BIZIATO, D., DI PUPPO, F., FERRARI, S., DE PALMA, M., MANFREDI, A. A. & ROVERE-QUERINI, P. 2011. Proangiogenic Tie2(+) Macrophages Infiltrate Human and Murine Endometriotic Lesions and Dictate Their Growth in a Mouse Model of the Disease. *The American Journal of Pathology,* 179**,** 2651-2659.

CAPOBIANCO, A. & ROVERE-QUERINI, P. 2013. Endometriosis, a disease of the macrophage. *Frontiers in Immunology,* 4**,** 9.

CASSETTA, L., CASSOL, E. & POLI, G. 2011. Macrophage Polarization in Health and Disease. *TheScientificWorldJournal,* 11**,** 2391-2402.

CHAKRABORTY, C., SHARMA, A. R., SHARMA, G., SARKAR, B. K. & LEE, S.-S. 2018. The novel strategies for next-generation cancer treatment: miRNA combined with chemotherapeutic agents for the treatment of cancer. *Oncotarget,* 9**,** 10164-10174.

CHAND, A. L., MURRAY, A. S., JONES, R. L., HANNAN, N. J., SALAMONSEN, L. A. & ROMBAUTS, L. 2007. Laser capture microdissection and cDNA array analysis of endometrium identify CCL16 and CCL21 as epithelial-derived inflammatory mediators associated with endometriosis. *Reprod Biol Endocrinol,* 5**,** 18.

CHEN, C. Z., LI, L., LODISH, H. F. & BARTEL, D. P. 2004. MicroRNAs modulate hematopoietic lineage differentiation. *Science,* 303.

CHEN, J., GU, L., NI, J., HU, P., HU, K. & SHI, Y.-L. 2015a. MiR-183 Regulates ITGB1P Expression and Promotes Invasion of Endometrial Stromal Cells. *BioMed Research International,* 2015**,** 340218.

CHEN, Q., WANG, H., LIU, Y., SONG, Y., LAI, L., HAN, Q., CAO, X. & WANG, Q. 2012. Inducible microRNA-223 down-regulation promotes TLR-triggered IL-6 and IL-1beta production in macrophages by targeting STAT3. *PLoS One,* 7**,** e42971.

CHEN, S., WANG, L., FAN, J., YE, C., DOMINGUEZ, D., ZHANG, Y., CURIEL, T. J., FANG, D., KUZEL, T. M. & ZHANG, B. 2015b. Host miR155 promotes tumor growth through a myeloid-derived suppressor cell-dependent mechanism. *Cancer research,* 75**,** 519-531.

CHEN, X., LIU, J., HE, B., LI, Y., LIU, S., WU, B., WANG, S., ZHANG, S., XU, X. & WANG, J. 2015c. Vascular endothelial growth factor (VEGF) regulation by hypoxia inducible factor-1 alpha (HIF1A) starts and peaks during endometrial breakdown, not repair, in a mouse menstrual-like model. *Hum Reprod,* 30**,** 2160-70.

CHENG, C. W., LICENCE, D., COOK, E., LUO, F., ARENDS, M. J., SMITH, S. K., PRINT, C. G. & CHARNOCK-JONES, D. S. 2011. Activation of mutated K-ras in donor endometrial epithelium and stroma promotes lesion growth in an intact immunocompetent murine model of endometriosis. *J Pathol,* 224**,** 261-9.

CHO, S., CHO, H., NAM, A., KIM, H. Y., CHOI, Y. S., PARK, K. H., CHO, D. J. & LEE, B. S. 2008. Neutrophil-to-lymphocyte ratio as an adjunct to CA-125 for the diagnosis of endometriosis. *Fertil Steril,* 90**,** 2073-9.

CHO, S., CHOI, Y. S., JEON, Y. E., IM, K. J., CHOI, Y. M., YIM, S. Y., KIM, H., SEO, S. K. & LEE, B. S. 2012. Expression of vascular endothelial growth factor (VEGF) and its soluble receptor-1 in endometriosis. *Microvasc Res,* 83**,** 237-42.

CHO, S., MUTLU, L., GRECHUKHINA, O. & TAYLOR, H. S. 2015. Circulating microRNAs as potential biomarkers for endometriosis. *Fertil Steril,* 103**,** 1252-60 e1.

CHRISTOPHER, A. F., KAUR, R. P., KAUR, G., KAUR, A., GUPTA, V. & BANSAL, P. 2016. MicroRNA therapeutics: Discovering novel targets and developing specific therapy. *Perspectives in clinical research,* 7**,** 68-74.

CHUANG, P. C., LIN, Y. J., WU, M. H., WING, L. Y., SHOJI, Y. & TSAI, S. J. 2010. Inhibition of CD36-dependent phagocytosis by prostaglandin E2 contributes to the development of endometriosis. *Am J Pathol,* 176**,** 850-60.

CLEMENT, P. B. 2007. The pathology of endometriosis: a survey of the many faces of a common disease emphasizing diagnostic pitfalls and unusual and newly appreciated aspects. *Adv Anat Pathol,* 14**,** 241-60.

COMINELLI, A., GAIDE CHEVRONNAY, H. P., LEMOINE, P., COURTOY, P. J., MARBAIX, E. & HENRIET, P. 2014. Matrix metalloproteinase-27 is expressed in CD163+/CD206+ M2 macrophages in the cycling human endometrium and in superficial endometriotic lesions. *Mol Hum Reprod,* 20**,** 767-75.

COMMONWEALTH OF AUSTRALIA DEPARTMENT OF HEALTH 2018. National action plan for endometriosis Australia.

CORLISS, B. A., AZIMI, M. S., MUNSON, J., PEIRCE, S. M. & MURFEE, W. L. 2016. Macrophages: An Inflammatory Link between Angiogenesis and Lymphangiogenesis. *Microcirculation (New York, N.Y. : 1994),* 23**,** 95-121.

CORVINO, V., MARCHESE, E., ZARKOVIC, N., ZARKOVIC, K., CINDRIC, M., WAEG, G., MICHETTI, F. & GELOSO, M. C. J. N. R. 2011. Distribution and Time-Course of 4-Hydroxynonenal, Heat Shock Protein 110/105 Family Members and Cyclooxygenase-2 Expression in the Hippocampus of Rat During Trimethyltin-Induced Neurodegeneration. 36**,** 1490-1500.

COSAR, E., MAMILLAPALLI, R., ERSOY, G. S., CHO, S., SEIFER, B. & TAYLOR, H. S. 2016. Serum microRNAs as diagnostic markers of endometriosis: a comprehensive array-based analysis. *Fertil Steril,* 106**,** 402-9.

COULEAU, N., FALLA, J., BEILLEROT, A., BATTAGLIA, E., D'INNOCENZO, M., PLANCON, S., LAVAL-GILLY, P. & BENNASROUNE, A. 2015. Effects of Endocrine Disruptor Compounds, Alone or in Combination, on Human Macrophage-Like THP-1 Cell Response. *PLoS One,* 10**,** e0131428.

COUSINS, F. L., MURRAY, A., ESNAL, A., GIBSON, D. A., CRITCHLEY, H. O. & SAUNDERS, P. T. 2014. Evidence from a mouse model that epithelial cell migration and mesenchymal-epithelial transition contribute to rapid restoration of uterine tissue integrity during menstruation. *PLoS One,* 9**,** e86378.

COXON, L., HORNE, A. W. & VINCENT, K. 2018. Pathophysiology of endometriosis-associated pain: A review of pelvic and central nervous system mechanisms. *Best Pract Res Clin Obstet Gynaecol,* 51**,** 53-67.

CRAMER, D. W., WILSON, E., STILLMAN, R. J., BERGER, M. J., BELISLE, S., SCHIFF, I., ALBRECHT, B., GIBSON, M., STADEL, B. V. & SCHOENBAUM, S. C. 1986. The relation of endometriosis to menstrual characteristics, smoking, and exercise. *Jama,* 255**,** 1904-8.

CRITCHLEY, H. O., KELLY, R. W., BRENNER, R. M. & BAIRD, D. T. 2001. The endocrinology of menstruation--a role for the immune system. Clin Endocrinol (Oxf), 55, 701-10.

CULLEY, L., LAW, C., HUDSON, N., DENNY, E., MITCHELL, H., BAUMGARTEN, M. & RAINE-FENNING, N. 2013. The social and psychological impact of endometriosis on women's lives: a critical narrative review. *Hum Reprod Update,* 19**,** 625-39.

CUMMINGS, A. M., HEDGE, J. M. & BIRNBAUM, L. S. 1999. Effect of prenatal exposure to TCDD on the promotion of endometriotic lesion growth by TCDD in adult female rats and mice. *Toxicol Sci,* 52.

CUMMINGS, A. M., METCALF, J. L. & BIRNBAUM, L. 1996. Promotion of endometriosis by 2,3,7,8-tetrachlorodibenzo-p-dioxin in rats and mice: time-dose dependence and species comparison. *Toxicol Appl Pharmacol,* 138.

D'HOOGHE, T. M., BAMBRA, C. S., RAEYMAEKERS, B. M. & HILL, J. A. 1999. Pelvic inflammation induced by diagnostic laparoscopy in baboons. *Fertil Steril,* 72**,** 1134-41.

D'HOOGHE, T. M., BAMBRA, C. S., RAEYMAEKERS, B. M. & KONINCKX, P. R. 1996a. Increased prevalence and recurrence of retrograde menstruation in baboons with spontaneous endometriosis. *Hum Reprod,* 11**,** 2022-5.

D'HOOGHE, T. M., BAMBRA, C. S., XIAO, L., PEIXE, K. & HILL, J. A. 2001. Effect of menstruation and intrapelvic injection of endometrium on inflammatory parameters of peritoneal fluid in the baboon (Papio anubis and Papio cynocephalus). *Am J Obstet Gynecol,* 184**,** 917-25.

D'HOOGHE, T. M., HILL, J. A., OOSTERLYNCK, D. J., KONINCKX, P. R. & BAMBRA, C. S. 1996b. Effect of endometriosis on white blood cell subpopulations in peripheral blood and peritoneal fluid of baboons. *Hum Reprod,* 11**,** 1736-40.

D'HOOGHE, T. M., KYAMA, C. M., CHAI, D., FASSBENDER, A., VODOLAZKAIA, A., BOKOR, A. & MWENDA, J. M. 2009. Nonhuman primate models for translational research in endometriosis. *Reprod Sci,* 16**,** 152-61.

DAS, L. M., TORRES-CASTILLO, M. D. L. A., GILL, T. & LEVINE, A. D. 2013. TGF-[beta] conditions intestinal T cells to express increased levels of miR-155, associated with down-regulation of IL-2 and itk mRNA. *Mucosal Immunol,* 6**,** 167-176.

DAVIDSON, E. P., COPPEY, L. J., HOLMES, A., LUPACHYK, S., DAKE, B. L., OLTMAN, C. L., PETERSON, R. G. & YOREK, M. A. 2014. Characterization of Diabetic Neuropathy in the Zucker Diabetic Sprague-Dawley Rat: A New Animal Model for Type 2 Diabetes %J Journal of Diabetes Research. 2014**,** 7.

DE ARELLANO ML, B. & MECHSNER, S. 2014. The peritoneum--an important factor for pathogenesis and pain generation in endometriosis. *J Mol Med (Berl),* 92**,** 595-602.

DE BARROS, I. B. L., MALVEZZI, H., GUEUVOGHLANIAN-SILVA, B. Y., PICCINATO, C. A., RIZZO, L. V. & PODGAEC, S. 2017. "What do we know about regulatory T cells and endometriosis? A systematic review". *J Reprod Immunol,* 120**,** 48-55.

DE LA PAZ SÁNCHEZ-MARTÍNEZ, M., BLANCO-FAVELA, F., MORA-RUIZ, M. D., CHÁVEZ-RUEDA, A. K., BERNABE-GARCÍA, M. & CHÁVEZ-SÁNCHEZ, L. 2017. IL-17-differentiated macrophages secrete pro-inflammatory cytokines in response to oxidized low-density lipoprotein. *Lipids in health and disease,* 16**,** 196-196.

DE LAS CASAS-ENGEL, M., DOMINGUEZ-SOTO, A., SIERRA-FILARDI, E., BRAGADO, R., NIETO, C., PUIG-KROGER, A., SAMANIEGO, R., LOZA, M., CORCUERA, M. T., GOMEZ-AGUADO, F., BUSTOS, M., SANCHEZ-MATEOS, P. & CORBI, A. L. 2013. Serotonin skews human macrophage polarization through HTR2B and HTR7. *J Immunol,* 190**,** 2301-10.

DEBROCK, S., VANDER PERRE, S., MEULEMAN, C., MOERMAN, P., HILL, J. A. & D'HOOGHE, T. M. 2002. In-vitro adhesion of endometrium to autologous peritoneal membranes: effect of the cycle phase and the stage of endometriosis. *Human Reproduction,* 17**,** 2523-2528.

DECHAUD, H., WITZ, C. A., MONTOYA-RODRIGUEZ, I. A., DEGRAFFENREID, L. A. & SCHENKEN, R. S. 2001. Mesothelial cell-associated hyaluronic acid promotes adhesion of endometrial cells to mesothelium. *Fertil Steril,* 76**,** 1012-8.

DEHOUX, J.-P., DEFRÈRE, S., SQUIFFLET, J., DONNEZ, O., POLET, R., MESTDAGT, M., FOIDART, J.-M., VAN LANGENDONCKT, A. & DONNEZ, J. 2011. Is the baboon model appropriate for endometriosis studies? *Fertility and Sterility,* 96**,** 728-733.e3.

DELA CRUZ, C. & REIS, F. 2015. The role of TGFβ superfamily members in the pathophysiology of endometriosis. *Gynecological Endocrinology***,** 1-5.

DENTON, G. W., SCHOFIELD, J. B. & GALLAGHER, P. 1990. Uncommon complications of laparoscopic sterilisation. *Ann R Coll Surg Engl,* 72**,** 210-1.

DERRICK-ROBERTS, A. L., PANIR, K., PYRAGIUS, C. E., ZARRINKALAM, K. H., ATKINS, G. J. & BYERS, S. 2016. Reversal of established bone pathology in MPS VII mice following lentiviral-mediated gene therapy. *Mol Genet Metab,* 119**,** 249-257.

DIAMOND, M. P., CARR, B., DMOWSKI, W. P., KOLTUN, W., O'BRIEN, C., JIANG, P., BURKE, J., JIMENEZ, R., GARNER, E. & CHWALISZ, K. 2014. Elagolix treatment for endometriosis-associated pain: results from a phase 2, randomized, double-blind, placebo-controlled study. *Reprod Sci,* 21**,** 363-71.

DIAMOND, M. P. & SHAVELL, V. I. 2012. Surgical Therapies: Peritoneal Endometriosis Surgery. *Endometriosis.* Wiley-Blackwell.

DINULESCU, D. 2012. Molecular Mechanisms Underlying Endometriosis and Endometriosis-Related Cancers. *Endometriosis.* Wiley-Blackwell.

DINULESCU, D. M., INCE, T. A., QUADE, B. J., SHAFER, S. A., CROWLEY, D. & JACKS, T. 2005. Role of K-ras and Pten in the development of mouse models of endometriosis and endometrioid ovarian cancer. *Nat Med,* 11**,** 63-70.

DMOWSKI, W. P., DING, J., SHEN, J., RANA, N., FERNANDEZ, B. B. & BRAUN, D. P. 2001. Apoptosis in endometrial glandular and stromal cells in women with and without endometriosis. *Human Reprod,* 16.

DODDS, K. N., BECKETT, E. A. H., EVANS, S. F. & HUTCHINSON, M. R. 2019. Spinal Glial Adaptations Occur in a Minimally Invasive Mouse Model of Endometriosis: Potential Implications for Lesion Etiology and Persistent Pelvic Pain. *Reprod Sci*, 1933719118773405.

DOGAN, E., SAYGILI, U., POSACI, C., TUNA, B., CALISKAN, S., ALTUNYURT, S. & SAATLI, B. 2004. Regression of endometrial explants in rats treated with the cyclooxygenase-2 inhibitor rofecoxib. *Fertility and sterility,* 82 Suppl 3**,** 1115-1120.

DORGAN, J. F., REICHMAN, M. E., JUDD, J. T., BROWN, C., LONGCOPE, C., SCHATZKIN, A., CAMPBELL, W. S., FRANZ, C., KAHLE, L. & TAYLOR, P. R. 1995. Relationships of age and reproductive characteristics with plasma estrogens and androgens in premenopausal women. *Cancer Epidemiol Biomarkers Prev,* 4**,** 381-6.

DOS ANJOS CASSADO, A. 2017a. F4/80 as a Major Macrophage Marker: The Case of the Peritoneum and Spleen. *Results Probl Cell Differ,* 62**,** 161-179.

DOS ANJOS CASSADO, A. 2017b. F4/80 as a Major Macrophage Marker: The Case of the Peritoneum and Spleen. *In:* KLOC, M. (ed.) *Macrophages: Origin, Functions and Biointervention.* Cham: Springer International Publishing.

DRURY, J. A., PARKIN, K. L., COYNE, L., GIULIANI, E., FAZLEABAS, A. T. & HAPANGAMA, D. K. 2018. The dynamic changes in the number of uterine natural killer cells are specific to the eutopic but not to the ectopic endometrium in women and in a baboon model of endometriosis. *Reprod Biol Endocrinol,* 16**,** 67.

DUNAND-SAUTHIER, I., IRLA, M., CARNESECCHI, S., SEGUÍN-ESTÉVEZ, Q., VEJNAR, C. E., ZDOBNOV, E. M., SANTIAGO-RABER, M.-L. & REITH, W. 2014. Repression of Arginase-2 Expression in Dendritic Cells by MicroRNA-155 Is Critical for Promoting T Cell Proliferation. *The Journal of Immunology,* 193**,** 1690.

DUNSELMAN, G. A., VERMEULEN, N., BECKER, C., CALHAZ-JORGE, C., D'HOOGHE, T., DE BIE, B., HEIKINHEIMO, O., HORNE, A. W., KIESEL, L., NAP, A., PRENTICE, A., SARIDOGAN, E., SORIANO, D. & NELEN, W. 2014. ESHRE guideline: management of women with endometriosis. *Hum Reprod,* 29**,** 400-12.

DUNSELMAN, G. A. J. & BEETS-TAN, R. G. H. 2012. Diagnosis of Endometriosis: Imaging. *Endometriosis.* Wiley-Blackwell.

DUNSELMAN, G. A. J., GROOTHUIS, P. G., DE GOEIJ, A. F. P. M. & EVERS, J. L. H. 2001. The Mesothelium, Teflon or Velcro?: Mesothelium in endometriosis pathogenesis. *Human Reproduction,* 16**,** 605-607.

EGGERMONT, J., DONNEZ, J., CASANAS-ROUX, F., SCHOLTES, H. & VAN LANGENDONCKT, A. 2005. Time course of pelvic endometriotic lesion revascularization in a nude mouse model. *Fertil Steril,* 84**,** 492-9.

EL-BROLOSY, M. A., KONTARAKIS, Z., ROSSI, A., KUENNE, C., GÜNTHER, S., FUKUDA, N., KIKHI, K., BOEZIO, G. L. M., TAKACS, C. M., LAI, S.-L., FUKUDA, R., GERRI, C., GIRALDEZ, A. J. & STAINIER, D. Y. R. 2019. Genetic compensation triggered by mutant mRNA degradation. *Nature,* 568**,** 193-197.

ELMEN, J., LINDOW, M., SCHUTZ, S., LAWRENCE, M., PETRI, A., OBAD, S., LINDHOLM, M., HEDTJARN, M., HANSEN, H. F., BERGER, U., GULLANS, S., KEARNEY, P., SARNOW, P., STRAARUP, E. M. & KAUPPINEN, S. 2008. LNA-mediated microRNA silencing in non-human primates. *Nature,* 452**,** 896-9.

ELMESMARI, A., FRASER, A. R., WOOD, C., GILCHRIST, D., VAUGHAN, D., STEWART, L., MCSHARRY, C., MCINNES, I. B. & KUROWSKA-STOLARSKA, M. 2016. MicroRNA-155 regulates

monocyte chemokine and chemokine receptor expression in Rheumatoid Arthritis. *Rheumatology (Oxford),* 55**,** 2056-2065.

ENDOACTIVE & ERNST & YOUNG, A. 2019. The cost of endometriosis in Australia.

EVANS, S. 2015. Management of persistent pelvic pain in girls and women. *Australian Family Physician,* 44**,** 454-459.

EVANS, S., MOALEM-TAYLOR, G. & TRACEY, D. J. 2007. Pain and endometriosis. *Pain,* 132 Suppl 1**,** S22-5.

EYHOLZER, M., SCHMID, S., SCHARDT, J. A., HAEFLIGER, S., MUELLER, B. U. & PABST, T. 2010. Complexity of miR-223 regulation by CEBPA in human AML. *Leuk Res,* 34**,** 672-6.

FACCHIN, F., BARBARA, G., DRIDI, D., ALBERICO, D., BUGGIO, L., SOMIGLIANA, E., SAITA, E. & VERCELLINI, P. 2017. Mental health in women with endometriosis: searching for predictors of psychological distress. *Hum Reprod,* 32**,** 1855-1861.

FALCONE, T. & FLYCKT, R. 2018. Clinical Management of Endometriosis. *Obstet Gynecol,* 131**,** 557-571.

FANG, H., SHUANG, D., YI, Z., SHENG, H. & LIU, Y. 2016. Up-regulated microRNA-155 expression is associated with poor prognosis in cervical cancer patients. *Biomed Pharmacother,* 83**,** 64-69.

FARAONI, I., ANTONETTI, F. R., CARDONE, J. & BONMASSAR, E. 2009. miR-155 gene: a typical multifunctional microRNA. *Biochim Biophys Acta,* 1792**,** 497-505.

FAZI, F. & NERVI, C. 2008. MicroRNA: basic mechanisms and transcriptional regulatory networks for cell fate determination. *Cardiovasc Res,* 79**,** 553-61.

FAZI, F., ROSA, A., FATICA, A., GELMETTI, V., DE MARCHIS, M. L., NERVI, C. & BOZZONI, I. 2005. A minicircuitry comprised of microRNA-223 and transcription factors NFI-A and C/EBPalpha regulates human granulopoiesis. *Cell,* 123**,** 819-31.

FAZLEABAS, A. T. 2012. Models of Endometriosis: Animal Models II – Non-Human Primates. *Endometriosis.* Wiley-Blackwell.

FERRERO, S., ANSERINI, P., REMORGIDA, V. & RAGNI, N. 2005. Body mass index in endometriosis. *Eur J Obstet Gynecol Reprod Biol,* 121**,** 94-8.

FERRERO, S., REMORGIDA, V., MAGANZA, C., VENTURINI, P. L., SALVATORE, S., PAPALEO, E., CANDIANI, M. & LEONE ROBERTI MAGGIORE, U. 2014. Aromatase and endometriosis: estrogens play a role. *Ann N Y Acad Sci,* 1317**,** 17-23.

FILIGHEDDU, N., GREGNANIN, I., PORPORATO, P. E., SURICO, D., PEREGO, B., GALLI, L., PATRIGNANI, C., GRAZIANI, A. & SURICO, N. 2010. Differential expression of microRNAs between eutopic and ectopic endometrium in ovarian endometriosis. *J Biomed Biotechnol,* 2010**,** 369549.

FINN, C. A. & POPE, M. 1984. Vascular and cellular changes in the decidualized endometrium of the ovariectomized mouse following cessation of hormone treatment: a possible model for menstruation. *J Endocrinol,* 100**,** 295-300.

FISCHER, S., HANDRICK, R., ASCHRAFI, A. & OTTE, K. 2015. Unveiling the principle of microRNA-mediated redundancy in cellular pathway regulation. *RNA Biol,* 12**,** 238-47.

FISHER, C., HICKMAN, L., ADAMS, J. & SIBBRITT, D. 2018. Cyclic Perimenstrual Pain and Discomfort and Australian Women's Associated Use of Complementary and Alternative Medicine: A Longitudinal Study. *J Womens Health (Larchmt),* 27**,** 40-50.

FÖRSTER, R., DAVALOS-MISSLITZ, A. C. & ROT, A. 2008. CCR7 and its ligands: balancing immunity and tolerance. *Nature Reviews Immunology,* 8**,** 362.

FUKAO, T., FUKUDA, Y., KIGA, K., SHARIF, J., HINO, K., ENOMOTO, Y., KAWAMURA, A., NAKAMURA, K., TAKEUCHI, T. & TANABE, M. 2007. An Evolutionarily Conserved Mechanism for MicroRNA-223 Expression Revealed by MicroRNA Gene Profiling. *Cell,* 129**,** 617-631.

FULCI, V., SCAPPUCCI, G., SEBASTIANI, G. D., GIANNITTI, C., FRANCESCHINI, D., MELONI, F., COLOMBO, T., CITARELLA, F., BARNABA, V., MINISOLA, G., GALEAZZI, M. & MACINO, G. 2010. miR-223 is overexpressed in T-lymphocytes of patients affected by rheumatoid arthritis. *Hum Immunol,* 71**,** 206-11.

FUNG, J. N., ROGERS, P. A. & MONTGOMERY, G. W. 2015. Identifying the biological basis of GWAS hits for endometriosis. *Biol Reprod,* 92**,** 87.

GABRILOVICH, D. I., OSTRAND-ROSENBERG, S. & BRONTE, V. 2012. Coordinated regulation of myeloid cells by tumours. *Nat Rev Immunol,* 12**,** 253-68.

GARMENDIA, J. V. & DE SANCTIS, J. B. 2012. Perspectives of new therapies for endometriosis. *Recent Pat Endocr Metab Immune Drug Discov,* 6**,** 218-23.

GARRY, R., HART, R., KARTHIGASU, K. A. & BURKE, C. 2010. Structural changes in endometrial basal glands during menstruation. BJOG: An International Journal of Obstetrics & Gynaecology, 117, 1175-1185.

GAUDET, A. D., MANDREKAR-COLUCCI, S., HALL, J. C. E., SWEET, D. R., SCHMITT, P. J., XU, X., GUAN, Z., MO, X., GUERAU-DE-ARELLANO, M. & POPOVICH, P. G. 2016. miR-155 Deletion in Mice Overcomes Neuron-Intrinsic and Neuron-Extrinsic Barriers to Spinal Cord Repair. *The Journal of neuroscience : the official journal of the Society for Neuroscience,* 36**,** 8516-8532.

GAUNT, A., HEARD, G., MCKAIN, E. S. & STEPHENSON, B. M. 2004. Caesarean scar endometrioma. *Lancet,* 364**,** 368.

GEORGANTAS, R. W., 3RD, HILDRETH, R., MORISOT, S., ALDER, J., LIU, C. G., HEIMFELD, S., CALIN, G. A., CROCE, C. M. & CIVIN, C. I. 2007. CD34+ hematopoietic stem-progenitor cell microRNA expression and function: a circuit diagram of differentiation control. *Proc Natl Acad Sci U S A,* 104**,** 2750-5.

GILABERT-ESTELLES, J., BRAZA-BOILS, A., RAMON, L. A., ZORIO, E., MEDINA, P., ESPANA, F. & ESTELLES, A. 2012. Role of microRNAs in gynecological pathology. *Curr Med Chem,* 19**,** 2406-13.

GIUDICE, L. C. 2010. Clinical practice. Endometriosis. *N Engl J Med,* 362**,** 2389-98.

GIUDICE, L. C. & KAO, L. C. 2004. Endometriosis. *Lancet,* 364**,** 1789-99.

GMYREK, G. B., SIERADZKA, U., GOLUDA, M., GABRYS, M., SOZANSKI, R., JERZAK, M., ZBYRYT, I., CHROBAK, A. & CHELMONSKA-SOYTA, A. 2008. Differential flow cytometric detection of intracellular cytokines in peripheral and peritoneal mononuclear cells of women with endometriosis. *Eur J Obstet Gynecol Reprod Biol,* 137**,** 67-76.

GONCALVES, A. V., BARROS, N. F. & BAHAMONDES, L. 2017. The Practice of Hatha Yoga for the Treatment of Pain Associated with Endometriosis. *J Altern Complement Med,* 23**,** 45-52.

GONCALVES, A. V., MAKUCH, M. Y., SETUBAL, M. S., BARROS, N. F. & BAHAMONDES, L. 2016. A Qualitative Study on the Practice of Yoga for Women with Pain-Associated Endometriosis. *J Altern Complement Med,* 22**,** 977-982.

GORDON, S. & PLÜDDEMANN, A. 2017. Tissue macrophages: heterogeneity and functions. *BMC Biology,* 15**,** 53.

GORDON, S. & TAYLOR, P. R. 2005. Monocyte and macrophage heterogeneity. *Nat Rev Immunol,* 5**,** 953-64.

GORDTS, S., KONINCKX, P. & BROSENS, I. 2017. Pathogenesis of deep endometriosis. *Fertility and Sterility,* 108**,** 872-885.e1.

GRACIAS, D. T., STELEKATI, E., HOPE, J. L., BOESTEANU, A. C., DOERING, T. A., NORTON, J., MUELLER, Y. M., FRAIETTA, J. A., WHERRY, E. J., TURNER, M. & KATSIKIS, P. D. 2013. The microRNA miR-155 controls CD8(+) T cell responses by regulating interferon signaling. *Nat Immunol,* 14**,** 593-602.

GRAHAM, A., FALCONE, T. & NOTHNICK, W. B. 2015. The expression of microRNA-451 in human endometriotic lesions is inversely related to that of macrophage migration inhibitory factor (MIF) and regulates MIF expression and modulation of epithelial cell survival. *Hum Reprod,* 30**,** 642-52.

GREAVES, E., COUSINS, F. L., MURRAY, A., ESNAL-ZUFIAURRE, A., FASSBENDER, A., HORNE, A. W. & SAUNDERS, P. T. 2014. A novel mouse model of endometriosis mimics human phenotype and reveals insights into the inflammatory contribution of shed endometrium. *Am J Pathol,* 184**,** 1930-9.

GREAVES, E., CRITCHLEY, H. O. D., HORNE, A. W. & SAUNDERS, P. T. K. 2017. Relevant human tissue resources and laboratory models for use in endometriosis research. *Acta Obstetricia et Gynecologica Scandinavica,* 96**,** 644-658.

GREEN, D., DALMAY, T. & CHAPMAN, T. 2016. Microguards and micromessengers of the genome. *Heredity,* 116**,** 125-134.

GREENBERG, L. H. & SLAYDEN, O. D. 2004. Human endometriotic xenografts in immunodeficient RAG-2/gamma(c)KO mice. *Am J Obstet Gynecol,* 190**,** 1788-95; discussion 1795-6.

GROOTHUIS, P. G. 2012. Angiogenesis and Endometriosis. *Endometriosis.* Wiley-Blackwell.

GROOTHUIS, P. G., NAP, A. W., WINTERHAGER, E. & GRÜMMER, R. 2005. Vascular development in endometriosis. *Angiogenesis,* 8**,** 147-56.

GRÜMMER, R. 2006. Animal models in endometriosis research. *Hum Reprod Update,* 12**,** 641-9.

GRÜMMER, R. 2012. Models of Endometriosis: In vitro and In vivo Models. *Endometriosis.* Wiley-Blackwell.

GRÜMMER, R., SCHWARZER, F., BAINCZYK, K., HESS-STUMPP, H., REGIDOR, P. A., SCHINDLER, A. E. & WINTERHAGER, E. 2001. Peritoneal endometriosis: validation of an in-vivo model. *Hum Reprod,* 16**,** 1736-43.

GUO, Y., HE, B., XU, X. & WANG, J. 2011. Comprehensive analysis of leukocytes, vascularization and matrix metalloproteinases in human menstrual xenograft model. PLoS One, 6, e16840.

GUO, S.-W. 2012. Pathogenesis: Epigenetics. *Endometriosis.* Wiley-Blackwell.

GUPTA, D., HULL, M. L., FRASER, I., MILLER, L., BOSSUYT, P. M., JOHNSON, N. & NISENBLAT, V. 2016. Endometrial biomarkers for the non-invasive diagnosis of endometriosis. *Cochrane Database Syst Rev,* 4**,** CD012165.

GWAK, J. M., KIM, H. J., KIM, E. J., CHUNG, Y. R., YUN, S., SEO, A. N., LEE, H. J. & PARK, S. Y. 2014. MicroRNA-9 is associated with epithelial-mesenchymal transition, breast cancer stem cell phenotype, and tumor progression in breast cancer. *Breast Cancer Res Treat,* 147**,** 39-49.

HAFFNER-LUNTZER, M., KOVTUN, A., RAPP, A. E. & IGNATIUS, A. J. C. M. B. R. 2016. Mouse Models in Bone Fracture Healing Research. 2**,** 101-111.

HAIDER, B. A., BARAS, A. S., MCCALL, M. N., HERTEL, J. A., CORNISH, T. C. & HALUSHKA, M. K. 2014. A critical evaluation of microRNA biomarkers in non-neoplastic disease. *PLoS One,* 9**,** e89565.

HALD, A., NEDERGAARD, S., HANSEN, R. R., DING, M. & HEEGAARD, A.-M. 2009. Differential activation of spinal cord glial cells in murine models of neuropathic and cancer pain. *European Journal of Pain,* 13**,** 138-145.

HALME, J., BECKER, S. & HASKILL, S. 1987. Altered maturation and function of peritoneal macrophages: possible role in pathogenesis of endometriosis. *Am J Obstet Gynecol,* 156**,** 783-9.

HALME, J., HAMMOND, M. G., HULKA, J. F., RAJ, S. G. & TALBERT, L. M. 1984. Retrograde menstruation in healthy women and in patients with endometriosis. *Obstet Gynecol,* 64**,** 151-4.

HAND, T. W., VUJKOVIC-CVIJIN, I., RIDAURA, V. K. & BELKAID, Y. 2016. Linking the Microbiota, Chronic Disease, and the Immune System. *Trends Endocrinol Metab,* 27**,** 831-843.

HANEKLAUS, M., GERLIC, M., O'NEILL, L. A. & MASTERS, S. L. 2013. miR-223: infection, inflammation and cancer. *J Intern Med,* 274**,** 215-26.

HANEY, A. F., MUSCATO, J. J. & WEINBERG, J. B. 1981. Peritoneal fluid cell populations in infertility patients. *Fertil Steril,* 35**,** 696-8.

HARADA, T., IWABE, T. & TERAKAWA, N. 2001. Role of cytokines in endometriosis. *Fertil Steril,* 76**,** 1-10.

HARP, D., DRISS, A., MEHRABI, S., CHOWDHURY, I., XU, W., LIU, D., GARCIA-BARRIO, M., TAYLOR, R. N., GOLD, B., JEFFERSON, S., SIDELL, N. & THOMPSON, W. 2016. Exosomes derived from endometriotic stromal cells have enhanced angiogenic effects in vitro. *Cell and tissue research,* 365**,** 187-196.

HARRIS, N. L. E., VENNIN, C., CONWAY, J. R. W., VINE, K. L., PINESE, M., COWLEY, M. J., SHEARER, R. F., LUCAS, M. C., HERRMANN, D., ALLAM, A. H., PAJIC, M., MORTON, J. P., AUSTRALIAN PANCREATIC CANCER GENOME, I., BIANKIN, A. V., RANSON, M., TIMPSON, P. & SAUNDERS, D. N. 2017. SerpinB2 regulates stromal remodelling and local invasion in pancreatic cancer. *Oncogene,* 36**,** 4288.

HARVEY, B. K., RICHIE, C. T., HOFFER, B. J. & AIRAVAARA, M. J. J. O. N. T. 2011. Transgenic animal models of neurodegeneration based on human genetic studies. 118**,** 27-45.

HAWKINS, S. M., CREIGHTON, C. J., HAN, D. Y., ZARIFF, A., ANDERSON, M. L., GUNARATNE, P. H. & MATZUK, M. M. 2011. Functional microRNA involved in endometriosis. *Mol Endocrinol,* 25**,** 821-32.

HAYES, J., PERUZZI, P. P. & LAWLER, S. 2014. MicroRNAs in cancer: biomarkers, functions and therapy. *Trends Mol Med,* 20**,** 460-9.

HE, M., XU, Z., DING, T., KUANG, D. M. & ZHENG, L. 2009. MicroRNA-155 regulates inflammatory cytokine production in tumor-associated macrophages via targeting C/EBPbeta. *Cell Mol Immunol,* 6**,** 343-52.

HE, S., YANG, L., LI, D. & LI, M. 2015. Kruppel-Like Factor 2-Mediated Suppression of MicroRNA-155 Reduces the Proinflammatory Activation of Macrophages. *PLoS One,* 10**,** e0139060.

HEARD, M. E., SIMMONS, C. D., SIMMEN, F. A. & SIMMEN, R. C. M. 2014. Krüppel-like factor 9 deficiency in uterine endometrial cells promotes ectopic lesion establishment associated with activated notch and hedgehog signaling in a mouse model of endometriosis. *Endocrinology,* 155**,** 1532-1546.

HERINGTON, J. L., BRUNER-TRAN, K. L., LUCAS, J. A. & OSTEEN, K. G. 2011. Immune interactions in endometriosis. *Expert Rev Clin Immunol,* 7**,** 611-26.

HEY-CUNNINGHAM, A. J., PETERS, K. M., ZEVALLOS, H. B., BERBIC, M., MARKHAM, R. & FRASER, I. S. 2013. Angiogenesis, lymphangiogenesis and neurogenesis in endometriosis. *Front Biosci (Elite Ed),* 5**,** 1033-56.

HIRATA, T., OSUGA, Y., HAMASAKI, K., YOSHINO, O., ITO, M., HASEGAWA, A., TAKEMURA, Y., HIROTA, Y., NOSE, E., MORIMOTO, C., HARADA, M., KOGA, K., TAJIMA, T., SAITO, S., YANO, T. & TAKETANI, Y. 2008. Interleukin (IL)-17A stimulates IL-8 secretion, cyclooxygensase-2 expression, and cell proliferation of endometriotic stromal cells. *Endocrinology,* 149.

HIRATA, T., OSUGA, Y., TAKAMURA, M., KODAMA, A., HIROTA, Y., KOGA, K., YOSHINO, O., HARADA, M., TAKEMURA, Y., YANO, T. & TAKETANI, Y. 2010. Recruitment of CCR6-expressing Th17 cells by CCL 20 secreted from IL-1 beta-, TNF-alpha-, and IL-17A-stimulated endometriotic stromal cells. *Endocrinology,* 151**,** 5468-76.

HIRATA, T., OSUGA, Y., YOSHINO, O., HIROTA, Y., HARADA, M., TAKEMURA, Y., MORIMOTO, C., KOGA, K., YANO, T., TSUTSUMI, O. & TAKETANI, Y. 2005. Development of an experimental model of endometriosis using mice that ubiquitously express green fluorescent protein. *Hum Reprod,* 20**,** 2092-6.

HO, H.-Y., LIN, Y.-T., LIN, G., WU, P.-R. & CHENG, M.-L. 2017. Nicotinamide nucleotide transhydrogenase (NNT) deficiency dysregulates mitochondrial retrograde signaling and impedes proliferation. *Redox biology,* 12**,** 916-928.

HOEK, J. B. & RYDSTRÖM, J. 1988. Physiological roles of nicotinamide nucleotide transhydrogenase. *The Biochemical journal,* 254**,** 1-10.

HONG, K. & CHOI, Y. 2018. Role of estrogen and RAS signaling in repeated implantation failure. *BMB reports,* 51**,** 225-229.

HORNE, A. & CRITCHLEY, H. O. D. 2012. Medical Therapies: Progestins. *Endometriosis.* Wiley-Blackwell.

HORNUNG, D., BENTZIEN, F., WALLWIENER, D., KIESEL, L. & TAYLOR, R. N. 2001. Chemokine bioactivity of RANTES in endometriotic and normal endometrial stromal cells and peritoneal fluid. *Molecular Human Reproduction,* 7**,** 163-168.

HORNUNG, D. & VON WUSSOW, U. 2012. Inflammation and Endometriosis. *Endometriosis.* Wiley-Blackwell.

HSIAO, K. Y., WU, M. H., CHANG, N., YANG, S. H., WU, C. W., SUN, H. S. & TSAI, S. J. 2015. Coordination of AUF1 and miR-148a destabilizes DNA methyltransferase 1 mRNA under hypoxia in endometriosis. *Mol Hum Reprod,* 21**,** 894-904.

HSU, C. Y., HSIEH, T. H., TSAI, C. F., TSAI, H. P., CHEN, H. S., CHANG, Y., CHUANG, H. Y., LEE, J. N., HSU, Y. L. & TSAI, E. M. 2014. miRNA-199a-5p regulates VEGFA in endometrial mesenchymal stem cells and contributes to the pathogenesis of endometriosis. *J Pathol,* 232**,** 330-43.

HUANG, K., DONG, X., SUI, C., HU, D., XIONG, T., LIAO, S. & ZHANG, H. 2014. MiR-223 suppresses endometrial carcinoma cells proliferation by targeting IGF-1R. *Am J Transl Res,* 6**,** 841-9.

HULL, M. L., CHARNOCK-JONES, D. S., CHAN, C. L., BRUNER-TRAN, K. L., OSTEEN, K. G., TOM, B. D., FAN, T. P. & SMITH, S. K. 2003. Antiangiogenic agents are effective inhibitors of endometriosis. *J Clin Endocrinol Metab,* 88.

HULL, M. L., ESCARENO, C. R., GODSLAND, J. M., DOIG, J. R., JOHNSON, C. M., PHILLIPS, S. C., SMITH, S. K., TAVARE, S., PRINT, C. G. & CHARNOCK-JONES, D. S. 2008. Endometrial-peritoneal interactions during endometriotic lesion establishment. *Am J Pathol,* 173**,** 700-15.

HULL, M. L., GUN, M. T. & RITOSSA, M. 2006. Hook-wire insertion facilitates the excision of scar endometriosis. *Bjog,* 113**,** 744-6.

HULL, M. L., JOHAN, M. Z., HODGE, W. L., ROBERTSON, S. A. & INGMAN, W. V. 2012. Host-derived TGFB1 deficiency suppresses lesion development in a mouse model of endometriosis. *Am J Pathol,* 180**,** 880-7.

HULL, M. L. & NISENBLAT, V. 2013. Tissue and circulating microRNA influence reproductive function in endometrial disease. *Reprod Biomed Online,* 27**,** 515-29.

HULL, M. L. & PRINT, C. G. 2012. MicroRNAs in Endometriosis. *Endometriosis.* Wiley-Blackwell.

HUME, D. A. 2006. The mononuclear phagocyte system. *Current Opinion in Immunology,* 18**,** 49-53.

HWANG, B., LEE, J. H. & BANG, D. 2018. Single-cell RNA sequencing technologies and bioinformatics pipelines. *Experimental & Molecular Medicine,* 50**,** 96.

ISMAIL, N., WANG, Y., DAKHLALLAH, D., MOLDOVAN, L., AGARWAL, K., BATTE, K., SHAH, P., WISLER, J., EUBANK, T. D., TRIDANDAPANI, S., PAULAITIS, M. E., PIPER, M. G. & MARSH, C. B. 2013. Macrophage microvesicles induce macrophage differentiation and miR-223 transfer. *Blood,* 121**,** 984-95.

ITALIANI, P. & BORASCHI, D. 2014. From Monocytes to M1/M2 Macrophages: Phenotypical vs. Functional Differentiation. *Frontiers in Immunology,* 5**,** 514.

IWABE, T. & HARADA, T. 2014. Inflammation and Cytokines in Endometriosis. *In:* HARADA, T. (ed.) *Endometriosis: Pathogenesis and Treatment.* Tokyo: Springer Japan.

JABLONSKI, K. A., GAUDET, A. D., AMICI, S. A., POPOVICH, P. G. & GUERAU-DE-ARELLANO, M. 2016. Control of the Inflammatory Macrophage Transcriptional Signature by miR-155. *PLoS One,* 11**,** e0159724.

JACKSON, J. B., LEUNG, J. H., STOUT, C. D., SCHURIG-BRICCIO, L. A. & GENNIS, R. B. 2015. Review and Hypothesis. New insights into the reaction mechanism of transhydrogenase: Swivelling the dIII component may gate the proton channel. *FEBS Lett,* 589**,** 2027-33.

JANSSEN, W. J. & HENSON, P. M. 2012. Cellular regulation of the inflammatory response. *Toxicol Pathol,* 40**,** 166-73.

JANTSCH, J., BINGER, K. J., MULLER, D. N. & TITZE, J. 2014. Macrophages in homeostatic immune function. *Front Physiol,* 5**,** 146.

JENKINS, S., OLIVE, D. L. & HANEY, A. F. 1986. Endometriosis: pathogenetic implications of the anatomic distribution. *Obstet Gynecol,* 67**,** 335-8.

JENKINS, S. J., RUCKERL, D., COOK, P. C., JONES, L. H., FINKELMAN, F. D., VAN ROOIJEN, N., MACDONALD, A. S. & ALLEN, J. E. 2011. Local macrophage proliferation, rather than recruitment from the blood, is a signature of TH2 inflammation. Science, 332, 1284-8.

JENSEN, J. R., WITZ, C. A., SCHENKEN, R. S. & TEKMAL, R. R. 2010. A potential role for colony-stimulating factor 1 in the genesis of the early endometriotic lesion. *Fertil Steril,* 93**,** 251-6.

JIA, C. Y., LI, H. H., ZHU, X. C., DONG, Y. W., FU, D., ZHAO, Q. L., WU, W. & WU, X. Z. 2011. MiR-223 suppresses cell proliferation by targeting IGF-1R. *PLoS One,* 6**,** e27008.

JIA, S. Z., YANG, Y., LANG, J., SUN, P. & LENG, J. 2013a. Plasma miR-17-5p, miR-20a and miR-22 are down-regulated in women with endometriosis. *Hum Reprod,* 28**,** 322-30.

JIA, W., WU, Y., ZHANG, Q., GAO, G., ZHANG, C. & XIANG, Y. 2013b. Identification of four serum microRNAs from a genome-wide serum microRNA expression profile as potential non-invasive biomarkers for endometrioid endometrial cancer. *Oncol Lett,* 6**,** 261-267.

JOHAN, M. Z., INGMAN, W. V., ROBERTSON, S. A. & HULL, M. L. 2019. Macrophages infiltrating endometriosis-like lesions exhibit progressive phenotype changes in a heterologous mouse model. *J Reprod Immunol,* 132**,** 1-8.

JOHANSSON, J., BERG, T., KURZEJAMSKA, E., PANG, M. F., TABOR, V., JANSSON, M., ROSWALL, P., PIETRAS, K., SUND, M., RELIGA, P. & FUXE, J. 2013. MiR-155-mediated loss of C/EBPbeta shifts the TGF-beta response from growth inhibition to epithelial-mesenchymal transition, invasion and metastasis in breast cancer. *Oncogene,* 32**,** 5614-24.

JOHANSSON, K., MALMHALL, C., RAMOS-RAMIREZ, P. & RADINGER, M. 2017. MicroRNA-155 is a critical regulator of type 2 innate lymphoid cells and IL-33 signaling in experimental models of allergic airway inflammation. *J Allergy Clin Immunol,* 139**,** 1007-1016.e9.

JOHNNIDIS, J. B., HARRIS, M. H., WHEELER, R. T., STEHLING-SUN, S., LAM, M. H., KIRAK, O., BRUMMELKAMP, T. R., FLEMING, M. D. & CAMARGO, F. D. 2008. Regulation of progenitor cell proliferation and granulocyte function by microRNA-223. *Nature,* 451**,** 1125-9.

JOHNSON, K. L., CUMMINGS, A. M. & BIRNBAUM, L. S. 1997. Promotion of endometriosis in mice by polychlorinated dibenzo-p-dioxins, dibenzofurans, and biphenyls. *Environ Health Perspect,* 105.

JOHNSON, M. C., TORRES, M., ALVES, A., BACALLAO, K., FUENTES, A., VEGA, M. & BORIC, M. A. 2005. Augmented cell survival in eutopic endometrium from women with endometriosis: Expression of c-myc, TGF-beta1 and bax genes. *Reproductive Biology and Endocrinology,* 3**,** 1-8.

JOHNSON, N. P. 2012. Medical Therapies: Randomized Controlled Trials/Traditional Medical Therapies. *Endometriosis.* Wiley-Blackwell.

JOHNSON, N. P. & HUMMELSHOJ, L. 2013. Consensus on current management of endometriosis. *Hum Reprod,* 28**,** 1552-68.

JONES, H. E., GODDARD, L., GEE, J. M., HISCOX, S., RUBINI, M., BARROW, D., KNOWLDEN, J. M., WILLIAMS, S., WAKELING, A. E. & NICHOLSON, R. I. 2004. Insulin-like growth factor-I receptor signalling and acquired resistance to gefitinib (ZD1839; Iressa) in human breast and prostate cancer cells. *Endocr Relat Cancer,* 11**,** 793-814.

JOSHI, N. R., SU, R. W., CHANDRAMOULI, G. V., KHOO, S. K., JEONG, J. W., YOUNG, S. L., LESSEY, B. A. & FAZLEABAS, A. T. 2015. Altered expression of microRNA-451 in eutopic endometrium of baboons (Papio anubis) with endometriosis. *Hum Reprod,* 30**,** 2881-91.

KALU, E., SUMAR, N., GIANNOPOULOS, T., PATEL, P., CROUCHER, C., SHERRIFF, E. & BANSAL, A. 2007. Cytokine profiles in serum and peritoneal fluid from infertile women with and without endometriosis. *J Obstet Gynaecol Res,* 33**,** 490-5.

KAMAT, B. R. & ISAACSON, P. G. 1987. The immunocytochemical distribution of leukocytic subpopulations in human endometrium. The American journal of pathology, 127, 66-73.

KASTINGSCHAFER, C. S., SCHAFER, S. D., KIESEL, L. & GOTTE, M. 2015. miR-142-3p is a novel regulator of cell viability and proinflammatory signalling in endometrial stroma cells. *Reprod Biomed Online,* 30**,** 553-6.

KEENAN, J. A., CHEN, T. T., CHADWELL, N. L., TORRY, D. S. & CAUDLE, M. R. 1995. IL-1 beta, TNF-alpha, and IL-2 in peritoneal fluid and macrophage-conditioned media of women with endometriosis. *Am J Reprod Immunol,* 34**,** 381-5.

KHAMMASH, M. R., OMARI, A. K., GASAIMEH, G. R. & BANI-HANI, K. E. 2003. Abdominal wall endometriosis. An overlooked diagnosis. *Saudi Med J,* 24**,** 523-5.

KHAN, K. N., KITAJIMA, M., HIRAKI, K., FUJISHITA, A., NAKASHIMA, M. & MASUZAKI, H. 2014. Visible and occult microscopic lesions of endometriosis. *Gynecology and Minimally Invasive Therapy,* 3**,** 109-114.

KHAN, K. N., KITAJIMA, M., HIRAKI, K., FUJISHITA, A., SEKINE, I., ISHIMARU, T. & MASUZAKI, H. 2010. Changes in tissue inflammation, angiogenesis and apoptosis in endometriosis, adenomyosis and uterine myoma after GnRH agonist therapy. *Hum Reprod,* 25**,** 642-53.

KHAN, K. N., MASUZAKI, H., FUJISHITA, A., KITAJIMA, M., SEKINE, I. & ISHIMARU, T. 2004. Higher activity by opaque endometriotic lesions than nonopaque lesions. 83**,** 375-382.

KHANJANI, S., AL-SABBAGH, M. K., FUSI, L. & BROSENS, J. J. 2012. Role of Steroid Hormones: Progesterone Signaling. *Endometriosis.* Wiley-Blackwell.

KHORRAM, O., TAYLOR, R. N., RYAN, I. P., SCHALL, T. J. & LANDERS, D. V. 1993. Peritoneal fluid concentrations of the cytokine RANTES correlate with the severity of endometriosis. *Am J Obstet Gynecol,* 169**,** 1545-9.

KIM, D., LANGMEAD, B. & SALZBERG, S. L. 2015. HISAT: a fast spliced aligner with low memory requirements. *Nature methods,* 12**,** 357-360.

KIM, H. Y., KWON, H. Y., HA THI, H. T., LEE, H. J., KIM, G. I., HAHM, K. B. & HONG, S. 2016. MicroRNA-132 and microRNA-223 control positive feedback circuit by regulating FOXO3a in inflammatory bowel disease. *J Gastroenterol Hepatol,* 31**,** 1727-1735.

KIM, N. H., KIM, H. S., KIM, N. G., LEE, I., CHOI, H. S., LI, X. Y., KANG, S. E., CHA, S. Y., RYU, J. K., NA, J. M., PARK, C., KIM, K., LEE, S., GUMBINER, B. M., YOOK, J. I. & WEISS, S. J. 2011. p53 and microRNA-34 are suppressors of canonical Wnt signaling. *Sci Signal,* 4**,** ra71.

KIM, T. H., YOO, J.-Y., CHOI, K.-C., SHIN, J.-H., LEACH, R. E., FAZLEABAS, A. T., YOUNG, S. L., LESSEY, B. A., YOON, H.-G. & JEONG, J.-W. 2019. Loss of HDAC3 results in nonreceptive endometrium and female infertility. 11**,** eaaf7533.

KLEMMT, P. A. B. & STARZINSKI-POWITZ, A. 2012. Biology of Eutopic and Ectopic Endometrium in Women with Endometriosis. *Endometriosis.* Wiley-Blackwell.

KLENTZERIS, L. D., BULMER, J. N., LIU, D. T. & MORRISON, L. 1995. Endometrial leukocyte subpopulations in women with endometriosis. *Eur J Obstet Gynecol Reprod Biol,* 63**,** 41-7.

KNAPP, V. J. 1999. How old is endometriosis? Late 17th- and 18th-century European descriptions of the disease. *Fertil Steril,* 72**,** 10-4.

KONG, W., YANG, H., HE, L., ZHAO, J. J., COPPOLA, D., DALTON, W. S. & CHENG, J. Q. 2008. MicroRNA-155 is regulated by the transforming growth factor beta/Smad pathway and contributes to epithelial cell plasticity by targeting RhoA. *Mol Cell Biol,* 28**,** 6773-84.

KONINCKX, P. R., BARLOW, D. & KENNEDY, S. 1999. Implantation versus Infiltration: The Sampson versus the Endometriotic Disease Theory. *Gynecologic and Obstetric Investigation,* 47(suppl 1)**,** 3-10.

KONINCKX, P. R., KENNEDY, S. H. & BARLOW, D. H. 1998. Endometriotic disease: the role of peritoneal fluid. *Hum Reprod Update,* 4**,** 741-51.

KONINCKX, P. R., USSIA, A. & ADAMYAN, L. 2012. The role of the peritoneal cavity in adhesion formation. *Fertil Steril,* 97**,** 1297.

KONINCKX, P. R., USSIA, A., ADAMYAN, L., WATTIEZ, A., GOMEL, V. & MARTIN, D. C. 2018. Pathogenesis of endometriosis: the genetic/epigenetic theory. *Fertil Steril*.

KOZOMARA, A. & GRIFFITHS-JONES, S. 2014. miRBase: annotating high confidence microRNAs using deep sequencing data. *Nucleic Acids Res,* 42**,** D68-73.

KRALICKOVA, M., FIALA, L., LOSAN, P., TOMES, P. & VETVICKA, V. 2018. Altered Immunity in Endometriosis: What Came First? *Immunol Invest,* 47**,** 569-582.

KRÁLÍČKOVÁ, M. & VETVICKA, V. 2014. Endometriosis and ovarian cancer. *World Journal of Clinical Oncology,* 5**,** 800-805.

KRÁLÍČKOVÁ, M. & VETVICKA, V. 2015. Immunological aspects of endometriosis: a review. *Annals of Translational Medicine,* 3**,** 153.

KRIKUN, G. 2012. Endometriosis, Angiogenesis and Tissue Factor. *Scientifica,* 2012**,** 306830.

KUOHUNG, W., JONES, G. L., VITONIS, A. F., CRAMER, D. W., KENNEDY, S. H., THOMAS, D. & HORNSTEIN, M. D. 2002. Characteristics of patients with endometriosis in the United States and the United Kingdom. *Fertility and Sterility,* 78**,** 767-772.

KUROWSKA-STOLARSKA, M., ALIVERNINI, S., BALLANTINE, L. E., ASQUITH, D. L., MILLAR, N. L., GILCHRIST, D. S., REILLY, J., IERNA, M., FRASER, A. R., STOLARSKI, B., MCSHARRY, C., HUEBER, A. J., BAXTER, D., HUNTER, J., GAY, S., LIEW, F. Y. & MCINNES, I. B. 2011. MicroRNA-155 as a proinflammatory regulator in clinical and experimental arthritis. *Proc Natl Acad Sci U S A,* 108**,** 11193-8.

KUROWSKA-STOLARSKA, M., HASOO, M. K., WELSH, D. J., STEWART, L., MCINTYRE, D., MORTON, B. E., JOHNSTONE, S., MILLER, A. M., ASQUITH, D. L., MILLAR, N. L., MILLAR, A. B., FEGHALI-BOSTWICK, C. A., HIRANI, N., CRICK, P. J., WANG, Y., GRIFFITHS, W. J., MCINNES, I. B. & MCSHARRY, C. 2017. The role of microRNA-155/liver X receptor pathway in experimental and idiopathic pulmonary fibrosis. *J Allergy Clin Immunol,* 139**,** 1946-1956.

KUSUME, T., MAEDA, N., IZUMIYA, C., YAMAMOTO, Y., HAYASHI, K., OGURI, H., NISHIMORI, Y. & FUKAYA, T. 2005. Human leukocyte antigen expression by peritoneal macrophages from women with pelvic endometriosis is depressed but coordinated with costimulatory molecule expression. *Fertil Steril,* 83 Suppl 1**,** 1232-40.

KYAMA, C. M., DEBROCK, S., MWENDA, J. M. & D'HOOGHE, T. M. 2003. Potential involvement of the immune system in the development of endometriosis. *Reprod Biol Endocrinol,* 1**,** 123.

KYAMA, C. M., MIHALYI, A., CHAI, D., SIMSA, P., MWENDA, J. M. & D'HOOGHE, T. M. 2007. Baboon model for the study of endometriosis. *Womens Health (Lond),* 3**,** 637-46.

KYAMA, C. M., OVERBERGH, L., MIHALYI, A., CUNEO, S., CHAI, D., DEBROCK, S., MWENDA, J. M., MATHIEU, C., NUGENT, N. P. & D'HOOGHE, T. M. 2008. Effect of recombinant human TNF-binding protein-1 and GnRH antagonist on mRNA expression of inflammatory cytokines and adhesion and growth factors in endometrium and endometriosis tissues in baboons. *Fertil Steril,* 89**,** 1306-13.

LAFFONT, B. & RAYNER, K. J. 2017. MicroRNAs in the Pathobiology and Therapy of Atherosclerosis. *Can J Cardiol,* 33**,** 313-324.

LAGOS-QUINTANA, M., RAUHUT, R., YALCIN, A., MEYER, J., LENDECKEL, W. & TUSCHL, T. 2002. Identification of tissue-specific microRNAs from mouse. *Curr Biol,* 12**,** 735-9.

LANDGRAF, P., RUSU, M., SHERIDAN, R., SEWER, A., IOVINO, N., ARAVIN, A., PFEFFER, S., RICE, A., KAMPHORST, A. O. & LANDTHALER, M. 2007. A mammalian microRNA expression atlas based on small RNA library sequencing. *Cell,* 129.

LANFRANCONE, L., BORASCHI, D., GHIARA, P., FALINI, B., GRIGNANI, F., PERI, G., MANTOVANI, A. & PELICCI, P. G. 1992. Human peritoneal mesothelial cells produce many cytokines (granulocyte colony-stimulating factor [CSF], granulocyte-monocyte-CSF, macrophage-CSF, interleukin-1 [IL-1], and IL-6) and are activated and stimulated to grow by IL-1. *Blood,* 80**,** 2835-42.

LASCHKE, M. W. & MENGER, M. D. 2007. In vitro and in vivo approaches to study angiogenesis in the pathophysiology and therapy of endometriosis. *Hum Reprod Update,* 13**,** 331-42.

LAUDANSKI, P., CHARKIEWICZ, R., KUZMICKI, M., SZAMATOWICZ, J., CHARKIEWICZ, A. & NIKLINSKI, J. 2013. MicroRNAs expression profiling of eutopic proliferative endometrium in women with ovarian endometriosis. *Reproductive Biology and Endocrinology,* 11**,** 1-7.

LAW, C. W., ALHAMDOOSH, M., SU, S., SMYTH, G. K. & RITCHIE, M. E. 2016. RNA-seq analysis is easy as 1-2-3 with limma, Glimma and edgeR. *F1000Research,* 5**,** 1408-1408.

LAWSON, C., AL-AKOUM, M., MAHEUX, R. & AKOUM, A. 2007. Increased expression of interleukin-1 receptor type 1 in active endometriotic lesions. *Reproduction,* 133.

LEBOVIC, D. I., BENTZIEN, F., CHAO, V. A., GARRETT, E. N., MENG, Y. G. & TAYLOR, R. N. 2000. Induction of an angiogenic phenotype in endometriotic stromal cell cultures by interleukin-1beta. *Mol Hum Reprod,* 6**,** 269-75.

LEBOVIC, D. I., MUELLER, M. D. & TAYLOR, R. N. 2001. Immunobiology of endometriosis. *Fertil Steril,* 75**,** 1-10.

LEE, K.-S., BAEK, D.-W., KIM, K.-H., SHIN, B.-S., LEE, D.-H., KIM, J.-W., HONG, Y.-S., BAE, Y.-S. & KWAK, J.-Y. 2005. IL-10-dependent down-regulation of MHC class II expression level on monocytes by peritoneal fluid from endometriosis patients. *International immunopharmacology,* 5**,** 1699-1712.

LEE, M., REY, K., BESLER, K., WANG, C. & CHOY, J. 2017. Immunobiology of Nitric Oxide and Regulation of Inducible Nitric Oxide Synthase. *Results Probl Cell Differ,* 62**,** 181-207.

LENG, R. X., PAN, H. F., QIN, W. Z., CHEN, G. M. & YE, D. Q. 2011. Role of microRNA-155 in autoimmunity. *Cytokine Growth Factor Rev,* 22**,** 141-7.

LEYENDECKER, G., HERBERTZ, M., KUNZ, G. & MALL, G. 2002. Endometriosis results from the dislocation of basal endometrium. *Hum Reprod,* 17**,** 2725-36.

LI, H. P., ZENG, X. C., ZHANG, B., LONG, J. T., ZHOU, B., TAN, G. S., ZENG, W. X., CHEN, W. & YANG, J. Y. 2013. miR-451 inhibits cell proliferation in human hepatocellular carcinoma through direct suppression of IKK-beta. *Carcinogenesis,* 34**,** 2443-51.

LI, J., ZHANG, J., GUO, H., YANG, S., FAN, W., YE, N., TIAN, Z., YU, T., AI, G., SHEN, Z., HE, H., YAN, P., LIN, H., LUO, X., LI, H. & WU, Y. 2018. Critical Role of Alternative M2 Skewing in miR-155 Deletion-Mediated Protection of Colitis. *Front Immunol,* 9**,** 904.

LI, T., MORGAN, M. J., CHOKSI, S., ZHANG, Y., KIM, Y. S. & LIU, Z. G. 2010. MicroRNAs modulate the noncanonical transcription factor NF-kappaB pathway by regulating expression of the kinase IKKalpha during macrophage differentiation. *Nat Immunol,* 11**,** 799-805.

LI, X., NAIR, A., WANG, S. & WANG, L. 2015. Quality control of RNA-seq experiments. *Methods Mol Biol,* 1269**,** 137-46.

LI, X., SANDA, T., LOOK, A. T., NOVINA, C. D. & VON BOEHMER, H. 2011. Repression of tumor suppressor miR-451 is essential for NOTCH1-induced oncogenesis in T-ALL. *J Exp Med,* 208**,** 663-75.

LIANG, C. C., LIOU, B., TSAI, C. C., CHEN, T. C. & SOONG, Y. K. 1998. Scar endometriosis. *Int Surg,* 83**,** 69-71.

LIAO, Y., SMYTH, G. K. & SHI, W. 2014. featureCounts: an efficient general purpose program for assigning sequence reads to genomic features. *Bioinformatics,* 30**,** 923-30.

LIDDIARD, K., ROSAS, M., DAVIES, L. C., JONES, S. A. & TAYLOR, P. R. 2011. Macrophage heterogeneity and acute inflammation. *Eur J Immunol,* 41**,** 2503-8.

LIN, S. C., LI, Y. H., WU, M. H., CHANG, Y. F., LEE, D. K., TSAI, S. Y., TSAI, M. J. & TSAI, S. J. 2014. Suppression of COUP-TFII by proinflammatory cytokines contributes to the pathogenesis of endometriosis. *J Clin Endocrinol Metab,* 99**,** E427-37.

LIN, S. C., WANG, C. C., WU, M. H., YANG, S. H., LI, Y. H. & TSAI, S. J. 2012. Hypoxia-induced microRNA-20a expression increases ERK phosphorylation and angiogenic gene expression in endometriotic stromal cells. *J Clin Endocrinol Metab,* 97**,** E1515-23.

LIN, Y. J., LAI, M. D., LEI, H. Y. & WING, L. Y. 2006. Neutrophils and macrophages promote angiogenesis in the early stage of endometriosis in a mouse model. *Endocrinology,* 147**,** 1278-86.

LIU, D., LIU, C., WANG, X., INGVARSSON, S. & CHEN, H. 2014. MicroRNA-451 suppresses tumor cell growth by down-regulating IL6R gene expression. *Cancer Epidemiol,* 38**,** 85-92.

LIU, G. & ABRAHAM, E. 2013. MicroRNAs in immune response and macrophage polarization. *Arterioscler Thromb Vasc Biol,* 33**,** 170-7.

LIU, S., ZHU, B., SUN, Y. & XIE, X. 2015a. MiR-155 modulates the progression of neuropathic pain through targeting SGK3. *Int J Clin Exp Pathol,* 8**,** 14374-82.

LIU, Y., WANG, R., JIANG, J., YANG, B., CAO, Z. & CHENG, X. 2015b. miR-223 is upregulated in monocytes from patients with tuberculosis and regulates function of monocyte-derived macrophages. *Mol Immunol,* 67**,** 475-81.

LOLMEDE, K., CAMPANA, L., VEZZOLI, M., BOSURGI, L., TONLORENZI, R., CLEMENTI, E., BIANCHI, M. E., COSSU, G., MANFREDI, A. A., BRUNELLI, S. & ROVERE-QUERINI, P. 2009. Inflammatory and alternatively activated human macrophages attract vessel-associated stem cells, relying on separate HMGB1- and MMP-9-dependent pathways. *J Leukoc Biol,* 85**,** 779-87.

LONG, M., WAN, X., LA, X., GONG, X. & CAI, X. 2015. miR-29c is downregulated in the ectopic endometrium and exerts its effects on endometrial cell proliferation, apoptosis and invasion by targeting c-Jun. *Int J Mol Med,* 35**,** 1119-25.

LOUAFI, F., MARTINEZ-NUNEZ, R. T. & SANCHEZ-ELSNER, T. 2010. MicroRNA-155 targets SMAD2 and modulates the response of macrophages to transforming growth factor-{beta}. *J Biol Chem,* 285**,** 41328-36.

LOUIS, C. A., REICHNER, J. S., HENRY, W. L., JR., MASTROFRANCESCO, B., GOTOH, T., MORI, M. & ALBINA, J. E. 1998. Distinct arginase isoforms expressed in primary and transformed macrophages: regulation by oxygen tension. *Am J Physiol,* 274**,** R775-82.

LOUSSE, J. C., VAN LANGENDONCKT, A., GONZALEZ-RAMOS, R., DEFRERE, S., RENKIN, E. & DONNEZ, J. 2008. Increased activation of nuclear factor-kappa B (NF-kappaB) in isolated peritoneal macrophages of patients with endometriosis. *Fertil Steril,* 90.

LUCAS, T., WAISMAN, A., RANJAN, R., ROES, J., KRIEG, T., MULLER, W., ROERS, A. & EMING, S. A. 2010. Differential roles of macrophages in diverse phases of skin repair. *J Immunol,* 184**,** 3964-77.

LUCK, M. E., MULJO, S. A. & COLLINS, C. B. 2015. Prospects for Therapeutic Targeting of MicroRNAs in Human Immunological Diseases. *Journal of immunology (Baltimore, Md. : 1950),* 194**,** 5047-5052.

LV, X., CHEN, P. & LIU, W. 2015. Down regulation of MiR-93 contributes to endometriosis through targeting MMP3 and VEGFA. *Am J Cancer Res,* 5**,** 1706-17.

MA, J., CHEN, T., MANDELIN, J., CEPONIS, A., MILLER, N. E., HUKKANEN, M., MA, G. F. & KONTTINEN, Y. T. 2003. Regulation of macrophage activation. *Cell Mol Life Sci,* 60**,** 2334-46.

MA, Y. L., MA, Z. J., WANG, M., LIAO, M. Y., YAO, R. & LIAO, Y. H. 2015. MicroRNA-155 induces differentiation of RAW264.7 cells into dendritic-like cells. *Int J Clin Exp Pathol,* 8**,** 14050-62.

MAAS, J. W., CALHAZ-JORGE, C., TER RIET, G., DUNSELMAN, G. A., DE GOEIJ, A. F. & STRUIJKER-BOUDIER, H. A. 2001. Tumor necrosis factor-alpha but not interleukin-1 beta or interleukin-8 concentrations correlate with angiogenic activity of peritoneal fluid from patients with minimal to mild endometriosis. *Fertil Steril,* 75**,** 180-5.

MACHADO, D. E., PALUMBO, A., JR., SANTOS, J. M., MATTOS, R. M., DOS SANTOS, T. A., SEABRA, S. H., BOLDRINI LDA, C., PERINI, J. A. & NASCIUTTI, L. E. 2014. A GFP endometriosis model reveals important morphological characteristics of the angiogenic process that govern benign and malignant diseases. *Histol Histopathol,* 29**,** 903-12.

MAK, A. & UETRECHT, J. 2019. Involvement of CCL2/CCR2 macrophage recruitment in amodiaquine-induced liver injury. *J Immunotoxicol***,** 1-6.

MAKIEVA, S., GIACOMINI, E., OTTOLINA, J., SANCHEZ, A. M., PAPALEO, E. & VIGANO, P. 2018. Inside the Endometrial Cell Signaling Subway: Mind the Gap(s). *Int J Mol Sci,* 19.

MAKITA, K., ISHITANI, K., OHTA, H., HORIGUCHI, F. & NOZAWA, S. 2005. Long-term effects on bone mineral density and bone metabolism of 6 months' treatment with gonadotropin-releasing hormone analogues in Japanese women: comparison of buserelin acetate with leuprolide acetate. *J Bone Miner Metab,* 23**,** 389-94.

MANGAT, R., BORTHWICK, F., HAASE, T., JACOME, M., NELSON, R., KONTUSH, A., VINE, D. F. & PROCTOR, S. D. 2018. Intestinal lymphatic HDL miR-223 and ApoA-I are reduced during insulin resistance and restored with niacin. *Faseb j,* 32**,** 1602-1612.

MARTIN, J. D., JR. & HAUCK, A. E. 1985. Endometriosis in the male. *Am Surg,* 51**,** 426-30.

MARTINEZ-NUNEZ, R. T., LOUAFI, F. & SANCHEZ-ELSNER, T. 2011. The interleukin 13 (IL-13) pathway in human macrophages is modulated by microRNA-155 via direct targeting of interleukin 13 receptor alpha1 (IL13Ralpha1). *J Biol Chem,* 286**,** 1786-94.

MARTINEZ, F. O. & GORDON, S. 2014. The M1 and M2 paradigm of macrophage activation: time for reassessment. *F1000Prime Rep,* 6**,** 13.

MARTINEZ, F. O., SICA, A., MANTOVANI, A. & LOCATI, M. 2008. Macrophage activation and polarization. *Front Biosci,* 13**,** 453-61.

MARUYAMA, T. & YOSHIMURA, Y. 2008. Molecular and cellular mechanisms for differentiation and regeneration of the uterine endometrium. *Endocr J,* 55**,** 795-810.

MASAKI, S., OHTSUKA, R., ABE, Y., MUTA, K. & UMEMURA, T. 2007. Expression patterns of microRNAs 155 and 451 during normal human erythropoiesis. *Biochem Biophys Res Commun,* 364**,** 509-14.

MATARESE, G., DE PLACIDO, G., NIKAS, Y. & ALVIGGI, C. 2003. Pathogenesis of endometriosis: natural immunity dysfunction or autoimmune disease? *Trends Mol Med,* 9.

MAYBIN, J. A., CRITCHLEY, H. O. & JABBOUR, H. N. 2011. Inflammatory pathways in endometrial disorders. *Mol Cell Endocrinol,* 335**,** 42-51.

MAYBIN, J. A., BARCROFT, J., THIRUCHELVAM, U., HIRANI, N., JABBOUR, H. N. & CRITCHLEY, H. O. 2012. The presence and regulation of connective tissue growth factor in the human endometrium. Hum Reprod, 27, 1112-21.

MCCARTHY, D. J., CHEN, Y. & SMYTH, G. K. 2012. Differential expression analysis of multifactor RNA-Seq experiments with respect to biological variation. *Nucleic acids research,* 40**,** 4288-4297.

MCKINNON, B., BERSINGER, N. A., HUBER, A. W., KUHN, A. & MUELLER, M. D. 2010. PPAR-gamma expression in peritoneal endometriotic lesions correlates with pain experienced by patients. *Fertility and sterility,* 93**,** 293-296.

MCLAREN, J., PRENTICE, A., CHARNOCK-JONES, D. S., MILLICAN, S. A., MULLER, K. H., SHARKEY, A. M. & SMITH, S. K. 1996. Vascular endothelial growth factor is produced by peritoneal fluid macrophages in endometriosis and is regulated by ovarian steroids. *J Clin Invest,* 98**,** 482-9.

MCLARREN, K. W., COLE, A. E., WEISSER, S. B., VOGLMAIER, N. S., CONLIN, V. S., JACOBSON, K., POPESCU, O., BOUCHER, J.-L. & SLY, L. M. 2011. SHIP-deficient mice develop spontaneous intestinal inflammation and arginase-dependent fibrosis. *The American journal of pathology,* 179**,** 180-188.

MEHEDINTU, C., PLOTOGEA, M. N., IONESCU, S. & ANTONOVICI, M. 2014. Endometriosis still a challenge. *Journal of Medicine and Life,* 7**,** 349-357.

MEHTA, A. & BALTIMORE, D. 2016. MicroRNAs as regulatory elements in immune system logic. *Nature Reviews Immunology,* 16**,** 279.

MEISTER, G. 2013. Argonaute proteins: functional insights and emerging roles. *Nat Rev Genet,* 14**,** 447-59.

MELE, A., FONZINO, A., RANA, F., CAMERINO, G. M., DE BELLIS, M., CONTE, E., GIUSTINO, A., CONTE CAMERINO, D. & DESAPHY, J.-F. 2016. In vivo longitudinal study of rodent skeletal muscle atrophy using ultrasonography. *Scientific Reports,* 6**,** 20061.

MELOCHE, J., LE GUEN, M., POTUS, F., VINCK, J., RANCHOUX, B., JOHNSON, I., ANTIGNY, F., TREMBLAY, E., BREUILS-BONNET, S., PERROS, F., PROVENCHER, S. & BONNET, S. 2015. miR-223 reverses experimental pulmonary arterial hypertension. *Am J Physiol Cell Physiol,* 309**,** C363-72.

MEOLA, J., ROSA E SILVA, J. C., DENTILLO, D. B., DA SILVA, W. A., JR., VEIGA-CASTELLI, L. C., BERNARDES, L. A., FERRIANI, R. A., DE PAZ, C. C., GIULIATTI, S. & MARTELLI, L. 2010. Differentially expressed genes in eutopic and ectopic endometrium of women with endometriosis. *Fertil Steril,* 93**,** 1750-73.

MILEWSKI, Ł., BARCZ, E., DZIUNYCZ, P., RADOMSKI, D., KAMIŃSKI, P., ROSZKOWSKI, P. I., KORCZAK-KOWALSKA, G. & MALEJCZYK, J. 2008. Association of leptin with inflammatory cytokines and lymphocyte subpopulations in peritoneal fluid of patients with endometriosis. *Journal of reproductive immunology,* 79**,** 111-117.

MILEWSKI, L., DZIUNYCZ, P., BARCZ, E., RADOMSKI, D., ROSZKOWSKI, P. I., KORCZAK-KOWALSKA, G., KAMINSKI, P. & MALEJCZYK, J. 2011. Increased levels of human neutrophil peptides 1, 2, and 3 in peritoneal fluid of patients with endometriosis: association with neutrophils, T cells and IL-8. *J Reprod Immunol,* 91**,** 64-70.

MIRA, T. A. A., BUEN, M. M., BORGES, M. G., YELA, D. A. & BENETTI-PINTO, C. L. 2018. Systematic review and meta-analysis of complementary treatments for women with symptomatic endometriosis. *Int J Gynaecol Obstet,* 143**,** 2-9.

MIRZA, R., DIPIETRO, L. A. & KOH, T. J. 2009. Selective and specific macrophage ablation is detrimental to wound healing in mice. *Am J Pathol,* 175**,** 2454-62.

MISSMER, S. A., HANKINSON, S. E., SPIEGELMAN, D., BARBIERI, R. L., MALSPEIS, S., WILLETT, W. C. & HUNTER, D. J. 2004. Reproductive history and endometriosis among premenopausal women. *Obstet Gynecol,* 104**,** 965-74.

MONTAGNANA, M., BENATI, M., DANESE, E., GIUDICI, S., PERFRANCESCHI, M., RUZZENENETE, O., SALVAGNO, G. L., BASSI, A., GELATI, M., PAVIATI, E., GUIDI, G. C., FRANCHI, M. & LIPPI, G. 2017. Aberrant MicroRNA Expression in Patients With Endometrial Cancer. *Int J Gynecol Cancer,* 27**,** 459-466.

MONTGOMERY, G. W., NYHOLT, D. R., ZHAO, Z. Z., TRELOAR, S. A., PAINTER, J. N., MISSMER, S. A., KENNEDY, S. H. & ZONDERVAN, K. T. 2008. The search for genes contributing to endometriosis risk. *Hum Reprod Update,* 14**,** 447-57.

MOON, C. E., BERTERO, M. C., CURRY, T. E., LONDON, S. N., MUSE, K. N., SHARPE, K. L. & VERNON, M. W. 1993. The presence of luteinized unruptured follicle syndrome and altered folliculogenesis in rats with surgically induced endometriosis. *Am J Obstet Gynecol,* 169**,** 676-82.

MOORE, J. S., GIBSON, P. R., PERRY, R. E. & BURGELL, R. E. 2017. Endometriosis in patients with irritable bowel syndrome: Specific symptomatic and demographic profile, and response to the low FODMAP diet. *Aust N Z J Obstet Gynaecol,* 57**,** 201-205.

MORI, H., SAWAIRI, M., NAKAGAWA, M., ITOH, N., WADA, K. & TAMAYA, T. 1992. Expression of interleukin-1 (IL-1) beta messenger ribonucleic acid (mRNA) and IL-1 receptor antagonist mRNA in peritoneal macrophages from patients with endometriosis. *Fertil Steril,* 57**,** 535-42.

MOROTTI, M., VINCENT, K. & BECKER, C. M. 2017. Mechanisms of pain in endometriosis. *European Journal of Obstetrics & Gynecology and Reproductive Biology,* 209**,** 8-13.

MOSSER, D. M. & EDWARDS, J. P. 2008. Exploring the full spectrum of macrophage activation. *Nat Rev Immunol,* 8**,** 958-69.

MOUSA, N. A., BEDAIWY, M. A. & CASPER, R. F. 2007. Aromatase inhibitors in the treatment of severe endometriosis. *Obstet Gynecol,* 109**,** 1421-3.

NA, Y. J., YANG, S. H., BAEK, D. W., LEE, D. H., KIM, K. H., CHOI, Y. M., OH, S. T., HONG, Y. S., KWAK, J. Y. & LEE, K. S. 2006. Effects of peritoneal fluid from endometriosis patients on the release of vascular endothelial growth factor by neutrophils and monocytes. *Hum Reprod,* 21**,** 1846-55.

NAGARKATTI, M., ZHOU, J., LESSEY, B. A. & NAGARKATTI, P. 2015. *Leukocyte MicroRNAs for use in diagnosis and treatment of endometriosis*. USA patent application 14/662574.

NAGASE, H., VISSE, R. & MURPHY, G. 2006. Structure and function of matrix metalloproteinases and TIMPs. *Cardiovasc Res,* 69**,** 562-73.

NAP, A. W. 2012. Theories on the Pathogenesis of Endometriosis. *Endometriosis.* Wiley-Blackwell.

NAP, A. W., DUNSELMAN, G. A., GRIFFIOEN, A. W., MAYO, K. H., EVERS, J. L. & GROOTHUIS, P. G. 2005. Angiostatic agents prevent the development of endometriosis-like lesions in the chicken chorioallantoic membrane. *Fertil Steril,* 83**,** 793-5.

NAP, A. W., GROOTHUIS, P. G., DEMIR, A. Y., MAAS, J. W., DUNSELMAN, G. A., DE GOEIJ, A. F. & EVERS, J. L. 2003. Tissue integrity is essential for ectopic implantation of human endometrium in the chicken chorioallantoic membrane. *Hum Reprod,* 18**,** 30-4.

NEUDECKER, V., HANEKLAUS, M., JENSEN, O., KHAILOVA, L., MASTERSON, J. C., TYE, H., BIETTE, K., JEDLICKA, P., BRODSKY, K. S., GERICH, M. E., MACK, M., ROBERTSON, A. A. B., COOPER, M. A., FURUTA, G. T., DINARELLO, C. A., O'NEILL, L. A., ELTZSCHIG, H. K., MASTERS, S. L. & MCNAMEE, E. N. 2017. Myeloid-derived miR-223 regulates intestinal inflammation via repression of the NLRP3 inflammasome. *J Exp Med,* 214**,** 1737-1752.

NI, N., GAO, Y., FANG, X., MELGAR, M., VINCENT, D. F., LYDON, J. P., BARTHOLIN, L. & LI, Q. 2018. Glandular defects in the mouse uterus with sustained activation of TGF-beta signaling is associated with altered differentiation of endometrial stromal cells and formation of stromal compartment. *PloS one,* 13**,** e0209417-e0209417.

NISENBLAT, V., BOSSUYT, P. M., SHAIKH, R., FARQUHAR, C., JORDAN, V., SCHEFFERS, C. S., MOL, B. W., JOHNSON, N. & HULL, M. L. 2016a. Blood biomarkers for the non-invasive diagnosis of endometriosis. *Cochrane Database Syst Rev***,** CD012179.

NISENBLAT, V., PRENTICE, L., BOSSUYT, P. M., FARQUHAR, C., HULL, M. L. & JOHNSON, N. 2016b. Combination of the non-invasive tests for the diagnosis of endometriosis. *Cochrane Database Syst Rev,* 7**,** CD012281.

NISENBLAT, V., ROBERTSON, S. A., EVANS, S. F. & HULL, L. M. 2012. Plasma miRNAS as non-invasive biomarkers for endometriosis. *Fertility and Sterility,* 98**,** S217-S218.

NISENBLAT, V., SHARKEY, D. J., WANG, Z., EVANS, S. F., HEALEY, M., OHLSSON TEAGUE, E. M. C., PRINT, C. G., ROBERTSON, S. A. & HULL, M. L. 2019. Plasma microRNAs display limited potential as diagnostic tools for endometriosis. *J Clin Endocrinol Metab*.

NOTHNICK, W. B. 2001. Treating endometriosis as an autoimmune disease. *Fertil Steril,* 76**,** 223-31.

NOTHNICK, W. B. 2017. MicroRNAs and Endometriosis: Distinguishing Drivers from Passengers in Disease Pathogenesis. *Semin Reprod Med,* 35**,** 173-180.

NOTHNICK, W. B., AL-HENDY, A. & LUE, J. R. 2015. Circulating Micro-RNAs as Diagnostic Biomarkers for Endometriosis: Privation and Promise. *Journal of Minimally Invasive Gynecology,* 22**,** 719-726.

NOTHNICK, W. B., FALCONE, T., JOSHI, N., FAZLEABAS, A. T. & GRAHAM, A. 2017. Serum miR-451a Levels Are Significantly Elevated in Women With Endometriosis and Recapitulated in Baboons (Papio anubis) With Experimentally-Induced Disease. *Reprod Sci,* 24**,** 1195-1202.

NOTHNICK, W. B., GRAHAM, A., HOLBERT, J. & WEISS, M. J. 2014. miR-451 deficiency is associated with altered endometrial fibrinogen alpha chain expression and reduced endometriotic implant establishment in an experimental mouse model. *PLoS One,* 9**,** e100336.

NOTHNICK, W. B. & HEALY, C. 2010. Estrogen induces distinct patterns of microRNA expression within the mouse uterus. *Reprod Sci,* 17**,** 987-94.

NOVAK, M. L. & KOH, T. J. 2013. Macrophage phenotypes during tissue repair. *J Leukoc Biol,* 93**,** 875-81.

NYHOLT, D. R., LOW, S. K., ANDERSON, C. A., PAINTER, J. N., UNO, S., MORRIS, A. P., MACGREGOR, S., GORDON, S. D., HENDERS, A. K., MARTIN, N. G., ATTIA, J., HOLLIDAY, E. G., MCEVOY, M., SCOTT, R. J., KENNEDY, S. H., TRELOAR, S. A., MISSMER, S. A., ADACHI, S., TANAKA, K., NAKAMURA, Y., ZONDERVAN, K. T., ZEMBUTSU, H. & MONTGOMERY, G. W. 2012. Genome-wide association meta-analysis identifies new endometriosis risk loci. *Nat Genet,* 44**,** 1355-9.

O'CONNELL, R. M., RAO, D. S. & BALTIMORE, D. 2012. microRNA regulation of inflammatory responses. *Annu Rev Immunol,* 30**,** 295-312.

O'CONNELL, R. M., TAGANOV, K. D., BOLDIN, M. P., CHENG, G. & BALTIMORE, D. 2007. MicroRNA-155 is induced during the macrophage inflammatory response. *Proceedings of the National Academy of Sciences,* 104**,** 1604-1609.

O'NEILL, L. A., SHEEDY, F. J. & MCCOY, C. E. 2011. MicroRNAs: the fine-tuners of Toll-like receptor signalling. *Nature Reviews Immunology,* 11**,** 163.

OERTELT-PRIGIONE, S. 2012. Immunology and the menstrual cycle. *Autoimmun Rev,* 11**,** A486-92.

OHLSSON TEAGUE, E. M., VAN DER HOEK, K. H., VAN DER HOEK, M. B., PERRY, N., WAGAARACHCHI, P., ROBERTSON, S. A., PRINT, C. G. & HULL, L. M. 2009. MicroRNA-regulated pathways associated with endometriosis. *Mol Endocrinol,* 23**,** 265-275.

OKADA, H., KOHANBASH, G. & LOTZE, M. T. 2010. MicroRNAs in immune regulation--opportunities for cancer immunotherapy. *Int J Biochem Cell Biol,* 42**,** 1256-61.

OKAMOTO, M., NASU, K., ABE, W., AOYAGI, Y., KAWANO, Y., KAI, K., MORIYAMA, M. & NARAHARA, H. 2015. Enhanced miR-210 expression promotes the pathogenesis of endometriosis through activation of signal transducer and activator of transcription 3. *Hum Reprod,* 30**,** 632-41.

OOSTERLYNCK, D. J., CORNILLIE, F. J., WAER, M. & KONINCKX, P. R. 1993. Immunohistochemical characterization of leucocyte subpopulations in endometriotic lesions. *Arch Gynecol Obstet,* 253**,** 197-206.

OOSTERLYNCK, D. J., CORNILLIE, F. J., WAER, M., VANDEPUTTE, M. & KONINCKX, P. R. 1991. Women with endometriosis show a defect in natural killer activity resulting in a decreased cytotoxicity to autologous endometrium. *Fertil Steril,* 56**,** 45-51.

OSBORN, B. H., HANEY, A. F., MISUKONIS, M. A. & WEINBERG, J. B. 2002. Inducible nitric oxide synthase expression by peritoneal macrophages in endometriosis-associated infertility. *Fertil Steril,* 77**,** 46-51.

OSTEEN, K. G., YEAMAN, G. R. & BRUNER-TRAN, K. L. 2003. Matrix metalloproteinases and endometriosis. *Semin Reprod Med,* 21**,** 155-64.

PAINTER, J. N., ANDERSON, C. A., NYHOLT, D. R., MACGREGOR, S., LIN, J., LEE, S. H., LAMBERT, A., ZHAO, Z. Z., ROSEMAN, F., GUO, Q., GORDON, S. D., WALLACE, L., HENDERS, A. K., VISSCHER, P. M., KRAFT, P., MARTIN, N. G., MORRIS, A. P., TRELOAR, S. A., KENNEDY, S. H., MISSMER, S. A., MONTGOMERY, G. W. & ZONDERVAN, K. T. 2011. Genome-wide association study identifies a locus at 7p15.2 associated with endometriosis. *Nat Genet,* 43**,** 51-4.

PAINTER, J. N., NYHOLT, D. R., KRAUSE, L., ZHAO, Z. Z., CHAPMAN, B., ZHANG, C., MEDLAND, S., MARTIN, N. G., KENNEDY, S., TRELOAR, S., ZONDERVAN, K. & MONTGOMERY, G. W. 2014. Common variants in the CYP2C19 gene are associated with susceptibility to endometriosis. *Fertility and sterility,* 102**,** 496-502.e5.

PARASAR, P., OZCAN, P. & TERRY, K. L. 2017. Endometriosis: Epidemiology, Diagnosis and Clinical Management. *Current obstetrics and gynecology reports,* 6**,** 34-41.

PARAZZINI, F., VERCELLINI, P. & PELUCCHI, C. 2012. Endometriosis: Epidemiology, and Etiological Factors. *Endometriosis.* Wiley-Blackwell.

PAREKH, V. V., WU, L., OLIVARES-VILLAGOMEZ, D., WILSON, K. T. & VAN KAER, L. 2013. Activated invariant NKT cells control central nervous system autoimmunity in a mechanism that involves myeloid-derived suppressor cells. *J Immunol,* 190**,** 1948-60.

PARISI, L., GINI, E., BACI, D., TREMOLATI, M., FANULI, M., BASSANI, B., FARRONATO, G., BRUNO, A. & MORTARA, L. 2018. Macrophage Polarization in Chronic Inflammatory Diseases: Killers or Builders? *J Immunol Res,* 2018**,** 8917804.

PARK, J. M., GRETEN, F. R., WONG, A., WESTRICK, R. J., ARTHUR, J. S., OTSU, K., HOFFMANN, A., MONTMINY, M. & KARIN, M. 2005. Signaling pathways and genes that inhibit pathogen-induced macrophage apoptosis--CREB and NF-kappaB as key regulators. *Immunity,* 23**,** 319-29.

PARK, Y. R., LEE, S. T., KIM, S. L., LIU, Y. C., LEE, M. R., SHIN, J. H., SEO, S. Y., KIM, S. H., KIM, I. H., LEE, S. O. & KIM, S. W. 2016. MicroRNA-9 suppresses cell migration and invasion through downregulation of TM4SF1 in colorectal cancer. *Int J Oncol,* 48**,** 2135-43.

PATHIVADA, S. & D'HOOGHE, T. 2012. Endometriosis and Autoimmunity. *Endometriosis.* Wiley-Blackwell.

PATTERSON, C., PERRELLA, M. A., ENDEGE, W. O., YOSHIZUMI, M., LEE, M. E. & HABER, E. 1996. Downregulation of vascular endothelial growth factor receptors by tumor necrosis factor-alpha in cultured human vascular endothelial cells. *The Journal of clinical investigation,* 98**,** 490-496.

PAZHOHAN, A., AMIDI, F., AKBARI-ASBAGH, F., SEYEDREZAZADEH, E., FARZADI, L., KHODARAHMIN, M., MEHDINEJADIANI, S. & SOBHANI, A. 2018. The Wnt/beta-catenin signaling in endometriosis, the expression of total and active forms of beta-catenin, total and inactive forms of glycogen synthase kinase-3beta, WNT7a and DICKKOPF-1. *Eur J Obstet Gynecol Reprod Biol,* 220**,** 1-5.

PELCH, K. E., SCHRODER, A. L., KIMBALL, P. A., SHARPE-TIMMS, K. L., DAVIS, J. W. & NAGEL, S. C. 2010. Aberrant gene expression profile in a mouse model of endometriosis mirrors that observed in women. *Fertil Steril,* 93**,** 1615-1627 e18.

PERANZONI, E., ZILIO, S., MARIGO, I., DOLCETTI, L., ZANOVELLO, P., MANDRUZZATO, S. & BRONTE, V. 2010. Myeloid-derived suppressor cell heterogeneity and subset definition. *Curr Opin Immunol,* 22**,** 238-44.

PEREIRA, S., GIBBS, R. A. & MCGUIRE, A. L. 2014. Open Access Data Sharing in Genomic Research. *Genes,* 5**,** 739-747.

PETRACCO, R., GRECHUKHINA, O., POPKHADZE, S., MASSASA, E., ZHOU, Y. & TAYLOR, H. S. 2011. MicroRNA 135 regulates HOXA10 expression in endometriosis. *J Clin Endocrinol Metab,* 96**,** E1925-33.

PLATTEEUW, L. & D'HOOGHE, T. 2014. Novel agents for the medical treatment of endometriosis. *Curr Opin Obstet Gynecol,* 26**,** 243-52.

POH, A. R. & ERNST, M. 2018. Targeting Macrophages in Cancer: From Bench to Bedside. *Front Oncol,* 8**,** 49.

PONPUCKDEE, J. & TANEEPANICHSKUL, S. 2005. The effects of implanon in the symptomatic treatment of endometriosis. *Journal of the Medical Association of Thailand = Chotmaihet thangphaet,* 88 Suppl 2**,** S7-10.

POROPATICH, C., ROJAS, M. & SILVERBERG, S. G. 1987. Polymorphonuclear leukocytes in the endometrium during the normal menstrual cycle. Int J Gynecol Pathol, 6, 230-4.

PRAME KUMAR, K., NICHOLLS, A. J. & WONG, C. H. Y. 2018. Partners in crime: neutrophils and monocytes/macrophages in inflammation and disease. *Cell Tissue Res,* 371**,** 551-565.

QUINN, S. R., MANGAN, N. E., CAFFREY, B. E., GANTIER, M. P., WILLIAMS, B. R., HERTZOG, P. J., MCCOY, C. E. & O'NEILL, L. A. 2014. The role of Ets2 transcription factor in the induction of microRNA-155 (miR-155) by lipopolysaccharide and its targeting by interleukin-10. *J Biol Chem,* 289**,** 4316-25.

RAHMIOGLU, N., MACGREGOR, S., DRONG, A. W., HEDMAN, A. K., HARRIS, H. R., RANDALL, J. C., PROKOPENKO, I., NYHOLT, D. R., MORRIS, A. P., MONTGOMERY, G. W., MISSMER, S. A., LINDGREN, C. M. & ZONDERVAN, K. T. 2015. Genome-wide enrichment analysis between endometriosis and obesity-related traits reveals novel susceptibility loci. *Hum Mol Genet,* 24**,** 1185-99.

RAHMIOGLU, N., NYHOLT, D. R., MORRIS, A. P., MISSMER, S. A., MONTGOMERY, G. W. & ZONDERVAN, K. T. 2014. Genetic variants underlying risk of endometriosis: insights from meta-analysis of eight genome-wide association and replication datasets. *Hum Reprod Update,* 20**,** 702-16.

RAI, D., KIM, S. W., MCKELLER, M. R., DAHIA, P. L. & AGUIAR, R. C. 2010. Targeting of SMAD5 links microRNA-155 to the TGF-beta pathway and lymphomagenesis. *Proc Natl Acad Sci U S A,* 107**,** 3111-6.

RAMON, L. A., BRAZA-BOILS, A., GILABERT-ESTELLES, J., GILABERT, J., ESPANA, F., CHIRIVELLA, M. & ESTELLES, A. 2011. microRNAs expression in endometriosis and their relation to angiogenic factors. *Hum Reprod,* 26**,** 1082-90.

RAZZI, S., LUISI, S., CALONACI, F., ALTOMARE, A., BOCCHI, C. & PETRAGLIA, F. 2007. Efficacy of vaginal danazol treatment in women with recurrent deeply infiltrating endometriosis. *Fertil Steril,* 88**,** 789-94.

REKKER, K., SAARE, M., ROOST, A. M., KAART, T., SORITSA, D., KARRO, H., SORITSA, A., SIMON, C., SALUMETS, A. & PETERS, M. 2015. Circulating miR-200-family micro-RNAs have altered plasma levels in patients with endometriosis and vary with blood collection time. *Fertil Steril,* 104**,** 938-946 e2.

REKKER, K., SAARE, M., ROOST, A. M., SALUMETS, A. & PETERS, M. 2013. Circulating microRNA Profile throughout the menstrual cycle. *PLoS One,* 8**,** e81166.

RESUEHR, D., GLORE, D. R., TAYLOR, H. S., BRUNER-TRAN, K. L. & OSTEEN, K. G. 2012. Progesterone-dependent regulation of endometrial cannabinoid receptor type 1 (CB1-R)

expression is disrupted in women with endometriosis and in isolated stromal cells exposed to 2,3,7,8-tetrachlorodibenzo-p-dioxin (TCDD). *Fertil Steril,* 98**,** 948-56.e1.

RIBATTI, D., NICO, B., VACCA, A., RONCALI, L., BURRI, P. H. & DJONOV, V. 2001. Chorioallantoic membrane capillary bed: a useful target for studying angiogenesis and anti-angiogenesis in vivo. *Anat Rec,* 264**,** 317-24.

RICCIO, L., SANTULLI, P., MARCELLIN, L., ABRAO, M. S., BATTEUX, F. & CHAPRON, C. 2018. Immunology of endometriosis. *Best Pract Res Clin Obstet Gynaecol,* 50**,** 39-49.

RICHTER, O. N., DORN, C., ROSING, B., FLASKAMP, C. & ULRICH, U. 2005. Tumor necrosis factor alpha secretion by peritoneal macrophages in patients with endometriosis. *Arch Gynecol Obstet,* 271**,** 143-7.

RIER, S. E. 2002. The potential role of exposure to environmental toxicants in the pathophysiology of endometriosis. *Ann N Y Acad Sci,* 955.

RIER, S. E., MARTIN, D. C., BOWMAN, R. E., DMOWSKI, W. P. & BECKER, J. L. 1993. Endometriosis in rhesus monkeys (Macaca mulatta) following chronic exposure to 2,3,7,8-tetrachlorodibenzo-p-dioxin. *Fundam Appl Toxicol,* 21.

RIER, S. E., TURNER, W. E., MARTIN, D. C., MORRIS, R., LUCIER, G. W. & CLARK, G. C. 2001. Serum levels of TCDD and dioxin-like chemicals in Rhesus monkeys chronically exposed to dioxin: correlation of increased serum PCB levels with endometriosis. *Toxicol Sci,* 59**,** 147-59.

RITCHIE, M. E., PHIPSON, B., WU, D., HU, Y., LAW, C. W., SHI, W. & SMYTH, G. K. 2015. limma powers differential expression analyses for RNA-sequencing and microarray studies. *Nucleic acids research,* 43**,** e47-e47.

ROBERTO, V. P., TIAGO, D. M., GAUTVIK, K. & CANCELA, M. L. 2015. Evidence for the conservation of miR-223 in zebrafish (Danio rerio): Implications for function. *Gene,* 566**,** 54-62.

ROBINSON, M. D., MCCARTHY, D. J. & SMYTH, G. K. 2010. edgeR: a Bioconductor package for differential expression analysis of digital gene expression data. *Bioinformatics (Oxford, England),* 26**,** 139-140.

RODRÍGUEZ, A. E., HERNÁNDEZ, J. Á., BENITO, R., GUTIÉRREZ, N. C., GARCÍA, J. L., HERNÁNDEZ-SÁNCHEZ, M., RISUEÑO, A., SARASQUETE, M. E., FERMIÑÁN, E., FISAC, R., DE COCA, A. G., MARTÍN-NÚÑEZ, G., DE LAS HERAS, N., RECIO, I., GUTIÉRREZ, O., DE LAS RIVAS, J., GONZÁLEZ, M. & HERNÁNDEZ-RIVAS, J. M. 2012. Molecular characterization of chronic lymphocytic leukemia patients with a high number of losses in 13q14. *PloS one,* 7**,** e48485-e48485.

ROGERS, P. A., ADAMSON, G. D., AL-JEFOUT, M., BECKER, C. M., D'HOOGHE, T. M., DUNSELMAN, G. A., FAZLEABAS, A., GIUDICE, L. C., HORNE, A. W., HULL, M. L., HUMMELSHOJ, L., MISSMER, S. A., MONTGOMERY, G. W., STRATTON, P., TAYLOR, R. N., ROMBAUTS, L., SAUNDERS, P. T., VINCENT, K. & ZONDERVAN, K. T. 2016. Research Priorities for Endometriosis: Recommendations From a Global Consortium of Investigators in Endometriosis. *Reprod Sci*.

ROSSI, M., SHARKEY, A. M., VIGANO, P., FIORE, G., FURLONG, R., FLORIO, P., AMBROSINI, G., SMITH, S. K. & PETRAGLIA, F. 2005. Identification of genes regulated by interleukin-1beta in human endometrial stromal cells. *Reproduction,* 130**,** 721-9.

RUAN, Y., QIAN, W. P., ZHANG, C. H., ZHOU, L. & HOU, Z. H. 2013. [Study on microRNA expression in endometrium of luteal phase and its relationship with infertility of endometriosis]. *Zhonghua Fu Chan Ke Za Zhi,* 48**,** 907-10.

RUBI-KLEIN, K., KUCERA-SLIUTZ, E., NISSEL, H., BIJAK, M., STOCKENHUBER, D., FINK, M. & WOLKENSTEIN, E. 2010. Is acupuncture in addition to conventional medicine effective as pain

treatment for endometriosis? A randomised controlled cross-over trial. *Eur J Obstet Gynecol Reprod Biol,* 153**,** 90-3.

SALAMONSEN, L. A., ZHANG, J. & BRASTED, M. 2002. Leukocyte networks and human endometrial remodelling. J Reprod Immunol, 57, 95-108.

SAMPSON, J. 1927. Peritoneal endometriosis due to the menstrual dissemination of endometrial tissue into the peritoneal cavity. *Am J Obstet Gynecol,* 14.

SAPKOTA, Y., FASSBENDER, A., BOWDLER, L., FUNG, J. N., PETERSE, D., O, D., MONTGOMERY, G. W., NYHOLT, D. R. & D'HOOGHE, T. M. 2015a. Independent Replication and Meta-Analysis for Endometriosis Risk Loci. *Twin Res Hum Genet,* 18**,** 518-25.

SAPKOTA, Y., LOW, S. K., ATTIA, J., GORDON, S. D., HENDERS, A. K., HOLLIDAY, E. G., MACGREGOR, S., MARTIN, N. G., MCEVOY, M., MORRIS, A. P., TAKAHASHI, A., SCOTT, R. J., KUBO, M., ZONDERVAN, K. T., MONTGOMERY, G. W. & NYHOLT, D. R. 2015b. Association between endometriosis and the interleukin 1A (IL1A) locus. *Hum Reprod,* 30**,** 239-48.

SAPKOTA, Y., STEINTHORSDOTTIR, V., MORRIS, A. P., FASSBENDER, A., RAHMIOGLU, N., DE VIVO, I., BURING, J. E., ZHANG, F. & EDWARDS, T. L. 2017. Meta-analysis identifies five novel loci associated with endometriosis highlighting key genes involved in hormone metabolism. 8**,** 15539.

SCHENKEN, R. S. 2018. *Endometriosis: Pathogenesis, clinical features, and diagnosis* [Online]. Waltham, MA: UpToDate Inc. Available: http://www.uptodate.com [Accessed 20th November 2018].

SCHJENKEN, J. E., PANIR, K., ROBERTSON, S. A. & HULL, M. L. 2019. Exosome-mediated intracellular signalling impacts the development of endometriosis-new avenues for endometriosis research. *Mol Hum Reprod,* 25**,** 2-4.

SCHNEIDER, C., KÄSSENS, N., GREVE, B., HASSAN, H., SCHÜRING, A. N., STARZINSKI-POWITZ, A., KIESEL, L., SEIDLER, D. G. & GÖTTE, M. 2013. Targeting of syndecan-1 by micro-ribonucleic acid miR-10b modulates invasiveness of endometriotic cells via dysregulation of the proteolytic milieu and interleukin-6 secretion. *Fertility and sterility,* 99**,** 871-881.e1.

SCHRODT, G. R., ALCORN, M. O. & IBANEZ, J. 1980. Endometriosis of the male urinary system: a case report. *J Urol,* 124**,** 722-3.

SCHUBERT, M., LINDGREEN, S. & ORLANDO, L. 2016. AdapterRemoval v2: rapid adapter trimming, identification, and read merging. *BMC research notes,* 9**,** 88-88.

SCHULKE, L., BERBIC, M., MANCONI, F., TOKUSHIGE, N., MARKHAM, R. & FRASER, I. S. 2009. Dendritic cell populations in the eutopic and ectopic endometrium of women with endometriosis. *Hum Reprod,* 24**,** 1695-703.

SCUTIERO, G., IANNONE, P., BERNARDI, G., BONACCORSI, G., SPADARO, S., VOLTA, C. A., GRECO, P. & NAPPI, L. 2017. Oxidative Stress and Endometriosis: A Systematic Review of the Literature. *Oxidative Medicine and Cellular Longevity,* 2017**,** 7265238.

SERACCHIOLI, R., MABROUK, M., MANUZZI, L., VICENZI, C., FRASCA, C., ELMAKKY, A. & VENTUROLI, S. 2009. Post-operative use of oral contraceptive pills for prevention of anatomical relapse or symptom-recurrence after conservative surgery for endometriosis. *Hum Reprod,* 24**,** 2729-35.

SERACCHIOLI, R., MONTANARI, G., MABROUK, M. & NASSIF, J. 2014. Endometriosis: Novel Models, Diagnosis, and Treatment. *BioMed Research International,* 2014**,** 2.

SHA, G., WU, D., ZHANG, L., CHEN, X., LEI, M., SUN, H., LIN, S. & LANG, J. 2007. Differentially expressed genes in human endometrial endothelial cells derived from eutopic endometrium of

patients with endometriosis compared with those from patients without endometriosis. *Hum Reprod,* 22**,** 3159-69.

SHA, Y., PHAN, J. H. & WANG, M. D. 2015. Effect of low-expression gene filtering on detection of differentially expressed genes in RNA-seq data. *Conference proceedings : ... Annual International Conference of the IEEE Engineering in Medicine and Biology Society. IEEE Engineering in Medicine and Biology Society. Annual Conference,* 2015**,** 6461-6464.

SHAH, D. K., CORREIA, K. F., VITONIS, A. F. & MISSMER, S. A. 2013. Body size and endometriosis: results from 20 years of follow-up within the Nurses' Health Study II prospective cohort. *Hum Reprod,* 28**,** 1783-92.

SHEA-DONOHUE, T., ZHAO, A. & ANTALIS, T. M. 2014. SerpinB2 mediated regulation of macrophage function during enteric infection. *Gut microbes,* 5**,** 254-258.

SHELTON, D. N., FORNALIK, H., NEFF, T., PARK, S. Y., BENDER, D., DEGEEST, K., LIU, X., XIE, W., MEYERHOLZ, D. K., ENGELHARDT, J. F. & GOODHEART, M. J. 2012. The role of LEF1 in endometrial gland formation and carcinogenesis. *PloS one,* 7**,** e40312-e40312.

SHEMI, A., KHVALEVSKY, E. Z., GABAI, R. M., DOMB, A. & BARENHOLZ, Y. 2015. Multistep, effective drug distribution within solid tumors. *Oncotarget,* 6**,** 39564-77.

SHEN, L., YANG, S., HUANG, W., XU, W., WANG, Q., SONG, Y. & LIU, Y. 2013. MicroRNA23a and microRNA23b deregulation derepresses SF-1 and upregulates estrogen signaling in ovarian endometriosis. *J Clin Endocrinol Metab,* 98**,** 1575-82.

SHI, L., FISSLTHALER, B., ZIPPEL, N., FRÖMEL, T., HU, J., ELGHEZNAWY, A., HEIDE, H., POPP, R. & FLEMING, I. 2013. MicroRNA-223 Antagonizes Angiogenesis by Targeting β1 Integrin and Preventing Growth Factor Signaling in Endothelial Cells. *Circulation Research,* 113**,** 1320-1330.

SHI, R., ZHOU, X., JI, W.-J., ZHANG, Y.-Y., MA, Y.-Q., ZHANG, J.-Q. & LI, Y.-M. 2015. The Emerging Role of miR-223 in Platelet Reactivity: Implications in Antiplatelet Therapy. *BioMed research international,* 2015**,** 981841-981841.

SHI, X. Y., GU, L., CHEN, J., GUO, X. R. & SHI, Y. L. 2014. Downregulation of miR-183 inhibits apoptosis and enhances the invasive potential of endometrial stromal cells in endometriosis. *Int J Mol Med,* 33**,** 59-67.

SHI, Y. L., LUO, X. Z., ZHU, X. Y. & LI, D. J. 2007. Combination of 17beta-estradiol with the environmental pollutant TCDD is involved in pathogenesis of endometriosis via up-regulating the chemokine I-309-CCR8. *Fertil Steril,* 88**,** 317-25.

SHIGESI, N., KVASKOFF, M., KIRTLEY, S., FENG, Q., FANG, H., KNIGHT, J. C., MISSMER, S. A., RAHMIOGLU, N., ZONDERVAN, K. T. & BECKER, C. M. 2019. The association between endometriosis and autoimmune diseases: a systematic review and meta-analysis. *Hum Reprod Update,* 25**,** 486-503.

SHUKLA, G. C., SINGH, J. & BARIK, S. 2011. MicroRNAs: Processing, Maturation, Target Recognition and Regulatory Functions. *Molecular and cellular pharmacology,* 3**,** 83-92.

SICA, A. & MANTOVANI, A. 2012. Macrophage plasticity and polarization: in vivo veritas. *J Clin Invest,* 122**,** 787-95.

SIGNORELLO, L. B., HARLOW, B. L., CRAMER, D. W., SPIEGELMAN, D. & HILL, J. A. 1997. Epidemiologic determinants of endometriosis: a hospital-based case-control study. *Ann Epidemiol,* 7**,** 267-741.

SIMITSIDELLIS, I., GIBSON, D. A. & SAUNDERS, P. T. K. 2018. Animal models of endometriosis: Replicating the aetiology and symptoms of the human disorder. *Best Pract Res Clin Endocrinol Metab,* 32**,** 257-269.

SIMOENS, S., DUNSELMAN, G., DIRKSEN, C., HUMMELSHOJ, L., BOKOR, A., BRANDES, I., BRODSZKY, V., CANIS, M., COLOMBO, G. L., DELEIRE, T., FALCONE, T., GRAHAM, B., HALIS, G., HORNE, A., KANJ, O., KJER, J. J., KRISTENSEN, J., LEBOVIC, D., MUELLER, M., VIGANO, P., WULLSCHLEGER, M. & D'HOOGHE, T. 2012. The burden of endometriosis: costs and quality of life of women with endometriosis and treated in referral centres. *Hum Reprod,* 27**,** 1292-9.

SLAYDEN, O. D. 2013. Induced endometriosis in nonhuman primates. *Biol Reprod,* 88**,** 43.

SMITH, K. A., PEARSON, C. B., HACHEY, A. M., XIA, D. L. & WACHTMAN, L. M. 2012. Alternative activation of macrophages in rhesus macaques (Macaca mulatta) with endometriosis. *Comp Med,* 62**,** 303-10.

SMYTH, G. K. 2005. Limma: linear models for microarray data. *In:* GENTLEMAN, R., CAREY, V., HUBER, W., IRIZARRY, R. & DUDOIT, S. (eds.) *Bioinformatics and Computational Biology Solutions Using R and Bioconductor.* New York: Springer.

SOFO, V., GÖTTE, M., LAGANÀ, A. S., SALMERI, F. M., TRIOLO, O., STURLESE, E., RETTO, G., ALFA, M., GRANESE, R. & ABRÃO, M. S. 2015. Correlation between dioxin and endometriosis: an epigenetic route to unravel the pathogenesis of the disease. *Archives of Gynecology and Obstetrics,* 292**,** 973-986.

SOHLER, F., SOMMER, A., WACHTER, D. L., AGAIMY, A., FISCHER, O. M., RENNER, S. P., BURGHAUS, S., FASCHING, P. A., BECKMANN, M. W., FUHRMANN, U., STRICK, R. & STRISSEL, P. L. 2013. Tissue remodeling and nonendometrium-like menstrual cycling are hallmarks of peritoneal endometriosis lesions. *Reprod Sci,* 20**,** 85-102.

SOLIMAN, A. M., FULDEORE, M. & SNABES, M. C. 2017. Factors Associated with Time to Endometriosis Diagnosis in the United States. *J Womens Health (Larchmt),* 26**,** 788-797.

STAMATOPOULOS, B., MEULEMAN, N., HAIBE-KAINS, B., SAUSSOY, P., VAN DEN NESTE, E., MICHAUX, L., HEIMANN, P., MARTIAT, P., BRON, D. & LAGNEAUX, L. 2009. microRNA-29c and microRNA-223 down-regulation has in vivo significance in chronic lymphocytic leukemia and improves disease risk stratification. *Blood,* 113**,** 5237-45.

SU, J., ZHANG, A., SHI, Z., MA, F., PU, P., WANG, T., ZHANG, J., KANG, C. & ZHANG, Q. 2012. MicroRNA-200a suppresses the Wnt/beta-catenin signaling pathway by interacting with beta-catenin. *Int J Oncol,* 40**,** 1162-70.

SUDA, K., NAKAOKA, H., YOSHIHARA, K., ISHIGURO, T., TAMURA, R., MORI, Y., YAMAWAKI, K., ADACHI, S., TAKAHASHI, T., KASE, H., TANAKA, K., YAMAMOTO, T., MOTOYAMA, T., INOUE, I. & ENOMOTO, T. 2018. Clonal Expansion and Diversification of Cancer-Associated Mutations in Endometriosis and Normal Endometrium. *Cell Rep,* 24**,** 1777-1789.

SUGATANI, T. & HRUSKA, K. A. 2009. Impaired micro-RNA pathways diminish osteoclast differentiation and function. *J Biol Chem,* 284**,** 4667-78.

SUN, H., YUAN, M., LI, N., ZHEN, Q., LI, Q., WANG, G. & LI, D. 2018. Macrophages alternatively activated by endometriosis-exosomes contribute to the development of lesions in mice. *MHR: Basic science of reproductive medicine,* 25**,** 5-16.

SUNDQVIST, J., FALCONER, H., SEDDIGHZADEH, M., VODOLAZKAIA, A., FASSBENDER, A., KYAMA, C., BOKOR, A., STEPHANSSON, O., PADYUKOV, L., GEMZELL-DANIELSSON, K. & D'HOOGHE, T. M. 2011. Endometriosis and autoimmune disease: association of susceptibility to moderate/severe endometriosis with CCL21 and HLA-DRB1. *Fertil Steril,* 95**,** 437-40.

SURREY, E. S. 1999. Add-back therapy and gonadotropin-releasing hormone agonists in the treatment of patients with endometriosis: can a consensus be reached? Add-Back Consensus Working Group. *Fertil Steril,* 71**,** 420-4.

SURYAWANSHI, S., VLAD, A. M., LIN, H. M., MANTIA-SMALDONE, G., LASKEY, R., LEE, M., LIN, Y., DONNELLAN, N., KLEIN-PATEL, M., LEE, T., MANSURIA, S., ELISHAEV, E., BUDIU, R., EDWARDS, R. P. & HUANG, X. 2013. Plasma microRNAs as novel biomarkers for endometriosis and endometriosis-associated ovarian cancer. *Clin Cancer Res,* 19**,** 1213-24.

SZYLLO, K., TCHORZEWSKI, H., BANASIK, M., GLOWACKA, E., LEWKOWICZ, P. & KAMER-BARTOSINSKA, A. 2003. The involvement of T lymphocytes in the pathogenesis of endometriotic tissues overgrowth in women with endometriosis. *Mediators Inflamm,* 12**,** 131-8.

TAIBI, F., METZINGER-LE MEUTH, V., MASSY, Z. A. & METZINGER, L. 2014. miR-223: An inflammatory oncomiR enters the cardiovascular field. *Biochim Biophys Acta,* 1842**,** 1001-9.

TAJIMA, M., HARADA, T., ISHIKAWA, T., IWAHARA, Y. & KUBOTA, T. 2012. Augmentation of arginase expression in the human endometrial epithelium in the secretory phase. *J Med Dent Sci,* 59**,** 75-82.

TAKAMURA, M., KOGA, K., IZUMI, G., URATA, Y., NAGAI, M., HASEGAWA, A., HARADA, M., HIRATA, T., HIROTA, Y., WADA-HIRAIKE, O., FUJII, T. & OSUGA, Y. 2016. Neutrophil depletion reduces endometriotic lesion formation in mice. *Am J Reprod Immunol,* 76**,** 193-8.

TAN, Y., YANG, J., XIANG, K., TAN, Q. & GUO, Q. 2015. Suppression of microRNA-155 attenuates neuropathic pain by regulating SOCS1 signalling pathway. *Neurochem Res,* 40**,** 550-60.

TANIGUCHI, F. & HARADA, T. 2014. Endometriosis in Experimental Models. *In:* HARADA, T. (ed.) *Endometriosis: Pathogenesis and Treatment.* Tokyo: Springer Japan.

TARIVERDIAN, N., SIEDENTOPF, F., RUCKE, M., BLOIS, S. M., KLAPP, B. F., KENTENICH, H. & ARCK, P. C. 2009. Intraperitoneal immune cell status in infertile women with and without endometriosis. *J Reprod Immunol,* 80**,** 80-90.

TAYLOR, J. A., RISTAU, B., BONNEMAISON, M., VOZNESENSKY, O. S., HEGDE, P., KUCHEL, G. A. & PILBEAM, C. C. 2009. Regulation of the prostaglandin pathway during development of invasive bladder cancer in mice. *Prostaglandins & Other Lipid Mediators,* 88**,** 36-41.

TEAGUE, E. M., PRINT, C. G. & HULL, M. L. 2010. The role of microRNAs in endometriosis and associated reproductive conditions. *Hum Reprod Update,* 16**,** 142-65.

THIRUCHELVAM, U., DRANSFIELD, I., SAUNDERS, P. T. & CRITCHLEY, H. O. 2013. The importance of the macrophage within the human endometrium. J Leukoc Biol, 93, 217-25.

THOMSON, A. J., JARVIS, S. K., LENART, M., ABBOTT, J. A. & VANCAILLIE, T. G. 2005. The use of botulinum toxin type A (BOTOX) as treatment for intractable chronic pelvic pain associated with spasm of the levator ani muscles. *BJOG,* 112**,** 247-9.

TILI, E., MICHAILLE, J. J., WERNICKE, D., ALDER, H., COSTINEAN, S., VOLINIA, S. & CROCE, C. M. 2011. Mutator activity induced by microRNA-155 (miR-155) links inflammation and cancer. *Proc Natl Acad Sci U S A,* 108**,** 4908-13.

TOLOUBEYDOKHTI, T., PAN, Q., LUO, X., BUKULMEZ, O. & CHEGINI, N. 2008. The expression and ovarian steroid regulation of endometrial micro-RNAs. *Reprod Sci,* 15**,** 993-1001.

TRANGUCH, S., DAIKOKU, T., GUO, Y., WANG, H. & DEY, S. K. 2005. Molecular complexity in establishing uterine receptivity and implantation. *Cell Mol Life Sci,* 62**,** 1964-73.

TRISSAL, M. C., DEMOYA, R. A., SCHMIDT, A. P. & LINK, D. C. 2015. MicroRNA-223 regulates granulopoiesis but is not required for HSC maintenance in mice. *PLoS One,* 10**,** e0119304.

TSAI, E. M., WANG, Y. S., LIN, C. S., LIN, W. Y., HSI, E., WU, M. T. & JUO, S. H. 2013. A microRNA-520 mirSNP at the MMP2 gene influences susceptibility to endometriosis in Chinese women. *J Hum Genet,* 58**,** 202-9.

TSAI, S. J., WU, M. H., CHEN, H. M., CHUANG, P. C. & WING, L. Y. 2002. Fibroblast growth factor-9 is an endometrial stromal growth factor. *Endocrinology,* 143**,** 2715-21.

TUGAL, D., LIAO, X. & JAIN, M. K. 2013. Transcriptional control of macrophage polarization. *Arterioscler Thromb Vasc Biol,* 33**,** 1135-44.

TURCHINOVICH, A., WEIZ, L., LANGHEINZ, A. & BURWINKEL, B. 2011. Characterization of extracellular circulating microRNA. *Nucleic Acids Res,* 39**,** 7223-33.

TURNER, M. & VIGORITO, E. 2008. Regulation of B- and T-cell differentiation by a single microRNA. *Biochem Soc Trans,* 36**,** 531-3.

UDOU, T., HACHISUGA, T., TSUJIOKA, H. & KAWARABAYASHI, T. 2004. The role of c-jun protein in proliferation and apoptosis of the endometrium throughout the menstrual cycle. *Gynecol Obstet Invest,* 57**,** 121-6.

UGUR, M., TURAN, C., MUNGAN, T., KUSCU, E., SENOZ, S., AGIS, H. T. & GOKMEN, O. 1995. Endometriosis in association with mullerian anomalies. *Gynecol Obstet Invest,* 40**,** 261-4.

UNO, S., ZEMBUTSU, H., HIRASAWA, A., TAKAHASHI, A., KUBO, M., AKAHANE, T., AOKI, D., KAMATANI, N., HIRATA, K. & NAKAMURA, Y. 2010. A genome-wide association study identifies genetic variants in the CDKN2BAS locus associated with endometriosis in Japanese. *Nat Genet,* 42**,** 707-10.

VAN FURTH, R., RAEBURN, J. A. & VAN ZWET, T. L. 1979. Characteristics of human mononuclear phagocytes. *Blood,* 54**,** 485-500.

VAN LANGENDONCKT, A., CASANAS-ROUX, F., DOLMANS, M. M. & DONNEZ, J. 2002a. Potential involvement of hemoglobin and heme in the pathogenesis of peritoneal endometriosis. *Fertil Steril,* 77**,** 561-70.

VAN LANGENDONCKT, A., CASANAS-ROUX, F. & DONNEZ, J. 2002b. Iron overload in the peritoneal cavity of women with pelvic endometriosis. *Fertil Steril,* 78**,** 712-8.

VAN SCHAIK, T. A., KOVALEVSKAYA, N. V., PROTOPAPAS, E., WAHID, H. & NIELSEN, F. G. G. 2014. The need to redefine genomic data sharing: A focus on data accessibility. *Applied & Translational Genomics,* 3**,** 100-104.

VASQUEZ-DUNDDEL, D., PAN, F., ZENG, Q., GORBOUNOV, M., ALBESIANO, E., FU, J., BLOSSER, R. L., TAM, A. J., BRUNO, T., ZHANG, H., PARDOLL, D. & KIM, Y. 2013. STAT3 regulates arginase-I in myeloid-derived suppressor cells from cancer patients. *J Clin Invest,* 123**,** 1580-9.

VELLA, V. & MALAGUARNERA, R. 2018. The Emerging Role of Insulin Receptor Isoforms in Thyroid Cancer: Clinical Implications and New Perspectives. *Int J Mol Sci,* 19.

VERCELLINI, P. 1997. Endometriosis: what a pain it is. *Semin Reprod Endocrinol,* 15**,** 251-61.

VERCELLINI, P., DE BENEDETTI, F., ROSSI, E., COLOMBO, A., TRESPIDI, L. & CROSIGNANI, P. G. 1993. Tumor necrosis factor in plasma and peritoneal fluid of women with and without endometriosis. *Gynecol Obstet Invest,* 36**,** 39-41.

VERCELLINI, P., ESKENAZI, B., CONSONNI, D., SOMIGLIANA, E., PARAZZINI, F., ABBIATI, A. & FEDELE, L. 2011. Oral contraceptives and risk of endometriosis: a systematic review and meta-analysis. *Hum Reprod Update,* 17**,** 159-70.

VERCELLINI, P., VIGANO, P., SOMIGLIANA, E. & FEDELE, L. 2014. Endometriosis: pathogenesis and treatment. *Nat Rev Endocrinol,* 10**,** 261-75.

VIGANÒ, P., SOMIGLIANA, E., PARAZZINI, F. & VERCELLINI, P. 2012. Endometriosis and Cancer: Epidemiology. *Endometriosis.* Wiley-Blackwell.

VINATIER, D., ORAZI, G., COSSON, M. & DUFOUR, P. 2001. Theories of endometriosis. *Eur J Obstet Gynecol Reprod Biol,* 96**,** 21-34.

WANG, C., ZHANG, C., LIU, L., A, X., CHEN, B., LI, Y. & DU, J. 2017. Macrophage-Derived mir-155-Containing Exosomes Suppress Fibroblast Proliferation and Promote Fibroblast Inflammation during Cardiac Injury. *Mol Ther,* 25**,** 192-204.

WANG, J., YANG, K., ZHOU, L., MINHAOWU, WU, Y., ZHU, M., LAI, X., CHEN, T., FENG, L., LI, M., HUANG, C., ZHONG, Q. & HUANG, X. 2013a. MicroRNA-155 promotes autophagy to eliminate intracellular mycobacteria by targeting Rheb. *PLoS Pathog,* 9**,** e1003697.

WANG, L., HUANG, W., REN, C., ZHAO, M., JIANG, X., FANG, X. & XIA, X. 2016. Analysis of Serum microRNA Profile by Solexa Sequencing in Women With Endometriosis. *Reprod Sci,* 23**,** 1359-70.

WANG, N., LIANG, H. & ZEN, K. 2014a. Molecular Mechanisms That Influence the Macrophage M1–M2 Polarization Balance. *Frontiers in Immunology,* 5.

WANG, W. T., ZHAO, Y. N., HAN, B. W., HONG, S. J. & CHEN, Y. Q. 2013b. Circulating microRNAs identified in a genome-wide serum microRNA expression analysis as noninvasive biomarkers for endometriosis. *J Clin Endocrinol Metab,* 98**,** 281-9.

WANG, X. Q., YU, J., LUO, X. Z., SHI, Y. L., WANG, Y., WANG, L. & LI, D. J. 2010. The high level of RANTES in the ectopic milieu recruits macrophages and induces their tolerance in progression of endometriosis. *J Mol Endocrinol,* 45**,** 291-9.

WANG, Y., ADILA, S., ZHANG, X., DONG, Y., LI, W., ZHOU, M. & LI, T. 2014b. MicroRNA expression signature profile and its clinical significance in endometrioid carcinoma. *Zhonghua Bing Li Xue Za Zhi,* 43**,** 88-94.

WARSHAMANA-GREENE, G. S., LITZ, J., BUCHDUNGER, E., GARCIA-ECHEVERRIA, C., HOFMANN, F. & KRYSTAL, G. W. 2005. The insulin-like growth factor-I receptor kinase inhibitor, NVP-ADW742, sensitizes small cell lung cancer cell lines to the effects of chemotherapy. *Clin Cancer Res,* 11**,** 1563-71.

WAYNE, P. M., KERR, C. E., SCHNYER, R. N., LEGEDZA, A. T., SAVETSKY-GERMAN, J., SHIELDS, M. H., BURING, J. E., DAVIS, R. B., CONBOY, L. A., HIGHFIELD, E., PARTON, B., THOMAS, P. & LAUFER, M. R. 2008. Japanese-style acupuncture for endometriosis-related pelvic pain in adolescents and young women: results of a randomized sham-controlled trial. *J Pediatr Adolesc Gynecol,* 21**,** 247-57.

WEI, S., XU, H. & KUANG, Y. 2015. Systematic enrichment analysis of microRNA expression profiling studies in endometriosis. *Iranian Journal of Basic Medical Sciences,* 18**,** 423-429.

WILKOSZ, S., PULLEN, N., DE-GIORGIO-MILLER, A., IRELAND, G. & HERRICK, S. 2011. Cellular exchange in an endometriosis-adhesion model using GFP transgenic mice. *Gynecol Obstet Invest,* 72**,** 90-7.

WINTERHAGER, E. 2012. Role of Steroid Hormones: Estrogen and Endometriosis. *Endometriosis.* Wiley-Blackwell.

WONG, Q. W., LUNG, R. W., LAW, P. T., LAI, P. B., CHAN, K. Y., TO, K. F. & WONG, N. 2008. MicroRNA-223 is commonly repressed in hepatocellular carcinoma and potentiates expression of Stathmin1. *Gastroenterology,* 135**,** 257-69.

WORM, J., STENVANG, J., PETRI, A., FREDERIKSEN, K. S., OBAD, S., ELMEN, J., HEDTJARN, M., STRAARUP, E. M., HANSEN, J. B. & KAUPPINEN, S. 2009. Silencing of microRNA-155 in mice during acute inflammatory response leads to derepression of c/ebp Beta and down-regulation of G-CSF. *Nucleic Acids Res,* 37**,** 5784-92.

WU, M. H., HSIAO, K. Y. & TSAI, S. J. 2019. Hypoxia: The force of endometriosis. *J Obstet Gynaecol Res,* 45**,** 532-541.

WU, M. H., SUN, H. S., LIN, C. C., HSIAO, K. Y., CHUANG, P. C., PAN, H. A. & TSAI, S. J. 2002. Distinct mechanisms regulate cyclooxygenase-1 and -2 in peritoneal macrophages of women with and without endometriosis. *Mol Hum Reprod,* 8**,** 1103-10.

WU, M. Y., CHAO, K. H., YANG, J. H., LEE, T. H., YANG, Y. S. & HO, H. N. 2003. Nitric oxide synthesis is increased in the endometrial tissue of women with endometriosis. *Hum Reprod,* 18**,** 2668-71.

WYNN, T. A. & BARRON, L. 2010. Macrophages: master regulators of inflammation and fibrosis. *Semin Liver Dis,* 30**,** 245-57.

WYNN, T. A., CHAWLA, A. & POLLARD, J. W. 2013. Macrophage biology in development, homeostasis and disease. *Nature,* 496**,** 445-55.

YAMAMOTO, Y., MAEDA, N., IZUMIYA, C., KUSUME, T., OGURI, H., KAWASHIMA, M., HAYASHI, K., NOMURA, A., YAMASHITA, C. & FUKAYA, T. 2008. Decreased human leukocyte antigen-DR expression in the lipid raft by peritoneal macrophages from women with endometriosis. *Fertil Steril,* 89**,** 52-9.

YAN, G. J., YU, F., WANG, B., ZHOU, H. J., GE, Q. Y., SU, J., HU, Y. L., SUN, H. X. & DING, L. J. 2014. MicroRNA miR-302 inhibits the tumorigenicity of endometrial cancer cells by suppression of Cyclin D1 and CDK1. *Cancer Lett,* 345**,** 39-47.

YANG, H., LIU, J., FAN, Y., GUO, Q., GE, L., YU, N., ZHENG, X., DOU, Y. & ZHENG, S. 2016. Associations between various possible promoter polymorphisms of MMPs genes and endometriosis risk: a meta-analysis. *Eur J Obstet Gynecol Reprod Biol,* 205**,** 174-88.

YANG, X., DONG, Y., ZHAO, J., SUN, H., DENG, Y., FAN, J. & YAN, Q. 2007. Increased expression of human macrophage metalloelastase (MMP-12) is associated with the invasion of endometrial adenocarcinoma. *Pathol Res Pract,* 203**,** 499-505.

YANG, Z., ZHONG, L., XIAN, R. & YUAN, B. 2015. MicroRNA-223 regulates inflammation and brain injury via feedback to NLRP3 inflammasome after intracerebral hemorrhage. *Mol Immunol,* 65**,** 267-76.

YARMOLINSKAYA, M. I., MOLOTKOV, A. S., BEZHENAR, V. F., SHVED, N. Y., IVASCHENKO, T. E. & BARANOV, V. S. 2014. Matrix metalloproteinases's association of polymorphisms of MMP3 and MMP9 with development of genital endometriosis. *Russian Journal of Genetics,* 50**,** 205-210.

YE, D., ZHANG, T., LOU, G. & LIU, Y. 2018. Role of miR-223 in the pathophysiology of liver diseases. *Exp Mol Med,* 50**,** 128.

YIN, H., SONG, S. & PAN, X. 2017. Knockdown of miR-155 protects microglia against LPS-induced inflammatory injury via targeting RACK1: a novel research for intracranial infection. *J Inflamm (Lond),* 14**,** 17.

YING, W., TSENG, A., CHANG, R. C.-A., MORIN, A., BREHM, T., TRIFF, K., NAIR, V., ZHUANG, G., SONG, H., KANAMENI, S., WANG, H., GOLDING, M. C., BAZER, F. W., CHAPKIN, R. S., SAFE, S. & ZHOU, B. 2015. MicroRNA-223 is a crucial mediator of PPARγ-regulated alternative macrophage activation. *The Journal of Clinical Investigation,* 125**,** 4149-4159.

YOO, A. S., SUN, A. X., LI, L., SHCHEGLOVITOV, A., PORTMANN, T., LI, Y., LEE-MESSER, C., DOLMETSCH, R. E., TSIEN, R. W. & CRABTREE, G. R. 2011. MicroRNA-mediated conversion of human fibroblasts to neurons. *Nature,* 476**,** 228-31.

YOUNG, V. J., AHMAD, S. F., DUNCAN, W. C. & HORNE, A. W. 2017. The role of TGF-beta in the pathophysiology of peritoneal endometriosis. *Hum Reprod Update,* 23**,** 548-559.

YOUNG, V. J., BROWN, J. K., MAYBIN, J., SAUNDERS, P. T., DUNCAN, W. C. & HORNE, A. W. 2014a. Transforming growth factor-beta induced Warburg-like metabolic reprogramming may underpin the development of peritoneal endometriosis. *J Clin Endocrinol Metab,* 99**,** 3450-9.

YOUNG, V. J., BROWN, J. K., SAUNDERS, P. T., DUNCAN, W. C. & HORNE, A. W. 2014b. The peritoneum is both a source and target of TGF-beta in women with endometriosis. *PLoS One,* 9**,** e106773.

YOUNG, V. J., BROWN, J. K., SAUNDERS, P. T. & HORNE, A. W. 2013. The role of the peritoneum in the pathogenesis of endometriosis. *Hum Reprod Update,* 19**,** 558-69.

YU, J., WANG, Y., ZHOU, W. H., WANG, L., HE, Y. Y. & LI, D. J. 2008. Combination of estrogen and dioxin is involved in the pathogenesis of endometriosis by promoting chemokine secretion and invasion of endometrial stromal cells. *Hum Reprod,* 23**,** 1614-26.

YU, Y. H., ZHANG, L., WU, D. S., ZHANG, Z., HUANG, F. F., ZHANG, J., CHEN, X. P., LIANG, D. S., ZENG, H. & CHEN, F. P. 2013. MiR-223 regulates human embryonic stem cell differentiation by targeting the IGF-1R/Akt signaling pathway. *PLoS One,* 8**,** e78769.

YUAN, X., BERG, N., LEE, J. W., LE, T. T., NEUDECKER, V., JING, N. & ELTZSCHIG, H. 2018. MicroRNA miR-223 as regulator of innate immunity. *J Leukoc Biol,* 104**,** 515-524.

ZAJAC, E., SCHWEIGHOFER, B., KUPRIYANOVA, T. A., JUNCKER-JENSEN, A., MINDER, P., QUIGLEY, J. P. & DERYUGINA, E. I. 2013. Angiogenic capacity of M1- and M2-polarized macrophages is determined by the levels of TIMP-1 complexed with their secreted proMMP-9. *Blood,* 122**,** 4054-67.

ZAMAH, N. M., DODSON, M. G., STEPHENS, L. C., BUTTRAM, V. C., JR., BESCH, P. K. & KAUFMAN, R. H. 1984. Transplantation of normal and ectopic human endometrial tissue into athymic nude mice. *Am J Obstet Gynecol,* 149**,** 591-7.

ZENG, Y., ZHANG, X., KANG, K., CHEN, J., WU, Z., HUANG, J., LU, W., CHEN, Y., ZHANG, J., WANG, Z., ZHAI, Y., QU, J., RAMCHANDRAN, R., RAJ, J. U., WANG, J. & GOU, D. 2016. MicroRNA-223 Attenuates Hypoxia-induced Vascular Remodeling by Targeting RhoB/MLC2 in Pulmonary Arterial Smooth Muscle Cells. *Scientific Reports,* 6**,** 24900.

ZHANG, C., MAEDA, N., IZUMIYA, C., YAMAMOTO, Y., KUSUME, T., OGURI, H., YAMASHITA, C., NISHIMORI, Y., HAYASHI, K., LUO, J. & FUKAYA, T. 2006. Killer immunoglobulin-like receptor and human leukocyte antigen expression as immunodiagnostic parameters for pelvic endometriosis. *Am J Reprod Immunol,* 55.

ZHANG, D., CUI, Y., LI, B., LUO, X., LI, B. & TANG, Y. 2017a. A comparative study of the characterization of miR-155 in knockout mice. *PLoS One,* 12**,** e0173487.

ZHANG, D., LI, Y., TIAN, J., ZHANG, H. & WANG, S. 2015. MiR-202 promotes endometriosis by regulating SOX6 expression. *Int J Clin Exp Med,* 8**,** 17757-64.

ZHANG, F., WANG, H., WANG, X., JIANG, G., LIU, H., ZHANG, G., WANG, H., FANG, R., BU, X., CAI, S. & DU, J. 2016a. TGF-β induces M2-like macrophage polarization via SNAIL-mediated suppression of a pro-inflammatory phenotype. *Oncotarget,* 7**,** 52294-52306.

ZHANG, N., FU, L., BU, Y., YAO, Y. & WANG, Y. 2017b. Downregulated expression of miR-223 promotes Toll-like receptor-activated inflammatory responses in macrophages by targeting RhoB. *Mol Immunol,* 91**,** 42-48.

ZHANG, Q., LIU, X. & GUO, S.-W. 2017c. Progressive development of endometriosis and its hindrance by anti-platelet treatment in mice with induced endometriosis. *Reproductive BioMedicine Online,* 34**,** 124-136.

ZHANG, T., DE CAROLIS, C., MAN, G. C. W. & WANG, C. C. 2018. The link between immunity, autoimmunity and endometriosis: a literature update. *Autoimmun Rev,* 17**,** 945-955.

ZHANG, X., KE, X., PU, Q., YUAN, Y., YANG, W., LUO, X., JIANG, Q., HU, X., GONG, Y., TANG, K., SU, X., LIU, L., ZHU, W. & WEI, Y. 2016b. MicroRNA-410 acts as oncogene in NSCLC through downregulating SLC34A2 via activating Wnt/beta-catenin pathway. *Oncotarget,* 7**,** 14569-85.

ZHANG, X., LI, M., ZUO, K., LI, D., YE, M., DING, L., CAI, H., FU, D., FAN, Y. & LV, Z. 2013. Upregulated miR-155 in papillary thyroid carcinoma promotes tumor growth by targeting APC and activating Wnt/beta-catenin signaling. *J Clin Endocrinol Metab,* 98**,** E1305-13.

ZHANG, Y., ZHANG, M., LI, X., TANG, Z., WANG, X., ZHONG, M., SUO, Q., ZHANG, Y. & LV, K. 2016c. Silencing MicroRNA-155 Attenuates Cardiac Injury and Dysfunction in Viral Myocarditis via Promotion of M2 Phenotype Polarization of Macrophages. *Scientific Reports,* 6**,** 22613.

ZHAO, A., YANG, Z., SUN, R., GRINCHUK, V., NETZEL-ARNETT, S., ANGLIN, I. E., DRIESBAUGH, K. H., NOTARI, L., BOHL, J. A., MADDEN, K. B., URBAN, J. F., JR., ANTALIS, T. M. & SHEA-DONOHUE, T. 2013. SerpinB2 is critical to Th2 immunity against enteric nematode infection. *J Immunol,* 190**,** 5779-87.

ZHAO, M., TANG, Q., WU, W., XIA, Y., CHEN, D. & WANG, X. 2014a. miR-20a contributes to endometriosis by regulating NTN4 expression. *Mol Biol Rep,* 41**,** 5793-7.

ZHAO, Y.-N., CHEN, G.-S. & HONG, S.-J. 2014b. Circulating MicroRNAs in gynecological malignancies: from detection to prediction. *Experimental Hematology & Oncology,* 3**,** 1-5.

ZHAO, Z. Z., CROFT, L., NYHOLT, D. R., CHAPMAN, B., TRELOAR, S. A., HULL, M. L. & MONTGOMERY, G. W. 2011. Evaluation of polymorphisms in predicted target sites for micro RNAs differentially expressed in endometriosis. *Mol Hum Reprod,* 17**,** 92-103.

ZHENG, B., XUE, X., ZHAO, Y., CHEN, J., XU, C. Y. & DUAN, P. 2014. The differential expression of microRNA-143,145 in endometriosis. *Iran J Reprod Med,* 12**,** 555-60.

ZHENG, W., CAO, L., XU, Z., MA, Y. & LIANG, X. 2018. Anti-Angiogenic Alternative and Complementary Medicines for the Treatment of Endometriosis: A Review of Potential Molecular Mechanisms. *Evid Based Complement Alternat Med,* 2018**,** 4128984.

ZHOU, H. C., FANG, J. H., LUO, X., ZHANG, L., YANG, J., ZHANG, C. & ZHUANG, S. M. 2014. Downregulation of microRNA-100 enhances the ICMT-Rac1 signaling and promotes metastasis of hepatocellular carcinoma cells. *Oncotarget,* 5**,** 12177-88.

ZHU, N., ZHANG, D., CHEN, S., LIU, X., LIN, L., HUANG, X., GUO, Z., LIU, J., WANG, Y., YUAN, W. & QIN, Y. 2011. Endothelial enriched microRNAs regulate angiotensin II-induced endothelial inflammation and migration. *Atherosclerosis,* 215**,** 286-93.

ZHUANG, G., MENG, C., GUO, X., CHERUKU, P. S., SHI, L., XU, H., LI, H., WANG, G., EVANS, A. R., SAFE, S., WU, C. & ZHOU, B. 2012. A novel regulator of macrophage activation: miR-223 in obesity-associated adipose tissue inflammation. *Circulation,* 125**,** 2892-903.

ZHUANG, Z., XIAO, Q., HU, H., TIAN, S. Y., LU, Z. J., ZHANG, T. Z. & BAI, Y. L. 2015. Down-regulation of microRNA-155 attenuates retinal neovascularization via the PI3K/Akt pathway. *Mol Vis,* 21**,** 1173-84.

ZONDERVAN, K. T., BECKER, C. M., KOGA, K., MISSMER, S. A., TAYLOR, R. N. & VIGANO, P. 2018. Endometriosis. *Nat Rev Dis Primers,* 4**,** 9.